Reclamation of red mud (RM) through microbial and vermi-technology- A lead towards sustainability

A thesis submitted to

Jadavpur University

In partial fulfilment of the requirements for the degree of

Doctor of Philosophy (Science)

by

Kasturi Charan (M.Sc.)

(Index No. 52/16/Life Sc./24)

Department of Life Science and Biotechnology

Jadavpur University

and

Agriculture and Ecological Research Unit

Indian Statistical Institute, Kolkata

June 2023

INDIAN STATISTICAL INSTITUTE

Pradip Bhattacharyya, PhD
Associate Professor
Biological Science Division
Agricultural & Ecological Research Unit

Rose Villa, New Barganda
Giridih, Jharkhand - 815 301, India
06532-226688 (O), (91) 09859986548 (mobile)
pradip.bhattacharyya@gmail.com

Dated: 17.06.2023

Certificate from the supervisor

This is to certify that the thesis entitled **"Reclamation of red mud (RM) through microbial and vermi-technology- A lead towards sustainability"** submitted by **Smt. Kasturi Charan** who got her name registered on **20.04.2016** for the award of **Ph.D. (Science)** Degree of **Jadavpur University, Department of Life Science and Biotechnology**, is absolutely based upon her work under the supervision of **Dr. Pradip Bhattacharyya** and that neither this thesis nor any part of it has been submitted for either any degree/ diploma or any other academic award anywhere before.

Pradip Bhattacharyya

Pradip Bhattacharyya, Ph.D
Associate Professor
Agricultural and Ecological Research Unit
Indian Statistical Institute
New Barganda, Giridih-815301
Jharkhand, India

Thank you, Krishna, …

Dedicated to my baba, maa, and beloved bonu…..

DECLARATION OF ORIGINALITY

I Kasturi Charan, **Index No.: 52/16/Life Sc./24**, hereby declare that this Ph.D. thesis entitled "**Reclamation of Red-mud through microbial and vermi technology – A lead towards sustainability**" represents my original work carried out as a doctoral scholar at **Indian Statistical Institute, Giridih, Jharkhand**. The work contained in the thesis is original and has been done by myself under the supervision of my supervisor, **Dr. Pradip Bhattacharyya, AERU, Giridih**. To the best of my knowledge, it does not contain any material previously published or written by any other person. The work has not been submitted to Jadavpur University or any other Institute for any other degree or diploma. Any input from sources other than myself or others with whom I have collaborated on this study has been acknowledged. I have given due credit to them by citing them in the text of the thesis and giving their details in the references. When I have used writing from another source, I have always put it in quotation marks and give credit where credit is due by citing the source and providing all necessary information in the references.

Kasturi Charan

Date: 17.06.2023 (Kasturi Charan)

ACKNOWLEDGEMENT

I want to take this opportunity to offer my sincere appreciation to everyone who has supported me this far in whatever form. First and foremost, my deepest sense of gratitude goes to my boss Dr. Pradip Bhattacharyya, Associate Professor, Indian Statistical Institute, without whom this degree would not have been a reality. His in-depth scrutiny of the topic, insightful ideas, and degree of expertise in the subject illuminated my path of journey. At several points in my research, his perceptive remarks and creative observations incited thought in me and enabled me to sharpen my focus. He allowed me the freedom to go exploring on my own while also providing the direction I needed to go back on track when my steps stumbled. To say that his advice, compassion, support, and extraordinary patience have been indispensable along this research journey.

I would also like to acknowledge Dr. Abhishek Mukherjee, Associate Professor, Indian Statistical Institute, Dr. Satya Sundar Bhattacharya, Assistant Professor, Tezpur University, and Dr. Jajati Mandal, University of Salford, UK, for their valuable ideas, knowledge, and moral support during the high and lows of this research expedition.

I would like to express my gratitude to my lab attendants, specifically late Hari da, Chotte bhaiya, Aslam da, Devsan da, and Suman da, Rashid Da for their constant assistance during laboratory work and field studies. A note of appreciation to my seniors Dr. Ananya Mondal and Dr. Saibal Ghosh for their help and cooperation whenever I required. My juniors Sonali, Suvasri, Shreya, Sonam, Rupsha, Ishita, Sumit, Gourav, and Riddhi especially deserve my gratitude for their cooperation, assistance, and contribution for providing a pleasant atmosphere at work. I will always treasure the time I spent with them at events and on other occasions while I was on this research journey. A special mention to Dr. Sandip Mondal, Post-Doctoral Scholar, The Ohio State University, Dr. Debasish Rana, Executive Product Development Officer, UPL Ltd., and Mrs. Kajori Saha, Junior Research Fellow, Indian Statistical Institute for their help and suggestion during my crop trial time. I also want to thank Nibedeeta di and Krishna for their helpful input on my work.

I convey my gratitude to Indian Statistical Institute, Kolkata for the financial assistance. I extend my sincere thanks to Amrit Dutta, Consultant, Tea Research Association for assisting in some field studies at the early stage of my research life. I would like to acknowledge Punjab University for providing FESEM-EDX and FTIR facilities.

Friends allegedly don't reciprocate thanks. I must then thank my own good fortune to have friends like Dr. Shreosi Chatterjee, Dr. Sandip Mondal, Dr. Kishalay Adhikari, Soumavo, Suchismita, Shibani, Rajarshi, and Aritra for their constant motivation and academic help. Most importantly, they have honestly stood by me during the best and worst of times. I “thank you all” for everything. I am also very much thankful to Adrija di, for giving me company during my thesis writing days.

Aboveground, I want to express my deepest sense of appreciation to my teachers who laid a strong base for my personal development from the beginning of my formal education. Words are not enough to express my thanks to them. I want to thank Mr. Pradip Samanta, sir, and Dr. Arpita Patra, ma'am, in particular, for inspiring my passion for my subject, microbiology, and encouraging me to pursue a career in research.

Finally, and certainly, not least, I must express my gratitude to Indian Statistical Institute, Agriculture and Ecological Research Unit, Giridih, Jharkhand for providing me with the chance to do my research.

Before I finish, I want to express my immense gratefulness to my father Dr. Kartick Chandra Charan, my mother KumKum Charan, and my aunty Namita Goswami for their unending encouragement, love, and enthusiasm, which kept me motivated toward my goals. No amount of thankfulness could ever fully express my appreciation for my dearest sisters' (Kausiki Charan) love, care, and support.

Above all, I thank my “Krishna”, the almighty being with me always and leading me on.

Date: 17.06.2023

Kasturi Charan

(Kasturi Charan)

ABSTRACT

This thesis illustrates how the hazardous aluminum industry waste known as red mud (RM) is managed sustainably. In this work waste (RM) was explored from two different perspectives in terms of their utilization: firstly, used as a vermicompost for agricultural applications, and secondly, as a port for harbouring numerous extremophilic bacteria with a wide range of utility. In present study, we investigated the metal remediation potential of one polyextremophilic bacteria isolated from RM, which may help in wastewater treatment. On a global scale, >100 million tons of RM are being produced annually with which India contributes approximately 10 million tons annually. Consequently, the global inventory of disposal is rising sharply, however, by 2015, it was past 4 billion tonnes. Effective post-production treatment and subsequent disposal are burning issues worldwide in regard to their environmental impact. High alkalinity, disproportionate Na concentration, and elevated presence of heavy metal coupled with radioactive elements are alarming if not adequately managed. Management of this lethal waste following international standards in developing countries requires experts with sound knowledge and experience. Moreover, the aluminum industries should follow international waste management standards and environmental protection policies. Regrettably, India failed not to sustain its pollution control measures, and as a result, it is ranked as the 7th most environmentally hazardous country.

Therefore, the repository of alkaline sodic red mud is in dire need of clean sustainable technology to alleviate the risk from its disposal and storage. One of the most trustworthy bioprocessing techniques, vermitechnology involves the quick stabilization and conversion of stubborn waste materials into friable and nutrient-rich organic fertilizer through the mutually beneficial actions of earthworms and microbes. Although a wide category of solid waste (brick kiln ash, municipal solid waste, tannery sludge, oil industry sludge, etc.) is managed through vermitechnology, however, use of vermitechnology in managing RM is not gaining momentum due to its threatening Na concentration. Under this context, we opted for a pretreatment technique that includes the use of calcium sulfate ($CaSO_4.2H_2O$) and calcium chloride ($CaCl_2.2H_2O$) in a 6 g/kg dose, followed by leaching (1:10 ratio) using a siphonic approach. The study's ultimate goal was to offer a vermistabilized RM with an appropriate field-scale agricultural application. The study was commenced by thoroughly analysing the RM and its effects on the environment and human health. Such in-depth research produced some crucial data and information needed to standardize vermitechnology. As harmful metals including Cr, Cd, Pb, and Ni are known to be abundant in RM, the earthworm species *Eisenia fetida* was chosen as a candidate species due to their extensive popularity in managing noxious waste. In the end, the vermicomposted RM was used as a source of crucial nutrients and a plant growth stimulant for the production of rice in red-lateritic soil. RM was characterized by highly sodic (Na+ 6.5%±0.5), elevated electrical conductivity (12.2 ±2.1 mS/cm) with high pH (11.5 ±1.9) and elevated toxic metal concentration which ranged as follows: 392 ±46.66 mg/kg (Cr), 9.71 ±1.37 mg/kg (Cd), 139.68 ±12.74 mg/kg (Ni) and 228.64 ±16.66 mg/kg (Pb). FESEM- EDX study revealed the aggregated structure with an elemental abundance of Fe_2O_3, TiO_2, Al_2O_3, SiO_2, and Na_2O. According to FTIR results Fe-O, Ti-O, Al-O, and Mg-O type bonds were largely present, while the XRD- study described their partial crystalline structure enriched with Fe_2O_3, Al_2O_3, quartz, and cristobalite. Environmental impact indices analysed that RM is posing a high pollution load to the environment (Pollution Index= 2.68) with severe

ecological risk (Ecological Risk Index = 587.86). Enduring exposure to Cr, Pb, and Ni from RM poses a serious risk to human health. Since RM is aluminum industry-generated waste, so, in our study, we also compared their characteristics with native bauxite ore (BO; chief commercial ore of Al^{3+}) to evaluate the degree of deviation after industrial Bayer extraction of aluminum. The study revealed an exclusive result that implied a drastic increase in Na and Ca content, DTPA-available metal including the enhancement of leaching characteristics of metals (TCLP study) in RM. Furthermore, microbial presence was largely reduced in RM compared to native BO indicating a dramatic fall of microbial load, confirmed by some microbial indicator enzymes viz., dehydrogenase (DHG), fluorescein diacetate hydrolysing activity (FDA), and microbial biomass C.

Following this thorough investigation, we conducted an RM-vermicomposting experiment with four distinct waste-to-bulking agent ratios (RM: CD), namely 1:1 (RM: CD), 1:2 (RM: CD), 1:3, and 1:4. In order to investigate the role of earthworms in altering the bioavailability of metal concentration, plant nutrients, organic matter content, and enhancement of microbial activity, a parallel traditional aerobic composting was carried out to evaluate the efficacy of vermicompost. Each ratio for vermicomposting inoculated with *Eisenia fetida* @ 10 worms per kg of substrate and incubated under a shaded vermicompost unit for 90 days, maintaining 50%- 60% moisture content with adequate aeration. Simultaneously, another series of aerobic composting was maintained using the same treatment combinations without earthworm inoculation. The result disclosed that exorbitant alkalinity was pacified to neutrality in all E. fetida-based feedstock with a considerable reduction in TOC, Na^{+}, and Ca^{2+} and increased NPK availability. Greater improvement in C_{mic}, respiration, and enzymatic activity was evidenced in vermireactors. Water soluble and exchangeable fractions of metal reduced by >55% (Cu, Cr, Pb, Ni, and Cd) in vermibeds. Fatty acid profiling (PLFA) and species diversity analysis (alpha diversity, E-var, E-PLFA) outlined that community distribution was significantly impacted by RM proportion in feedstock however it was proficiently compensated in VC2 (1RM:2CD) and VC3 (1RM:3CD). A switch from P to N limitation to microbial requisite in the reactors is an important scientific observation from vector analysis. Pearson's correlation statistics signify that metal availability was efficiently compressed by microbial activity at the end of incubation. Lastly, the field trial with monsoon rice (*Oryza sativa* L.) showed the most prolific vermicompost mixture was 1:2 and 1:3 which produced the highest yield of 4.2 tons/ha, when substituted with 50% NPK (50% RM-VC+ 50% NPK). A concurrent soil health analysis (available NPK, TOC, and microbial activity) revealed an improvement in RM-VC treated plots. In terms of the metal uptake results, rice roots accumulated metal less than untreated plots on average, however, shoot and grain did not accumulate any metal.

Focusing on the second direction of work, initially the RM was explored for its biological characteristics through enzymatic analysis which showed incredibly poor activity. Nevertheless, a 16S V3-V4 Metagenome study revealed the presence of microbes that mostly belonged to the genera *Bacillus*, *Halomonas*, *Alcanovorax*, *Indibacter*, *KSA 1*, etc. Proteobacteria, Bacteroidetes, Planctomycetes, and Actinobacteria were the predominant phylum. The total heterotrophic bacterial count showed the fresh residue was completely barren, however, long-term deposited RM was obtained by 1.4 X 102- 2.9 X 102 cfu/g. A total of 20 alkaliphilic isolates were obtained and

biochemically characterized. Focusing on objective of the study of finding metal-tolerant alkaliphilic bacteria, five isolates were selected based on their minimum inhibitory concentration (MIC). Out of these five isolates *Bacillus xiamenensis* ISIGRM16 showed their wide range of pH, temperature, and NaCl concentration, thus selected as polyextremophilic bacteria, which subsequently explored for their metal adsorption ability for three predominant metal (Cd^{2+}, Ni^{2+}, Cr^{6+}) species of the wastewater stream. The dried biomass biosorbent was able to remove Cd^{2+}(>99%), Ni^{2+}(>85%), and Cr^{6+}(>40%) from the aqueous solution under different temperatures, pH, ion concentration, salinity, and time exposure. The interaction mechanism followed both Freundlich (Cd^{2+}) and Langmuir (Cr^{6+}, Ni^{2+}) isotherm models in accordance with pseudo-2nd-order kinetics. The reaction was both exothermic (Cd^{2}+, Ni^{2+}) and endothermic (Cr^{6+}) based on the choice of metal. Maximum loading capacities were 31.99 mg/g, 29.30 mg/g, and 13.68 mg/g for Cd^{2+}, Ni^{2+}, and Cr^{6+} respectively. In multi-component systems, adsorption capacity remained most consistent for Ni^{2+} followed by Cd^{2+} and Cr^{6+} confirmed by their relative adsorption capacity (R_i). FT-IR reveals that the carboxyl, amide, and hydroxyl are accountable for host-guest interaction. FESEM-EDAX analysis closely divulged the morphological alteration along with the adsorbed metal. A sequential adsorption-desorption study confirmed significant removal efficacy conservation up to 3rd cycle ($p<0.05$) making it gainful for commercial scale.

Keywords: *Eisenia fetida*, red mud, toxic metal, PLFA, soil health, crop growth, extremophilic, relative adsorption, isotherm, kinetics, thermodynamics, heavy metals.

Kasturi Charan 17.06.2023
(Signature of Student)

Pradip Bhattacharyya 17.06.2023
(Signature of Supervisor)

Pradip Bhattacharyya, Ph.D
Associate Professor
Agricultural and Ecological Research Unit
Indian Statistical Institute
New Barganda, Giridih-815301
Jharkhand, India

LIST OF ABBREVIATIONS

AAS: Atomic Absorption Spectroscopy

ANOVA: Analysis of variance

ANOSIM: Analysis of similarity

As: Arsenic

FTIR: Attenuated total reflectance Fourier-transformed infrared

ATSDR: Agency for Toxic Substances and Disease Registry

BaF: Bioaccumulation factor

BLAST: Basic Local Alignment Search Tool

BO: Bauxite ore

Ca: Calcium

Cd: Cadmium

CDA: Czapek Dox Agar

CD: Cow dung

Cd: Cadmium

CEC: Cation exchange capacity

CFU: Colony formation unit

CR: Compost respiration

CR: Cancer risk

Cr: Chromium

Cu: Copper

CQQ: Compost quality quotient

DTPA: Diethylenetriaminepentaacetic acid

EC: Electrical conductivity

ECM: Extracellular matrix

EDX: Energy-dispersive X-ray spectroscopy

EDI: Estimated daily intake

EPS: Extra polymeric substances

ERI: Ecological risk index

FESEM: Field emission scanning electron microscopy

FYM: Farm Yard Manure

FIAM: Free ion activity model

FS: Forest soil

Hg: Mercury

HI: Hazard Index

HQ: Hazard quotient

I_{geo}: Geo-accumulation index

IARC: International Agency for Research on Cancer

JCPDS-ICCD: Joint Committee on Powder Diffraction Standards-International Centre for Diffraction Data

K: Potassium

K_b: Biodegradability quotient

LSD: Least significant difference

MBC: Microbial biomass carbon

MCT: Micro centrifuge tube

Mg: Magnesium

MF: Mobility factor

MIC: Minimal inhibitory concentration

MUFA: Mono unsaturated fatty acid

MDL: Method detection limit

N: Nitrogen

NFB: Nitrogen fixing bacteria

NaOAc: Sodium acetate

NCBI: National Center for Biotechnology Information

Ni: Nickel

OD: Optical density

PCA: Principal component analysis

PLFA: Phospholipid fatty acid analysis

PERMANOVA: Permutational multivariate analysis of variance

PCF: Phyto concentration factor

PF: Phytoaccumulation factor.

PLI: Pollution load index

PTE: Potentially toxic element

Pb: Lead

PBS: Phosphate buffer saline

PCR: polymerase chain reaction

PUFA: Polyunsaturated fatty acid

qCO_2: Metabolic quotient.

QC: Quality control

QA: Quality assurance

RQ: Respiration quotient

R^2: Correlation coefficient

REE: Rare earth element

RM: Red mud

RM: Relative mobility

RM-VC: Red mud vermicompost

RBD: Randomized block design

R_fD: Reference dose

SIMPER: Similarity percentage analysis

SRM: Standard reference material

SOC: Soil organic carbon

SR: Soil respiration

TOC: Total organic carbon

TF: Translocation factor

TSS: Total soluble sugar

USEPA: United States Environmental Protection Agency

XRD: X-ray Diffraction

Zn: Zinc

$\Delta G°$: Gibbs free energy

$\Delta H°$: Enthalpy

$\Delta S°$: Entropy

LIST OF FIGURES

LIST OF TABLES

NOTATIONS

°C: Degree Celsius

K: Kelvin

%: Percentage

g: Gram

mg: Milligram

µg: Microgram

h: Hour

min: Minute

mm: Millimeter

µm: Micrometer

nm: Nanometer

Å: Angstrom

Km^2: Kilometer square

ml: Milliliter

L: Liter

µl: Microliter

g/L: Gram per liter

mg/L: Milligram per liter

µg /L: Microgram per liter

mol/L: Mole per liter

mg/kg: Milligram per kilogram

mg/g: Milligram per gram

mS/cm: Milli siemens per centimeter

min^{-1}: Minute inverse

$L.mg^{-1}$: Liter per milligram

µg $gram^{-1}h^{-1}$: Micro gram per hour.

M: Molar

mM: Millimolar

CFU/ml: Colony forming unit per milliliter

CFU/g: Colony forming unit per gram

cmol kg^{-1}: Centimole per kg

mV: Millivolt

KV: Kilovolt

w/v: Weight per volume

v/v: Volume per volume

2θ: 2 thetas

rpm: Revolution per minute

ppm: Parts per million

TABLE OF CONTENTS

Chapter 1

General Introduction

Chapter 1

General Introduction

1. Introduction

1.1. The scenario

Advancement of civilization experiences spectacular progress in different industrial sectors. The boost in industrialization paves the way to fortify economic growth and progress of any nation. Such progression leads to a proficient lifestyle in any society. Implementation of society's requirements is appreciable yet many factors are not overcome by them successfully and one of that is safe disposal and utilization of waste generating at the end. Increasing industrial activities like transportation, consumption, manufacturing, and downstream processing of the product not only disrupts the natural biodiversity but also put stress on environment by accumulating waste beyond its capacity. Unscientific management of waste specifically in developing countries adversely affects the quality of environment, presently becoming a threat towards sustainability. In the race of globalization, environmental awareness was the least concerned issue in the early 19^{th} century, however, in the late 1980s environmental pollution and public health has become a thoughtful subject around the globe. Due to dense population and high demand for commodity in developing countries, waste generation, and its management has not been handled in accordance with international standards, consequently, India is listed as the 7^{th} most environmentally hazardous country in the world (Liu et al., 2014; Li et al., 2021)

Like any other industry, alumina, and aluminum industry plays a revolutionary role in globalization. This lightweight metal was introduced long before to mankind when it was considered to be an unknown metal that resembles silver. However, this unfamiliar metal has now become an inevitable part of life. It has gained significant interest owing to its diversified application in different sectors. It is the second most widely used metal after steel (Sanders, 2002). This metal has seldom utilization in its pure form, instead has an inclusive application in alloy form. The strength of the alloys, which are mostly created with magnesium, copper, silicon, and manganese, is increased by about 15 times when compared to their pure form (Ramaswamy et al., 2019). India is the 2^{nd} largest aluminum producer after China, sharing nearly 5.3% of global aluminum output. Six different industries broadly use aluminum and can be categorized by sectors: 23% in transportation, trailed by construction (22%), packaging

(13%), electrical (12%), machinery and equipment (8.5%), consumer durables (4.5%), and other segments (4%). The metal is incredibly adaptable, inexpensive, and attractive for widespread application (Pandey & Prakash, 2020). The only precursor of aluminum on this earth is bauxite and the most common economic process of extraction of alumina from bauxite ore is the Bayer process availed by maximum refineries/industries across the world. During the Bayer process, bauxite ore is digested with Sodium hydroxide (NaOH) under elevated temperature and pressure, in which bauxite is converted to soluble sodium aluminate, and the insoluble part, generated after extraction is called "red mud" or "bauxite residue". The reaction that turns bauxite into aluminum is given below (Deshpande et al., 2017)

$2NaOH + Al_2O_3.3H_2O = 2NaAlO_4 + 4H_2O$ + Red Mud

The amount of high-volume aluminum by-product, "red mud", generated during extraction process depends on two factors. First is the ore quality and second is the processing condition. In general, 1-2 tons of red mud is produced per ton of alumina extraction. According to some authors, the appraised volume of red mud might range from 0.3 tons for each ton of supreme-quality bauxite to 2.5 tons for each ton of lower-graded bauxite (Kurniawan et al., 2006; Qaidi et al., 2022). Based on statistical data the global inventory of bauxite residue (red mud) reached to estimated 4 billion tons and is expected to increase with current generation which is more than 150 million tons. China is the largest global inventory creditor, registered an estimated 0.6 billion tons, and is still generating with an annual increase of 70 million tons (Wang et al., 2019). Australia, India, Brazil, and Greece are next top four red mud-producing countries (Swain et al., 2022). India has reached 10 million tons of red mud generation annually. There are six functioning and two closed alumina industry that are/were generating red mud and their annual production of red is described in Table 1.1. Discharge and management of red sludge have been a problem for ages. There are two traditional disposal methods viz. closed cycle disposal (CCD) and modified closed cycle disposal (MCCD) exist, however, presently a new method dry stacking (DS) has emerged to manage this waste which requires less land area. Apart from these, currently, some other disposal procedures have been employed by industries like lagooning, sea water discharge, etc., (Qi, 2021).

Table 1.1. Generation of RM from 2015-2020 across Indian aluminum unit.

Unit Name	Yearly generation of red mud (Metric Ton)				
	2015-16	**2016-17**	**2017-18**	**2018-19**	**2019-20**
Hindalco, Muri, Jharkhand	525332	590959	610020	542855	143368
Utkal Alumina International Ltd.	1914000	1974000	2049000	2082000	INF
Vedanta Ltd. Odisha	1497733	1626194	1694693	1758462	INF
NALCO Ltd., Odisha	2789160	3137853	3096637	3057509	INF
Hindalco Industries Ltd., Uttar Pradesh	928515	972319	968029	946208	933599
Hindalco Industries Ltd. Belgaum	356878	434358	443910	468399	412017

*INF- Information not found.

Source: Central Pollution Control Board, 2021.

Red mud, as its name suggests, is brick-red in colour, appears slimy, and has an average particle size of 10 m. Many times, this bauxite residue is brown in colour instead of red, known as brown mud. The diasporic-derived residue is more blackish in appearance compared to red and brown colour (Li et al., 2017). Red colour of red mud comes from iron oxide (Fe_2O_3). Besides that, the other major constituent of red mud is silica, sodium, titanium, and aluminum oxide. Precisely, the prime constituents of red mud are as follows: Fe_2O_3 (30−60%), Al_2O_3 (10−20%), SiO_2 (3−50%), Na_2O (2−10%), CaO (2−8%) and TiO_2 (trace−10%) (Tom et al., 2022). Red mud also acts as source of rare earth elements (Sc, Y, La, Nd) and radioactive elements (U, Th, V, Lanthanides, etc.). Due to presence of a high concentration of iron, red mud is also used as low-grade iron ore. Characteristically it is viscous alkaline bearing pH 11-13, and contain a high amount of Na, thereby typically sodic-alkaline in nature. The solid composition of red mud is influenced by a variety of factors such as bauxite parent material, climate, age, and topography. Hence geological identity of bauxite ore is the defining factor for elemental composition of red mud and its corresponding concentration (Nie et al., 2020). The residual alkalinity, presence of metallic species and radioactive elements make it a thrust area for the researcher to develop an exploitation strategy in order to minimize the disposal cost and protect the environmental health.

1.2. Pollution aspect of bauxite residue or red mud (RM)

Bauxite residue generated from the aluminum industry projected a serious threat to the immediate environment, including soil, water, vegetation, and aquatic life, if not appropriately managed. Irrespective of colour whether red or brown, chemical and mineralogical composition of the residue is extremely impactful, and registered a considerable load to the

environment. The degree of red colour depends on the amount of iron oxide (Fe_2O_3), while the alkalinity comes from Na-containing compounds like Na_2O, Na_2CO_3, $NaHCO_3$ etc. The amount of alkali reaches 2-3 g/L resulting high pH of red mud between 10-13, however, the untreated red mud bears pH ranges between 11-13. Approximate 2 tonnes of RM liquor with a significant alkalinity of 5–20 g/L caustic soda (as Na_2CO_3) accompanies every tonne of dry mud (Kauben & Friedrich, 2016; Rai et al., 2012). Such high pH values and high Na content make the red mud extremely eroding. Stockpiling of red mud invited a number of problems to the environment. The major concern is its persistent alkalinity and high sodicity where, in a few cases, the pH value of the fresh residue exceeds 13. In addition to its caustic nature, it also comprises different toxic metals like Cr, Cd, Ni, As, Pb, Cu, and radionuclides (Swain et al., 2022; Kavas, 2006). In general, industries transport bauxite residue or red sludge to the tailing region and hold a greater water content with 30%-40% solids having a high ionic strength. Owing to its liquid/viscous nature, large lagoons of red mud are formed, like dams while, dried or semi-dried disposal occupy a vast area of land. Such wide landfilling is a major limitation. Long-term storage of red mud slurry, or dry stacking incurred hazardous effects as alkali, heavy metals other radioactive contaminants percolate through soil pores that lead to groundwater pollution in case of heavy rainfall. Problems with RM dams frequently include low hydraulic conductivity, a high volume-to-weight ratio, and waterlogging characteristics of RM particles. Exorbitant alkalinity and polymetallic species presence degrade the soil quality and structure. Beside seepage of toxic elements leading to the deterioration of surface /sub-surface water quality. Toxic metals like As, Al, and V, in RMs show a greater migration ability under alkaline environments (Kishan et al., 2018; Gräfe & Klauber, 2011). Moreover, the fine particles of dried red mud dispersed in the air through wind, trigger air pollution causing numerous airs borne diseases in workers including the people in a closer vicinity. The particle size of the RM is less than 10 µm with specific surface area ranges between 10-25 m^2/g, depending upon the processing temperature. The alkaline dust not only degrades the air quality but also put a detrimental impact on the surrounding vegetation. Infiltration of liquid discharged from dumped sites containing a high amount of Na^+ and Al^{3+} destroys the biological health of the soil, retarded plant growth, and reduced their productivity. Inclusion of RM dust and slurry on water bodies threatens aquatic life, biological distribution, and community diversity. During seawater discharge, the fine particles of RM mixed with seawater make it turbid and disrupt the marine ecosystem. Presence of radioactive elements in RM is another fatal concern. Long-term exposure to these elements through RM leads to genetic alteration of the species (Lyu et al., 2021; Power et al., 2011; Ghosh et al., 2011; Rubinos & Barral, 2013).

Apart from direct detrimental impact, natural catastrophic events (rainfall, windstorm, flood, etc.) have an immense effect on red mud landfills like dam collapse, sewage outflow, etc. In October 2010, Ajka village of Hungary evidenced a disastrous spillage in which 700 000 m^3 of red mud was dispensed to the surrounding area, due to which, 10 people were killed and hundreds of people were injured, and, 40 km^2 of agricultural land was devasted. Likewise, in January 2018 another disaster happened in Belem, Brazil. Excessive rainfall caused red mud storage overflow, and contaminated soil and drinking water with high levels of lead (Pb) and aluminum (Al). Another important accident occurred in Henan province of China in the year 2005, where, red mud storage was busted in the form of a mud landslide. The wall of the contaminant suddenly ruptured and silt along with stones from mountainside rushed out. Although there was no such report of causality, it destroyed huge farmland of the nearby villages due to its high alkalinity (Mukiza et al., 2019; Liu & Naidu, 2014; Gelencsér et al., 2011; Rai et al., 2020; Souza et al., 2019).

The hazard rules of different countries categorized red mud into different classes viz. hazardous waste, by-product, non-hazardous waste, etc., however, India government termed its high-volume low affect waste. Altogether, the mishandling and poor management strategy of red mud by different industries is a fatal concern for the environment in the current scenario.

1.3. Chemical and mineralogical constituents of red mud (RM)

The chemical and mineralogical constituents of bauxite broadly depend on the bauxite ore used in the extraction process. In general, the Bayer process is used in most of the country for aluminum production. The process is highly recommended and achievable to extract alumina from top-grade bauxite ore having composite properties of Al_2O_3/SiO_2 (A/S) (>7-10), while, Sintering process is used if the quality of bauxite is poor (Liu & Zhang, 2011). Red mud generated through Bayer process contains a high amount of Fe_2O_3 and Al_2O_3 whereas in the case of sintering process presence of CaO and SiO_2 is more. Considering the chemical composition of the global red mud deposition it is extremely diversified due to the usage of different kinds of extraction process and bauxite quality. In India, Bayer process is availed by aluminum industries since it is the most economical process with greater production. Irrespective of production process the major chemical constituents of red mud are Fe_2O_3, Al_2O_3, TiO_2, SiO_2, Na_2O, and CaO. The range of these oxides is as follows., Fe- 20-50%, Al 15-25%, Si 5-25%, Na- 5-10%, Ca-5-10%, Ti 15-20% (Qaidi et al., 2022; Bray et al., 2018). It also contains different metallic species such as Cr, Pb, Ni, Cu, Cd, Fe, Mn, Zn, etc. Aside from

metallic contents, red mud also acts as a source of trace amounts of radioactive elements viz. Th, Sc, U, Rh, etc., and a few rare earth elements. Naturally occurring radioactive elements such as thorium and uranium are present in a little higher amount due to their geogenic presence in bauxite ore during the time of extraction. As stated earlier red mud is highly alkaline (pH10-13), finely grained, strictly sodic (exchangeable sodium percentage, ESP-53-91%) with raised electrical conductivity (1.4-28.4 mS/cm) (Jones & Haynes, 2011; Xue et al., 2016). Such high pH resulted from generation of sodalite, and hydrate garnet during the time of Bayer process when NaOH and lime were added. HCO_3^-, CO_3^{2-}, Al $(OH)_4^-$, and OH^- are major alkaline anions found in red mud. Presence of organic carbon (TOC) is considerably low and varies from traceto 0.3% depending upon the age of deposits.

Mineralogical composition of the red mud widely differs owing to variations in the parent bauxite ore. More mineralogical compounds are found in red mud as it is not uniform. Gibbsite (Al (OH)3), goethite (FeO (OH)), hematite (Fe_2O_3), anatase (TiO2), calcite (CacO3), quartz (SiO_2) is the major mineralogical compound of the red generated through Bayer process, while in the case of sintering process, the compounds are majorly β-$2CaO.SiO_2$, calcite ($CaCO_3$), aragonite ($CaCO_3$), hematite (Fe_2O_3), gibbsite Al $(OH)_3$), and perovskite ($CaTiO_3$) (Cusack et al., 2019; Swain et al., 2022).

1.4. Microbial characteristics of red mud (RM)

Since NaOH is the prime component during Bayer extraction of alumina, the bauxite residue/red mud becomes extremely alkaline, pH ranges between 11-13. Such high alkaline pH along with high electrical conductivity, and greater Na content make the residue immensely hostile to microbial growth and survival. Iron oxide, silica, unreacted alumina, and residual NaOH as Na_2CO_3, are the core ingredients of red mud. Alkali is present in chemically bonded form as sodalite, ferrite, etc. Extreme sodicity, high pH, and soluble ions like sodium and carbonate lock the available nutrient thereby creating a limiting condition for microbial uptake. Microbial populations found in alkaline environments are known as alkaliphilic organisms. In general, microbes play a major role in the transformation of organic carbon and other nutrient-cycling process which helps improvement of nutrient dynamics. Microbial communities are first to respond to changing environments compared to other components of any ecosystem, thereby, they offer a preliminary assessment of the course of recovery. Hence, a study on microbial community structure, diversity, and their contribution could be beneficial to study

any ecological restoration process (Krishna et al., 2014; Zampieri et al., 2019; Feigl et al., 2017).

Many authors have studied the microbial diversity of different natural alkaline environments like soda lake and other alkaline environments that showed numerous microbial diversities. However, red mud is characteristically different from natural soda lakes considering its origin, chemical composition, and nutrient availability. This man-made industrial waste is so hostile, that the freshly generated residue can be completely barren due to high alkalinity (pH>13) (Joshi et al., 2008; Naykodi et al., 2022). The high temperature and pressure during Bayer process make the red mud more complex and dreadful. Sustenance of microbes in immediately generated waste is scanty, nonetheless, the presence of microbes is likely to be a result of human handling or aging of the waste. The harsh environment of red mud provides an extreme habitat that can harbour halo-alkaliphilic, metal-tolerant bacteria capable of growing at high pH, high electrical conductivity (EC), and metallic presence. The organism, that is able to grow and survive in such a harsh environment may have some unique adaptation mechanisms, which provide resistance against several stressors. (Dubnovitsky et al., 2009)

Studies on the microbial diversity of some noxious industrial waste, having extreme habitat will explore information on different extremophilic/poly extremophilic indigenous bacteria that could be applicable for reclamation of waste-dumped sites, metal recovery, bioremediation purposes, etc. In addition to it, red mud can also be a good precursor of oligotrophic bacteria with extreme adaptability of pH, high Na concentration, and heavy metals that could have different biotechnological applications. There are very few investigations on microbes in artificially alkaline environments like bauxite residues, thus findings and critical evaluation of microbial diversity of red mud and their potential use in different fields could have greater prospects towards sustainability (Hamdy & Williams, 2001; Krishna et al., 2005).

1.5. Utilization possibilities of red mud (RM)

Red mud possesses unique physical and chemical properties which make it usable in several aspects. Although there are comprehensive utilization possibilities in different fields yet their employment rate is poor considering the massive production. Even if there are so many prospects in different sectors, nevertheless, very few are put into practice due to the economic condition. The utilization of red mud has been in practice either on a pilot scale or commercial scale in various sectors. It has extensive usage in the construction industry for production of bricks, building components, blocks, concrete aggregates, cement, etc. On

account of an appropriate ratio of iron oxide and aluminum oxide, it is widely used in making Portland cement or used as a stabilizer to make distinct types of cement, however, the use of red mud for manufacturing process is restricted to up to 15% wt due to its high alkalinity (Schwarz & Lalík, 2012). Red mud is widely applied in glass and ceramic industry. Characteristically red mud belongs to pozzolanic material, which after lime treatment gets hardened and forms a steady durable compound. A proportionate mixture of red mud and clay is used in production of ceramic glass (Sglavo et al., 2000; Yalcın & Sevinc, 2000). Red mud has an extensive utilization in chemical industry. It is greatly used as a catalyst in different chemical reactions viz., as a hydrogenation catalyst in organic synthesis. Sometimes, the red mud gets modified and used as catalyst for petrochemical industry, in dichlorination reactions, as a catalytic converter, in selective catalytic reactions of nitrogen oxide, in methane catalytic incineration, in removing hydrogen chloride, carbon monoxide, etc. (Hasoda et al., 1995; Khalafalla & Haas, 1972; Ordonez et al., 2001; Alvarez et al., 1999; Eamsiri et al., 1922).

Red mud, either native or activated form broadly used in pollution mitigation. Given the size and surface area of waste mud, it is used as low cost adsorptive agent which opens up its wide scale of application in waste management. It is a promising agent for removal of toxic metals (Cu^{2+}, Pb^{2+}, Cd^{2+}, Zn^{2+}, Ni^{2+}, Cr^{6+}) and metalloids (As^{3+} and As^{5+}), inorganic ions (PO_4^{3-}, F^-, NO^{3-}), different pigments and dyes (rhodamine B, congo red, methylene blue, reactive blue 19, fast green etc.) and organic pollutants like phenols, chlorinated phenols etc. Red mud is exclusively used in sequestration of greenhouse gases. It has adsorptive efficacy of noxious gases like H_2S, SO_2 etc., (Zhang et al., 2018). A significant presence of iron oxide (20-50%), in consort with titanium oxide (5-15%) makes the red mud a befitting agent for materials recovery. Due to this high presence of iron oxide, red mud is presently used as low-grade ore of iron. As previously mentioned, red mud reservoirs a number of rare earth elements (Sc, U, Ga, Tl, V, Ce, Y etc.), which are extracted through an acid medium followed by an ion exchange method (Ochsenkühn-Petropoulou et al., 2002; Gheorghita & Sirbu, 2009).

Other than these, red mud is also used in soil remediation and other contaminated site. Owing to its high alkalinity red mud is used in bulk in treating contaminated sites like acid mine drainage, which is another dreadful waste generated from coal and copper mine that load a considerable toxic effect on the environment. Using the alkaline properties, red mud is used to mitigate the acidification of soil (Gray et al. 2006). It not only increases the pH; it also binds the toxic metals through its adsorptive ability. Addition of red mud to soil transforms chemisorption of metal ions into iron oxide form. In heavy metal-contaminated soil, addition

of red mud restricts the metal mobility, as well as leachability when coupled with acidity (Brunori et al., 2005). In addition, many authors reported that long-term addition of red mud to the soil improves the texture and structure of soil (van Beers et al., 2009). Overall red mud has a multi-scale application prospect if it can be properly disposed of and used in a scientific manner.

1.6. Prospect of red mud in agriculture

Although red mud has a diversified application in different sectors, however utilization of RM in agriculture is scarce. The red mud produced in alumina industry is immensely alkaline (pH 10-13). This highly alkaline waste is often used in acidic soil to alleviate the acidity, however, the limitation of using the waste for plant growth and development is high sodicity, occurrence of toxic metals (Cd, Cr, Pb, Ni), and metalloids (As, Si,). High alkalinity, elevated Na concentration, salinity, unbalanced texture, poor water holding capacity, and low availability of nutrients is an additional constraint for establishment of vegetation/ agricultural activity in red mud waste areas. It contains the many vital nutrient ions that plants need, such as Ca^{2+}, Mg^{2+}, Fe^{3+}, Zn^{2+}, Mn^{2+}, and Cu^{2+}, but they are unavailable because of their insolubility in the mud's high pH levels (Gautam & Agrawal, 2019; Fuller et al., 1982). Furthermore, the major obstacle of RM associated with plant nutrition is its inert nature due to poor availability of nutrients and lower organic carbon content that leads to retardation of microbial activity, resulting in RM being barren. Application of readily mineralizable organic residue is already reported to increase microbial activity, thereby, addition of organic matter is expected to be productive in improving microbial activity, since OM provide nutrient for sustenance of microbial growth and proliferation (Rao and Chonkar, 1998). Incorporation of an adequate amount of organic matter into the RM likely improves the nutrient dynamics in regard to plant nutrition. The increased microbial activity in presence of organic matter leads to the acid extraction of nutrients from insoluble forms in RM during organic matter decomposition, similar to how organic matter accumulated throughout different stages of soil development causing rocks to disintegrate (Brady, 1995).

1.7. Vermitechnology: Importance and practicability

Considering the current status, management of red mud using a biological agent for beneficial purposes likely reduce environmental risks related to exposed disposal problems and also mitigate their toxicity. Nowadays, bio-conversion is the preferred way to convert any toxic waste into non-toxic energy-rich organic manure. Vermicomposting is one such eco-

biotechnological process, that has emerged in the recent past, and possesses the ability to transform and stabilize different kinds of solid waste (Suthar et al., 2012). It is a sluggish biodegradable progression in which solid wastes are slowly degraded by the synergistic action of earthworms and microorganisms and converted into a nutrient-rich, stabilized, and aesthetically pleasant material. Moreover, vermicomposting and decomposition are characterized by control-donor dynamics, in which the detrital input is the chief influencing factor within the decomposer community (Yadav & Garg, 2019). In general, surface-dwelling epigeic earthworms are mostly used for composting processes which as well reserve a rich concentration of diverse microorganisms, enzymes, and hormones. Due to their voracious feeding habit, the earthworms ingest the waste material which gets pulverized into finer particles through their gizzard actions. Including, worm intestinal microflora gets benefits from gizzard actions of earthworms for extracting nutrients into their mineralized form. The partially digested food material released as vermicast in the reactors is loaded with active microbial species, available nutrients, enzymes, hormones, and other biomolecules in significant amounts that eventually make it a value-added product. Their peat-like appearance, porosity, aeration, and high-water retention capacity enhance their applicability as compost (Sharma & Garg, 2017).

Vermicomposting is a technique often used to detoxify waste, containing high concentrations of toxic metals. This is due to the metal sequestration ability of earthworms. They have a special kind of cysteine-rich protein namely metallothionein (MT) in their intestine that helps to accumulate metals. Interestingly, the presence of metals in the substrate amplifies the synthesis of MT isoform in their intestine (Maity et al., 2009). It is a ubiquitous metal-binding protein, that plays an important role in maintaining metal ion homeostasis and redox chemistry within cells (Chiaverini and Ley, 2010). A recent report by Goswami et al. (2016) illustrates Cd exposure triggers the synthesis of metal-binding protein in the intestine of *Eisinia fetida*.

In recent years vermicomposting has been extensively used to detoxify several industrial wastes viz. tannery waste (Ravindran et al., 2016), paper and pulp industry waste (Kaur et al., 2010), textile industry waste (Chakraborty et al., 2022), dairy waste (Desai et al., 2016), food industry waste (Yadav & Garg, 2013), petrochemical industry waste (Banu et al., 2005), municipal solid waste (Sahariah et al., 2015), lignocellulosic waste (Devi et al., 2020) using numerous earthworm species like, *Eisenia fetida, Eudrillus euginae, Lumbricus rubellus, L. terrestris, Lampito mauritii, Ponthoscolex corethrurus, Perionyx excavates*. These

earthworm species efficiently detoxify and alleviate the waste material. Considering the above-mentioned qualities vermicomposting is not only an eco-friendly approach to enhance nutrient bioavailability, including, it is great detoxifier to metal-containing waste. In this context, the detoxification of red mud (RM) through vermicomposting is zilch, thereby, we are assuming that vermitechnology could be a successful means of recycling RM and its possible use as compost in agriculture.

1.8. Research gaps and major issues

After an extensive literature survey, I found there is scarcity of information on characteristics, environmental toxicity and eco-friendly management of red mud. Based on that a few research gaps have been identified with some vital inquiries, described below:

- There is currently a lack of knowledge on the physicochemical and microbial characteristics of red mud (RM), their solubility dynamics, and potential effects on soil environment.
- No such information is available on the characteristics of bauxite ore and how it is different from bauxite residue.
- There hasn't been enough research done on how potentially harmful metals are distributed in RMs, including any potential risks to human health, the environment, or pollution.
- Very poor information is available microbial diversity of red mud
- The potential of vermicomposting technology for remediation has not yet been tested with RMs.
- To date, there have been no extensive field-based experiments to assess the effects of vermicomposted RM on soil health and crop growth.

Using the aforementioned research gaps as a starting point, the following important inquiries were framed:

1. What are the physicochemical characteristics of bauxite residue (RM)?
2. What are the environmental impacts of bauxite residue?
3. How bauxite residue is different from its ore?

4. Can bauxite residue be a good source of extremophilic microbes?

1.9. Research objectives

Based on these key questions the major objectives of this research are given below:

1. To characterize the native bauxite ore and processed bauxite residue (red mud) in terms of the physicochemical properties and evaluate their probable impact on the environment.
2. To explore the microbial composition of red mud and evaluation of their growth parameters, metal tolerance ability, and special emphasis on the biosorption potential of metal.
3. To examine the effectiveness of vermicomposting technology in removing pollutants from red mud, as well as in improving nutrient supply and microbial quality.
4. To utilize the vermicomposted-Red Mud (VC-RM) in agriculture as a source of essential bio-compost through field application.

1.10. Research plan

Research plan is schematically presented in Fig. 1.1. According to the research goals the work is segregated into four different phases. To address and accomplish the proposed research objectives, in the first phase the red mud samples were collected from an aluminum plant located at Muri, Jharkhand in the year 2021, January. A detailed physicochemical characterization (pH, EC, TOC, availability of N, P, K, different labile and non-labile fractions of Fe, Mn, Zn, Cu, Pb, Cr, Ni, Cd etc) was done including XRD, FT-IR, and FESEM-EDX analysis was carried out in the first phase of the study. Assessments of the potential for contamination and the factors that could threaten human health as a result of RM exposure were also done using authentic indices.

In the second phase of work, the crude bauxite ore sample was collected from a bauxite mine located in the Lohardaga district of Jharkhand. The sample was characterized in a detailed way. Physicochemical parameters viz. pH, EC, TOC, availability of N, P, K, different labile and non-labile fractions of Fe, Mn, Zn, Cu, Pb, Cr, Ni, Cd, etc., and microbial quality parameters(FDA, MBC, microbial respiration), enzyme activities were checked. In addition to that, XRD, FT-IR, and FESEM-EDX were carried out to understand the mineralogical composition,

distribution of functional groups, and surface morphology of the ore body. Lastly, a brief illustration was made of characteristic changes before and after alumina extraction of bauxite.

During the third phase of the study, red mud was explored from the microbial perspective. A metagenomic study was carried out to know microbial diversity and their community distribution in RM. In addition, the other microbial parameters like FDA, MBC, and enzymatic activity were checked to disclose whether this harsh toxic waste is able to harbour any microorganism, and if so, then how strong the activity is. Apart from that, a total heterotrophic count was taken. Furthermore, the waste was also used to find out indigenous metal-tolerant bacteria, that could have appreciable tolerance to higher metal concentrations. Such attempt was taken to develop a metal-tolerant polyextremophilic bacterial biosorbent that could be used in wastewater treatment.

The fourth phase of the study dealt with sanitization potential of vermitechnology in terms of nutrient recovery and metal detoxification of red mud. The experiment was carried out in four different ratios (RM+ Cow dung) by using the epigeic earthworm species *Eisenia fetida*. At the end of experiment, the final product underwent nutrient dynamics study and metal detoxification analysis. The earthworms were sacrificed to assess their metal sequestration ability. Finally, the favourable outcome of the vermicomposting experiment gave the confidence to conduct field studies on the widespread usability of vermiconverted RMs using rice and green gram as the test crop. Green gram was conducted through a pot experiment and rice was done through a field experiment. The efficacy of the formulation was assessed in relation to farm yard manure (FYM) and various concentrations of synthetic fertilizers. The nutrient-supplying capacity of vermiconverted RM was determined in relation to crop growth, productivity, and quality of the harvested product. The changes in soil quality parameters were examined. As a result, the current analysis was an attempt to provide some unique facts regarding many environmental aspects associated with red mud produced by the aluminum industry. The thorough investigation of the effectiveness of vermicomposting technology with *E. fetida* may also serve as a foundation for the in-situ management of this waste.

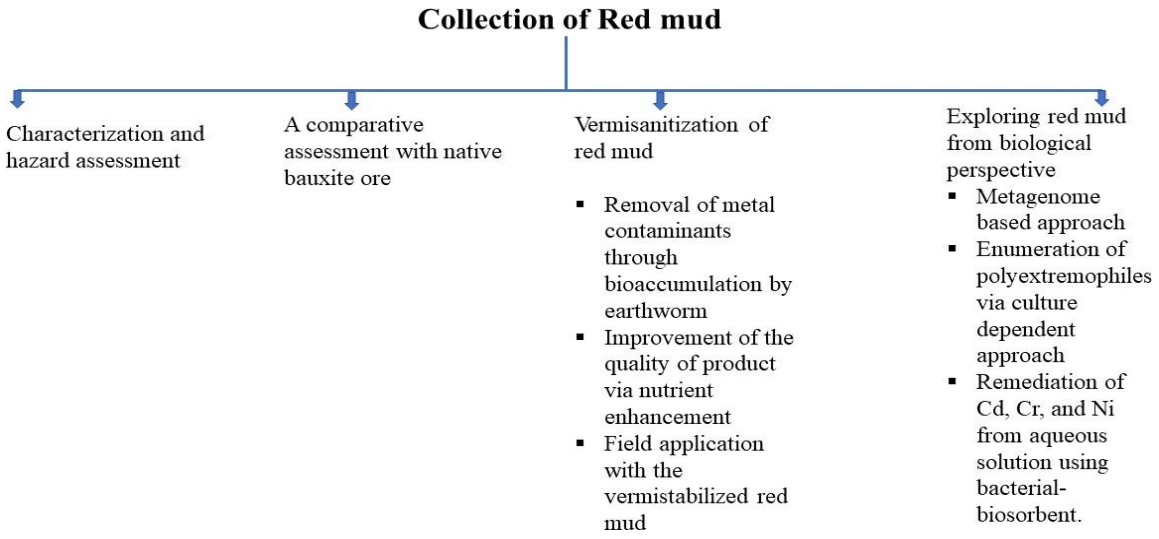

Fig. 1.1. Schematic representation of the research plan

1.11. Thesis outline

The contents of different chapters are narrated briefly in the following section:

Chapter 1: In the first chapter, the research problem and the primary goals for this thesis are introduced in the context of the relevant scientific literature. This chapter describes the overall problem and present status of the problem in a nutshell.

Chapter 2: This chapter includes a thorough analysis of the pieces of literature compiled prior to the start of the study. This quick evaluation of the literature helped us develop our research plan, spot any gaps in the literature, and support the inimitability of the study.

Chapter 3: This chapter explains the fundamental technique used to carry out the study's specific objectives. The chapter also describes the tools utilized and the quality control checks carried out during the course of the investigation.

Chapter 4: The complete findings of the experiments and studies conducted to define the RM and determine their likely effects on human health and the environment are presented in this chapter.

Chapter 5: This chapter demonstrates a thorough characterization of native bauxite ore and also outlines their characteristic deviations from RM.

Chapter 6: This chapter broadly discusses the microbial quality, characteristics, and microbial diversity of RMs. In addition, it also includes isolation and characterization of alkaliphilic

bacteria and their metal sequestration property (Cd^{2+}, Ni^{2+}, and Cr^{6+}) and optimization of metal removal potential from aqueous solution.

Chapter 7: This chapter deal with the vermi-sanitization of RMs using *Eisenia fetida*. A brief introduction is followed by a review of the pertinent literature, in-depth comments on the experimental procedures, and finally a discussion of the chapter's key findings. The outcomes have been shown as figures or in tabular format.

Chapter 8: This chapter includes references to the crop experiment. The chapter involves a two-crop trial on green gram (*Vigna radiata L.*) and rice (*Oryza sativa*). It begins with a brief introduction, a review of the relevant research, the experimental procedures used, and a discussion of the key outcomes. The outcomes have been shown as figures or in tabular format.

Chapter 9: This part of the thesis wraps up the entire research work with significant findings made during this investigation, future scope and limitation of the study.

Chapter 2

Review of Literature

Chapter 2

Review of literature

2.1. RM processing and generation from global perspective

Urbanization, industrialization, and waste generation, three of these phenomena are harmonizing with each other. The evolution of mankind and the corresponding expansion of civilization direct revolutionary progress in the industrial sector. Throughout the history of human civilization, the process of urbanization and industrialization have always remained intertwined to give rise to any advanced society. To meet up the demand for industrial requisites the minerals found in the earth's crust continually served as raw material from the ancient period. Minerals and mining activity are indispensable inputs for the economic growth of any industrial sector like civil engineering, defense, aerospace, energy production, agriculture, etc. In this current era of industrial insurgency aluminum is the second most demanding metal after steel in 21st century with an annual consumption of 88 million tones. It is the most emerging metal since late 20th century (Parbat et al. 1996; Mishra et al.2020). As a result of it, the large-scale industrial waste generation and the issues associated with its proper management and disposal are the primary adverse impacts of these global operations. The lack of available land, materials, and resources for ongoing construction projects, including infrastructure, and environmental quality deterioration is the second issue, presently the world is dealing with (Edraki et al., 2014).

Bauxite, which has the highest concentration of alumina and contains silica, iron oxide, and other impurities in minor or trace amounts, is the type of aluminum ore that is mined for commercial purposes. The Bayer process, developed by an Austrian chemist Karl Bayer in 1887, is used to refine bauxite into alumina, which is then used in the Hall-Heroult process to smelt alumina into aluminum. These three steps make up the primary aluminum production process (Sutar et al., 2014). It is the most economical process for alumina extraction opted by industries worldwide. The alumina minerals in bauxite are converted in this process into the soluble compound tetrahydroxoaluminate Al $(OH)_4$. It is then converted into soluble sodium aluminate. The residual mineral remains in the bauxite are insoluble and separated in solid phase. Following separation, this solid phase is dumped as bauxite residue waste which is otherly known as red mud (RM), due to its brick-red colour (Zhang, 2013). Reaction involved in alumina production is depicted below

Gibbsite: $Al_2O_3.\ 3H_2O + 2NaOH \xrightarrow{105^0C\text{-}150^0C} 2NaAlO_2 + 4H_2O$

Boehmite: $Al_2O_3.\ 3H_2O + 2NaOH \xrightarrow{240^0C} 2NaAlO_2 + 2H_2O$

Diaspore: $Al_2O_3.3H_2O + 2NaOH \xrightarrow{280^0C} 2NaAlO_2 + 2H_2O.$

Other than Bayer process, Bayer-sintering, and sintering process is used among aluminum industries, however,>90% of aluminum is extracted through Bayer process, due to low energy consumption and easy handling. In sintering process of aluminum extraction, prime component is soda lime for sintering raw materials like bauxite, nepheline (Feng & Yang, 2018). The red mud generated after aluminum extraction is slurry usually deposited in red mud ponds and impoundments presently dry mud disposal, solar drying another rising disposal method, etc. In general Bayer red mud has finer particles similar to engineered clay particles with high water content, low permeability, and poor strength, while the sintering red mud has a coarse particle with greater sand content and hardened during filtering process (Feng & Yang, 2018). This rustycolour of red mud comes from iron oxide (Fe_2O_3) encompassing almost 20% to 30% of its mass(Evans et al., 2012). Approximately 1- 2 tons of red mud is produced during aluminum extraction; however, it is primely dependent on the quality of the bauxite ore used in the process. Based on statistical reports the global deposit of RM has so far reached 4 billion tons by 2015 and continually increasing with an annual generation of 150 million tons, out of which China accounted for 60% of total red mud production (Liu & Naidu, 2014; Wang et al., 2019; Zeng et al., 2020). According to Swain et al. (2022), in the last decade, China, Australia, Brazil, India, and USA have been the leading contributor of the global bauxite residue deposit (BRDA), however in another study by Mukiza et al. (2019) showed along with these previously mentioned countries Greece is another topmost contributor of RM in the global stockpile. Considering the Indian contribution to this global stockpiling is about 9 million tons annually. The annual generation of red mud by different countries in the world is presented in Table 2.1.

Table 2.1. Annual production of RM in top five countries in the world. Source: Mukiza et al. (2019)

Country	RM production (in million tons)
China	90
Australia	30
India	10
Brazil	10.6
Greece	0.7

Reviewing the Indian scenario, the aluminum sector largely deals with the companies viz., NALCO, HINDALCO, and Vedanta (Misra & Pandey, 2005). Alumina production and corresponding red mud generation by these industries are presented in Table. 2.2.

Table 2.2. Annual aluminum production and red mud generation by Indian companies. Source: Rai et al. (2020)

Company	Aluminum production (million tons/year)	Red mud Generation (million tons/year)
NALCO	2.275	3.096
HINDALCO, Utkal	1.499	2.049
HINDALCO, Belgaum	0.185	0.4439
HINDALCO, Muri	0.3394	0.61
HINDALCO, Renukoot	0.684	0.9697
VEDANTA, Lanjigarh	1.8	2

2.2. Properties of RM

The chemical properties of bauxite are related to the ore quality and their extraction technology. CaO, Fe_2O_3, SiO_2, Al_2O_3, and TiO_2 are major constituents of RM. Red mud (RM) generated from Bayer process has more amount of Fe_2O_3 and Al_2O_3, while the RM generated through sintering process possesses more amount of silicon and calcium. The major phase of the RM produced by the combined process and sintering process, 2Ca SiO_2, has a mass ratio near 50% and is characterized by significant calcium and silicon content. From the mineralogical background, the major mineral found in Bayer red mud is boehmite, anorthite, perovskite, goethite, cancrinite, sodium aluminosilicate, calcite, anatase, sodalite, and rutile as reported by many researchers (Liu & Naidu, 2014; Samal et al., 2013; Wang et al., 2019). Free soda and bound sodium are the two main types of sodium in red mud. Free sodium is the caustic soda that gets incorporated throughout the digesting process and stays with the red mud despite repeated washings. It is present in the entrained liquid of red mud slurry. The free sodium mainly exists as NaOH, Na_2CO_3, and $NaAlO_2$. High sodicity and alkaline pH mainly come from freely existing sodium. On the other hand, the desilication phase used in the Bayer process to remove kaolinitic silica from bauxite is responsible for the bound soda in the red mud. In the form of sodalite, the complex can be recognized as "NAS" phase $3(Na_2OAl_2O_32SiO_2)$ Na_2X ($X=CO_2^{2-}$, $2OH^-$, $SO4^{2-}$,$2Cl^-$)[7] (Sutar et al., 2014). The major constituents of RM generated

from three different types of extraction processes (Bayer process, Sintering process, and Combined process) are presented in Table 2.3.

Table 2.3. Major constituents of RM in three different extraction processes (%).Source: Chen and Wu (2012); Qaidi et al. (2022)

Extraction process	CaO	Fe_2O_3	Al_2O_3	SiO_2	TiO_2	Na_2O	K_2O	MgO	Nb_2O_5	Sc_2O_3	TREO	LOSS
Bayer Process	3-9	35-65	12-22	4-20	0.2-10	03-10	-	-	-	-	-	13.88
Sintering process	45-49	06-Oct	4-7	22-23	2.6-3.0	2.5-3.2	0.3-0.4	1.3-1.6	0.0193	0.02	0.25	16.96
Combined process	43.8-46.8	6.2-7.5	5.5-7.5	20.2-20.5	6.2-7.7	2.7-3.0	0.4-0.7	1.77	-	-	-	11.77

In India aluminum is dominantly extracted by Bayer process, thus the major constituents of Bayer RM are Fe_2O_3 (20-30%), Al_2O_3 (10%-20%), Na_2O (2%-10%), SiO_2 (10%-20%), however, the amount of the constituents can be altered slightly according to a different industrial operation. The compositional difference across the aluminum industries of India is tabulated in Table 2.4.

Table 2.4. Chemical constituents of Indian red mud (%).Source: Sutar et al. (2014); Raghubanshi et al. (2022)

Industries	Al_2O_3	Fe_2O_3	Na_2O	CaO	TiO_2	SiO_2
BALCO, Korba	16-18	35-37	5-6	2-3	17-19	6-7
NALCO, Damanjodi	17-20	51-57	3-5	1-2	3-3	4-6
HINDALCO, Muri	19-21	44-46	3-4	1-2	17-19	5-7
HINDALCO, Belagum	17-20	44-47	3-5	1-3	8-11	7-9
MALCO, Metturdam	18-22	40-26	4-5	1-3	3-4	12-16
HINDALCO, Renukoot	17-19	48-54	5-6	3-5	14-16	7-9

The typical particle size of red mud ranges from 10 µm to 20 µm, with significant variation in both content and particle size (Liu et al., 2011). Red mud is crystalline in form, with a real density of about 3.30 g/cm3, and a large surface area in the range of 10 to 30 m2/g depending on how much the bauxite was ground up before digestion. Table 2.5 shows the variations in

the chemical constituent of red mud produced in several countries throughout the world which differs in amounts of chemical composition due to the difference in the extraction process.

Table 2.5. Difference in chemical composition of red mud (wt.%) in different countries. Source: Wang et al. (2008); Qaidi et al. (2022)

Country name	Fe_2O_3	Al_2O_3	TiO_2	SiO_2	Na_2O
Hungary	38.5	15.2	4.6	10.15	8.12
Jamaica	50.9	14.2	6.27	3.4	3.18
Surinam	24.81	19	12.15	11.9	9.29
Taiwan	41.3	20.21	2.9	17.93	3.8
Australia	36.25	17.15	3.95	28.85	1.65
Brazil	45.5	15.2	4.25	15.5	7
China	31.25	18.5	6.2	8.3	3.25
Germany	44.9	16.2	12.33	5.4	5.22
Greece	44.57	15.66	7.08	6.95	3.25
Indonesia	50.3	24.1	2.8	20.4	
Russia	49.8	12.7	4.66	8.8	3.4
Spain	37.1	12.1	20.05	9.2	5.2
UK	46.01	20.05	5.1	20.1	8.5
USA (ALCOA Mobile)	30.4	16.2	10.11	11.14	2
USA (Arkansas)	55.6	12.15	4.5	4.5	1.5-5.0
USA (Sherwon)	50.54	11.5	Trace	2.59	9

Similar to the chemical constituents, the mineralogical composition of RM differs based on the extraction process. The major mineral composition of red mud boehmite AlO(OH), calcite ($CaCO_3$), gibbsite ($Al(OH)_3$), calcium aluminium hydrate(x.CaO.yAl_2O3.zH_2O), rutile (TiO_2), anatase (TiO_2),CaTiO3, Na_2TiO_3, kaolinite $Al_2O_3.2SiO_2.2H_2O$, sodalites, aluminum silicates, cancrinite ($NaAlSiO_4$)6$CaCO_3$and hydrogarnet $Ca_3Al2(SiO_4)n(OH)12-4n$. The compositional dissimilarity among the extraction process is presented in below mentioned Table 2.6.

Table 2.6. Major mineralogical variation in Bayer, Sintering, and Combined process of aluminum extraction. Source: Rai et al. (2012); Nie et al. (2020); Wang et al., (2019).

Mineral composition	Bayer process	Sintering process	Combined process
Boehmite	21		143
Calcite	19	26	10
Anthrothite	20	5	2
Sodium aluminosilicate	20	4	4
Calcite	19	14	10
Diaspore	2	-	-
Illite	2	-	-
Cancrinite	12.3	-	-
Perovskite	13.6	3	-

Studies by Romano et al. (2019) suggested the presence of sodalite which originated from caustic soda used during the time of digestion and original ore mineral like hematite, calcite, goethite, etc. In another study Alekseev et al. (2019) mentioned that hematite and quartz are largely present, however, they found magnetite in their study. In the red mud, Manfroi et al. (2014) found chantalite, cancrinite, gibbsite, hematite, quartz, and calcite. 100% of the particles were less than 18 µm, according to the particle size distribution. Overall, red mud is extremely diverse and complex in terms of its chemical constituents and mineralogical composition.

Considering the chemical properties of red mud, it is alkaline with high sodicity. Due to the presence of greater amounts of salt like Na, Ca, Mg, and K, the RM bears high electrical conductivity > 10 mS/cm. In general, Na found in bauxite residue seldom exists in soluble form. Compared to the total Na concentration, the soluble Na is less and usually generated from the NaOH used in the extraction process. Although refineries try to recover this Na for their reuse, the residual soluble Na remains as sodium aluminate and sodium carbonate making the residue extremely sodic. This Na interacts with CO2 over time, primarily producing sodium carbonate (Evans, 2016). A study by Rao and Reddy (2017) also observed that RM is dominated by Na and possesses a compacted structure (high bulk density). Furthermore, RM exhibited an agglomerated structure of uniformly dispersed particles, having an average particle size of < 10 µm. Additionally, RM act as a sink of different trace element and radioactive elements. Being the aluminum industry by-product, it contains high amounts of Al, Fe, and Si. Zhu et al. (2012) reported that RM contains a wide range of Fe from 4.5 to 50.6%

depending upon bauxite quality, besides they also found that more than 51% Fe can be recovered from RM, which can give good competition to the iron ore. Another study by Liu and Naidu (2014) revealed the presence of different toxic elements like Cr, Ni, Cd, Pb, Zn, Mn, and radioactive elements and rare earth elements like U, Th, Zr, Sc, Ga V, etc. Consequently, the RM becomes an obstacle to industrial application due to the presence of this typical rare earth and radioactive element. Table 2.7 depicted the trace element of RM along with their measured concentration by previous researchers.

Table 2.7. Major elements, Trace elements, Rare-earth elements, and Radio-active elements of RM. Source: Khairul et al. (2019); Wang et al. (2013); Sun et al. (2019); Foday, (2019).

Element	Concentration (%)
Fe	4.5-50.6
Al	4.42-16.06
Si	2.16-14.86
Ti	0.98-5.34
Cr	497
Ni	31
Cd	0.3-2.3
Pb	50-230
As	0.4-1.26
Cu	30-71
Zn	20
Mn	85
U	50-60
Ga	60-80
Zr	1230
Th	20-30
Sc	60-120
Y	60-150
Lanthanides	0.1-1

2.3. Disposal, Storage, and Reuse: History and Trends

Due to the fact that safe disposal is the primary goal of all alumina industries, bauxite residue/ red mud management is a topic of concern around the globe. Over the years, bauxite residue management and storage techniques have progressed. In the early stage, the residue was hardly deposited on site or in nearby areas. According to Evans, 2016**,** abandoned/depleted mines or quarry sites were the foremost choices for residue dumping. Since bauxite residue/red mud has a slurry appearance, a fine silt-to-clay proportion, pH>11 with high Na content possesses a high dispersive property. Rai et al. (2020) reported that red mud emitted as slurry

deposited in high dams which were made extremely deep to avoid large area requirements, however, disposal in lakes, natural ponds, or artificial impoundments/red mud ponds were into practice. In other cases, the waste was dumped in neighbouring estuaries or marine lagoons, and as the nearby convenient sites filled up, valleys were dammed to hold the steadily increasing amounts of waste. Verma et al. (2017) informed that before slurry disposal in impoundments, NaOH was separated through a dewatering process, which thickened and increase the solid content of the RM up to 15% to 30%. Another preventive measure used to take by industries is the bottom sealing of impoundments with clay to prevent any leakage. Alkaline solution seepage, however, continued to be an issue for long-term storage. Jones and Haynes (2011) stated that to over this issue, researchers suggested a drain disposal method that increased storage efficiency. Solar drying was another approach that was extensively used in hot and dry climate countries, though in the rainy season, this method faced obstacles. In between the 1940s-1960s, a disposal technique became popular among European countries viz., France, Germany, Greece, Ireland, Scotland, and Japan from South-East Asia, where they used to discharge the red mud slurry into the sea or rivers or estuaries, according to availability (Evans, 2016**)**.

Over the past few decades, new disposal techniques have been incorporated because industries are currently more focused on the sustainable manufacturing and management of waste. In the present context, dry mud stacking is widely used, where moisture content is reduced by employing pressure filters thus converting the slurry into mud cake which is then deposited as dry mud stacking (Rai et al., 2020). This dry staking was adopted 75 years ago in UK and almost 50 years ago in Germany, but, now this method of red mud dumping is widely used by industries across the world. In India, this dry mud stacking is an extensively employed method for residue management. Table 2.8. and Table 2.9 presented the disposal practices used by the companies.

Table 2.8. Disposal methods used by Indian companies. Source: Data as reported by respective alumina refineries.

Companies	Disposal practice
NALCO, Damanjodi	Bauxite residue is disposed of using the Thickened Tailings Disposal (TTD) system from 2001, which has a solid composition of 55–57% by weight.
HINDALCO, Muri	After treatment with a pressure filter, dry disposal into a storage area is used to raise the solids percentage. The residue is excellent for dry stacking after filter pressing. For storage, the ponds are surrounded by gabion walls.
HINDALCO, Renukoot	Traditional CCD method of impoundment was used. In late 1979 dry disposal method was implemented. After five stages of counter-current washing, the solid is filtered (70% solids) and disposed of in the pond
BALCO, Korba	After settling, the residue is currently filtered and washed in four stages. The filtered cake is dropped into the pond after being repulped with water from the pond. utilizes a modified CCD disposal system. The currently in-use pond's barriers are made of stone, a well-protected polythene liner, and a layer of clay.
HINDALCO, Belgaum	In 1985, the factory shifted from wet slurry disposal to dry disposal. The mud is dumped off by dumpers at the pond site after clarifying, six-stage counter-current washing, and filtering (65% solids). In order to encourage green growth, the dry area of the pond is covered with a 15 cm thick layer of black cotton soil.
Vedanta Ltd. Lanjigarh	Dry disposal is done by lowering the moisture content to 25% and then depositing the waste using the gradual rise and step deposition method, which is typically employed in mountainous or heavily sloped areas. The bauxite residue management method reduces the need for land by 50–60% and reduces caustic usage by 10–15 kg/ton of alumina.

Table 2.9. Disposal practices are used by different countries across the world. Source: Evans, (2016); Samal et al. (2013); Peng et al. (2005); Liu et al. (2009); Hyun et al. (2005).

Country	Disposal practice
Australia	Filter pressing followed by dry stacking coupled with seawater or CO_2 neutralization.
USA	En route to lake, bottom deposition in the lakes followed by top water discharged from lakes or reused. Dry stacking is also opted.
China	Disposal to landfills, few portions were recycled for metal recovery and also used for raw material for bricks production.
Japan	Sea disposal by partial pre-treatment i.e., Acid neutralization.
Greece	100% dry disposal.

Although the disposal methods are continually modified to reduce accidental and contamination risk nevertheless, some merits and demerits remained there. The advantages and disadvantages are presented in below mentioned Table 2.10.

Table 2.10. Different disposal methods with their pros and cons. Source: Pradhan et al. (1999); Prasad (2006); Samal et al. (2013).

Disposal method	Advantages	Disadvantages
Dry stacking	Eco-friendly, lower space requirement, seepage reduction	High investment for concentrating slurry, high machinery cost, high energy, requirement of hot climate, impracticable in rainy season.
Lake/sea disposal	Zero expenditure on pond making, lower expenditure for machinery and lower energy.	Destruction of aquatic environment, less recovery of caustic soda since no return, extensive pipeline mandatory.
Slurry disposal	Recovery of caustic soda, lower transportation cost, lower infrastructure	Large space requirement, high cost, potentially hazardous, high expenditure in making ponds and their enlargement from time to time.
Sun drying	Reduce soluble soda loss, Reduce groundwater contamination	Required hot weather, drainage of rainwater, not feasible in rainy season.

Modification in disposal methods is unable to reduce their enormously high sodicity, besides seepage of the alkaline solution from storage is a serious concern for the environment. High pH and sodicity is an obstructions of RM for its further utilization. Thus, to alleviate the sodicity industries used different neutralization techniques. According to the Australian and New Zealand Environment and Conservation Council (ANZEX) and Agriculture and Resource Management Council of Australia and New Zealand (ARMCANZ), the accepted pH of the liquor should be 8 after treatment. Since the pH reduction coupled with Na declination is costly industries barely use it. Different kind of neutralization techniques has existed, reported by

many authors (Rai et al., 2012; Qi, 2021; Kannan et al., 2021 Patel et al., 2018**).** Acid neutralization, seawater neutralization, and CO_2 neutralization are mostly used however, Qui et al. (2021) reported CaO neutralization technique. In another study by Xue et al. (2016) and Ahn and Reddy (2011) on the biological neutralization of RM where microorganisms are used for the reduction of pH. In

In acid neutralization, the aqueous acid solutions are used. Carbonic acid, oxalic acid, sulphuric acid, hydro choleric acid is used. A study by Zeng et al. (2019) informed that sulphuric acid showed a 91.09% of dealkalization rate while another investigation reported by Li et al. (2020) showed that dealkalization rate of oxalic acid is more than 95% when used in 15% concertation at temperature 80^0C. Apart from direct acid, acidic industrial effluent is also used to neutralize RM. One such example is reported by Rai et al. (2012), the acidic spent pickling solution generated from steel making process provides a coagulant. On the other hand, CO_2 or CO_2-containing gas bubbled through slurries to produce carbonic acid which will be used for dealkalization. Carbonic acid reacts with basic components thus reducing pH (Khaitan et al., 2009). Sea water neutralization is another cost-effective popular method for neutralization. When seawater is mixed with caustic RM, it precipitates out hydroxide, carbonate, or hydroxy carbonate, thereby reducing pH. Instead of eliminating caustic compounds, it converts the readily soluble component into a partially soluble and weakly alkaline solid (Palmer et al., 2010; Sahu et al., 2010). Zhou et al. (2019) and Qi, (2021) suggested alkali recovery using CaO and MgO with hydrothermal method. The principle behind the method is to replace Na^+ with Ca^{2+} or Mg^{2+}. Ca^{2+} replaced the Na^+ and react with less soluble and more stable cancrinite. Apart from these chemical treatments Xue et al. (2016) and Ahn and Reddy (2011) investigate the potential of bacteria/fungus to mitigate the alkalinity by producing organic acid. A study by Hamdy and Williams (2001), investigated RM neutralization efficacy of 150 bacterial isolates, out of them, *Lactobacillus*, *Leuconostoc*, and *Bacillus* played crucial for the synthesis of organic acids which lowers the pH of RM from 13 to 7. A fungal species *Aspergillus tubingensis* reported by Ahn and Reddy (2011) is capable of lowering the pH of RM, which subsequently supported growth of Bermuda grass and supports vegetation. In a recent study Patel et al. (2018) reported that cow dung too is good neutralizer of RM. Patel and group stated that 80 g of cow dung is optimum for 10g of RM neutralization. It also minimizes the alkalinity and supports the growth of microflora and vegetation thus illuminating an eco-friendly way of RM neutralization.

Disposal of solid waste is not always an environmental burden, but sometimes it can have an extensive utilization. Green Gross Domestic Product (Green GDP), is an index that determines the positive and negative side of industrial growth (Rai et al., 2012). For a long time, red mud was thought to be a useless by-product for aluminum industries. However, the related financial expenses and environmental hazards have prompted industrialists and researchers to look for eco-friendly options to reduce the waste amount. Considerable use of RM in different sectors like building and construction, catalyst synthesis, metal recycling wastewater treatment, etc is previously reported in the literature. Since it contains a greater amount of Fe, Si, Al, and Ti they are widely used in the metallurgical industry. 10% -20% of aluminum and 6%-7 % of Si make them suitable for the building and construction sector. The huge presence of Fe_2O_3 (30%-60%) captivated the attention of researchers for using it as low-grade Fe ore for Fe extraction. Pig iron production is done by smelting RM in an electric blast furnace (Verma et al., 2017). Geng et al. (2020) and his group made an alloy and cleaned slag from the co-reduction of a mixture of solid waste incinerated fly ash and red mud. Large-scale use of RM was in road making and cement production. Owing to the presence of Fe and Al, the RM is utilized to make Portland cement which has added benefit of CO_2 emission reduction markedly (Evans, 2016). It also acts as a binder, additive, clay material during the production of Portland cement (Sneff et al., 2011). RM act as an adsorbent in catalytic industries to clean industrial gases (Paredes et al., 2004; Silveira et al., 2021). In the chemical industry, catalysts are needed for chemical processes like hydrogenation, hydride chlorination, and hydrocarbon oxidation in order to speed up the process and improve the outcome. By appropriately altering its characteristics, bauxite residue can be utilized in place of expensive catalysts (Ordóñez et al., 2001; Zhang et al., 2007). RM is an excellent material for making ceramic. 51%-91% weighed RM is mixed with 49-10% weighed of silicate bearing minerals and heated at temperatures 950^0C-1250^0C to make the ceramic product. RM is also broadly used in geopolymerisation. Solid aluminosilicate is transferred to liquid gel through an alkaline leaching solution, followed by nucleation and condensation of the gel to a solid binder. The generated product remains amorphous under 500^0C and crystalline above 500^0C. In this process, RM is used to make that alkaline solution to develop geopolymer for constructing blocks, massive bricks, cement, etc. (Zhang et al., 2010; Somlai et al., 2008; Dimas et al., 2009). As RM harbours different rare earth elements (REE) viz., scandium (Sc), lanthanum (La), cerium (Ce), and neodymium (Nd) thus it is also used to extract these valuable elements. Apart from these, Al, Ti is also recovered from RM which gives an economic benefit. Steel industries use RM for iron recovery and use them as an alternative to Fe ore. Other than these sectors RM

is broadly used in different kinds of environmental applications, such as landfill capping, soil remediation, waste water treatment etc (Ni et al., 2012; Wang et al., 2015). French and American trials of covering municipal landfills with bauxite residue have been conducted. Although usage in France varies greatly from year to year, it is estimated to be between 40,000 and 100,000 tonnes of RMs are utilized annually. Though they are used in capping and covering yet dust generation, leaching of heavy metals makes hindrances during transportation. Owing to the fact of metal adsorption, RMs are well applied for metal adsorption in heavy metal-contaminated soil. Additionally, due to their alkaline nature, they are used in acidic soil on a large-scale basis for buffering. Besides it also acts as a disinfectant and stabilizing agent for municipal sewage (Paramguru et al., 2004; Evans,2016). Another major utilization of RM in wastewater treatment reported by many researchers. Due to their porous structure, they can easily adsorb a wide category of anions (F^-, NO^{3-}, PO^{4-}, BO^{3-}, $[Fe\ (CN)_6]^{3-}$) and cations (As, Cr, Pb, Cu), radioactive ions (Cs-137, Sr-90, and U) and organic pollutant. Their sufficiency, low cost, and easy operation make them popular as an adsorbent (Wang & Liu, 2021).

2.4. Environmental hazards and calamity associated with RM

High alkalinity (pH >13) and a substantial amount of potentially toxic elements limit the ecological disposal and resource use of RM. The practice of stockpiling involves numerous risks to the environment. Chemical properties like sodicity, alkalinity, high electrical conductivity, poor organic carbon, and deprivation of essential plant nutrients restrict the occurrence of vegetation. Both soluble and insoluble Na, and the hazardous elements make RM biologically barren (Lyu et al., 2019; Wang, et al., 2019; Di Carlo et al., 2019). The RM particles are extremely fine, due to which the dust generated from waste dump area pollutes the air and the minuscule largely deposited inside the respiratory system and finally causes health hazards to the people of the nearby area. High volume-to-weight ratio, low hydraulic conductivity, and waterlogging are common glitches of the red dam. The mobility of Al, V, and As is high under alkali environments. In addition to that the alkali cations viz., Na, Ca, K migrate faster (Burke et al., 2012). The outfall and outflow of RM liquor thus pose toxicity to the surrounding community. Mixing RM in the aquatic system (sea, river, estuary, lake) threatens life inside the water with its profound detrimental impact. Seepage from the dry stacked RM contains a considerable amount of alkalinity and hazardous metal which finally contaminate groundwater. This hard alkaline solution not only percolates through soil pores, it additionally degrades the soil structure. Through leaching the radioactivity present in RM is dispersed which directly influences the flora and fauna of the ecosystem. Due to the presence of toxic and radioactive

elements, cement, bricks, and ceramic material made up by using RM, bear environmental threats (Gu et al., 2012; Somlai et al., 2008; Power et al., 2011).

Many catastrophes take place in the recent past related to dam collapses, pond bursts, overspills, pond failures, explosions, etc. Century's worst ecological disaster took place in Ajka, Hungary, where the reservoir wall ruptured, and the RM slurry dispersed all the nearby areas. It almost travels 160 km from the site of the accident. According to the reports, 10 people died and 150 people were injured, however, the environmental damage was vast and long-term. Almost 400 hectares of agricultural land was destroyed and the nearby aquatic system was badly affected due to the mixing of alkaline RM. It destroys aquatic life because of its high alkalinity and salinity (Silveira et al., 2021). Another natural calamity takes place in China, where similarly the reservoir wall cracked, and the silt with stone above the mountains rolled down and finally ruptured the wall. The accident was so catastrophic that it destroyed the adjacent villages and agricultural land (Mukiza et al., 2019;). In 2018 Brazil faced the red mud catastrophe, which primely caused due to power fluctuation and voltage failure. The HINDALCO aluminum in Muri, Jharkhand had a similar kind of red mud incident in 2019, which also affected the adjacent area. The agricultural land located on the southeastern side of Muri is mostly affected. An excessive burden was the prime reason behind this explosion. These disasters not only damaged the environment in the short term, but they additionally placed future hazards to both human health and the environment (Gomes et al., 2016; Rai et al., 2020). Many studies reported that after Ajka, Hungary disaster, trace metal availability increased in RM-flooded areas. Along with that, the salinity increased potentially. A study by Milačič et al. (2012) reported Al concentration was excessively elevated, although the soluble fraction Al was 1% of total Al. The toxic highly mobile $[Al(OH)_4]^-$ species were dominantly present in the water-soluble fraction. In addition to that, the author mentioned the presence of Cr (> 0.10 mg/kg). The hyper alkalinity created a hindrance in the endurance of the indigenous vegetation of the red mud flooded area. It affected root elongation. High leaching of RM reduced plant productivity. Increased pH and increased Na change the soil's physical structure as well as soil chemistry. In another study, Mayes et al. (2016) reported that immediately after the Ajka disaster the fugitive dust increased the risk of air quality deterioration. The physical characterization of spill material projected, the particle size was predominantly PM_{10} class, sized between 3-8μm, and only a little portion belonged (PM2.5 and PM1: with diameters less than 2.5 and 1 lm, respectively, which researchers concluded were similar to the urban dust. However, a follow-up study on PM10 fraction aerosol indicated no such breaches in air quality

parameters. Mayes et al. (2011) analyzed the residual leachates after a month of Ajka spill and found an elevation in pH (>13.1) and alkalinity (6600 mg/L as Na_2CO_3) and enrichment of a range of potentially hazardous elements that include a series of oxyanion forming elements mostly soluble at high pH viz., Al, V, As, Cr, Mo. The particulate and dissolved phases received portions of the elements' bulk concentration. Mo, P, and V were primarily found in the dissolved phase, where they may be readily bioavailable to the environment. A speciation study by Burke et al. (2012) reported that Cr and As mostly exist in Cr^{3+} and As^{5+} while V was found in its most toxic form V^{5+} (as vanadate) in the RM leachate. The authors additionally found that RM leachate was oversaturated with Ba-arsenate ($Ba_3(AsO_4)_2$) while undersaturated with Ca-arsenate and Al-arsenate. At high pH, Ba-arsenate has less solubility. However, according to them, the neutralization approach after a disaster may have consequences. Although it lowered the pH (around 8.5), where Al-oxyhydroxide got precipitated Cr^{6+} became more soluble at this pH. Likewise at near neutral pH arsenate was prospectively affected by other anions like phosphate, and bicarbonate. The RM-deposited Marshes faced As^{3+} due to the reducing condition which promotes arsenate to As^{3+} (Cornelis et al., 2008; Islam et al., 2004). the concentration of these elements (As, Cr, Ni, V) crossed the aquatic life standards in aquatic system, which was threatening to inside water environment. Another oxyanion-forming element P was increased which was distributed in particulate, dissolved, and colloidal fractions, and have a significant impact on environment. The most dreadful effect is the aquatic system. Eros (2015) investigated through an electrofishing survey after Ajka spill, where he surveyed 4 species with 59 specimens, and the sudden influx of caustic solution created an imbalance in the ionic strength. There was also a decline in the planktonic rotifer population. One fluvial hyphomycetes population capable of degrading leaf litter reduced its ability to degrade after the spill ascribed to its minimization in the population. Overall the calamity or mishandling and long-term effect of RM are derogatory to the environment.

The RM Depository not only impacts the environment but also put a potential economic burden on the industries and causes environmental safety risks. Crude RM is so harsh that not a patch of vegetation can grow. The area around the plant loses its natural balance and is readily affected by landslides and dust. Many disasters happened previously which costs huge for the recovery of the accidental area. Furthermore, the industries have to spend a lot on disposal for its accelerating occupancy of land area and transport. So, large-scale RM management has emerged as one of the world's most pressing issues that need to be solved.

2.5. Microbiota, vegetation, rehabilitation strategy: A glimpse behind.

Microbe-plant-soil continuum is important for making an ecosystem. All ecosystems depend on microorganisms, which are essential for pedogenesis, the growth of soil, and plant nourishment. It can be challenging to separate interactions between microbial populations and the ecosystems they live in since they have complex impacts on one another. In order to understand the directions and relative magnitude of microbial and geochemical processes that contribute to remediation and how these might change over time. This is especially true in a geochemically dynamic and extreme environment such as tailings. RM is one of the man-made extreme environments that have complex chemical and physical characteristics. The extreme geochemical characteristics put pressure on community for the natural selection, for instance, the community that could be selected naturally and survive in RM is haloalkaliphilic or haloalkalitolerant owing to the high salinity and alkaline environment of RM. Such extremophiles can exist within a narrow range compared to others, nevertheless, their adaptability toward changing environments is impressive. Survivability is mostly related to metabolic alteration. Autotrophic archaea and bacteria are prevalent in such extreme conditions, however, when the threshold reaches, their growth is also compromised, which is an indication of starting rehabilitation of the site. At that critical point, a holistic remedial approach should be introduced in a different way (microbial strategy, vegetation,) in consort with organic and inorganic amendments, which will support the heterotrophic population also (Santini et al., 2015; Schmalenberger et al., 2013).

Along with its high metal and metalloid content, RM is well-known for more contaminants than just its enhanced Na concentration. The metal and metalloids that are predominant in RM are Cd, Cr, Ni, Pb, Zn, As, V, etc. Previously many authors attempted to explore the microbial diversity of RM through both culture-dependent and culture-independent approaches (Schmalenberger et al., 2013; Krishna et al., 2014). In general, the community structure of the RM is slightly different from those of naturally alkaline environments reported by a study by Joshi et al., 2008, and Yang et al., 2010. The predominant family prevails in RM are *Chitinophagaceae*, *Beijerinckiaceae*, *Xanthomonadaceae*, and *Acetobacteraceae* ar mostly oligotrophic, metal-tolerant early colonizing communities. Schmalenberger et al. (2013) had seen that, there was a shift in community structure in the reclaimed RM heap. The reclamation is through vegetation with gypsum amendment. *Nocardioidaceae*, *Acidobacteriaceae*, *Nitrosomonadaceae*, *Caulobacteraceae*, and *Anaeroplasmataceae* family dominate the microbial community. Santini et al. (2015) reported in their investigation that *Bacillius* is the

predominant genus found in such hyper alkaline environments because of their cellular adaptability. In their cell wall along with peptidoglycan, they have some acidic polymers such as phosphoric acid, glutamic acid, gluconic acid, aspartic acid, and galacturonic acid which promote negative charges and aid in adsorbing the sodium and hydronium ions and repulse hydroxide aion, which provide them survivability in such alkaline condition (Aono & Horikoshi, 1983). *Proteobacteria* and *Firmicutes* are dominant phyla according to Santini et al. (2015). In the year of 1995, Agnew et al. worked on bauxite residue in search of some novel alkaliphilic bacteria, which they isolated and marked as JaA, JaH and JaD. The isolated obligate alkaliphiles and JaH were identified *Bacillus veddari*. This same species was isolated by Nogueira et al. (2017) while working on bauxite residue from Brazil. Additionally, they have also isolated *Bacillus cohnii, Bacillus pseudofirmus, and Bacillus polygoni* which are gram-positive and tolerate up to 50^0C of temperature and 17% of NaCl concentration. Far before, Hamdy and Williams (2001) isolated 150 isolates from treated bauxite residue of Alcoa deposits using the minimal medium. The isolates were largely gram-positive and belonged to a diversified genus viz., *Bacillus*, *Lactobacillus*, and *Leuconostoc*, *Micrococcus*, *Staphylococcus*, *Pseudomonas*, *Flavobacterium*, *Enterobacter*, Proteus. Focusing on the Indian bauxite deposit and their diversity, Krishna et al. (2008) isolated 57 bacterial isolates from NALCO, Damajodi, using different mediums and growth conditions. The bacteria were capable of utilizing a wide range of carbon sources and can tolerate up to 10% of NaCl and 50^0C belonged from genera *Kochuria* spp. This same research group Krishna et al. (2014) later on worked on NALCO Damanjodi bauxite residue and isolated 57 isolates having high pH tolerance (pH 12) and wide range of carbohydrate utilization patterns. They investigated both cultivable and non-cultivable populations. 16srDNA sequencing identified the cultivable isolate were *Agromyces indicus*, *Bacillus litoralis, Bacillus anthracis, Chungangia koreensis*, *Kokuria flava*, *Kochria polaris*, *Microbacterium hominis*, *Planococcus plakortidis*, *Pseudomonas alcaliphila* and *Salinococcus roseus*, while study on non-cultivable bacterial diversity relvealed presence of three major phyla *Gammaproteobacteria* (41.1%), *Betaproteobacteria* (37.5%), and *Bacteroidetes* (21.4%). Qu et al. (2019) isolated one chemoheterotrophic bacterium *Acetobacter* sp. from 20 years residue deposit of Chinalco, in southwest China. A very recent study by Dey & Paul, (2021) conducted on bauxite deposit of different restoration history of HINDALCO, Muri, where they identified alkaliphillic metal tolerant isolates, which were mostly from the genus *Bacillus* along with some other genera namely, *Paenibacillus*, *Halomonas*, *Ochrobactrum*, *Salinococcus*, *Pseudomonas*, and *Kurthia*. On the other hand, the culture-independent study by Santini et al. (2015) found the presence of

Proteobacteria, *Firmicutes*, *Actinobacteria*, and *Bacteroidetes* and *Ascomycota* was predominant in the case of the fungal population. Wu et al. (2020) did a widespread investigation on bauxite residue disposal area (BRDA) in Zibo City, Shandong Province, China, where the residue was restored for the past 50 years. They sequenced the DNA through Illumina MiSeq 250 platform. Total of 44 phyla they detected, out of which four were predominant viz., *Firmicutes* (6.1–33.8%), *Actinobacteria* (8.9–32.3%), *Chloroflexi* (6.8–25.3%), and *Proteobacteria* (10.9–19.5%). *Bacilli*, *Actinobacteria, Acidobacteria, Alphaproteobacteria*, *Thermomicrobia*, KD4-96, *Planctomycetacia*, *Gemmatimonadetes, Gammaproteobacteria*, *Deinococci*, *Phycisphaerae*, Gitt-GS-136, and *Anaerolineae* were all reported to be found. According to them, Firmicutes were more prevalent in poorly restored residue (PR), while, *Chloroflexi*, *Acidobacteria*, and *Planctomycetes* were more prevalent in well-restored residue (WR). These extreme ecological niches can harbour phylogenetic diversity, where alkaliphilic microorganisms, therefore, may exist in the following three domains: Archaea, Eukarya, and Bacteria. The organism can be both aerobic and anaerobic. The aerobic alkaliphilic bacteria include Bacillus, Micrococcus, Pseudomonas, Streptomyces, and Eukarya comprise yeast, and filamentous fungi (Duckworth, 1996). Contrastingly, Groth et al. (1997) reported some anaerobic alkaliphiles namely *Clostridium* sp, *Anaerobranca horikoshii*, *Amphibacillus xylanus*, *Thermococcus alcaliphilus*, *Thermococcus* sp. Almost all authors agreed that the newly deposited residue was devoid of microbial activity, even though the research had found a variety of microbial species. Overall, the microbial community of bauxite residue (RM) is extremely diverse and needs an extensive study to explore its detailed characteristics.

Even while long-term accumulated residue (RM) contains a variety of microbes, the amount of natural flora on the RM heap is limited. Researchers have recently proposed a variety of rehabilitation options, with microbially driven processes, vegetation, and chemical additives becoming more and more popular in the modern era for the rehabilitation of bauxite residues. High pH, sodicity, and salinity are reduced gradually with the age of disposal, thus gypsum becomes a very common amendment for reducing the enhanced Na concentration residue. Subsequently, the heaps are seeded with different kinds of vegetation preferably the alkali-tolerant grass family. As residue gets older, and mud particle deposition occurs, common plants grown in RM heaps include *Sonchus asper, Sachharaum bengalense,* and *Launaea asplenifolia.* (Dey, 2021). *Agrostis stolonifera*, *Holcus lanatus*, *Lolium perenne*, *Trifolium repens* and *Trifolium pratense* are the common grassland species used for vegetation in gypsum-amended

bauxite residue (Courtney et al., 2020). The author, also informed that this vegetation helped to improve the structural, physical, and chemical properties of RM, which in turn, helped to improve the faunal community such as an increase in nematode and earthworm populations, etc. Fresh bauxite residue, according to a study by Di Carlo et al. (2020) is extremely noxious, inhibits the germination of *Lepidium sativum*, *Sinapis alba*, and *Sorghum saccharatum* seeds, and negatively impacts the growth of *Lolium perenne* seedlings, which exhibit visible stress symptoms like chlorosis on the leaves. They also mentioned that revegetated BRs exhibited improved chemical characteristics demonstrating the beneficial effects of amendments and/or weathering in reducing the BR's plant-limiting characteristics (such as alkalinity and sodicity, as well as the high availability of non-essential elements). The three test plant species (*L. sativum*, *S. alba*, and *S. saccharatum*) were not inhibited. The pH (9.2) and ESP (30%) reached a significant decline in the revegetated BRs; however, root elongation was slowed down in comparison to the control soil. According to Jonnes and Haynes, 2011, nutrient deficiency, high exchangeable sodium percentage (ESP), high SAR (sodium adsorption), low organic matter, and high alkalinity are hindrances to vegetation, thus stabilization is the first step toward vegetation. The two approaches are widespread: (1) the cap and cover technique, by using soil/sand or soil-like material to provide plant growth and medium, (2) improvement of physical and chemical properties using different amendments (gypsum, compost or solid) and another is direct vegetation (Tordoff et al., 2000). A study was done on European bauxite residue disposal area (BRDA) by Courtney and Xue (2019), where they reported vegetation growth, especially by grass family. They used to check the growth of two grass families Poaceae and Fabaceae on differently amended (organic waste) bauxite residue heap. The grassland species *Agrostis stolonifera, Festuca rubra, Holcus lanatus, Lolium perenne, Trifolium repens*, and *Trifolium pratense* at a rate of 100 kg/ha were chosen, and they observed after one year of vegetation nutrient scarcity develops, that finally outnumbered those species which are sensitive to nutrient deficient condition.

Other than revegetation, sand or soil layering, and amendment addition, presently the indigenous microbes are gaining popularity for the rehabilitation of red mud (RM) otherly bauxite residue. Microbial bioremediation involved a variety of organisms include bacteria, fungi, and archaea. These organisms participated in a wide variety of metabolic processes, which led to the production of several types of organic acids that aid in lowering pH, salinity, and other environmental factors. Additionally, many of them can produce extra polymeric substances which help in an aggregation of particles that finally facilitate aeration.

Characteristically RM has a high concentration of Na ions, which occupy the cation exchange site and have a very high exchangeable sodium percentage. Reducing the amount of exchangeable sodium promotes the production of aggregates that are better suited for plant growth and, ultimately, bioremediation. A wide range of bacterial and fungal species such as *Penicillium* sp., *Athrobacter* sp., *Aspergillus* Sp., *Bacillus* sp., *Lactobacillus* sp. *Candida* sp., *Propionibacter* sp. were reported to produce different kinds of organic acids (Wu et al., 2011; Kubicek et al., 1987; Liao et al., 2018; Wu et al., 2019). These bacteria are capable of reducing the alkalinity of the RM. In an amended bauxite deposit, Courtney & Kirwan (2012) revealed the presence of arbuscular mycorrhizal fungi and described their crucial function in residue regeneration. Some chemolithotrophic and chemoheterotrophic bacteria produce inorganic acids like H_2SO_4. They are mainly iron and sulfur-oxidizing bacteria that produce sulfuric acid thereby facilitating pH reduction (Sorokin et al., 2011). In extreme environments bacteria/fungi develop different strategies to cope. Synthesis of extra polymeric substance (EPS) or extracellular matrix (ECM) is one such mechanism, which not only helps in their survivability but also helps in development of well-aerated soil by forming particle aggregation thereby facilitating residue remediation. Lünsdorf et al. (2000) reported the development of soil particle aggregation through EPS production in saline-sodic soil and polychlorinated biphenyl-contaminated soil. Additionally, these polysaccharides possess several functional groups like COO^-, PO_4^-, and OH^-, that help in adsorbing metal (Cd, Ni, Cr, Pb, As) (Guibaud et al., 2005; Li et al., 2006). Consequently, it also helps in metal remediation from bauxite residue.

2.6. Metal-Microbe interaction

Metal and metalloids are always stress factors for microbiota. However, the metals are classified as (1) Essential metals, (2) Toxic metals and metalloids, (3) non-essential nontoxic metals. They are chemical compounds that can cause harm through a variety of mechanisms such as oxidative damage by generation of reactive oxygen species (ROS), protein deactivation, DNA damage, etc. (Osman et al., 2019). However, to mitigate such stress microbes develop diverse mechanisms. Through metabolic processes, alterations in pH or redox status, the secretion of chelating agents, or passive sorption, they can solubilize or precipitate the metal. The microbe can either resist or detoxify the heavy metal. Based on their integral ability to withstand the metal concentration, microbes retort to heavy metals. In general, their response can be categorized into two arrays: (1) a general mechanism, which provides resistance but doesn't require any inducement through metallic species. (2) another mechanism entails metal stress for its activation. The mechanisms can be both, metabolically

dependent or metabolically independent. Microbes require energy to either uptake metal or provide resistance to it. For instance, microbial precipitation of metal is referred to as biomineralization, and solubilization of metal is referred to as bioleaching which in other way called biomining, and alteration in the redox state of metal is referred to as bioreduction (Newsome & Falagán, 2021). Briefly, microbial action to a metallic constituent is either/or mobilization or immobilization. Mobilization includes redoxolysis, acidolysis, complexolysis, and alkylation, while immobilization includes biosorption, bioaccumulation, complex formation, and redox reaction. In redoxolysis microbes either oxidize or reduce metal during oxidation-reduction reaction, while acidolysis is proton-induced metal solubilization, where the synthesis of proton by microbes changes the mobility of metal. Complexolysis is ligand-induced metal solubilization, where microbial chelation determines the metal mobility. Alkylation is otherly known as metal volatilization, where enzymatic transfer of alkyl groups takes place that is covalently bounded with metal. Conversely, immobilization occurs through biosorption where the microbial (dead/ altered) surface active functional groups are responsible for metal binding. In the case of bioaccumulation, metals are actively transported through metabolic pathways and accumulated within the cell as solid particles or in vacuoles (Brandl, 2002; Brandl, 2001; Ledin, 1996). The metal microbe interplay is very intricate. They can both cause or resolve problems. Metals are released from sulphide mine wastes generating acid mine drainage, which is caused by microbial oxidation of Fe (II)- and sulfide-bearing rocks. This is a major environmental issue that significantly pollutes terrestrial and aquatic habitats with metals. Production of organic acid during respiration and fermentation may enhance the mobility of metal (Newsome & Falagán, 2021). Conversely, they can also remove metals from aquatic systems, thereby restraining the impact on human and terrestrial ecosystems. They have the ability to sequester metal by precipitating them as sulphide, oxalate, carbonate, or phosphate mineral (McMahon & Chapelle, 1991). A number microbial agent has the ability to metal sequestration including bacteria, fungus, algae, and actinomycetes. Cumberland et al. (2016) reported that *Thiobacillus thiooxidans* and *Thiobacillus ferrooxidans* can do enzymatic oxidation of a radioactive element U. Hg, which is enormously toxic at low concentrations, can be uptake by Cyanobacteria, many algae and diatoms. It is believed that passive diffusion is the primary means by which a neutral-Hg complex diffuses into the cytoplasm (Zhong & Wang, 2009; Cain et al., 2008). Cd^{2+} and As^{3+} are other two metal and metalloid which poses toxicity at relatively low concentration. Aspergillus niger is reported to reduce As(V) to As(III). As detoxification primely involved efflux, intracellular sequestration, or methylation, while most of it's a reduction mechanism which further transported extracellularly via efflux protein

(Cánovas et al., 2003). Cd resistance is mostly associated with efflux pump viz., plasmid-encoded *cad* gene found in *Staphylococcus aureus* (Nucifora et al., 1989) or through biosorption (Manasi et al., 2014). Table 2.11**.** on microbe-mediated remediation and associated mechanism.

Table 2.11. Microbe-mediated remediation and resistance mechanism of heavy metals. Source: Xiu et al. (2015); Pande et al. (2022); Newsome and Falagán (2021); Verma and Kuila (2019).

Group	Heavy metal	Organism	Resistance Mechanism
Bacteria	Cadmium	*Pseudomonas aeruginosa*	Biosorption
	Lead	*Bacillus subtilis* X3	Bioimmobilization
	Cadmium and Lead	*Pseudomonas aeruginosa* and *Bacillus cereus*	Bioaugmentation
	Cadmium	*Cupria vidus* sp. Strain Cd^{2+}	Bioprecipitation
	Nickel	*Bacillus* sp. KL1	Biosorption
	Copper, Cadmium, Zinc	*Desulfovibrio desulfuricans*	Extracellular sequestration
	Copper, palladium, Zinc	*Pseudomonas aeruginosa*	
	Cadmium, Zinc	*Synechococcus* sp.	Intracellular sequestration
	Mercury, Cadmium, Zinc, Mercury	*Escherichia coli*	Active export
	Arsenic (V)	*Pseudomonas* sp. Strain GE1	Co-precipitation
	Arsenic (III)	*Pseudomonas* sp. Strain GE2	Biosorption
	Mercury	*Geobacter sulfurreducens*	Hg^{2+} methylation
	Chromium	*Turbinaria vulgaris*	Bioaccumulation
	Nickel	*Thiocapsa roseopersicina* and *Pseudomonas* strain MBR	Bioreduction
	Zinc	*Bacillus licheniformis, Bacillus cereus, Bacillus alevi*	Bioaccumulation
	Fe	*Bacillus licheniformis, Bacillus cereus, Bacillus alevi*	Bioaccumulation

Algae	Cadmium, Zinc, Lead, Nickel	*Asparagopsis armata*	Biosorption
	Lerad, Nickel, and Cadmium	*Cystoseira barbata*	
	Lead, Nickel, Cadmium, Zinc	*Codium vermilara*	
	As(V)	*Lessonia nigrescens*	
Fungi	Copper, Lead, and Chromium (VI)	*Aspergillus niger*	Biosorption
	Lead	*Botrytis cinereal*	
	Copper	*Rhizopus oryzae*	
	Silver	*Pleurotus platypus*	
	Aluminum (III)	*Acremonium* sp.	

2.6.1. Cellular mechanisms involved heavy metal sequestration

Persistent exposure to heavy metals can have a number of deadly effects on microorganisms, including cellular disruption, macromolecule destruction, and disruption of cellular function and growth. Depending on the type of metal, the concentration of metal, and the environmental conditions surrounding them, microbes evolved both internal and extracellular defence mechanisms to reduce the toxicity of metals inside the cell. The extracellular method entails the sequestration of metal ions via cell wall components, whereas the intracellular mechanism involves metal ions forming complexes with microbial protein and other biomolecules inside the cell (Siddiquee et al., 2015, Priyadarshini et al., 2021). The defense mechanisms of bacteria have been classified into four processes, which are biosorption, bioaccumulation, metal chelation, and efflux transportation, as depicted in Fig 2.1.

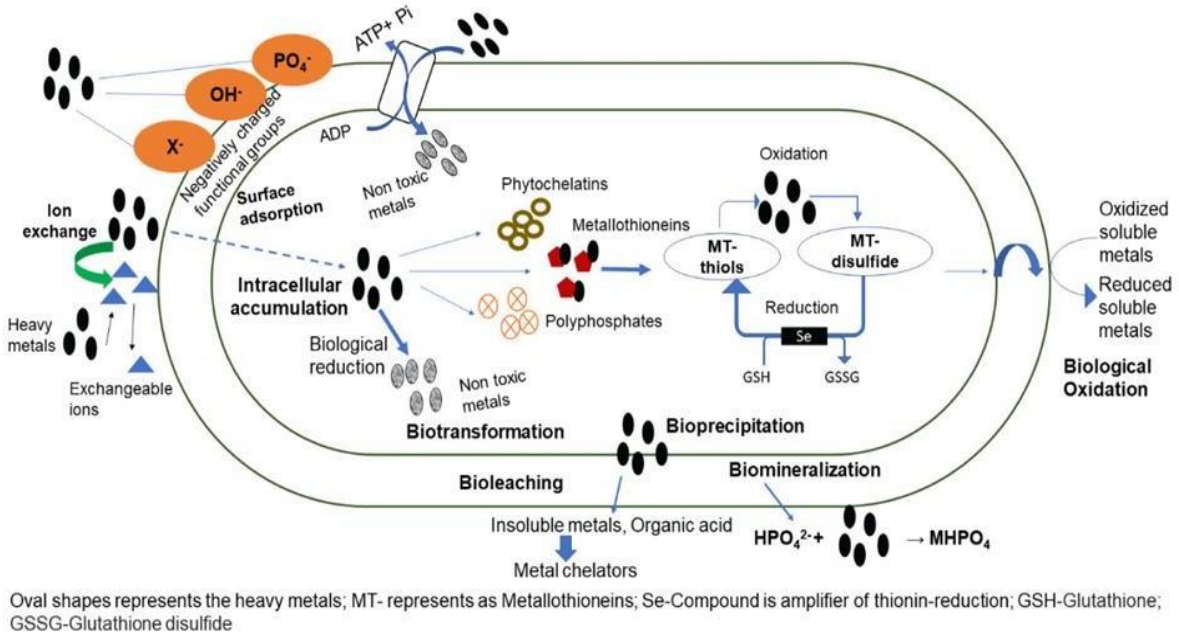

Fig. 2.1. Extracellular and intracellular mechanisms involved in the mitigation of heavy metal toxicity including biosorption, intracellular accumulation, biotransformation to a non-toxic state, bioreduction, immobilization by organic acid, and metal ion chelation by metal-binding proteins. Source: Jeyakumar et al. (2022).

I. Biosorption:

The interactive mechanism involves non-specific metal ion binding with polysaccharides and proteins present on the cell surface (Fig. 2.2). It can be accomplished by both living and dead microbial biomass. It is a metabolically independent process in which negatively charged functional groups like carboxyl, phosphate, hydroxyl, carbonyl, and amine found in cell wall proteins, lipids, and polysaccharides attract cationic heavy metals, facilitating extracellular metal-binding via electrostatic force (Das et al., 2008). Presence of peptidoglycan is a characteristic feature of both Gram +ve and Gram -ve bacteria, however it is thicker and have more layer in Gram +ve bacteria while in Gram -ve, there is only one layer. This layer comprises glycoprotein, lipopolysaccharide and phospholipids which act as ligand for meta binding. On the other hand, presence of teichoic acid in peptidoglycan of Gram +ve have more functional group like COO^-, OH^- which play a decisive role in adsorbing metal onto its surface. Thus Gram +ve bacteria are more promising for metal adsorption compared to Gram -ve (Ayangbenro & Babalola, 2017; Nanda et al., 2019; Fomina & Gadd, 2014; Gupta et al., 2015). An actinobacteria *Streptomyces rimosus* has good metal binding affinity for Pb and Fe

(Sahmoune, 2018). Rahman et al. (2019) investigated lead-resistant bacteria *Staphylococcus hominis* strain AMB-2 and reported that it could be used for biosorption of Pb and Cd. A coral associated solubilizing bacteria *Cronobacter muytjensii* KSCAS2 found to be resistant against multiple ple heavy metals (Saranya et al., 2018). Synthesis of extra polymeric substance (EPS) is a distinct characteristic feature that aids in metal binding owing to the abundance of negatively charged functional groups. Due to their strong binding ability, they do not allow heavy to enter inside the cell thereby protecting cell from heavy metal toxicity. According to reports, *Micrococcus luteus* and *Azotobacter* sp. create EPS and have higher resistance to metal stress (Osman et al., 2019).

II. Bioaccumulation

Metal ions are taken up inside the cell during bioaccumulation either by a proton-driven transport pathway or through simple diffusion (Fig. 2.2). Bioaccumulation, in contrast to biosorption, is a metabolically dependent process that can only be carried out by living cells. Metal ions are compartmentalized once they enter the cell inside numerous cellular organelles, such as vacuoles, which precipitate metals in a non-toxic form. Mechanisms for heavy metal bioaccumulation in the bacterial membrane include endocytosis, ion channels, carrier-mediated transport, complex permeation, and lipid permeation (Geva et al., 2016; Shahpiri & Mohammadzadeh, 2018; Ahemad, 2012). Using transmission electron microscopy (TEM), Rani and colleagues observed that *Pseudomonas putida* 62 BN exhibited intracellular and periplasmic accumulation of the metal (Rani and Goel., 2009). More recently, Naskar et al. (2020) showed that developing *Bacillus cereus* M116 cells had an intracellular nickel (II) buildup of 20%.

III. Biotransformation

Biotransformation involves structural alteration of a chemical compound leading to the synthesis of a compound with more polarity (Asha & Vidyavathi, 2009; Pervaiz et al., 2013)). The metals and organic compounds are transformed from toxic to non-toxic forms (Fig. 2.2). Microbes have developed a mechanism to assist them in adapting to environmental changes. Condensation, hydrolysis, the generation of new carbon bonds, isomerization, development of functional groups, oxidation, reduction, and methylation are the mechanism of accomplishment. The reaction may even lead to volatilization of metal and diminish the toxicity (Siddiquee et al., 2015). The process leads the metal to volatilize and reduces its toxicity. Different kinds of pollutants can be biotransformed such as hydrocarbon, pharmaceuticals, and

heavy metals (Karigar & Rao, 2011). there are reports on oxidation As (III) to As (V) by *Acinetobacter* Sp. and *Micrococcus* Sp (Nagvenkar & Ramaiah, 2010). Thatoi et al.(2014) reported on Cr(VI) to Cr (III) reduction by *Bacillus* sp. using NADPH- dependent reductase. Lloyd and Lovley (2001) reported biotransformation of radionuclide U(VI) to U(III).

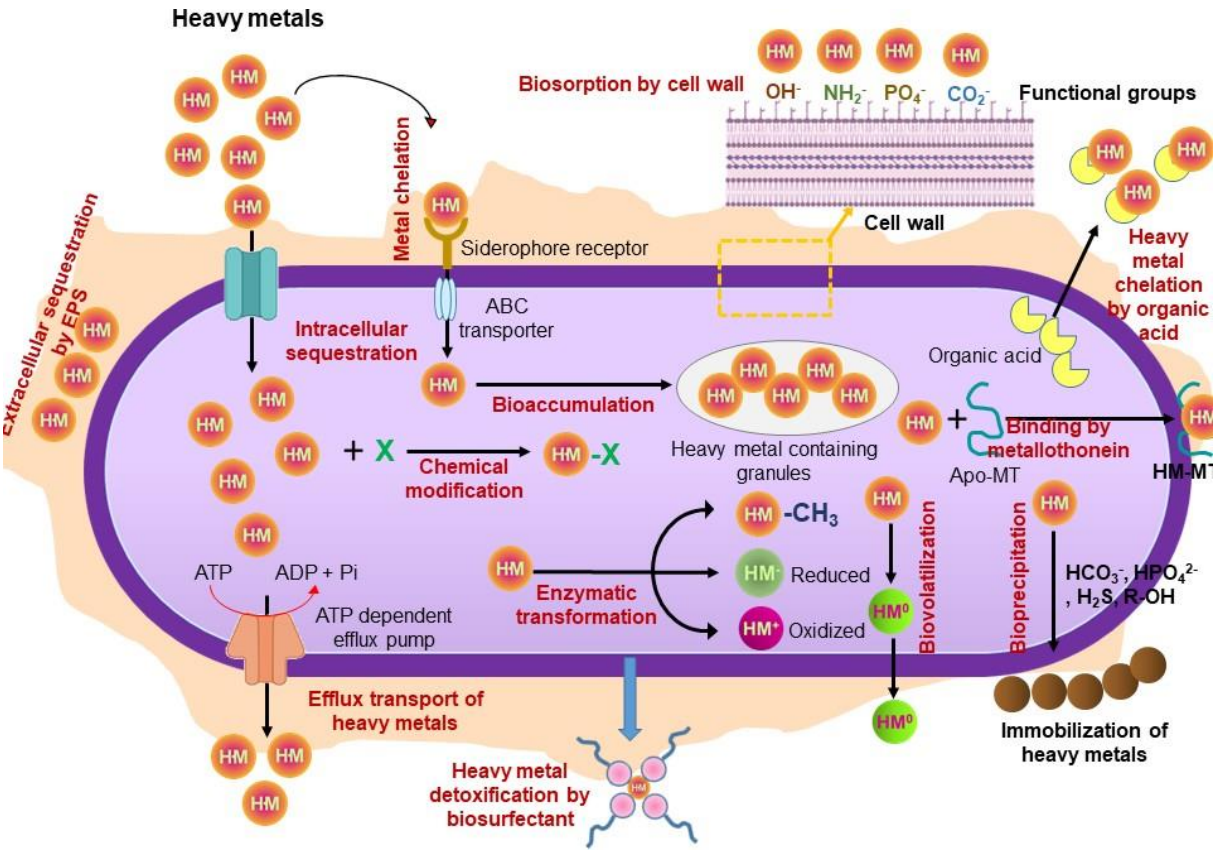

Fig. 2.2. Cellular mechanisms involved in metal sequestration.

2.6.2. Mechanisms involved in heavy metal resistance

In order to mitigate the meta stress several mechanism bacteria develop which includes (i) extracellular barrier, (II) Efflux transportation, (III) extracellular sequestration, (IV) intracellular sequestration, and (V) metal speciation.

(I) Extracellular barrier

Multiple safeguards bacteria can develop to prevent the entry of heavy metals into the cytosol. Cell wall, plasma membrane, and some specialized characteristic i.e., development like biofilm formation, and extrapolymeric substance secretion which prevents the intracellular entry of metal (Fig. 2.2). They adsorb the metal and act as a barrier. Kumar et al. illustrated many bacteria and fungi can adsorb metal. Teitzel and Parsek (2003) reported that

Pseudomonas aeruginosa can give protection to its cellular integrity against Cu, Pb, and Zn by forming a biofilm. *Rhodotorula mucilaginosa* increases metal removal efficiency from 91.71% to 95.25% by biofilm formation. In another study, Kazy et al (2002) observed EPS production confers the copper resistance to Pseudomonas aeruginosa. The Cu-resistant strain produces double amount of EPS compared to its sensitive strain. Additionally, by altering the plasma membrane's permeability, metal ion entry into the cells can be avoided.

(II) Efflux transportation

In general, a non-specific transport system allows bacteria to simultaneously absorb both essential and non-essential elements. However, particular efflux systems discharge surplus metal ions that regulate metal concentration inside the cell if the concentration of essential metals inside the cells exceeds the threshold amount (Fig. 2.2). Additionally, the efflux system prevents harmful metal ions from entering the interior of the cell, giving it the ability to resist heavy metals. Heavy metals are removed through efflux pumps, which also maintain homeostasis. A chromate ion transporter protein called ChrA87. from the *Bacillus* sp. SFC 500-1E facilitates the efflux of harmful chromate ions Cr(VI) (Rasulov et al., 2013). The *ars* operon system in Gram-positive and Gram-negative bacteria codes for the ATPase pump, ArsA/ArsB, and ArsC (arsenic reductase). As part of the efflux mechanism, arsenite is exported from cells through the plasma membrane, and ArsC is known to convert arsenate to arsenite in the cytoplasm. Rosen, (2002) reported a trivalent metalloid transporter GlpF and phosphate transporters (Pst and Pit pumps) in gram-negative arsenic-resistant *E. coli* which they use for arsenate and arsenite uptake.

(III) Extracellular sequestration

This mechanism encompasses the formation of a metal ion complex with components located in the periplasmic space (Fig. 2.2.). Additionally, it involves the formation of insoluble compounds due to metal-ion complexation (Be et al., 2018). A copper-resistant strain *Pseudomonas syringae* was reported to form blue colour colonies after binding with Cu ions and accumulating them. This was due to sysnthesis of copper-inducible protein (Cha & Cooksey, 1991). Another study by Sharma et al. (2000) showed thiosulphate is converted to hydrogen sulphide by *Klebsiella planticola*, and insoluble sulphides of cadmium are precipitated. A similar kind of activity was observed in *Desulfovibrio desulfuricans* by Yin et al. (2019), forming hydrogen sulphide in the extracellular environment through metal-ion precipitation to protect the host cell against the toxicity of heavy metals.

(IV) Intracellular sequestration

Intracellular sequestration demonstrates the involvement of metal-binding peptides in the cytoplasm for metal complexation. Two types of metal-binding peptides are found-metallothioneins and phytochelatins. They are inducible cysteine-rich metalloproteins that have an affinity for metal binding, expressed in presence of metal ions. A cyanobacterium *Synechococcus* sp. PCC 7942, was reported to synthesize metallothioneins for which *smtA* and *smtB* were accountable for its synthesis. In *Mycobacterium* sp. *Mymt* and in *Oscillatoria brevis* BmtA gene is responsible for metallothionein synthesis (Chatterjee et al., 2020). Plants and fungi contain peptides called phytochelatins that have a low molecular weight. They are created from glutathione and include 5–11 residues of amino acids. A study by Talukdar et al. (2020) revealed that cellular entry Cr (VI) in *Aspergillus* sp., is sequestered by glutathione and converted into a less toxic form.

(V) Metal speciation

Metals and metalloids exist in a wide range of oxidation states. They can be oxidized or reduced through numerous enzymatic actions, and converted from toxic to non-toxic form. These metallic species act as electron donors or acceptors to generate energy in microorganisms. Oxidized form of metal can act as a terminal electron acceptor during anaerobic respiration in bacteria. Many studies in the literature, reported that a number of bacteria from different ecological niches are capable of reducing chromate, vanadate, and molybdate (Ianieva, 2009). According to Ma et al. (2019), a bacterial consortium converted chromium (IV) to a less hazardous form. Another noteworthy example is the detoxification of mercury ions by the mercuric reductase encoded by the *mer* operon. Fig. 2.2. illustrate the machinery.

2.7. Role of earthworm intervention in waste management: A lead toward circling economy

Aristotle, the world-famous Greek philosopher once referred to earthworm as “the intestine of earth and restoring agent of soil fertility”. This terrestrial invertebrate belonging to the phylum Annelida, originated 600 million years ago, during the Pre-Cambrian era (Piearce et al., 1990). They inhabit a variety of habitats and exhibit efficient action by promoting chemical and physical changes in the soil which increase soil fertility. They play an influential role in maintaining the balance of soil-water environment. Because of their intrinsic ability to increase soil fertility, they are regarded as soil engineers and used as candidate species of

vermitechnology or vermicomposting. Vermitechnology accelerates biodegradation by the combined activity of microorganisms and earthworms. It is an efficient method for turning various types of solid waste into beneficial fertilizers and improving the condition of the soil. Bouche (1977) classified earthworms into three categories: (i) Epigeic, (ii) anecic, and (iii) endogenous depending upon their habitat preference. However, Lee, (1995) classified them into two categories detrivorous and geophagous based on their feeding habits. Epigeic earthworms are litter feeders that reside on the soil's surface. Anecics earthworms are a species of topsoil that dig vertical burrows in the soil and feed on the leaf litter that has been mixed in with the soil. Endogeic earthworms prefer to dig horizontal burrows and eat more soil than epigeic or anecic species because humus provides them with nutrition. Epigeic earthworms are broadly used in vermitechnology followed by anecics and endogeics. In short, earthworms feed upon organic waste and are a great decomposer, however, not all the earthworm are avid decomposer, only a few of them qualified for the process, example include, Eisenia fetida, *Eudrillus euginae*, *Lumbricus rubellus*, *Lampito terrestris*, *Lampito mauritii*, *Ponthoscolex corethrurus*, *Metaphire posthuma*, and *Perionyx excavates* (Bhattacharya & Kim, 2016). A list is provided in Table 2.12. that are widely used in vermicomposting worldwide.

Table 2.12. Earthworms largely used in vermicomposting. Source: Das et al. (2020); Zhang et al. (2021)

Earthworm species	Ecological category	Viability (%)	Life Span (Days)
Eisenia fetida	Epigeic	73 to 80	45 to 51
Eudrilus eugeniae	Epigeic	75 to 84	50 to 70
Perionyx excavates	Epigeic	~90	40-50
Drawida nepalensis	Endogeic	75 to 80	100 to 120
Aporrectodea calignosa	Endogeic	91 to 95	120-150
Lampito mauritii	Anecic	~98	100 to 105
Lumbricus rubellus	Anecic	60 to 70	120 to 170

* Viability is expressed in terms of cocoon hatching rate

The efficiency of vermicomposting is measured with some quality control parameters of end product, which include texture, odour, colour, bulk density, particle size, porosity, water holding capacity and C:N ratio, available nitrogen (N), phosphorus (P), potassium (K), organic matter content, high porosity, high microbial activity etc. The foremost benefits of vermitechnology, however, are its (i) low cost, (ii) low maintenance, (iii) accessibility to earthworms, (iv) quick detoxification, (v) nutrient-rich final product, and (vi) eco-friendly agricultural application. Vermicomposting employed on many types of solid waste previously.

Table 2.13 represented formerly used solid waste for vermicomposting. Even while earthworms can consume organic waste, they also require certain environmental qualities for growth and survival, namely, pH 5-8, moisture content 40-55%, and C: N ≤ 30. When the waste does not meet up the properties to warrant their growth and survivability, it needs to mix bulking agents or some kind of pre-treatment Das et al. (2020). Dried cow dung is dominantly used as bulking agent owing to its availability, easy usage, and supports high proliferation of earthworm, etc. However, presently rice husk, mustard husk, fruit peel, and saw dust is also used as a bulking agents (Chang & Chen, 2010; Lim et al., 2011). Pre-treatment is typically necessary before vermicomposting. For instance, dried cow dung is frequently utilized as an amendment, whereas fresh cow dung is not conducive to earthworm growth (Qi, 2012). Therefore, cow dung must be pre-treated before vermicomposting by being dried in natural sunshine for one week with frequent rotation (Lv et al., 2013).

Table 2.13. Stabilization of different industrial waste using different earthworm species. Source: Vig and Singh (2018); Das et al. (2020); Zhang et al. (2021).

Earthworm species	Waste type (proportion)	Bulking agent	Time taken (day)	Ratio
Eisenia fetida	Wastewater treatment plant sludge	Cow dung + swine manure	60	1:4
Eisenia fetida	Sewage sludge	Biochar	126	23:2
Eisenia fetida	Bakery industry waste	Cow dung	105	1:9
Eisenia fetida	Biogas digestate	Wheat straw	150	3:2
Eisenia fetida	Municipal solid waste-organic fraction	Cow dung	56	3:2
Eisenia fetida	Bagasse waste	Cattle dung	135	1:1
Eisenia fetida	Waste carbide sludge (NA)	Vegetable waste+ Cow dung+ saw dust (NA)	45	-
Eisenia fetida	Distillery sludge	Cattle dung	150	1:1
Eisenia fetida	Press mud	Cow dung	120	1:3
Eisenia fetida	Dyeing sludge	Cattle dung	90	1:3
Eisenia fetida	Milk industry sludge	Cow dung+ sugarcane waste+ wheat straw	90	1:1
Eisenia fetida	Thermal power plant fly ash	Cattle dung	90	1:3
Eisenia fetida	Tannery sludge	Cattle dung	120	1:3
Eisenia fetida, Lampito mauritii	Tea industry coal fly ash	Cow dung	60	1:1
Metaphire posthuma	Jute mill waste	Cow dung+ vegetable waste	80	1:1
Perionyx excavates, P. sansibarins	Anaerobic digestate	Cattle dung	60	-

Successful utilization of different kinds of earthworms for the stabilization of different industrial waste is mentioned in the literature. The complex food mixtures are ground to the finest sizes in the earthworm's strong, thick-walled gizzard, thereby expanding the feed mixture's surface area. Earthworms consume organic waste voraciously, and while they only use a small fraction of it for body synthesis, they expel a substantial quantity of it in a partially digested state, called vermicast (Sharma et al., 2005). Earthworms' intestine is enriched with diverse microorganism, enzymes, hormones, etc. which trigger faster digestion in the earthworm gut. These partially metabolized materials decompose quickly and become vermicompost in a short period (Sharma et al., 2005). Humification, the last step in the vermi-processing and degradation of organic matter, involves transforming the big organic particles into a complex amorphous colloid that contains "phenolic" components. Only about one-fourth of the organic matter is converted into humus Sinha et al. (2010). Earthworms can survive in a wide range of temperatures from 5^0C to 29^0C, however, they prefer to live in dark, moist habitats with temperatures 20^0C to 25^0C, and moisture content 60%-75%. With favourbale growth conditions and sufficient feeding material, they can grow 2^8 times every six weeks. Their average lifespan is 220 days and can produce 300-400 offspring within one life span (Hand 1988; Sinha et al., 2010). Earthworms can use their gizzard to grind the food they consume into even smaller pieces. Every day, they swallow a sizable amount of food. According to Sinha et al. (2010), the body wall of an earthworm can passively collect dissolved chemical species from the substrate. Following swallowing and absorption, intestinal fluids combine with the food components, acting as a repository for bacteria and enzymes. A variety of enzymes, including amylase, xylanase, cellulose, cellobiose, nitrate reductase, acid phosphatase, and alkaline phosphatase, are produced by earthworms and their gut microflora, which has an important industrial significance (Prabha et al., 2007; Shweta, 2012). Several different earthworm species have been used in vermicomposting technology. Epigeic earthworms, such as *Eisenia fetida*, *Eudrilus eugeniae*, and *Perionyx excavates*, have, nevertheless, been used extensively in the conversion and reuse of various types of industrial and household waste as they are r-strategist (short life with high reproductive rate). Although the surface dwellers' contribution to the development of soil structural stability and physical qualities is determined to be minimal, they are effective at breaking down complicated waste compounds. However, numerous studies have shown that such epigeic earthworms are helpful for soil health and crop growth (Wang et al., 2010; Ansari and Ismail, 2012; Singh et al., 2012). Although endogeics like *Metaphire posthuma* are claimed to increase soil health through increased microbial diversity, but, deep burrower anecics *Lampito mauritii* are not shown to be

effective composters (Ismail, 1997; Sahariah et al., 2015). In the context of this recycling economy, today's worldwide scientific community is looking for a technology that is "socially acceptable," "economically viable," and "environmentally sustainable." And here the vermitechnology based upon using earthworms meets all the virtue.

2.8. Earthworm: The sanitizer

Due to their greater resilience to a variety of environmental conditions and large reproductive potential, earthworms are reputed as ardent colonizers. They play a major role in preserving the fertility, productivity, and sustainability of the soil. Their most fascinating trait is their unique sanitizing potential of the numerous pollutants, making them a dependable agent in this eon of sustainable waste remediation. Owing to their voracious feeding habit, they feed on, digest and transform the chemical nature of waste/ waste-bulked material within a short span of time. The majority of these physical changes occur in the earthworm's gut, where many gut-residing microorganisms aid in the biochemical processes and breakdown. A wide variety of microflora (fungi, bacteria, protozoa) harboured by earthworm gut has previously been reported by many authors in the literature (Hussain et al., 2016; Hussain et al., 2018; Ali et al., 2015). Popular microbial species include *Stenotrophomonas maltophilia*, *Pseudomonas aeruginosa*, *P. monteilii*, *P. fluorescens*, *Bacillus pumilis*, *B. subtilis*, *B. flexus*, *Microbacterium schleiferi*, *Acinetobacter calcoaceticus*, *A. baumannii*, *A. junii*, *A. schindleri* etc., (Medina-Sauza et al., 2019). As Das et al. 2020 reported that the earthworm gut provides a conducive environment for growth and proliferation of microbes, which include a neutral pH range of 6.4-7.7, C: N=7:1, sugar 3-137 mM, total C 80-110 mg/kg, total N 9.1-11 mg/kg, free amino acid 400-410 mM, fatty acid 3.2-3.8 µmol/g. Many N_2-fixing and P-solubilizing bacteria are also found in the gut environment. In the recent past, Hussain et al., 2016 identified N_2 fixing and P-solubilizing bacteria belonging to the genus *Bacillus*, *Serratia*, *Burkholderia*, and *Kluyvera*. They claimed the performance of two genera *Bacillus* and *Serratia* was extremely promising, even significantly better than commercially availed biofertilizers with respect to N and P availability. These organisms play a crucial role in transformation of the pollutant during vermicomposting. Humification and mineralization are two processes which are responsible for transformation of an unstable waste compound into a stable bioactive compound. Chelation and interference of phytohormonal elements stabilized the reactions in earthworm gut and finally released a stabilized end product as vermicast that can be readily applicable for soil fertility. The process also reduces the pathogenic organism load after vermicomposting. For instance, when vermicomposting has opted for, pathogens like *E. coli* and other coliforms are

reduced (Ali et al., 2015; Medina-Sauza et al., 2019; Goswami et al., 2016; Hill & Baldwin, 2012; Yadav et al., 2010). Fig. 2.3 represents the internal gut stabilization process of the waste.

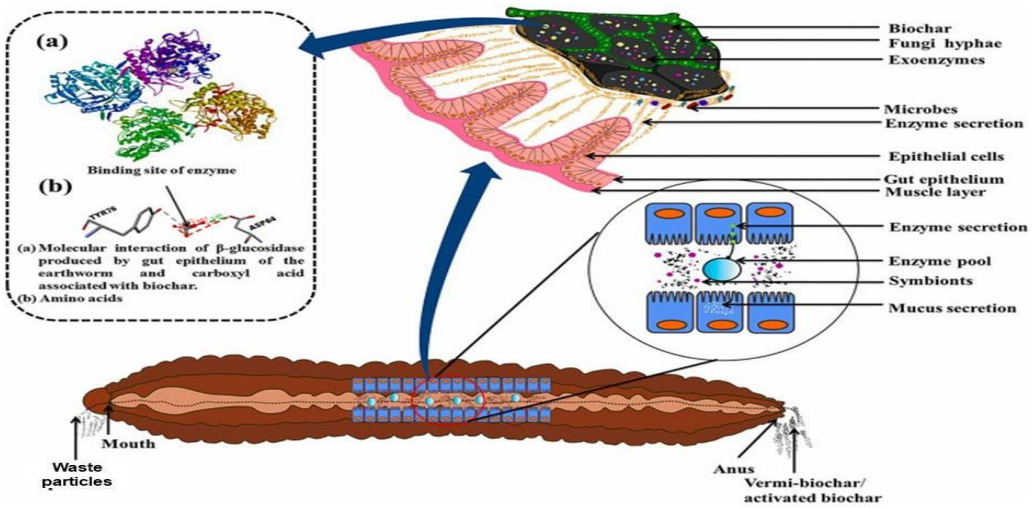

Fig. 2.3. Stabilization process inside the earthworm gut.

Source: Yuvaraj et al. (2021)

As stated earlier, in the recent past earthworms were exposed to different kinds of waste material, where they faced a wide range of pollutants, and successfully neutralized them. This is however made possible due to the mixing of the organic bulking agent with waste at different ratios. For instance, dried cow dung, poultry manure, sawdust, vegetable waste, or wheat straw were the primarily chosen option (Suthar, 2007). Table 2.14 represent the removal efficiency of numerous earthworms when dealing with a different type of pollutant.

Table 2.14. Potent earthworms in the removal of harmful organic contaminants and heavy metals. Source: Zeb et al. (2020).

Earthworm species	Type of pollutant	Removal efficiency (%)	Exposure time (days)
Eisenia fetida	Hydrocarbon (organic)	43 to 52%	90
E. fetida	Phenanthrene, pyrene (organic)	(10.5%), (6.2%)	150
E. andrei	Polycyclic aromatic hydrocarbon (organic)	85.70%	35
Pontoscolex corethrurus	Benzo-a-pyrene (organic)	36.1	122
Hyperiodrilus africanus	Hydrocarbon (organic)	38.9 to 90.3	84
Consortium of *E. fetida* & *Lumbricus terrestris*	Chlorpyrifos (organic)	93	90
E. fetida	Cd, Cr, Cu, Pb (Polluted soil)	32-37	60
E. fetida	Zn, Fe, Mn (Polluted soil)	18-58	90
E. fetida	Cu, Pb, Fe, Mn, Cr, Zn (Brick kiln ash)	41-74	60
E. fetida	Cu, Pb, Fe, Mn, Cr, Zn (Beverage industry sludge)	10-17	120
E. fetida	Cu, Pb, Fe, Mn, Cr, Zn (Food industry waste)	29-40	105
E. fetida	Cu, Pb, Fe, Mn, Cr, Zn (Sewage sludge)	17-84	105
Eudrilus eugeniae	Cu, Pb, Fe, Mn, Cr, Zn (Tannery sludge)	79-89	90
Perionyx ceylanesis	Cu, Pb, Fe, Mn, Cr, Zn (Press mud)	24-84	60

Vermicompost is a multifunctional substance with many useful properties. It was found to be helpful in the micro-remediation of contaminated soil and to promote plant growth simultaneously. Vermicompost is also renowned for locking a number of harmful heavy metals that would otherwise pollute the environment because it is a highly humified substrate. In this context, earthworms can be considered helpful in the rehabilitation of soil with heavy metal contamination (Santana et al., 2019; Ahadi et al., 2020). A specialized tissue called chloragogenous tissue confers the ability to detoxify the heavy metal. The cation exchange system is the mechanism in which the metals are trapped and retained without causing any harm to earthworms. However, the genetic aspect of metal resistance is explored by many researchers, yet the detailed underlying mechanisms are lesser known (Goswami et al., 2016; Hussain et al., 2021). Metallothionein and phytochelatin are low molecular weight metal-induced proteins found in terrestrial organisms, that get expressed in response to metallic

presence. These proteins contribute to maintaining the balance of metal ion homeostasis and chemistry in cells through an effective binding with a variety of metals (Cd^{2+}, Cu^{2+}, Mn^{2+}, and Zn^{2+}). The ionic (i.e., bioavailable) forms of the metals are captured by these cysteine-rich proteins, which then store them in the chloragogenous tissues that float freely in the coelomic fluid of the colon (Stürzenbaum et al., 2013; Vijver et al., 2007). As a result, these inert metal forms are immobilized as harmless and nonreactive substances for extraordinarily extended times (Chiaverini & De Ley, 2010; Irvine et al., 2013). Fig. 2.4. illustrate the detoxification mechanism inside earthworm gut.

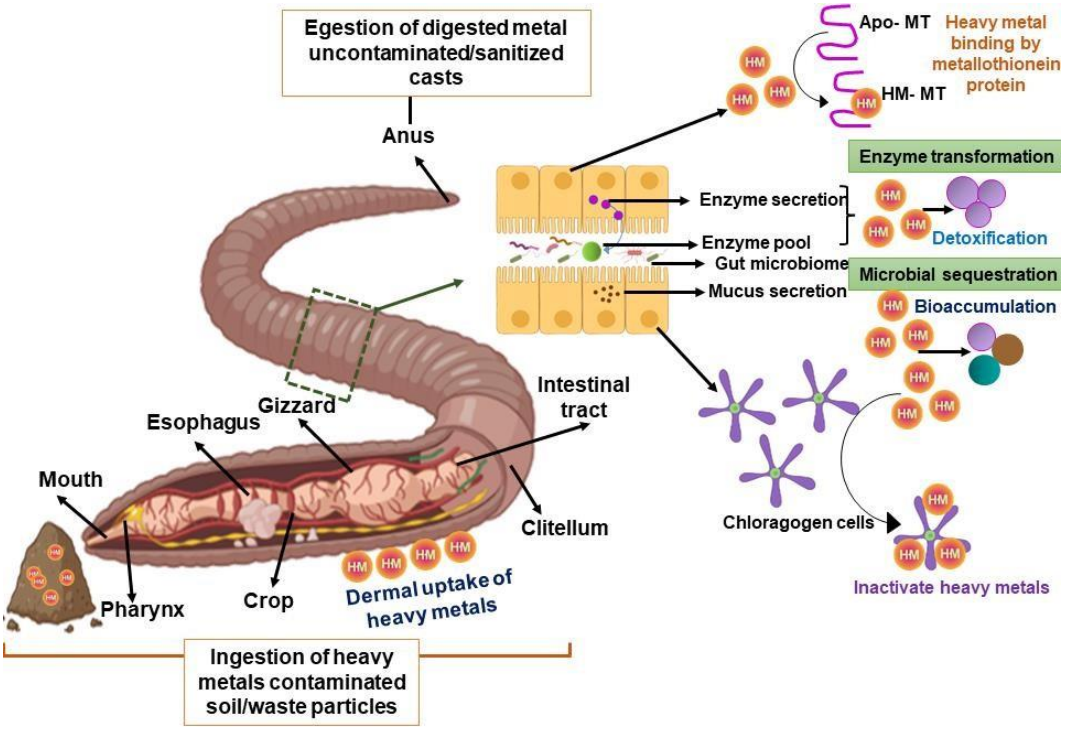

Fig. 2.4. Detoxification mechanism inside the earthworm gut, including the involvement of chloragogenous tissue, and metallothionein protein.

The behaviour of earthworms in vermicomposting reactors is largely different from that of natural soil because of some factors viz., aeration, temperature, moisture, and substatre composition. The presence of a bioavailable fraction of metal is an important influencing factor in regard to their growth and fecundity (Hussain et al., 2018). As stated early in Table 2.14, many authors have successfully vermicomposted metal-rich waste mostly using the epigeic earthworm species *E. fetida* or *E. eugeniae* reported that the formation of recalcitrant complexes with oxides, carbonates, minerals, and humic compounds during the process of

organic matter degradation is the main cause of the reduction in bioavailable metal forms in vermicomposting systems (Easha et al., 2015; Vig et al., 2018). While increased metallothionein expression was seen in the intestines of earthworms when they were exposed to metal-rich feedstocks. The correlation between metallothionein expression and metal reduction validates their role in the metal detoxification mechanism of earthworms. Non-metallothionein metal binding protein was also discovered in E. fetida, according to Goswami et al., 2016, who also provided this information.

2.9. Pristine red mud (RM) or vermistabilized red mud (RM-VC): Agricultural prospect

After a thorough review of the literature, we learned that red mud, a by-product of the aluminum industry, is highly sodic and has high levels of alkalinity, electrical conductivity, the presence of potentially harmful metals, including radioactive materials, and is biologically inert. In consideration of their massive global production, RM usage is inadequate. Their high sodicity and the presence of hazardous metals combined with radioactive components provide the most challenges in this situation. RM is currently used mainly in the chemical industry, road and building construction, ceramic industry, iron recovery, rare earth element recovery, land restoration, wastewater treatment, etc., but no attempt has yet been made to use it in the agricultural sector. This is likely caused by the increased Na content, poor nutritional status, and low organic carbon levels. Attempts have been made in the current situation to restore the RM disposal site through vegetation, however, due to their high Na concentration, only plants in the grass family that can withstand high alkali concentrations mainly survive. The heaps are amended with gypsum, compost, or stacked with soil and sand to get over this. In regards to the use of red mud in agriculture, nothing is known as of yet. Additionally, there have been no attempts to use RM as compost. Moreover, metal recovery and neutralization are the only techniques used for reducing metal toxicity and sodicity, but in-situ remediation is not given the same attention. It is unknown whether RM can be bioremediated or biotransformed before being used in agriculture by earthworms. A few scientists, like Hackenberger et al. (2019) and Di Carlo et al. (2020), investigated the impact of various RM doses on earthworm survival rates as well as the genetic consequences of those RM doses on earthworm, but the chemical status of RM in post earthworm treatment was overlooked. Therefore, in this work, we tried to convert RM into compost using the earthworm *Eisenia fetida* and subsequently used it for a crop trial.

Chapter 3

Methodology and Instrumentation

Chapter 3

Methodology and Instrumentation

3.1. Orientation of the work

The present thesis edifies the two directions of work for the sustainable management of noxious waste. To reach the goal this chapter gives a quick review of the experimental planning and procedures used to achieve success for the proposed aim of the study. The work plan of this study was categorized into four phases. In the first phase the red mud (RM) samples were collected from the HINDALCO alumina plant located in Muri, Jharkhand, India. The waste was undergone a thorough environmental characterization. Additionally, the solubility patterns of several elements were assessed in order to understand the long-term effects of RMs on the nearby soil and water habitats. Additionally, a variety of reliable metrics were used to evaluate the potential effects on both human health and the overall health of the environment. In the second phase of the work, a sample of raw bauxite ore was taken from a Bagru bauxite mine in Lohardaga, Jharkhand. The sample was characterized in detail from a physicochemical and microbial perspective and also underwent a relative study with soil to check its quality difference in terms of environmental impact. Finally, a simple representation of the characteristics before and after alumina extraction from bauxite ore was provided. In the third stage, the study was investigating red mud from a microbiological standpoint. To understand microbial diversity and their community dispersion in RM, a metagenome-based approach was conducted. Other microbiological characteristics, including FDA, MBC, and enzymatic activity, were also examined to determine whether or not this harsh toxic waste is capable of harboring any microorganisms and, if so, what kind and how active they are. In addition, a complete heterotrophic count was performed. Additionally, the waste was utilized to identify native bacteria with metal sequestration ability. Such an effort was made to create a polyextremophilic biomass-biosorbent that could be suitable for wastewater treatment. In the last phase, the epigeic earthworm *Eisenia fetida was* used to evaluate the potential of vermicomposting technology for converting hazardous RMs into sanitized vermicompost with high nutrient value and low heavy metal concentration. Though the first stage of the study report unveiled the harsh characteristics of RM, yet, we opted for vermicomposting technology a little skeptically, and finally, we achieved success after some kind of pre-processing. Being extremely sodic this waste was not much appreciated previously for bio-composting; thus, we

took the challenge to provide a sustainable way of management using earthworms. Vermibeds made consisting of various combinations of RMs and cow dung (CD) were used in two distinct crop trials (Pot and field conditions). Regarding nutrient enrichment, end-product maturity, and the removal of hazardous metals, vermicomposting technology was compared against aerobic composting to determine which method was more effective.

For this study, a work plan was divided into four phases. These are presented below

Step 1: Collection of red mud and collection of native bauxite ore

Step 2: (a) Characterization of physico chemical parameters and microbial parameters

(b) Heavy metal concentration determination

(c) Environmental risk assessment

Step 3: (a) Searching for alkaliphilic metal tolerant bacteria; Biochemical characterization and molecular identification of the isolate; Biosorption efficacy of the three potentially toxic metal Cd, Ni, Cr.

(b) Vermiconversion of the red mud (RM); Insight to metal remediation assessment; Microbial quality assessment; Physico-chemical assessment of the vermiconverted product.

Step 4: Field study of the rice and pot experiment of the green gram using vermiconverted red mud (RM); Soil parameters analysis; Yield analysis and agronomic parameter analysis.

3.2. Phase I of the work

This phase encompasses a thorough characterization of collected red mud. They were collected from the dump site of HINDALCO alumina plant with different ages of disposal histories. They were brought in clean sterile zip locks from the sampling site. As they were dry cake-like and also muddy-slurry type, so, initially, they were air dried, ground, and sieved through 2mm and 0.2 mm mesh and stored in an air-tight container. All the physicochemical analyses done in the first phase are presented in the below-mentioned flowchart:

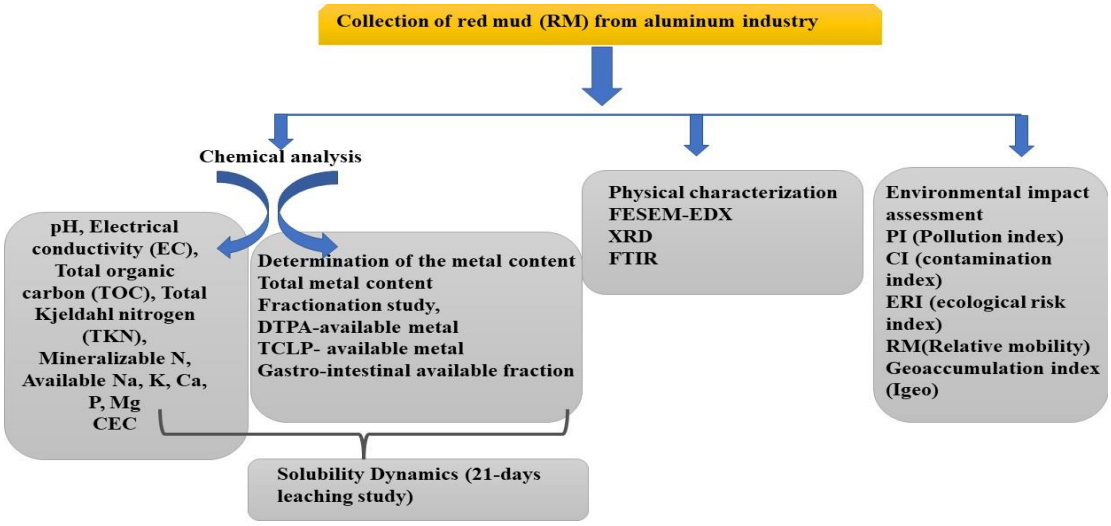

Fig 3.1. Flowchart of the work done under phase I.

By using standardized procedures, pH, electrical conductivity (EC), available potassium (Av. K), available calcium (Av. Ca), available phosphorus (Av. P), available sodium (Av. Na), available magnesium (Avl. Mg), total organic carbon (TOC), and total Kjeldahl nitrogen (TKN), mineralizable nitrogen, cation exchange capacity (CEC) was measured (Page et al. 1982; Lindsay and Norvell 1978; Tessier et al. 1979). In the RMs, the bioavailable forms of several metals (such as Cd, Cr, Mn, Pb, Zn, Cu, Ni, and Fe) were extracted through different extracts (Diethylene Triamine Penta Acetic acid for DTPA, glacial acetic acid for TCLP, pepsin and pancreatin for gastro-intestinal availability) in order to quantify their availability and accessibility and corresponding detrimental effect. Metal was measured in AA S- 816, Systronics, India. Subsequently, total metal content and fractionation study were done to check their distribution in the red mud. Finally, to quantify their mobility in water extract, a solubility study was carried out and the cations, anions, and metal content in the extract were checked.

To explore their surface morphology, elemental composition FESEM- EDX study was done. FTIR was to check their functional group distribution, and XRD was employed to visualize their physical appearance whether crystalline or amorphous. Additionally, XRD revealed their mineralogical composition.

3.3. Phase II of the work

This phase includes a detailed characterization of the gathered bauxite ore. They were carried in from the sampling site in a clean, sterile zip lock. They were initially air dried, ground, sieved through 2mm and 0.2mm mesh, and stored in an airtight container. In the flowchart below, all of the analyses performed during the second phase are shown.

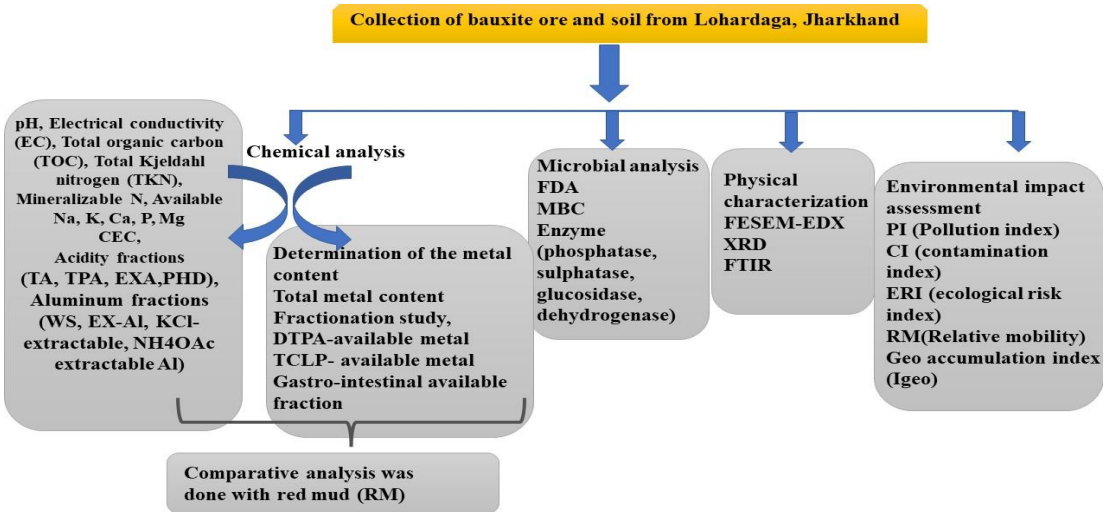

Fig 3.2. Flowchart of the work done under phase II.

In this stage, likewise, following the standardized method I carried out all the physicochemical characteristics (pH, EC, TOC, Available N, Na, Ca, K), CEC (Page et al. 1982; Lindsay and Norvell 1978; Tessier et al. 1979). Additionally, I carried out an acidity fractionation study because it was found that the nearby forest soil and bauxite ore were both acidic. Next step, I also checked the aluminum fraction by extracting it into different extracts (water, KCl, NH_4OAc) to find out their availability. Similar to RM the ore sample was also characterized through FESEM-EDX, FTIR, and XRD to elucidate their structure, elemental composition, and mineralogical distribution. Lastly, the characteristic deviation of RM from natural ore was evaluated.

In addition, I also carried out a detailed study on microbial parameters of the sampling site viz. fluorescein diacetate hydrolyzing activity (FDA), β-D -glucosidase activity, acid phosphatase, aryl sulphatase, dehydrogenase, and microbial biomass carbon (MBC) (Tabatabai, 1994).

3.4. Phase III of work

In this stage, RM was methodically explored from a microbiological perspective. Initially, I have done the enzymatic analysis (FDA, alkaline phosphatase, glucosidase, sulphatase) to get an idea of the microbial presence (Tabatabai, 1994). Next, I conducted a metagenome based (16s V3-V4 sequence-based analysis) study to know the microbial diversity (genus and species abundance). This study was outsourced from CLEVERGENE, a Hyderabad-based company. It was a culture-independent approach to exploring the microbial diversity of the RM. Subsequently, I carried out a culture-dependent study in order to achieve

alkaliphilic metal-tolerant organism (bacteria) for making a biosorbent for metal adsorption. The isolation, purification and molecular identification of the isolate is discussed thoroughly in Chapter 6 (section 6.2.2). An alkali-specific medium named HoriKoshi was used for isolation purposes. The composition of the media is given below:

Glucose 10g/L
Yeast extract 5g/L
Peptone 5g/L
K_2HPO_4 1 g/L
$MgSO_4$ 0.2 g/L
Na_2CO_3 10%
Agar agar 20 g/L
the pH of the medium 10.5 (pH adjusted by 1 (N) NaOH)
All the precursor components were purchased from Hi-Media.

For biochemical assay, I used KB013 Hi-Bacillus^{TM} identification kit, while to know the carbohydrate utilization pattern KB009- Hi carbo^{TM} kit (KB009A/ KB009B1/ KB009C) was used. All the kit was purchased from Hi-media. Following this, we checked the multimetal tolerance and minimum inhibitory concentration assay (MIC) for identifying the potent metal-tolerant bacteria. to carry out the MIC assay, we selected five metals viz., Cd, Cr, Ni, As, and Cu. The precursor salt used in the assay were Cd $(NO_3)_2$, $K_2Cr_2O_7$, Ni $(NO_3)_2$, $(NaAsO_2)$, and Cu $(NO_3)_2$ purchased from Merck, Germany. The stock solution of the metal was prepared by using these precursor salt. The broth medium was supplemented with this stock solution with varying concentrations to achieve the MIC value of the isolates. Subsequently, we selected the most potent isolate based on MIC and growth optimization assay (pH, NaCl, and temperature tolerance) to prepare the biosorbent for metal adsorption study. The preparation of biosorbent, in a nutshell, 48 hours culture grown in Hori Koshi medium (pH 10.5) was spun down, washed with PBS, and oven dried at 45^0C to 50^0C. This oven-dried sample was preserved at -20^0C for use in the biosorption experiment. After adsorption, the residual metal was measured by atomic absorption spectrophotometer (AA S-816 Systronics, India). The entire work briefly summarizes through a flow chart.

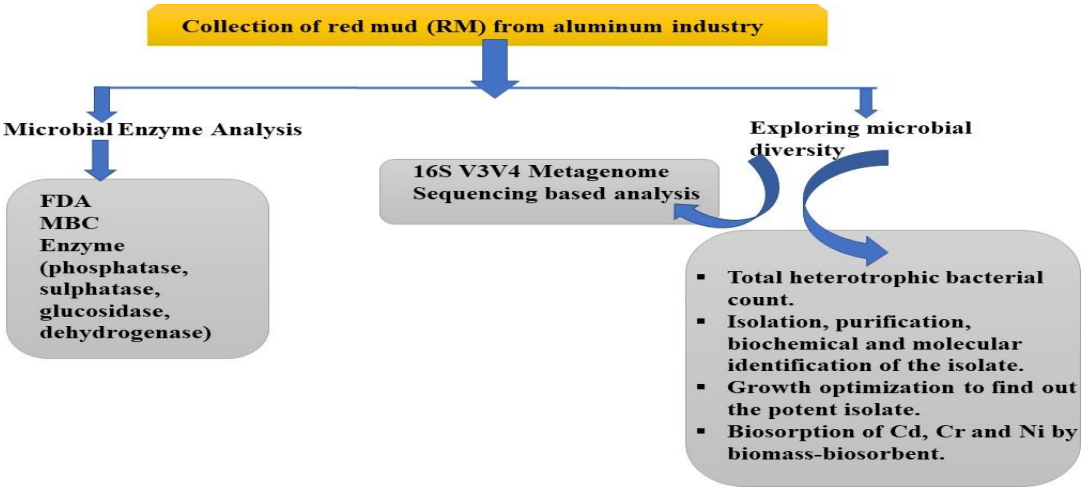

Fig. 3.3. Flowchart of the work done under phase III.

Diagrammatically the biosorption study is presented below:

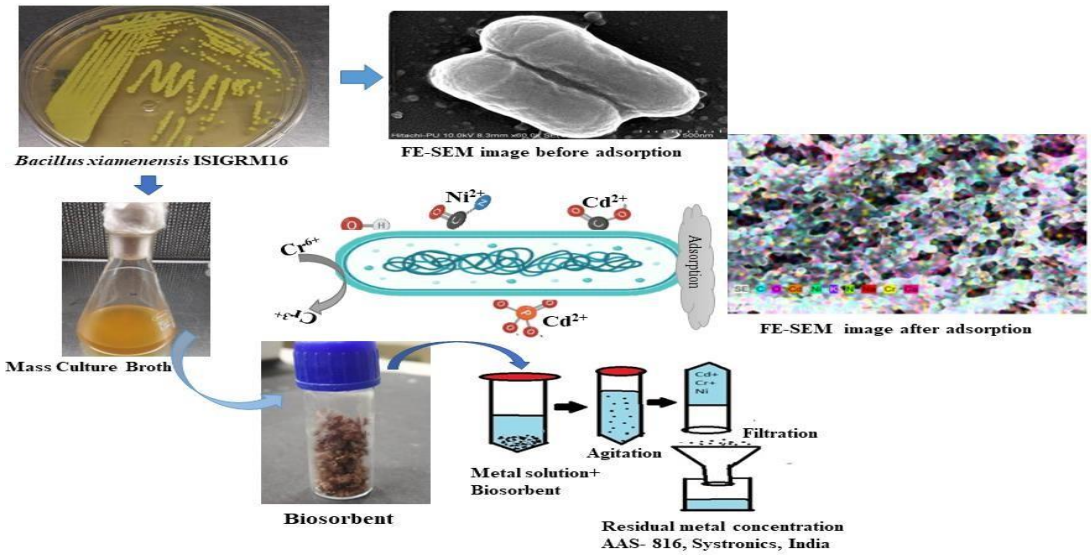

Fig. 3.4. Cd^{2+}, Ni^{2+} and Cr^{6+} adsorption by *Bacillus xiamenensis* ISIGRM16.

3.5. Phase IV of work

In Fig.3.3, the work accomplished during phase III of the study is presented schematically. In this phase, an effort was made to comprehend the bioconversion of red mud (RM) using earthworm *Eisenia fetida* in order to sanitize the waste. *Eisenia fetida*'s potential for vermicomposting was evaluated in contrast to aerobic composting in feedstocks made with various RM and cow dung treatment combinations. The experimental setup is depicted in the flowchart presented below:

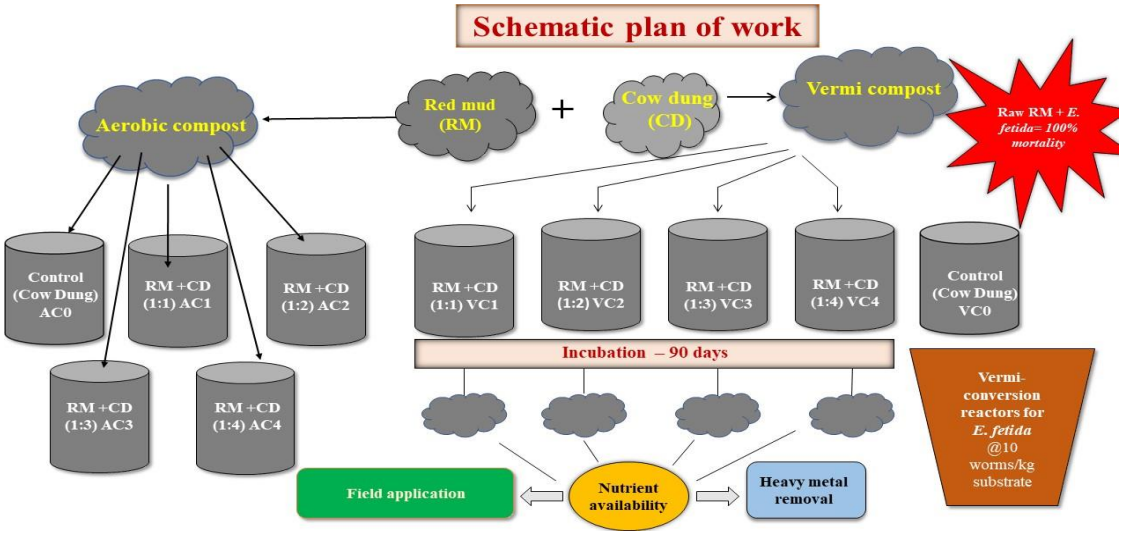

Fig 3.5. Experimental setup for composting and vermicomposting of RM

The concentrations of metals (Cd, Cr, Pb, Cu, Mn, Zn, Fe, etc.) in the vermibeds and earthworm intestines were evaluated before and after the incubation using conventional extraction and analytical techniques (Page et al., 1982). Also, to check the efficacy and success of vermicomposted RM the following attributes were checked routinely: pH, EC, TOC, microbial biomass carbon, available nitrogen, C:P ratio, urease activity, available P, phosphatase activity, glucosidase, dehydrogenase, sulphatase exchangeable K, and metals (Cd, Cr, Ni, Cu, and Pb) (Page et al. 1982; Lindsay and Norvell 1978; Tessier et al. 1979; Tabatabai and Bremner, 1982).

Since, the study's primary goal was to assess how well vermiremediated RMs work on crop growth, productivity, and soil health. The combination (ratio of RM+CD) of vermicompost for large-scale production was chosen based on the findings of the pot and field scale investigation. So, to attain this objective we checked that, the vermicomposted RM was found to be more promising compared to aerobically composted RM for agricultural application purposes, thus, I conducted a pot experiment of this vermicompost taking *Vigna radiata L.* as a test crop. After a success on pot scale application, I proceeded for large scale field application taking the staple crop of the subcontinent, rice (*Oryza sativa L.*) as a test crop to check how well the vermicomposted red mud affect crop growth and soil fertility. I also kept a raw CD as organic manure positive control to compare the efficiency of vermi-converted RM. Different physicochemical properties of soil viz., pH, EC, available NPK, and DTPA available metal were measured before and after vermicomposted treatment. Soil microbial quality was checked temporally during the experiment in order to assess the microbial density. Different

agronomic parameters were measured in post-harvested crops. Finally, yield was calculated by using standard formula. The crop trial procedure is thoroughly discussed in Chapter 8.

3.6. Quality assurance and quality control

All elemental analyses were carried out in accordance with the broad quality control (QC) recommendations made public by Indian Statistical Institute, Agriculture and Ecological Research Unit. Below is a definition of quality assurance and quality control. A measurement program's ability to be quantified and produce data of known quality is ensured by a set of coordinated efforts, such as plans, specifications, and procedures, known as quality assurance. "The routine use of procedures designed to achieve and maintain a specified level of quality for a measurement system" is the definition of quality control. Without sufficient QA/QC, a monitoring system faces the risk of being unable to control the data quality and ensure precision and accuracy.

3.7. Sample storage and preservation

Upon collection, samples of soil, plants, and vermicompost were air-dried, powdered, and sieved in line with NCR 13 and AOAC requirements. Samples that had been air-dried were kept in plastic bottles that had dates and numbers on them. Before use, each of these vials was properly cleaned, washed with reagent water, and dried. The majority of the samples were examined within two to three days following collection. Samples were kept at 4° C for a maximum of 28 days after collection in cases where storage was necessary.

3.8. Purity of chemicals, reagents, and lab wares

All of the chemicals were GR grade (guaranteed reagent) and had a purity level of 90–98%. To prepare the reagents, ultrapure water was employed. The reagent was newly made on the day of the analysis. Prior to each usage, the glassware and plastic items were cleaned with reagent water, rinsed with double-distilled water, and oven-dried.

3.9. Calibration procedures

Prior to usage, all of the analytical equipment was calibrated and adjusted. Before analyzing a fresh set of samples, the calibration was checked. There would be multiple criteria and at least one blank in the method. Numerous standards were taken on a regular basis for some instruments, such as pH meters, which do not require blanks. To guarantee the accuracy of the analysis, standard reference materials (SRMs) that provide certified values of analytes

were employed throughout the tests. The highest level of purity was maintained for all standards (for pH meters, electrical conductivity meters, UV-Vis's spectrophotometers, and AAS-816). The accuracy value was calculated from the certified and the experimental values of each heavy metal (Table 3.1). Briefly, with a relative standard deviation (RSD) of 10%, we conducted a triplicate analysis of the mean values of each metal. Except Cd (range 0.1 to 1 mg/L), calibration standards ranging from 0.1 to 10 mg/L were employed with standard stock solutions of the individual metal ions (1000 mg L^{-1}, Sigma-Aldrich grade) in 1% (v/v) HNO3. Based on the range of each PTE, a standard curve was drawn, and analysis was then done. Three steps completed the metal analysis: the addition of reagent, a continuous calibration verification (CCV), and an initial calibration verification (ICV) using a 1 mg/L standard (tested for > 95% recovery). The accuracy and reproducibility of the tested samples were evaluated using certified reference material SRM 2710 in 1% (v/v) HNO_3. The recovery % of metals in tested samples provided accurate data. In order to determine the accuracy of the technique for PTEs, the certified material was ultimately digested in an ultrapure combination of acids and the acquired findings were discriminated against using SRM2710 values. Given that the standard reference solution had its PTEs content validated, it had been diluted three times, and the measured concentration was compared to it. The percentage recovery for each heavy metal, i.e., the analytical accuracy of the instrument, was ranging from 97.65–98.24% which suggested no technical contamination during the AAS-816 analysis.

Table 3.1. Accuracy value of Standard Reference Materials (SRM 2710) analyzed in AAS- 816.

PTEs	SRM 2710 (mg kg^{-1})	AAS measured (mg kg^{-1})	Recovery (%)
Cr	17	17.3	98.2659
Ni	10	10.24	97.65625
Pb	5104	5195	98.24832
Cu	2700	2730	98.9011
Cd	19	19.51	97.38596

3.10. Initial demonstration of performance

Prior to studies, the technique detection limits are determined using the initial demonstration of performance to characterize instrument performance (definition of linear calibration ranges) and laboratory performance.

3.11. Linear calibration range (LCR)

Every six months or whenever a significant change in instrument response was noticed, the LCR was originally determined and validated for important instruments such as the UV-vis spectrophotometer, Kjeltec N analyzer, and AAS-816. Generally speaking, 1 blank and 3 standards were used to verify linearity.

3.12. Instruments and equipment

- **Operations and maintenance**

  All instruments and equipment were kept in top working order and had complete records of their proper use, calibration, and troubleshooting. The following rules are followed when using the used laboratory equipment on a daily basis: Equipment includes balances, automatic pipettes, pH meters, UV-VIS spectrophotometers, and electrical conductivity meters.

- **Calibrations**

UV-VIS Spectrophotometers: Following initial instrument warm-up. For every 50 samples that were analyzed, the calibration was verified.

Maintenance-Maintenance yearly once by professionals.

AAS- 816: After an initial warm-up of the instrument. Verification of calibration was done after every 50 samples analyzed. A recalibration was conducted if periodic QC samples fail to be within control limits

Maintenance-Maintenance yearly once by professionals

pH Meter: For every 100 samples, calibrate the instrument at pH 4, 7, and 9 with standard solutions.

Maintenance- Checking probes regularly and ensuring that electrodes are filled.

Conductivity Meter: The conductivity probes were cleaned with double distilled water before and after every use. The surfaces of the probes were usually wiped with high-absorbent paper towels to ensure their dryness. The instrument was frequently calibrated with known solutions supplied by the instrument

Maintenance- Checking of probes regularly as specified by the manufacturer.

Balances: Every day before use, the balances were checked. The balances were kept in airtight cabinets to eliminate measurement mistakes. The precision of the balances was routinely checked by weighing authentic weighs.

Maintenance- After every use necessary cleaning was performed with ethanol. The dust and fallen chemicals during weighing were cleared. The instrument was serviced and calibrated by certified company engineers once a year.

Automated Pipettes: Used to be calibrated every 15 days.

Maintenance- Adequate cleaning after every use

Laminar Airflow: The machine is kept in an air-conditioned microbial inoculation room properly separated by the glass door. Before starting the culture work the machine is left for 15-20 minutes UV exposure with HEPA filtration.

Maintenance- Adequate cleaning before and after use, UV exposure, and yearly maintenance of the HEPA filter.

BOD-Incubator: The machine is kept in an air-conditioned microbial inoculation room properly separated by the glass door. Appropriately cleaned with 70% alcohol each time before and after incubating culture plates/ broth.

Maintenance – Checking compressor for 6 months at professionals' intervals for proper upkeeping of the required temperature.

Centrifuge: Kept in an air-conditioned room. Properly cleaned before and after use of the rotor head.

Maintenance – Maintenance yearly once by professionals.

Autoclave: To prevent any form of accident and ensure that the medium is properly sterilized during autoclaving, the water level and pressure relief valve are both properly checked.

Maintenance- Maintenance yearly once by professionals.

Chapter 4

Characterization, pollution potential, and ecological impact of red mud (RM)

Chapter 4

Characterization, pollution potential, and ecological impact of red mud (RM)

4.1. Introduction

Red mud is a high-volume by-product of the aluminum industry generated during alumina extraction through Bayer process. About 90% of the aluminum is produced through Bayer process worldwide (Liu et al., 2007). Globally 150-170 million tons of red mud is produced annually. In general, 1-2 tons of red mud is formed to extract 1 ton of alumina, however, the volume generation of RMs largely depends on the grade quality of bauxite ore (Bray et al., 2018; Evans, 2016; Hackenberger et al., 2019). Bauxite is the only precursor of alumina on the earth. Almost 85% of the bauxite can be converted to aluminum. In the Bayer process, this bauxite ore is digested with sodium hydroxide (NaOH) at high temperature and pressure, which results in the soluble sodium aluminate and leaves the insoluble residue behind with immense impurities (Cho et al., 2019). This insoluble leftover is termed bauxite residue or red mud. The name itself indicates its appearance which is brick- red colour and silty texture owing to an abundance of iron oxide (Fe_2O_3). The global inventory deposits of red mud have by now exceeded 4.6 billion tons which are expected to increase shortly, representing a potential source of contamination on-site or off-site. Wet disposal method like red mud pond is still the prevalent way of dumping, however, dry stacking/semi-dry stacking are very in nowadays considering their lethal impact on the environment (Li et al., 2018). Considering the Indian scenario, ~9 million tons of red mud have been produced annually, covering 5% of worldwide generation. However, the generation is also constantly rising as a result of rising per-person alumina/aluminum consumption. The extraction of the highest-quality bauxite sources has led to a decline in the class of bauxite ore hence it is anticipated that the generation of red mud will increase corresponding to its ore quality deterioration (Hua et al., 2017). The majority of dumping occupies either large landfills or is dumped into the sea. As of now, bauxite residue is kept in land-based bauxite residue disposal sites (BRDAs) (Burke et al., 2013; Zhu et al., 2016). Such massive accumulation of this highly alkaline (> pH 12) RM may result in ecological and environmental issues due to the possibility of spills, leaks, and even the collapse of storage ponds during intense rainfall.

Characteristically RM is highly alkaline (pH>12), saline, and sodic, contains a high amount of water-soluble and absorbed sodium, and residual mineral of bauxite in the form of an oxide (Obhodas et al., 2012). It has high electrical conductivity (>10 dS/mt), and exchangeable sodium percentage (ESP). It lacks structural stability that causes seal and crust formation, resulting in obstacles in air and water movement and also root penetration, etc. (Wang et al., 2019; Zhu et al., 2016; Li, et al., 2016). Furthermore, the lower particle size of red mud is responsible for its low hydraulic conductivity, porosity, and meager water-holding capacity. Due to its extremely fine texture, it easily forms dust that leads to harm the nearby residing communities and downwind areas (Kong et al., 2017). Apart from that, the residue act as a sink of numerous toxic metals and metalloids like Cd, Cr, Pb, As, Ni, V and low levels of micronutrients viz., K, Zn, Mn, etc. (Gautam et al., 2018). Seepage from the residue landfill area contaminates the surrounding soil, groundwater, surface, and subsurface water through alkalization (high Na content of leachate). Importantly, long-term exposure to toxic metals may have an immediate/passive impact on the ecosystem Additionally, the increased deposition of heavy metals mobilized from RM in plants and sediment would pose major threats to human health in the long run (Wang et al., 2019; Cho et al., 2019).

Although red mud is used in different sectors (chemical industry, metallurgy, cement, and bricks production, waste-water treatment, etc.), presently a little portion is used in soil specifically acid soil amelioration however use of red mud in agriculture is scarce (Bhatnagar et al., 2011; Dimas et al., 2009; Van Beers et al., 2009). Thus, it is crucial to understand how harmful metals and sodicity of red are alleviated during soil application. The literature has hardly explored the fate of metals and their possible distribution in soil amended with red mud. Additionally, the physico-chemical properties of RM have not yet been researched from an agricultural perspective. In general, RM is loaded with different kinds of toxic metals (Gautam et al., 2018). Many researchers have previously explored the sorption behaviour of red mud for metal and other toxicant removals (dye) from aqueous solution, but no study is available on the dissolution kinetics of indigenous metal of red mud that may greatly enhance the pollutant load of the surface soil/water.

Usually, the distribution of metals in their soluble and/or resistant forms has a significant impact on the environmental risk and trajectory of metals. Therefore, it is also required to evaluate the probability of metal accumulation in geological strata. Understanding the environmental fates of RMs through geochemical model-based techniques is crucial since contaminant solubility in any solid waste limits their leaching processes based on the

adsorption-dissolution equilibrium over time (Sahariah et al., 2015). Earlier, solubility study was used to predict the leaching behaviours and stabilization process of ions in coal ash, solid waste, and textile sludge, however, this model has not yet been applied to know the saturation profile of ions in RM (Bhattacharyya et al., 2011; Sahariah et al., 2015). Estimating the effect of bioavailable metal forms derived from RM on human health status is important to be explored. As a result, the constant influx of metals from industrial effluents into the environment poses a risk to human health in terms of the skin, lungs, and cancer. There is currently no information in the literature regarding the risk to human health linked with the speciation behavior of metals in the RM.

Keeping an eye on these viewpoints, the present research was conducted to develop a comprehensive understanding of the characteristics of RM and their probable impact on the environment and human health. The major objectives of the work are narrated below:

1. Characterize RM based on their originating material using Principal Component analysis (PCA).
2. Evaluate the distribution of different metal fractions in the RM.
3. Solubility dynamics study of elements.
4. List the environmental and health risks that RM could pose.'

The distribution and physical properties RM were examined, and several potential hazard indices affecting ecological and human health were computed. To comprehend the long-term environmental effects of RM, the patterns of existence of various metals were also evaluated.

4.2. Material and methods

4.2.1. Sample Collection and Processing

The red mud samples were collected from the age-old dump of the HINDALCO aluminum plant located in Muri, Jharkhand (Fig 4.1). The samples were taken from 12 different hips with different age disposal histories. Samples were labelled RM1-RM12. We adopted a simple random sampling technique for collecting composite and representative samples from the selected dumped sites. The collected RM samples from each site were ground to powder mechanically, sieved via 2mm and 0.2 mm mesh, and mixed properly to form a representative sample for each site. All parameters were analysed taking three replicates.

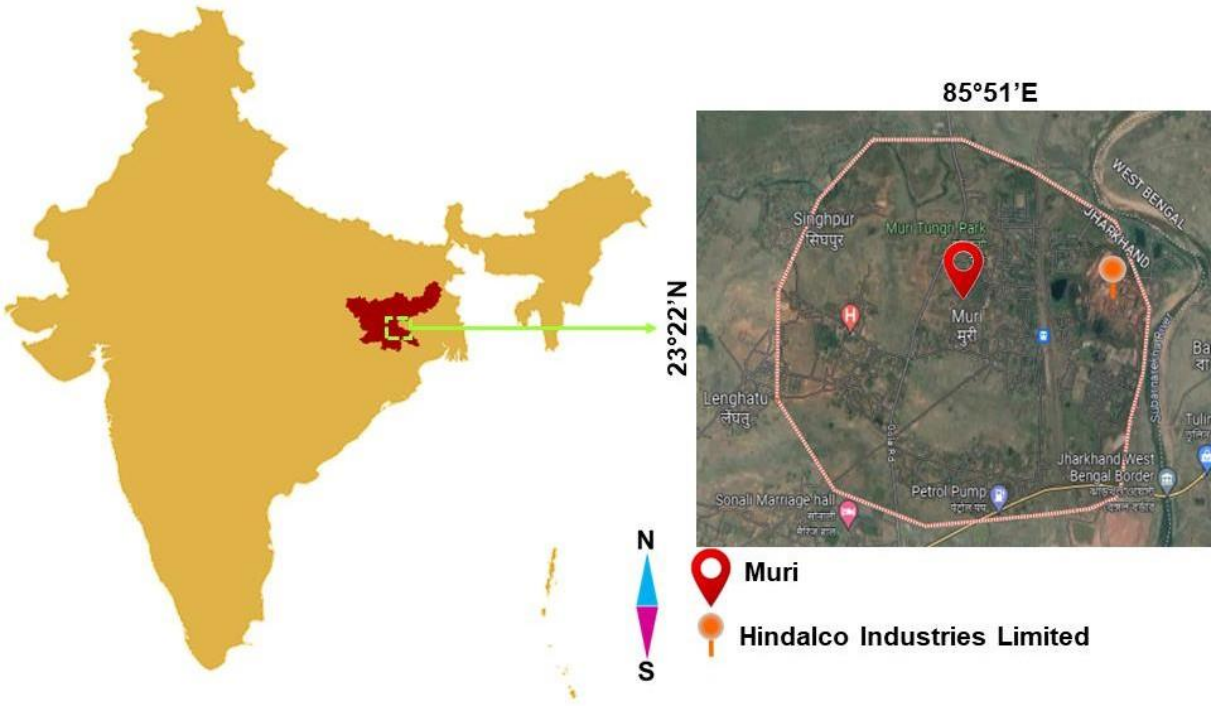

Fig. 4.1. Location map of sampling site with details, HINDALCO, Muri, Jharkhand.

4.2.2. Physico-chemical analysis of RM

Following the standard procedures, the physicochemical characteristics of the BKCA samples were assessed, including pH, electrical conductivity (EC), bulk density (BD), water holding capacity (WHC), cation exchange capacity (CEC), available Ca, Na, P, and K, and total organic C (TOC), total N, easily mineralizable N (Page et al., 1982). To examine the structural and elemental characteristics of the RM sample, we used energy-dispersive X-ray spectroscopy (EDX) and scanning electron microscopy (SEM). The abundance pattern of functional groups was also determined using FTIR spectroscopy. XRD was used to find out the mineralogical compositions. Below is a detailed description of the techniques.

A. Measurement of pH

To measure pH of the samples, a 1:2.5 solution was prepared by mixing 10g sample with 25ml distilled water. The solution was then intermittently stirred with a glass rod uniformly for about 30 minutes. Finally, the pH of the suspension was recorded with the help of digital pH meter (Systronics).

B. Measurement of electrical conductivity (EC)

To measure EC of the samples, a 1:5 solution was prepared by mixing a 10g sample with 50 ml distilled water in a 100 ml beaker. The solution was stirred with a glass rod uniformly and then left for 30 minutes. The suspension was left to stand until the sample's particles had settled. After that, a digital conductivity meter (Systronics Conductivity Metre 307) was used to record the EC of the suspension.

C. Estimation of Total organic carbon (%) (Modified Walkley and Black method, 1934)

Reagents:

1. 1N Potassium dichromate solution ($K_2Cr_2O_7$)

2. 0.5 Ferrous ammonium solution {$FeSO_4$. $(NH_4)2SO_4.6H_2O$}

3. Diphenylamine indicator 4. 85% Orthophosphoric acid (H_3PO_4)

5. Conc. Sulphuric acid (H_2SO_4).

Procedure:

1.1g of RM sample was taken in a 250 ml conical flask.

2. 10ml potassium dichromate was added to the sample followed by addition of 20ml of conc. H_2SO_4.

3. The conical flask kept undisturbed for 30 minutes in dark incubation

4. After incubation 30 ml of distilled water and 1 ml of 85% orthophosphoric acid was added.

6. Afterwards, 6 drops of ferroin indicator was added and finally titrated with ferrous ammonium sulphate solution (0.5 M).

7. A baff pink colour is obtained at the endpoint.

Calculation:

Total organic carbon (%) = $Vk\times (1-Vs\ Vb)\ W \times Sk \times 0.3$

Where,

Vk: Volume of $K_2Cr_2O_7$ solution

Vs: Titrant reading

Vb: Blank reading

Sk: Strength of $K_2Cr_2O_7$ solution

W: Weight of RM sample

D. Total Kjeldahl Nitrogen (TKN) estimation

Reagents:

1. $CuSO_4$
2. K_2SO_4
3. Conc. H_2SO_4
4. H_2SO_4 (0.1N)
5. NaOH (0.1N)
6. Mixed indicator

Procedure:

1. Digestion procedure:
    a. In a digestion tube, 12ml of concentrated H_2SO_4 was added together with 1g of sample, 0.8g of Copper sulphate, and 7g of Potassium sulphate. The tube was then digested in the Foss Kjeltec Techtor TM digestor at 420^0 C for one hour.
2. Distillation procedure:
    a. The Kjeltec TM 8100's distillation chamber was used for the distillation process. Following digestion, the tube was first cooled and subsequently used for distillation. The distillate was then collected in a conical flask with 20 ml of 0.1 N H_2SO_4 and 2 to 3 drops of mixed indicator before being titrated with 0.1 N NaOH.

Calculation: Total nitrogen (%) = $\frac{Titre\ value x\ 0.014x100}{W}$

Titre value = [(Volume of H_2SO_4× Strength) – (Burette reading of NaOH × Strength ×0.014×100] ÷W

W: Dry weight of the sample

E. Easily mineralizable nitrogen estimation (available N)

Reagents:

1. 0.32% $KMnO_4$: 3.2 g of $KMnO_4$ was added to distilled water and made the volume up to 1 liter.
2. 2.5 % NaOH: 25 g of NaOH pellets was dissolved in distilled water and made volume up to 1 liter

3. 0.8 % NaOH: 0.8 g of NaOH pellets was dissolved in 1 liter of distilled water.
4. N/50 N H_2SO_4: 550 µL of H_2SO_4 was dissolved in 1 liter of distilled water.
5. Liquid paraffin wax: 4 to 5 drops.
6. Methyl red indicator: 0.3 g of bromocresol green + 0.2 g of methyl red were dissolved in 400 ml of 90% ethanol. The indicator colour will change from red in acid solution to blue in the alkaline solution.

Procedure:

1. A 2.5 g sample was taken in a distillation tube of Kjeltech N analyzer and 40 ml 0.32% $KMnO_4$, 40 ml 2.5% NaOH, and 20 ml distilled water was added.
2. Then the digestion tube was fitted well in KjeltecTM 8100 distillation unit for distillation. 20 ml of N/50 H_2SO_4 along with a few drops of methyl red indicator was taken in a 250ml conical flask.
3. The flask was then fitted to the ammonia exhaust pipe and then the contents of the tube were distilled and collected in N/50 H_2SO_4 solution in the conical flask containing N/50 H_2SO_4.
4. After distillation was completed, the collected ammonia solution was titrated with N/50 NaOH to original straw yellow colour. A blank was carried out without sample following the same procedure.

Calculation: Total N mg/kg = $W (V_b - Vs) \times 0.28 \times 1000$

Where, W = Weight of the sample taken. V b = Volume of N/50 NaOH solution consumed in the titration in the blank Vs = Volume of N/50 NaOH solution consumed in the titration in the sample.

F. Available sodium, calcium, potassium (mg kg^{-1}) estimation

The estimation of available Na, K, Ca was carried out by Flame photometric method

Reagents:

1. Ammonium acetate (1N): 77.08g of Ammonium acetate was taken and dissolved in distilled water and the volume was made up to 1L. The pH of the solution was adjusted to 7 by the addition of either Acetic acid or Ammonium solution.

Procedure:

1. 5 g of TPW sample was taken in a 250 ml conical flask.
2. 50 ml of 1 N CH_3COONH_4 (pH 7) solution was added.
3. The flask was shaken for 30 minutes on a mechanical shaker.
4. Supernatant was filtered with Whatman No. 1 filter paper.

5. The filtrate was then examined in Flame photometer.

Calculation: Available Ca (mg kg-1) = Ca concentration × dilution factor

Available Na (mg kg-1) = Na concentration × dilution factor

Available K (mg kg-1) = K concentration × dilution factor

G. DTPA extractable micronutrients & toxic metals estimation (Lindsay and Norvell, 1978):

The bio-available metals of the samples were extracted using the diethylene triamine penta acetic acid (DTPA) extraction technique. Following Lindsay and Norvell's (1978) directions, a heavy metals AAS analysis of Fe, Cu, Mn, Zn, Pb, Cd, and Cr was carried out.

Reagents:

1. DTPA extract
2. 20-25 ml of double distilled water (DDW) was added to it
3. Next, 100 ml of DDW and 13.3 ml of triethanolamine (TEA) were also added.
4. The pH was adjusted to 7.3 and the volume was made up to 1L. The extraction of several trace elements still present in bio-available forms was done using the solution.

Procedure:

1. 10 g of sample was taken in a 250 ml of conical flask.
2. 50 ml of DTPA extract was added to it.
3. It was then shaken in the mechanical shaker for 2 hrs. and then filtered.
4. Estimations of these elements were carried out with the help of Systronics AAS 816.

H. *In vitro* method for metal accessibility (Bio-accessibility of metal)

The physiological-based extraction test (PBET) method was employed to determine the bioaccessible fraction of metal proposed by Ruby et al., (1996) with slight modifications. *In vitro,* synthetic gastro-intestinal solutions were used to identify the physiological metal intake of two phases viz. gastric and intestine.

1. Gastric phase: 1 gm of the dry sample was extracted with 150 ml. of the synthetic gastric solution containing pepsin and NaCl, followed by a 1-hour water bath at 37^0C. The pH of the solution was adjusted to 1.5-1.8 by HCl. Finally, 10-40ml of solution was filtered and kept at 4^0C up to analysis.
2. Intestine phase: 525mg of bile salt and 52.5 mg of pancreatin were added to the residual gastric phase and the pH of the solution was adjusted to 7 by $NaHCO_3$. Again, the solution was kept for another 1 hour at 37^0C, and lastly filtered and stored for analysis.

Bioaccessible % has been calculated by using the following formula (Kabir et al., 2022)

$$\text{Bioaccessible \%} = (C_{bioaccessible} / C_{total}) \times 100$$

I. Determination of toxicity characteristics leaching procedure (TCLP)

The TCLP test using the USEPA SW-846 Method 1311 was used to determine the potential toxicity of heavy metals. Reagent 1 is used when the pH of a soil is more than 5. When the pH of a soil is less than 5, reagent 2 is used.

Reagent:

1. Solution 1- Glacial acetic acid ($CH_3\,CH_2OOH$) 5.7 mL diluted in 1 L of water is the reagent 1. Using 1 M HNO3 or 1 M NaOH, the pH of this extractant was brought down to 2.88.
2. Solution 2- 5.7 mL of glacial acetic acid (CH_3CH_2OOH) and 64.3 mL of 1M NaOH were combined to create this extractant, which has a pH of 4.93.

Procedure:

1. 2 g of soil and 40 mL of extractants (soil to solution ratio: 1:20) were put into a 50 mL centrifuge tube for extraction, and the tube was mechanically shaken for 18 hours at a speed of 30 2 rpm.
2. After an 18-hour extraction period, the fluid in each jar was vacuum-filtered through 0.8-micron-pore glass fibre filter paper to remove the solid phase. After determining the pH of the TCLP extracts, all extracts were acidified with HNO3 until they had 1% HNO3 (v/v) for long-term preservation. AAS was used to calculate the concentration of Zn, Cu, Ni, Pb, and Cd in the extracts.

J. Metal fractionation

To determine the distribution of various soluble and recalcitrant metal forms (Cd, Cr, Cu, Fe, Zn, Mn, and Pb) in the TPW samples, the metal fractionation investigation was carried out. Following Tessier et al. (1979), six distinct metal fractions (water soluble, exchangeable, carbonate bound, oxide bound, organic matter bound, and residual) were calculated. To calibrate the ICP-MS, standard solutions for each of the target metals were made from the stock solution (1000 mg L-1, Merck grade) in 1% (v/v) HNO_3. Certified reference material (SRM 2710) and blank extract were utilized for general QA-QC. The reference material was then digested on a hotplate at atmospheric pressure using an ultrapure $HF/HNO_3/HClO_4/H_2O_2$ combination. Comparing the results with approved SRM values subsequently allowed us to verify the analytical procedure's accuracy. Speciation of particulate trace metals is accomplished through sequential extraction.

Reagents:

1. 0.5M Mg $(NO_3)_2$ (pH 7.0).
2. 1M CH_3COONa (pH 5)

3. 0.04 M $NH_2OH.HCl$
4. 0.02 M HNO_3
5. 30% H_2O_2
6. 3.2M CH_3COONH_4
7. Conc. HNO_3

Procedure:

1. Taken 1g of the sample (TPW)). Added 40 ml of deionized water (Shaken for 30 minutes, kept overnight). Filtered and the filtrate analysed for water-soluble (F1). And
2. Next to the residue, 40 ml of 1 M $MgCl_2$ added. (Continuous agitation for 30 minutes, kept overnight) filtered and filtrate analysed for exchangeable (F2). And to the residue
3. Next to the residue 40 ml of 1 M CH_3COONa was added (Continuous agitation for 5 h, kept overnight) filtered and filtrate analysed for carbonate bound (F3).
4. And to the residue 40 ml of $NH_2OH.HCl$ was added (Kept at $96^0C \pm 3$ for 6 h, kept overnight) filtered and filtrate analyzed for oxide bound (F4).
5. And to the residue Added 3 ml 0.02 M HNO3 + 5 ml of 30% H_2O_2 (Heated at $85^0C \pm 3$ for 5 h initially, a second aliquot of 3 ml 30% H_2O_2 added and heated for another 3 h. After cooling, 5 ml of 3.2 M NH_4COOCH_3 added, content was diluted to 20 ml and continuous agitation for 30 minutes) filtered and filtrate analysed for organic matter bound (F5).
6. And to the residue 25 ml conc. HNO_3 (Kept until content dries at 105^0C, to the dried content 25 ml of deionized water added) filtered and filtrate analysed for residual (F6).

Calculation:

AAS detected value× (volume taken in ml/1000) = amount in mg in given sample S g i.e., let D mg. Therefore, S g contains D mg of metal. Hence, 1000 g of sample contain D/S× 1000 mg of metal i.e., mg kg^{-1} .

K. Estimation of available phosphorus (Jackson., 1973) (mg kg^{-1})

Based on the pH and kinds of soil, there are primarily two ways for determining the amount of accessible phosphorus in soil. It's them, 1. Bray and Kurtz method (for soil with a pH below 6 that is acidic) Olsen's technique, which is used for soils that are neutral, alkaline, or calcareous (pH over 6).

Bray and Kurtz method

Reagents:

1. 0.03 N NH_4F solution: 1.11g NH_4F was dissolved in distilled water and made the volume up to 1000ml.

2. 1.5% ammonium molybdate solution: 15g ammonium molybdate [$(NH_4)6Mo_7O.4H_2O$] was dissolved in 300 ml concentrated HCl and made the volume up to 1000 ml with distilled water in volumetric flask.

3. 5% stannous chloride solution ($SnCl_2$): 2.5g stannous chloride ($SnCl_2.2H_2O$) was added in 5ml conc. HCl and made the volume up to 50 ml with warm distilled water.

4. 4N NH_4OH: 27 ml ammonia hydroxide (NH_4OH) was dissolved in distilled water and made the volume up to 1000 ml.

5. 4N HCl: 34.5 ml conc. HCl was dissolved in distilled water and made the volume up to 100 ml.

6. Phosphorus free charcoal.

7. Standard P solution: As described in Olsen method.

Procedure:

1. In a 250 ml conical flask, a 1.2.5 g sample was obtained. 1 g of P-free charcoal and 50 ml of the extractant solution (0.5 M $NaHCO_3$; pH 8.5) were added to the sample. For 30 minutes, flasks were continuously shaken in a mechanical shaker.

2.Sample solution was filtered using Whatman (no. 42) filter paper after 30 minutes. A 50 ml volumetric flask containing 5 ml of filtrate was pipetted, and 4 to 5 drops each of dinitrophenol, 4N NH_4OH, and 4N HCl were added.

3. Then, each flask received 10 ml of ammonium molybdate, 2–3 drops of (5%) stannous chloride, and 50 ml of distilled water to bring the volume up to 50 ml.

4.The mixture of the solution and the reading was taken in the Systronics 117 UV spectrophotometer (Double beam) at 660 nm.

Calculation:

Available P (mg kg-1) = P concentration × dilution factor

Olsen's method (for neutral, alkaline and Calcareous soils i.e. pH above 6)

Reagents:

1. 0.5 M $NaHCO_3$ (pH 8.5) solution (Olsen extractant): 42g $NaHCO_3$ was dissolved in distilled water and made the volume up to 1000ml.

2. Charcoal

3. Ammonium molybdate solution (1.5 %): 15g ammonium molybdate [$(NH_4)6Mo7O.4H_2O$] was dissolved in 301ml con HCL and made up the volume with distilled water up to 1000ml in volumetric flask.

4. Stannous chloride solution (5 %): 2.5g Stannous chloride ($SnCl_2.2H_2O$) was dissolved in 5ml con HCl and made the volume up to 50 ml with warm distilled water.

5. 4N NH_4OH: 27ml Ammonia hydroxide (NH_4OH) was dissolved in distilled water and made the volume up to 100ml.

6. 4 N HCl: 34.5 ml conc. HCl was dissolved in distilled water and made the volume up to 100 ml.

7. 2, 4 dinitrophenol indicator: 2, 4 dinitrophenol was dissolved in distilled water and made the volume up to 250 ml, filter and used the solution.

8. Standard P solution: 400 ml of distilled water were used to dissolve 0.2196 g of potassium orthophosphate (KH_2PO4) in order to create a 50-ppm stock solution. The solution was then diluted up to 1 L using 25 ml of 7N H_2SO_4. To create a 2-ppm standard P solution, 20 ml of the stock solution were transferred to a 500 ml volumetric flask and diluted with distilled water until the desired consistency was reached.

Standard curve preparation: Individual 50 ml volumetric flasks were pipetted with 1, 2.5, 5.0, 7.5, 10.0, 12.5, 15.0, and 20.0 ml of a 2-ppm standard P solution. To each flask, 3 drops of dinitrophenol were added. Drop by drop, 4 N NH_4OH was added to each solution until a yellow colour was visible. Then, drop by drop, 4 N HCl was added until the yellow tint vanished, at which point the pH of each solution was changed to 3. 10 ml of the $(NH_4)6Mo7O.4H_2O$ solution and two to three drops of the SnCl2 solution were added to each flask. The volume was appropriate. Readings were taken using a Systronics 117 UV-Visible spectrophotometer at 660 nm against a blank solution. Following that, a curve was formed by plotting the optical density reading against the standard concentration.

Procedure:

1. A 2 gm sample was placed in a 250 ml conical flask together with 1 g of P-free charcoal and 20 ml of an extracting 0.5 M $NaHCO_3$ (pH 8.5) solution.

2. After that, the flask containing the sample was left in the mechanical shaker for 30 minutes. Sample solution was filtered using Whatman (no. 42) filter paper after 30 minutes.

3. Next, 5 ml of the filtrate was combined with 4 to 5 drops of 2, 4-dinitophenol, 4 N NH_4OH, 4 N HCl, 5 ml of ammonium molybdate, and 5 ml of stannous chloride to make a volume that was 50 ml in total.

4. After mixing the solution, a reading at 660 nm is taken using the Systronics 117 UV-spectrophotometer (Double beam).

Calculation: Total P = P concentration × 10(dilution factor)

L. Cation Exchange Capacity (CEC)

Reagents:

1. 1N acetic acid (CH_3COONa) solution: 136 g acetic acid trihydrate was dissolved in 750 ml distilled water and made the volume up to 1L. pH was adjusted to 8.2 with dilute NaOH.
2. Ethyl alcohol (95%)
3. 1N ammonium acetate (CH_3COONH_4) solution: 57 ml concentrated acetic acid was added in 750 ml distilled water and 68 ml conc. ammonium hydroxide and made the volume up to 1L. pH was adjusted to 8 by adding dilute NH_4OH or CH_3COOH as required.

Procedure:

1. 5 g soil sample was taken in a 250 ml bottle and 100 ml of 1N Sodium Acetate was added and shaken for half an hour. The bottles were kept horizontally overnight and the supernatant was decanted on the next day very carefully.
2. 35 ml of ethanol was added to the bottle shaken well and filtered. This step was repeated three times and the same filter paper was used for all the filtrations of the same sample.
3. The filter paper was put inside the bottle along with the sample and 100 ml of 1 N ammonium acetate was added to the bottle and shaken for half an hour.
4. The total contents of the bottle were filtered in a clean 1L volumetric flask and the volume of the filtrate was made up to 1L with distilled water. After that the concentration of sodium ions was determined in a flame photometer.

Calculation:

If concentration of Na+ ions in extracted solution is 'x' ppm then CEC of the soil will be $\frac{20x}{23}$meq per 100g soil.

M. Solubility study

Following Bhattacharyya et al. (2011) and Goswami et al. (2014), the concentration of various components in water in the MSW samples of both cities was examined. Conical flasks were used to collect the samples, which were then combined (1:10 (w/v)) with distilled deionized water. Every seven days, samples were taken in order to conduct analyses. The results from the 7-, 14-, and 21-day solubility studies are utilised to evaluate their solubility dynamics.

Analysis of cations

The following cations were examined using conventional techniques.

Sodium: The flame photometric method (Systronics Flame Photometer 128) was used to measure sodium (Na^+). Stock Na^+ solution was made by combining 2.542 g of dried sodium chloride, dried at 140 °C, with 1000 mL of deionized water. This solution has a 1000 mgL-1 strength.

Potassium: The Systronics Flame Photometer 128 was used to analyse potassium (K^+). Standardisation was done using KCl (Merck A.R grade). In order to create a stock solution with a 1000 mgL^{-1} strength, 1.907g of dried KCl was dissolved in 1000 mL of deionized water at 110 ^{O}C.

Atomic absorption spectroscopy (Systronics AAS-816) was used to analyse the following elements: calcium (Ca), zinc (Zn), lead (Pb), manganese (Mn), and copper (Cu), chromium (Cr), cadmium (Cd), nickel (Ni).

Analysis of anion:

For this investigation, Cl^-, SO_4^{2-}, PO_4^{3-}, and NO^{3-} were the anions examined. Anion analysis followed the recommended standard methods.

Bicarbonate: Using the potentiometric titration method, the bicarbonate (HCO^{3-}) level was ascertained.

Chloride: The water samples were measured using the argentometric method. This technique used potassium chromate as an indicator to titrate with standard silver nitrate (AgNO3) to estimate the amount of silver in water samples.

Reagents:

1. Potassium Chromate (K_2CrO_4) indicator: 5g of $K2CrO_4$ was dissolved in 75 ml distilled water and added dropwise AgNO3 solution to form a red precipitate. The suspension was then filtered and diluted to 100 ml.
2. Standard Silver Nitrate (AgNO3) solution: 4.791 g AgNO3 was weighed and dissolved in 1 L distilled water producing a solution 1 ml equivalent to 1 mg of Cl
3. Standard NaCl solution: 1.648 g NaCl dissolved in 1L distilled water.

Procedure: Standardization of AgNO3 solution: 10 ml of standard NaCl solution was taken, 2-3 drops of K2CrO4 indicator was added and titrated with standard AgNO3 solution until appearance of permanent red precipitate. The factor of strength of AgNO3 solution was standardized with the help of titre value.

If F be the factor of AgNO3 concentration and V be the volume required for titration, then, F=10/V

Cl^-estimation: 25 ml of sample was titrated with standard AgNO3 solution till appearance of permanent red precipitate.

25 ml of sample was titrated with standard AgNO3 solution till appearance of permanent red precipitate. Calculation: Concentration of Cl^- (ppm) $= \frac{x\ X\ FX1000}{V}$

Where, X: titre value (ml), F: Factor, V: aliquot volume.

Fl^- estimation: The water sample was measured directly through a benchtop ion-selective electrode (Orion, STARA 214 PH/ISE Benchtop meter, Software version 3.04)

Standard Curve Preparation: The standard curve was prepared with 1 mg/L, 5 mg/L, and 10 mg/L, which was prepared from the 100-ppm stock solution of Thermo Fisher Scientific. The average slope value of the calibration curve -58.2 mV/dec. (The recommended range of accuracy is -54 mV/dec. to – 60 mV/dec.)

Procedure:

1. 1 ml sample was mixed with 100µl TISAB (total ionic strength adjustment buffer).
2. Reading was noted with the average slope in mg/L (ppm)

NO^{3-} estimation: The water sample was measured directly through a benchtop ion-selective electrode (Orion, STARA 214 PH/ISE Benchtop meter, Software version 3.04)

Standard Curve Preparation: The standard curve was prepared with 1 mg/L, 5 mg/L, and 10 mg/L, which was prepared from the 100-ppm stock solution of Thermo Fisher Scientific. The average slope value of the calibration curve -56.1 mV/dec. (The recommended range of accuracy is -54 mV/dec. to – 60 mV/dec.)

Procedure:

1. 1 ml sample was mixed with 1 ml NISS (nitrate interference suppressor solution).
2. Reading was noted with the average slope in mg/L (ppm)

Alkalinity:

Water samples containing measurable OH^- or CO_3^{2-} ions turn pink to phenolphthalein indicator (Mohr's rapid titration). This water turns colourless at pH below 8.4, when titrated with acid to convert these ions to HCO_3^- form. Again, sample with only HCO_3^- can be titrated to critical pH level of 5.3 with acid by using yellow to faint orange colour of methyl orange indicator. Both the indicators used for total alkalinity.

Reagents:

1. Phenolphthalein solution: 0.5 g phenolphthalein dissolved in 50 ml 95% ethanol.
2. Methyl orange indicator: 0.5 g methyl orange is dissolved in 100 ml distilled water.

3.Standard (0.02 N) Sulphuric acid solution: 1.4 ml of Grade pure (Merck) H_2SO_4 (36 N) mixed in 1 L water.

Procedure:

5 ml of sample solution diluted to 25 ml with distilled water. 2-3 drops of phenolphthalein indicator were added. If red colour appears, it was titrated against 0.02N H_2SO_4 acid till colour disappears. Reading was recorded. Then, again, 2-3 drops of methyl orange indicator were added to the solution and titrated against standard H_2SO_4 acid solution till yellow colour turn into rosy red. The reading was recorded

Calculation: Carbonate (mel^{-1}) $= \frac{PRX2XNX\ 1000}{V}$;

PR; phenolphthalein reading, N: H_2SO_4 normality, V: aliquot volume.

Bicarbonate (mel^{-1}) $= \frac{(MR-PR)X\ 2X\ NX1000}{V}$;

MR: Methyl orange reading, PR: phenolphthalein reading.

4.2.3. Fourier Transform Infrared (FTIR) spectroscopy

The substance (fraction 0.63 mm) was pulverised in a pestle for spectroscopic investigations in order to ensure good repeatability of the captured spectra. Using KBr (FTIR grade) (1:100) and 2 mg of the pulverised sample, a pellet was created (Panias et al., 2007). The spectrometer's transmission mode was used to measure the pellet right away after it had been prepared. The measurements were made using a Perkin Elmer FTIR spectrophotometer (Model 1000) in the mid-infrared band between 4000 cm1 and 400 cm1. 32 scans were recorded with a resolution of 4 cm1, averaged for each spectrum, and corrected for background air. In the majority of the images, spectra were moved parallel to the wave number axis. Band heights were measured in relation to a selected baseline using with the Perkin Elmer software (Spectrum lite). In order to compare various. To emphasise the relative change in the samples, the relative intensities of several bands were determined.

4.2.4. SEM-EDX sample preparation

The standard methodology for sample preparation for SEM-EDX analysis was followed (Kutchko and Kim, 2006). After sieving, the sample was examined using a scanning electron microscope (JEOL, JSM-6390 LV Japan, 15 KV) with a magnification range of 3000-10,000 X to characterise the surface morphology and analyse the composition of the microstructure. Energy Dispersive X-ray Microanalysis System (EDX) (INCA X-sight, Oxford Instruments, Model 7582) was used to analyse the elemental compositions of samples in the energy range of 0–20 KeV. With a detection limit of 0.1 wt.

4.2.5. XRD- sample preparation

The collected red mud is utilised to characterise the mineral phase using the X-Ray Diffraction (XRD) technique. The Rietveld refining techniques, which were applied to the collected red mud for usable classification of the mineral phases and quantitative approximation of mineralogical composition, are referenced by the X-ray diffraction method. For X-ray diffraction examination, red mud sample powder was dried at 105°C following (Bish & Post, 1989). For mineral phase detection, red mud powder is first taken. A complete transit through a Philips diffract metre equipped with a Cu K radiation source and a single crystal graphite monochromator characterises the powdered material. The angular range is provided throughout at 10-70° of 2 values in 0.1° increments.

4.2.6. Ecological assessment

Different known indices were used to evaluate the potential hazards to the environment and to human health from the toxic element-loaded RM. Typically, the amount of harmful metal poisoning depends on the combined effect of all the instead of a single, dominant element. In order to determine the cumulative effect of the potentially harmful substances, the pollution index (PI) was computed as follows. The tolerance limits recommended by Kabata-Pendias (2001) were adopted for Cd (3 mg/kg), Cr (100 mg/kg), Cu (100 mg/kg), Mn (300 mg/kg), Ni (100 mg/kg), Pb (100 mg/kg) and Zn (300 mg/kg). PI>1 indicates RM have significantly high contamination potential.

$$PI = \frac{\frac{Cd}{3} + \frac{Cr}{100} + \frac{Cu}{100} + \frac{Ni}{100} + \frac{Mn}{300} + \frac{Pb}{100} + \frac{Zn}{300}}{7} \text{...}$$

Mobility of heavy metals in soil is a distinct attribute making eco-toxicity in environment and can be measured by calculating the mobility factor (MF) following the equation proposed by Kabala and Singh 2001.

To understand the level of pollution and the risk associated with the cumulative effect of the discovered metals, the contamination index (CI) and the ecological risk index (ERI) were calculated. These metrics aid in determining the overall eco-toxicological potential of environmental samples. CI was determined using (Leenaers et al., 1990) as shown

Where Cn is the metal concentration in RMs and Bn is the metal concentration in pristine (undisturbed) soil. While the ecological risk index (ERI) was generated using the equation provided by Yang et al. 2009 taking into account the toxicological factor together with the pollution factor.

$$ERI=\sum T_i \times \frac{Cn}{Bn}$$

Here, Ti is the toxic response factor for a given metal (for Cd, Cr, Cu, Fe, Mn, Pb, and Zn, Ni; Ti was 30, 2, 5, 1, 1, 5, 1 and 5 respectively).

Furthermore, a geo-accumulation index (I_{geo}) has been computed following Mondal 2017 to assume several metals' possible accumulation patterns in the forthcoming period.

$$I_{geo} = \log_2 \frac{Cn}{1.5Bn}$$

where Cn indicates the concentration of any metal, Bn is the concentration of a similar metal in the adjacent soil, and the constant 1.5 is used to study the natural discrepancy of the element in the sample related to its anthropogenic history. The reference values for Bn of different metals (Mn, Cu, Cd, Cr, Pb, Ni and Zn) were implemented from different literature report (Adimalla 2019). The I_{geo} values have been categorized in to seven classes of contamination levels according to Muller 1969. The seven classes of contamination levels are given below.

Classification standard of Igeo values (Muller, 1969).

Igeo Classes	Contamination level
Igeo ≤ 0; Class 0	uncontaminated
Igeo0–1; Class 1	uncontaminated to moderately contaminated
Igeo1–2; Class 2	moderately contaminated
Igeo2–3; Class 3	moderately to highly contaminated
Igeo3–4; Class 4	highly contaminated
Igeo4–5; Class 5	highly to very highly contaminated
Igeo ≥ 5; Class 6	very highly contaminated

To determine the non-carcinogenic toxicity three exposure pathways viz. oral intake (intake ingestion), intake of re-suspended particulates emitted from the soil through mouth and nose (Intake inhalation) and intake through skin exposure (Intake dermal) have been computed and also taken for calculating the hazard quotient (HQ) and hazard index (HI) (Adimalla 2019)

$$HQ = \frac{\text{Intakes (Ingestion or Inhalation or Dermal)}}{\text{RfD}}$$

$$HI = \sum HQexP$$

The exPs denote different exposure pathways ($Intake_{ingestion}$, $Intake_{inhalation}$ and $Intake_{dermal}$). While, the R_fD indicates the limit of exposure to the pollutant which is supposed to be harmless

during a lifetime. The risk for significant non-cancer health hazards is seemingly high when HI is > 1. Additionally, the carcinogenic risk was assessed as the incremental possibility of cancer during a lifetime due to exposure to various carcinogens via different routes (viz. ingestion, inhalation, dermal). Cancer risk (CR) was computed by following equation (USEPA 2002)

$$CR = ADD \times SF_i$$

$$TCR = \sum CR$$

where ADD is average daily intake (ingestion/ inhalation/ dermal) and SF_i is the cancer slope factor (mg $kg^{-1}day^{-1}$) through oral ingestion, dermal contact, and inhalation of each metal and total cancer risk (TCR) is represented as sum of CR. CR value ranges from $1x\ 10^{-6}$ to 1×10^{-4} are considered to be harmless for human health (USEPA 2002) ones the value exceeds 1×10^{-4}, it represents a lifetime carcinogenic risk to the human body.

4.2.7. Statistical analysis

The mean and the standard deviation was used to represent the data of solubility studies. The mean and standard error was used to present the physicochemical attributes of study are. Principal component (PCA) was done to physicochemical attributes of RM to find out dominant factors. Prior to this the data were all log-transformed following the formulae

$$Zi = \frac{Xi - \bar{X}}{S} \quad \ldots\ldots\ldots\ldots\ldots\ldots\ldots\ldots$$

where Zi = standard score of the sample i; Xi = value of sample i; $\bar{X}$= mean; S = standard deviation.Least significant difference (LSD) was calculated to assess any significant variance is present or not among days (temporal variation) for solubility dynamics of RM. The statistical analysis was carried in SPSS 25.

4.3. Result and Discussions

4.3.1. Physico-chemical properties of red mud (RM)

The composition and physicochemical properties of RM widely vary due to their bauxite ore composition and the operational technology of the alumina plant. Table 4.1 provides concise information on the physico-chemical characteristics of RM collected from the aluminum plant of Muri, Jharkhand. We found a variation in the pH value where; freshly dumped residue showed the highest pH 13.1 and a few years old dumped exhibited a little reduction in pH (10.6). Such high pH may arise from inadequate washing of the residue material like NaOH, Na_2CO_3, $NaAl(OH)_4$, which remains in residue and makes them alkaline (Kirwan et al., 2013). Electrical conductivity (EC) indicates the presence of soluble cations, which was considerably high, varied from 9.8-15.7 mS/cm (mean 12.2 ±1.1). Presence of a

high concentration of Na and Na-bearing solids causes the high EC of RM. However, from the result it was quite evident that fresh disposal had a higher EC (15.7) compared to few years old one. A similar kind of result is reported by Liu et al., 2007, who observed an analogous trend in RM of aluminum plant located in China. Comparatively high pH and EC primely accredited to the use of caustic soda and slaked lime in Bayer process and their inappropriate handling before disposal leads to the generation of hydroxide, carbonate and aluminate salt, which remains more or less same regardless of their restoration age trigger salinity/alkalinity of the residue (Kong et al., 2017). Total organic carbon (TOC) was significantly lower varying between 0.18%-0.28% (mean 0.22% ±0.08). Likewise, total N content ranged between 0.01-0.02% (mean ±0.013%). Inadequate amounts of mineralizable organic carbon and nitrogen corresponding to lower vegetation and reduced microbial activity are major decisive factors of reduced carbon-nitrogen content (Pandey et al., 2014). A study by Courtney et al. (2009) also found poor organic carbon content (trace-0.3%) in red mud, likewise, Wong and Ho (1994) illustrated the meager N content (0.02%) which is in agreement with our observation. Although there was a variation in TOC and TN content, nevertheless, prominent evidence of relative increment in TOC and TN content was found in a few years old deposited residue. Establishment of natural plant routes in the surface layer or improvement of microbial colonization with age may be the reason for the increment in carbon-nitrogen content. The bioavailability of P (13-18 mg/kg; mean 14.1 ±2.9) and N (11.56-19.89 mg/kg; mean 12.21 mg/kg) was also very scanty.

4.3.2. Salinity and sodicity of RM

The salinity of any sample primely depends on the presence of soluble cations. The result of exchangeable cations of the present study is depicted in Table 4.1. The concentration of exchangeable cations was as follows Na >Ca >K >Mg, where exchangeable Na accounted for 72.83% of total exchangeable cations. Since Na accounted for the highest percentage, it is clear that Na dominates in the bauxite residue. Liu et al. (2007) stated in their study that, about 78% of exchangeable Na governs among total exchangeable cations of RM dumped by a Chinese aluminum plant. However, aging of the RM alleviates the sodicity by facilitating the reduction of exchangeable Na with exchangeable Ca. Concurrently exchangeable Na percentage (ESP) also declined with increasing disposal history. Although, the concentration of K and Mg was relatively low, yet, natural evolution processes like mineral weathering causes a diminution of alkalinity and prompted the release of Ca, K, and Mg (Zhu et al., 2016).

The ability of a material to retain, release, and exchange positive ions with its medium is known as the CEC. CEC determined for RM varied from 7.7-25.2 meq/100g (mean 19.7 ±1.7). It is

also noted that CEC decreased over time. The highest CEC was shown by newly dumped residue (25.2 meq/100g), while a 40-year-old residue exhibited lowest CEC. This could be explained by a gradual decline in pH, which causes the negatively charged colloids to lose some of their negative charges. The hydronium ions (H+) were tightly bound to the surface of the material's particles at low pH levels, but at high pH, the formation of exchange sites to capture cations promoted their dissociation (Gray et al., 2016). A gradual decrease in pH leads to the leaching of NaOH and also precipitates $Ca(OH)_2$ which could also be the reason for such variation in CEC.

$[Al\ (OH)^6]^3+[Na^+ + Ca^{2+}]^{3+} \rightarrow [Al(OH)3]^0 + NaOH(leaching) + Ca(OH)^2(precipitation)$

In the equation above, the initially negatively charged $[Al\ (OH)^6]^3$ loses three OH to become the zero-charged $[Al\ (OH)^3]^0$ due to the leaching of NaOH and precipitation of $Ca\ (OH)^2$. This could help to partially explain the decline in CEC. Due to the proportion of exchangeable Na, Ca, and Mg, the exchangeable sodium percentage (ESP) corresponds to the composition of cation exchange sites on the residue surface. ESP was found to be considerably high ranging from 135%- 75% (72.83% ±4.9). In accordance with early mentioned attributes, ESP also decreased with the age of disposal. Since sodium ion takes time to get dehydrated compared to Ca or Mg, thus gets a stable hydration layer with bauxite residue particles, however, with passing time it eventually precipitated out as soda ash. Thereby the recently dumped site has higher ESP, consequently, bauxite residue does not aggregate well and has a proclivity to be crusted and eroded well (Courtney et al., 2013).

Table 4.1: Physico-chemical characteristics of red mud (RM) collected from different age of dump from HINDALCO alumina plant. Muri, Jharkhand. Values represent the range and average ±SE of the studied parameters.

Parameters	Range	Mean
pH	13.1-10.6	11.5 ±1.9
EC mS/cm	9.8-15.7	12.2 ±2.1
CEC meq/100g	7.7-25.2	19.7 ±2.9
TOC (%)	0.18-0.28	0.22 ±0.05
TKN (%)	0.01-0.02	0.013 ±0.001
Available Na mg/kg	6190-14204	7990.04 ±983.86
Available K mg/ kg	136-406	196 ±20.98
Available Ca mg/kg	880.78-3265.87	2426.65 ±211.04
Available Mg mg/kg	177.88-657.7	374.23 ±51.92
Available P mg/kg	13-18.09	15.34 ±2.6
Mineralizable N mg/kg	11.56-19.89	12.21 ±2.9
Total Cr mg/kg	184-526.08	392 ±46.66
Total Cd mg/kg	9.4-14.89	9.71 ±1.37
Total Ni mg/kg	67.11-176.8	139.68 ±12.74
Total Pb mg/kg	119.09-283.71	228.64 ±16.66
Total Cu mg/kg	49.44-144.62	87.67 ±12.99
Total Mn mg/kg	62.20-195.69	137.37 ±11.13
Total Zn mg/kg	28.83-105.46	68.17 ±6.52
Total Fe mg/kg	134567-263421	195200 ±51897
DTPA extractable Cr mg/kg	1.9-6.7	3.89 ±0.58
DTPA extractable Pb mg/kg	1.13-8.5	4.76 ±0.81
DTPA extractable Cd mg/kg	0.4-1.1	0.78 ±0.006
DTPA extractable Ni mg/kg	1.13-5.8	2.08 ±0.66
DTPA extractable Cu mg/kg	1.4-8.7	3.45 ±0.82
DTPA extractable Mn mg/kg	11.12-26.14	16.42 ±1.95
DTPA extractable Zn mg/kg	8.1-13.7	11.29 ±3.2
DTPA extractable Fe mg/kg	29.65-41.88	34.89±6.9

4.3.3. Surface morphology, elemental composition (FESEM-EDX) and surface chemistry

The surface morphology of the bauxite residue is depicted in Fig. 4.2. FESEM micrograph of RM sample revealed that particle arrangement of the RM is relatively loose with high porosity and small particle size. In present study the size of the RM varies from 0-1 µm. Ahead of this, Liu et al. (2009) reported that the average RM particle size is less than 10 µm. Majority of particle were 200-500 nm. The following sizes have been reported by other writers in other samples of RM: less than 75 µm and less than 5 µm (Ye et al., 2014). Structurally RM

particles are unshaped, irregular, agglomerated. However, in some cases, they are spherical with round shape and in some cases, they are little angular. They also showed a poor crystalline structure. Visibly they are amorphous and form aggregates. In line with the present study, Das et al. (2015) reported about irregular shapes and different size of RM particle from NALCO, Koraput, India. During alkali digestion process, the desilication phases generated and deposited on the mineral surface present in bauxite and remail are visibly distinguished. Based on morphological investigation RMs, are interlocked and chemically bonded resulting in poor liberation characteristics (Agrawal et al., 2018). Concerning the elemental composition the EDX analysis ensures the presence of Si, Fe, Al, Na, Ti, O. Na, Fe, Si, and Al were found to be copious. However, the abundance of O is an indication of the presence of metal oxide. The finding of our study is consistent with many of the formerly reported studies (Özden et al., 2019).

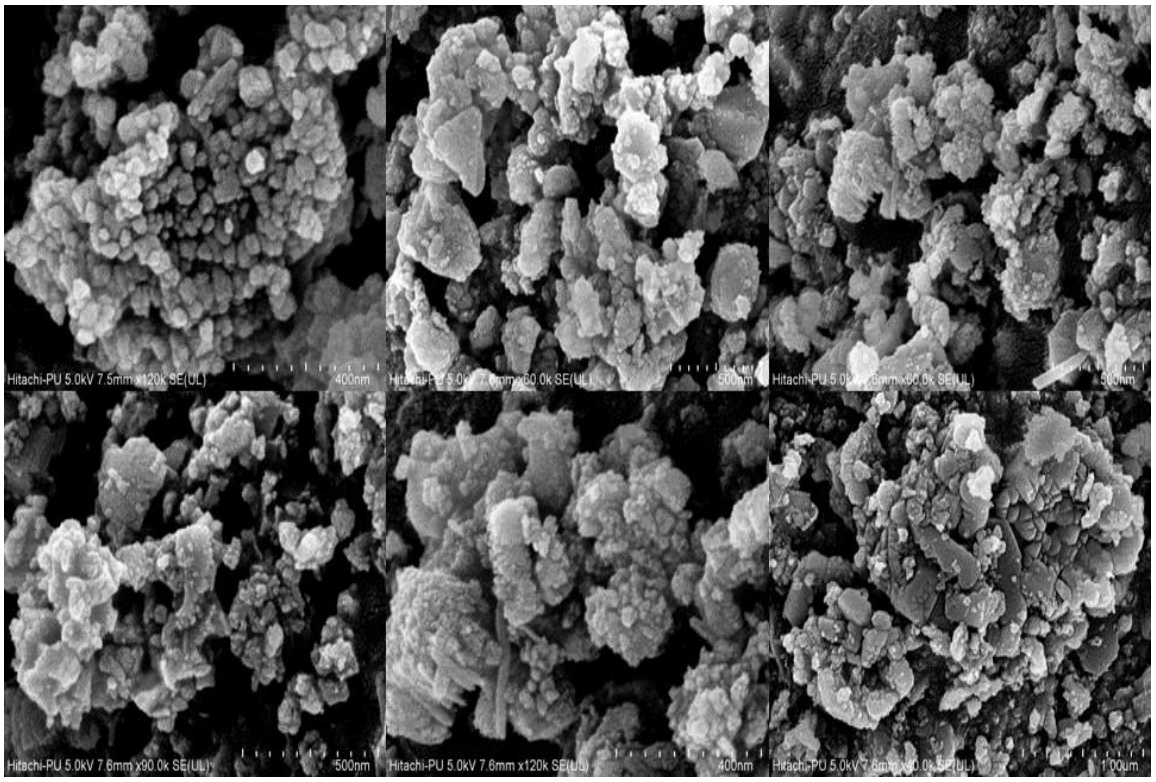

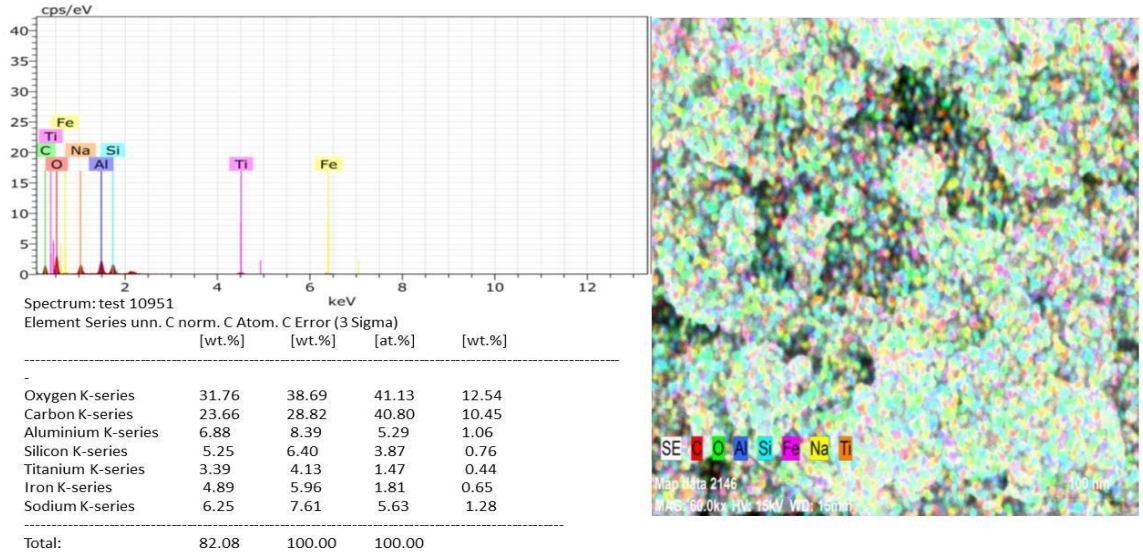

Spectrum: test 10951
Element Series unn. C norm. C Atom. C Error (3 Sigma)

	[wt.%]	[wt.%]	[at.%]	[wt.%]
Oxygen K-series	31.76	38.69	41.13	12.54
Carbon K-series	23.66	28.82	40.80	10.45
Aluminium K-series	6.88	8.39	5.29	1.06
Silicon K-series	5.25	6.40	3.87	0.76
Titanium K-series	3.39	4.13	1.47	0.44
Iron K-series	4.89	5.96	1.81	0.65
Sodium K-series	6.25	7.61	5.63	1.28
Total:	82.08	100.00	100.00	

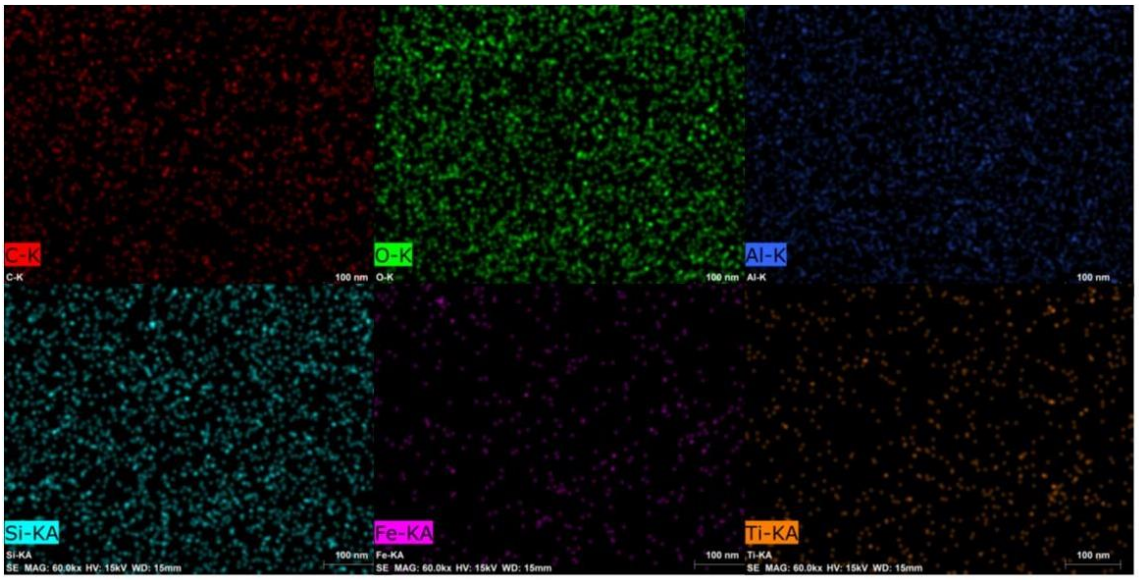

Fig. 4.2. FESEM images of red mud (RM) with EDX elemental spectra showing a clear indication of aggregate formation.

The FTIR spectrum is shown in Fig. 4.3. A broad band was observed around 3413.85 cm-1, which is possibly due to starching vibration of O-H bond and H-O-H bending vibration for interlayer adsorbed H_2O (Sahu et al., 2011). The band around 1411.85 cm^{-1} and 1455.17 cm^{-1} was possibly attributed to C=O due to the presence of carbonate groups. Chemisorbed CO_2 in RM possibly accounted for this. The signal around 1386.89 cm^{-1} may correspond to CaO (Ramírez et al., 2022). The signals near 479.23 cm-1 and 622.06 cm-1 emerged in the vicinity corresponding to Fe-O, Ti-O, Al-O, and Mg-O type bonds. A broad peak generated

around 995.37 cm^{-1} which is attributed to Si-O, confirms the presence of a silicate group. Signals generated near 622.06 is an indication of the presence of Mg-O (Madejová, 2003).

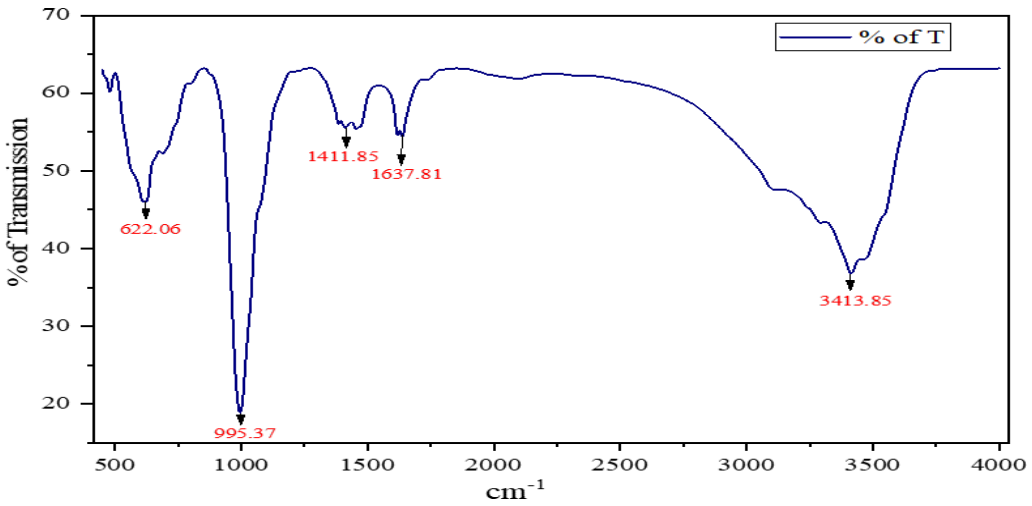

Fig. 4.3. Distribution of functional group in red mud (RM)

4.3.4. Mineralogical composition of RM

An X-ray diffraction investigation was conducted in order to investigate the mineralogical distribution of bauxite mine tailing, and the results are shown in Fig. 4.4. The diffraction pattern was recorded from 10º - 80º (2θ) with a step size of 0.02º by means of Cu Ka (k = 1.542 Å) as a radiation source and an operation at 40 kV–30 mA. The sharp peak at different 2θ positions indicates the crystalline structure of the sample. An analysis of X-ray diffractograms reveals the presence of numerous minerals, including gibbsite (Al (OH)3), hematite (Fe2O3), and quartz, all of which are distinguished by their d-spacing (Å) and position (2θ). Although the elemental analysis and phase characterization, yet data of the composition is not uniform. The composition of RM largely depends on the type of bauxite ore used in the extraction process. The spectra of the present study revealed that RM is dominated by iron oxide (Fe_2O_3) followed by Al $(OH)_3$. The presence of quartz and silicon oxide is also detected. The findings of XRD are consistent with the EDX study, where we found a dominant presence of Fe, Al, O, etc. In addition to that smaller number of peaks also indicate its amorphous nature, which we previously detected from our FE-SEM micrograph analysis. Our results XRD study is in line with Rout et al. (2013) and Fahad et al. (2019).

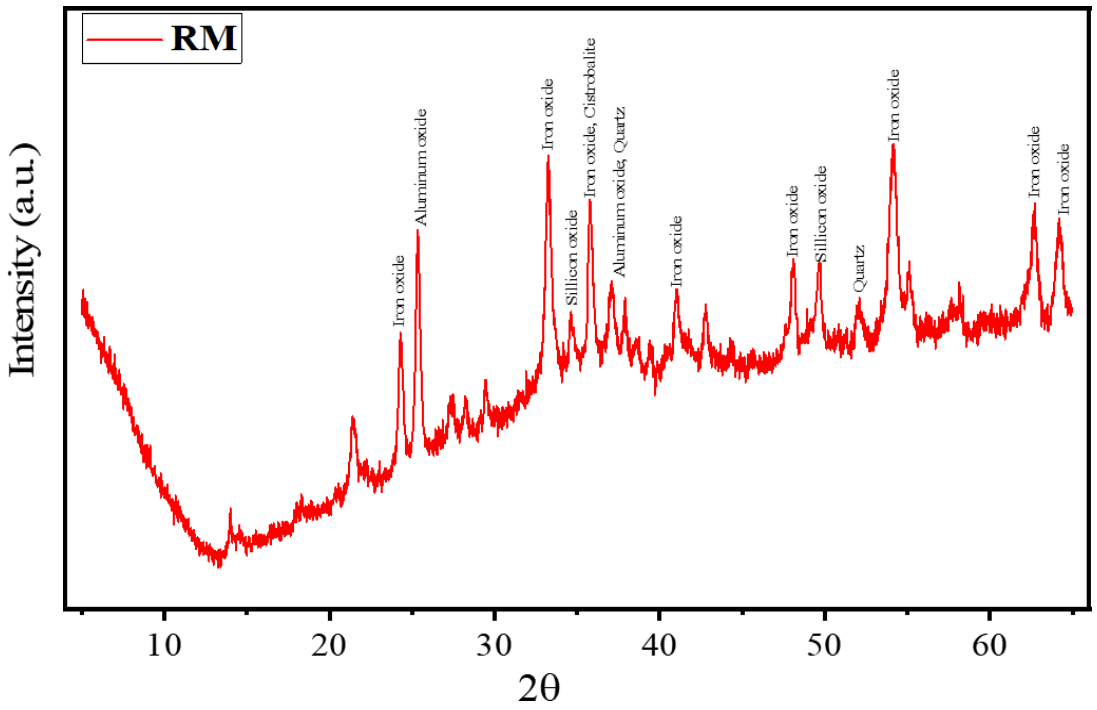

Fig. 4.4. Phase analysis detect diffraction peaks indicating dominant presence of iron oxide (Fe_2O_3), silicon oxide (SiO_2) and aluminum oxide (Al_2O_3).

4.3.5. Potential toxic element (PTEs) and their mobility (Fractionation study), bioavailability (DTPA-extractable)

Other than high sodicity, RM harbours numerous toxic elements. In present study, we assessed the total concentration of PTEs along with their distribution among different pools. Since a little part of an element is regarded as bioavailable, mobile, labile, or potentially toxic to the environment thus total concentration is unable to comprehend the degree of pollution. In this context, the fractionation study proposed by Tessier et al. (1979), and DTPA-available (Lindsay & Norvell, 1978) were carried out for a better understanding. Occurrence of PTEs viz. Cd, Cr, Pb, Ni, in RM, is tabulated in Table 4.1 and was ordered as Cr >Pb >Ni >Cd, however, the other micronutrient i.e., Cu, Zn, Fe, and Mn was in the following manner: Fe >Mn >Cu>Zn. Each PTE's concentration varies significantly. Cr occurred highest, ranging between 184-526 mg/kg with the maximum mean of 392 mg/kg ±46.66. Following Pb showed its considerable presence (119-283 mg/kg; 228 mg/kg ±16.66) followed by Ni and Cd. In line with our findings, Mayes et al. (2016) also noted a higher concentration of Cd, Cr, and Pb in RM. Fe (19.25%) dominates the micronutrient content of red mud, while Mn, Zn, and Cu are present but in relatively smaller amounts. It is consistent with the current study that Gautam

and Agrawal (2017) and Xue et al. (2016) also found relatively lower concentrations of Zn, Cu, Mn, and Mg in RM.

Understanding the mobility of RM has great significance in the case of its soil application or long-term toxicity to environment. The mobility of PTEs showed a wide variation in RM, however, pH is governing factor behind metals mobility. 12 RM samples were sequentially extracted in the current study and are shown in Fig. 4.5. Surprisingly, the bioavailability of metal (water soluble+ exchangeable) was comparatively lower in freshly dumped RM, while was considerably higher in those RM disposed of long ago. This is possibly due to a decrease in pH, however, the lowering of pH is seldom as low as the extractant, thus the mobility of RM in case of soil application is predicted to be lower, though, should be analysed in a site-specific manner (Hua et al., 2017). Pb and Ni showed greater mobility (WS+Ex) followed by Cr, Zn, Mn, Cu, and Fe. Mn was mainly found in oxide bound or reducible phase. The oxide or the reducible phase of metals readily solubilizes under anoxic conditions as a result of its thermodynamic instability (Yuan et al., 2011). The result of the present study is little deviated from Rubinos and Barral (2013) who observed a predominant residual fraction and a low amount of reducible fraction for Mn. Although Cr and Pb were highest in residual fraction accounting for 180 and 136 mg/kg respectively, yet, a considerable presence was detected in water-soluble, exchangeable, and acid-soluble fractions. A considerable incidence of water-soluble Cr indicates the labile species (Cr^{6+}) in the material, however, the (WS+Ex; F1 & F2) together occupy <30% of total, and were substantially distributed in F4, F5, and F6 demonstrating its overall low bioavailability of the metal. A similar kind of metal distribution pattern was found by Paul et al. (2023) in the case of textile industry sludge. In the instance of Cu, it is primely associated with acid-soluble and oxide-bound fractions which indicate that Cu could be potentially mobilizable under acidic conditions. There is evidence reported by Lockwood et al. (2015) >80% of Cu leached by a series of weakly acidic solutions. Ni and Cd are predominant in the carbonate bound/acid soluble fractions followed by residual fractions. The residual fractions of metal comprise primary and secondary minerals that could bind the metals inside their crystal structure. Thus, it is considered to be stable and does not possess any dissolving tendency over a long period under normal conditions (Lasheen & Ammar, 2009). Zn was largely distributed in oxide bound or reducible fraction followed by a residual fraction.

Although reducible fractions are relatively insoluble, however, they are readily subjected to degradation thereby posing a threat to the environment. Fe was distributed primarily in Fe/Mn oxide-bound and residual fractions.

In DTPA- extract micronutrients were more available (Table 4.1). The availability was as follows: Fe> Mn> Zn> Pb> Cr> Cu> Ni> Cd. Although DTPA majorly focuses the micronutrient availability for plants (Lindsay and Norvell, 1978), nevertheless in our study we applied them in the case of PTEs to check the PTEs plant availability. DTPA-extractable metal which is also considered plant-available metals, was found to be comparatively higher for Fe, Zn, and Mn, followed by Pb, Cr, Ni, and Cd. In general, metal's bioavailability is greatly influenced by the soil's pH, Fe, Mn, and Al oxides, competitive behaviour of the metals in the soil, microbial activity, organic matter concentration, etc. Xue et al. (2016). Concerning the present study, the DTPA-extractable metals are considerably poor in the case of micronutrients, on the other hand, the reduced availability of PTEs like Pb, Cr, Ni, and Cd is a benefit to the environment. Less availability is primely owing to RMs high pH, and greater presence of hematite and cancrinite which helps the red mud for strong adsorption of metal on the surface. Although sometimes aging leads to the reduction of alkalinity, nevertheless presence of iron/aluminum oxide supports long-term in situ stabilization (Lombi et al., 2003). In fact, under neutral to alkaline soil conditions, the amount of soluble and mobile metals decreases as a result of precipitation and adsorption onto charged colloids of mud red (Gautam & Agrawal, 2017).

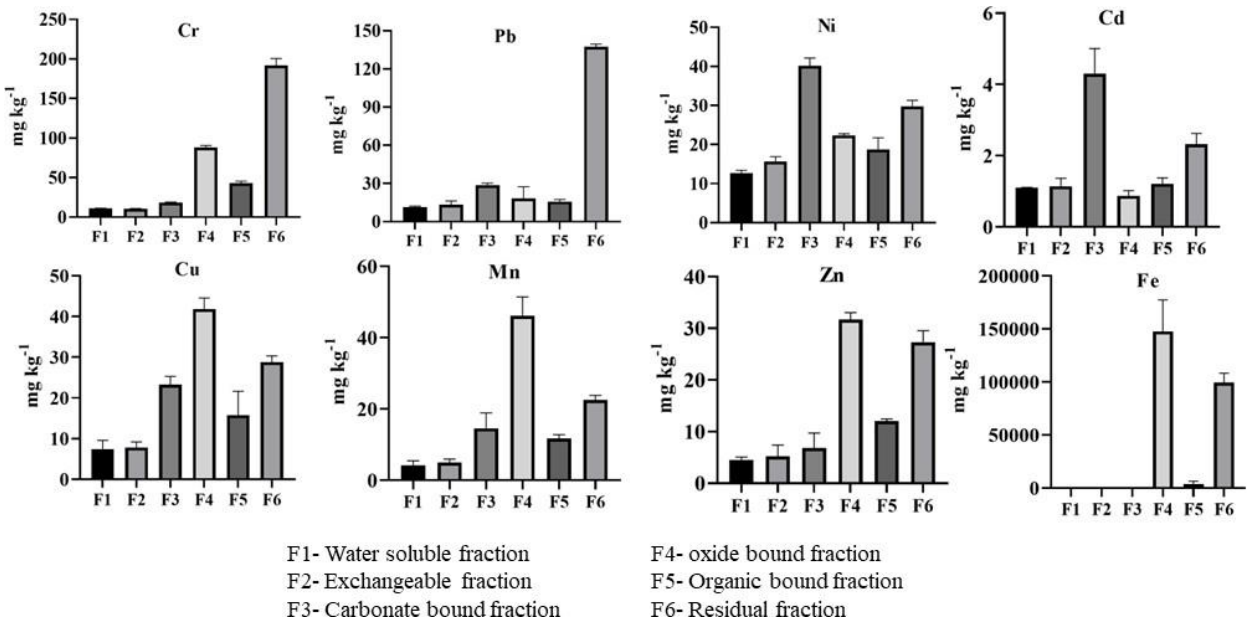

Fig. 4.5. Distribution of various metal in red mud (RM) collected from HINDALCO alumina plant, Muri, Jharkhand.

4.3.6. Toxicity characteristics leaching procedure (TCLP) and bioaccessible fraction

Toxicity characteristics leaching procedure is an important method developed by US-EPA (1997) to assess the leaching potential of RM and its possible consequence to human health and living organism. Presence of PTEs in the leachate helps to understand the degree of toxicity posed by RM. The presence of hazardous PTEs in the TCLP – leachate is listed in Table 4.2. The results are evaluated in comparison with TCLP and WHO standards. A high presence Pb (7.2 mg/L ±0.78), Cd (0.89 mg/L ±0.06) and Cr (8.2 mg/L ±0.42), Ni (3.2 mg/L ±0.66), Cu (4.9 ±0.98) detected which crossed the TCLP-threshold limit as well WHO standard limit for drinking limit. It was found in many previously studies that concentrations of metals in leachate were mere, however, in present study we detected significant amount of PTEs which is inconsistent with earlier mentioned results by Ke et al. (2021) and Chandra & Krishnaiah (2022). Interestingly we found that more concentration of metal in the leachate of with long disposal history, while the lately/immediately dumped site showed less release from the residue which may be due to a relative reduced alkalinity of the long-disposed RM encouraged the mobility of metals. The result is consistent with our fractionation study. Thus, it can be said that RM leachate had high potential of toxicity to living organism of the system.

The inorganic pollutants' bioavailability is what causes them to be hazardous to living things. The physiologically based extraction test (PBET) or in vitro experiment using synthetic gastrointestinal juices present an apparent perspective of the bio-accessibility of hazardous metals through stomach and gastrointestinal absorption. Although there are considerably fewer bio-accessible portions when compared to the total concentration, this suggests that the total concentration has little effect on the bioaccessibility of metals. Five different metals have been examined (Table 4.2). Out of the five metals examined, Pb, and Ni exhibited greater bioaccessibility in the gastric phase (GP) than the intestine phase (IP). This might be as a result of the gastric juice's acidic pH (1.5), which makes metals more likely to release and cause a higher absorption rate (Han et al. 2020). An earlier work (Dong et al. 2020) also supports the relatively high bioaccessibility of Ni in the stomach phase. The bioaccessibility of Pb from GP to IP was significantly reduced by a sudden rise in pH from 1.5 to 7 due to the rapid rate of metal precipitation in a neutral to alkaline environment. Because there are fewer H+ ions available to compete for the binding site as pH rises, Pb adsorption increases; yet, the presence of $NaHCO_3$ in intestinal juice may contribute to Pb adsorption onto clay edges and the formation of Pb carbonate mineral (Han et al., 2020). In contrast, Cu and Cr have demonstrated greater intestine phase bioavailability. Such Copper behaviour suggests that at pH values close to neutral, a strong combination between organic molecules and Cu has formed. It demonstrates

a significantly increased solubility in water as a result of the development of such a complex with digestive solutions (bile salt, pancreatin) (Jiao et al., 2015). Therefore, study from the bioaccessible fractions uncovers that long-term consumption of metal could lead to severe health hazards due to metals probable solubility in gastric and intestinal juice.

Table 4.2. Presence of PTEs in TCLP leachate and bioaccessibility of PTEs from RM. Value represent mean ±SE

Metals (mg/L)	TCLP Leachate (mg/L)	Bio-accessible (mg/L)	
		Gastric available	Intestine available
Cr	8.2 ±0.42	90.9 ±6.74	129.87 ±13.37
Cd	0.89 ±0.06	---	---
Ni	3.2 ±0.66	33.99 ±4.4	17.1 ±1.14
Pb	7.2 ±0.78	73.78 ±8.4	61.08 ±7.9
Cu	4.9 ±0.98	13.36 ±1.19	45.73 ±3.12

4.3.7. Dissolution-precipitation dynamics of ions: solubility experiment

Fig. 4.6-4.7 represent the result of solubility dynamics. Changes in pH, cations and anions, and metal concentration were found in the RM sample after the 21-day experiment. The chemical composition of MSW leachates is typically influenced by a number of variables, including waste types, quantities of trash dumped, the age of the landfill, and environmental conditions. The leaching of metals and non-metals is often regulated by solubility and is reliant on precipitation, adsorption, and dissolution equilibrium. (Bhattacharyya et al., 2011; Zhang et al., 2008). The pH of the RM showed a slight decrease after 7 days, while after 21 days the decline was sharp, from 11.5 to 9.2 (LSD= 0.28; p=0.025). During the initial phase, the EC was rising. This gradual and steady increment was continued in RM leachate till the end of experiment, which was found to be significant at 5% level(p=0.004). The elevated pH of the RM leachate was an indicative of high alkalinity, since, RM is dominated by Na-ions, thus high pH of the solution perhaps attributed to prevalence of bases like Na^{+}. Alkalinity of any solution mainly depends upon predominance of HCO^{3-}/CO^{3-} (Goswami et al., 2014). The CO^{3-} was initially increased between 7 to 14 days and subsequently decreased, while HCO^{3-} decreased between 7 to 14 days and thereafter increase. Presence of fluoride and nitrate was also detected in RM leachate. A continual acceleration of fluoride (F^{-}) and chloride (Cl^{-}) was observed till the end of experiment while, NO^{3-} showed an increment between 7-14 days afterward

decreased. These are possibly the underlying causes of pH reduction. As mentioned earlier that Na^+ is the predominant ion, consequently, solubility was much higher than for Ca^{2+} and K^+. Solubility of Na^+ steadily increase over time, while K^+ and Ca^{2+} were accelerated at an early stage followed by a slight decline and subsequently increased. The increment for Ca^{2+} between 7 to 14 days was not so commendable, while the increase was sharp for K^+ (Fig. 4.6).

Changes in metal concentration during solubility studies is depicted in Fig. 4.7. Interestingly solubility of all the metals (Cr, Pb, Ni, Mn, Cu, Fe) increased over time, except Zn and Cd that showed a midway flection. These elements (Cd and Zn) may have precipitated in insoluble forms as a result of changes in the system's redox potential or sometimes microbially induced precipitation (Goswami et al., 2014; Martínez et al., 2020). As earlier stated, RM contains >15% of iron oxide (Fe_2O_3), thereby solubility of Fe was highest among all. Solubility of Cr and Pb was spectacular, which is probably due to their higher occurrence in the waste. A considerable increment in Cr solubility suggested that recalcitrant Cr species may be converted to readily soluble ones in the leachate over time, which is alarming because of their probable toxicity towards the ecosystem. On the other hand, the steady increase in solubility of Pb is likely due to soluble $PbCl^-$ or $PbCl_2$ (Zhang et al., 2008). The next most abundant metal in RM was Ni, which consequently showed an increasing solubility till the end of experiment. Inclusively, the increase in solubility of these toxic metals over time in RM leachate is a potential concern for the environment.

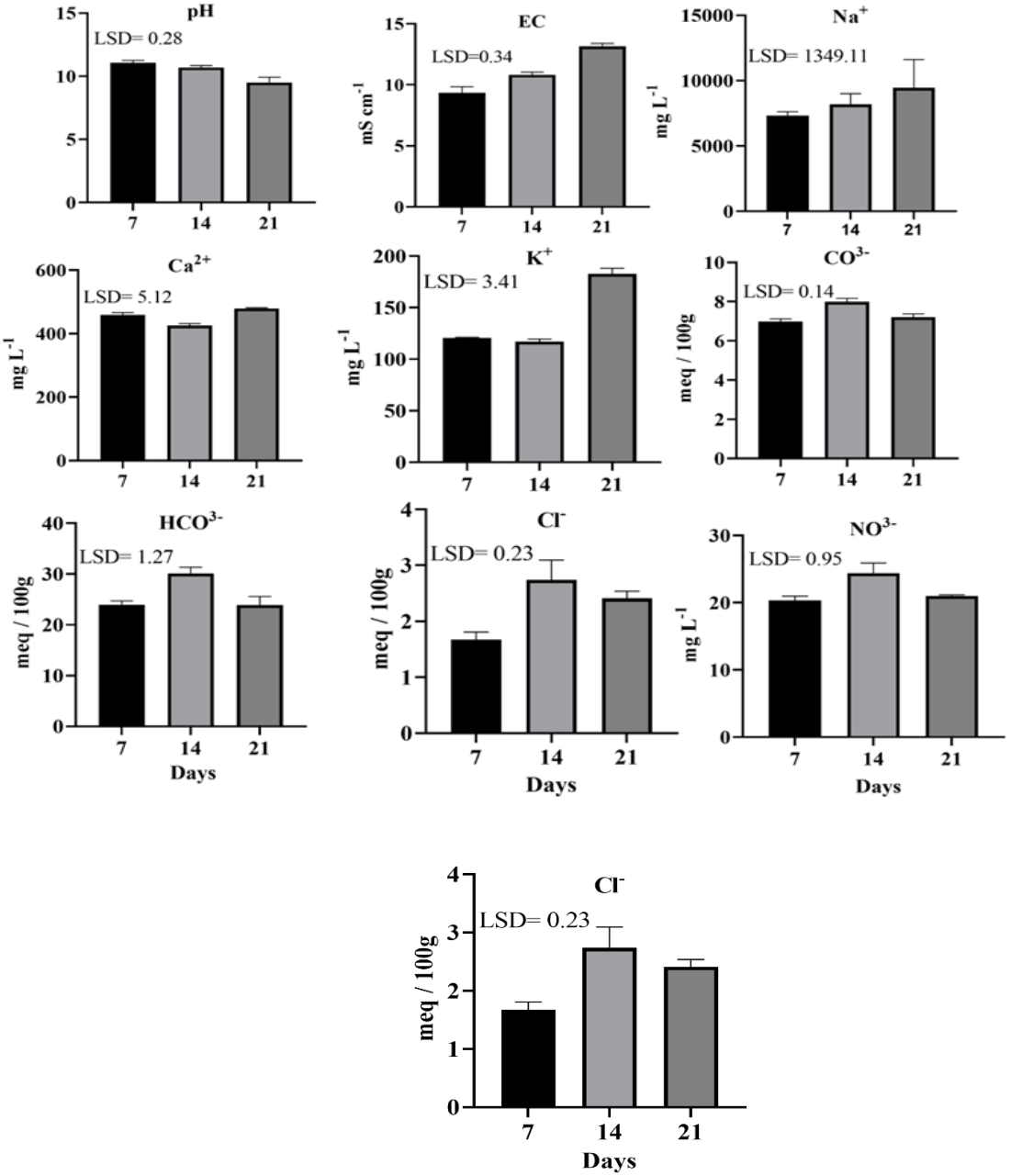

Fig. 4.6. Temporal variation in pH, EC, and solubility of major cations and anions in RM leachate (value represented in mean ±SD).

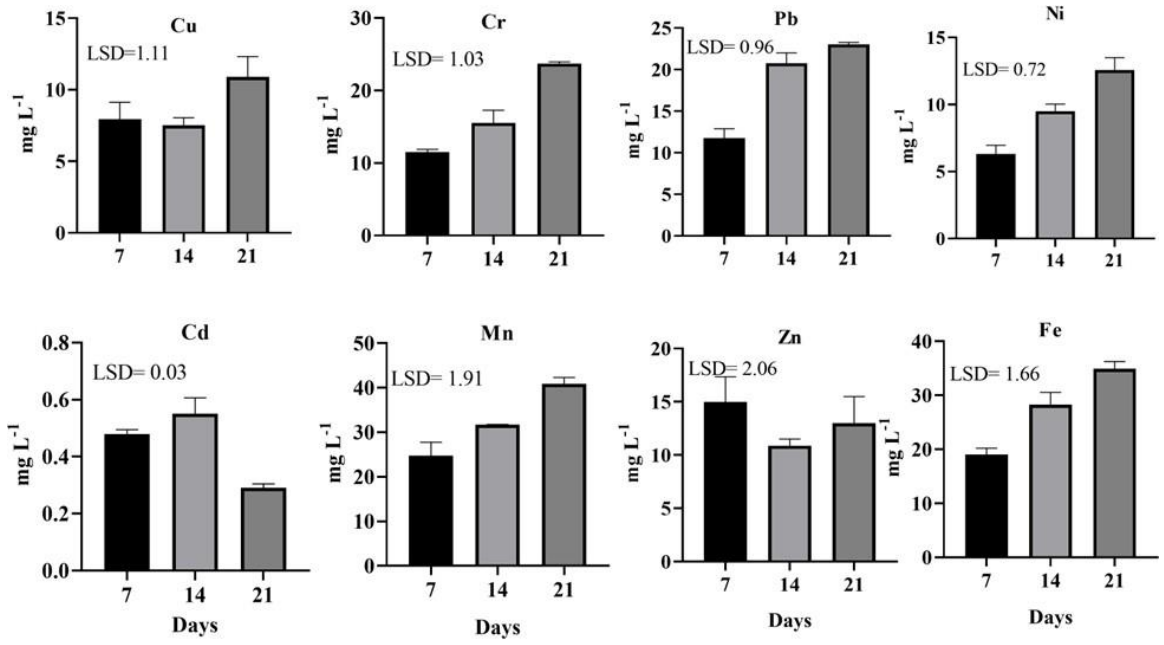

Fig. 4.7. Solubility dynamics of various metallic ions in RM leachates (values represented in mean ± standard deviation).

4.3.8. Principal component analysis

Principal component analysis was done to summarise the dominant attributes creating the variation in the RM physicochemical properties (Fig. 4.8.). The results accommodated in three components out of which PC1 covered 34.86%, PC2 covered 18.82% and PC3 covered 12.23%. Strong positive loadings of Cu, Cr, Ni, Zn, and physicochemical properties like, pH, EC, available Na, and Ca in PC1 was observed, while, moderate negative loadings of Pb, Cd and physicochemical properties like, TOC, TKN indicating uniqueness of the source of the material. PC1 has strongest positive loading of available Na (r=1.56) followed by Zn (r= 1.49), Mn (1.45), Cu (r=1.20) EC(r=1.23), and Cr (r=0.77). Available Na occupied highest is possibly due to high presence of incompletely washed caustic soda. While, a strong negative loading for TOC (r=-1.40), TKN (r= -1.0), CEC (r= -0.55). This makes sense given that metal bioavailability is known to be inversely correlated with pH and CEC. The findings are generally in line with our earlier reports (Sahariah et al., 2015). The second PC described 18.82 % of the variance. PC2 has the highest positive loading for Ni (r= 1.41), Pb (r=1.34), available Mg (r= 1.19); EC (r=1.21) it was negatively loaded with available N (r=0.74) and available K (r=0.23). PC3 described 12.56% of the total variance, where the highest positive loading factor was available Ca (r=1.20). Overall PCA analysis substantiated the probable metal contamination of

RM. The PCA also showed that available N, and Cd acted as independent may not have any significant effect on other chemical attribute.

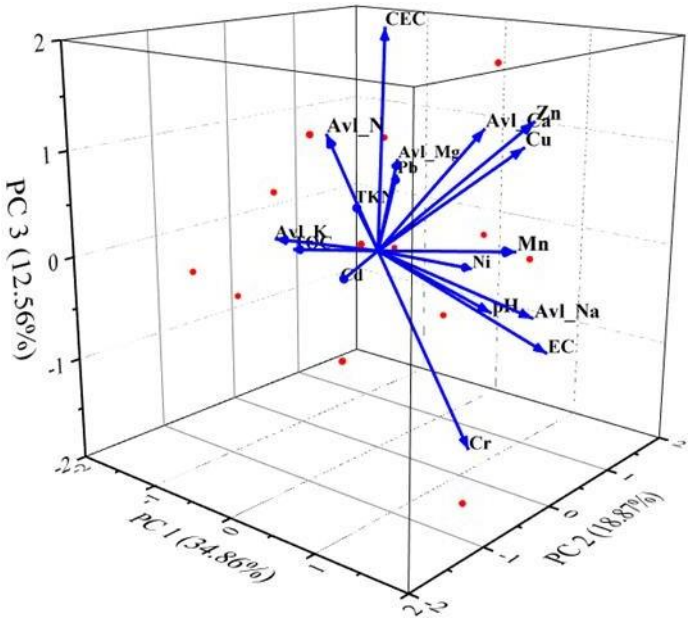

Fig. 4.8. Principal component analysis relating physicochemical properties of red mud based on log-transformed data.

4.3.9. Ecological impact assessment and human health hazards

In the majority of developing countries, landfills and agricultural soils are the primary sites where RM is disposed. Metal contamination from the open dumping of RMs on land is therefore an inevitable result. By assessing relative mobility (RM), pollution index (PI), contamination index (CI), ecological risk index (ERI), and geo-accumulation index (Igeo) for the examined metals in RM, I attempted to address these concerns. The results of these indices are presented in Table. 4.3.

The relative mobility outlines an idea of immediate toxicity of the metals present in RM towards environment. The assessment exhibited that Cd has the highest relative mobility followed by Pb, Ni and Cr. This is possibly attributed to their greater presence in bioavailable fraction, as well as their high occurrences in the RM sample. The mobility of other elements like Zn, Mn, and Cu was relatively low compared to the PTEs. Since it was already found in our study that RM harbours different kinds of toxic metals, so, the pollution index (PI) assessment provides the pollution load of environment posed by RM. The PI determines the

multi-element contamination potential, and a number greater than 1 denotes that the area requires remedial action because the substance (in this example, RM) is severely polluted and the gross metal concentration is over the permissible limit (Kim & Chon, 2001). Consequently, PI for RM was >1 implying its high-risk pollution load towards environment. The geo-accumulation index (I_{geo}) is another important directory that helps to assess soil contamination. Based on the geo-accumulation index (I_{geo}) and contamination level, RM samples were divided into seven classes. The RM dump can be divided as extremely contaminated due to high Cr and Ni occurrence and heavily contaminated due to preponderance of Cd, and Pb. The RM poses a hazard due to its extremely high contamination index (241.20). In general, ecological risk <300 suggests low risk, however in our case, the ecological risk was 587.76, which was high. ERI >600 indicates significant potential risk (Özden et al., 2019), and the recorded ERI 587.76 was a matter of concern in regard to the disposal of RM.

Table 4.3. Pollution, contamination, ecological, and accumulation indices-based assessment of environmental hazard potential of RM

Pollution Indices	
Relative mobility of Cd	1.61
Relative mobility of Cu	0.23
Relative mobility of Cr	0.53
Relative mobility of Pb	0.91
Relative mobility of Ni	0.5
Relative mobility of Mn	0.17
Relative mobility of Zn	0.3
Contamination index	241.01
Pollution index	2.63
Ecological risk index	587.86
Geo-accumulation index (I_{geo}) Cu	2.72
Geo-accumulation index (I_{geo}) Cr	6.73
Geo-accumulation index (I_{geo}) Cd	3.23
Geo-accumulation index (I_{geo}) Pb	3.97
Geo-accumulation index (I_{geo}) Ni	5.67
Geo-accumulation index (I_{geo}) Mn	0.96
Geo-accumulation index (I_{geo}) Zn	1.32

The non-carcinogenic and carcinogenic health risk associated with metal exposure was evaluated and presented in Table 4.4. The non-carcinogenic hazard was calculated in terms of hazard index (HI). Three routes of exposure viz., ingestion, inhalation, and dermal are considered. Overall HI was higher in children compared to adults, and ingestion was found to

be the most detrimental route of exposure. In general HI>1 is considered to have high health risk, but, in present study HI was <1 for all the metals, never the less, Cr and Pb, both the metal showed probable risk to adults and children. High intake of Cr and Pb leads to neurological disorder coupled with growth and developmental dysfunctionality in particular close to the "safe" level HI=1 (Ferreira-Baptista & De Miguel, 2005). Considering the cancer risk, which was high for Ni in the case of children. Therefore, the RM is a potential health hazard for both adults and children.

Table 4.4. Carcinogenic (ingestion, inhalation, dermal and non-carcinogenic risk (inhalation, ingestion, dermal) from RM in adults and children.

Metal	Adult					Child				
	HQ ingestion	HQ inhalation	HQ dermal	HI	CR	HQ ingestion	HQ inhalation	HQ dermal	HI	CR
Ni	0.006859	9.79E-07	0.000101	0.006961	8.79E-05	0.054872	1.49E-06	0.000569	0.055442	0.000171
Cu	0.003503	5.15E-07	0.000466	0.003969		0.028022	7.83E-07	0.002727	0.03075	
Cr	0.074063	0.00038	0.014775	0.029739	4.47E-05	0.592501	0.000578	0.08295	0.225343	8.5E-05
Cd	0.004702	6.91E-07	0.001876	0.006579	8.06E-07	0.037617	1.05E-06	0.010533	0.04815	1.61E-06
Pb	0.080494	4.71E-06	0.000858	0.081357	6.88E-06	0.643953	7.16E-06	0.004817	0.648777	3.55E-06
Zn	0.000363	5.34E-08	7.24E-06	0.00037		0.002905	8.12E-08	4.07E-05	0.002946	
Mn	0.004505	0.002131	0.000449	0.007086		0.036043	0.00324	0.002523	0.041806	

4.4. Conclusion

RM was critically examined for their ecological and environmental effects based on their morphology, physicochemical characteristics, PCA, metal fractionation, pollution indices, and human health hazard indices. Morphologically they are unshaped, irregular, and agglomerated. XRD studies revealed their partial amorphous structure with a predominance of iron oxide (Fe_2O_3) and aluminum oxide (Al_2O_3). The RM was extremely alkaline with high sodicity and also overloaded with many hazardous elements, such as Cd, Cr, P, and Ni, both in terms of overall content and bioavailability. Consequently, it poses a deleterious effect on both environment and human health. PCA analysis illustrated this high Na content and noxious metals primely govern the variation of the physicochemical attributes. In line with that, it is extremely poor in carbon-nitrogen content. Despite its sodicity and harmful metal content, it contains several micronutrients such as Mg, Mn, Zn, Fe, Cu, K, etc. that might deliver a good agriculture benefit, if it can be managed through a bio-composting process. In light of the substantial research on the RM's physicochemical properties done in the current work, we anticipate applying this RM in agriculture by turning it into bio-compost using vermitechnology, which will be further covered in subsequent chapters.

Chapter 5

Deciphering the physicochemical attributes of bauxite ore (BO) and its characteristic deviation from red mud (RM)

Chapter 5

Deciphering the physicochemical attributes of bauxite ore (BO) and its characteristic deviation from red mud (RM)

5.1. Introduction

The present thesis is primely focused on management of aluminum industry waste sustainably. In the previous chapter, I illustrated a detailed physicochemical characteristic of alumina industry-generated waste named red mud (RM). As we know that bauxite is the only precursor of aluminum extraction, so, I also conducted a study on native bauxite ore to observe any characteristic deviation exists following alumina extraction in order to perceive the impact of industrial scale-up. Since bauxite formation is a geogenic phenomenon, the present work additionally focused on the distinctive chemical properties that set them apart from virgin soil. This chapter is an embellishment of the physicochemical properties of native bauxite ore and their distinctiveness from virgin soil (here forest soil), subsequently, a thorough illustration of its alteration after being processed by alumina industries.

Bauxite is a residual rock formed due to a lateritic weathering process where alkalis, alkali earth and silicon show higher mobility as compared to Al, and Fe under the influence of humid, tropical and sub-tropical climates. It consists of mainly hydrates of aluminum oxide (27-80%), iron oxide (20-30%), and a trace amount of silicon oxide (3-6%) (Jiang, 2014). From the geological perspective, it is the product of intense continental subaerial weathering, influenced by distinct climatic and tectonic conditions (Meyer 2004). The parent rock of bauxite is different igneous rocks, metamorphic classic-sedimentary derivatives that undergoes numerous chemical and mineralogical modification to form bauxite under suitable climatic condition. The modification process includes kaolinization followed by laterization and bauxitization (Donoghue 2014). A large amount of rainfall triggers the breakdown of clay particles and supports leaching out the more mobile elements and leaving behind relatively immobile aluminum, and iron with a little amount of silicon and titanium. In addition, the presence of pyrite in bauxite ore/gaunge is the source of sulfide which in turn oxidized when exposed to atmospheric oxygen and leads to the acidity of bauxite mine and mine seepage (Mishra and Das 2021; Sahoo et al., 2010). Precisely the release of sulfur by weathering of sulfide rock generates sulfuric acid which is another source of production of acid mine water in bauxite mine. At reduced pH level, metal, and metallic contaminants present in ore body

dissolves, leaches out, and dispersed into different environmental component like soil, water bodies, agricultural land etc. The metal-rich acidic mine water contaminates groundwater of the mine area by sluggish percolation through intra-particular space. Lower pH not also increases the metal availability (Sahoo et al., 2010). Since Al_2O_3 and Fe_2O_3 are the key minerals of bauxite, Al plays a dominant role in acidic condition by prevailing in different forms such as exchangeable, non-exchangeable, soluble, and complex oxide forms (Pal et al. 2007). A high concentration of Al^{3+} creates considerable damage to the soil flora and fauna. Many researchers demonstrated aluminum (Al^{3+}) as an acidic cation, and a combined effect of Al^{3+} and H^+ i.e., has a significant effect on nutrient cycling and biochemical activity of organisms (Kunito et al. 2016; Pal et al. 2007). Al^{3+} can exclusively reduce the microbial respiration, nitrification, and microbial uptake of ammonium in forest ecosystem (Kunito et al. 2016). As bauxite ore is a rock, so organic matter is expected to be less as per literature survey. In general, rock is very different for soil, and their formations are also two different geogenic processes. Rock is mainly made up of minerals. They are cohesively linked natural mineral aggregates, whereas soil is created when rock breaks down through natural weathering. The soil particles also generated from dead and decomposition of plant and animal matter (Tripathy & Raha, 2019).

Other than these fundamental difference, unscientific mine excavation activity is a root cause of structural alteration of mine site and the probable damage to the ecosystem. Though, formation of bauxite ore and mine is a natural activity, yet, their composition, mishandling, prolonged excavation, overburden/tailing deposition at nearby location of mine put stress to the environment (Keita and Traore 2020). Consequently, their characteristics, properties and long-term impact on environment seems to be different from a soil. So, through our study we tried to identify, how much characteristic difference, and environmental damage takes place in bauxite ore/ mine/mine overburden compared to a virgin soil.

Additionally, as stated earlier that red mud (RM) is by product during aluminum extraction through Bayer process, where high amount of NaOH is used. This NaOH /caustic soda is the prerequisite of Bayer process, which even after aluminum extraction remains in high amount. So, it is predicted that there may be a massive difference between bauxite ore and bauxite residue (alternatively RM). As I have previously explored the characteristics of RM, thus, this chapter illustrates a comparative assessment between bauxite ore and bauxite residue (RM).

5.2. Material and Methods

5.2.1. Study area and site description

The sampling site, Bagru bauxite mine (23.4734^{0}N to 84.6243^{0}E) is situated at an elevation of 2,100 feet in the Lohardaga district of Jharkhand state in India (Fig. 5.1). It is an open-pit surface mining operation and one of the oldest mines in India. The mining operation has begun in the year of 1933. Approximately 3.5 tons of bauxite are mined annually. The climate is tropical monsoonal and differs from humid subtropical in the northern region to tropical wet and dry in the southeast. It is one of the warmest regions with an average temperature of 33^{0}C. Based on the atmospheric conditions, three seasons prevail throughout the year, summer from April to June with an average temperature of 37^{0}C, monsoon from June to October with an annual rainfall of 1000 mm, and winter from November to February with a daily average of 24^{0}C. The relative humidity varied from 41% in summer to 89% during monsoon.

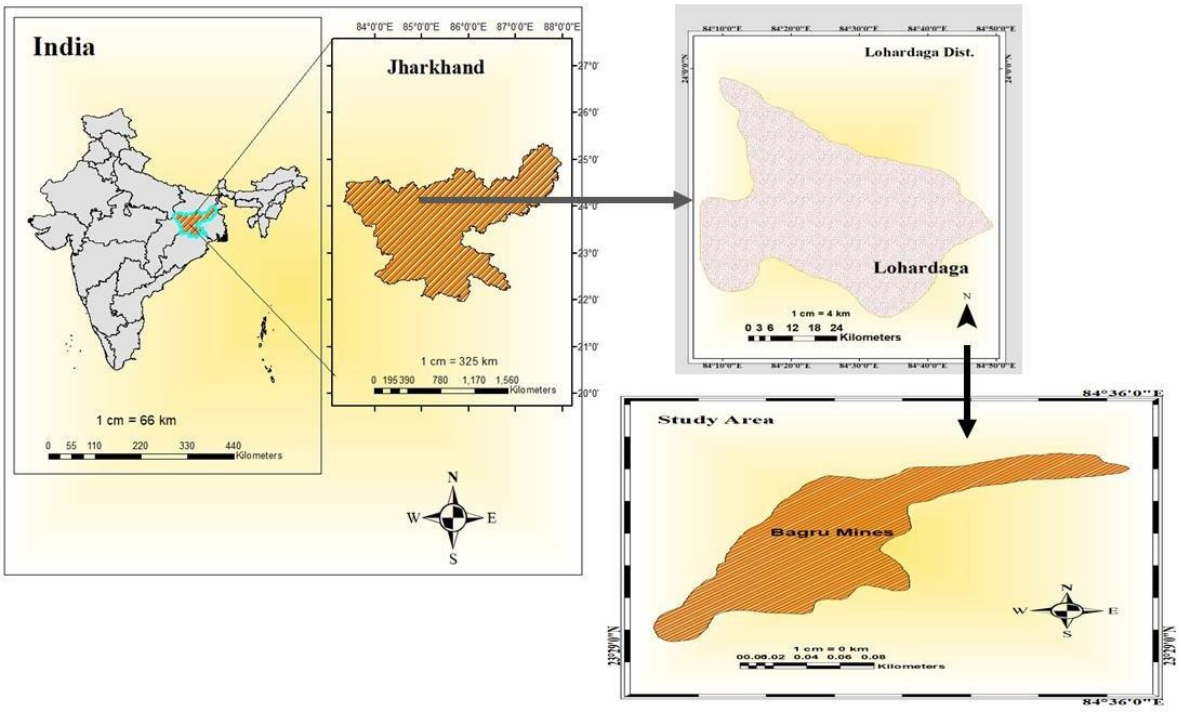

Fig. 5.1. Map showing the bauxite mine (sampling site) located in Jharkhand.

5.2.2. Sampling and Preparation

A total of 18 samples were collected from the surface (<10 cm in depth) of two different sites of the mine and nearby forest area in April 2021. Among them, 9 samples were collected from the mine/tailing and 9 from a natural forest area located close to the mine. The deposited mine/tailing samples are primarily rock types, while, forest soil is clay loam in texture. Samples were brought to the laboratory in a labelled and sealed polythene bag and kept at 4^0C in the refrigerator for further analysis. For physicochemical analysis, samples were air-dried, sieved through 2 mm and 0.2 mm and stored in a vial for future study. For microbial and biochemical parameters moist samples had been used. Chemical, microbiological and biochemical parameters were expressed on a moisture-free basis.

5.2.3. Physicochemical properties and different forms of acidities

According to the procedure described by Page et al. (1982), the obtained samples were tested for pH, electrical conductivity (EC), total organic carbon (TOC), available N, cation exchange capacity (CEC), available phosphorous (P), available potassium (K), available calcium (Ca), With the use of A AS 816 Systronics, India, metals were extracted using the sequential extraction method of Tessier et al., 1979. DTPA extractable metal were checked by following Lindsey & Norvell, 1978. TCLP was done following USEPA SW-846. Bio-accessible fraction was done following Ruby et al., 1996. Acidity and aluminum were measured following Mclean, 1965 and Peech, 1962.

A. pH- Description detailed in Chapter 4 (Section 4.2.2)

B. EC- Description detailed in Chapter 4 (Section 4.2.2)

C. TOC- TOC was measured following the Modified Walkley and Black method, 1934. Description detailed in Chapter 4 (Section 4.2.2)

D. Easily mineralizable nitrogen estimation (avl. N) - Description detailed in chapter 4 (Section 4.2.2)

E. Cation exchange capacity (CEC)- Description detailed in Chapter 4 (Section 4.2.2)

F. Available P- Description detailed in Chapter 4 (Section 4.2.2)

G. Available Na^+, K^+, Ca^{2+}- Description detailed in chapter 4 (Section 4.2.2)

H. Different forms of acidities and aluminum

Total Acidity

Reagents

1. 1(N) NaOAC solution adjusted to pH 8.2
2. 0.1(N) NaOH solution
3. Phenolphthalein indicator

Procedure

1. Weighing of 40g air-dried soil passed through a 2mm sieve into a 250ml conical flask.
2. Addition of 100ml of 1(N) NaOAc solution.
3. Shake for an hour and filter.
4. Titration of filtrate against 0.1(N) NaOH using 2-3 drops phenolphthalein indicator until
5. a persistent pink colouration is obtained.

Calculation

Let Volume of 0.1(N) NaOH required for sample titration = VI ml

Therefore, meq of total acidity in 100 ml extract = 0.1 × VI

Thus 40 g soil contains total acidity of (0.1 × VI) meq.

Hence, 100 g soil contains total acidity of= 0.1 X V_I X 100/40 meq

Thus, total acidity of the soil = 0.1 X V_I X 100/40 meq/100g

Exchangeable Acidity

Reagents

1. Potassium chloride solution 1(N). Prepare from analytical grade reagent by dissolving
2. 74.56 g in one litre distilled water.
3. Potassium fluoride solution 1(N). Dissolve 58 g potassium fluoride in about 900 ml
4. distilled water. Add a few drops of phenolphthalein. If the solution is not pink, add
5. 0.1(N) NaOH in drops till it turns pink. Discharge the colour by adding 0.1(N) H_2SO_4
6. in drops. This eliminates the necessity for blank for the second titration. Dilute to one
7. litre.
8. Standard sodium hydroxide solution, 0.1(N)
9. Standard sulphuric acid solution 0.1(N)

10. Phenolphthalein solution 0.1% in 95% ethanol.

Procedure

1. Weighing 10 g airdry sample into a 100 ml conical flask.
2. Addition 50 ml of the KCl-solution. Mix thoroughly and then allow to stand for 30 min.
3. Filtered through Whatman No. 40 filter paper into a 100 ml volumetric flask.
4. Leach the soil four times with 10.0 ml portions of KCl solution.
5. Dilute to the volume with the KCl solution.
6. Transferred to a 250 ml conical flask, add 6-8 cc phenolphthalein indicator.
7. Titrated against the standard NaOH solution to a pink colour that persists for at least 30 seconds.
8. Preserved the solution for the second titration.
9. Determined the blank correction for the KCl by titrating 100 ml of the KCl solution with the NaOH to an identical end point.
10. To determine exchangeable aluminium, added one drop 0.1 N sulphuric acid to the titrated solution, if required to discharge the pink colour, added 10 ml of the KF solution into the flask and mix well.
11. Titrated against the standard sulphuric acid till the pink colour disappears.
12. Left aside for ten minutes and continue titrating to a lasting colourless endpoint.
13. This step is followed because the release of the last of the hydroxyl from Al(OH)3 takes place slowly.
14. Standardise the NaOH versus Oxalic acid and H_2SO4 versus standard NaOH.

Calculation

Exchangeable acidity (H + Al), meq/100 gm soil= $(V_1 - B) \times N_1 \times {}^{100}/_{w}$

Exchangeable Al, meq/100 gm soil= = $V_2 \times N_2 \times 100/w$

where V1 = volume of standard NaOH required for sample titration (ml)

B = volume of standard NaOH for blank titration (ml)

N_1 = normality of standard NaOH

N_2 = normality of standard acid

V_2 = volume of standard acid required for sample (ml)

Total potential acidity

Reagents

1. 1(N) $BaCl_2$ solution
2. 0.2 (N) HCl
3. Buffer extractant of 0.5(N) $BaCl_2$ plus triethanolamine (pH 8-8.2): Dilute 25 ml of triethanolamine (sp.gr.1.126, normality 8) to 250 ml with water and adjust the pH to 8.0-8.2 with HCl (approx.90 ml 1(N) HCl is required for this partial neutralization process). Dilute the solution to 500 ml and then mix it with 500 ml of 1(N) $BaCl_2$ solution. The final solution must be kept free of CO_2.
4. Bromocresol green-methyl red indicator: Dissolve 0.5 g bromocresol green and 0.1 g methyl red in 100 ml of 95% ethanol and adjust the pH to 4.5.

Procedure

1. Weighed 10 g of soil and take it in a 250 ml conical flask.
2. Added 100 ml of extracting buffer solution and shake for half an hour and keep
3. overnight.
4. Transferred the contents to a Buchner funnel fitted with a Whatman No. 42 filter paper and carry out gentle suction filtration.
5. Rinsed the conical flask with an additional extracting solution so that no soil particles is left over in the flask.
6. Now, transferred the leachate to a 250 ml volumetric flask and make up the volume with the extracting solution.
7. Poured the leachate into a conical flask and add a few drops of mixed indicator into it.
8. Titrated with 0.2 (N) HCl until the endpoint colouration (pink) is obtained.
9. Performed a blank keeping all conditions identical except soil.

Calculation

Let Volume of 0.2(N) HCl required for blank titration = B ml

Volume of 0.2(N) HCl required for sample titration = S ml.

So 100g soil has total potential acidity = $\frac{(B-S)X0.2X100}{10}\ meq$

Thus, total potential acidity [2(B-S)] meq/100 g.

pH-dependent acidity

pH-dependent soil acidity mainly comprises acidity arising from the dissociation of protons from functional groups, viz. carboxyl groups (R–COOH) and phenolic hydroxyl groups (R–OH) on soil organic matter as well as weakly acidic proton on soil mineral edges (OH-groups exposed on broken edges of 1: 1 kaolinitic mineral) due to an increase in soil pH.

Calculation

pH-dependent acidity = total potential acidity – exchange acidity.

Determination of Available Aluminum in Soil:

Estimation: Colorimetric method with Aluminon.

Procedure:

1. Weigh 5 gm soil in a 100 ml conical flask, add 50 ml of 1N Kcl, and shake for 30 mins. Filter the suspension with Whatman 42.
2. Pippete 2 ml of aliquot to a 50 ml Vol. Flask and add 4 ml of 1N Hcl.
3. Add 2 ml of 2% Thioglycolic Acid and add about 15 ml of distilled water and heat at least for 30 mins. in a water bath at 80-90 deg. C.
4. Cool the solution and dilute to about 35 ml with dist. water. Add 10 ml of Aluminon Acetate buffer and make up the volume and shake thoroughly. The pH should be 3.7 to 4.0.
5. Measure the colour intensity after 2 hrs. at 530 nm.

Reagents:

1. 1N Potassium chloride (KCl): Dissolve 74.56 gm KCl (AR grade) in 1 lit. distilled water.
2. Aluminon Acetate Buffer: Dilute 120 ml of glacial acetic acid to about 800 ml of dist. water. Add 24 gm of NaOH and mix, dissolve 0.35 gm of Aluminon in the solution, and make volume to 1 lit with dist. water and mix.
3. 1 N HCl: Add 84 ml of a con. HCl to 1 lit. dist. water.
4. 2% Thioglycolic Acid: Add 2 ml of Thioglycolic Acid to 100 ml dist. water.

Standard Curve for Al 3+:

Dissolve 4.942 gm of Aluminum Chloride (AR grade) in 1000 ml dist. water to make 1000 ppm of Al 3+. Then take 5 ml (from 1000 ppm solution) in 1000 ml of dist. water to make 5

ppm of Al 3+. Then take 2, 4, 6, 8, 10, and 20 ml from the 5-ppm solution to 50 ml vol. Flask to have to contain 0.2, 0.4, 0.6, 0.8, 1.0, and 2.0 ppm Al^{3+} per ml respectively for preparation of Standard Curve.

(Rest the procedure is same as above (starting from Procedure no. 2) after taking the solution in 50 ml vol. flask.)

5.2.4. Ecological assessment

Discussed detailed in Chapter 4 (section 4.2.6)

5.2.5. Microbial analysis

Microbial biomass carbon (MBC) was analyzed following Jenkinson, 1988. FDA and other enzyme activities (Acid phosphatase, aryl sulphatase, β-D- glucosidase, dehydrogenase) was measured.

A. FDA- Description detailed in Chapter 6 (section 6.1.2.2.)
B. β-D glucosidase- Description detailed in Chapter 6 (section 6.1.2.2.)
C. Dehydrogenase- Description detailed in Chapter 6 (section 6.1.2.2.)
D. Acid phosphatase- Description detailed in Chapter 6 (section 6.1.2.2.)
E. Aryl sulphatase- Description detailed in Chapter 6 (section 6.1.2.2.)
F. Microbial biomass carbon (MBC) (Jenkinson, 1988)

Reagents

1. Ninhydrin reagent: Dissolved 0.8 g ninhydrin and 0.12 g hydrindantin in 30ml dimethyl sulfoxide and added 10ml of lithium acetate buffer to it. Used always fresh reagents for analysis of MBC.
2. Lithium-acetate buffer: 168g lithium hydroxide ($LiOH.H_2O$) was mixed in 500 ml distilled water. Dissolved about half of the ingredient by continuous stirring and add 293ml of glacial acetic acid and made the volume up to 1L. pH was adjusted to 5.2 ± 0.05 either with acetic acid or lithium hydroxide. Allow the solution to cool overnight and then made the volume up to 1L.
3. Ethanol – water: 165 ml ethanol was diluted to 300ml by adding distilled water
4. Potassium chloride solution (2M KCl): 149g potassium chloride was dissolved in distilled water and volume made up to 1L.

5. Chloroform: HPLC grade chloroform stabilized with 0.006%. 2-methyl -2- butane and used for this analysis.
6. Nitrogen standards: 47mg of Leucine was dissolved in 2 M KCl and made up to 50 ml. This contained 100 (μg N ml^{-1}). This solution was serially diluted to 0, 2, 4, 8, and 16 μg Nml-1 with 2 M KCl solution.

Required instruments

1. Spectrophotometer
2. Water bath at 100ºC

Procedure

1. 10g of moist soil was immediately collected from the experimental pot for both fumigated and unfumigated carbon analysis
2. Unfumigated: Soil samples were taken in a 250ml conical flask and 40ml of 2M KCl was added. Then shaken for half an hour on mechanical shaker and filtered. 1 ml of filtrate was taken in each test tube and 0.5 ml of Ninhydrin was added. Then the solution was heated in a water bath for some time and after cooling 9.5 ml ethanol–water was added and thoroughly mixed and absorbance was measured at 570 nm against the blank (KCl solution).
3. Fumigated: Soil samples were placed in a vacuum desiccator preloaded with 10g of soda lime, 25 ml of chloroform, and boiling chips in a beaker. Evacuated for 2 minutes till chloroform boils and kept for 24 hours. The next day, a beaker containing chloroform was removed by repeated evacuation. Then transferred the soil in a 250 ml conical flask and extracted the same as the unfumigated process.

Determination of ninhydrin-reactive N:

Calibration:

1 ml of each leucine standard was taken in a 50 ml test tube and then slowly added 0.5 ml of ninhydrin reagent. After mixing all contents, thoroughly heated all the standard solutions in a boiling water bath. After cooling of a test tube, added 9.5 ml of ethanol-water to each of the test tubes and mixed thoroughly. Absorbance was measured in a spectrophotometer at a wavelength of 570nm with KCl solutions as the blank. Calibration curve was drawn with the absorbance against N- concentration. In a similar fashion colors of the samples were developed. Concentration of the extract was determined with the help of a standard curve.

Calculation:

Initial calculation:

MBC (μg g-1) = [(Fumigated concentration – Unfumigated concentration) x DF] Oven dry soil wt. difference

Oven dry soil wt. the difference means if moist wt. was 10 g and oven dry wt. = 9.23 g,

Hence the difference would be 10 – 9.23 = 0.77

Microbial Biomass C (μg g-1 oven dry soil) = 31 × ninhydrin N

Microbial Biomass N (μgg-1 oven dry soil) = 4.6 × ninhydrin N

5.2.6. Statistical analysis

Mean ±standard error was used to represent the physicochemical properties of the bauxite and forest soil. All analysis was carried out in triplicates. Statistical analyses like Pearson correlation analysis and T-test were carried out to analyze any significant differences between the variables and the linear relationship among them. Raw data were used to make the box whisker plot, which is a convenient way of graphically presenting the dataset that consists of the smallest observation, lower quartile, median, upper quartile, and largest observation; additionally, the boxplot specifies those observations, if any, that are considered unusual, or outliers. All of these statistical analyses were done by using the SPSS version 26 statistical software package

5.3. Result and Discussion

5.3.1. Physicochemical properties of bauxite ore and soil

Physicochemical properties of two different sites of BM (mine site, forest site) are depicted in (Table 5.1) The pH (water) of the soil samples was found to be acidic ranging from 4.2 – 4.9 (mean 4.48) at the mine site, 4- 4.4 (mean 4.18) at the forest site. The trend of organic carbon (TOC) and available N was somewhat opposite to the pH values. TOC is high at forest sites ranging from 1.5-2.1% (mean 1.8%) followed by mine sites (0.15-0.37% mean 0.27%). Higher organic C at forest sites is an indication of the accumulation of a high amount of organic matter. Following the organic C trend mineralizable N was also found to be highest at forest sites (0.007-0.01% mean 0.01%) while mine sites were considerably poor with a mean of 0.002%.

Acidic soils are considered to be high in acidic cations like H^+ and Al^{3+} compared to the alkali cations viz. calcium (Ca^{2+}), magnesium (Mg^{2+}), potassium (K^+), and sodium (Na^+). Such conditions can be caused by geogenic parent material, the disintegration of organic matter, leaching and rainfall, etc. (Sanyal 1991). The cationic constituents are loosely bounded and highly leachable near low pH, thereby the presence of alkali cations is found in lesser quantities than acidic ones. In our case, total cationic content of the core mine site was, $Mg^{2+}>Na^+>K^+>Ca^{2+}$, while forest site contained a high amount of Ca^{2+} (170.31 ±11.09). Under an acidic environment, basic ions are likely to replace by H^+ and Al^{3+} ions through cation exchange capacity (CEC) (Goulding 2016). CEC is one of the most important properties that retain the nutrient and make it available to plants. It is maximum at forest soil 20.46 cmol/kg, which might be due to its clay texture and high organic matter that more efficiently adsorb the positive charge cations. On a contrary note, mine/ore exhibited a lower CEC, average of 6.28 cmol/kg respectively. A highly significant positive correlation between TOC and CEC (r =0.94 significant at 1% level) demonstrated that organic matter is responsible for higher CEC in soil. Additionally, the dissociation of H^+ from humic constituents may be another reason for it. CEC is largely dependent on clay, organic matter content, and pH, any change in one or more of these factors will significantly impact CEC.

Table 5.1. The comparison between physicochemical properties between bauxite ore and soil (forest soil). Values represent mean ± SE

Parameters	Bauxite ore/mine	Forest soil
pH	4.48 ±0.42	4.46 ±0.51
CEC meq/100g	6.28 ±1.08	20.46 ±2.27
TOC (%)	0.27 ±0.01	1.89 ±0.19
Available Na mg/kg	13.09 ±1.69	24.11 ±2.28
Available K mg/ kg	9.49 ±1.41	119.4 ±8.41
Available Ca mg/kg	7.47 ±2.8	170.31 ±11.09
Available Mg mg/kg	25.66 ±4.65	71.55 ±1.58
Available P mg/kg	3.09 ±0.12	5.92 ±0.98
Mineralizable N mg/kg	27.48 ±3.86	102.81 ±13.59
Total Cr mg/kg	458.78 ±116.04	39.09 ±7.84
Total Cd mg/kg	8.57 ±0.9	1.61 ±0.21
Total Ni mg/kg	355.11 ±34.01	119.3 ±4.27
Total Pb mg/kg	684.52 ±90.59	130.81 ±6.09
Total Cu mg/kg	256.48 ±32.88	51.29 ±2.81
Total Mn mg/kg	1177.57 ±212.37	14.15 ±14.15
Total Zn mg/kg	189.68 ±13.95	113.45 ±3.01
Total Fe mg/kg	171946 ±25489.7	47801.6 ±1106.06
DTPA extractable Cr mg/kg	0.6 ±0.001	1.6 ±0.08
DTPA extractable Pb mg/kg	2.08 ±0.19	4.03 ±0.98
DTPA extractable Cd mg/kg	0.01 ±0.008	0.08 ±0.003
DTPA extractable Ni mg/kg	1.28 ±008	2.9 ±0.1
DTPA extractable Cu mg/kg	0.8 ±0.06	2.67 ±0.98
DTPA extractable Mn mg/kg	1.39 ±0.99	16.09 ±0.67
DTPA extractable Zn mg/kg	2.3 ±0.05	4.14 ±0.33
DTPA extractable Fe mg/kg	11.46 ±1.06	28.46 ±0.45

5.3.2. Mineralogical Characterization and surface chemistry of bauxite ore

The elemental composition of any sample is highly required to know for its physical representation. An elemental map needs to be generated with spatially resolved data pointing

to the incidence of existing elements' location and what other elements they are accompanied with. It helps to understand the ore body with respect to its textural associations, and distribution of metal across the deposits. A somewhat reliable evaluation was done through FESEM-EDX analysis (Fig. 5.2.). FESEM micrograph revealed its surface morphology, illustrating its granular structure having an irregular shape, ranging between 100-1000 nm. where a maximum of the granular structure varied between 400-500nm. These irregular flaky-shaped grains exist by forming aggregates. The agglomerate structures differed in their size, sometimes they were densely packed, large, and occasionally loosely bounded. Sahoo et al. 2017 well observed the collomorphous or vesicular texture of bauxite in the sundargarh district of Orissa which somewhat resembles our observed structures. Further proceedings of EDX analysis disclosed the elemental abundance of the ore body. The major element detected in bauxite ore was O, Al, Fe, Ti, and Si, out of which O, Al, and Fe were predominant. The presence of O along with Al, and Fe was indicating the existence of metal oxides like aluminum oxide (Al_2O_3) and iron oxide (Fe_2O_3). A minor quantity of SiO_2 is evidence of robust leaching during bauxitization (Balabantaray et al. 2020).

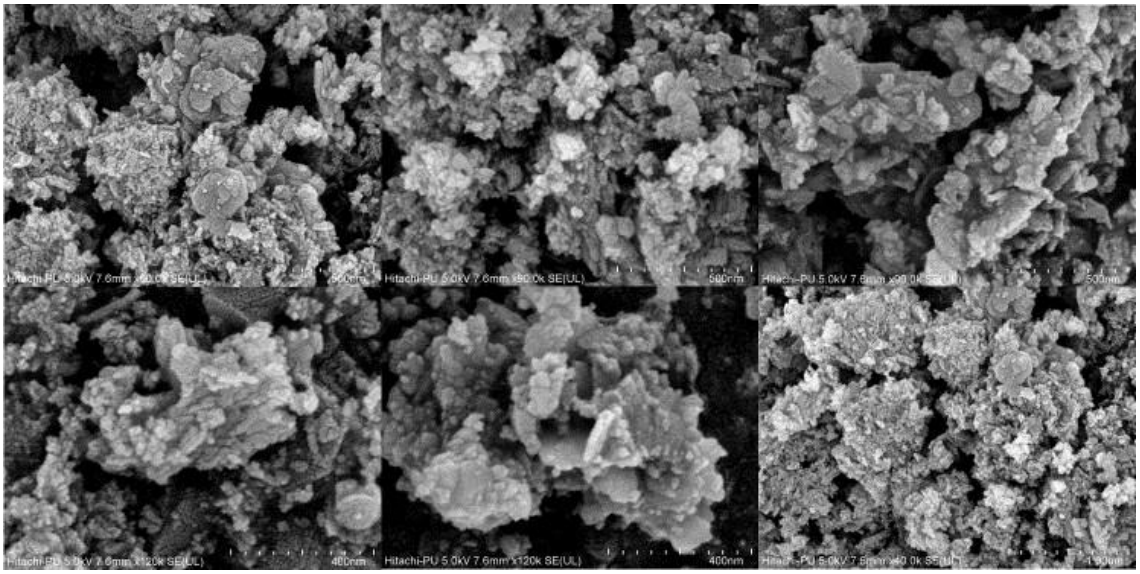

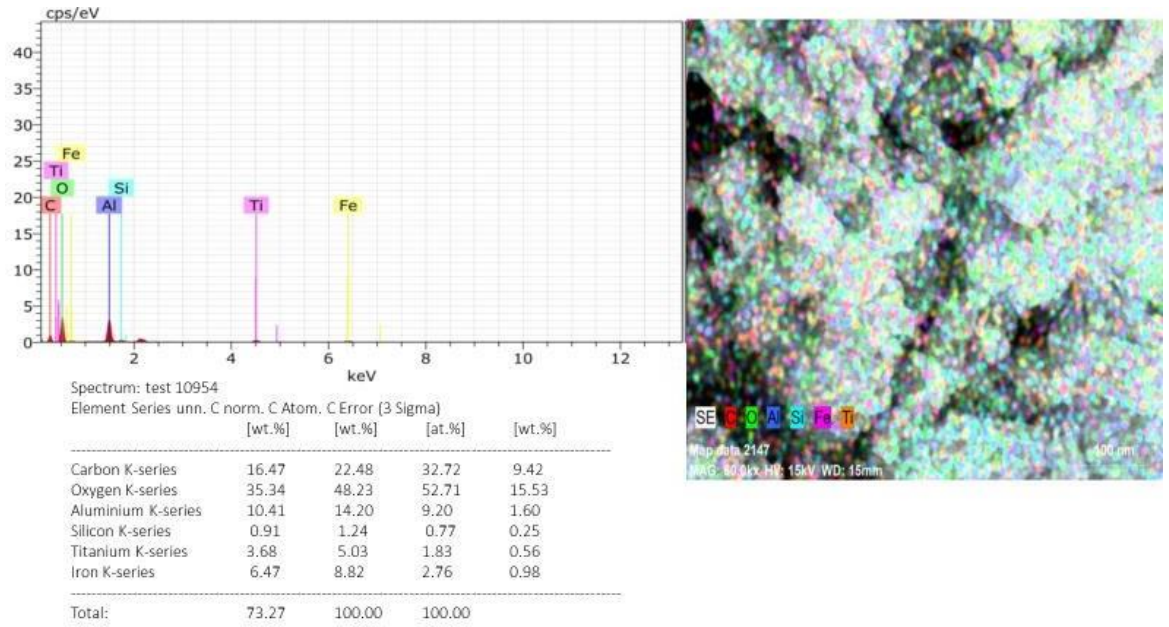

Spectrum: test 10954
Element Series unn. C norm. C Atom. C Error (3 Sigma)

	[wt.%]	[wt.%]	[at.%]	[wt.%]
Carbon K-series	16.47	22.48	32.72	9.42
Oxygen K-series	35.34	48.23	52.71	15.53
Aluminium K-series	10.41	14.20	9.20	1.60
Silicon K-series	0.91	1.24	0.77	0.25
Titanium K-series	3.68	5.03	1.83	0.56
Iron K-series	6.47	8.82	2.76	0.98
Total:	73.27	100.00	100.00	

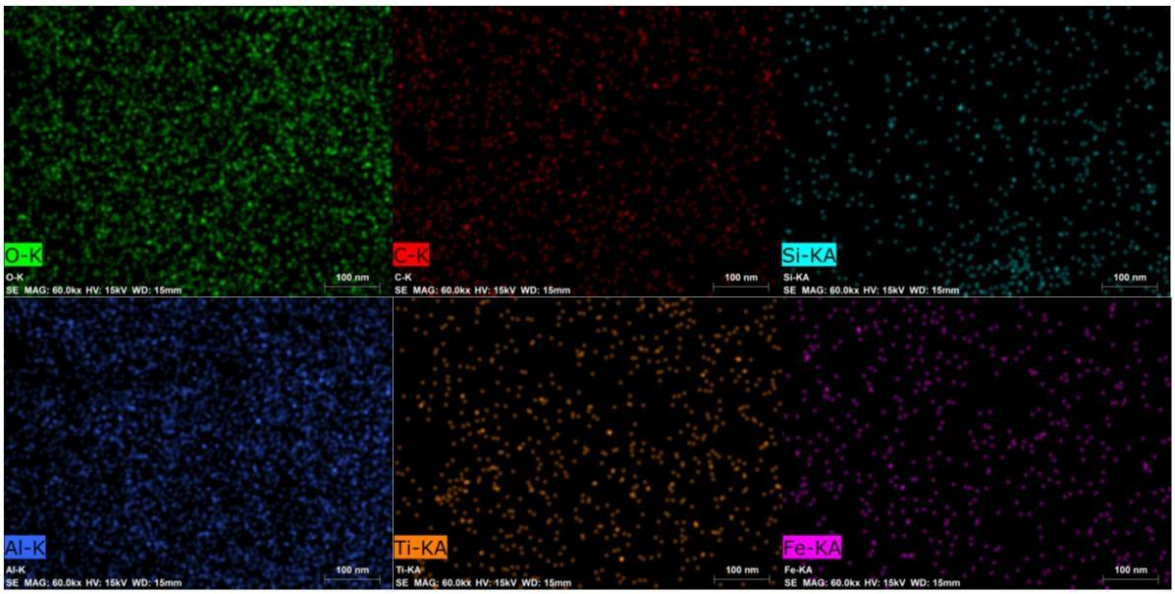

Fig. 5.2. FESEM image of bauxite ore with EDX elemental spectra.

Fourier transform infrared spectroscopy (FTIR) is a convenient tool for defining the chemical profile of different environmental samples (Fig. 5.3). Vibrational bands between the mid to low range (1500-400) were primarily associated with Al and Si indicated the presence of Al and Si bearing minerals (Opiso et al., 2021). The IR spectra included extensive peaks between 700- 1400 cm^{-1} suggesting the asymmetric stretching vibration of Si-O- Al or Al-O-Si, furthermore, Si-O-Al^{3+} vibration was detected at 748 cm^{-1}. The sharp peak at 803 cm^{-1} pointing the asymmetrical bending vibration of Si-O (Opiso et al., 2021). The Al-OH absorption peak lied between 851-915. The studied sample band at 912 cm^{-1} corresponds to the

Al-OH, which is also supported by the observation of Saikia et al (2010) in kaolinite. A band at 1035 cm^{-1} was presenting Si-O-Si stretching of a non-bridging oxygen atom. A strong Si-O-Si bending vibration was detected at 554 cm^{-1} and 476 cm^{-1}. In this same range, Si-O bending vibration was also observed by Mondal et al. (2017). The band at 1618 cm^{-1} was pointing toward hydration H-O-H deformation. Peaks of O-H stretch between 3600-3800 seed to those related to clay minerals. More precisely band around 3600cm^{-1} showed a crystalline hydroxyl group (Saikia et al. 2010). A sharp peak at 3452cm^{-1} indicated H-O stretching, which might be the hydroxyl bonds of gibbsite, according to Arhin et al. (2013) who observed a band near 3426 cm^{-1} was associated with the hydroxyl group of gibbsite. The band at 3621 cm^{-1} might be assigned for the inner hydroxyl group.

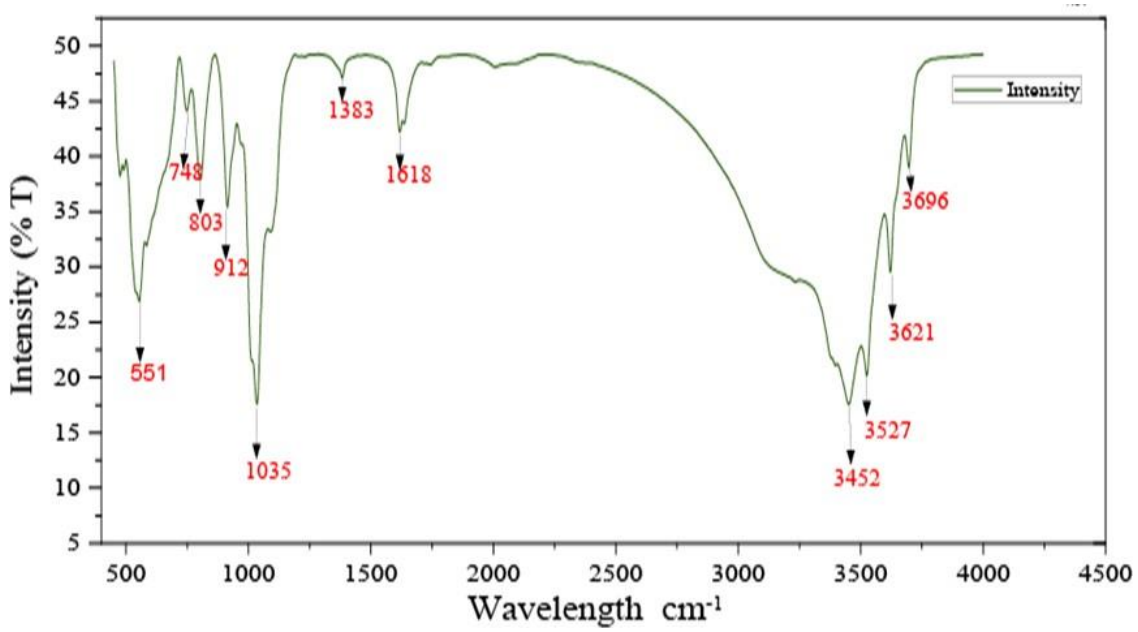

Fig. 5.3. Distribution of functional group in bauxite ore.

In order to explore the mineralogical distribution of bauxite ore, an X-ray diffraction study was carried out. The diffraction pattern was recorded from 10^0 - 80^0 (2θ) with a step size of 0.02^0 by means of Cu Ka (k = 1.542 Å) as a radiation source and an operation at 40 kV–30 mA. The sharp peak at different 2θ positions indicated the crystalline structure of the sample. X-ray diffractogram study uncovered the mineral richness like gibbsite, and hematite with concurrence of cristobalite, and quartz that are identified by their d-spacing (Å) and position (2θ) (Fig. 5.4). The intensity of diffractogram peak together with their corresponding inter planner spacing (d spacing) was calculated and matched with theoretical values from the Joint Committee on Powder Diffraction Standards-International Centre for Diffraction Data

(JCPDS-ICDD) database. An abundance of gibbsite (Al $(OH)_3$) (JCPDS card no. 01-0264) and hematite (Fe_2O_3) (JCPDS Card No. 13-0534) in sample, was strongly revealing the laterization of bauxite formation (Sahoo et al. 2017; Balabantaray et al. 2020). High amount of gibbsite (Al $(OH)_3$) structurally made the bauxite ore monoclinic, while hematite was accountable for its rhombohedral lattice. The presence of quartz (JCPDS card no. 83-2469) and cristobalite (JCPDS card no. 75-1544) commonly known as silicon oxide (SiO_2) also held responsible for its diversified crystal (hexagonal and cubic) structure.

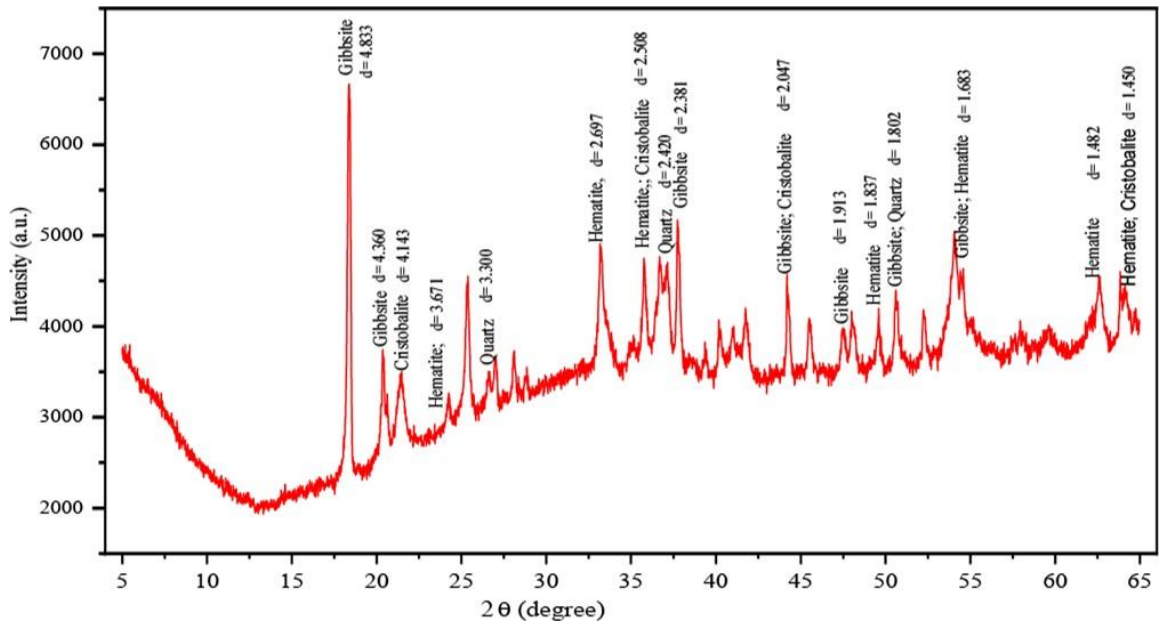

Fig. 5.4. Phase analysis detect diffraction peaks indicating dominant presence of hematite (Fe_2O_3), quartz, and gibbsite [Al $(OH)_3$].

5.3.3. Metallic constituents of bauxite ore and forest soil

Soils are the natural reservoir of metals and metalloids. A large part of metallic contaminants is released due to anthropogenic activity. They can exist from easily leachable to recalcitrant forms on account of critical interaction with the soil matrix. Thereby total concentration of metal is not sufficient to provide a comprehensive index for assessing their impact on soil ecophysiology (Sahoo et al. 2010). The acidic nature of bauxite mines has an immense influence on the mobility of metallic pollutants. Trace elements are relatively more soluble at acidic pH conditions due to their lower adsorption and high desorption capacity. A minute change in the pH values can have a large impact on metal leachability (Krol et al. 2020). The total concentration of elemental profile is represented in Table 5.1. The observed data showed an elevated total concentration of potentially toxic metals (PTMs) viz Cr, Cd, Pb, Ni,

at mine overburden while micronutrients like Cu, Zn, Fe, and Mn showed more presence in forest soil. The total concentration of metals is unable to evaluate their noxious effect on the ecosystem thus they are seldom strictly correlated to their bioavailability which is understated in maintaining ecological health (Sahoo et al. 2010).

Metal leachability is one of the significant routes of groundwater and aquifer region contamination. A trace but mobile part of metal is way more detrimental to the ecosystem than a high amount of inert part. The mobility and toxicity are largely related to the chemical form of the metal (Tripathi et al., 2014). Toxicity characteristics leaching procedure (TCLP) is the standardized method developed by USEPA used to quantify the mobile part of metal that poses toxicity to the environment. It was employed to determine the migration of the contaminants that accumulate in soil via the leaching process (Zhou et al. 2014). In accordance with leachability studies, it also had a high leaching potential of toxic metals like Pb (mean 10.03 mg/kg), Ni (mean 2.5 mg/kg), and Cr (mean 1.3 mg/kg) (Table 5.2.).

DTPA extractable metal (mostly plant-available) fraction of all heavy metals exhibited poor dynamism (Table 5.1.). It may be due to organic matter that holds metal fractions through an ion-exchange mechanism or by specific adsorption. Mn and Fe since micronutrients projected a higher availability ranging from 1-36 mg/kg and 7-19 mg/kg respectively. Mobility of Fe in humus-rich acidic forest soil might be influenced by its clay texture and humic acid that shows a higher affinity to Fe-oxide thereby altering the toxicity and bioavailability (Kungolos et al.2006). Likewise, Mn becomes more accessible to the plant at lesser pH. The reduced form of Mn (II) remains in a substantial amount in soil solution because of the complexation with organic ligands.

Table 5.2. Presence of PTEs in TCLP leachate and bioaccessibility of PTEs from bauxite ore and soil. Value represents mean ±SE

Metal (mg/L)	TCLP		Bio-accessible			
			Gastric available		Intestine available	
	Bauxite ore	Forest soil	Bauxite ore	Forest soil	Bauxite ore	Forest soil
Cr	1.3 ±0.99	1.5 ±0.65	10.06 ±2.32	59.88±6.78	34.77 ±4.77	71.99 ±11.32
Cd	0.8 ±0.00	2.4 ±0.78	---	---	----	---
Ni	2.5 ±0.087	1.7 ±0.61	7.05 ±1.8	12.95±3.11	7.2 ±1.11	12.41±1.99
Pb	5.8 ±0.67	10.03 ±1.87	11.98 ±3.1	41.51±5.87	9.08 ±1.05	37.88±3.65
Cu	0.43 ±0.08	0.49 ±0.00	6.08 ±1.10	25.59±2.12	17.55 ±3.65	64.91±9.08

5.3.4. Fractionation of Potentially Toxic Metal (PTMs) and their ecotoxicity

The toxicity of metals is largely subjected to their bioavailability and mobility in the environment. Therefore, sequential extraction is the most promising technique to explore the occurrences related to ecotoxicity (Mondal et al. 2017). Total metal content is somewhat unable to provide contamination load and their corresponding influence ecosystem, thus fractionation study offers a precise understanding of their distribution and bio-availability (Bhattacharyya et al. 2008). The particle size of the mine dust is another reason behind the metal mobility, Different metal fractions of the investigated site are given in Fig. 5.5. From the current study, it was evident that oxide bound (OXD) and the residual fractions (RS) are dominant over other fractions except for Cd which was found to be more allied with carbonate bound (CBD) followed by exchangeable phases (EX). Even though Cd content is low compared to others, being in the mobile fraction has more chances to get accessible for soil microflora and easily pass onto the water-soluble phase, thereby conferring toxicity to the food chain (Tripathy et al., 2014). All forms of metals were significantly higher at the bauxite mine/ore, except the oxide and organically bound Fe and Mn which are highest at the forest soil. Among the studied metals Cu, Ni, Cr, and Pb were mostly present in residual fraction, which bears a strong association with the crystalline structure of minerals and is hard to separate. Similar fractional distribution of Pb was described in soils of mining. Cu in the residual fraction was most likely for its chemisorption property or inherent incorporation with clay minerals areas (Forghani et al.,

2015). Residual fraction of Cr was high due to replacement of Fe^{3+} and Al^{3+} by Cr^{3+} in silicate clay mineral. Mn is mainly present in the reducible fraction (Fe &Mn oxide bound) and exceptionally high soil. It is likely the acidic pH of the forest soil where most of the Mn remains in dissolved phases. It is the second most mobile fraction after acid-soluble and exchangeable phases (Yuan et al. 2011). Oxide-bound phases are considered to be reservoirs for heavy metals because of their numerous occurrences as the combination of precipitation, adsorption, surface complex formation, and ion exchange. Metals retained by this phase have a high probability of emerging contamination as they can easily dissociate with changing redox status of soil (Tripathy et al., 2014). The poor organically bound form is possibly due to less amount of organic matter in the bauxite ore because natural organic matter (NOM) and dissolved organic matter (DOM) both are accountable for the deposition and fractional interchanging of heavy metals (Yuan et al. 2011).

Water-soluble (WS) and exchangeable (EX) are the two most fluctuating fractions which impose a significant impact on soil microflora and enzymatic activity. These are the fraction having the most labile union with a solid matrix consequently posing a risk to the environment (Tripathy et al., 2014).

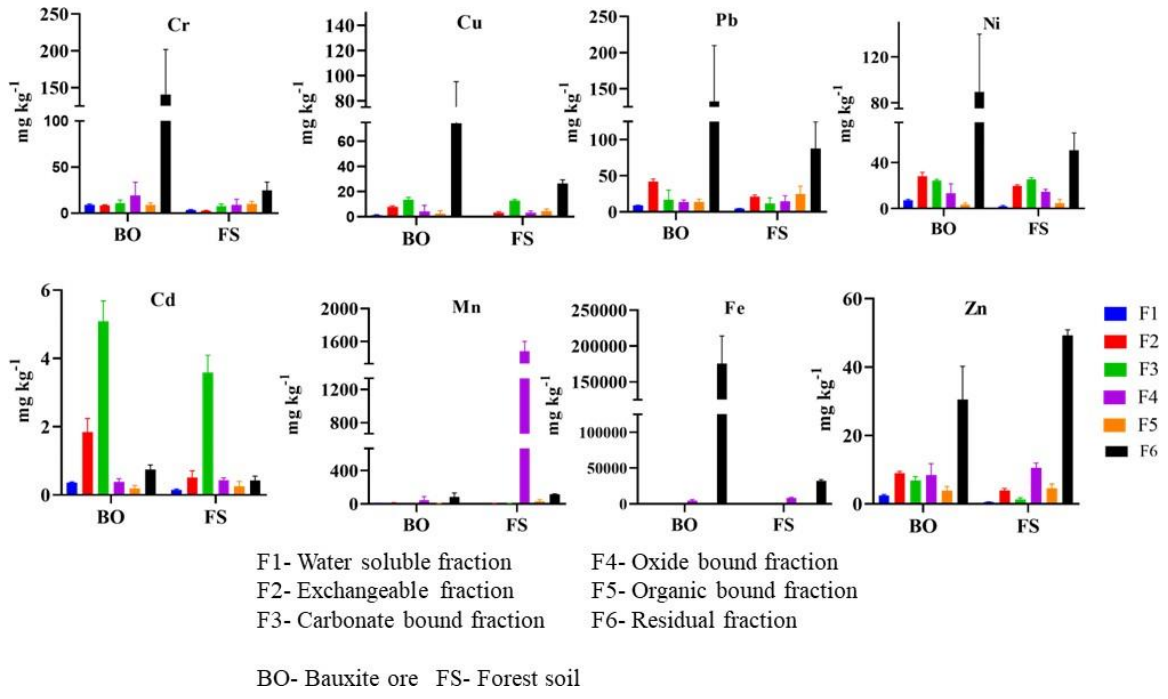

Fig.5.5. Distribution of various metal fractions in bauxite ore and forest soil. Error bars represent standard deviation.

5.3.5. In vitro metal availability

Bioavailability of the inorganic contaminants is responsible for conferring toxicity in living organisms. *In vitro* assay using synthetic gastro-intestinal juices, alternatively, physiologically based extraction test (PBET) provides an apparent view of the bio-accessibility of toxic metals through gastric and gastrointestinal absorption. Although, bio-accessible portions are much less, considering the total concertation which implies that total concentration has the least impact on metals' bioaccessibility. A total of five metals have been checked, out of which Pb, Zn, and Ni showed more bioaccessibility in the gastric phase (GP) compared to the intestine phase (IP) (Table 5.2). This may be due to the acidic pH (1.5) of the gastric juice where metals are more prospective to release, thereby triggering an elevated absorption rate (Han et al. 2020). Relatively high bioaccessibility of Zn and Ni in the gastric phase was also supported by a previous study (Dong et al. 2020). A sharp increase in the pH from 1.5 to 7, reduced the bioaccessibility of Pb from GP to IP because of the high precipitation rate of metal in a neutral to an alkaline environment. The Pb adsorption increased with the rise of pH due to lesser H^+ ions available to compete for the binding site, on the other hand, presence of $NaHCO_3$ in intestinal juice likely contributed to Pb adsorption onto clay edges and give rise to Pb carbonate mineral. The neutral pH of the intestinal juice aid in pepsin precipitation which may be the cause of lowered intestinal availability (Dong et al. 2020). Similar findings of reduction from GP to IP in the case of Pb were reported by a number of researchers, among many of them who found that co-precipitation with Fe and sorption to the amorphous Fe via surface complexation could be a possible reason for decreased intestinal availability. The lowest bioaccessible fraction of Pb in forest soil is consistent with other findings that corroborated the clay fraction exhibits lower bioaccessibility on account of a stable Pb-humus complex attached to clay particles. The observation done by Han et al. (2020) is fairly similar to our observation, which noticed the lowest bioaccessible % of Pb in contaminated sites, which matched with our findings having 9.8% bioaccessibility in bauxite mine while 41.6% in uncontaminated forest soil.

Contrastingly, Cu and Cr showed more bioavailability in the intestinal phase. Such behaviour of Cu is pointing to the formation of a strong complex between organic compounds-Cu at near-neutral pH. Due to the formation of such complex with digestive solutions (bile salt, pancreatin), it exhibited comparatively higher solubility in water (Han et el., 2020). In that same way, Cr showed more intestinal bioaccessibility in a silicon-rich environment. The lower availability of Cr in GP is supported by Kabir et al. (2022) who observed reduced GP fraction

in road dust, which might be due to chromium developing a residual form and not readily absorbed by gastric fluid. Cd did not show any bioaccessibility in our study irrespective of extractant, which diminished the risk of any accidental ingestion of this element**.**

5.3.6. Total Potential Acidity & pH-Dependent Acidity

Total potential acidity (TPA) bearing the largest pool that sums up all fractions of acidity. Along with another form, it as well includes the weakly acidic functional groups associated with organic matter and partly neutralized Al-hydroxyl polymer present even in soil pH >7. TPA value was ranging from 15-55 cmol/kg. The TPA was high in forest soil (mean 49 cmol/kg) and comparatively low in bauxite mine (23 cmol/kg) respectively (Fig. 5.6.a.). High organic matter content of forest soil may be accountable for the elevated concentration of TPA that contributed to TPA through their functional groups like R-COOH and R-OH groups (Sahoo et al 2010).

The subtracted fraction of exchangeable acidity from TPA is stated as pH-dependent acidity (PHD) ranging from 15-50 cmol/kg thus occupying a greater proportion towards TPA (Fig. 5.6a). It followed the same manner as TPA, which was high in forest soil (47 cmol/kg) followed by mine soil (24.1 cmol/kg). A high proportion of the acidity pool contributed by PHD might be due to the higher value of pH-dependent charges that are linked with elevated concentrations of Fe and Al- oxide accompanied by the high amount of organic matter (Sanyal, 1991).

5.3.7. Total Acidity & Exchangeable acidity

Total acidity (TA) varied from 0.22 to 6.25 cmol/kg, while the exchangeable acidity (EXA) ranged from 0.2- 2.9 cmol/kg which is much less than TPA and PHD. Following another acidity (TPA & PHD) fraction, TA and EXA were consistently high at the forest soil (mean TA 6.12; EXA 2.4 cmol/kg) bauxite mine (mean TA 0.45 cmol/kg) (Fig. 5.6a). Total acidity specifies the active form of acidity indicating the amount of H^+ and Al^{3+} retained by the adsorptive complex, and projects an unswerving impact on plant and soil microbiota, whereas EXA comprises exchangeable H^+ and Al^{3+} occupied at the permanent charge site of the soil exchange complex (McLean 1965). Increased EXA of forest soil might be due to high organic matter, humic content and clay texture that leads to the strong adsorption of H^+ and Al^{3+} in the exchange site of the clay lattice (Stehouwer 2004). High positive significant correlation between EXA and CEC (r =0 .85 p<0.01) implied the dominant role of organic colloids and mineral exchange sites accountable for making EXA.

Exchangeable Al contributed a significant part of exchangeable acidity ranging from 0.3-0.5 (mean 0.45); 2.5-3.2 (mean 2.8) respectively for bauxite mine and forest soil Fig. 5.6b. EXA showed a highly significant positive correlation (r = 0.95, p<0.01) with exchangeable Al^{3+} inferring the dominant role of aluminum in making EXA in soil. At lower pH usually below 5 or 4.5, aluminum exists as Al^{3+} and basic cations that are adhered at the exchange site are replaced by Al^{3+} and H^{+} which can further hydrolyze to produce species like Al $(OH)^{2+}$, Al $(OH)_2^{+}$, Al $(OH)_3$, Al $(OH)_4$ (Sahoo et al. 2010). A positive significant correlation among CEC & exchangeable Al (r = 0.86, p<0.01) supported the competition of soil exchange site between acidic (Al^{3+} & H^{+}) and basic (Na^{2+}, Ca^{2+}, Mg^{2+}, K^{+}) cations. In that way, the highest CEC of forest soil directly influences the presence of the increased amount of exchangeable Al leading to the formation of an organic complex in acidic forest soil (Stehouwer 2004).

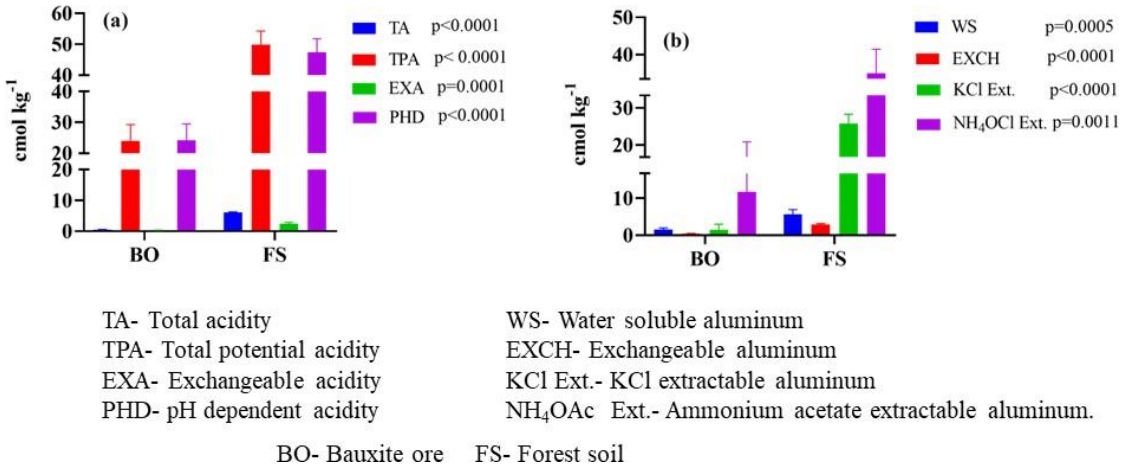

Fig. 5.6. Different fractions of acidity (a) and aluminum (b) in bauxite ore and forest soil. Error bars represent standard deviation.

5.3.8. Extractable Al

Extractable Al is determined by using two extractants i.e., 1(N) KCl and 1(N) NH_4OAc (pH 4.8) by the aluminon reagent method. Aluminum extracted by 1(N) NH_4OAc was a little higher than extraction by 1(N) KCl. KCl extraction usually brings out the leachable aluminum, while the NH_4OAc extraction at pH 4.8 emphasizes exchangeable Al^{3+} and some soluble hydroxyl aluminum monomers and polymers that may be adsorbed by colloidal structure (Sahoo et al. 2010). KCl-aluminon extractable aluminum varied from 0.05-28.86 cmol/kg, however, the NH_4OAc-aluminon extraction ranged from 2.2-44.15 cmol/kg. Fig. 5.6b

presented that a high amount of Al^{3+} has been extracted from forest soil (mean 25.68 KCl; mean 34.85 NH_4OAc) in both KCl & NH_4OAc extraction compared to mine (mean 1.47KCl; mean 11.72 NH_4OAc) while total aluminum was high at bauxite mine 5287 cmol kg^{-1} (Fig. 5.6b). A positive significant correlation of TOC with KCl & NH_4OAc extractable Al^{3+} (r =0.94 & r = 0.82 p<0.01) pointed toward the presence of organic matter making a stable complex thereby justifying the high value of extractable Al^{3+} in forest soil. A stable organo-Al complex is formed under high organic matter content, and cannot be readily extracted by KCl, contrastingly, NH_4OAc (pH 4.8) evidenced a greater extraction of Al^{3+}. The connection between OM and Al^{3+} is previously established by several authors (Pal et al. 2007). A plentiful reason supports this relatedness i.e., mobilized Al re-adsorbed via an insoluble organic complex that can again be desorbed by extraction solution. Low molecular weight organic molecule (e.g., citrate) make a soluble complex with Al and produce an organo-Al complex. The degree of decomposition of organic matter and its content might alter according to soil pH and Al-availability (Sahoo et al. 2010).

5.3.9. Relation between organic carbon and acidity and Al solubility

A negative correlation between pH in H_2O and exchangeable acidity is an indication of a contradictory connection between EXA and pH. On a contrary note, the significant positive correlation between TOC and different acidity fractions viz. TPA (r =0.90), PHD (r =0.88), EXA (r =0.91), TA (r =0.96) unveiled the conspicuous role of organic carbon in formation of acidity, results due to the generation of numerous charges from phenolic and carboxylic group arises from organic matter decomposition (Maison et al., 2000). The association of clay content and organic matter might be responsible for facilitating acidity, which can originate from the mineralization of organic matter on surfaces under subtropical climatic conditions in forest soil (Stehouwer, 2004). Increased acidity and high OM have an immense effect on Al solubility. A significant positive correlation between TOC and a different fraction of Al (Al_{ws} r = 0.90; Al_{Ex} r =0.92; Al_{KCl} r =0.94; Al_{NH4OAc} r =0.82) suggests the bioavailability and toxicity of Al in soil, are regulated on diverse chemical interlinkage with OM. Aluminum is highly reactive in the aqueous phase and interacts with both soluble and insoluble organic molecules with high to low molecular weight. High molecular humic substance retains Al through electrostatic forces. The specific binding site on organic ligands might be another reason for the distribution of Al in OM-rich soil compared to OM-deprived bauxite mine (Maison et al., 2000). The increasing and decreasing manner of ligand controls aluminum solubility by affecting the aluminum ligand complex and its tendency to persist in solution or get precipitated. Al solubility sturdily

depends on reactive Al species, which might have a direct or indirect relation with OM. Although the reactive Al phase occupied a smaller amount and got an easy depletion upon adding a large amount of acid, nevertheless, at below pH 4.1 complexation reaction with OM seemed to control Al^{3+} activity (Maison et al., 2000). The significant positive correlation amidst all forms of acidity viz. TA, EXA, TPA, & PHD acidity with different pools of Al (Fig 5.7), is illustrating that aluminum mobility is directly involved in the acidified condition which is encouraged by interaction with soil OM. In present study, the bauxite mine is deprived of OM thus soluble aluminum was poor in bauxite mine.

TA- Total acidity
TPA- Total potential acidity
EXA- Exchangeable acidity
PHD- pH dependent acidity
WS- Water soluble aluminum
EXCH- Exchangeable aluminum
KCl Ext.- KCl extractable aluminum
NH_4OAc Ext.- Ammonium acetate extractable aluminum.

Fig. 5.7. Correlation plot between different fractions of acidity and aluminum.

5.3.10. FDA Activity

FDA activity has long been regarded as a potential biological indicator to determine soil microbial activity. It is a non-fluorescent, non-polar derivative that is easily transported to the cell, where it has been hydrolysed into polar fluorescein by several enzymes viz. lipase, esterase, protease, that are involved in organic matter decomposition (Tripathy et al., 2014; Nannipieri et al., 2003). Active cells are capable of converting the FDA into fluorescein. When

the cells are unable to hold the fluorescein, it eventually gets out of the cell and is measured spectrophotometrically.

FDA activity was significantly high at the forest site (46.12-65.36 µg/g) than mine site (7-9.6 µg/g) Fig. 5.8. A strong positive linear regression was found between TOC and FDA (R^2=0.903), suggesting a highly significant positive correlation (r= 0.834, p<0.01) between the organic carbon pool and fluorescein released. Similar findings reported by Tripathy et al. 2014 showed that high organic matter and clay content are the two major contributing factors behind higher FDA activity. This strongly indicates that hydrolytic enzymatic actions are greatly associated with organic matter decomposition by microbes. It is evident from Fig.5.9 that acidity does affect enzyme hydrolysis, nonetheless, the high organic carbon content of soil concealed acidity disturbances and thereby exhibited a promising microbial activity. A positive correlation between FDA and TOC inferred that microbial activity was precisely associated with organic carbon and may be partially influenced by the clay texture of the soil, and stabilized by enzyme-organic matter-clay complex (Sahoo et al., 2010). However, the negative correlation between acidity fractions and FDA/OC indicates the saviour role of TOC in soil.

5.3.11. Soil Microbial Biomass-C (MBC)

Soil microbial biomass plays a crucial role in any ecosystem's biogeochemical cycling and nutrient turnover dynamics (Anderson & Domsch, 1990). MBC is recognized as the most sensitive and distinctive parameter to determine soil quality. The MBC varied from 113-589 mg kg^{-1} being high in forest soil (mean 567.74) compared to mine (mean 144.39) site (Fig. 5.8). Regardless of high acidity coupled with lower pH value, a substantial quantity of MBC is attributed due to the high organic matter content of the forest soil. An abundance of numerous substrates from plant sources such as chemicals from root exudates, secondary plant metabolite, lignin, cellulose, hemicellulose content, labile carbon, and nutrient availability encourages microbial decomposition (Schmidt et al., 2011). MBC showed a significant positive correlation with OC (r = 0.96, p<0.01). MBC acts as a living component and provides a sink for nutrients usually occupying 5% of the total OC pool (Anderson & Domsch, 1990). The MBC/OC ratio is an important index to validate any soil quality. Powlson et al., 1987 corroborated that microbial biomass C is a useful index to monitor any significant change in soil organic carbon pool. Precisely, a minute change in biomass carbon provides an early warning of soil quality deterioration. The MBC/OC ratio is significantly and negatively correlated with the different fractions of acidity ana Al^{3+}, representing the deleterious effect of

acidity (Fig. 2b). Perhaps, the high acidity of the soil turns down the substrate utilization efficacy of the microbiota, since more substrate is being utilized for catabolic activity instead of anabolism, resulting in a lower MBC/OC ratio (Pal et al. 2007).

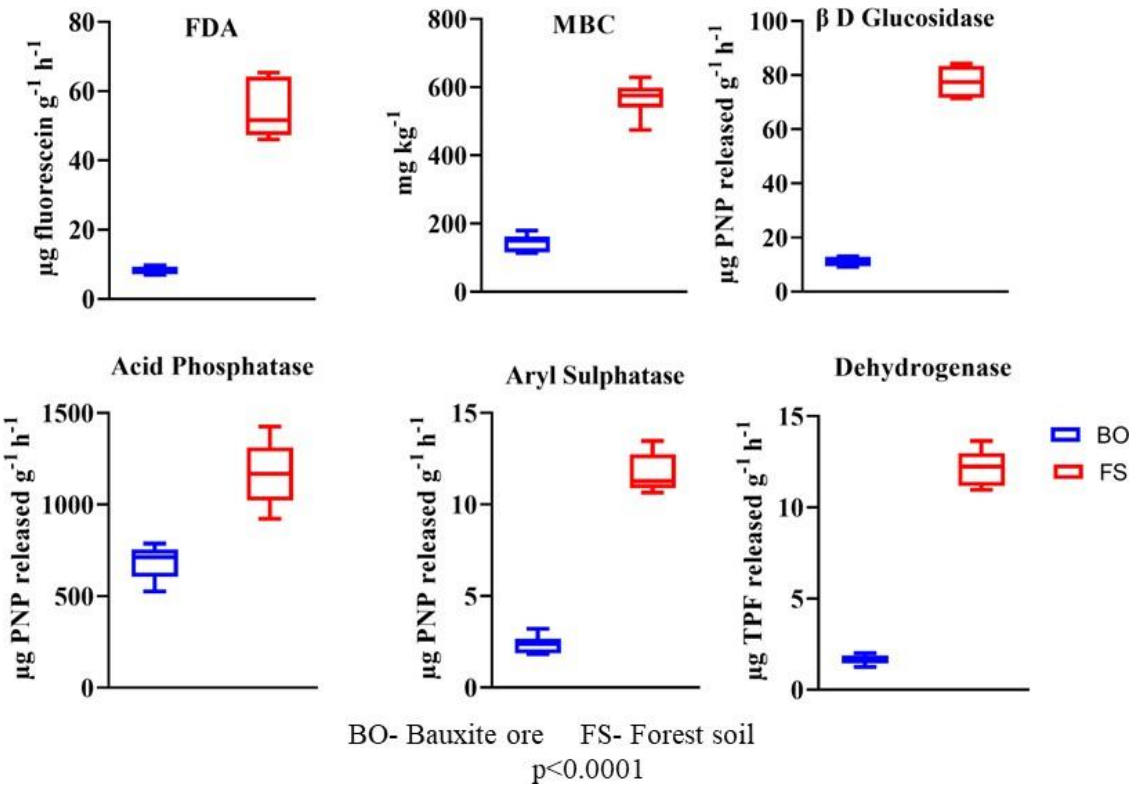

Fig. 5.8. Microbial and biochemical properties of bauxite ore and forest soil. Error bars represent standard deviation.

5.3.12. Enzymatic Activities

Soil enzymatic activities play a pivotal role to explore soil nutrient dynamics. They are the key component of catalytic reactions of organic matter decomposition and nutrient distribution via regulating carbon, nitrogen, and phosphorus turnover (Bueis et al.2018). Microbes are the chief controlling agent of enzymatic regulations; thus, they have the potential to respond to any environmental changes and provide detailed information on enzyme catalytic reactions associated with the biological process. They serve as an indicator of soil health quality. Soil enzymes can be both intracellular and extracellular. Intracellular one is liberated after cell death, and together with extracellular enzymes makes a stabilized organo-mineral complex that remains active for a long period (Nannipieri et al. 2003).

The enzyme activities varied significantly (Fig. 5.8). Enzymes such as phosphatase, β-Glucosidase, and sulfatase are noticeably high in forest soil than in bauxite mines. Dehydrogenase activity in soil is a reliable indicator of a microbial redox system and is accounted as an efficacious measure of microbial oxidative activities in soil (Tabatabai, 1994). They belong to the oxidoreductase group that, oxidizes organic compounds by moving electrons between substrate and acceptors. The enzyme is completely intracellular and does not accumulate outside of the cell (Tabatabai 1994), hence providing a brief index of soil microbial load. The result of the current study showed an enhanced dehydrogenase concentration, indicating a luxurious microbial activity in forest soil ranging from 10-12 mg kg^{-1} (Fig. 4g) The significant positive correlation between soil MBC, TOC, and dehydrogenase ($r_{MBC} = 0.94$; $r_{TOC} = 0.91$, $p<0.01$) activity was stipulating the dominant role of organic matter and labile C pool. Furthermore, a positive linear relationship between TOC and mineralizable N ($R^2 = 0.885$) was reflected in the positive correlations among dehydrogenase activity, TOC and mineralizable N ($r_{TOC} = 0.91$; $r_{min.N} = 0.73$ $p<0.01$), which was validating an elevated microbial activity in soil. Contrastingly, the reduced organic matter, poor mineralizable N, and an elevated concentration of toxic metal might be the prime hindrances behind the poor enzymatic activity in bauxite mines.

Additionally, β-Glucosidase regulates the carbohydrate release in soil, which serves as a prime substrate for soil microorganisms. A positive correlation between soil OC and MBC with β-Glucosidase indicated the advantageous role of soil organic matter (Tripathy et al., 2014). Following the same trend, arylsulfatase and acid phosphatase are significantly and positively correlated with organic carbon at 1% level suggesting a firm association of organic carbon. Acid phosphatase is the only enzyme that shows greater activity with decreasing pH and is affected by organic matter. The large production of acid phosphatase might be due to the procurement of P from organic sources in P-limited conditions of acid soil (Kunito et al. 2016). Therefore, it was portrayed from the result, that expressing enzymatic activity on an rganic carbon basis will deliver a better understanding of soil microbial actions under acidity stress (Sahoo et al. 2010).

Although, all the enzyme activities are significantly and positively correlated, nevertheless the significant negative correlation between enzyme/OC ratio and exchangeable Al and acidity fractions signifies the detrimental effect of labile Al on soil microbial community (Pal et al. 2007) (Fig 5.9).

5.3.13. Relationship between microbial parameters with different forms of aluminum and acidity fraction

From the correlation matrix, (Fig. 5.9) it was evident, that all forms of acidity are significantly and positively correlated with each other expressing a dynamic equilibrium among them. A small change in one fraction can be recovered by another. Alongside, a concurrent positive significant correlation between acidity fractions and different pools of aluminum is revealing the role of Al^{3+}, in the formation of soil acidity (Fig. 5.7). As Al^{3+} is the predominant exchangeable cation of acid soil, and a positive correlation between exchangeable Al^{3+} and exchangeable acidity might be the result of podzolization, where clay hydrolysis causes destabilization of 2:1 lattice and resulting in some Al^{3+} cations into the exchangeable site. The significant positive correlation between acidity and different forms of Al unmasking the offstage performance of Al in making acidity. In spite of high acidity and different soluble Al, an elevated microbial biomass and enzyme activities in soil may be the result of increased organic carbon content. The two antagonistic phenomena are responsible for such contradictory results of this study. Firstly, OC augments the microbial growth in soil, other hand acidity and Al unitedly detain the cellular progress. Here, organic carbon is stabilizing the negative effect of acidity and soluble Al in soil, by precipitating Al as an insoluble composite with organic carbon, producing a humus-enzyme complex that progresses the enzyme steadiness thus defending the microbial development.

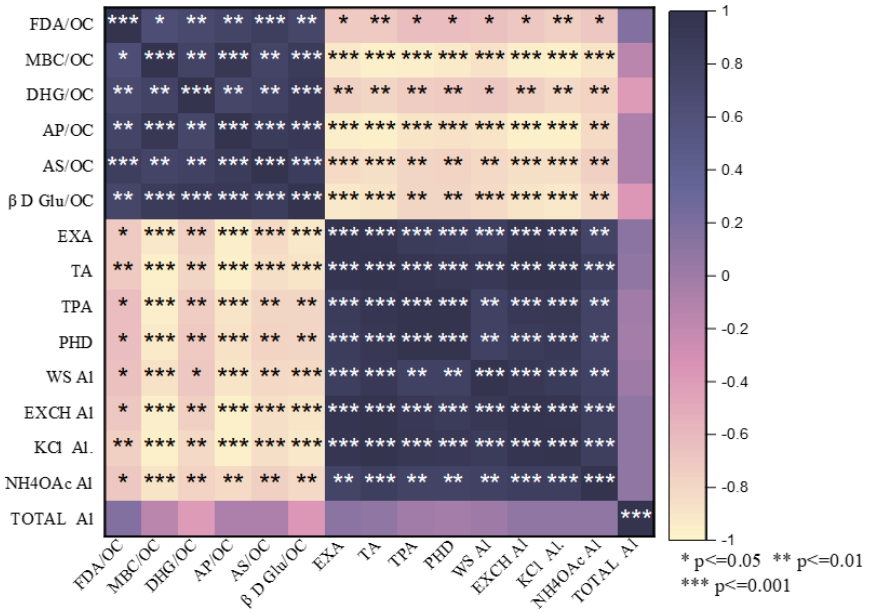

Fig. 5.9. Correlation matrix of microbial parameters/OC with different fraction aluminum (Al^{3+}) and acidity.

5.3.14. Risk assessment

The constant exposure of heavy metals to the environment due to unscientific mine excavation activity and their residual mine overburden increases the risk of contamination several folds. Recurrent subjection of trace elements to human beings has become a life-threatening issue nowadays. The health hazards related to this exposure (ingestion or inhalation or dermal) have been evaluated by a risk assessment study. Table 5.3 represent metal-oriented cancer and non-cancer risk in human subjects including children and adults. The resultant HQ and HI values for the estimation of non-cancerous risk were different for each toxic metal, nonetheless, on a general note, the HQ values for all metals < 1, in adults, were showing no such significant effects on health whereas, the higher HQ and HI i.e., > 1 values for toxic metals like Pb and Cr in children is a matter of concern. Children are the most subtle part of any population to geogenic contamination. Although many studies have previously informed that HQ values of toxic metals for children remain twelve times higher than adults in all land-use areas (Mihankhah, 2020), however, the concurrent exposure of toxic metals like Pb, and Cr might be an alarming health worry due to their comparative high HQ values than other toxic elements. Pb is mostly bioavailable through ingestion when associated with carbonates and Mn-oxides (Ettler et al., 2019), since children have higher digestion capacity, absorption rate, and more haemoglobin sensitivity therefore high intake of Pb leads to develop neurological disorders, improper development, haematopoietic complications, cardio-vascular difficulties etc (Kabir et al. 2022; Mondal et al. 2017). In our study, the maximum HI value was recorded for children for the metal Pb (6.29) followed by Cr (2.2). Pb is high in both sites, while Cr (2.2) crossed its limit only in bauxite mine.

Likewise, the carcinogenic risks (CR) are primely developed by Ni followed by Cr, Pb and Cd. In contrast, the CR of Mn, Zn, Fe and Cu could not be identified due to a lack of slope factor (SF). Total carcinogenic risk (TCR) has been calculated by summation of CR of three different pathways of ingestion, inhalation and dermal, and the value, if, lies between 1.00E-4 to 1.00E-6 considered to be safe according to USEPA. The carcinogenic risk executed by Ni crossed the safer limit in both children and adults bearing the value 4.04E-04 and 7.8E-04 respectively. Following the course, Cr showed TCR of 2.9E-04 for children and 1.4E-04 for adults. Since, the carcinogenic risk of Pb and Cd bears its value within range thereby does not impose such health risks on humans. Additionally, Ni and Cr have already been listed as two strong carcinogens according to International Agency for Research on Cancer (Kabir et al., 2022). So, their constant exposure to the human subject will bring significant alteration in cell

growth and development. Comparing bauxite ore/mine, it can be undoubtedly concluded that, the mine is more contaminated with hazardous elements compared to forest soil indicating a significant risk of continual acquaintance.

Table 5.3. A comparative carcinogenic (ingestion, inhalation, dermal) and non-carcinogenic risk (inhalation, ingestion, dermal) analysis of bauxite ore with respect to soil.

		Adult					Child				
Site	**Metal**	**HQ ingestion**	**HQ inhalation**	**HQ dermal**	**HI**	**CR**	**HQ ingestion**	**HQ inhalation**	**HQ dermal**	**HI**	**CR**
Bauxite ore	Ni	0.028	4.05E-06	0.0004	0.0288	0.000364	0.227	0.0006	0.0024	0.2300	0.000708
	Cd	0.014	2.02E-06	0.0055	0.0192	2.35E-06	0.110	0.0000	0.0307	0.1403	4.7E-06
	Cr	0.244	3.77E-03	0.0488	0.2969	0.000148	1.955	0.0057	0.2737	2.2344	0.000281
	Cu	0.010	1.51E-06	0.0001	0.0104		0.082	0.0000	0.0008	0.0828	
	Mn	0.041	1.94E-02	0.0041	0.0643		0.327	0.0294	0.0229	0.3796	
	Pb	0.781	4.57E-05	0.0083	0.7898	6.68E-05	6.251	0.0001	0.0468	6.2982	9.56E-05
	Zn	0.001	1.49E-07	0.0000	0.0010		0.008	0.0000	0.0001	0.0082	
Forest soil	Ni	0.010	1.36E-06	0.0001	0.0097	0.000122	0.076	0.0002	0.0008	0.0773	0.000238
	Cd	0.003	3.80E-07	0.0010	0.0036	4.43E-07	0.021	0.0000	0.0058	0.0265	8.86E-07
	Cr	0.021	3.21E-04	0.0041	0.0253	1.26E-05	0.166	0.0005	0.0233	0.1902	2.39E-05
	Cu	0.002	3.01E-07	0.0000	0.0021		0.016	0.0000	0.0002	0.0166	
	Mn	0.022	1.04E-02	0.0022	0.0346		0.176	0.0158	0.0123	0.2042	
	Pb	0.149	8.73E-06	0.0016	0.1509	1.28E-05	1.195	0.0000	0.0089	1.2036	1.83E-05
	Zn	0.001	8.89E-08	0.0000	0.0006		0.005	0.0000	0.0001	0.0049	

It’s not only an unhurried destroyer of living creatures but also of the environment. Their cumulative depositions in the environment and likely impact have been assessed by using different pollution indices. Deployed contamination directories confirmed that PI represents the multi-metal contamination potential and the value > 1 indicates the heavy pollution of that substance and their gross metal concentration is above the permissible limit (Kim and Chon 2001). A high PI (>1) of 3.56 of the studied mines, indicated an extensive gross metal concentration compared to forest soil (0.91) (Table 5.4). The geo-accumulation index (I_{geo}) is another important directory that helps to assess soil contamination. The studied bauxite mine site comes under seven geo-accumulation categories, where mine tailing deposition has shown moderate to heavily contamination due to the prevalence of Cd, Mn, Zn, and Cu followed by reclaim and forest soil, and heavy to extremely contaminated due to occurrence of Cr, Pb, and Fe (Fig.7d). Likewise, the contamination index (CI) of native forest soil was reasonably poor due to a lesser amount of Cr, Mn, Zn, Pb, etc. Moreover, the degree of metal concentration was maximum at the bauxite mine. The ecological risk factor (ER) is one more vital attribute of the pollution indices that provide a brief idea about the potential damage caused due to heavy metals. Relative mobility (RM) was also high for bauxite ore compared to soil. The ecological risk index (ERI) provides the cumulative effect of heavy metals in soil. ERI values were illustrated in Table 5.4 which clearly showed an elevated ERI value at bauxite mine overburden (1341-2210) suggesting a high ecological risk due to extensive PTM exposure. This ERI value was considerably low in forest soil (454-525). ERI <300 is suggesting a low to moderated risk, caused due to an average exposure of PTMs, while >600 indicated significant potential risk (Jiao et al., 2015).

Table 5.4. A comparative chart on environment hazard potential of bauxite ore with respect to soil.

Pollution Indices	Bauxite ore	Forest Soil
Relative mobility of Cd	0.85	0.79
Relative mobility of Cu	0.23	0.32
Relative mobility of Cr	0.37	0.27
Relative mobility of Pb	0.52	0.46
Relative mobility of Ni	0.64	0.41
Relative mobility of Mn	0.19	0.01
Relative mobility of Zn	0.3	0.08
Contamination index	473.81	131.12
Pollution index	3.56	0.91
Ecological risk index	1849.56	502.09
Geo accumulation index (I_{geo}) Cu	3.53	1.27
Geo accumulation index (I_{geo}) Cr	4.96	1.5
Geo accumulation index (I_{geo}) Cd	2.89	0.44
Geo accumulation index (I_{geo}) Pb	4.31	1.97
Geo accumulation index (I_{geo}) Ni	7.01	5.46
Geo accumulation index (I_{geo}) Mn	2.64	1.91
Geo accumulation index (I_{geo}) Zn	2.15	1.43

5.3.15. Bauxite ore /mine and forest soil- a contrasting natural phenomenon

As I stated earlier that bauxite ore precisely bauxite mine is geochemically different from soil as their formation process is dissimilar. So, the present study was a detailed evaluation of how much diverse soil can be from rock in terms of their physicochemical and microbial properties. Bauxite mine and soil both were highly acidic primely because of the aluminum. Al toxicity in acid soil and an acidic environment is a major limitation for plant growth, productivity, and microbial diversity, previously established by many authors (Rahman et al., 2018; Wright, 1989trip). Additionally, acidity is another important limitation for microbial growth and proliferation. In present study, both the soluble aluminum and acidity were far higher compared to the bauxite mine, nevertheless, the high organic carbon of soil played a

saviour and protect soil microbial health despite aluminum and acidity stress. Organic carbon/organic matter is a key factor in soil microbial activity. Including, the organic matter is crucial for metal lability. The more organic matter, the less metal availability. Thus, we found a greater metal availability in mine compared to soil. So, lack of organic matter in bauxite mines is a disadvantage, which makes it a threatening factor for environment. Though both are natural formations, yet, mine/rock/ore pose a greater risk towards the environment/ecosystem.

5.3.16. A comparative analysis between native bauxite ore and processed bauxite residue (RM)

After extensive work done on physicochemical, and biological properties of bauxite ore and bauxite residue (RM), I have come up with some exclusive findings (Table 5.5). The conversion is immensely contrasting. Native bauxite ore is extremely acidic (pH 4.2-4.8) while after aluminum extraction it completely converted to a highly alkaline product (pH 10-13). It is due to the Bayer extraction process where caustic soda is used and subsequently dumped as by-product after incomplete wash, thus making the residue sodic. The other cations like K^+, Mg^{2+}, Ca^{2+} get a considerable increment. Concerning metallic contaminants, the total metal content is much higher in both products, however, the leaching of metal (TCLP) is more in the residue. The fractionation infers that metals are more mobile in acidic bauxite mine compared to bauxite residue. This is due to high alkalinity of bauxite residue that barely tends to form soluble phosphate or carbonate, while in acidic conditions they exist in available ionic forms (Adamczyk-Szabela & Wolf, 2022). The presence of organic carbon is more or less poor in both, however, in terms of microbial characteristics (enzyme activity, MBC, FDA) the bauxite ore is relatively better compared to bauxite residue. Such high sodicity and alkalinity are the leading hindrances of microbial activity. The structural alteration also takes place after Bayer treatment elucidated from FESEM micrograph and X-ray diffractogram study. The native ore is irregularly flaky-shaped aggregated, while after extraction, it becomes slightly amorphous, some angular or round shaped structures were also found, while XRD reveales that, it partially loses its typical crystalline nature after processing and becomes slightly amorphous. Lastly, the bauxite residue is more dispersive and has extremely poor water retention ability, which is another fatal concern for environment. In terms of pollution load, both pose a considerable threat toward the environment/ ecosystem.

Table 5.5. A comparative chart on chemical and biological characteristics of bauxite before and after alumina extraction (bauxite ore and bauxite residue).

Chemical characteristics	Red Mud	Bauxite ore
pH	11.5	4.48
EC (mS/cm)	12.2	0.6
TOC %	0.22	0.27
Available Na	7990.04	13.09
Available K	196	9.49
Available Ca	2426.65	7.47
TCLP-Cr	8.2	1.3
TCLP-Cd	0.89	0.8
TCLP- Ni	3.2	2.5
TCLP-Pb	7.2	10.03
TCLP- Cu	4.9	0.43
DTPA-Cr	3.89	0.6
DTPA- Cd	0.78	0.01
DTPA- Ni	2.08	1.28
DTPA Pb	4.76	2.08
DTPA-Cu	3.45	0.8
Microbial characteristics	**Red Mud**	**Bauxite ore**
FDA (µg/g/hr)	4.95	8.15
MBC (mg/kg)	------	144.38
Dehydrogenase (µg TPF /g/hr)	0.96	1.65
glucosidase (µg PNP /g/hr)	8.34	11.02
Aryl sulphatase (µg PNP /g/hr)	1.3	2.36
Phosphatase (acid/alkaline) (µg PNP/g/hr)	74	685.56

5.4. Conclusion

This study provided a clear view of bauxite ore, and how it is different from soil in terms of physicochemical and microbial properties. The ore is immensely poor in organic matter content and other microbial and enzyme activity. It also has less acidity than soil but concerning metal concentration, toxic metal like Cd, Cr, Pb, and Ni, were high while micronutrient concentration viz., Cu, Zn, Mn, and Fe was in moderate difference with soil. As a result, the bauxite mine damages the environment and has a higher pollutant load than soil. The DTPA available micronutrient Fe, Mn in soil, while the leaching fraction (TCLP) was greater in the bauxite mine. Lastly, from a comparative analysis perspective, bauxite ore faced a huge alteration in terms of its chemical and biological characteristics after aluminum

extraction. The bauxite ore and bauxite residue both bear an entirely dissimilar characteristic which narrated the adverse role of using high amounts of NaOH during aluminum production and the subsequent negligence of industries for their improper waste management strategy.

Chapter 6

Assessment of microbial diversity in red mud: A search for metal detoxifying alkaliphilic microorganism

Chapter 6

Assessment of microbial diversity in red mud: A search for metal detoxifying alkaliphilic microorganism

6.1. Exploring the biological characteristics of red mud (RM)

6.1.1 Introduction

Very little is known about the biological properties of bauxite leftovers. Due to its harsh characteristics, it is almost barren. According to many authors, fresh bauxite residue or red mud (RM) deposits have no biological characteristics because Bayer's technology operates at extremely high temperatures and pressures with high amounts of NaOH (Dey, 2021). As a result of which, it does not exhibit any biological characteristics instantaneously. Despite high soda content, they are very different from samples of naturally occurring soda lakes, including the Lonar and Sambhar Lakes in India, where the pH ranges from 9 to 12 and the salinity is high. High alkalinity, Na-concentration, presence of toxic metal is the major fence of biological activity in RM. Insufficient information is provided about enzymatic activity, microbial activity, or establishment of vegetation of disposal. In general, microorganisms are an important and largest community in soil, familiar to undertake a wide range of tasks, such as biogeochemical cycling, energy flow, matter circulation, decomposition of plant residue, plant growth promotion, bioremediation and balancing ecosystem thus their scantiness is alarming (Caravaca et al., 2002; Ke et al., 2021). As mentioned before, the alkaline-sodic characteristic of RM is the prime constraint of biological activity, thereby it lacks soil properties. Another piece of evidence in support of biological properties is enzymatic activity (alkaline phosphatase, dehydrogenase, fluorescein diacetate hydrolyzing activity) which approves the sustenance of microorganisms. Reports on the enzymatic activity and other microbial properties, diversity, and community abundance of RM are scanty, however, a few researchers reported on a trace amount of enzymatic activity such as FDA, alkaline phosphatase, β-D-glucosidase with long disposal history (Mishra & Pandey, 2019; Dey & Paul, 2021). Nevertheless, immediately disposed of RMs are devoid of microbial activity; if so, the occurrence is rare. It is only after storage, human intervention, rehabilitation, transportation, etc. that microbial activity is expected to occur (Banning et al., 2011).

Generally, early colonization of microbes is surprising due to their poor organic matter content, high alkalinity, high sodicity, and presence of toxic metals (Cr, Ni, Pb, Cd, Hg, As, V, Cu, Th, U), poor water retention ability, yet, a chance of heterogenous assemblage of genetical and functional diversity of microbes likely to occur because of its extreme physicochemical nature. Microbial colonization that evolves within a short span of dumping is generally oligotrophic metal tolerant and mostly belongs to *Chitinophagaceae, Beijerinckiaceae, Xanthomonadaceae*, and *Acetobacteraceae*. Joshi et al. (2008) and Tiago et al. (2004) reported in their studies that numerous alkaliphilic bacteria are prevalent and can be found in both naturally sodic-alkaline environments and artificially hyper-alkaline environments. The present state of the art emphasizes indigenous alkaliphilic/ extremo-alkaliphilic organisms which have a widespread application in different biotechnological/industrial fields. Including they can be used for contaminated site reclamation, waste valorisation, wastewater treatment, etc. thus gaining importance. Hence, studies on the diversity and community structure of the extreme environment, and waste dump sites, have a chance to light on indigenous extremophiles that has a prospect in pollution mitigation.

RM is slowly weathered with age and generates mud and dust particles, also the leaching of metals, cations (Na^+, K^+, Ca^{2+}, Mg^{2+}), and anions (Cl^-, CO^{3-}, HCO^{3-},) occurs due to rainfall to which gradually lightens their alkalinity. All these things make a soil-like layer on top of it which allows natural vegetation (mostly plant grows in extreme habitat and alkali tolerant) like *Lolium perenne, Fescue longifolia*, *Holcus lanatus* (Mishra & Pandey, 2019). Plant growth and vegetation promote microbial activity in their rhizospheric zone which gradually recovers these ecological calamitous environments. These rhizosphere harbouring microorganisms are inherently alkaliphilic, metal resistant, and tolerate high pH and a good concentration of Na (Dey & Paul, 2021). In general, many microbes are well-organic acid producers, concerning their alkaliphilic nature they could have the ability to produce organic acid which can neutralize RM by lowering the pH. In addition to that, they can produce secondary metabolites which enhance the organic matter generation and may lead to harbour micro-eukaryotes which can help to improve the physical structure of bauxite residue (Ke et al., 2021).

Moreover, microbially-driven policies for waste management are more successful when using native microbial communities in contaminated sites since they easily thrive in harsh environments owing to their unique metabolisms developed through natural selection (Ma et al., 2019; Sajjad et al., 2020). Additionally, microorganisms are quite familiar with their

composite machinery and respond strongly during any environmental fluctuations compared to axenic culture. A next-gen-based metagenomic study is an efficient tool to explore the community dynamics of the target site associated with ecological process/restoration (Macías-Pérez et al., 2022). Focusing on the need for microbe-assisted waste management, a present study carried out a metagenomic study on red mud to find out the diversity and abundance of pioneer species which could be used for bioremediation purposes. To date, studies concerning bauxite residue or red mud primely focused on isolating single species and their potential use, here, we adopted the two approaches i.e., culture-dependent and culture-independent methods using molecular technology to get the idea of microbial diversity and potent microbe for wastewater treatment. The culture-dependent study was done in search of novel alkaliphiles with poly-extremophilic characteristics useful for metal sequestration from wastewater while the culture-independent metagenome-based study was focused on microbial communities involved in ecological restoration process overlooking their active participation in the process.

6.1.2. Material and Methods

6.1.2.1. Sample collection and processing

The red mud sample used for this study was collected from HINDALCO alumina plant, Muri, Jharkhand. Sample collected from different disposal histories. Field moist sample was collected in a sterile zip lock and brought to the laboratory and kept at -20^{0}C for subsequent analysis.

6.1.2.2. Enzymatic analysis

A. Estimation of phosphatase activity of sample (RM) (Tabatabai 1994):

Principle of the method:

The method is based on the determination of p-nitrophenol released after the incubation of soil with p-nitrophenyl phosphate for 1h at 37^{0}C.

Reagents:

1. Toluene
2. Modified Universal Buffer (MUB) stock solution.
3. 3.025gTris, 2.9g maleic acid, 3.5g citric acid and1.575g boric acid were dissolved in about 125ml 1 (M) NaOH and diluted to 250ml with distilled water.

4. MUB, pH 6.5 [or 11]: 100ml of MUB stock solution was titrated to pH 6.5 [or11] with 0.1 (M) HCl [or 0.1(M) NaOH] and diluted to 500ml by distilled water.
5. p-nitrophenyl phosphate solution, pnpp [0.115 (M)]: 1.067g of p-nitrophenyl phosphate, hexahydrate was dissolved in 20ml MUB (pH 6.5 / 11) and brought up to 25ml with buffer of the same pH.
6. $CaCl_2.2H_2O$, 0.5 (M): 18.375g of $CaCl_2.2H_2O$ was dissolved in 250ml of distilled water.
7. NaOH, 0.5(M): 5g NaOH was dissolved in 250ml of distilled water.
8. Standard p-nitrophenol solution: 0.1g p-nitrophenol was dissolved in about 70ml of distilled water and diluted to 100ml with distilled water and stored at 4^0C.

Procedure:

The samples were examined in triplicate, and the average of the three results was calculated. A 50-ml Erlenmeyer flask containing 1g of sample (either soil or compost) was treated with 0.25ml of toluene, 4ml of MUB (pH 6.5/11), and 1ml of pnpp solution produced in the same buffer. The flasks' contents were combined and then incubated at 370C for an hour after being stoppered. Following the incubation, 4ml of 0.5(M) NaOH and 1ml of CaCl2 were added. Filter paper, Whatman No. 42, was used to combine and filter the contents. At 400 nm, the absorbance was measured. Before filtering the soil suspension, 1ml of pnpp solution was added, along with 1ml of 0.5 (M) CaCl2 and 4ml of 0.5 (M) NaOH, to perform the controls.

Calibration curve:

In a volumetric flask, distilled water was used to dilute 1ml of the standard p-nitrophenol solution to 100ml. Following that, aliquots of this diluted standard solution of 0, 1, 2, 3, 4, and 5 ml were pipetted into Erlenmeyer flasks (50 ml). The volume was increased by adding distilled water to make it 5ml. Then each flask received 4ml of 0.5 (M) NaOH and 1ml of 0.5 (M) CaCl2. Contents were thoroughly combined, filtered, and shaken briskly. At 400 nm, absorbance was measured.

Calculation:

Phosphatase activity (μg p-nitrophenol released/g oven dry sample/h at 37^0C)

$$= \frac{C \times V}{d_{wt} \times SW \times t}$$

Where,

C = Measured concentration of p-nitrophenol (μg/ml filtrate);

d_{wt} = Oven dry weight of 1g sample;

V = Total volume of the sample suspension (ml);

SW = The weight of the sample used (1g);

t = The incubation time (1hour).

B. Estimation of β-D-glucosidase activity (Tabatabai, 1994)

Principle of the method:

The method is based on the determination of p-nitrophenol released after the incubation of soil with p-nitrophenyl phosphate for 1h at 37^0C.

Reagents:

1. Toluene
2. Modified Universal Buffer (MUB) stock solution: 3.025gTris, 2.9g maleic acid, 3.5g citric acid and1.575g boric acid were dissolved in about 125ml 1 (M) NaOH and diluted to 250ml with distilled water.
3. MUB, pH 6: 100ml of MUB stock solution was titrated to pH 6 with 0.1 (M) HCl
4. p-nitrophenyl β-D glucopyranoside -solution, (PNG) [0.115 (M)]: 0.377 of PNG was dissolved in 40ml MUB (pH 6) and brought up to 50 ml with the buffer of the same pH.
5. $CaCl_2.2H_2O$, 0.5 (M): 18.375g of $CaCl_2.2H_2O$ was dissolved in 250 ml of distilled water.
6. NaOH, 0.5(M): 5g NaOH was dissolved in 250 ml of distilled water.
7. Standard p-nitrophenol solution: 0.1g p-nitrophenol was dissolved in about 70ml of distilled water and diluted to 100ml with distilled water and stored at 4^0C.

Procedure:

The samples were examined in triplicate, and the average of the three results was calculated. A 50-ml Erlenmeyer flask containing 1g of sample (either soil or compost) was treated with 0.25ml of toluene, 4ml of MUB (pH 6), and 1ml of png solution produced in the same buffer. The flasks' contents were combined and then incubated at 37^0C for an hour after being stoppered. Following the incubation, 4ml of 0.5(M) NaOH and 1ml of CaCl2 were added. Filter paper, Whatman No. 42, was used to combine and filter the contents. At 400 nm, the absorbance was measured. Before filtering the soil suspension, 1ml of png solution was added, along with 1ml of 0.5 (M) $CaCl_2$ and 4ml of 0.5 (M) NaOH, to perform the controls.

Calibration curve:

In a volumetric flask, distilled water was used to dilute 1ml of the standard p-nitrophenol solution to 100ml. Following that, aliquots of this diluted standard solution of 0, 1, 2, 3, 4, and 5 ml were pipetted into Erlenmeyer flasks (50 ml). The volume was increased by adding distilled water to make it 5ml. Then each flask received 4ml of 0.5 (M) NaOH and 1ml of 0.5 (M) CaCl2. Contents were thoroughly combined, filtered, and shaken briskly. At 400 nm, absorbance was measured.

Calculation:

Glucosidase activity (μg p-nitrophenol released/g oven dry sample/h at 37^0C)

$$= \frac{C \times V}{d_{wt} \times SW \times t}$$

Where,

C = Measured concentration of p-nitrophenol (μg/ml filtrate);

d_{wt} = Oven dry weight of 1g sample;

V = Total volume of the sample suspension (ml);

SW = The weight of the sample used (1g);

t = The incubation time (1hour).

C. Estimation of sulphatase activity (Tabatabai,1994)

Principle of the method:

The method is based on the determination of p-nitrophenol released after the incubation of soil with p-nitrophenyl phosphate for 1h at 37^0C.

Reagents:

1. Toluene
2. Acetate Buffer solution: 68g sodium acetate trihydrate was dissolved in about 700ml of dH_2O and adjust the pH 5.8 with concentrated acetic acid. Finally, volume brought upto1000 ml.
3. p-nitrophenyl sulphate solution, (PNS) [0.25mM)]: 0.312 of PNG was dissolved in 40ml acetate buffer (pH 5.8) and brought up to 50ml with buffer of the same pH.
4. $CaCl_2.2H_2O$, 0.5 (M): 18.375g of $CaCl_2.2H_2O$ was dissolved in 250ml of distilled water.
5. NaOH, 0.5(M): 5g NaOH was dissolved in 250ml of distilled water.
6. Standard p-nitrophenol solution: 0.1g p-nitrophenol was dissolved in about 70ml of distilled water and diluted to 100ml with distilled water and stored at 4^0C.

Procedure:

The samples were examined in triplicate, and the average of the three results was calculated. A 50-ml Erlenmeyer flask containing 1g of sample (either soil or compost) was treated with 0.25ml of toluene, 4ml of acetate buffer (pH 5.8), and 1ml of pns solution produced in the same buffer. The flasks' contents were combined and then incubated at 37^0C for an hour after being stoppered. Following the incubation, 4ml of 0.5(M) NaOH and 1ml of CaCl2 were added. Filter paper, Whatman No. 42, was used to combine and filter the contents. At 400 nm, the absorbance was measured. Before filtering the soil suspension, 1ml of pns solution was added, along with 1ml of 0.5 (M) CaCl2 and 4ml of 0.5 (M) NaOH, to perform the controls.

Calibration curve:

In a volumetric flask, distilled water was used to dilute 1ml of the standard p-nitrophenol solution to 100ml. Following that, aliquots of this diluted standard solution of 0, 1, 2, 3, 4, and 5 ml were pipetted into Erlenmeyer flasks (50 ml). The volume was increased by

adding distilled water to make it 5ml. Then each flask received 4ml of 0.5 (M) NaOH and 1ml of 0.5 (M) CaCl2. Contents were thoroughly combined, filtered, and shaken briskly. At 400 nm, absorbance was measured.

Calculation:

Sulphatase activity (μg p-nitrophenol released/g oven dry sample/h at 37^0C)

$$= \frac{C \times V}{d_{wt} \times SW \times t}$$

Where,

C = Measured concentration of p-nitrophenol (μg/ml filtrate);

d_{wt} = Oven dry weight of 1g sample;

V = Total volume of the sample suspension (ml);

SW = The weight of the sample used (1g);

t = The incubation time (1hour).

D. Estimation of fluorescein diacetate hydrolyzing activity (FDA) (Schnurer and Roswall 1982)

Principal of the method:

The method is based on estimation of fluorescein produced in soil treated with fluorescein diacetate solution and incubated at 24^0C.

Reagents

1. Sodium orthophosphate buffer (60mM, pH 7.6)- Adjust to 7.6 with HCl
2. Acetone
3. Fluorescein diacetate solution (2mg/ml)
4. Fluorescein standard solution (5mg/ml)

Procedure

1g sample is placed in 50 ml conical flask treated 25ml phosphate buffer, then FDA added and the mixture incubated in a rotary shaker for 3 hr. After 3hr of incubation reaction is

stopped adding acetone to reach a final concentration of 50%. The suspension was then filtered and measured at 490 nm.

Calibration curve

It was prepared by taking 0.1, 0.2, 0.4, 0.6, 0.8, 1, 1.5 ml of 1000ppm fluorescein. It was diluted to 10 ml with acetone (10,20,40,60,80, 100, 150). 1ml of this solution was taken and mixed with 24ml buffer and 25 ml acetone, filtered and OD taken at 490nm.

Calculation:

FDA activity (μg p-fluorescein released/g oven dry sample/h at 37^0C)

$$= \frac{C \times V}{d_{wt} \times SW \times t}$$

Where,

C = Measured concentration of fluorescein (μg/ml filtrate);

d_{wt} = Oven dry weight of 1g sample;

V = Total volume of the sample suspension (50 ml);

SW = The weight of the sample used (1g);

t = The incubation time (3hour).

E. Estimation of dehydrogenase activity (Casida et al., 1964)

Principle of the method:

The method is based on estimation of triphenyl formazan (TPF) released after the incubation of soil with triphenyl tetrazolium chloride (TTC) for 24hr at 37^0C.

Reagents

1. Calcium carbonate
2. 2,3,5, - triphenyl tetrazolium chloride
3. Triphenyl formazan
4. Methanol

Procedure

10g soil was mixed with 0.1g CaCO3 thoroughly. A 6g soil mixture was accurately weighed and taken in a test tube. 1 ml of 3% TTC was added to the soil followed by the addition of 2.5 ml of water. The test tube was properly sealed with a stopper and incubated at 37^0C for 24 hr. The TPF was extracted and filtered with methanol. The filtrate was collected in a 100 ml. volumetric flask. And additional methanol was added till the disappearance of the reddish colour. The volume was made up to 100 ml. and the colour intensity was examined at 485nm spectrophotometrically.

Calibration curve

A 100µg/ml of TPF in methanol was prepared and preserved in a refrigerator in dark. On the day of work, the stock solution was diluted to give 5, 10, 20, and 40 µg/ml of TPF in methanol. The absorbance of the individual dilution was noted and standard was prepared by taking OD.

Calculation:

Dehydrogenase activity (µg TPF/g oven dry sample/h at 37^0C)

$$= \frac{C \times V}{d_{wt} \times SW \times t}$$

Where,

C = Measured concentration of p-nitrophenol (µg/ml filtrate);

d_{wt} = Oven dry weight of 1g sample;

V = Total volume of the sample suspension (100ml);

SW = The weight of the sample used (6g);

t = The incubation time (1day).

6.1.2.3. Taxonomic diversity analysis

25 ng of DNA was used to amplify 16S rRNA hypervariable region V3-V4. The reaction includes KAPA HiFi Hot Start Ready Mix and 100 nm final concentration of modified 341F and 785R primers. The PCR involved an initial denaturation of 95°C for 5 min followed by 25 cycles of 95°C for 30s, 55°C for 45s, and 72°C for 30s, and a final extension at 72°C for

7 min. The amplicons were purified using Ampure beads to remove unused primers. Additional 8 cycles of PCR were performed using Illumina barcoded adapters to prepare the sequencing libraries.

V3-V4 primer sequences---(Primer sequence 5→3)

V3V4F: CCTACGGGNGGCWGCAG

V3V4R: GACTACHVGGGTATCTAATCC

The sequence data was generated using Illumina MiSeq. Data quality was checked using FastQC and MultiQC software.

- Data Analysis

The reads were trimmed (20bp) from 5' end to remove the degenerate primers. The trimmed reads were processed to remove adapter sequences and low-quality bases using Trimgalore. The QC passed reads were imported into Mothur and the pairs were aligned with each other to form contigs. The contigs were screened for errors and only those between 300bp and 532bp were retained. Any contig with ambiguous base calls was rejected. The high-quality contigs were checked for identical sequences and duplicates were merged. Although the primers for the experiment were designed for 16s bacterial rRNA, there are good chances for non-specific amplification of other regions. To correct this, we align the contigs to a known database for 16s rRNA. Depending on the variable region being amplified, most of the contigs will align to its respective region on the database. Any ambiguous contigs aligning with other regions on the database were discarded. After this process, the gaps and the overhang at the ends from the contigs were removed and processed for chimera removal which may have formed due to pcr errors. UCHIME algorithm was used to flag contigs with chimeric regions. A known reference of all the chimeric sequences was used to identify and remove possible chimeric sequences. The filtered contigs were processed and classified into taxonomical outlines based on the GREENGENES v.13.8-99 database. The contigs were then clustered into OTUs (Operational Taxonomic Unit). After the classification, OTU abundance was estimated.

6.1.2.4. Isolation, identification, and characterization of alkaliphilic metal tolerant microbe

A. Isolation of bacterial strain from red mud slurry:

An alkaline-specific Hori Koshi (HK) medium (pH10.5) was used for microbiological purposes. The reagents were obtained from Hi-media laboratories, Merck, Sigma-Aldrich,

Invitrogen etc. The bacterial strain was isolated using HK medium through an enrichment technique followed by the spread plate method. The inoculated plates were incubated at 30^0C for 48-72 hours. At the end of incubation, the discrete colonies were picked up for preservation and also subjected to morphological, biochemical and molecular characterization. The isolation process was carried out in triplicates. Individual colony appeared on the plate were counted following eqatiuon.

$$Colony\ formig\ unit(CFU)perg\ of\ sample = \frac{No.of\ colonies\ per\ plate\ X\ dilution\ factor}{V}$$

Where V is the volume (ml) of diluted sample spread on the culture plate. Finally, the culture was preserved at 4^0C and maintained by a monthly subculturing technique during the study.

B. Identification of the bacteria

Out of the twenty colonies found on the plate, five isolates had been selected based on their unique extremophilic characteristics as RM1, RM5, RM6, RM16 and RM20. All twenty isolates were examined by their gram characteristics and followed by biochemical characterization viz. carbohydrate fermentation, citrate utilization, arginine production, ONPG, methyl red/Voges Proskauer test according to Bergey's Manual of Determinative Bacteriology.

C. Growth parameters optimization

To explore and optimize their favourable growth condition, the one factor at a time (OVAT) technique was chosen to check the effect of culture conditions such as pH (4-13), temperature (20^0C-55^0C), and NaCl concentration (10%-35%) affecting bacterial growth. The experiment was carried out by using glucose-yeast extract-peptone (GYP) broth inoculated with exponential phase culture and incubated for 48 hours. After incubation optical density was taken at 600 nm to evaluate the best growth condition for the culture.

D. Selection of the isolate based upon Minimum inhibitory concentration (MIC)

Three potentially toxic metals had been chosen for the study viz. Cd^{2+}, Cr^{6+}, and Ni^{2+}. The stock solution of the metal had been prepared by using its precursor salt. Cd^{2+} from Cd $(NO_3)_2$, Cr^{6+} from $K_2Cr_2O_7$, and Ni^{2+} from Ni $(NO_3)_2$. Apart from that tolerance to arsenic As^{3+} and Cu^{2+} were also checked by using their precursor solution obtained from salt sodium arsenite ($NaAsO_2$) and Cu $(NO_3)_2$. These metal stock solutions were added to the glucose -yeast extract-peptone (GYP) agar plate (broth dilution method) with varying concentrations ranging from 50 mg L^{-1} to 3500 mg L^{-1}(Yang et al., 2020). Approximately 1x 10^6 CFU/ml cells were inoculated and kept for 48 hours at 30^0C. After incubation, the growth of the isolates was confirmed by

measuring optical density at 600nm. Alongside, the isolate also went for molecular characterization.

E. Molecular characterization

- **Isolation of genomic DNA**

Genomic DNA was isolated by following the standard protocol (Sambrook & Russel, 2001). The exponential phase culture (OD ≥1 at 600 nm) was harvested to get the pellet which was lysed by a lysis buffer (Glucose- 20%, Tris-50 mM, and EDTA-50 mM), followed by lysozyme treatment at 37^0C for 30-40 minutes. Thereupon, the extraction was accomplished using 10% SDS for 1-2 hours at 37^0C and was completed by using an equal volume of PCI (Phenol: Chloroform: Isoamyl alcohol). Finally, the lysate was subjected to ethanol treatment to precipitate the DNA and dissolved in 30 µl TE (Tris: EDTA buffer). The DNA obtained by the procedure was evaluated for its quality checking using 1% agarose gel electrophoresis.

- **PCR amplification of 16SrDNA**

The fragment of 16SrDNA gene was amplified by using 27F and 1492R primers. When resolved on Agarose gel, a single discrete PCR amplicon band of 1500 bp was observed. The PCR amplicon was purified for the removal of contaminants. Subsequently, the gel purified amplicon was sequenced by commercial sequencing at Eurofins, genomics, Hyderabad, using BDT v3.1 Cycle sequencing kit on ABI 3730xl Genetic Analyzer. A consensus sequence of the 16S rDNA gene was generated from forward and reverse sequence data using aligner software. The 16SrDNA gene sequence was used to perform BLAST with the database of NCBI GenBank. The sequence was given in to NCBI GenBank to get accession no.

6.1.2.5. Statistical analysis

All the experiments performed in triplicates were expressed as mean±SD. All statistical analysis was performed using GraphPad (Prism Version 7.00). Mean and standard deviations were calculated to analyse the enzymatic activity of red mud, and growth parameter optimization of the potent isolates.

6.1.3. Results and Discussion

6.1.3.1. FDA Activity

For a very long time, FDA activity has been thought of as a potential biological identify for detecting soil microbial activity. It is a non-fluorescent, non-polar derivative that is readily

taken up by cells, where it is hydrolysed into polar fluorescein by various enzymes, including lipase, esterase, and protease, which are involved in the breakdown of organic materials (Tripathy et al. 2014; Nannipieri et al. 2003). The FDA can be changed into fluorescein by active cells. Fluorescein eventually leaks out of the cells when they are unable to contain it, and this allows for spectrophotometric measurement. The data from the FDA analysis is represented in Table. 6.1.1**.** The FDA activity of red mud was very poor ranging from 1.5-13.6 µg fluorescein/gram/hour (mean 4.95±0.99), indicating reduced microbial activity of RM. However, the dump disposed of long ago showed a little improved activity compared to the disposal of a short span. Surprisingly, the fresh residue did not show any FDA activity. The finding of the present study is consistent with Dey et al. (2021), who observed lower FDA activity in the RM sample.

6.1.3.2. Enzymatic activity (alkaline phosphatase, dehydrogenase, aryl sulphatase, β-D glucosidase,)

Enzymatic processes in the soil are crucial for understanding nutrient dynamics. By controlling the turnover of carbon, nitrogen, and phosphorus, they are the essential part of catalytic reactions that break down organic matter and distribute nutrients (Bueis et al. 2018). Since microbes are the primary factor in enzymatic regulation, they have the ability to adapt to environmental changes and provide comprehensive information on the enzyme catalytic reactions involved in biological processes. They act as a gauge of the state of the soil. Both internal and extracellular soil enzymes are possible. After a cell dies, the intracellular enzyme is released, and it joins forces with the extracellular enzyme to form a stabilized organo-mineral complex that is persistently active (Nannipieri et al. 2003).

The data of the enzymatic study of RM is presented in Table 6.1.1. Out of all the enzymes alkaline phosphatase (AP) was higher compared to other. It was ranging from 33-112 (µg p-nitrophenol released/g/h) with an average of 74 ±4.05. This is possibly due to lower P mineralization. Since RM contain negligible organic carbon and also poor microbial activity, thereby, phosphatase activity is also meager (Šarapatka, 2003). β-Glucosidase, the carbon (C) cycle enzyme controls the soil's release of carbohydrates, which is a key substrate for soil microorganisms. It was ranging from 3-36 (µg p-nitrophenol released/g/h), with a mean of 8.34 ±1.55. The activity was a little higher in RM hip disposed 35 to 40 years back. This site was slightly vegetated, which is perhaps the reason behind the high activity. Poor organic C is the

only reason for having reduced activity in RM sample. Likewise, aryl sulphatase activity was ranging from 0.9-4.1(µg p-nitrophenol released/g/h) with a mean of 1.3 ±0.47.

According to Tabatabai (1994), dehydrogenase activity in soil serves as a reliable indication of a microbial redox system and a useful indicator of microbial oxidative activities. They are oxidoreductases, which transfer electrons between the acceptors and the substrates to oxidise organic molecules. The enzyme provides a quick measure of soil microbial load because it is entirely intracellular and does not accumulate outside of the cell (Tabatabai 1994). Dehydrogenase activity was almost missing; however, a minute amount was released (0.96 µg TPF/ g/h) from the RM heap that bears some natural vegetation. This may be due to a little larger microbial activity because of plant growth. Overall, the enzymatic study reveals that lack of microbial activity is likely the reason behind lower enzymatic activity.

Table 6.1.1. Biological characteristics (FDA and enzymatic activity) of red mud (RM) collected from HINDALCO alumina plant, Muri, Jharkhand. Values represent in mean ±SE

Enzyme	Range	Mean
FDA (µg fluorescein/gram/hour)	1.5-13.6	4.95 ±0.99
Alkaline phosphatase (µg p-nitrophenol /gram/hour)	33-112	74 ±4.05
β-D-Glucosidase (µg p-nitrophenol /gram/hour)	3-36.78	8.34 ±1.55
Aryl sulphatase (µg p-nitrophenol /gram/hour)	0.91-4.1	1.3 ±0.47
Dehydrogenase (µg p-nitrophenol /gram/hour)	0.32- 1.33	0.96 ±0.06

6.1.3.3 Taxonomic diversity of RM (culture-independent)

Two samples were analysed for their taxonomic diversity. One sample was from a heap with 15-20 years of aging (sample designated as 35 normal) and another from 35-40 years of aging (sample designated as 35IIb), however the 35IIb sample bears little vegetation. From the rarefaction curve (Fig. 6.1.1), it is visible that OTU (Operational taxonomic unit) was much more distributed for 35IIb (622) than 35normal (423). This may be due to a more diverse species present in 35IIb sample. As it is mentioned earlier that this heap of RM contains little vegetation thus root exudates of plant enhance microbial diversity, however, the 35 normal samples possess little less diversity due to their extreme nature. Surprisingly, from the rarefaction curve it also seemed the presence of species was high in 35 normal, while the diversity was more in 35IIb. Although the 35nomal curve crossed more sequences but got

saturation, however, 35IIb was increasing and needed more sequence analysis to reach saturation. So, we can say that 35IIb was more diverse in terms of species while 35normal had more species. In support of this, alpha diversity measurement declared the richness and relative abundance of bacteria within the sample. Fig. 6.1.2 represents different alpha diversity indices of which Chao1 and ACE represent the richness of the sample and Shannon, Simpson, Inv-Simpson, and Fisher represent both richness and relative abundance. So, alpha diversity analysis exhibited that more species diversity takes place in the 35IIb sample.

The samples were dominated by phyla, *Proteobacteria, Bacteroidetes*, *Planctomycetes, Cyanobacteria, Actinobacteria*, and *Chloroflexi*. The result is consistent with (Macías-Pérez et al., 2022). At the genus level, the predominant species are *Halomonas*, *KSA1*, *Rhodobaca*, *Bacillus* etc. in both 35normal and 35IIb, however, abundance distribution of *Halomonas* (Fig. 6.1.3) was more in 35 normal. In 35IIb sample, the abundance of genus *Leptolyngbya* was highest (Fig. 6.1.3). Considering the species diversity was mostly *alkaliphilus* and *alkalitolerans* (Fig. 6.1.3). Inclusively the above data gave us an idea of taxonomic distribution in red mud. Moreover, presence of culture-independent alkaliphilic bacteria contributes a lot to the restoration of biological activity in the RM.

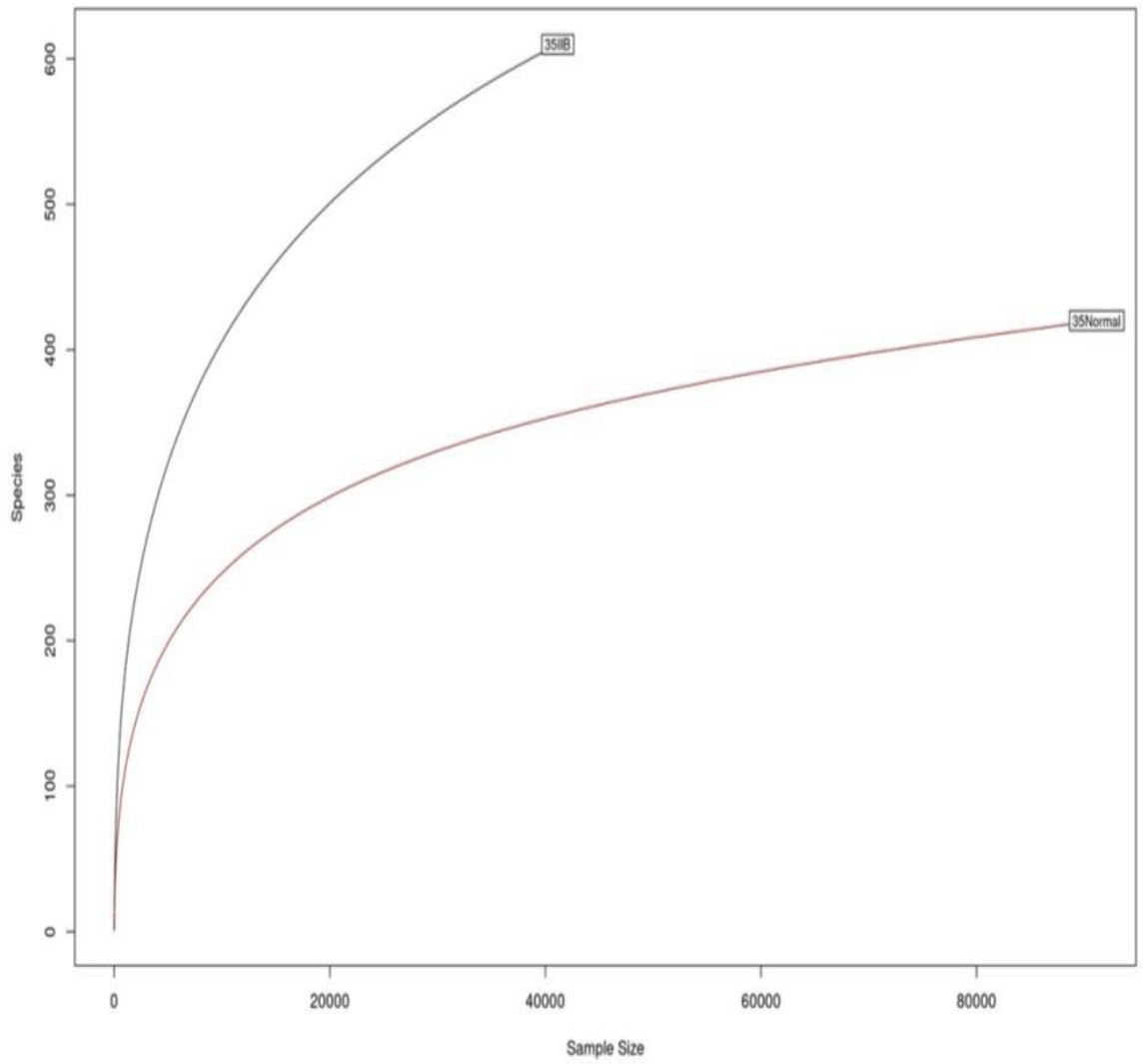

Fig. 6.1.1. The rarefaction curve of the four samples, 35 Normal and 35 IIB, is illustrated by the relationship between the reads and OTUs. The curve's impending plateau means there are enough reads to adequately describe the OTUs that represent the community.

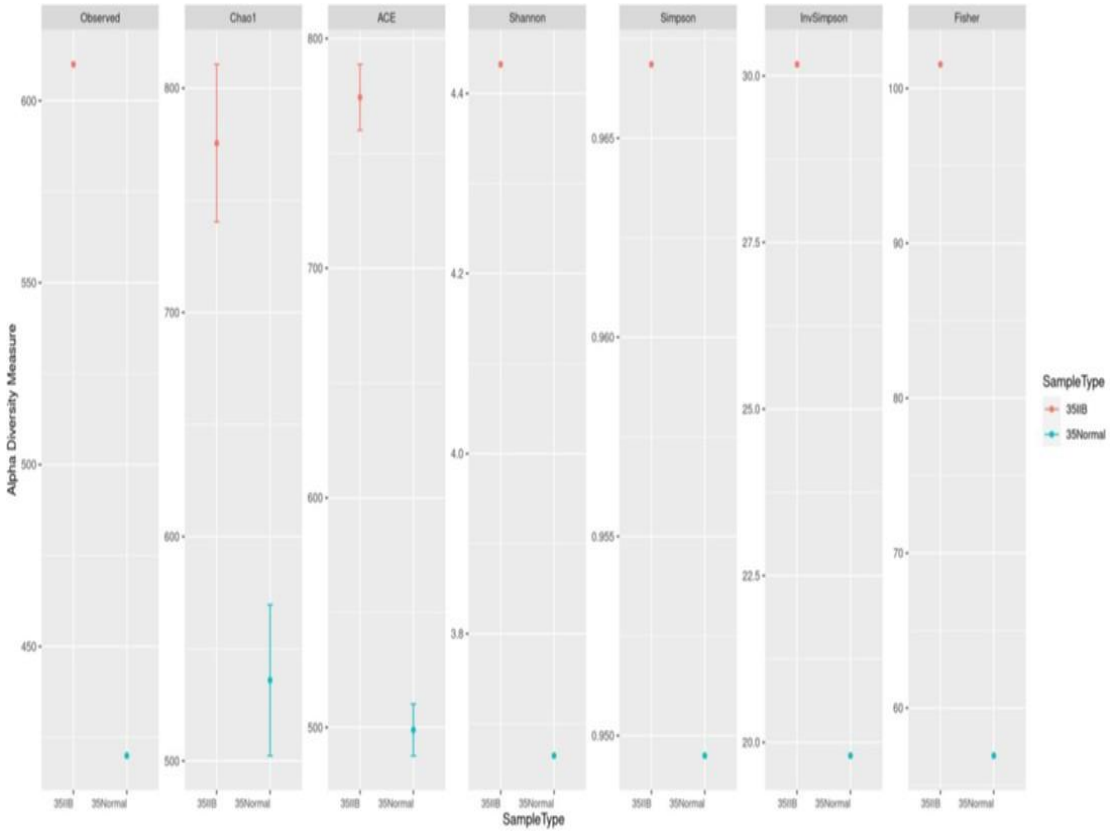

Fig. 6.1.2. Alpha diversity analysis of the two sample (35 Normal and 35IIb).

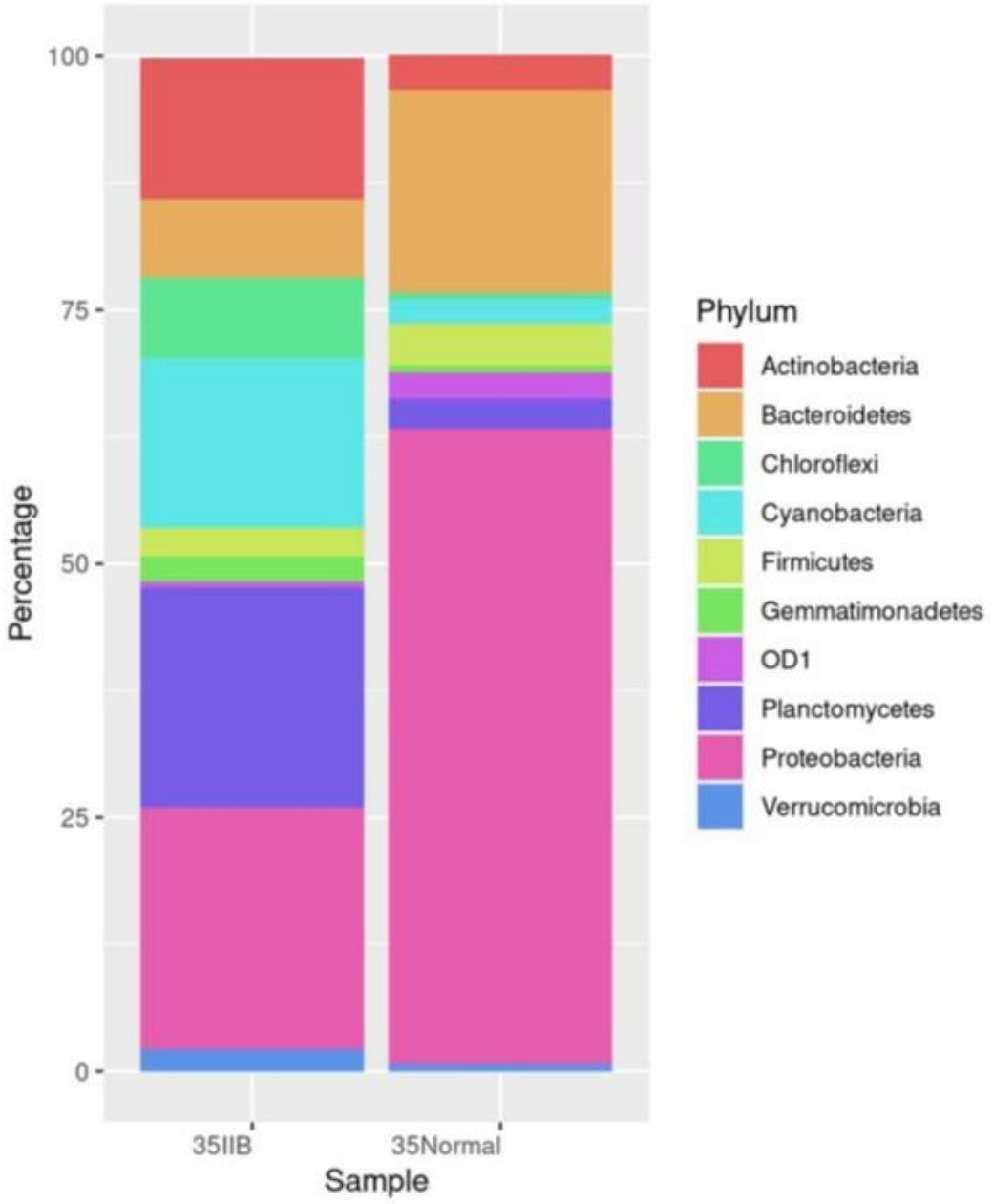
100
75
50
25
0
Percentage
35IIB
35Normal
Sample
Phylum
Actinobacteria
Bacteroidetes
Chloroflexi
Cyanobacteria
Firmicutes
Gemmatimonadetes
OD1
Planctomycetes
Proteobacteria
Verrucomicrobia

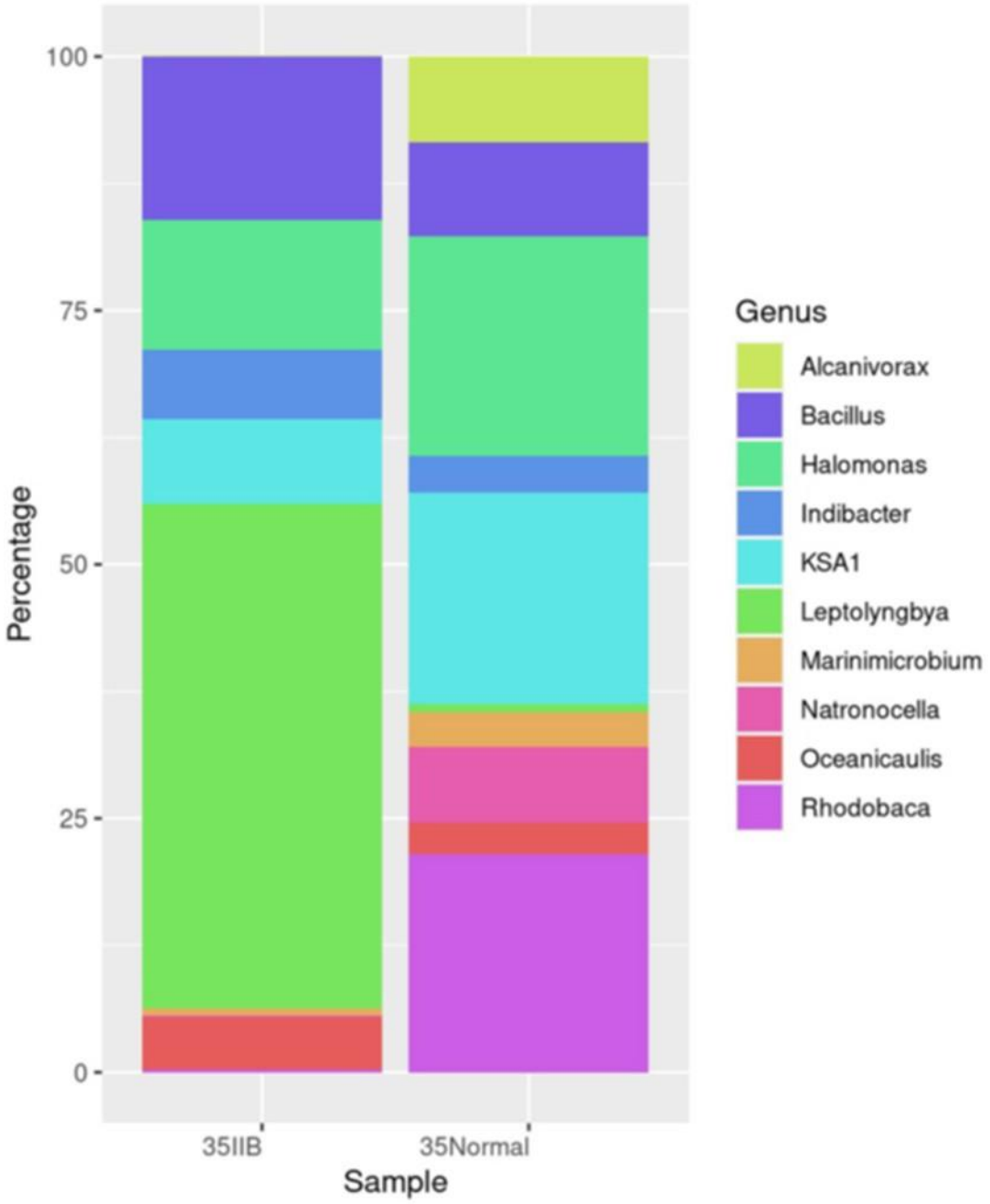
100
75
50
25
0
Percentage
35IIB
35Normal
Sample
Genus
Alcanivorax
Bacillus
Halomonas
Indibacter
KSA1
Leptolyngbya
Marinimicrobium
Natronocella
Oceanicaulis
Rhodobaca

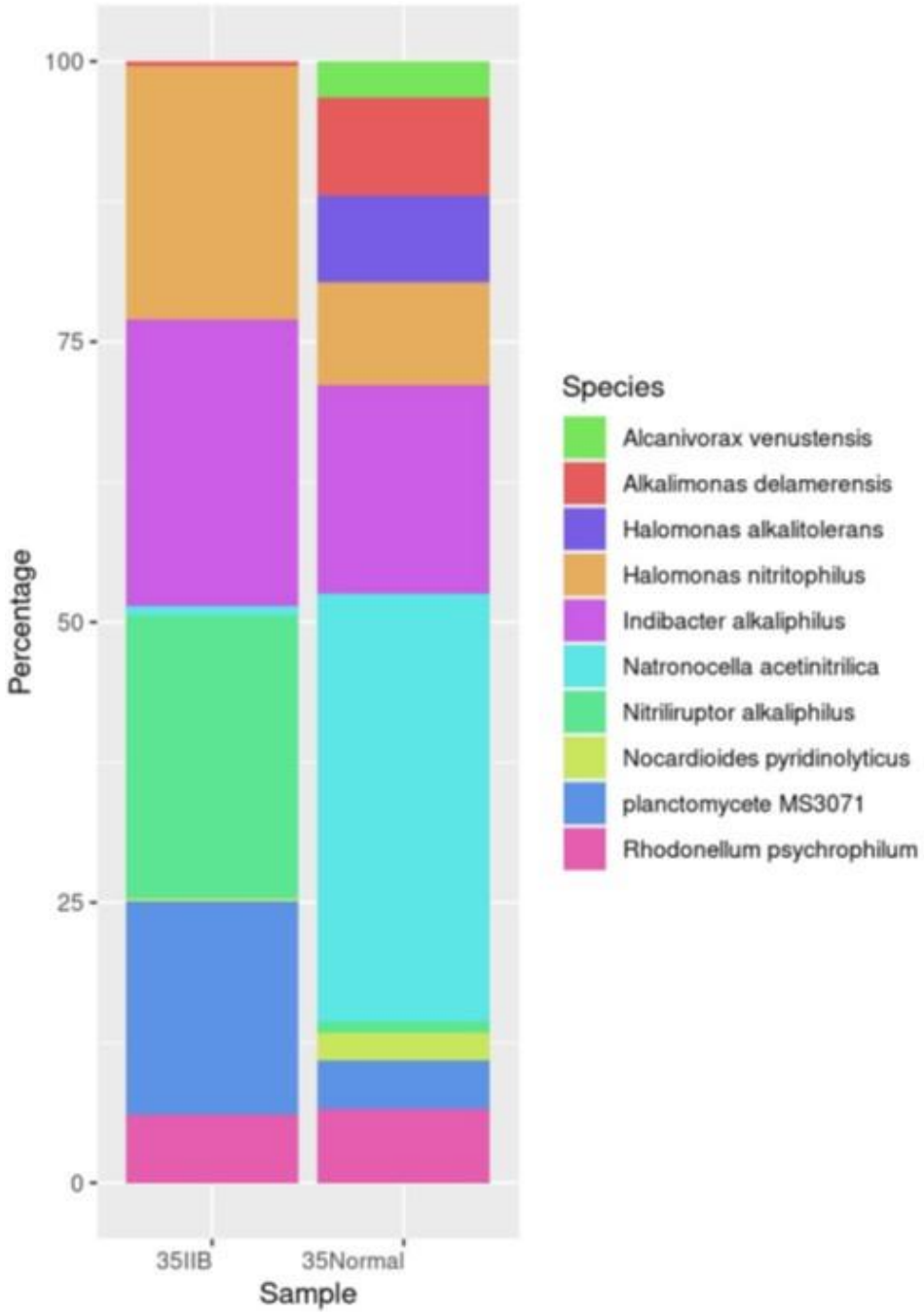

Fig.6.1.3. Taxonomic composition and relative abundance of ten most dominant bacterial phylum, genus, and species of the red mud sample (35 normal and 35IIB)

6.1.3.4. Isolation, characterization of metal tolerant alkaliphilic organism from RM (culture-dependent study)

A. Total heterotrophic microbial (bacteria & fungus) count, colony characteristics:

Since red mud is extremely alkaline, an alkaline-specific HoriKoshi (HK) medium (pH 10.5) supplemented with 10% Na_2CO_3 was used to isolate the total bacterial count. As stated

in earlier section that RM is extremely poor in microbial load (result from enzymatic assay), we categorized the RM into three parts to isolate the bacteria. The first one was fresh, the second was the short-term deposited part (approx. 20 years of deposition) and third was long-term deposited (>30 years). Overall microbial load was meager for all the sample; however, the fresh residue was completely deprived of microbial activity (no colony was found in plate). In second part of RM deposition, total bacterial count was average 1.4 $X10^2$ ±0.22 cfu/g of RM, while the third part deposition of showed a to some extent greater bacterial count i.e., 2.9 X 10^2 ±0.06 cfu/g of RM. This may be due to the long-term storage reducing the pH slightly, along with the leaching of metals, cationic species (Na^+, K^+, and Ca^{2+}, Mg^{2+}) and growth of some natural vegetation act as key factors for greater microbial activity. On the other hand, disproportionately high Na concentration (14000-18000 mg/kg) and negligible organic matter are the prime hindrances for scanty presence of microorganisms. A similar kind of observation was reported by Dey et al., 2021.

Morphologically the colonies were differently pigmented i.e., yellow, orange, and milky white, some were transparent while many of them were opaque. Marginally they were smooth and mostly round-shaped. Most of the colony was mucoid produce slime. Three different size ranges viz., small, medium and large colony appeared. Colonies were more or less flat in all the plates, however, a few of them were slightly convex. All together a total of 20 pure bacterial colonies were picked up based on their morphological distinctiveness. Concerning to the gram characteristics, majority of them were gram-positive, some gram-negative and three isolates remained undifferentiated through gram staining **(**Fig. 6.1.4 and Table 6.1.2). Cells were both in rods and cocci. They were found in both forms i.e., single and cluster. The result of the biochemical characteristics is tabulated in Table 6.1.3. Surprisingly, we did not find any fungus in any of the Czapek-dox/PDA plates. Since fungi are mostly acid-loving, mostly grows in a pH range of 3-8, thus the high alkalinity and elevated pH was probable obstacle to their growth in RM (Rousk et al., 2009).

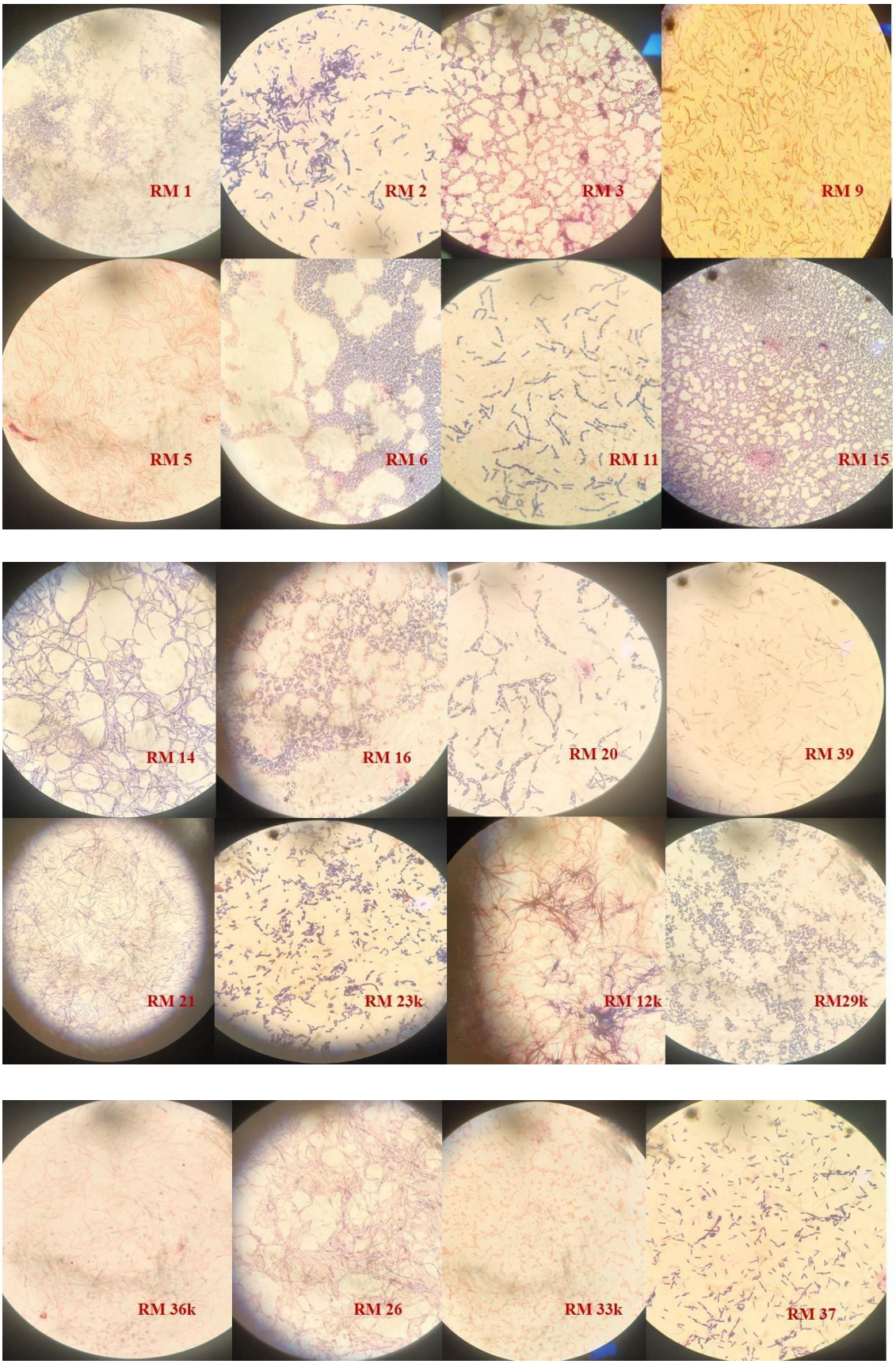

Fig. 6.1.4. Gram characteristics of 20 morphologically distinct isolates.

Table 6.1.2. Gram characteristics and morphological characteristics of the 20 isolates, isolated from red mud (RM).

Isolate Code	Gram Characteristics	Shape/ Colour/ Elevation
RM1	Gram Positive	Short rods, ivory white, flat
RM2	Gram positive	Rod, yellow, flat
RM3	Undifferentiated	Cocci, pale white, flat
RM9	Gram negative	Rod, transparent, flat
RM5	Gram positive	Strict rod, transparent, mild convex
RM6	Gram positive	Coccus, ivory white, flat
RM11	Gram positive	Rod, white, flat
RM15	Gram positive	Coccus, pale yellow, flat
RM14	Gram positive	Strict rod, pale white to transparent, flat
RM16	Gram positive	Short rod, ivory white, flat
RM20	Gram positive	Rod, pale white, flat
RM39	Gram positive	Rod, orange/yellow, flat
RM21	Gram positive	Rod, orange, flat
RM23K	Gram positive	Rod, yellow, slight concave
RM12K	Undifferentiated	Spiral, brownish white, slight concave
RM29K	Gram Positive	Cocci, pale yellow, flat
RM36K	Undifferentiated	Rod, pale white, flat
RM26	Gram positive	Rod, yellow, flat
RM33K	Gram negative	Cocci, pale white, flat
RM37	Gram positive	Rod, whitish, flat

Table 6.1.3. Biochemical characterization of the isolates, isolated from red mud (RM).

Sugar utilization	RM1	RM2	RM3	RM9	RM5	RM6	RM11	RM15	RM14	RM16	RM20
Glucose	Positive	Positive	Positive	Positive	Positive	Positive	Positive	Positive	Positive	Positive	Positive
Lactose	Negative	Positive	positive	Negative	Positive	Positive	Negative	Negative	Negative	Negative	Positive
Sucrose	Negative	Negative	Negative	Negative	Negative	Negative	Negative	Negative	Negative	Negative	Negative
Maltose	Positive	Positive	Positive	Positive	Positive	Negative	Positive	Positive	Negative	Positive	Positive
Fructose	Negative	Negative	Negative	Negative	Negative	Negative	Positive	Negative	Negative	Negative	Positive
Dextrose	Positive	Positive	Positive	Positive	Positive	Positive	Positive	Positive	Positive	Positive	Positive
Galactose	Negative	Negative	Negative	Negative	Negative	Negative	Negative	Positive	Negative	Negative	Positive
Xylose	Negative	Negative	Negative	Negative	Negative	Negative	Negative	Negative	Negative	Negative	Negative
Arabinose	Positive	ND	ND	ND	Positive	Positive	Negative	Negative	Negative	Negative	Positive
Raffinose	Negative	Negative	Negative	Negative	Negative	Negative	Negative	Negative	Negative	Negative	Negative
Trehalose	Positive	Positive	Positive	Positive	Positive	Positive	Negative	ND	ND	Positive	Positive
Mannose	Positive	Positive	Positive	Negative	Negative	Negative	Negative	Negative	Negative	Positive	Positive
Mannitol	Positive	ND	ND	ND	Positive	Positive	Negative	Negative	ND	Positive	Positive
Inositol	Positive	Positive	ND	ND	Positive	Positive	ND	Negative	Negative	Positive	Negative
Biochemical parameters											
Indole production	Negative	Negative	Negative	Negative	Negative	ND	Negative	Negative	Negative	Negative	Negative
Voges-Proskauer	Positive	Negative	Negative	Negative	Negative	Negative	Positive	Positive	Negative	Negative	Negative
Methyl Red	Positive	Positive	Positive	Positive	Positive	Positive	Positive	Positive	Positive	ND	Positive
Citrate utilization	Positive	Positive	Positive	Positive	Positive	Negative	Positive	Positive	Positive	Positive	ND
Arginine	Negative	ND	Negative	ND	Positive	Positive	ND	ND	Positive	Positive	Positive
Nitrate	Positive	Negative	Negative	Negative	Positive	Positive	Negative	Negative	ND	Negative	Positive
Urease	Positive	Positive	Negative	ND	Positive	Positive	Negative	ND	Positive	Negative	Negative
Phenylalanine deamination	Negative	Negative	ND	Negative	Negative	Negative	Negative	Negative	Negative	Negative	ND
H2S Production	Negative	ND	ND	ND	Negative	ND	Negative	Negative	ND	ND	Negative
ONPG	ND	Negative	Negative	Negative	Negative	ND	ND	Negative	ND	Negative	Negative

Sugar utilization	RM20	RM39	RM21	RM23K	RM12K	RM29K	RM36K	RM26	RM33K	RM37
Glucose	Positive	Positive	Positive	Positive	Positive	Positive	Positive	Positive	Positive	Positive
Lactose	Positive	Positive	Positive	Negative	Negative	Negative	Negative	Negative	Negative	Negative
Sucrose	Negative	Negative	Negative	Negative	Negative	Negative	Negative	Negative	Negative	Negative
Maltose	Positive	Positive	ND	Positive	Positive	Positive	Positive	Positive	Positive	Negative
Fructose	Positive	Positive	Negative	Negative	Positive	Negative	ND	Negative	ND	Negative
Dextrose	Positive	Positive	Positive	Positive	ND	Positive	Positive	Positive	Positive	Positive
Galactose	Positive	Positive	Negative	Negative	Negative	Negative	Negative	Negative	Positive	Negative
Xylose	Negative	Negative	Negative	Negative	Negative	ND	Negative	ND	Negative	Negative
Arabinose	Positive	Positive	Positive	ND	Negative	Positive	Negative	Positive	Positive	Negative
Raffinose	Negative	Negative	Negative	Negative	Negative	ND	Negative	Negative	Negative	Negative
Trehalose	Positive	Positive	Positive	Negative	Negative	Negative	Positive	Positive	Negative	Negative
Mannose	Positive	Negative	Negative	Negative	ND	Negative	Negative	Negative	Negative	Negative
Mannitol	Positive	Negative	Positive	Negative	Positive	Negative	Negative	Positive	Positive	Negative
Inositol	Negative	Negative	Positive	Positive	Positive	Negative	ND	ND	ND	
Biochemical parameters										
Indole production	Negative	Positive	Positive	Negative	Positive	Negative	Positive	Positive	Positive	Positive
Voges-Proskauer	Negative	Positive	Negative	Positive	Negative	ND	Negative	ND	Negative	Positive
Methyl Red	Positive	Positive	ND	Positive	Positive	Positive	ND	Positive	Negative	Positive
Citrate utilization	ND	Negative	Negative	Negative	ND	Positive	Positive	Negative	ND	ND
Arginine	Positive	Negative	Positive	Negative	Negative	Positive	ND	Positive	Negative	Negative
Nitrate	Positive	ND	Negative	Positive	Negative	Positive	Positive	Positive	ND	Positive
Urease	Negative	Negative	ND	ND	Negative	ND	Positive	Positive	Positive	ND
Phenylalanine deamination	ND	ND	Negative	Negative	Negative	Negative	ND	ND	Negative	Negative
H2S Production	Negative	ND	Negative	Negative	Negative	Negative	Negative	Negative	Negative	Negative
ONPG	Negative	ND	Nd	ND	ND	ND	Negative	Negative	Negative	Negative

*ND – Note detected

B. Screening of the metal-tolerant bacteria and molecular identification:

In support of the aim of the study I carried out minimum inhibitory concentration (MIC) to screen the metal-tolerant bacteria. The MIC value was checked for the metal Cd, Cr, Pb, Ni, As, and Cu and demonstrated in Fig. 6.1.5. According to the result, 5 isolates out of 20 were found to tolerate these five metals up to a high concentration. They were designated as RM1, RM5, RM6, RM16 and RM20. From the MIC study it was exhibited that all isolates showed lower tolerance for Cd (II) and maximum tolerance was seen for Cr (VI). This can be well justified with the native metal concentration of the red mud where Cr was highest (184-526mg/kg) and Cd was lowest (18 mg/kg). Additionally, Cd (II) is highly toxic in trace amounts for any cell (Shen et al., 2005; Raiesi & Sadeghi, 2019). Molecular identification through 16srDNA sequencing disclosed their identity. The majority of them belonged to the genus *Bacillus spp.* while one RM 6 was *Nesterenkonia spp*. BLAST analysis and GenBank submission revealed that five-metal tolerant isolate was as RM1 (*Bacillus inaquosorum* ISIGRM1, accession no. OP242829), RM5 (*Bacillus amyloliquifaciens* ISIGRM5, accession no. OR039758), RM6 (*Nesterenkonia aethiopica* ISIGRM6, accession no. OP245088), RM 16 (*Bacillus xiamenensis* ISIGRM16, accession no. OP243450) and RM 20 (*Sutcliffiella cohnii* ISIGRM20, accession no. OR039776). Subsequently, the growth parameter optimization (pH, % NaCl, temperature) test done on these five isolates is represented in Fig. 6.1.6. Based on these growth optimizations and MIC study, we selected *Bacillus xiamenensis* ISIGRM16, accession no. OP243450 for our further study in waste management (wastewater treatment).

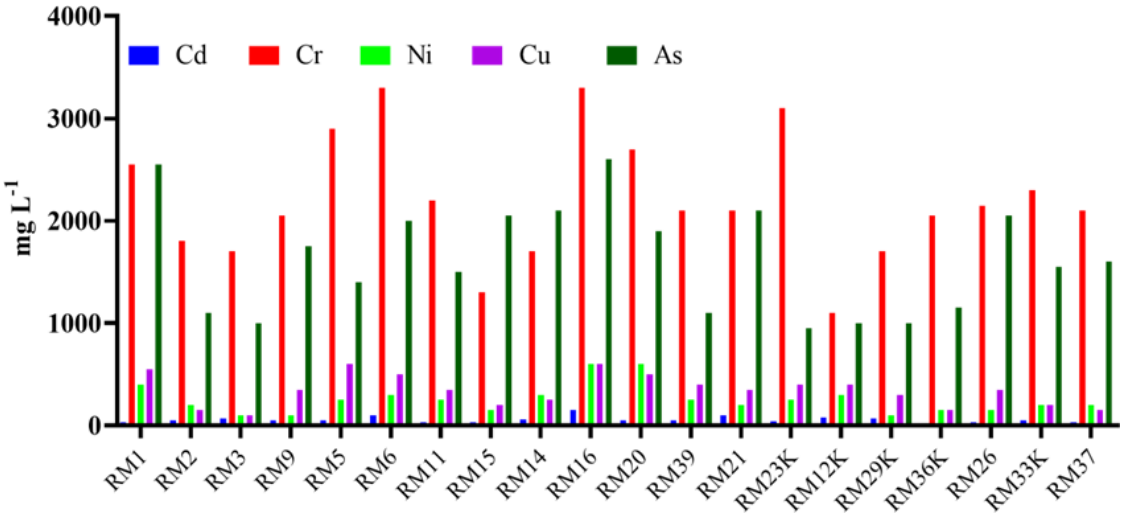

Fig. 6.1.5. Minimum inhibitory concentration of Cd (II), Cr (VI), Ni (II), Cu (II), As (III) against the bacterial isolate thriving in red mud (RM)

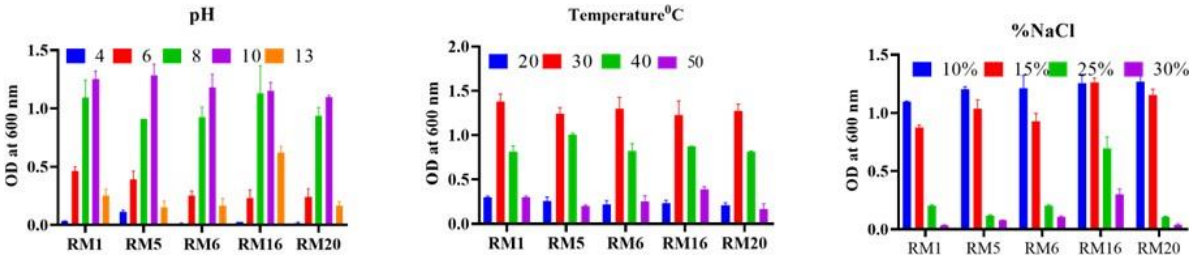

Fig. 6.1.6. Growth optimization of five metal tolerant isolates screened from MIC experiment.

6.1.4. Conclusion

In this study of exploring biological properties of RM, we found some exclusive fact. Biologically RM is destitute, however, we found it as a sink of extremophilic organism. The enzyme dynamics of the residue concludes a relatively better production of alkaline phosphatase, as compared to another enzyme. The metagenome based taxonomic diversity analysis deciphered the abundance of *Proteobacteria*, *Bacteroidetes*, *Planctomycetes*, and *Actinobacteria* in the phylum level, while *Bacillus*, *Halomonas* and *KSA1* were predominant in genera level. The total heterotrophic bacterial count divulges that aging of disposal has an impact on improvement/development of microbial activity in RM since long term disposal showed a greater count (2.9 X 10^2 cfu/g). A total of twenty alkaliphilic bacteria was isolated out of which, five bacteria carry multiple extremophilic characteristics (wide range pH tolerance, metal tolerance and temperature tolerance). Colony morphology, molecular identification and microscopic analysis revealed the gram-positive characteristics of isolates, and majority of the isolate belonged to *Bacillus*. Lastly, the isolate *Bacillus xiamenensis* ISIGRM16 showed maximum resistance to three potentially toxic metal Cd (II), Cr (VI) and Ni (II) with a wide range of pH, temperature and salinity. Thus, the metal sequestration ability of *Bacillus xiamenensis* ISIGRM16 was subsequently investigated, using it as biosorbent.

6.2. Detoxifying potential of novel polyextremophilic *Bacillus xiamenensis ISIGRM16* in mono and multi-metal system- A sorptive approach

6.2.1. Introduction

The advancement of civilization leads to meteoric progress of industries, agricultural activities, transport and other human doings that reached another level in the current century. This sudden boost in industrialization is generating an enormous amount of pollutants each year creating an alarming environmental impact. For instance, effluents from different industries, solid or muddy disposals, and sludges contaminated with various noxious metals, are commonly raising a threat to the environment and public health. Unlike organic pollutants, these inorganic contaminants are non-biodegradable, intrinsically persist for a long time, and finally accumulate through different biological systems. Heavy metals (HM) occupy a large part of inorganic contaminants as well are of prime concern due to their lethal consequence at relatively low concentrations known to be a potent carcinogen (Cherono et al., 2021). Additionally, anthropogenic factors are the natural source of toxic metals introduced to environment and water bodies. With passing time, HMs are becoming ubiquitous on account of accelerated waste generation coupled with geogenic activities, causing harmful effects on living organisms. Continual discharge of these pollutants to the catchments creates profound incorporation into the natural system in consort with forthcoming bioaccumulation proceeds towards biomagnification in higher trophic levels (Fathollahi et al., 2021).

Several toxic metals like Cr^{6+}, Cd^{2+}, and Ni^{2+} are mainly discharged from industrial dumped waste, pesticides, chemical fertilizers, and municipal solid waste. They are accumulated in soil that further leaches over time, contaminating surface and groundwater. Cr happens to stay in a wide range of oxidation states from -2 to +6, out of which Cr^{3+} is quite innocuous and less soluble while Cr^{6+} is a mobile, highly soluble and strong oxidizer that is of significant ecological concern. Cd^{2+} is highly sensitive to the living organism because of its greater lability and weak adsorbing nature with soil matrix prompting greater bioaccumulation (Borah et al., 2018). Correspondingly, Ni^{2+} also prevails over a mobile fraction of soil and remains stable in an aqueous solution for a long-time results noteworthy plant uptake. Moreover, the toxicity of HMs towards phytotoxicity follows the order Cd>Cr>Ni. According to ATDSR Cd^{2+} and Cr^{6+} are positioned as the 7^{th} and 17^{th} most hazardous elements for toxicological profile and are designated as two potent carcinogens by the International Agency for Research on Cancer (IARC) exhibiting mutagenic, carcinogenic and teratogenic properties

(ATSDR, 2012; Jaishankar et al., 2012). Likewise, Ni^{2+} accomplished all the criteria of being hazardous known for its potential to cross to the placenta in humans and other animals showing carcinogenicity, confirmed by ATDSR and IARC. Persistent exposure to these HMs leads to multiple dysfunctionalities in human subjects like bronchial damage, skin irritation, cancer, renal failure, abdominal cramps, loss of appetite etc. (Zhang et al., 2017).

These metal-laden industrial effluents consist of multiple components showing interactive behaviour based upon numerous factors viz. competition for binding sites among co-cations, metal concentration, the equilibrium concentration of ion species, pH, nature and dosage of biomass adsorbent. Treatment of such industrial waste streams is challenging (Jain et al., 2015). Over the decades several physical and chemical technologies including coagulation, reverse osmosis, precipitation, ion exchange, and chemical reduction have been used for wastewater treatment, although these conventional techniques are inefficient for a trace amount of metal removal, too expensive as well have some limitations in case of large-scale application. Additionally, these treatments generate a substantial amount of secondary toxicants demand further treatment thereby multiplying the operational cost (Zhang et al., 2017). Keeping an eye on these circumstances, there is an urgent need to develop a low-cost simple operational technology with environmental and economic sustainability as a resolute approach for treating wastewater on a large scale. Adsorption or more specifically biosorption could be a promising replacement for contemporary techniques, offers cost-effectiveness, higher metal retention capacity, efficiency in a lesser concentration of metal adsorption, adequate availability and is environment friendly. Biosorption illuminates a new avenue for the sustainable management of toxic metals in the aquatic system. The performance of any biosorbent is highly important due to its advanced surface area-to-volume ratio and polarity of the sorbent (Jain et al., 2015).

Microorganisms inhabit contaminated sites and are found to play a pivotal role in metal sequestration. The long persistence of metallic contaminants in the environment results in a paradigm shift in the existing microbial diversity. Consequently, resistance to high-concentration metal has evolved. In general, bacteria are used to adapt three different mechanisms to cope namely efflux of metals via transporter, conversion of the metal into non-toxic or less toxic forms and biosorption (Das et al., 2016). Synthesis of extra polymeric substance (EPS) is another mechanism that exerts a potential metal entrapment due to the presence of numerous anionic functional groups (carboxyl, hydroxyl, sulphate, phosphate and amine etc.) thus conferring metal resistance (Mathivanan et al., 2021). Several studies have

reported two mechanistically different approaches to use living cells and dead biomass for metal removal. Characteristically the former is metabolically dependent and the latter is metabolically independent. Bioaccumulation defines the metal integration inside the living biomass, while biosorption is accomplished through complex formation, chelation, ion exchange etc. Since, bioremediation by using living cells has some practical limitations like growth inhibition in excessive metal concentration, chances of contamination due to mishandling, environmental factors, and genetic alterations, on this ground the dead/dried biomass is easy to handle, has a higher surface to volume ratio, altered cellular structure due to killing influence increased adsorption process to a greater extent, hence gaining more acceptance over living one (Singh & Singh, 2017; Li et al., 2018). Bacteria thrive in a metal-rich environment, develop tolerance and are known to be good accumulators of metal ions, yet their role in the physical adsorption process has not been explored in detail. So far, bioaccumulation, EPS and biofilm-mediated metal sequestration are the foremost choices for wastewater treatment, nevertheless, the dried- biomasses of bacteria are slowly gaining importance as an effective means of remedial strategy because of their advantages over high metal toxicity or adversative operating condition (Mathivanan et al., 2021). To date, plenteous studies have already been published on mono-metal systems, which is a kind of limitation to wastewater treatment, where more than one metal ion species compete with each other. Multi-metal adsorption study could be the best possible answer to this problem where interaction among metal ions can be studied. A competitive adsorption study aids in assessing the interference of co-ions present in wastewater along with the competence of adsorbents to eliminate such contaminants (Jain et al., 2015). The present study is an embellishment of bacterial- biosorbent including the critical analysis of its sorption efficacy of some noxious metals like Cd^{2+}, Ni^{2+} and Cr^{6+} from the aqueous solution under different physicochemical parameters in single and multi-component systems. Growth optimization and metal tolerance were set out firstly to screen the potent isolate in regard to metal sequestration by competing with common cations and anions of wastewater. Along with this, a sequential adsorption-desorption study was accomplished to ascertain its persisting sorption potential up to a few treatments for confirmation of the biomass-biosorbent is worthwhile.

6.2.2. Material and Methods

6.2.2.1. Isolation, growth optimization, characterization, and molecular identification of bacterial strain from red mud slurry

An alkaline-specific Hori Koshi (HK) medium (pH10.5) was used for the isolation and maintenance of the bacterial strains. The potent isolate was examined by their gram characteristics and biochemical characterization. The one factor at a time (OVAT) technique was used for growth parameters optimization viz. pH (4-13), temperature (20^0C-55^0C), and NaCl concentration (10%-35%). The parameters were optimized by checking optical density at 600 nm for their best growth. To assess the metal tolerance ability Cu, Cr, Ni, As, Cd were considered and added to the glucose -yeast extract- peptone (GYP) broth with varying concentrations ranging from 50 mg L^{-1} to 3500 mg L^{-1}. Analysing the OD value at 600 nm isolate RM16 was chosen as the most resistant isolate to these metals and subjected biosorption experiments. Genomic DNA was isolated following the standard protocol (Sambrook, 2001). In the end, the obtained 16SrDNA gene sequence was used to perform BLAST with the database of NCBI GenBank. The sequence was given in to NCBI GenBank to get accession no.

6.2.2.2. Preparation of the biosorbent

The bacterial culture was prepared on a large scale for making biosorbent for our aimed study. Preparation of the cell suspension was achieved by growing the isolate RM16 in HK broth supplemented with 10% Na_2CO_3 incubated at 30^0C for 72 hours with constant shaking at 125 rpm. For biosorbent preparation, the late exponential cells were harvested by centrifugation at 8000 rpm for 20 minutes. The pellet was washed three times with PBS buffer of pH 7.4. Finally, the washed pellet was dried at 45^0C- 50^0C in a hot air oven. The dry biomass was used for the biosorption experiment.

6.2.2.3. Batch adsorption study and optimization of environmental factors

A batch adsorption experiment was performed to investigate the removal ability of biosorbent of three potentially toxic metals i.e., Cd^{2+}, Cr^{6+}, and Ni^{2+} from the aqueous solution. Optimization of the environmental factors viz. pH, temperature, adsorbent dosage, contact time, salinity and initial concentration, was carried out to find out the best suitable condition for removal purposes. The stock solutions of 1000 mg/L of the metals (Cd^{2+}, Ni^{2+} and Cr^{6+}) were prepared using their precursor salt from Merck, Germany.

- Mono-component study

A Batch mode of adsorption was carried out for each metal to investigate the behaviour of metal towards adsorbent under several physicochemical factors, along with findings of metal's affinity towards adsorbent. For each experiment, 10 ml of the reaction mixture of 100 mg/L was taken in a microcentrifuge tube (MCT) with an adsorbent dose of 3 g/L and continuously agitated for 120 minutes at room temperature 30^0C± at 150rpm. The influence of temperature was studied at four different temperatures viz. 20^0C, 30^0C, 400C and 45^0C by keeping the concentration of each metal fixed at 100 mg/L with a 3g/L adsorbent dosage. To understand the behaviour and metal availability of biosorption medium a pH-dependent (2-10) study was carried out. The pH was maintained by using 0.1(N) HCl and 0.1(N) NaOH. Three different doses of adsorbent (1g/L -3g/L) were used to determine the most effective one for maximal removal of the metal ions. In order to, check the efficacy of biomass- biosorbent, an initial concentration of 30 mg/L to 500 mg/L was taken and shaken at 150 rpm at room temperature 30^0C± for 120 minutes. To observe the saturation of biomass-biosorbent, a sorption process was conducted with different contact times (15-120 minutes). The study of salinity effect on the biosorption of metal ions was accomplished using different NaCl concentrations i.e., 2%, 4%, and 6% at 150 rpm for 60 minutes. All the experiments were performed in triplicate at optimum pH 6 for Cd^{2+} and Ni^{2+} and pH 2 for Cr^{6+}. After completion of each experiment, the biosorbent was separated by centrifugation at 5000×g for 15 minutes with a subsequent collection of filtrates in fresh MCT for residual concentration of metal measurement. Using their respective standards, the Systronics AAS 816 was used to quantify the remaining metal (Cd^{2+}, Cr^{6+}, and Ni^{2+}) concentration. The metal solution without bacterial biomass was taken as control. The metal loading capacity of biosorbent at equilibrium for each sorption system was calculated using the following equation (Jain et al., 2015).

$$qe = (Ci\text{-}Ce) \times V/m \ldots$$

Where Ci and Ce are the initial concentration and residual concentration of metal (mg/L) respectively, V is the volume of the reaction mixture (L) and m is the mass of adsorbent (g). The metal removal efficiency was evaluated by equation as given below:

$$\text{Removal (\%)} = (Ci\text{-}Ce)/Ci \times 100 \ldots$$

- Multi-component study

The role of co-cation greatly influences the sorption process, thereby a study was conducted to explore their behaviour. The impact of co-cations on Cd2+, Ni2+, and Cr6+ sorption was checked in a ternary system, where concertation of the target metal will be fixed at 100 mg/L and co-cation concentration will be variable. The experimental design used in this study was a ternary system viz. Cd+Ni+Cr, Ni+Cd+Cr, Cr+Ni+Cd. The concentration of co-cations varied from 100mg/L to 500mg/L. This multi-elemental biosorption process was completed by using previously optimized parameters obtained from a single component system viz. pH 6 for Cd^{2+}, and Ni^{2+} and pH 2 for chromium Cr^{6+}, adsorbent dose 3g/L for 120 minutes at room temperature 300C with constant shaking at 150 rpm.

6.2.2.4. Adsorption models for metal removal

- Adsorption models

For a better understanding of the adsorption process of metals by biomass-biosorbent, it is necessary to comprehend the adsorption equilibrium using different isotherm models. To summarize the equilibria adsorption characteristics four different isotherm models had been adopted viz. Langmuir, Freundlich, Dubinin–Radushkevich (D–R), and Temkin. The models are explained following.

Langmuir isotherm:

$$q_e = \frac{q\max k_L Ce}{1+k_L c_e}$$

The Langmuir isotherm was linearised to calculate the adsorptionparameters

$$\frac{1}{q_e} = \frac{1}{k_L q_{\max x}} . \frac{1}{c_e} + \frac{1}{q_{\max}}$$

Where q_{max} denoted the maximum adsorption capacity (mg/g), K_L (L/mg) is the Langmuir isotherm constant indicating the binding affinity between the metal and biomass-biosorbent. To determine the practicability of any adsorption process, the dimensionless R_L was calculated from the Langmuir model by using the following equation.

$$R_L = \frac{1}{1+C_i \times K_L}$$

The value of R_L determines whether the adsorption possibility is either favourable (0 < RL < 1), unfavourable (RL > 1), linear (RL = 1) or irreversible (RL =0).

Freundlich isotherm is represented and similarly the linear form of Freundlichisotherm was taken to figure out the adsorption equilibria characteristics.

$$q_e = K_f C_e^{\frac{1}{n}}$$

$$\text{Log}\, q_e = \text{Log}\, K_f + \frac{1}{n} \log C_e$$

where, K_f denotes Freundlich's constant and was used to estimate the adsorption capacity, and 1/n was the adsorption intensity. The value of 1/n reveals the nature of the adsorption process whether it is favourable (0.1 < 1/n < 1) or unfavourable (1/n > 2).

Temkin isotherm model reveals that the adsorption heat of all molecules in the layer reduces linearly with respect to coverage area as a result of the adsorbent-adsorbate interactions and is characterized by a homogeneous distribution of binding energies up to maximum binding energy (Hosseini et al., 2003). The equation is as follows:

$$q_e = \frac{RT}{b} \ln kT + \frac{RT}{b} \ln C_e$$

where "q_e" is the amount of solute adsorbed per unit weight of adsorbent at equilibrium (mg/g), "RT/b = B", "R" is the gas constant (8.314 J/mol K), "T" is the absolute temperature in Kelvin unit, "b" is associated to the heat of adsorption (J/mol), "K_T" is the Temkin constant (L/mg), and "C_e" the equilibrium concentration of the solute in bulk solution (mg/L).

Dubinin−Radushkevich (D−R) isotherm is another model through which surface interaction between biomass-biosorbent and metal was characterised. The equation is as follows

$$\ln q_e = \ln q_m - \beta\varepsilon^2$$

where β is D-R constant, and q_m is the maximum amount adsorbed. And Ɛ is derived from Eq. below

$$\varepsilon = RT \ln\left(1 + \frac{1}{C_e}\right)\ldots$$

- Adsorption kinetics

The uptake of metal by *Bacillus sp.* largely depends on contact time thereby study of the kinetics of adsorption is essential. The prediction of adsorption rate to support the model of

adsorption, kinetic parameters were investigated by employing pseudo-first-order and pseudo-second-order models (Chatterjee et al., 2020). The pseudo-first-order and second-order equation is represented in Eq. (12) and (13)

$\ln (q_e - q_t) = \ln q_e - K_1 t$ ....(12)

$\frac{t}{q_t} = \frac{1}{K_2 q_e^2} + \frac{1}{q_e} t$.. (13)

In pseudo-first-order equation, qt designates the adsorption capacity (mg/g) at time t while K_1 (min^{-1}) is the equilibrium rate constant while, in the case of the pseudo-second-order equation, K_2 (g $mg^{-1}min^{-1}$) is the equilibrium rate constants. The linear coefficient regression values (R^2) were evaluated and analysed to interpret the accuracy of the model by comparing the theoretical value of adsorption capacity with obtained one from the batch adsorption studies.

- Thermodynamics of the bio-sorption

For a better understanding of the adsorption behaviour of the metal-biomass-biosorbent at different temperatures (20^0C to 45^0C), thermodynamic parameters were assessed. The free energy of the sorption process (ΔG^0), changes in the enthalpy (ΔH^0) and entropy (ΔS^0) during the time of interaction are given by Vant -Hoff equation.

$\Delta G^0 = -RT \ln K$

$\ln k = \frac{-\Delta H^0}{RT} + \frac{\Delta S^0}{R}$

Where *k* is the equilibrium constant derived from the metal concentration adsorbed on the biosorbent to the residual concentration that remains in the solution. The ln*K* vs 1/T plot provides the ΔH^0 and ΔS^0 respectively.

6.2.2.5. Common ion effect on Cd, Ni, and Cr removal by biomass-biosorbent

Determination of common ion effect on Cd^{2+}, Cr^{6+}, and Ni^{2+} removal by biomass-biosorbent, a study was carried out following (Chatterjee et al., 2020), where the adsorption process takes place in presence of different cations (Na^+, K^+, Ca^{2+}, Mg^{2+}, Cu^{2+}, Pb^{2+}, Zn^{2+}) and anions (NO^{3-}, CO_3^{2-}, Cl^-, SO_4^{2-}). Briefly, 3g/L of biosorbent was added to a 100 mg/L concentration of metal solution (Cd^{2+}, Ni^{2+}, and Cr^{6+}) and kept under shaking conditions for up to 120 minutes at room temperature and at optimum pH (pH 6 for Cd^{2+} and Ni^{2+}, and pH 2 for Cr^{6+}). At the end of the experiment, the biosorbent was parted out by centrifugation at 5000 rpm followed by analysing residual metal concentration by AAS 816 Systronics, India.

6.2.2.6. Desorption and reusability study

To carry out the desorption study the metal-laden biosorbent was treated with 0.1(N) of basic and 0.5(N) acidic solution (NaOH, Na_2CO_3, HCl, HNO_3, and H_2SO_4) following

Masoudi et al. (2018). In a nutshell, a desirable amount of biomass was treated with metal solution for adsorption. After the adsorption study, the metal-adsorbed biomass was washed with double distilled water to eliminate any unbound or loosely attached metal ions. Subsequently, 10 ml of desorption solution was added to it and the reaction mixture was kept under shaking conditions for 2 hours. Lastly, reaction medium was separated by centrifugation and metal concentration was measured by AAS 816, Systronics, India. Desorption capacity was calculated by following equation and expressed in percentage (%).

$$\% \text{ of desorption} = \frac{amount\ of\ metal\ desorbed}{amount\ of\ metal\ adsorbed}\ X\ 100$$

Regeneration of the biosorbent is an important aspect to make them available for reusability which will somewhat make it cost-effective. Recycling efficiency of the biomass was investigated by a consecutive adsorption-desorption experiment up to five times. To carry out this 3g/L biomass dosage was chosen to treat a 100 mg/L metal solution. Three most effective desorption solutions for three different metals were used for desorption (0.1(N) NaOH for Cr^{6+}, 0.5(N) HCl for Cd^{2+} and 0.5(N) HNO_3 for Ni^{2+}). After each cycle the biomass was harvested by centrifugation, washed with distilled water, and semi-dried, to regenerate successfully for the subsequent adsorption-desorption experiment. The metal in solution was measured by AAS Systronics, India.

6.2.2.7. Characterization of the biomass-biosorbent

Surface morphology of the biosorbent is the most crucial attribute of adsorption process. Here, the detailed surface morphology of biomass-biosorbent was achieved by FESEM-EDAX analysis before and after the metal adsorption. For sample preparation, the pristine and metal-adsorbed biomasses were washed with PBS 7.4 to eliminate any unbound or loosely attached component followed by a fixation over a glass slide with 2.5% glutaraldehyde. The slides were kept at 4^0C for 12 h. The fixed slides were then dehydrated by using an increasing concentration of ethanol gradient and finally observed under Field Emission Scanning Electron Microscope (Hitachi SU8010) followed by EDAX mapping (Priyadarshanee et al., 2021). Presence of the functional group on the surface of biosorbent plays a pivotal role in metal adsorption. Thus, an FTIR analysis of biosorbent before and after adsorption was done to observe the surface-active groups and their probable role in metal interaction. Both the samples after and before interaction of metal were pelletized with IR grade KBr powder (Hi-media) and used for FT-IR analysis. The spectra were recorded within the wavenumber range between 400-4000 cm^{-1} using an FT-IR spectrometer (Perkin Elmer, USA, Model: Spectrum 400 FT-IR/FIR Spectrometer).

6.2.2.8. Statistical analysis

All the experiments executed in triplicates were expressed as mean±SD. The statistical analysis was performed using GraphPad (Prism Version 7.00). Two-way analysis of variance (ANOVA) followed by Tukey's multiple comparisons test was conducted to evaluate significant differences among parameters of batch adsorption. Further, for batch adsorption with variable pH and metal concentration and desorption studies, one-way ANOVA following Sidak's multiple comparisons test was carried out. One-way ANOVA following Dunnett's multiple comparisons test was assessed for reusability study. For the entire study, $P<0.05$ was referred statistically significant value.

6.2.3. Result and Discussion

6.2.3.1. Characterization of the isolate Bacillus xiamenensis ISIGRM 16

Morphologically the isolate *Bacillus xiamenensis* ISIGRM16 was yellowish, gummy, flat and marginally round in appearance. Gram reaction revealed its rod shape with CV-I complex retaining property. The other result of morphological, gram characteristics and biochemical identification experiments are presented in Table 6.1.2 and 6.1.3. Isolation and maintenance of the bacteria in a medium (Hori Koshi) bearing pH 10.5 demonstrated its typical alkaliphilic nature. Culture optimization revealed its best proliferation rate at 30^0C temperature after 24 hours of incubation (mean OD value 1.2), although they confirmed a descent tolerance of a wide stretch of temperature from 20^0C to 50^0C **(**Fig. 6.2.1). pH plays an influential role in homeostasis mechanism for cells in extremely high (basic) and low (acidic) ranges. Since the isolate was the resident of a saline-sodic environment thereby showed luxuriant growth in alkaline range of pH (pH 8-13) **(**Fig. 6.2.1) and optimal at pH10 (mean OD value 1.26). Salinity is a dreadful factor that creates ionic imbalance and leads to death of a viable cell via plasmolysis. Herein, the isolate was found to sustain greater osmotic potential with a widespread NaCl tolerance from 10% to 30**% (**Fig. 6.2.1) with a maximal proliferation rate at 10% (mean OD value 1.36) followed by 15%-25%. At 30% NaCl concentration the growth lessened and afterward reduced hence considered to be the maximum tolerance concentration. In earlier studies, Wu et al. (2019) reported one *Bacillus sp*. isolated from bauxite residue waste of China capable of growing at pH12, 45^0C temperature and 15% NaCl concentration, while Nogueira et al. (2017) isolated the bacteria of *Bacillus sp*. showed maximum growth at pH10, 40^0C and 10% NaCl which was lower than our isolated strain. Molecular characterization of 16srDNA sequencing disclosed the identity of the isolate by generating the 16srDNA gene sequence followed by BLAST analysis and submission to the NCBI GenBank database, which

showed that the isolate belongs to the genera *Bacillus sp*. with maximum similarity of a reported species *Bacillus xiamenensis* (accession no. NR_148244.1). The sequence of our findings received an accession number OP243450 for the isolate *Bacillus xiamenensis* ISIGRM16. Based on the maximum identity score first ten sequences have been selected and aligned using multiple align software program Clustal W and lastly, a phylogenetic tree was generated by using MEGA 7 (Fig. 6.2.2)

6.2.3.2 Multiple metal tolerance

Maximum metal tolerance acts as one of the most relevant screening parameters for this study. The isolate was found to be highly tolerant to toxic metals like Cr^{6+}, As^{3+}, Cd^{2+}, Ni^{2+} and Cu^{2+} (Fig. 6.2.1.) showed relatively greater tolerance to As^{3+} and Cr^{6+} up to 2400mg/L and 3000 mg/L respectively, while in the case of $Ni^{2+,}$ and Cu^{2+} it ceased its growth at 600 mg/L concentration. Previously, Priyadarshanee et al. (2021) showed maximum tolerance to Cr^{6+} 1900 mg/L of a strain of *Pseudomonas sp.* In another study, Dey et al. (2016) reported of a *Bacillus sp.* isolated from an arsenic-contaminated area tolerate up to 600 mg/L of As^{3+}. The isolate of present study exhibited a greater tolerance to Cr^{6+} and As^{3+} which is better than previously reported strain. In Cd^{2+} amended medium it showed effective proliferation up to 100 mg/L. Correspondingly, for Ni^{2+}, and Cu^{2+} the growth slowed down after 500 mg/L. Tolerance in such high concentrations with a wide range of metals may come from different factors like, metal-resistant gene located in chromosome or in an extrachromosomal part, production of extra polymeric substances etc. Many studies reported that plasmid-borne genes i.e., *cad* operon, *cop* operon are responsible for Cd and Cu resistance respectively. One enzyme machinery works better for Cr and As named chromate reductase and arsenic reductase confers the resistivity, while for Ni it is mostly an efflux mechanism (Das et. al., 2016).

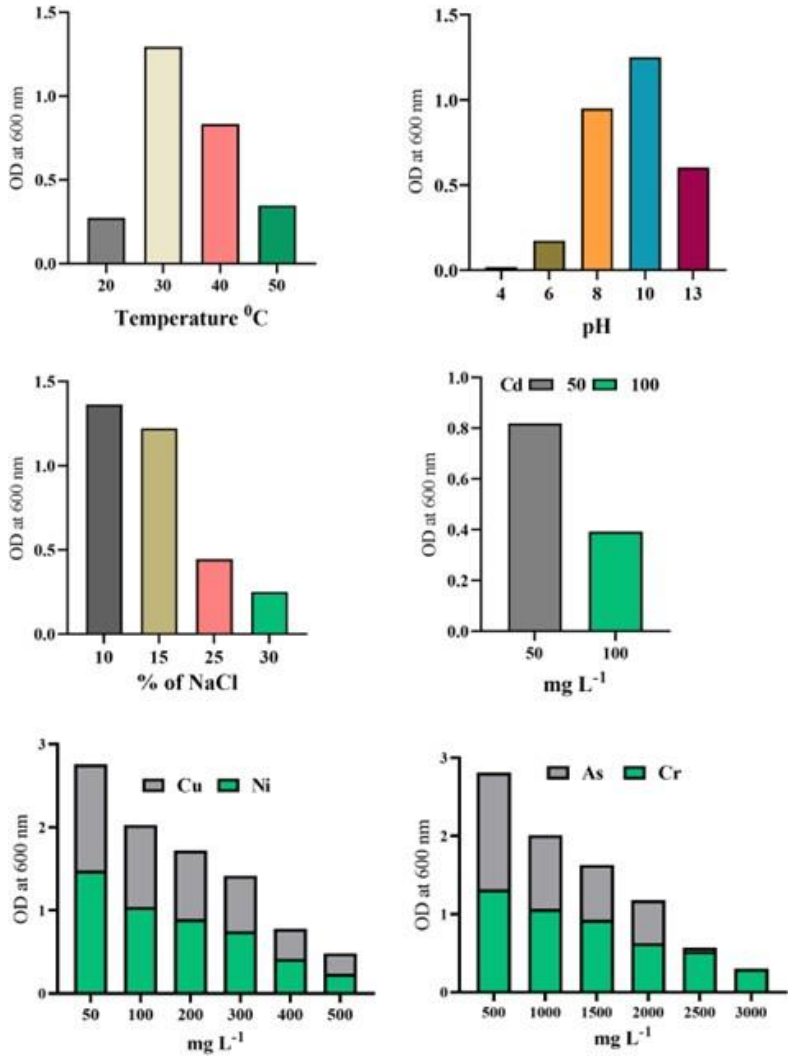

Fig. 6.2.1. Growth parameter and maximal metal tolerance by *Bacillus xiamenensis* ISIGRM16. (Values present in mean ±SD)

.

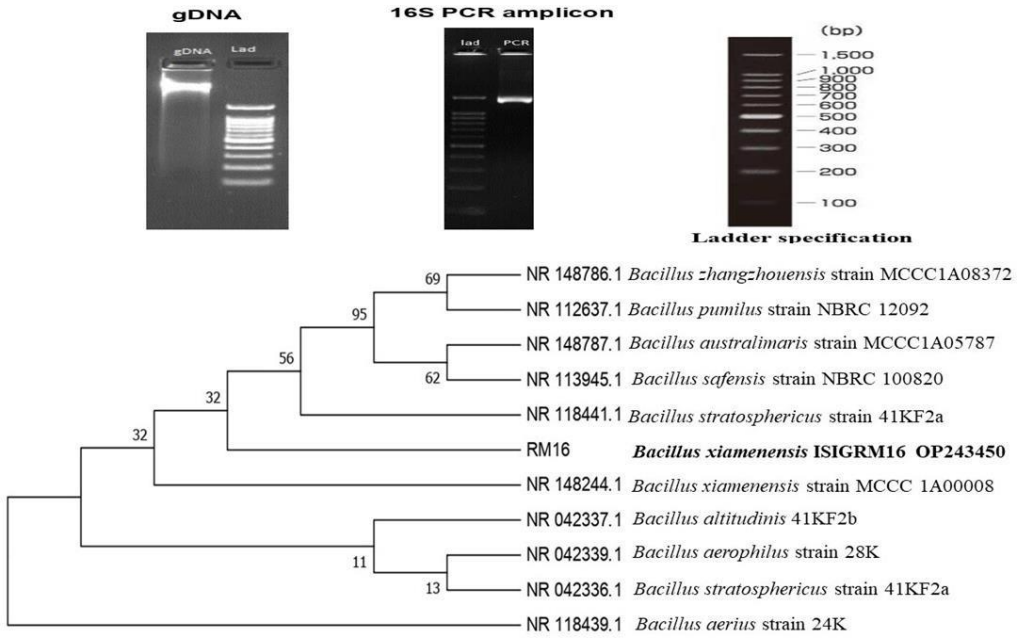

Fig. 6.2.2. Molecular identification of *Bacillus xiamenensis* ISIGRM16 by 16srDNA-based molecular methods and ISIGRM16 showed high similarity with *Bacillus xiamenensis* based on nucleotide homology and phylogenetic analysis

6.2.3.3. Surface morphology and spectral characterization of biosorbent

Investigation of the possible involvement of functional groups located on the bacterial surface. The pristine and metal adsorbed biomass were analyzed for FT-IR spectrometer. The recorded IR spectra are illustrated in Fig. 6.2.3 which clearly discriminate the metal-loaded and unloaded biomass. The unloaded biomass exhibited a number of peaks revealing complex structure of cell surface. The peak around 3400 cm^{-1} denoted the stretching vibration of the N-H bond of amino group and an indication of -OH group (Ozdemir et al., 2009). The linear stretching around 2900 cm^{-1} elucidated the asymmetric stretching of γC-H bond of the $-CH_2$ group combined with aliphatic methylene group. The peak at 1638 cm^{-1} specified the γC=O of amide I, while the peak at 1549 cm^{-1} designated γNH/γC=O bond of amide II indicating the presence of carboxyl group (Quintelas et al., 2009). A peak at 1081 cm^{-1} might be assigned for -C-O stretching vibrations. A P=O stretching vibrational peak was generated at 1400 cm^{-1} and might come from phosphoric acid. The peak around 1232 cm^{-1} identified the presence of C-N stretching vibration of the saccharide. The peak appeared at 400-1000 possibly the bending vibration within the polysaccharide molecule and near 599 may be ascribed to the deformation of modes of C−C=O groups in polysaccharides (Wiercigroch et al., 2017). Considering the

metal-laden biomass shifted in the peak position fairly defined the involvement of functional groups in adsorption. The peak near 1638 cm^{-1} was shifted to 1639 cm^{-1}, 1641$cm^{-1,}$ 1618^{-1} for Ni^{2+}, and Cd^{2+}, Cr^{6+} respectively. Following, metal adsorption peak near 3400 cm^{-1} shifted to 3465 cm^{-1}, 3467cm^{-1}, 3474 cm^{-1} for respective metals (Cd^{2+}, Ni^{2+} and Cr^{6+}). Change indicated the involvement of amino and hydroxyl groups. In the case of Ni^{2+} and Cr^{6+} an overlapping peak was generated at 3415 cm^{-1}. Two new peaks were generated at 480 cm^{-1} and 481cm^{-1} in Cr^{6+} and Ni^{2+} loaded biomass might be the result of the complexation/coordination reaction during adsorption. Peak near 1400 cm^{-1} slightly shifted to 1408 cm^{-1} for Cd^{2+}, and 1381cm^{-1}, and 1384 cm^{-1} for Ni^{2+} and Cr^{6+} respectively suggesting the participation of phosphate group. Metal sequestration critically changed biomass appearance. The ions bind to the functional group as ligands according to their preferences and availability of the functional group in the active site of biomass surface. Changes in the peak position indicated the involvement of carboxyl, phosphate, hydroxyl and amide groups, which coincide with Ozdemir et al. (2009); Mathivanan et al. (2021) who studied surface active groups of *Bacillus sp*. responsible for adsorption. Many other studies affirm similar to our findings (Priyadarshanee et al., 2021; Das et al., 2016). Although functional groups were majorly involved in adsorption nonetheless many other mechanisms could be responsible for new peak generation in metal-laden biomass. Chelation, coordination/complexations, and so on, thus, it's hard to conclude the exact mechanism of adsorption of the studied species. With the intention of investigating surface morphology of the biomass biosorbent FE-SEM microscopy gave a clear illustration concerning metal interactions **(**Fig. 6.2.4 and 6.2.5). The surface of the biosorbent appeared to be smooth, rod-shaped, dense, and shiny before metal interaction (Fig. 6.2.4) while under metal stress the surface appears to be rough, contracted and the adhesion of layers was caused owing to the action of metals. The crystal-like structure on the cell surface was possibly from the metal aggregates deposited on the cell surface (Fig. 6.2.5). A similar kind of crystal formation was corroborated by Li et al. (2021) in lactic acid bacteria after metal sorption. The aggregation of cells may arise from extra polymeric substances. EDAX spectra recorded the presence of carbon, hydrogen, nitrogen, phosphorus, sodium, calcium, and potassium coming from the cell wall component. Unloaded spectra did not indicate any signal of metals while the loaded one clearly defined the presence of Cd^{2+}, Ni^{2+}, and Cr^{6+}. Adsorption percentage on the cell surface is Ni^{2+}>Cd^{2+}>Cr^{6+}, which supports the findings obtained in multi-metal adsorption. A lower peak intensity of Ca in a loaded cell implied the release of Ca during metal adsorption, confirming the occurrence of ion-exchange mechanism (Li et al., 2018).

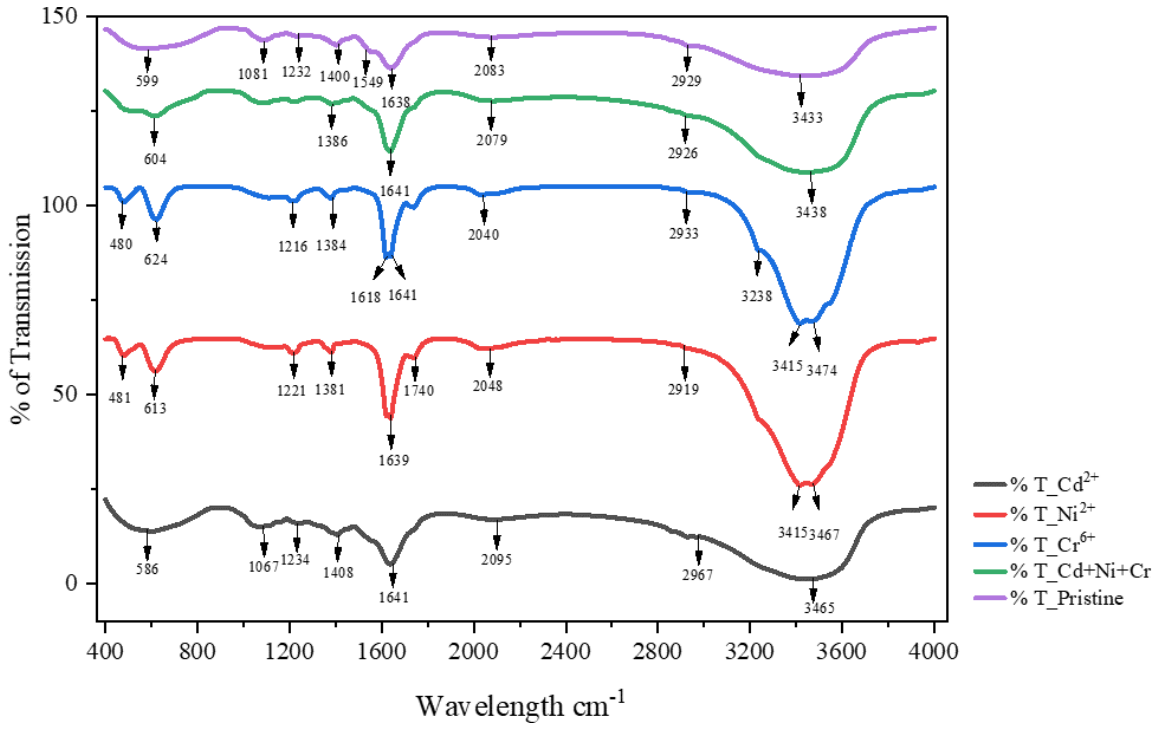

Fig. 6.2.3. FT-IR spectral analysis of biomass-biosorbent before and after adsorption (in single and ternary solution).

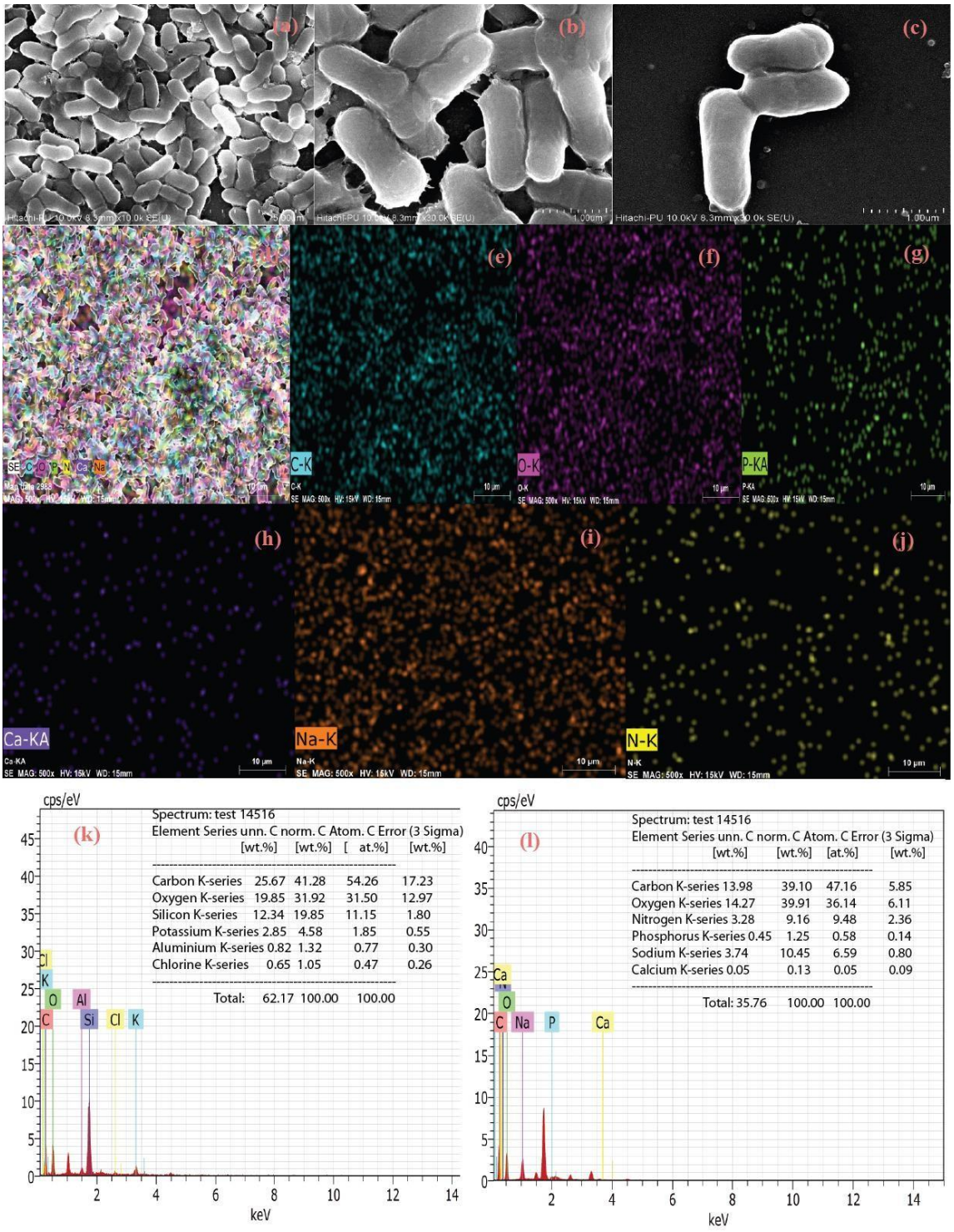

6.2.4. Field emission scanning electron microscopy-energy dispersive X-ray spectroscopy (FESEM-EDAX) of (a-l) bacterial cells without heavy metals. (a-c) represent the biomass-biosorbent surface morphology before metal adsorption and (d-l) represent elemental composition of biosorbent surface.

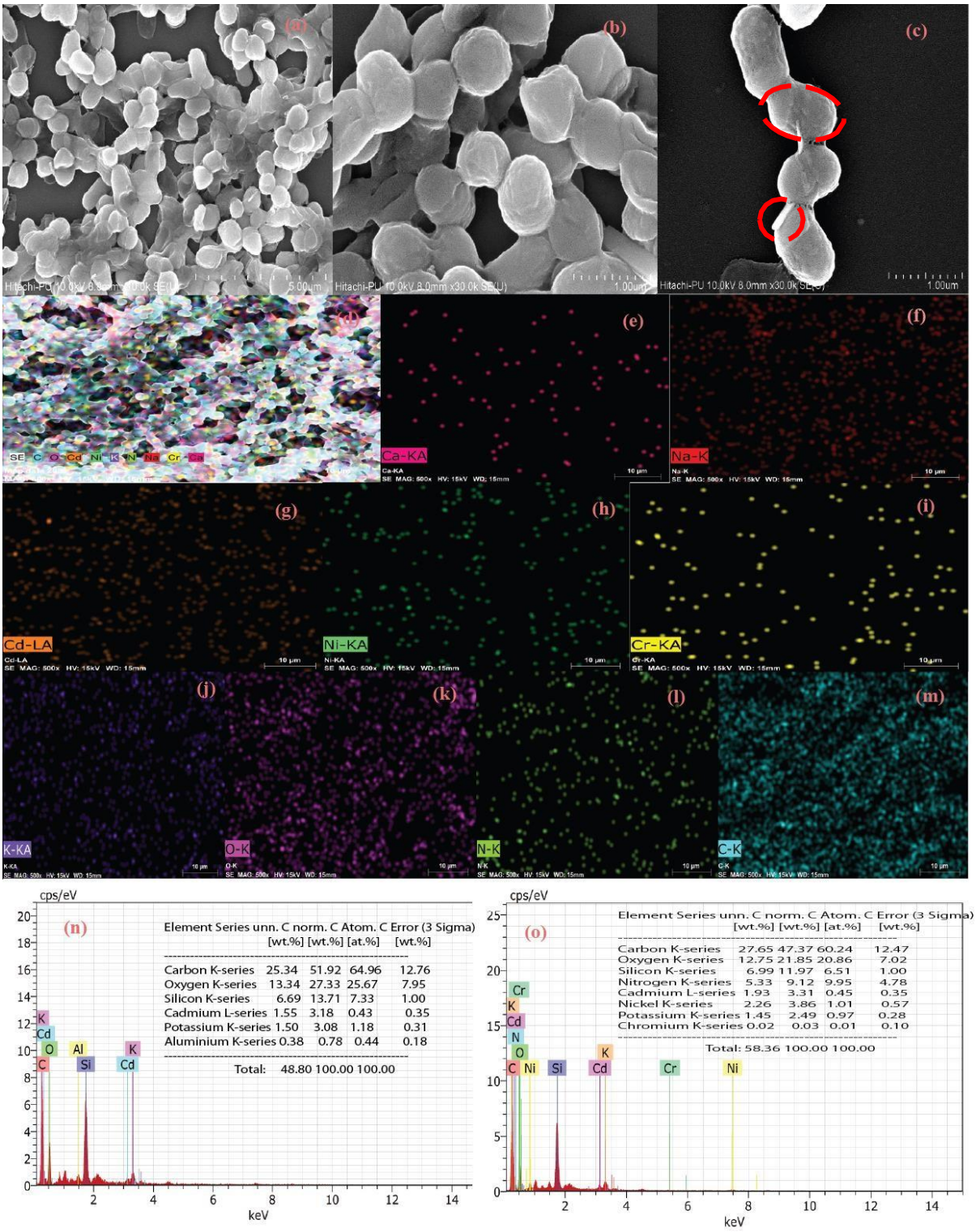

Fig. 6.2.5. Field emission scanning electron microscopy-energy dispersive X-ray spectroscopy (FESEM-EDAX) of (a-o) bacterial cells with heavy metals. (a-c) represent the biomass- biosorbent surface morphology after metal adsorption and (d-m) represent elemental composition of biosorbent which indicated the presence of Cd^{2+}, Cr^{6+} and Ni^{2+}. Red dotted line indicates the morphological alteration i.e., size reduction, crystal like structure formation etc.)

6.2.3.4. Batch experiments for metal (Cd^{2+}, Ni^{2+} and Cr^{6+}) removal

Investigation of the effect of different abiotic factors on adsorption process viz. pH, temperature, biomass dosage, contact time, initial concentration, and salinity in mono-metallic system clearly concluded a remarkable metal removal efficacy of the biomass-biosorbent under different environmental conditions. Optimum metal removal reaches after 60 minutes of interaction with 3g/L of dosage for Cd^{2+} while for Ni^{2+} and Cr^{6+} the equilibrium attains after 90 minutes of adsorption at 30^0C. From batch adsorption experiment results it is clearly perceived that biomass-biosorbent was more efficient for the removal of cationic species compare to the anions.

I. Effect of biomass dosage on biosorption with respect to temperature

Adsorbent-adsorbate interaction is highly influenced by adsorbent dosage owing to its different mechanisms of interaction i.e., adsorption, chelation, coordination, ion exchange etc. (Ren et al., 2015). In our study, we checked the removal (%) of a 100 mg/L metal solution with increasing biomass dosage i.e., 1g/L, 2g/L, 3g/L at three different temperatures 20^0C, 30^0C, and 45^0C for 2 hours (Fig. 6.2.6.). The result clearly depicted an increasing removal capacity with increased biomass dosage. For Cd^{2+}, maximum removal reached 99.55% ±0.51 after 60 minutes of interaction with biomass dose 3g/L while it decreased to 91.03% ±1.4 and 97.82% ±1.18 when biomass dosage was 1g/L and 2g/L respectively at 30^0C (Fig. 6.2.6.a). When reaction temperature lowered to 20^0C there were no significant changes in removal capacity 99.33% ±0.48 but with the rise in temperature at 45^0C the removal notably decreased to 92.33% ±2.4 ($p<0.0001$, two-way ANOVA, Tukey's multiple comparison test). In the case of Ni^{2+}, to reach the highest removal capacity it needed 90 minutes of interaction. After 90 minutes the removal was maximum of 89.37% ±0.78 at 30^0C for 3g/L dosage while it decreased at 45^0C showed 77.72% ±1.5 ($p<0.0001$). At 20^0C removal % was little less compared to its optimal removal at 30^0C ($p=0.0419$) (Fig. 6.2.6.b). Previously Cd^{2+} and Ni^{2+} adsorption by Ozdemir et al. (2009) on an extremophilic *Geobacillus* sp. recorded 82.2% removal while for Ni^{2+} 53.2% of removal at 100 mg/L of initial concentration implying that the investigated species of our study portrayed a greater efficiency. Contrastingly, removal of Cr^{6+} increased with the rise of temperature on 3g/L dose. Like the other two metals Cr^{6+} also showed an exponential removal from the aqueous medium with increasing biomass dosage. The removal capacity was maximum of 41.15% ±1.06 at 45^0C (Fig. 6.2.6.c). This increasing % removal with increased biomass dosage can be justified due to vacancy of more adsorption sites for complexation of metal ions. Although the efficacy of studied *Bacillus sp*. for Cr^{6+} adsorption was comparatively poor as Cr^{6+} is primely detoxified by bio-reduction mechanism, including the fact that Cr^{6+}

produce anionic species in aqueous medium and appear as $HCrO_4^-$ or $Cr_2O_7^{2-}$ ions at pH <6 and CrO_4^{2-} at pH>6 thus repealed by the bacterial surface which contain more negatively charged functional group (Ren et al., 2018).

In accordance with other studies, the present investigation evidenced a significantly decreased sorption capacity with increased biosorbent dose ($p<0.0001$) (Fig. 6.2.6 d-f). The capacity was highest for Cd^{2+} followed by Ni^{2+} and Cr^{6+}. Biosorption capacity of Cd^{2+} declined from 88.07 mg/g to 29.47 mg/g at 30^0C when the dose was increased from 1g/L to 3g/L at 30^0C. Similarly, Ni^{2+} adsorption capacity dropped from 42.12 mg/g to 27.82 mg/g when the dose was highest. At 45^0C Cr^{6+} the isolate portrayed the lowest adsorption capacity of 14.47 mg/g at 3g/L while highest 38.95 mg/g at 1g/L. The phenomenon can be well explained with the fact of aggregation and overlapping of binding site with increased biomass dose as well the inadequacy of metal ion concerning to binding site. A contradictory phenomenon was observed in the case of removal efficiency where it increased with biosorbent doses. (Nuhoglu et al., 2009; Wierzba et al., 2017).

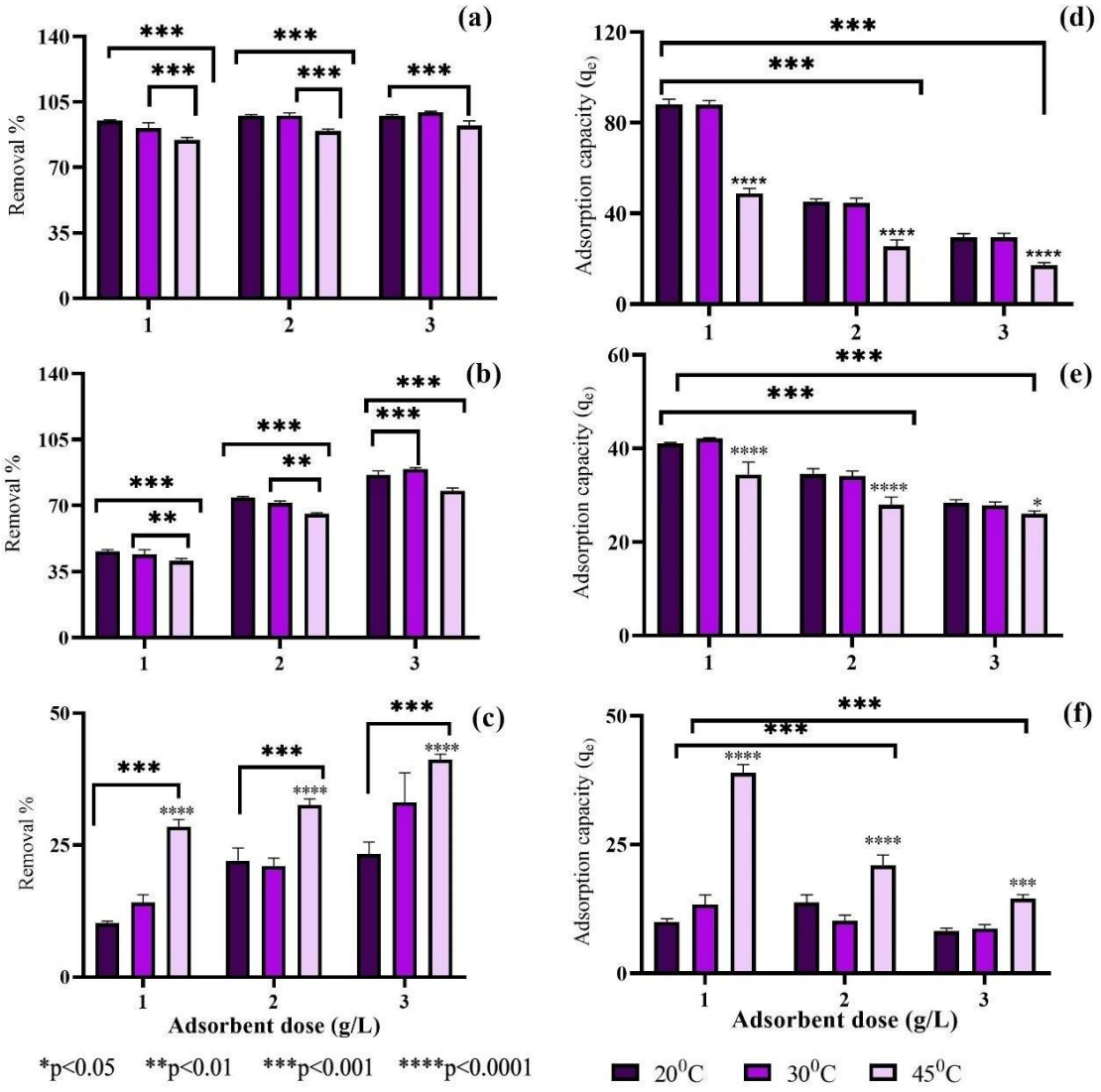

Fig. 6.2.6. Effect of biomass dose on the removal of Cd^{2+} (a), Ni^{2+} (b), Cr^{6+} (c) and adsorption capacity of Cd^{2+} (d), Ni^{2+} (e), and Cr^{6+} (f) with respect to temperature.

II. Effect of contact time on biosorption with respect to temperature

The effect of temperature with respect to incubation time critically influences the removal capacity of the biomass-adsorbent. Removal capacity was found to be enhanced with increasing time (0-120 minutes) by keeping the biomass dosage (3g/L) and initial concentration constant (100 mg/L) (Fig. 6.2.7); however, three different metals achieved saturation at different times. Out of the three metals, Cd^{2+} attained its equilibrium faster compared to Ni^{2+} and Cr^{6+} at 30^0C. Within 60 minutes of contact time, the biosorbent removed maximum Cd^{2+} (98.14% ±0.22) from the aqueous medium (Fig. 6.2.7a), while it took 90 minutes to reach the

equilibrium in the case of Ni^{2+} (maximum removal 87.81%±0.14) (Fig. 6.2.7b). The highest removal capacity for Cr^{6+} was also attained after 90 minutes of time (33.95% ±2.3) (Fig. 6.2.7c). However, any deviation in temperature had a significant impact on adsorption process ($P<0.0001$, two-way ANOVA and Tukey's multiple comparison test). Rising temperature significantly reduced removal capacity of both Cd^{2+} and Ni^{2+} while Cr^{6+} worked best at high temperature i.e., 45^0C. The removal efficiency of Cr^{6+} after 90 minutes of interaction increased from 33.95% ±2.3 to 41.76% ±1.63 ($p=0.0010$) whereas Cd^{2+} and Ni^{2+} decreased from 98.17% ±0.22 to 90.27% ±1.9 and 87.81% ±0.14 to 77.67% ±0.9 respectively ($p<0.0001$). Although reduction of temperature (20^0C) did not show any significant impact on Cd^{2+} and Ni^{2+} removal but it significantly reduced removal capacity of Cr^{6+} to 25.44% ±1.11 ($p<0.0001$). Attaining highest removal percentage at equilibrium was probably due to sorption accomplished through three stages, an initial rapid binding of metal ions or mass transfer tailed by intra-particular diffusion and lastly sorption of ions. After the equilibrium time, there was no such significant increase in removal percentage in all three metals might be due to the fact that at the initial state more vacant sites were available triggering enhanced sorption which further slowed down due to exhaustion of residual surface site and repulsive force between adsorbent-adsorbate interaction (Saravanane et al., 2002). In earlier studies by Nagarajan et al. (2015), and Quintelas et al. (2009), Ni^{2+} biosorption by using bacterial biomass took 120 minutes to 180 minutes to reach the equilibrium concentration, while the isolate of the present study showed a better performance. The lower biosorption of Cr^{6+} by the studied isolate is validated by the studies of Quintelas et al. (2009) who observed reduced Cr^{6+} adsorption in *E. coli*- biofilm and the phenomenon is truly justified by anionic dissociation of chromium in an aqueous medium.

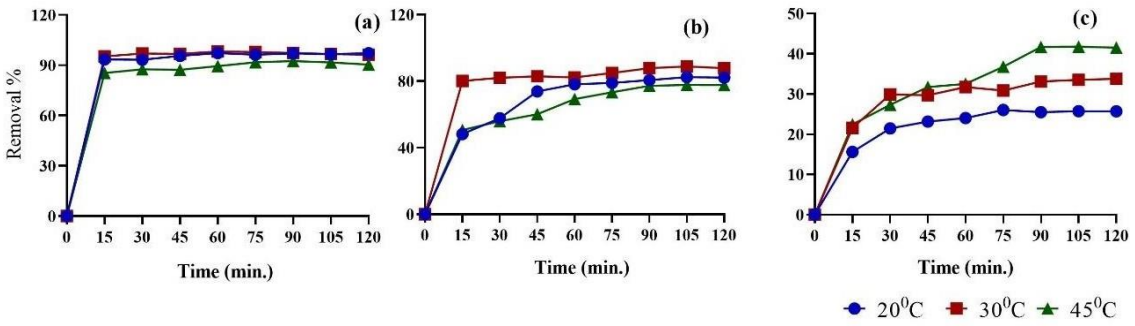

Fig. 6.2.7. Effect of contact time on removal of Cd^{2+} (a), Ni^{2+} (b), and Cr^{6+} (c) with respect to temperature.

III. Effect of pH on biosorption

The pH is the game changer of any reaction medium hence it is important to explore its effect on the adsorption system. pH alters the surface chemistry of the adsorbent as well as the metal speciation in the reaction medium thereby being considered an important parameter. The native pH of the solution was 5.2. Any increase and decrease in pH of the reaction medium was done using 0.1(N) NaOH and 0.1(N) HCl. To investigate the optimum pH for the adsorption of studied metals five different pH from acidic to basic range (2,4,6,8, and10) was taken, where the other parameters were constant like temperature (30^0C for Cd^{2+}, Ni^{2+} and 45^0C for Cr^{6+}), initial concentration (100mg/L) and time (2 hours) (Fig. 6.2.9a). Highest removal efficiency for metal Cd^{2+} and Ni^{2+} was achieved at pH 6, 98.24% ±1.0, and 86.30 ±0.2 respectively, while Cr^{6+} showed maximal removal at pH 2, 44.03% ±0.96. The removal efficiency of Cr^{6+} started decreasing with increasing pH value. The rise of pH from 2 to 4 removal of Cr^{6+} reduced significantly from 44.03% ±0.96 to 29.35% ±0.89 ($p<0.0001$, One-way ANOVA, Tukey's multiple comparison test). Beyond pH 4 the removal capacity fell drastically and at pH 10 and the removal was almost nil i.e., 5.58% ±1.04 ($p=0.0063$). As chromium produces negatively charged $HCrO_4^-$, $Cr_2O_7^{2-}$, CrO_4^{2-}, $Cr_4O_{13}^{2-}$ and $Cr_3O_{10}^{2-}$ in solution, it is more adsorbed when the surface of the biosorbent is protonated hence showed excellent removal at pH 2 (Ren et al., 2018).

In the case of $Cd^{2+,}$ the acidic pH turned out to be unfavourable for the adsorption exhibited 15.40% ±1.5 of removal at pH 2. The removal capacity started to increase from pH 4 65.91% ±1.1 to a maximum at pH 6 98.24% ±1.0. However, with a further increase in pH up to 10 the adsorption is more quantitative, nevertheless, there was a significant difference between removal capacity at pH 6 (98.24% ±1.0) and pH 10 (85.25% ±1.3) ($p= 0.0018$). Likewise, Ni^{2+} showed maximum removal at pH 6 (86.30% ±0.2) and minimum at pH 2 (1.6%± 0.7). Unlike Cd^{2+} beyond pH 6 removal of Ni^{2+} remarkably fell from 86.30% ±0.2 to 63.44% ±0.9 at pH 10 ($p<0.0001$) might be due to the precipitation of metal in hydroxide ion at higher pH. The acidity of the solution increases H^+ and H_3O^+ ions in the solution resulting in competition between metal cations and protons for binding sites leads to an inhibition of adsorption, while an increase in pH reduces the H^+ and availability of negative charge increases supports effective adsorption. Furthermore, the valence state, electronegativity, atomic weight, and ionic radius impact biosorption proficiency (Quintelas et al., 2009). Thus, a neutral range of pH had the optimal removal for Ni^{2+} from an aqueous medium. Similar findings were also reported in *Bacillus thuringiensis* by Oves et al. (2013).

IV. Effect of initial concentration of target metal on biosorption

The impact on initial concentration of the adsorbate is directly proportional to the adsorption capacity of adsorbent. The initial metal concentration for Cd^{2+} was 100 mg/L to 500 mg/L while for Ni^{2+} and Cr^{6+} the concentration was 30 mg/L to 500 mg/L. The results disclosed that with an increasing concentration, the removal efficacy of the bio-sorbent declined significantly (One-way ANOVA, Tukey's multiple comparison test) (Fig. 6.2.8) The removal % of Cd^{2+} was highest at 100 mg/L i.e., 99.34% ±0.21 and lowest at 500 mg/L, 80.24%±1.4 ($p<0.0001$) **(**Fig. 6.2.8a). In the same way, removal of Ni^{2+} significantly reduced at high concentrations ($p<0.0001$). The removal efficacy of biosorbent was well up to 100 mg/L, 87.58% ±0.4 with no significant decrease. Further enhancement in concentration depicted a decreasing order of removal; 56.11% ±0.51 (200 mg/L) > 40.28% ±0.45 (300 mg/L) > 33.68% ±2 (400 mg/L) > 29.30%±1.4 (500 mg/L) (Fig. 6.2.8b). Although the biomass-biosorbent performed well for Cd^{2+} and Ni^{2+} removal, yet, it showed the least performance on Cr^{6+} removal **(**Fig. 6.2.8c). The removal was maximum at 100 mg/L i.e., 32% ±1.3, and minimum at 500 mg/L i.e., 10.92% ±1.7. Like the other two metals, it also showed significantly reduced efficacy with elevated concentration ($p<0.0001$). Considering the adsorption capacity (q_e mg/g) which increased with the increased metal concentration. In all the metals the q_e (mg/g) was highest at 500 mg/L. For Cd^{2+} the adsorbed metal capacity (q_e mg/g) increased significantly ($p<0.0001$) following the order; 31.54 ±0.57 (100 mg/L) < 49.41 ±0.80 (200 mg/L) < 80.75 ±0.49 (300mg/L) < 100.88 ±0.33 (400 mg/L) < 124.11 ±1.26 (500 mg/L) (Fig. 6.2.8d). Ensuing the same trend, the uptake of Ni^{2+} also significantly increased ($p<0.0001$) with highest 54.20 ±0.99 at 500 mg/L and lowest 8.83 ±0.12 at 30 mg/L (Fig. 6.2.8e). Considering the poor removal capacity of Cr^{6+}, the metal uptake was correspondingly poor compared to former two, nevertheless, it also tracked in the same manner of lowest q_e 1.69 ±0.21; at lowest concentration, 30 mg/L and highest capacity 21.65 ±0.5 at highest concentration 500 mg/L ($p<0.0001$) (Fig. 6.2.8f). From the result, it can be concluded that the biosorbent was more efficient in removal of the Cd^{2+} followed by Ni^{2+} and Cr^{6+}. In another way, it can be said the biomass-biosorbent has more capacity to uptake cationic species compare to an anionic one in the aqueous medium.

This enhancement in sorption capacities might be due to an increase in electrostatic interactions, engrossment of sites with increasingly lower affinity for metal ions in addition to effective pore diffusivity at high concentrations. This behaviour is also supported by Hanif et al. (2007) who concluded that at lower concentrations the sorption sites were easily employed

by adsorbate while at higher concentrations the metal ion must diffuse through intra-particular diffusion sluggishly. Besides the higher driving force of higher initial concentration facilitate the uptake capacity adsorbent. In contrast, the percentage removal decreased with elevated concentration since most ions remain unadsorbed due to saturation of biosorption sites (Gupta and Kumar, 2019; Skodras et al., 2008).

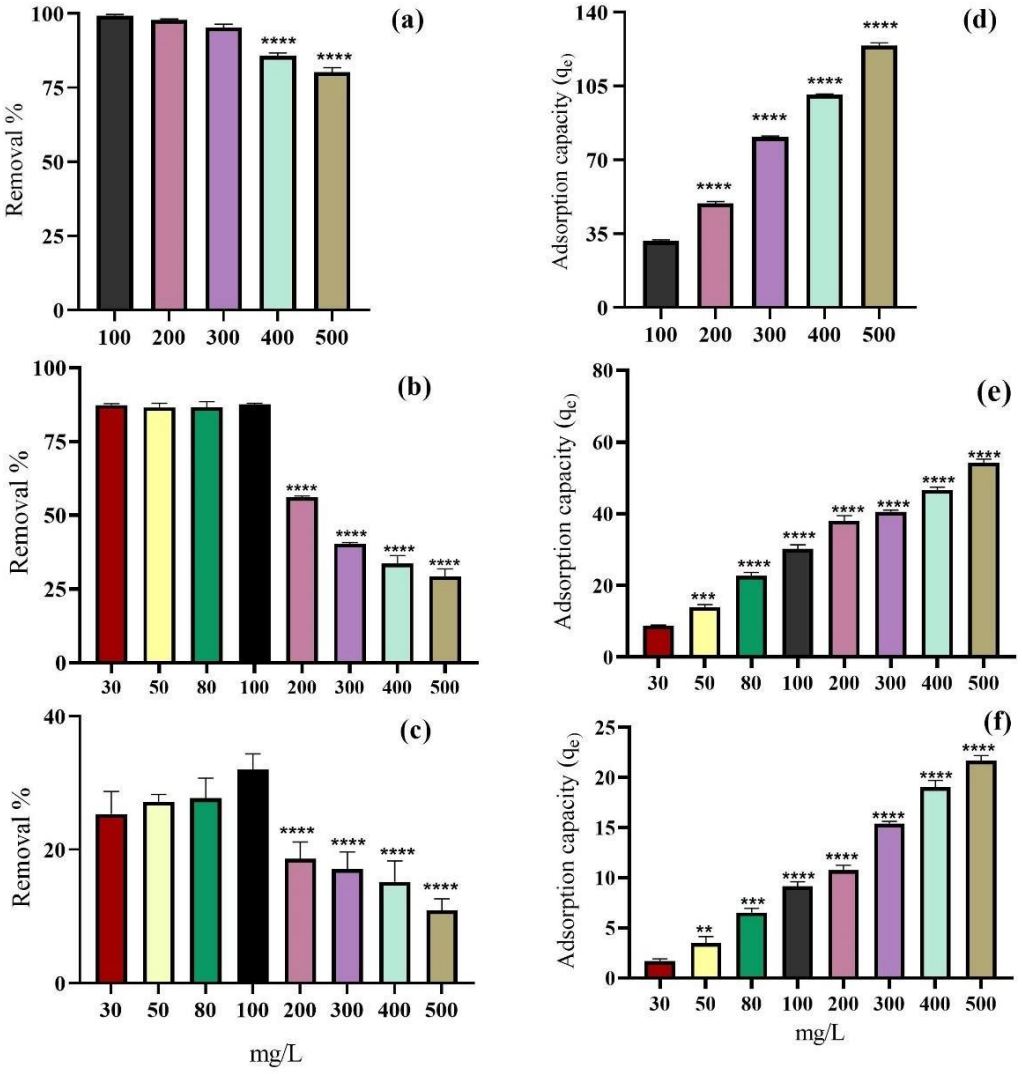

Fig. 6.2.8. Effect of initial concentration on removal of Cd^{2+} (a), Ni^{2+} (b), Cr^{6+} (c) and adsorption capacity of Cd^{2+} (d), Ni^{2+} (e), Cr^{6+} (f)

V. Effect of temperature on biosorption

Temperature is another important factor that has an immense influence on biosorbent capacity as well as metal solubility. Four different temperatures viz. 20^0C, 30^0C, 40^0C and 45^0C

were studied which comes to an interesting fact. In all the reaction systems the other parameter like initial concentration (100 mg/L), pH (6 for Cd^{2+} and Ni^{2+}; 2 for Cr^{6+}) time (2 hr) were kept fixed (Fig. 6.2.9b). The two metals Cd^{2+} and Ni^{2+} showed a greater removal capacity at lower temperatures while Cr^{6+} went in the opposite direction showed a greater percentage of removal at 40^0C to 45^0C. Removal of Cd^{2+} worked best at 20^0C and 30^0C where % of removal was 99.13 ±0.51, and 99.34% ±0.21 respectively. The efficacy lowered significantly when temperature rises up to 45^0C; (% of removal 92.39% ±2.01) (p=0.0099). This was perhaps the increasing kinetic energy between adsorbent-metal hindering the binding owing to higher molecular movement (Ahad et al., 2021). For Ni^{2+}, the biomass showed the best removal efficiency at 30^0C at 87.43% ±1.2 while an elevated temperature of 40^0C and 45^0C significantly dropped the removal efficiency to 79.97% ±1, 77.93% ±1.2 (p=0.0171, p= 0.0043) comparing with its optimal at 30^0C. This depreciation seems to be the result of elevated escaping tendency of cations from aqueous to bulk phase, including increased solubility of the cations at moderately high temperature (Arief et al., 2008). Interestingly, a higher temperature was found to be best for removal of Cr^{6+} where it showed its maximum removal 41.51% ±1.1 which was significantly higher (p=0.0001) compared to other temperatures.

VI. Effect of salinity on biosorption

Salinity is a vital factor and can have an influence on the adsorption process and here we found some exclusive facts on metal adsorption in saline solution. Keeping the other parameters constant viz. metal concentration (100 mg/L), temperature (30^0C for Cd^{2+}, Ni^{2+}, and 45^0C for Cr^{6+}), time (2h) three different % of saline solution viz. 2%,4%, and 6% solutions were taken to carry out the study (Fig. 6.2.9c). Both the metal Cd^{2+} and Ni^{2+} were moderately removed by the biomass up to 4% of NaCl concentration. The removal was maximum at 2% NaCl concentration, 54.85% ±1.3 for $Cd^{2+,}$ and 37.61% ±1.2 for Ni^{2+}. However, any additional increase in NaCl concentration drastically reduced removal efficiency ($p< 0.0001$). Our obtained result was supported by Mohapatra et al. (2019) who reported removal of another divalent cation Pb^{2+} by *Bacillus sp.* under NaCl concentration. In all the cases removal of Cr^{6+} was found to be extremely poor.

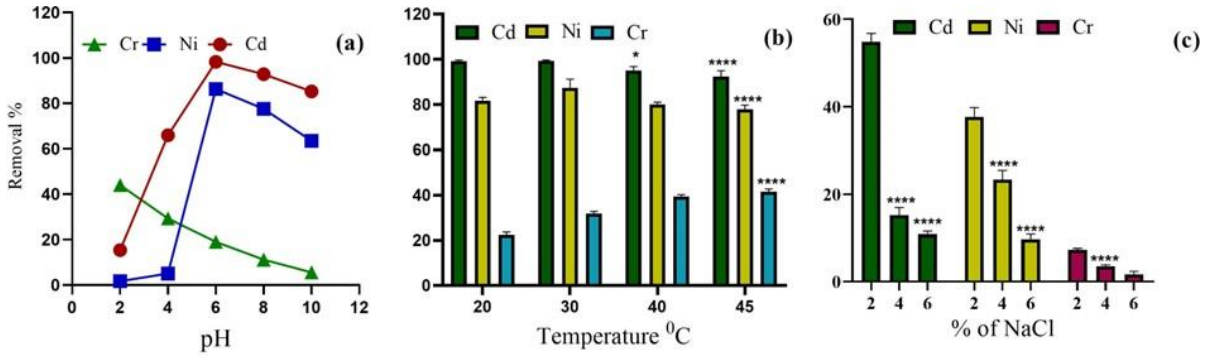

*p<0.05; **p<0.01, ***p<0.001, ****p<0.00001

Fig. 6.2.9. Effect of pH (a), temperature (b) and salinity (c) on adsorption

6.2.3.5. Adsorption Models

I. Adsorption isotherm

By keeping the initial concentration as the variable parameter for metal ions, the isotherm models are evaluated from the experiment done under a specific biosorbent dosage (3g/L), temperature 30^{0}C, pH of 6 for 90 minutes for Cd^{2+}. The time was 120 minutes for Ni^{2+}, and for Cr^{6+} pH was 2, and the time was 120 minutes. For a better comparison of experimental results four different isotherm models viz. Langmuir, Freundlich, Temkin and Dubinin-Radushkevich (D-R) isotherms were applied and the best-fitted model was declared based on the value of linear regression coefficient (R^2) **(**Fig. 6.2.10). The R^2 value closer to 1 represents fitness of the model. The linear form of equation and major parameters of four different isotherm models with respect to three different metals (Cd^{2+}, Ni^{2+} and Cr^{6+}) are listed in Table 6.2.1. The theoretic Langmuir isotherm model describes the monolayer adsorbate-sorption mechanism of homogenous sorption sites. It speculates the homogeneous nature of the surface of the biosorbent with a uniform distribution of binding sites sharing indistinguishable affinity facilitates absolute monolayer adsorption of metals on the surface of the biosorbent (Pakade et al., 2017). In our study, the R^2 value of Ni^{2+} (R^2>0.94) and Cr^6+(R^2>0.95) was found to be closer to 1 (Table 6.2.1). The maximum yielded adsorption capacity (q_{max}) was 58.20 mg/g which was near to that of calculated one and the coefficient of adsorption energy KL (L/mg) 0.053, derivated from intercept and slope of the plot 1/Ce vs 1/qe. The dimensionless RL 0.158 confirmed the favourability of the Ni^{2+} adsorption onto the bacterial surfaces. Relating to Cr^{6+} adsorption Langmuir isotherm showed very close agreement in experimental data approving

that one chromium molecule will be occupied by one singly active site (Ren et al., 2018). The maximum adsorption capacity q_{max} (mg/g) for Cr^{6+} was 85.9 and energy coefficient KL (L/mg) was derived from the slope and intercept of 1/Ce vs 1/qe plot. The favourability of the adsorption process was identified with a dimensionless separation factor RL value (0.001) lies lesser than 1 signifying the favourable adsorption process. The Freundlich isotherm model deals with the adsorbents that exhibit heterogeneous surfaces. It elucidates the bonding energy between adsorbent and adsorbate quantifying the amount of adsorbate adsorbed onto the heterogenous surface of the adsorbent (Ghaedi et al., 2014). Freundlich gave the goodness of fit for Cd^{2+} indicating bonding energy-driven multilayer heterogenous entrapment of cation onto the cell surface. In the present study correlation coefficient value (R^2 >0.97) being closer to 1 described the state of equilibrium in a better way. The Freundlich constant K_f related to adsorption capacity was 31.99 representing a closer agreement with experimental one (31.168 mg/g) and 1/n adsorption intensity derived from slope and intercept of Log q_e vs Log C_e plot was less than 1 was securing a favourable interaction between Cd^{2+} and biosorbent. Temkin isotherm determines the adsorption heat of all the molecules in the layer decrease linearly and based on electrostatic interaction (Mohi-Eldin et al., 2016). In the present study except for Cd^{2+}, the other metals poorly fit with the model. The correlation coefficient value (R^2) for Cd^{2+} is 0.97 while for Ni^{2+} and Cr^{6+} it's 0.92 and 0.94 respectively. The KT is the equilibrium binding constant corresponding to the maximum binding energy while B is related to the heat of the adsorption. The plot q_e vs ln C_e permits us to determine the isotherm constants B and KT from the intercept and slope correspondingly. For Cd^{2+} the calculated equilibrium binding constant KT (L/mg) was 20.54 and B (J/mol) 3.52. The D-R isotherm model was independent of Langmuir or Freundlich isotherm model and is common to describe the sorption mechanism of a single solute system (Dubinin et al., 1947). The parameters of the D-R isotherm are tabulated in Table 6.2.1. In the present study, all the metal barely followed the D-R isotherm due to their poor co-relation coefficient.

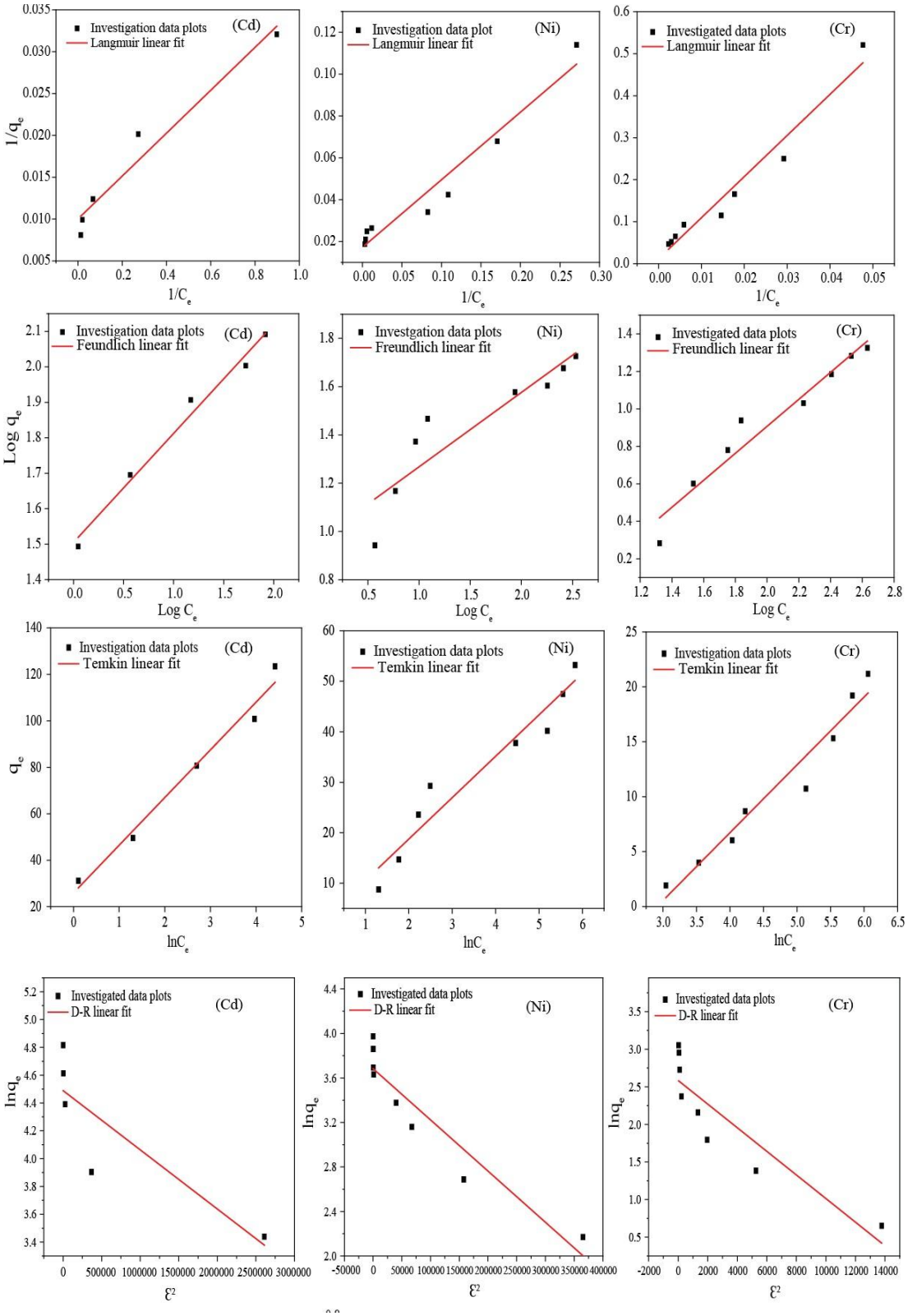

Fig 6.2.10. Illustration of isotherm models for Cd^{2+}, Ni^{2+} and Cr^{6+}. Langmuir, Freundlich, Temkin and Dubinin-Radushkevich linear model.

Table 6.2.1. Adsorption models parameters for biosorption of Cd^{2+}, Ni^{2+}, and Cr^{6+}

Adsorption models	Parameters	Test Metals								
		Cd^{2+}			Ni^{2+}			Cr^{6+}		
Langmuir Isotherm	q_{max} (mg/g)	99.800			58.207			85.98		
	K_L	0.390			0.053			8.78		
	R_L	0.026			0.158			0.001		
	R^2	0.942			0.941			0.953		
Freundlich Isotherm	K_f (L/mg)	31.995			9.122			0.292		
	1/n	0.307			0.307			0.720		
	R^2	0.979			0.806			0.938		
Temkin Isotherm	B (J mol^{-1})	20.540			8.204			6.177		
	K_T (L mg^{-1})	3.526			1.329			0.054		
	R^2	0.974			0.926			0.944		
Dubinin-Radushkevich Isotherm	q_e	89.041			39.77			13.25		
	E (KJmol^{-1})	1083.91			329.68			56.42		
	β (mol^2/K^2J^2)	4.25E-07			4.60E-06			1.5E-04		
	R^2	0.66			0.87			0.78		
		Cd^{2+}			**Ni^{2+}**			**Cr^{6+}**		
Kinetic Models		**20^0C**	**30^0C**	**45^0C**	**20^0C**	**30^0C**	**45^0C**	**20^0C**	**30^0C**	**45^0C**
$q_{e,\ exp}$ (mg/g)		31.42	31.16	30.01	23.63	29.30	23.17	7.50	8.67	13.68
Pseudo-first-order	$q_{e,\ cal}$ (mg/g)	2.39	0.66	1.61	5.34	2.27	5.21	1.55	1.13	2.88
	K_1 (min^{-1})	-0.0006	-0.0002	-5.9 x10^{-5}	-0.00009	-0.0002	-3.5 x10^{-5}	-0.0003	-0.0001	-0.0002
	R^2	0.808	0.709	0.115	0.146	0.688	-0.08	0.523	0.488	0.590
Pseudo-second-order	$q_{e,\ cal}$ (mg/g)	31.22	31.02	30.35	29.30	29.80	28.32	8.76	10.04	69.63
	K_2 (g $mg^{-1}min^{-1}$)	0.083	0.340	0.054	0.005	0.024	0.004	0.052	0.043	0.0002
	R^2	0.999	0.999	0.999	0.991	0.999	0.989	0.998	0.996	0.999

II. Kinetic models for the biosorption

Kinetic studies for biosorption are important to assess their mechanistic approach for interaction and the rate of biosorption process during mass transfer (Munoz et al., 2015). Two adsorption kinetic models i.e., pseudo-first-order and pseudo-second-order were investigated to evaluate the adsorbent-metal ion interaction in an aqueous medium at different temperatures (20^0C, 30^0C, 45^0C), and correlation coefficient (R^2) value closer to 1 demonstrated the fitness of model (Fig. 6.2.11). The respective equation and their constants are tabulated in Table 6.2.1**.** Considering the present study all three metals (Cd^{2+}, Ni^{2+} and Cr^{6+}) were well fitted with the pseudo-second-order kinetic models than pseudo-first-order owing to their R^2 values being closer to 1. The R^2 values for the Cd^{2+}, Ni^{2+} and Cr^{6+} were 0.999, 0.999, and 0.998 respectively at a temperature 30^0C (Fig. 6.2.11d-f). Furthermore, the equilibrium adsorption of the metals which was calculated from pseudo-second order i.e., $q_{e\ cal.}$ for Cd^{2+}, Ni^{2+} and Cr^{6+} were 31.02 mg/g, 29.80 mg/g, 10.04 mg/g respectively which was in high agreement with our experimental $q_{e\ exp}$ value (31.168 mg/g for Cd^{2+}, 29.300 mg/g for Ni^{2+}, and 8.675 mg/g for Cr^{6+}). Whereas, the $q_{e\ cal}$ of pseudo-first-order showed a large deviation with our experimental data as well the poor R^2 values rejecting the model for the present study (Fig. 6.2.11a-c). Moreover, the calculated rate constant ($K_{2\ cal}$) of pseudo-second-order kinetics of Cd^{2+}, Ni^{2+}, and Cr^{6+} were 0.34, 0.02, 0.009 correspondingly defining the biomass-biosorbent was more efficient in removing metal ions faster from aqueous solution, and the adsorption rate will be as follows Cd^{2+}> Ni^{2+}>Cr^{6+}, which again found to be consistent with our experimental outcomes. Under various experimental conditions described in literature, pseudo-second-order is the most fitted model widely for metal sorption (Khambhaty et al., 2009; Zhang et al., 2020; Nuhoglu et al., 2009). In contrast, the experimented decrease in the sorptive capacity of Cd^{2+} of biosorbent from 31.16 mg/g to 30.01 mg/g with an increase in temperature was satisfying the calculated decrease in rate constant K_2 (0.3 at 30^0C and 0.05 at 45^0C). A similar result was obtained for Ni^{2+} having a reduced sorptive capacity (29.30 mg/g at 30^0C and 23.17 mg/g at 45^0C) linearises with a reduction in K_2 value (0.02 at 30^0C and 0.004 at 45^0C). At 45^0C the number of bound ions decreased consequently the kinetic parameters do the same. As the sorbent is biological in nature, temperature rise might bring some changes in the surface that diminishes the adsorption of these divalent cations (Witek-Krowiak, 2012).

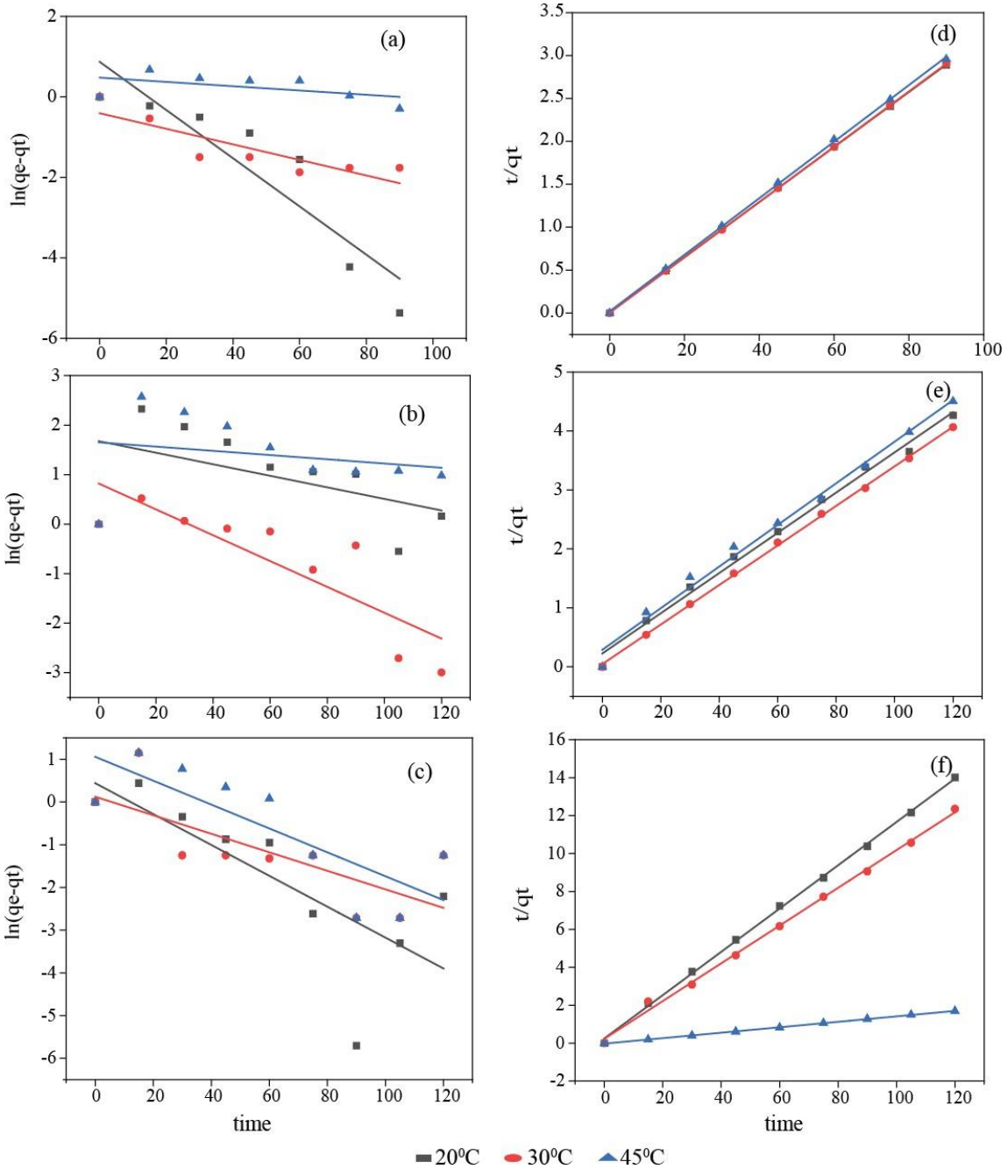

Fig. 6.2.11. Adsorption kinetics plots of biomass-biosorbent (a-c) pseudo-first-kinetics of Cd^{2+}, Ni^{2+}, Cr^{6+}; (d-f) pseudo-second-order kinetics for Cd^{2+}, Ni^{2+}, Cr^{6+}.

III. Thermodynamic analysis

Temperature is an important criterion that affects the adsorption process by determining its nature (exothermic or endothermic), spontaneity, and favourability (Mekonnen et al., 2015). The influence of temperature was studied at temperatures 20^0C, 30^0C, 40^0C, and 45^0C (Fig. 6.2.12) As per the first law of thermodynamics, it is postulated that energy cannot be generated

or lost and entropy is the only driving force in an isolated system (Nuhoglu et al., 2009). Hence, ΔG0, ΔH0, and ΔS0 are considered to be the most genuine parameters to interpret an adsorption process. The values of Gibbs free energy (ΔG0), enthalpy (ΔH0), and entropy (ΔS0) were calculated from lnK vs 1/t plot and summarised in Table 6.2.2. For Cd^{2+} and Ni^{2+} the value of ΔG0 was negatively directing the spontaneous nature of the process and with rising temperature, the decreasing value of ΔG0 was indicating unfavourable adsorption at higher temperatures while in Cr^{6+} the positive ΔG0 evinces the nonspontaneous nature of adsorption. A similar type of non-spontaneous behaviour was reported in metal and dye biosorption by plant biomass Amin et al. (2017). However, the non-spontaneity was decreased when the temperature was raised to 45^0C. The negative ΔH0 and ΔS0 declared the exothermic nature of reaction where randomness decreased at solid/liquid interface throughout adsorption process of Cd^{2+} and Ni^{2+} demonstrating sorption and decreasing on the successive increase in temperature. Contrastingly, the positive ΔH0 and positive ΔS0 was implying the endothermic reaction process with increased randomness at the solid/ suspension interface during adsorption of Cr^{6+}.

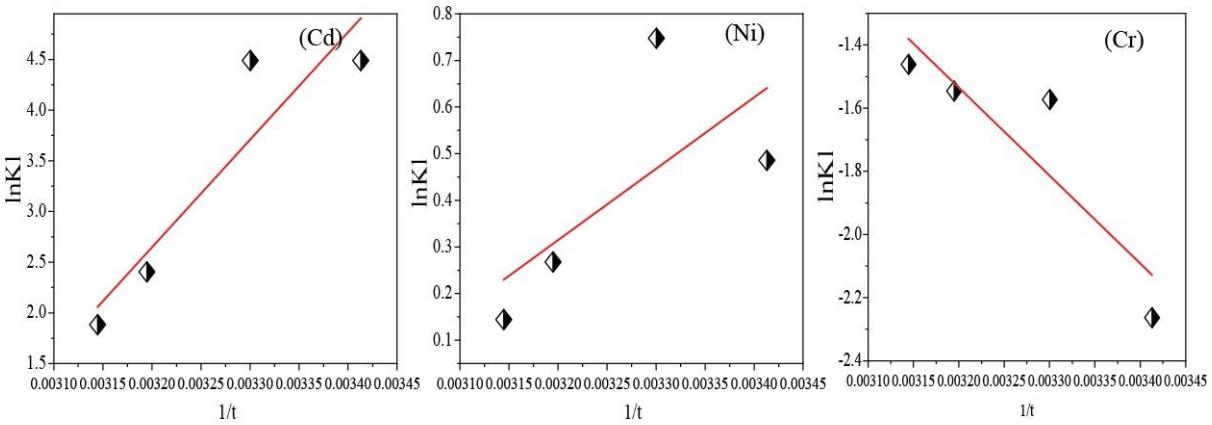

Fig. 6.2.12. The lnK vs 1/t plot against adsorption of Cd^{2+}, Ni^{2+}, and Cr^{6+}.

Table 6.2.2. Thermodynamic parameters for Cd^{2+}, Ni^{2+}, and Cr^{6+} adsorption

Test Metal	Temperature (^{0}C)	Temperature (K)	ΔG° (kJ.mole^{-1})	ΔH° (kJ.mole^{-1})	ΔS° (J.mole^{-1}.K^{-1})
Cd^{2+}	20^{0}C	293	-10.93	-88.22	-260.31
	30^{0}C	303	-11.30		
	40^{0}C	313	-6.25		
	45^{0}C	318	-4.97		
Ni^{2+}	20^{0}C	293	-1.18	-12.72	-38.09
	30^{0}C	303	-1.88		
	40^{0}C	313	-0.69		
	45^{0}C	318	-0.38		
Cr^{6+}	20^{0}C	293	5.51	23.16	61.35
	30^{0}C	303	3.96		
	40^{0}C	313	4.02		
	45^{0}C	318	3.86		

6.2.3.6. Biosorption in ternary system

In order to assess the degree of interference of neighbouring metal species in an adsorption process a multi-component adsorption experiment was done to check the efficacy of the biomass-biosorbent. The removal efficiency % and adsorption capacity of the biosorbent is given in Fig. 6.2.13a-b. As shown in Fig. 6.2.13a the removal of all three metals (Cd^{2+}, Ni^{2+}, and Cr^{6+}) faced a significant decrease in presence of co-ions, and when the concentration of co-ions increased from 100 mg/L to 500 mg/L each of the three metals in their respective system got a significant decrease ($p<0.001$). The removal capacity of Cd^{2+} in presence of Ni^{2+} and Cr^{6+} (Cd+Ni+Cr) get decreased to 84.33% ±0.61, and when the concentration of Cr^{6+} and Ni^{2+} increased up to 500 mg/L the removal capacity decreased significantly ($p<0.0001$; One way ANOVA; Tukey's multiple comparison test). The order of decrease of Cd^{2+} with increased concentration of Ni^{2+} and Cr^{6+} was as follows 84.33% ±0.61 (100 mg/L) > 73.14%±0.86 (200

mg/L) > 57.04%±0.37 (300 mg/L) > 49.01%±0.34 (400 mg/L) > 42.19±0.8 (500 mg/L) (Fig. 6.2.13a). Corresponding to removal percentage the adsorption capacity (q_e mg/g) of divalent Cd also decreased significantly from 27.61 ±0.9 to 12.90 ±1.3 (Fig. 6.2.13b). Following the same inclination removal of Ni^{2+} was found to be highest (81.075% ±0.04) when the co-ion (Cd^{2+} and Cr^{6+}) concentration was lowest (100 mg/L) and lowest (52.07%±0.8) when the co-ions were highest (500 mg/L) (Fig. 6.2.13a). The adsorption capacity (q_e mg/g) also declined at an elevated co-ion concentration (16.4 ±0.9). The biosorbent showed a similar proclivity for Cr^{6+} in presence of divalent Cd and Ni. Considering the co-ion concentration highest removal was 23% ±0.7 and the lowest was 11.76%±1.4 (Fig. 6.2.13a). In a ternary system, the adsorbent-adsorbate interaction can be expressed in a more classical way by calculating the relative adsorption capacity % (R_i) (Chang and Chen, 1998). Precisely it is the ratio of the adsorption capacity for one ion along with existence of the other ions, to the adsorption capacity for the same ion when exists alone in the solution. From the present study, we culminated that Ni^{2+} had the highest relative adsorption capacity (R_i) 92.57% followed by Cd^{2+} 90.66% and Cr^{6+} 82.46%. The competition whether antagonistic or synergistic was calculated by relative adsorption capacity (R_i). R_i >100% indicates the synergistic behaviour of metal, while R_i <100% denotes the antagonistic relations and R_i=100 validates non-interactive behaviour. Seeing outcomes, the R_i% of all three metals are <100% demonstrated that, they were antagonistic to each other might be due to the screening effect of metals present in the trio-mixture. So, it can be inferred that interaction among metals in natural systems is antagonistic. Similar findings were corroborated by Jain et al. (2015). Several factors could be responsible for this competitive behaviour viz. electronegativity, electrostatic attrition owing to charge-to-radius ratio, formation of metal hydroxide complex, suitable adsorption site etc. Comparing the performance of each metal in ternary solution with a gradual increase of co-ion's presence, Ni^{2+} performed most consistently up to the highest concentration of co-ions. It may be due to its smallest hydrated radius, highest reduction potential, and greater electronegativity influencing the strong attraction to the surface of adsorbents. However, compared to mono-metallic system the adsorption capacity decreased significantly in multi-metallic system might be the consequence of progressive interference of ions due to overlapping on the sorption site at higher concentrations (Srivastava et al., 2006).

`6.2.3.7. Desorption and reusability study

The desorption study was carried out in both acidic and basic mediums to determine the most effective one, which will be subsequently used for a reusability study (Gupta and Kumar, 2019; Chatterjee et al., 2020; Masoudi et al., 2018). Out of the five different mediums,

HCl was found to be the most efficient one for Cd^{2+} with 98.76% ±0.6 of recovery followed by HNO_3 and H_2SO_4; 97.6% ±0.57 and 96.74±0.47 respectively (Fig. 6.2.13c). HNO_3 showed the highest recovery rate for Ni^{2+} (97.73%±0.09) (Fig. 6.2.13c). For Cr^{6+} the basic medium turned out to be the best desorption solution with the highest desorption ability of 72.07% ±0.3 (Fig. 6.2.13c). The reusability study was accomplished using most effective desorbent solution for each metal and continued up to five cycles through a consecutive adsorption-desorption. After three cycles the adsorbent showed a significant decrease in removal of divalent Cd and Ni **(**Fig. 6.2.13d) while for Cr^{6+} the removal capacity significantly decreased ($p<0.05$; Sidak's multiple comparison test) after second cycle (Fig. 6.2.13d). After each cycle, the removal % was calculated, however after fourth cycle and fifth cycle the removal was decreased by 6% and 21% respectively for Cd^{2+}. Considering Ni^{2+} removal, at the end of fourth and fifth cycles of reusability study, the efficacy was reduced by 17% and 21%. For Cr^{6+} at end of fifth cycle removal % drastically fell and decreased by 44.15%. When metal-laden biomass (Cd^{2+}, Ni^{2+}, and Cr^{6+}) was desorbed into their respective eluent, the biomass showed successful removal of metal ions up to 3rd cycle. At 4th cycle, the biomass reduced its uptake capacity ($p<0.05$), while for Cr^{6+} the biomass can successfully be utilized up to 2nd cycle. Thus, the reusability study indicated the biomass of *Bacillus xiamenensis* ISIGRM16 can be reutilized for effective adsorption of metal ions.

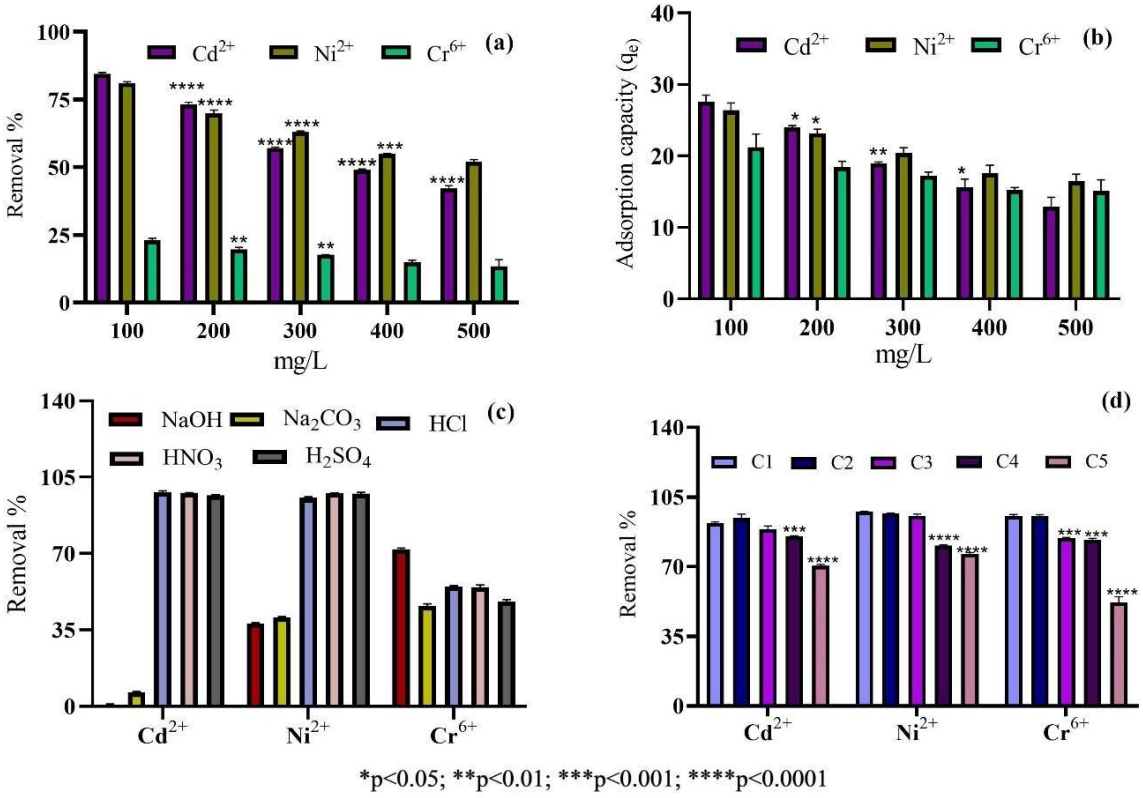

Fig. 6.2.13. Biosorption in ternary solution (a) removal percentage; (b) adsorption capacity; (c) desorption of metal using acidic and basic eluent; (d) regeneration study.

6.2.4. Comparative assessment with other strains

The strain of the present study was compared in terms of adsorption capacity with previously isolated different bacterial, fungal and algal biomass by various authors and presented in Table 6.2.3. The comparison fairly confirmed that the studied bacterium had good adsorption capacity for all three metals (Cd^{2+}, Ni^{2+}, Cr^{6+}) when compared with these formerly studied strains. Hence, this novel *Bacillus xiamenensis* ISIGRM16 is proved to be a potent biosorbent for those precarious metallic species.

Table 6.2.3. Comparison of biomass adsorption capacity of various bacterial, fungal, and algal strains.

Metal	Strain name	Adsorption capacity (mg/g)	Reference
Cd^{2+}	*Bacillus circulans* EB1	26.50	(Yilmaz & Ensari, 2005)
	Pseudomonas putida	8.00	(Pardo et al., 2003)
	Halomonas BVR 1	12.02	(Manasi et al., 2014)
	Actinomucor sp.	24.09	(Masoudi et al., 2018)
	Apergillus niger	1.31	(Kapoor et al., 1999)
	Caulerpa racemosa	10.40	(Tamilselvan et al., 2011)
	Geobacillus thermoleovorans sub.sp. stromboliensis	24.40	(Özdemir et al., 2009)
	Nostoc sp. JRD1	24.70	(Ahad et al., 2021)
	Spirogyra insignis	22.90	(Romera et al., 2007)
	***Bacillus xiamenensis* ISIGRM16**	**31.42**	**Present study**
Ni^{2+}	*Geobacillus thermoleovorans sub.sp. stromboliensis*	10.40	(Özdemir et al., 2009)
	Geobacillus toebii sub.sp. decanicus	21.10	(Özdemir et al., 2009)
	Yarrowia lipolytica	15.70	(Wierzba, 2017)
	Exiguobacterium sp. 27	28.50	(Amer et al., 2013)
	Rhodococcus opacus	12.69	(Cayllahua et al., 2009)
	Escherichia coli biofilm	6.90	(Quintelas et al., 2009)
	Exiguobacterium sp. ZM-2	20.10	(Alam & Ahmad, 2012)
	Aspergillus niger 405	14.10	(Filipović-Kovačević et al., 2000)
	***Bacillus xiamenensis* ISIGRM16**	**29.30**	**Present study**
Cr^{6+}	*Penicillium chrysogenum* (raw)	9.11	(Netzahuatl-Muñoz et al., 2015)
	Aspergillus niger ZH2 (dead biomass)	8.89	(Noreen et al., 2010)
	Aspergillus niger 405	7.2	(Filipović-Kovačević et al., 2000)
	Aspergillus flavus	0.53	(Riti Thapar, 2022)
	Aspergillus niger	11.72	(Mondal et al., 2017)
	***Bacillus xiamenensis* ISIGRM16**	**13.68**	**Present study**

6.2.5. Conclusion

The dried biomass of *Bacillus xiamenensis* ISIGRM16 proved to be an effective biosorbent and possesses removal efficacy in order > 99% Cd^{2}+, >85% Ni^{2+}, and>40% Cr^{6+}. FT-IR study validated the involvement of surface negative charges for biosorption. Optimized condition for removal of cationic and anionic contaminants was pH6 and pH2 respectively. Sorption potential was marginally affected at relatively higher concentrations of adsorbate (max. 500mg/L) and 3g/L biomass dosage worked best for adsorption. Satisfactory performance was observed in a multi-metal system with decent adsorption capacity (Ni^{2+}>Cd^{2+}>Cr^{6+}). The desorption and regeneration study disclosed a high recovery rate of all metals (>98% Cd^{2+}>97% Ni^{2+}>70% Cr^{6+}) and higher removal potential up to 3rd cycle making them cost-effective for commercial purposes. Usage of dried biomass turns out to be advantageous for remedial purposes as it eliminates the efflux of metal of living ones. Lastly, the metal affinity to the biomass was found to be in the sequence Cd^{2+}>Ni^{2+}>Cr^{6+} and the preference of biosorbent for metal can be elucidated based on the electronegativity of the metal ions and their cation/anion state.

Chapter 7

Vermisanitization of red mud (RM)

Chapter 7

Vermisanitization of red mud (RM)

7.1. Introduction

To fulfill the everyday need of this expanding population, from nib of a pen to a syringe of injection, to construction, transport, domestic purpose, and many other commodities- the aluminum industry is truly shaping our daily life. However, the unchecked release of this industrial waste has always been an environmental concern for decades. Red mud is a high-volume by-product generated by alumina refineries popular for its sodic-alkaline characteristics. Globally >100 million tons of red mud is produced each year, out of which India contributes 9 million tons annually. Red mud's high sodicity and alkalinity in association with toxic elements (Cr, Cd, Ni, Pb, Cu, V, As) impose a potential threat towards sustainability (Di Carlo et al., 2020; Bray et al., 2018). About 0.5-2 tons of bauxite residue (red mud; RM hereafter) is produced while one ton of alumina is extracted through Bayer process. This increasing accumulation of RM accelerates the global inventory of disposals. High salinity, alkalinity, and polymetallic species existence together with radioactive elements degrade the soil quality and structure besides continuous leaching of toxic elements leading to the deterioration of groundwater, and surface /sub-surface water quality (Dey, 2021). Moreover, the fine particles of dried red mud dispersed in the air, trigger air pollution causing numerous diseases in workers including the people in a closer vicinity. The infiltration of liquid discharged from dumped sites containing a high amount of Na destroys the biological health of soil, retarded plant growth, and reduced productivity. Although there is some use of red mud exists (construction material, brick, and cement production) nevertheless the utilization rate is very poor considering their massive production worldwide.

The present state of the art of rehabilitation techniques involves revegetation, dry mud stacking, seawater/CO_2 neutralization, addition of gypsum, treatment with acid, etc. The common end practice is to cover the dump with soil and establishment vegetation, yet, high operational cost of this cap and cover technique makes it unpopular to the industries. Abandoning the disposal without surface layering causes greater infiltration of rainwater and dust generation (Naykodi et al., 2022; Bray et al., 2018). As a consequence, industries are mainly focusing on direct revegetation by using some alkali-tolerant grass family plants, overlooking the internal soil health. However, many researchers currently suggest focusing on

restoration of soil health not only above the ground but also on enhancing the soil microbial community (Forey et al., 2018; Boyer & Wratten 2010). In such a challenging frame, amelioration through earthworm intervention may open a new avenue from the ecological viewpoint.

Earthworms are regarded as soil-engineer. Relating to soil health earthworms are unanimously considered soil indicators and were formerly utilized by many researchers in the restoration of degraded soil quality. Their voracious feeding habit, burrowing activity, and worm-microorganism interactions are the prime mechanisms of vermitechnology. This sustainable bio-engineered practice is gaining importance for pollution mitigation owing to the metal accumulation ability of earthworms. Only a few species are designated to be good bio-transformers of metal and metalloids such as *Eisenia fetida*, *E. andrei*, *Perionyx excavatus*, *Eudrilus eugeniae*, and *Lumbricus rubellus* among thousands of species (Roy et al., 2021). The earthworms consume metal-rich substrate as feeding material that eventually induces some unique metal-chelating cysteine-rich protein (metallothionine) in their gut thereby reducing the bioavailability of metal in the end product. Additionally, earthworms' ground and converted the waste product into a finer substance afterward their gut microflora mineralizes the essential nutrient and makes them bioavailable (Mondal et al., 2020). The feedstock composition of vermibed is a vital factor that regulates the performance of earthworms in the degradation of waste. Since red mud is extremely inhospitable for earthworms due to high alkalinity, lack of nutrients and reduced moisture content, a readily decomposable organic substrate (cow dung; CD hereafter) had been used as a bulking agent. Two types of composting processes (aerobic composting and vermicomposting) were used to opt for an eco-friendly sustainable amelioration of red mud. The involvement of earthworms in consort with their gut-associated microflora in vermicomposting plays a crucial role in bioconversion while indigenous microbial decomposition is the governing factor of aerobic composting. In the present study, *Eisenia fetida* was taken as candidate species for vermi-sanitization of alkaline waste on account of their short life span, high productivity, ease to handle, cultivable under laboratory conditions, and wide tolerance to environmental factors (temperature, pH, moisture content) additionally they do not provide any underestimation of ecotoxicological risk, unlike some native populations (Paul et al., 2018; Sahariah et al., 2015).

The compost quality can be effectually appraised by studying their microbial community structure. Phospholipid fatty acid (PLFA) analysis is an important gateway in assessing microbial diversity during composting and vermicomposting. They are an important

structural unit on the organism's plasma membrane that gets altered to adapt to any environmental fluctuation. Hence, PLFA profiling provides a comprehensive idea of behavioural changes of microorganisms towards bio-engineered feedstock. Microbes and earthworms combinedly degrade the waste-amended feedstock and end up with a value-added product. After an extensive literature survey, we have come up with numerous rehabilitation strategies for this momentous alkaline RM, nonetheless, except for revegetation, no attempt has been made to remediate the RM employing epigeic earthworm species. Considering the advantageous outcome of vermicomposting for the first time an attempt was made to introduce earthworms to that hostile RM, and finally, the sanitized and stabilized end product was used for agricultural application. Under this context, the present study was designed to estimate the practicability of vermitechnology in the stabilization of red mud into nutrient-rich compost along with metal detoxification potential of *E. fetida* from red mud to finished products. Different feedstock combinations were tested to find a suitable one for optimization of vermiculture in the long run. We hypothesized that earthworm-mediated degradation and mineralization would alter the microbial and physicochemical indices of different feedstock that can be well utilized for crop productivity.

7.2. Material and Methods

7.2.1. Procurement of cow dung, red mud, and earthworm species

The red mud (RM) waste was collected from an alumina plant located in Muri, Jharkhand. Urine-free cow dung (CD) used in this experiment was obtained from a local cowshed of Giridih. Initial physicochemical characteristics of RM were done following Page et al. (1982). 40 to 50 days old ciliated adult epigeic species of earthworm *Eisenia fetida*, weighing approximately 200-300 mg were procured from institutional vermiculture unit at Giridih, Jharkhand. RM was mixed with cow dung to generate different feedstock combinations to perform both aerobic and vermicomposting.

7.2.2. Feedstock preparation and treatment design

Two bio-composting techniques were adopted i.e., aerobic composting and vermi-composting. At first, the collected RM sample was pulverized into finer particles and subsequently homogenously mixed with the bulking agent (cow dung) in various ratios. The experimental mixtures were given below

Composting	Vermicomposting (*Eisenia fetida*)
CD- AC0	CD+ *Eisenia fetida* - VC0
RM+CD (1:1)- AC1	RM+CD (1:1) + *Eisenia fetida* - VC1
RM:CD (1:2)- AC2	RM:CD (1:2) + *Eisenia fetida* - VC2
RM:CD (1:3)- AC3	RM:CD (1:2) + *Eisenia fetida* - VC3
RM:CD (1:4)- AC4	RM:CD (1:4) + *Eisenia fetida* - VC4

Aerobic composting was done following Goswami et al. (2013). The CD-RM mixtures were left for 10-12 days for initial waste stabilization and microbial activation. This technique helps to thermostabilized the feedstock and satisfactorily prepares for earthworm employment to the mixture and their proliferation leading to an accelerated degradation process (Hussain et al., 2018). After achieving a stable pH (initial pH 9.8±1.9) and temperature (~35^0C) earthen pots designated for vermicomposting were inoculated with *Eisenia fetida* @ 10 worms per kg. The vessels were incubated for 90 days in partially dark humid conditions maintaining 50%-60% moisture with intermittent stirring. All the treatments were in triplicated form. Earthworms were also inoculated into only RM-based vermibed, but all the earthworms died within two days of inoculation hence the experiment for this treatment was withdrawn. The representative samples were drawn periodically at 0, 30, 60, and 90 days in adequate amounts for microbial and physicochemical analysis.

7.2.3. Growth and fecundity assessment of earthworm

Earthworms are well used in the bioconversion process owing to their robust adaptation and endurability towards substrate. They were taken periodically every 30 days and counted by a previously standardized method (Goswami et al., 2016). Briefly, feedstocks were put on aluminium trays, and earthworms were sieved via a mesh, manually counted, and reintroduced to the allocated vessel with the feedstock. Lastly, at the end of incubation period (i.e., 90 days) vermiprocessed feedstocks were withdrawn from the vessel and sieved to take the final count of juvenile and adult earthworms. However, earthworms introduced to crude RM were unable to survive, and replenishment did not make any difference in their survival. The mortality rate was calculated following equation (Garg & Gupta, 2011).

$$\text{Mortality rate}(\%) = \frac{E0-Et}{E0}$$

Where E0= initial number of worms and Et= final number of worms.

In due course, the earthworms were released to the stock vermiculture unit. The present study correspondingly arrayed their growth and fecundity in the RM-based feedstock deploying some formulae viz. reproduction rate, growth rate, biomass gain per unit of waste, etc., and presented following (Garg & Gupta, 2011).

$$\text{Reproduction rate} = \frac{C}{E}$$

Where R is the reproduction rate, C denotes cocoon produced and E is the initial number of earthworms.

$$G = \frac{B2-B1}{Txn}$$

where g = growth rate (mg/worm/day); *B*1 = initial worm biomass (mg); *B*2 = maximum biomass (mg); *T* = time (number of days); *n* = initial count inoculated.

$$\text{Biomass gain per unit of feed mixture} = \frac{B2-B1}{w}$$

Where W is the total quantity of waste taken (g).

7.2.4. Evaluation of physicochemical properties and microbial dynamics of the feedstock

The physicochemical dynamics of the feedstock composition of both aerobic and vermicomposting were analysed by following Page et al. (1982). The chemical attributes like pH, electrical conductivity (EC), easily mineralizable N, and total organic carbon (TOC) were analysed temporally while, P, K, Na^+, and Ca^{2+} were measured in both initial and matured feedstock (Description detailed in chapter 4, section 4.2.2). All analyses were performed according to the general quality control guideline using analytical grade chemicals (with more than 90% purity). The performance of two bio-composting (aerobic composting and vermicomposting) systems was evaluated by calculating their nutrient benefit ratio (NBR) and biodegradability coefficient (K_b) (Eq. 6) following Sahariah et al. (2015) and Diaz et al. (2002). BR will put light on the quality improvement and nutrient acquisition of composting process while K_b will exercise the degree of degradability. The variables such as available K, P, and

easily mineralizable N were taken for computation of nutrient benefit ratio following the formula by Sahariah et al. (2015).

$$\text{Nutrient benifit ratio} = \frac{Average\ conc.(90d) - average\ conc.(0d)}{Average\ conc.(0d)}$$

$$\text{Biodegradibility coefficient } (K_b) = \frac{(OMi - OMf)x100}{OMi(100 - OMf)}$$

Where OM_i is the initial organic matter content and OM_f is the organic matter at the end process.

To assess the temporal fluctuations in microbial biomass C (C_{mic}), compost respiration (glucose-induced respiration) fresh moist sample was taken at 30 days interval and measured according to Jenkinson, (1988) while enzymatic activities (urease, alkaline phosphatase, fluorescein-diacetate hydrolysing activity, dehydrogenase, aryl sulphatase) were measured following Tabatabai, (1994).

A. Alkaline phosphatase, fluorescein-diacetate hydrolysing activity (FDA), dehydrogenase, aryl sulphatase (Description detailed in chapter 6; section 6.1.2.2.).

B. Microbial biomass C (Description detailed in chapter 5; section 5.2.5)

C. Urease activity (Tabatabai 1994)

The method is based on determination of ammonia released after the incubation of soil samples with urea solution for 2h at 37^0C.

Reagents:

1. Toluene
2. THAM buffer (pH 9.0), 0.05 (M) – 6.1g Tris (hydroxy methyl aminomethane) was dissolved in about 700ml of water. The pH of the solution was brought to 9.0 by 0.2(M) sulphuric acid and diluted with water to 1L.
3. Urea solution, 0.2 (M) – 1.2g urea was dissolved in about 80ml of THAM buffer and the solution was diluted to 100ml with THAM buffer. The solution was stored in a refrigerator.
4. Potassium chloride, 2.5(M) + Silver sulphate (100 mg/L) solution – 100mg silver sulphate (reagent grade) was dissolved in about 700ml water. 188g potassium chloride (reagent grade) was dissolved in this solution and diluted to 1L.

5. Magnesium oxide
6. Mixed indicator – 0.66g bromocresol green and 0.33g methyl red were dissolved in 1L ethanol (95%).
7. Boric acid indicator solution – 20g pure boric acid (H_3BO_3) was dissolved in about 700ml hot water. The cooled solution was transferred to a 1L volumetric flask containing 200ml ethanol and 20ml mixed indicator solution. After mixing the contents of the flask, 0.05(N) NaOH (approximately) was continuously added until the colour was reddish purple. The volume was then made up to the mark with distilled water and mixed thoroughly.
8. 0.005 (N) H_2SO_4
9. 0.05 (N) NaOH
10. 0.1(N) Oxalic acid.

Procedure

1. The samples were tested in triplicate and mean of triplicate determinations were computed.
2. 5g sample was taken in a 50ml volumetric flask and 0.2ml toluene and 9ml THAM buffer were added to it.
3. The flask was swirled for few seconds to mix the contents. Then 1ml of 0.2 (M) urea solution was added and swirled again for few seconds. The flask was stoppered and placed in an incubator at 37^0C for 2 hours. After 2 hours, the stopper was removed.
4. Approximately 35ml KCl-Ag_2SO_4 solution was added and the flask was swirled for few seconds and allowed to stand until the contents had cooled to room temperature (5 minutes). The volume of the flask was made upto 50ml by addition of KCl-Ag_2SO_4 solution. For control, urea solution was added after the addition of KCl-Ag_2SO_4 solution.
5. To determine NH_4-N in the resulting soil suspension, a 20ml aliquot of the suspension was pipetted out into 100ml-distillation flask and 0.2g MgO was added to it. The contents of the flask were then distilled for 5 minutes and the distillate was collected in a 50ml conical flask containing 5ml boric acid indicator solution. The distillate was titrated with 0.005 (N) H_2SO_4.
6. 1ml of 0.005 (N) H_2SO_4 is equivalent to 70μg NH_4-N.

Calculation

Urease activity (μg urea hydrolyzed/g oven dry sample/h at 37^0C) = $\frac{C\ X\ 50\ X\ 2.144}{dwt\ X\ 5\ X\ 2\ X\ 20}$

C = Measured NH_4-N concentration (μg/ml) in sample – Measured NH_4-N concentration (μg/ml) in control sample;

d_{wt} = oven dry weight of 1g sample;

5 is the weight of sample used;

50 is the total volume of the sample suspension;

2 is the period of incubation;

20 is the volume of aliquot taken.

2.144 is the conversion factor for NH_4-N to urea.

D. Compost respiration (Epstein, 1997)

Compost respiration is the respiration of both the aerobic and anaerobic microbe present in composted samples, due to which organic materials are decomposed and release of CO2 in the atmosphere.

Reagents

1. NaOH (0.1N): Dissolved 4 g of NaOH in water and volume made up to one litre by adding distilled water.
2. HCl (0.05N): At first, prepared 1N HCl (By taking 50ml of HCl from the stock solution volume made up to one litre.)
3. BaCl2 (0.5M): Dissolved 122.14g of BaCl2 in one litter of distilled water.
4. Phenolphthalein indicator: 0.1g of phenolphthalein and 80ml of ethanol were mixed
5. and made the volume up to 100ml.

Procedure

1. 10g of moist sample was taken from each treatment in a 500ml conical flask.
2. In a test tube, 1ml of distilled water and 5ml of 0.1N NaOH were taken and closed the mouth of the conical flask by stopper after keeping the test tube inside the flask.
3. Samples were incubated for 24 hours at 250C.
4. After the 24 hours, test tubes were taken out from the flask.

5. Solution was transferred from the test tube to a 100ml conical flask and 5 ml of distilled water was added to it.
6. Now 5ml of BaCl2 was added in the solution along with 3 drops of phenolphthalein indicator to the solution and titrated with 0.05N HCl.
7. End point was recorded when the solution turned colourless from pink.

Calculation

CO_2 mg g-1 of oven dry soil=$\frac{V0-Vt\ X\ 100X\ 22X\ \delta}{(Mw-Md)Xt}$

Where, t= Time of incubation.

Vo= Blank titrated value.

Vt= Sample titrated value.

Mw= Weight of the moist soil.

Md= Weight of the oven dry soil.

δ = Strength of HCl

Moreover, total bacterial and fungal counts were taken after 3 days of incubation and, at the end of incubation using the spread plate method. Luria Bertani agar medium and potato dextrose agar medium were used for total bacterial and fungal colonies isolation respectively. Lastly, a modified index, compost quality quotient (CQQ) was generated using some pre-existing maturity indices to assess the quality of compost (Brinton, 2000). The quality produced relied upon cumulative changes in pH, available NPK, compost respiration, and C/P ratio. The formula adopted to generate CQQ is given below

$$Compost\ quality\ quotient\ (CQQ) =$$
$$\sum\left(\frac{\text{pH at t1}-\text{pH at t2}}{\text{pH at t2}}, \frac{\text{Avl.N at t2}-\text{Avl.N at t1}}{\text{Avl.N at t1}}, \frac{\text{Avl.P at t2}-\text{Avl.P at t1}}{\text{Avl.P t1}},\right.$$
$$\left.\frac{\text{Avl.K at t2}-\text{Avl.K t1}}{\text{Avl.K t1}}, \frac{\text{CR at t2}-\text{CR at t1}}{\text{CR at t1}}, \frac{\text{C/P ratio at t1}-\text{C/P ratio at t2}}{\text{C/P ratio at t2}}\right)$$

7.2.5. Evaluation of metal content

Metal concentrations in all the feedstock combinations were measured before and after composting following Tessier et al. (1979). The concentrations of five toxic metals viz. Cd, Cr, Pb, Ni, and Cu were checked. A metal fractionation study was carried out to assess the metal availability in mobile fraction as well the fate of metal in the compost. Likewise, the metal

bioaccumulation was also checked in the earthworm gut to get an idea of their detoxification potential. Gut accumulation was measured by digesting the sacrificed (gut evacuation followed by freezing) earthworm in di acid mixture 4:1 ratio (HNO_3:$HClO_4$). At first, the worms are washed with deionized water and left overnight for their gut evacuation by placing them on moist filter paper in a petri dish at (30^0C±2). Subsequently, they were sacrificed by freezing followed by digestion and finally underwent gut accumulated metal measurement in the atomic absorption spectrophotometer (AAS-Systronics).

7.2.6. Microbial community structure analysis: PLFA assay and alpha diversity analysis

Given the total bacterial and fungal count result, the dominance of bacterial proliferation in the final vermicompost product was observed. Hence, a detailed investigation of microbial community structure phospholipid fatty acid analysis (PLFA) was done, as described in our previous paper (Hussain et al., 2018). The assay is primarily based on lipid extraction followed by solid phase extraction and finally undergoes gas chromatographic analysis. The obtained PLFA result of microbial communities was detected by Sherlock software (Luo et al., 2016). The community structure obtained from fatty acid biomarkers underwent alpha diversity analysis using PAST 4.0 statistical software. A brief illustration of Shannon diversity (H_{PLFA}) and Shannon evenness (E_{PLFA}) was presented for a better understanding of species richness and relative abundances. The formula adopted to calculate the Shannon diversity and evenness is adopted from Shannon, (1948). Furthermore, the E_{var} index was computed following Smith and Wilson (1996) based on the variance in abundance.

Shannon diversity index (H_{PLFA})= $\sum_{i=1}^{n} pi\ lnpi$

where pi is the relative abundance of each community in the total sum and n is the number of detected species.

Shannon's evenness E (E_{PLFA}): = H/ lnS

Where S= number of species, if, E is closer to 1 denotes a more even community, while closer to 0 indicates a less even distribution.

Evar= 1 - 2/π arctan {∑ ln (xs)- ∑ ln(x1) /S)2/S}

where x is the relative abundance of species in the total sum and S is the total number of species.

7.2.7. Nutrient limitation assessment

Nutrient limitation of microorganism can be assessed through vector analysis where vector lengths and angles for enzymatic activity was calculated from the untransformed ratios of C:P, and C: N. A longer vector length depicts a higher C limitation and a vector with an angle $<45^0$C or $>45^0$C designates a relative constraint of N or P correspondingly. The below mentioned formulae were employed to calculate vector length (VL, dimensionless) and vector angle (VA, degree) following Moorhead et al. (2016).

$$\text{Length} = \text{SQRT}\,(x^2+y^2)$$

$$\text{Angle}\,(°) = \text{Degrees}\,(\text{ATAN2}(x, y))$$

where x and y represent the relative activity of C and N acquisition enzymes and relative activity of C and P acquisition enzymes respectively.

The significance of differences in enzyme activity in the end product was evaluated by permutational multivariate analysis of differences (PERMANOVA) and analysis of similarity (ANOSIM) based on Brays and Curtis similarity index after 9999 permutations. Subsequently, SIMPER (similarity percentage) analysis according to Brays Curtis similarity index was applied to measure the major contributing enzyme for observed dissimilarity among treatments (Siles et al., 2018). In addition, Shannon diversity (H_{Enz}), evenness (E_{Enz}), and E_{var}-Enz index were employed to describe the diverse role of enzyme richness among feedstock combinations.

7.2.8. Metal budget, accumulation and pollution load index (PLI), mobility factor (MF)

Changes in the metal concentration between initial and end product were computed in both aerobic and vermicomposting using removal efficiency indices, which will determine microorganism or earthworm/microorganism's ability to detoxify the substrate. On the other hand, bioaccumulation factor and pollution load index were also evaluated. The mobility factor designates the ratio of water-soluble, exchangeable, and carbonate-bound fractions to total metal. All these indices were calculated following Mondal et al. (2020) and Sahariah et al. (2015) and presented below

$$\text{Removal efficiency} = \frac{\text{Avrg. metal conc.initial} - \text{Avrg.metal conc.final}}{\text{Average metal concentration initial}}$$

$$\text{Bioaccumulation factor (BaF)} = \frac{\text{Metal in the earth worm gut}}{\text{Metal in the substrate}}$$

$$\text{Pollution load index (PLI)} = \frac{\text{Metal conc.in compost \& vermicompost}}{\text{Metal conc.in refence substrate}}$$

Reference substrate= metal concentration in pristine cow dung.

7.2.9. Statistical analysis

Two-way ANOVA was used to assess the data on physicochemical and biological parameters. However, one-way ANOVA was used to evaluate the alterations in the PLFA-derived microbial community architectures and fatty acid profiles in the vermibeds. Additionally, we carried out the least significant difference (LSD) post-hoc test to compare the effectiveness of the various treatments. Furthermore, Pearson's correlation statistics were used to understand the relationships between the vermireactors' microbial diversity and metal removal dynamics. The statistical program r-studio 4.1.1 and PAST statistics (4.0) were used for all statistical analyses.

7.3. Result and Discussion

7.3.1. Characterization of raw material

The alkaline bauxite residue popularly red mud (RM) is the disposal of aluminum industry and was taken as raw material. The properties of RM are charted are previously discussed elaborately in chapter 4. Inherently it was sodic alkaline in nature (pH 11.5±0.8). Such high alkalinity results from basic cations of caustic solution used in Bayer process, which got dumped before complete washing perhaps giving rise to alkaline elements in the residue. Likewise, high electrical conductivity (12.2 mS/cm) of RM is primely governed by elevated Na^+ (6.5%±0.5) (Kong et al., 2017). However, such basic pH got a considerable reduction during precomposting stage (10-12 days), but EC remained near its native value. Reduction of pH can be resulted from the biodegradation of alkaline elements, while the unchanged EC may come from presence of high Na. Such high Na plausibly leads to osmotic stress on earthworms, hence, to alleviate the sodicity, the crude RM was first treated with gypsum followed by leaching using a siphonic approach. The water-soluble Na leaches out due to substitution of Na by Ca from its exchangeable site, thereby the water-soluble Na lowered, and the addition of bulking agent (cow dung) to that of washed RM reduced EC and making it favourable for earthworm dwelling (Goncalo Filho et al., 2019). The waste was extremely low in bioavailable nutrients (C, N, P) including a greater presence of toxic metals (Cd, Pb, Ni, Cr, Cu) is of longer threat to the environment. The red colour of red mud was generated from its high Fe content (19.25%±1.02). High sodicity, poor humic content, and elevated presence of polymetallic

species of red mud make it extremely hostile. It poses a scientific challenge and emphasizes the need for reclamation through sustainable treatment technology.

7.3.2. Earthworm prolificacy, microbial propagation, and substrate compatibility

Survivability, growth, and reproduction rate are the foremost factor of successful vermicomposting which primarily depends upon substrate compatibility. The population dynamics of the earthworm during the course of VC are presented in Fig. 7.1(a-d). As previously mentioned, RM is extremely hostile to cellular survivability due to its high alkalinity and metallic presence, hence, the earthworm could not survive in solitary RM-based feedstock. An expected 100% mortality was observed within 48 hours of exposure which is consistent with some previous studies (Hackenberger et al., 2019; Courtney et al., 2020). In contrast, a significant ($p<0.05$) increase was observed in all the cow dung mixed RM feedstock (CD-RM). All the combinations (VC1, VC2, VC3, and VC4) evinced a decent increment in earthworm population (average 35-37%). The rate of proliferation was significantly greater during 30 to 60 days intervals compared to 0-30 days which might be due to substrate acclimatization. During 0-30 days the increment was highest in VC4 (45%) while between 30-60 days VC3 evidenced a greater proliferation (38%). Surprisingly, the rate of proliferation dropped down between 60-90 days intervals might be due to scarcity of food in the RM feedstock. At the end of 90 days, the earthworm count (including hatchlings) was in the order VC0> VC4> VC3> VC2> VC1 (LSD_D=1.20, LSD_T=1.34 p for the treatment x day =0.009). Despite high alkalinity and metal toxicity earthworms showed an appreciating reproduction rate in all the combinations, among them, VC3 reached its highest in between 30-60 days which to some extent crossed the reproductive rate of solitary CD-based feedstock (VC0), however, the growth rate was found to be highest in VC4 (9.84 mg/worm/day). Such high reproductivity in RM-CD feedstock can be attributed to some stress repair mechanism that exists at the genetic level which safeguards them in such hostile habitats (Vasseur & Bonnard, 2014). A two-way ANOVA revealed that the reproduction rate was significant among treatments and treatment-day interaction also (p for treatment x day =0.001; LSD_D=0.005; LSD_T=0.007). Losses in body weight of earthworms in metal-contaminated waste and soil were previously reported by many researchers (Courtney et al., 2020) who explained this phenomenon as energy shifting from growth to reproduction, nevertheless, our study did not evince any significant reduction in body weight compared to control. Contrastingly the earthworms were found to gain little weight in the feedstock VC1 and VC2 where the RM is less diluted with CD. Such an enlarged and swelled body could be the result of water accumulation to acclimate with osmotic stress, which

is a mechanism adopted by many earthworms to strive against dehydration process in a hyperosmotic environment. Although there are not many reports on water accumulation inside the body however Edwards, (2004) reported reabsorption ability of salt through excretory organs to equilibrate the osmotic pressure gradient between body and exterior environment. In terms of cocoon production *E. fetida* lodged maximum addition to VC4 where the percentage of CD was highest. Generally, earthworm needs simply digestible C-containing substrate as their food thus they showed more productivity in carbon-reached feedstock. A similar kind of result was reported by Paul et al., 2018 during silk industry sludge vermicomposting. Overall **E.** *fetida* are quite popular for their wide adaptability towards obstinate waste hence used as composting worms.

Microbial proliferation in both composting and vermicomposting are summarized in Fig. 7.1(e-f) which indicates that both bacterial and fungal counts were noticeably high in vermicomposting compared to composting. The bacterial count was in the order VC2>VC0>VC3>VC4>VC1>AC0>AC>AC2>AC4>AC1 (LSD_T= 0.10; P<0.05) while fungal count was highest in VC2 and lowest in AC1 (LSD_T= 0.057, p<0.05).

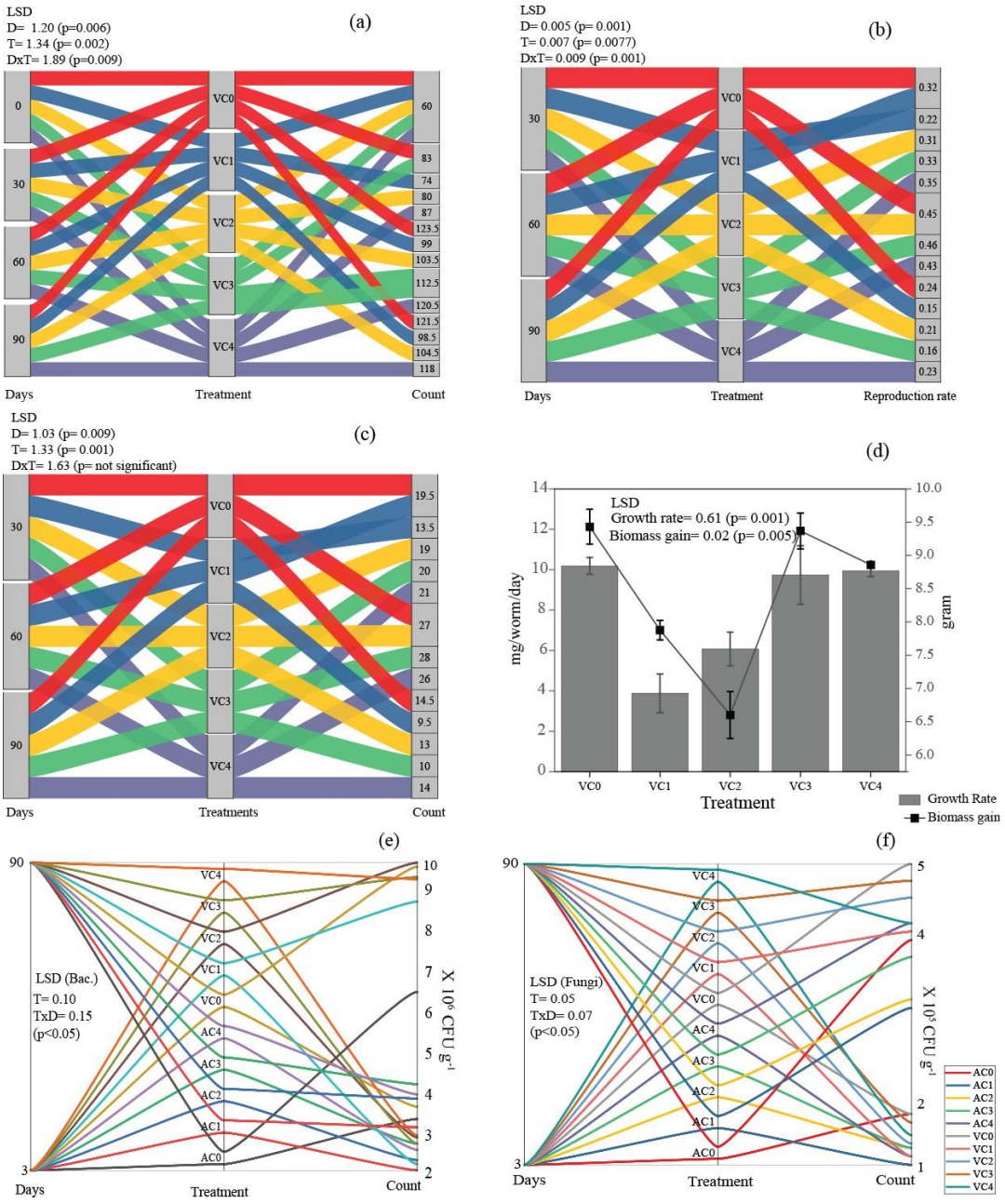

Fig. 7.1. (a-d) Growth and fecundity of earthworm population in vermireactors; (a) earthworm count (b) cocoon count (c) reproduction rate (d) Growth rate and biomass gain. (e-f) Variability in bacterial and fungal growth of the bioprocessing units. (LSD= Least significant difference; T= treatment, D= days).

7.3.3. Changes in pH, electrical conductivity (EC), mineralizable N, and total organic carbon (TOC)

The RM is intrinsically alkaline owing to the high presence of Na together with other alkaline elements viz. K, Ca, and Mg (Kong et al., 2017). Although gypsum treatment and precomposting reduced the pH yet, at the beginning of bio composting the pH of all the

feedstock combinations was in the alkaline range (8.1-9.7). During the course, the pH shifted towards neutrality, however, the shifting was more under vermicomposting than composting., (Fig. 7.2a) There was an average 17 % reduction compared to its initial stage, among which VC4 (23.81%±0.31) and AC4 (23.55.%±0.51) attained the highest (p for the treatment=0.0009, LSD_T=0.05). Production of humic acid due to organic matter degradation induces acidity while a simultaneous NH^{4+} production tends to raise the pH of the compost bed. Consequently, their opposing effect with each other kept the pH of compost at a near-neutral range (Paul et al., 2018). Interestingly, the result of EC was a little dubious (Fig. 7.2b). In both cases, composting and vermicomposting feed stock AC1, AC2, and VC1 VC2 evinced a significant increase while AC3, AC4, VC3, and VC4 got a significant reduction. In the mixture where RM was less diluted (1RM:1CD and 1RM:2CD), EC increased significantly ($p<0.05$). The overall increment was 107-125% compared to its initial stage, although increment was marginal between 60 to 90 days indicating the stabilization of compost. Both the control AC0 and VC0 got an increase of 47% and 58% respectively. This sharp increase could be attributed to the weight loss of organic matter that adds different mineral salts in the compost bed like ammonium, phosphate, and some inorganic ions (Deka et al., 2011). On the other hand, where the RM was largely diluted (1RM:3CD, 1RM:4CD), faced an average 30% reduction under composting (AC3, AC4) and a 50% of reduction under vermicomposting (VC3, VC4) which might result from insolubility, leaching, and microbial immobilization of salts during the course. The two-way ANOVA result declared the significant treatment x days (p=0.0033) interaction indicating that treatment was getting stabilized between 60-90 days. A similar kind reduction trend was reported by Roy et al. (2022) during biochar-based vermicomposting.

The contrasting trend of TOC and mineralizable N was detected in all the feedstock where a gradual decrease of TOC occurred, with a corresponding increase in mineralizable N content. It was higher at the beginning (Fig. 7.2d), but over the course, a substantial reduction was recorded in both vermi and aerobic compost bins ($p<0.05$). A sharp decline was noticed between 30 to 60 days while reduction was marginal between 60 to 90 days indicating the maturation of compost (p for the day =0.001; LSD_D= 0.23; p for day x treatment= 0.0008). The drop was markedly higher in vermibed (0.5-0.6-fold decrease) compared to aerobic bins (0.2-0.3-fold decrease). At the end of incubation, the TOC status of different feedstocks was in the order of AC3> AC1> AC4> AC0> AC2> VC4> VC1> VC0> VC2 (LSD_T=0.15). Accelerated mineralization of organically bound substrate (C, N, P), and loss of carbon as CO_2 through respiration are the prime contributing factor to TOC reduction (Paul et al., 2018). Moreover,

the loss in vermibed attributed to the increment in earthworm population that led to enhanced organic matter oxidation alongside the increased respiratory activity of earthworm and microorganism approved this greater loss of TOC in vermi bins than compost bed, which is in good agreement with Deka et al. (2011) and Suthar (2009). The steady increase in mineralizable N implied a good rate of nitrogenous compound decomposition in both composting systems however vermi bins had a greater activity of N mineralization (3.1-4.4-fold increment) compared to aerobic ones (Fig. 7.2c). After incubation, the nitrogen was significantly high in VC2 and VC3 (LSD_T=3.45; p for the treatment= 0.0043). The small increment in aerobic composting (2.1-2.4- fold) may be due to the sluggish activity of microflora, whereas in vermi bins the earthworms trigger N mineralization via their gut harbouring flora coupled with indigenous microbial population (N_2- fixing) of the system that secretes numerous hydrolytic enzymes accountable for the breakdown of complex nitrogenous macromolecule. In addition, the mucilaginous vermicast enriched with nitrogenous metabolite and other enzymes defecated from worms facilitates a greater amount of N availability in vermi reactors. The findings of present study concord with many other contemporary observations (Roy et al. 2022; Hussain et al., 2018; Chakraborty et al., 2022).

7.3.4. Macro and micronutrient dynamics

Data on availability of P, K, Na, and Ca are depicted in Fig. 2e-h. Availability of P in compost is highly recommended for suitable plant growth and development Suthar (2009). As shown in Fig. 7.2f the investigation exhibited a significant increase in phosphorus availability in both compost and vermicompost at the end of incubation. Initial P was poor in all the treatments except the experimental control (AC0 and VC0) which was ascribed to the initial alkalinity of the feedstock as P availability is highly pH specific. Any acidity and alkalinity restrict P availability (Sahariah et al., 2015). After 90 days of incubation, a noteworthy increment was seen in vermicompost (1.5-2.2-fold) compared to aerobic compost (0.7-1.0-fold). The P was significantly high in VC2 and VC3 ($p<0.05$;) and the availability was in the order VC2> VC0> VC3> VC1> VC4> AC0> AC3> AC4 >AC2>AC1(LSD_T=5.49, p for the treatment =0.0023). The neutrality of vermicompost possibly enhances the P content in vermi bins, moreover, phosphatase secretion by gut flora of earthworms including phosphate solubilizing bacteria in worm cast induces P mineralization (Chakraborty et al., 2022; Paul et al., 2018). Induction of nitrogen and phosphorus (urease and phosphatase) specific enzymes seems to play a key role in the liberation of organically bound N and P. Variation in availability among reactors might be the result of the varied proportion of bulking agents (CD) (Suthar,

2009). Concurrently, bioavailability of exchangeable K augmented in both composting (0.1-1.0-fold) and vermicomposting units (0.6-1.8-fold). In general, the cow dung, used in this experiment was highly enriched with K reflected in the initial K content of the feedstock where the experimental control (AC0, VC0) and the ratio 1:3 and 1:4 (VC3, VC4, AC3, AC4) was having a greater amount of CD, showed high exchangeable K (Fig. 7.2e). After 90 days of incubation, K in different RM mixture was in the order VC4> VC3> AC4> AC3> VC0> VC2> VC1> AC0> AC2> AC1 (LSD_T= 93.62; p for treatment= 0.0039; p for treatment x day= 0.000). A 4-fold increment after vermicomposting, reported by Deka et al., (2011), is in high concordance with our findings. Such augmentation may be attributed to mass and volume drop of the substrate during vermicomposting, K mineralization, or surface enhancement owing to the grinding action of worm gizzard (Yadav & Garg, 2019, Hussain et al., 2018). Exchangeable Na was a challenging factor in this study due to its larger intrinsic presence in RM hence, a contrasting result was achieved between composting and vermicomposting. In aerobic mixture, there was a 0.11-0.66 -fold increase with exception of experimental control (AC0) where Na decreased 0.03- fold after incubation (Fig. 7.2g) Simultaneously, all vermi bins evinced receding in Na content about 0.14 to 0.37- fold and were in the order of VC1> VC3> VC2> VC4> VC0. A two-way ANOVA suggested treatment day interaction was significant (p for treatment=0.006, LSD_T=77.39; p for the treatment X Day= 0.008), which implies leaching of soluble Na over time can be the reason for lowering. Accumulation of Na^+ in the earthworm gut may be another reason for Na^+ reduction. It was highest in VC1 (17.1) g/kg and lowest in VC4 (8g/kg). Similarly, Ca content also subsided across the compost bins (p for treatment = 0.003; p for day= 0.0022; LSD_T=53.90) probably due to the leaching or production of organic acid and evolution of CO_2 in the course of humification process (Paul et al., 2020). In a nutshell, the increment in available nutrients in different RM mixtures is credited to earthworms that dwindle the waste mass thereby uplifting the organic matter mineralization (Fernández-Gómez et al., 2010)

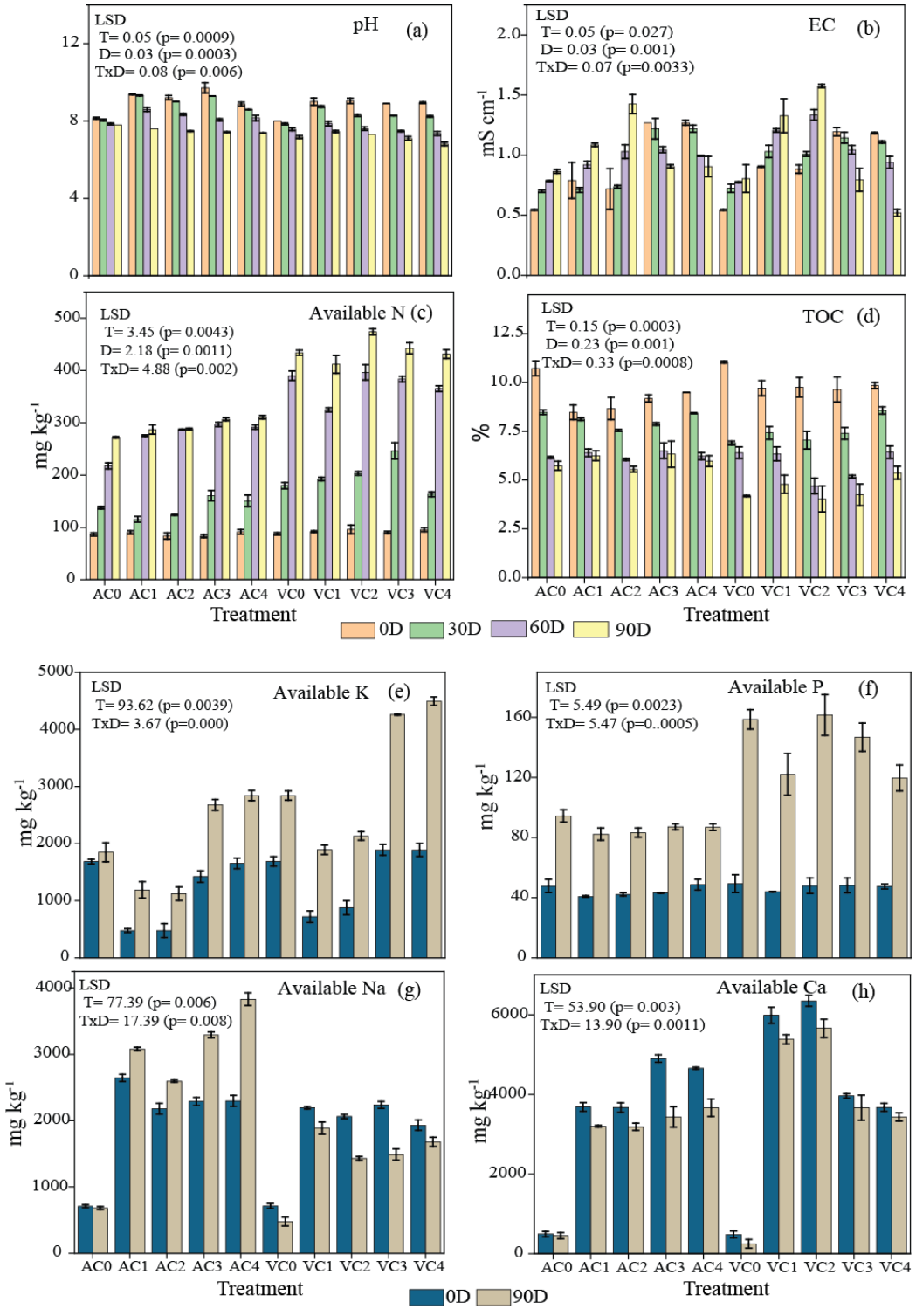

Fig. 7.2. (a-d) Temporal variation of physicochemical characteristics. (e-h) Variability in nutrient dynamics under various treatments during composting and vermicomposting process. (LSD= Least significant difference; T= treatment, D= days). Each error bar represents value ± standard error.

7.3.5. Enzyme dynamics

Changes in the enzymatic activities presented in Fig. 7.3a-f. Earthworm gut-secreted digestive enzymes coupled with microbial extra-intracellular exudation assist in the breakdown of macromolecules in the feed mixture (Karwal & Kaushik, 2020). FDA hydrolysis determines gross enzymatic profile of compost while DHG, an intracellular enzyme involved in oxidative phosphorylation, designates total microbial activity, hence, acceleration of these two attributes implies the improvement of microbial population thereby being recommended as OM stabilization indicator (Nikaeen et al., 2015). A gradual significant increase ($p<0.05$) was exhibited in vermi bins up to 60 days for FDA and DHG (FDA hydrolysis=1-3 fold; DHG= 3.5-6.2-fold), however, in aerobic units AC3 and AC4 got a decrease (0.1-0.3-fold) at 60 days compared to 30 days and subsequently increased. Similarly, FDA hydrolysis successively decreased after 30 days in aerobic unit. This could be for rapid hydrolysis in the early phase due to presence of bulky labile OM (Diaz-Burgos et al., 1993). Quick augmentation at initial phase followed by moderate increment in vermi bins up to 60 days likely due to readiness of macromolecules that induces microbial proliferation along with enzyme availability by earthworm gut-associated flora made the system conducive (Chakraborty et al., 2022). A significant increase was observed in VC2 and VC3 (p for the treatment for FDA= 0.0012; p for the treatment for DHG= 0.0010). Dearth of readily available substrate likely declined the microbial activity after 60 days. The two-way ANOVA indicates the treatment day interaction was highly significant (FDA-LSD_T=1.52; LSD_D=0.96, p for the treatment x day=0.0008; DHG-LSD_T=0.86; LSD_D=0.54; p for the treatment x day= 0.0044). The overall hydrolase activity of compost was quantified by measuring the nutrient cycle (C, N, P, S) enzyme. Urease is an N cycle participator that exhibited more pronounced activity in vermi reactors (1.4-3.2-fold increase) compared to their corresponding compost counterpart (1-2.4-fold increase). The activity was significantly ($p<0.001$) high in VC2 and VC3 (LSD_T=2.39; LSD_D= 1.54, p for the treatment =0.0088). Profuse burrowing activity accompanied by nitrogen-fixing bacteria (NFB) induces more aeration in vermibed, which seems to augment the N mineralization reasoned for greater urease production (Ge et al., 2020). On the other hand, alkaline phosphatase (AlP) is known to transform organic phosphate into its labile form, which significantly ($p<0.001$) amplified in both aerobic (0.5-1.0- fold) and vermicompost (1.2-3.4-fold) up to 60 days thereafter retarded significantly ($p<0.05$) till the end of the experiment. Increased mineral P possibly inhibits the phosphatase activity as the enzyme is highly sensitive to feedback inhibition (Lazcano et al., 2008). β-D glucosidase is the only one that showed a

progressive loss of activity till the end of incubation. In vermicomposting pile a significant reduction registered (0.4-0.6-fold) up to 60 days afterward became linear whereas the depreciation of the aerobic pile was prolonged (0.09-0.2-fold), indicating a treatment day interaction was significant (p=0.0004). This inducible cellulolytic enzyme acts on complex saccharide molecules which were highest at the initiation. Over time the decline ensued owing to microbial degradation of the substrate with earthworm intervention. At the end the enzyme was as follows VC3> VC2> VC4> VC0> VC1> AC1> AC4> AC0> AC2> AC3 (LSD_T= 11.10, LSD_D= 7.02; p for treatment x day =0.0004). A similar kind of finding was reported by Fernández-Gómez et al. (2013). Degradation of sulphur-ester by aryl-sulphatase (AS) followed the similar means as phosphatase and urease exhibited, an initial elevation followed by depreciation at a later stage. The post-incubation activity was in the order VC3=VC0 VC2> VC4> VC1> AC4> AC0> AC3> AC2> AC1 (LSD_T= 2.39; p=0.0012). Except for β-D glucosidase, all the enzymatic activity was found to have depreciation in between 60 to 90 days which may be due to deficiency of available substrate, inhibition by humic carbon, or feedback effect. The result is in high agreement with Karwal & Kaushik, (2020) who studied vermicompost of press mud with coal fly ash.

7.3.6. Changes in microbial biomass C (C_{mic}), compost respiration (CR), respiration quotient (RQ), and metabolic quotient (qCO_2)

The variation in C_{mic}, CR, RQ, and qCO_2 are plotted in Fig. 7.3g-j. C_{mic} considerably increased with time in all the RM mixtures of aerobic and vermi reactors until substrate scarcity arises. Although C_{mic} was highest in control at the initiation of the experiment, nevertheless a significant increment (1.8-2.9-fold) was noticed in vermi bins corresponding to their compost counterpart where increment was comparatively poor (0.4-1.4 -fold). Earthworm intestine is a reservoir of diversified microbes due to a conducive environment that in due course released as vermicast consequently loading high microbial biomass to the system (Paul et al., 2018). Metal richness, osmotic stress, and structural complexity might be the initial perturbation which latterly compensated through earthworm interference (Roy et al., 2022), however, at final stage, C_{mic} started to decrease may be due to poor worm activity. The energy expenditure of the process with concurrent compost stabilization was measured through compost respiration. With progression of the experiment increase in CR among treatments was found to be significant (p=0.0001, LSD_T= 1.16), having highest expenditure in VC3 and VC2 possibly due to greater earthworm population and their corresponding activity. Retardation in CO_2 evolution occurred at final stage of composing implying the exhaustion of substrate for further

microbial degradation, although, RQ provides most reliable insight to measure the stress of immediate environment. In the present study, we evidenced significantly high RQ ($p=0.0001$) at the beginning regardless of combinations, however, 90 days of incubation with CD perhaps enhanced the zymogenous population thus mitigating the stress produced from osmotic imbalance, noxious metal, and reactive compounds of RM-based feedstock. High qCO2 at initial stage supported this observation, which reflects, respiration for survivability was more precedence over development and proliferation (Chakraborty et al., 2022). Interestingly, both of these attributes considerably reduced over time (qCO_2- p for day = 0.009; RQ-p for day = 0.005, p for day x treatment= 0.001), and noticeably vermireactors had a more pronounced reduction than aerobic ones concluding that earthworm-microorganism association turns out more fruitful than solitary microbial action (aerobic) in such stress mitigation. The result is pretty much similar to some previous work by Devi et al. (2020) and Chakraborty et al. (2022).

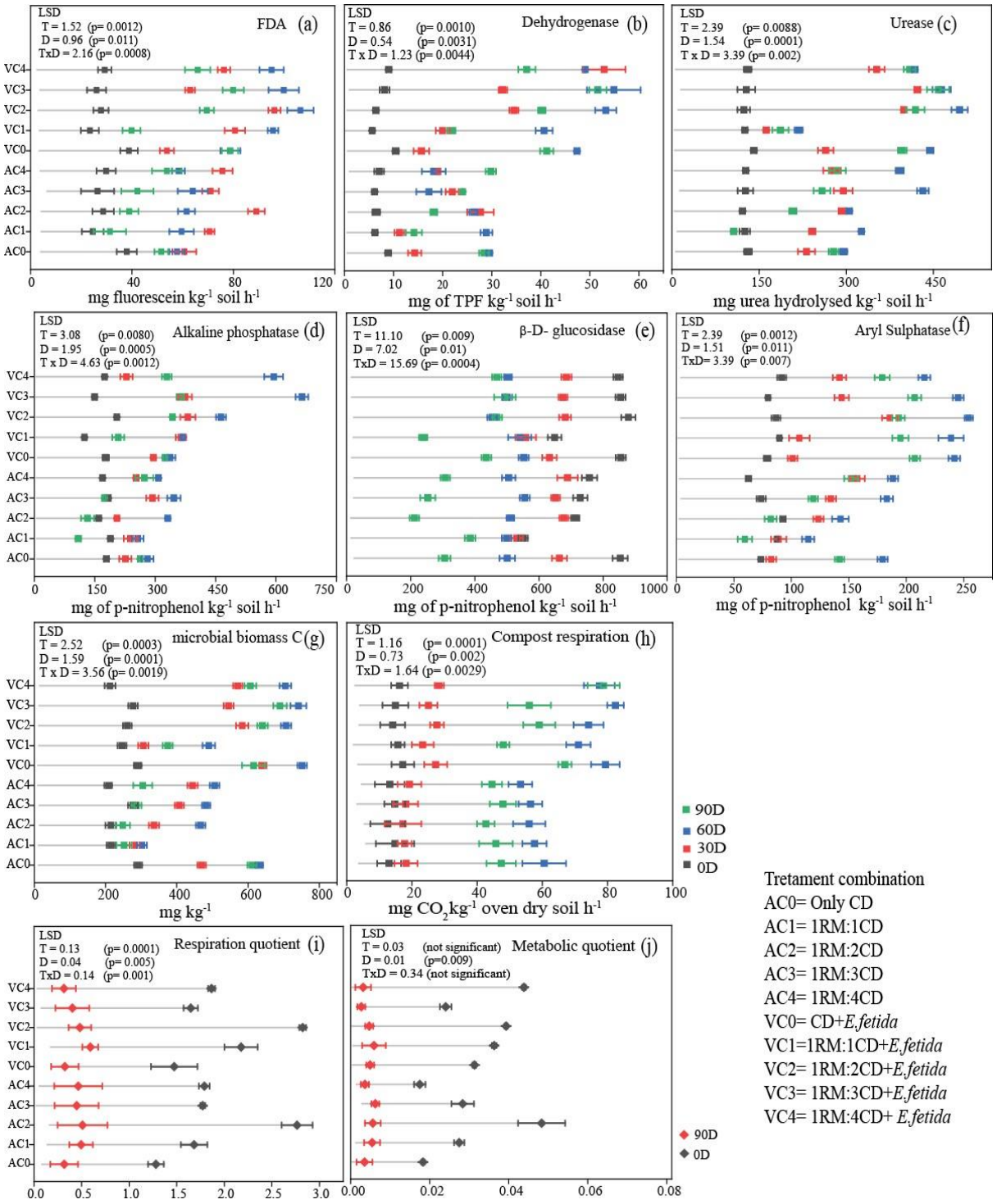

Fig. 7.3. (a-h) Temporal variation of enzyme activities under various treatments during composting and vermicomposting process. (LSD= Least significant difference; T= treatment, D= days). (i-j) Changes in respiration quotient and metabolic quotient. (LSD= Least significant difference; T= treatment, D= days). Each error bar represents value ± standard error.

7.3.7. Evolvement of microbial community - PLFA assay and alpha-diversity analysis

The impressive augmentation in microbial quality in vermi bins indulges exploring their distribution. Since the relative abundance of PLFA is considerably disparate and group-specific thus offers an easier understanding of the community's response in vermi bins to RM treatment. (Zhao et al., 2018). PLFA analysis unveiled (Fig. 7.4m) a wide variety of community structures among different ratios where total PLFA was in the order VC0> VC2> VC3> VC4> VC1 ($p=0.0002$; LSD= 9.34). The dominance of gram-positive bacteria across the vermibins suggests gainful feedstock compatibility (Fig. 7.4a-e). At the same time, poor presence of gram-negative bacterial PLFA was a definite stress-relieving phenomenon of earthworm-microorganism symbiosis however a comparatively higher presence of gram-negative bacteria in VC1 (1RM:1CD; Fig. 7.4b) indicated that 50% diluted feedstock was not adequately favourable for *E. fetida* mediated system as gram-ve are stress indicators (Eberlein et al., 2018). Actinomycetes and anaerobic bacteria were the next most abundant species followed by fungi and other eukaryotes. Actinomycetes are chemoorganotrophs capable of degrading complex cellulosic material was found to be highest in VC0 followed by VC2> VC4> VC3> VC1($p=0.009$; LSD=0.47). Similarly, fungi were also high in VC0. As VC0 is a solitary CD-based feedstock that explicitly holds a favourbale habitat for harbouring diverse microorganisms. The results are in line with our earlier study by Devi et al. (2020). Fatty acid profiling disclosed that monounsaturated fatty acid (MUFA), straight and branched chain fatty acid were highest in VC2 (Fig. 7.4f-j) while polyunsaturated fatty acid (PUFA) was highest in VC0 followed by VC4> VC3> VC1> VC2 ($P<0.05$). MUFA and straight-chain fatty acids mostly contribute to the indigenous microbial population (gram-positive and negative) while branched-chain serves for the anaerobe and sulfate-reducing microbes (Zhao et al., 2018). This implies, that VC2 feed mixture provided a favourable environment for microbial sustenance which was also detected in our experimental results. PUFA primarily represents microeukaryotes, with some distinguishing hallmark PUFA (18:19c) suggesting the presence of fungal colonies in the final product, which was consistent with the overall fungal count. MUFA and PUFA typically preserve membrane fluidity until any interference from environmental stressors destabilize membrane fluidity and ultimately create obstacles to the transport system that restricts cellular activity (Hussain et al., 2018). Precisely, MUFA, produced by gram-negative bacteria retards under stressful conditions which then transforms into cyclopropane (e.g., 17:0 cyclopropane and 19:0 cyclopropane) and acts as a stress Sindicator. The ratio between cy17:0 + cy19:0/16:1Ω7c +18:1Ω7c determines the degree of

stress where a bigger value signifies greater stress (Chakraborty et al., 2022). In current investigation, a significantly high stress ratio was observed in VC1 (p=0.001;) trailed by VC4>VC2>VC3 (LSD=0.058) (Fig. 7.4l). Reduction of stress ratio in feedstock (VC2, VC3, VC4) with a greater percentage of CD incorporation infers that worm-microbe interaction stabilizes the metal-induced toxicity profusely whereas sustainability under VC1 vermi bins (1RM:1CD ratio) was challenging in terms of stress ratio. Alpha diversity analysis including Shannon- Wiener index, Simpson 1-D, Barger-Parker, Brillouin, and Margalef index provides another array of comparisons among the feedstocks (Table 7.1). Interestingly H-PLFA (Shannon diversity) was highest in experimental control (VC0) followed by VC2> VC3> VC4>VC1, while E-PLFA (Shannon evenness) was in the order VC2> VC0> VC3> VC4> VC1. This suggests that, in terms of community evolution, VC2 (1RM:2CD) was as suitable as CD (Fig. 7.4k). Likewise, Simpson 1-D showed its maximum value for VC0 followed by VC3>VC2> VC4=VC1, indicating species richness of VC2 and VC3 were equally high as VC0. In contrast, the unchanged value of Margalef's index indicated there was no such relative diversity among the treatments. The Barger-Parker (B-P) index illustrates diversity in regard to species dominance. The higher B-P index value of VC2 indicated its species dominance than diversity while the lowest value of experimental control (VC0) turned out more diversified. In contrast, the Brillouin index is more biased toward rare species, which was highest in VC0 followed by VC3>VC2>VC1>VC4 (Stiling, 2011). Improvement of feedstock can be well understood by analysing the E-var PLFA index as it gives an insight into the response of any immediate change of microsomal habitat (Chakraborty et al., 2022). Interestingly this too followed the same as previous where highest evenness was showed by VC2 (1RM:2CD) after control (VC0) and lowest by VC1 (1RM:1CD), which again implies that dominance of RM is a threat to cellular sustenance. These diversity indices provide evidence of how the RM-induced risk in vermibins is offset by the earthworm–bacteria synergism.

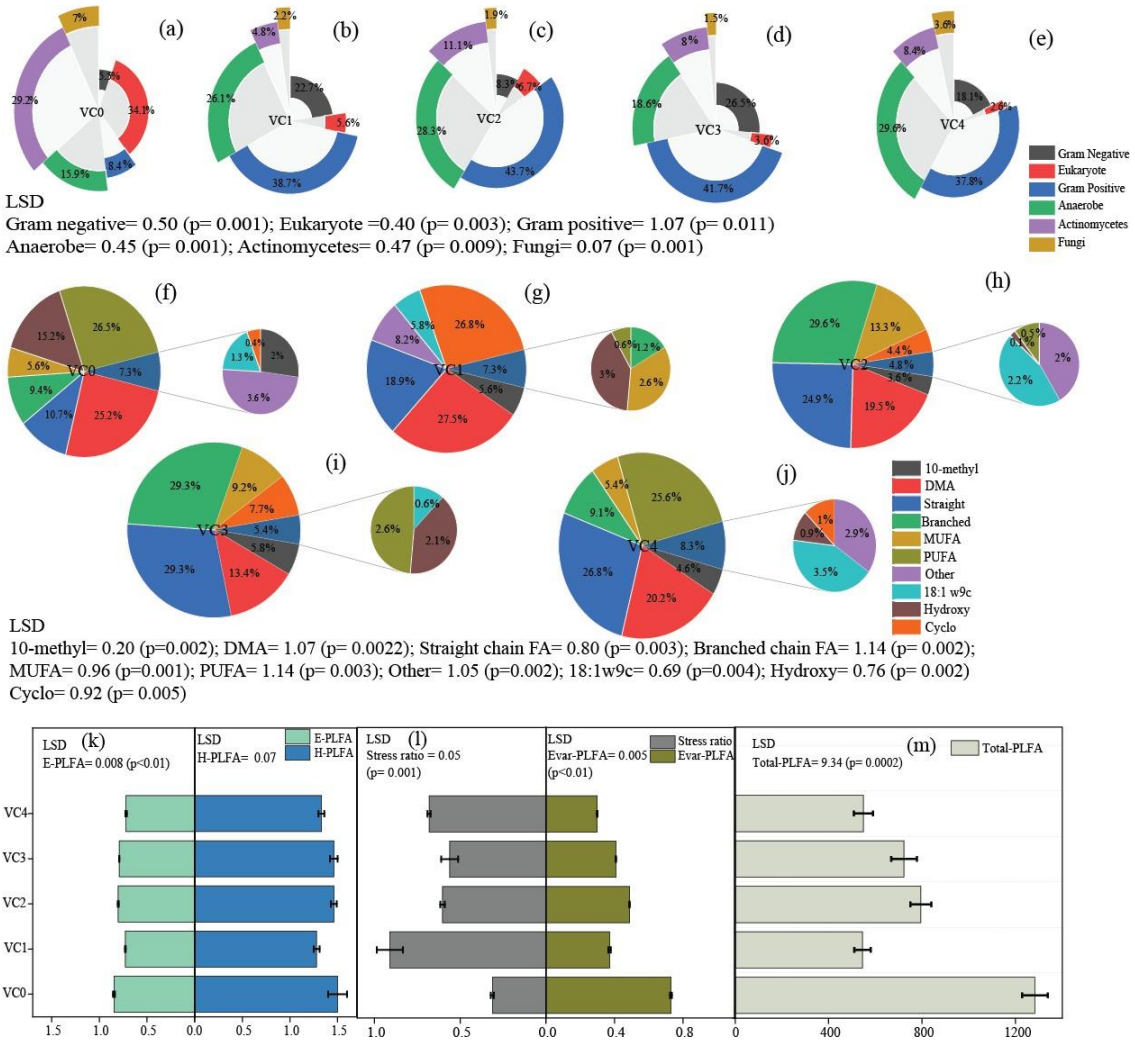

Fig. 7.4. (a-e) Distribution of PLFA-identified microbial groups across vermicomposting reactors. (f-j) Distribution of phospholipid fatty acid in vermicomposting unit. (k-o) Changes in Shannon diversity (H), evenness (E), and E-var of microbial groups during vermiconversion of red mud. (LSD= Least significant difference). Each error bar represents value ± standard error.

Table 7.1. Alpha diversity analysis of vermireactors.

Diversity index	VC0	VC1	VC2	VC3	VC4
Shannon Wiener	1.507	1.34	1.45	1.44	1.32
Simpson 1-D	0.74	0.69	0.71	0.72	0.69
Barger-Parker	0.37	0.42	0.43	0.41	0.42
Brillouin	1.3	1.08	1.13	1.16	1.06
Margalef	1.09	1.09	1.09	1.09	1.09

7.3.8. Insight into enzyme indices- diversity, SIMPER approach

Enzyme richness and evenness across the composting and vermicomposting reactors were critically evaluated by calculating H-enzyme (Shannon richness), E-enzyme (Shannon evenness), and E-var enzyme, which illuminate a pronounced and diversified activity in vermicompost process possibly from combined functionality of earthworm and microbes (Fig. 7.5a-b). Extensive burrowing, mucus secretion, and addition of beneficial microbe through excreta of earthworms substantiate the richness of enzymes in *E. fetida* system. Additionally, the E-var index offers the practicability of microbial adaptation to changing environment and its related impact on enzyme secretion. Interestingly we found almost all the vermibins managed the RM-induced stress except VC1 (1RM:1CD) where earthworm density and corresponding microbial propagation were limited thus enzyme richness was restricted (Fig. 7.5b). Alternatively, the in-situ population of aerobic reactors expenses more energy to acclimate instead progress, a concurrent nutrient limitation might be another contributing factor to their poor adjustment to the immediate environment. A similar kind of finding was reported in our previous study by Chakraborty et al. (2022) during tannery waste sludge vermicomposting.

In addition, the similarity percentage analysis (SIMPER) exhibited that the average difference in enzyme content between the groups (AC & VC) was 26.53%, with β-D glucosidase (C-cycle enzyme) being the highest, accounting for 29.41% of the overall difference (Table 7.**2**). PERMANOVA and ANOSIM approved this difference with a significant p-value (PERMANOVA p=0.0027, F= 13.51; ANOSIM p= 0.0017, R= 0.45). Although the difference was significant yet the degree of difference was not much stronger due to the moderate R-value (0.45, equally distant from 0 and 1). Urease and alkaline phosphatase were next in the line contributing 28.29% and 22.7% respectively. Dehydrogenase, like that of FDA, had the least contribution while aryl-sulphatase contributed moderately. The result highlighted that C, N, and P cycle enzymes were predominant and contributed >80% to the calculated functional dissimilarity. Due to the fact of using CD as a bulking agent, presence of organically bound C, N and P was a leading factor in extensive production of C, N, and P cycle enzymes compared to others. Moreover, the varied ratio of C, N, and P in the end-product might be another reason for their diverse abundance that creates the distance of presence. Between the groups, the abundance of enzyme was more in VC, as hypothesized, owing to the synergistic act of earthworm-microbes, however, the order of contribution to the dissimilarity index edifies the major drivers of the transformation process. Nikolova et al. (2023) reported

on β-D glucosidase and alkaline phosphatase's contribution to dissimilarity index in surface and sub-surface soil enzyme activity, nonetheless, no such report has yet been produced regarding compost enzyme drivers and their corresponding contribution towards dissimilarity matrix.

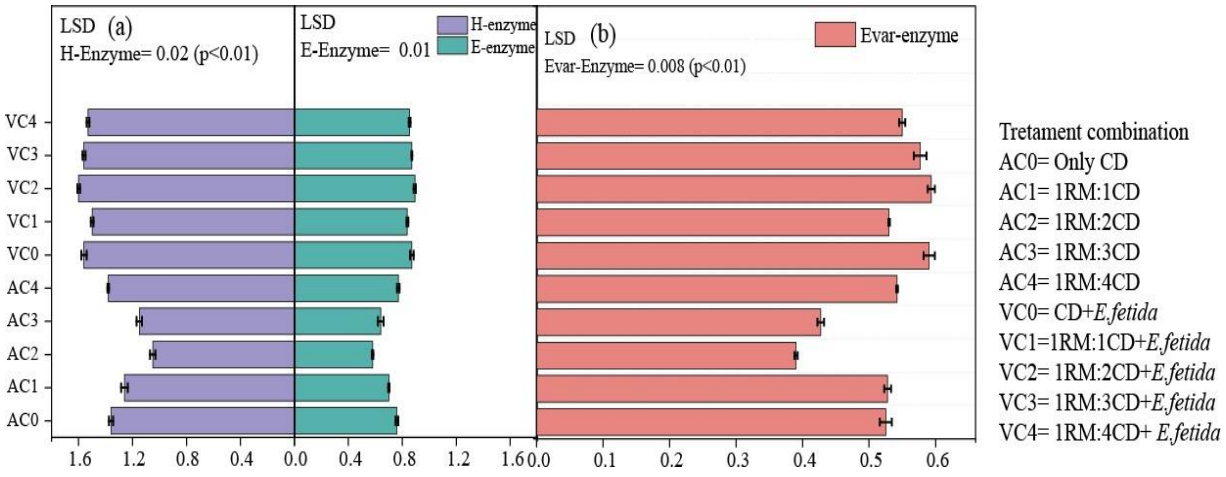

Fig. 7.5. Changes in Shannon diversity (H), evenness (E), and E-var of enzyme activities during vermiconversion of red mud. (LSD= Least significant difference). Each error bar represents value ± standard error.

Table 7.2. SIMPER analysis of enzyme activities contributing to the functional dissimilarity between composting and vermicomposting in the Bray-Curtis dissimilarity matrix.

Taxon	Average. dissimilarity	Contribution %	Cumulative %	Mean composting	Mean vermicomposting
β- D Glucosidase	7.804	29.41	29.41	253	419
URS	7.507	28.29	57.71	229	372
AP	6.023	22.7	80.41	191	314
AS	3.405	12.83	93.24	110	176
FDA	1.088	4.1	97.34	44.7	66.9
DHG	0.7045	2.655	100	23.4	38

7.3.9. Microbial nutrient limitation study- vector analysis approach

Vector analysis is an analytic approach to assess the nutrient limiting conditions of compost and vermicompost. A longer vector length (1.01-1.19) in all the treatments (both in

AC and VC) at initial stage of incubation indicated C limitation while it decreased significantly (p for the day=0.0004) at the end (0.73-0.79) (Fig. 7.6a). This is due to the presence of complex C compounds like cellulose, hemicellulose, and lignin in cow dung making the C limited to microbial population, though, such limitation latterly compensated, attributable to C mineralization. Besides, observed vector length >45^{0}C indicated the P limitation across the treatments (Fig. 7.6b) at the beginning while <45^{0}C revealed the N limitation at the end of trial. The P limitation of the initial stage occurred from the scarcity of available P because of more organically bound P which was further alleviated by P-mineralization. The N-limitation can be well explained by "microbial nitrogen mining" hypothesis proposed by Moorhead and Sisnabugh (2006), which adopts N-acquiring microbes use labile C to meet up their energy requirement to decompose recalcitrant organic matter for gaining N. Microbes were eager to utilise the large levels of labile C produced by C-mineralization in bioreactors, which led organic matter to breakdown slowly for N uptake. However, another conceptual model, priming effects elucidates the microbial shifting of community structure that occurred in N-limitation conditions in reactors at a later stage (negative priming effects) (Blagodatskaya & Kuzyakov, 2011). At end of incubation, the reactors became limited with the substrate which may have encouraged the growth of K-strategists (slow growers with restricted resources), that use existing labile C for N-requirement, supporting the "nitrogen mining hypothesis" in another way (Chen et al., 2014).

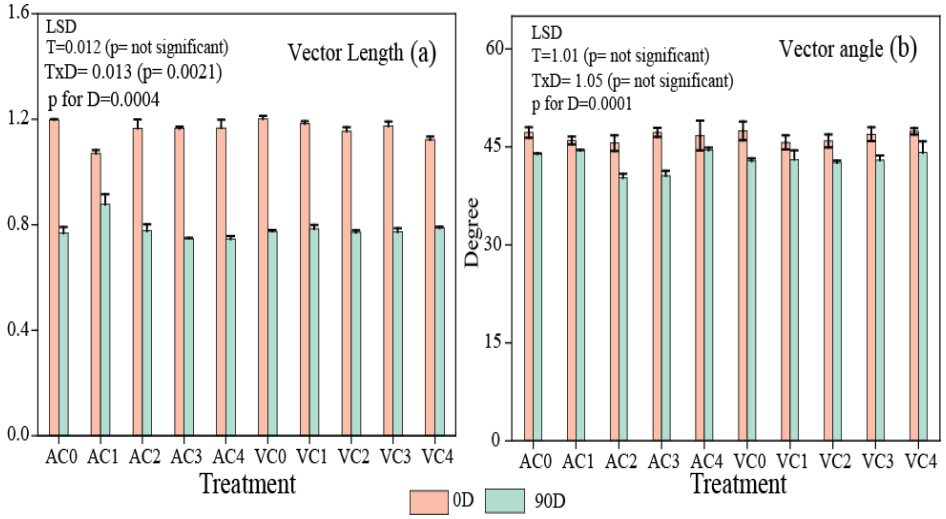

Fig. 7.6. Vector analysis of composting and vermicomposting reactors. (LSD= Least significant difference; T= treatment, D= days). Each error bar represents value ± standard error.

7.3.10. Metal budgeting, bioaccumulation, and removal efficiency

The bioavailability of metal is a doorway of inflowing toxic elements in the food chain thus drawing significant attention. Primarily five metals (Cu, Cr, Cd, Pb, Ni) were taken into consideration due to their elevated presence in the waste material. Initially, we measured the water-soluble (WS) and exchangeable (Ex) fractions, as they are more biologically dynamic. A significant decrease in their mobility was observed in both composting and vermicomposting reactors at the end of bioprocessing, however, change was more distinguishable in vermi reactors (Fig. 7.7a). Such reduction in vermi reactors could be the fact of mass and volume reduction of RM-CD-feedstock as a result of high decomposition and mineralization, and secondly, accumulation of metal in the earthworm gut (Yadav & Garg, 2019). The decrease was most remarkable for WS-Pb (10%-60%), Ex-Ni (31%-58%), WS-Cd (23%-64%), and Ex-Cd (47%-68%) ($p<0.05$) in vermi reactors compared to their composting counterpart, however, a little increment was found in some metals, viz. Cu (Ex), Pb (Ex), and Ni (WS) at end of composting. This may be due to weight loss and C loss during mineralization (Goswami et al., 2013). Interestingly VC3 showed highest reduction for WS-Pb (>60%), WS-Cr (55%), and WS & Ex-Cd (64.02% and 68.56%) while VC2 significantly reduced Ex-Cu (32.20%) and Ex-Cr (32.99%). Although, Cr concertation was highest in all the feedstock at the beginning nevertheless their decrease after the trial was not muchly appreciable, perhaps, due to its intricacies in oxidation state. Among the vermi reactors, the reduction was high in VC3 and VC2, followed by VC4 >VC1. Since VC4 (1RM:4CD) held a large part of CD, it had the least metal content after experimental control (VC0), whereas VC1 (1RM:1CD) had more part of waste thereby, contained more metal. Increased growth of earthworms in VC2 and VC3 seems to be responsible for a greater removal in respective systems. Passage of partially digested organic matter elevates the microbial activity in the gut which in turn helps in metal binding to the ingested material. This earthworm-mediated metal reduction can be more validated through their cellular adaption theory which delineates the formation of inclusion of nuclear bodies due to metal-bound nuclear protein and cytoplasmic synthesis of metal-binding protein in chloragogenous tissue (Cherian & Nordberg, 1983). The findings of this study are in good agreement with many previous studies by Goswami et al. (2013); Chakraborty et al. (2022); Karwal & Kaushik (2020). Fascinatingly a considerable tissue (gut/skin) deposition occurred in RM-based feedstock however it was negligible in control (VC0) except for metal Cu and Ni. The highest accumulation was found in VC1 and the lowest in VC4, however, it mostly depends on the metal concentration of the feedstock. Overall bioaccumulation was in the order of Cr>

Cu> Ni> Pb> Cd (Fig.7.7b). One-way ANOVA comprehends that accumulation among treatments was significant ($p<0.001$), where the minimum difference was as follows, Cu- LSD= 0.31, F=103.66; Pb-LSD=0.41, F=156.18; Ni-LSD=0.26, F=130.71; Cr-LSD=1.45, F=252.69; Cd-LSD=0.12, F=82.70). Such wide variation in gut/skin absorption is influenced by numerous factors like interspecific differences in element uptake, chemical characteristics of the feedstock (OM, pH, food palatability), ecological category, physiology and morphology of the species, season and other abiotic factors (moisture, aeration) (Usmani et al., 2017). Earthworms have a natural predisposition to accumulate metal, which they do by retaining metal in insoluble phosphate granules or chloragosomes without impeding cytosolic process. This, further chelate with sulphur donating ligand of metallothionein and gets relocated to the chlorogenous tissue, where it gets neutralized (Stürzenbaum et al., 2012). The linear regression analysis between bioavailable metal loss and tissue-absorbed metal strongly supported biotransformation (Cu-R^2=0.94, Pb-R^2=0.78, Ni-R^2=0.82, Cr-R^2=0.98, Cd-R^2=0.98). Suthar (2009) and Mondal et al. (2020) formerly reported on metal accumulation in *E. fetida* during vermi conversion of coal ash and sewage sludge which is quite analogous to our observation. A fractionation study provides a clear picture of metal switching from easily accessible to unavailable state.

Bioaccumulation factor (BaF) is a promising approach to quantifying the ingested pollutants inside the cell. This approach has been widely used assuming that organisms attain chemical equilibrium concerning the root of exposure (Hsu et al., 2006). In present investigation, we noted BaF ranges for Cr (0.04-0.90), Cd (0.04-0.8), Pb (0.14-0.30), Ni (0.13-0.36), Cu (0.05-0.17). It showed a significant difference among treatments for Cu (LSD=0.014, $p<0.001$), Pb (LSD= 0.016, $p=0.001$), Ni (LSD= 0.018; $p<0.001$), Cd (LSD= 0.028, $p<0.001$) except for Cr (LSD=0.05, $p=0.36$). From the result, it can be stated that higher metal concentration does not have any impact on accumulation factor, since the order of average accumulation was somewhat like Cr> Cd> Cu> Ni >Pb (Fig.7.7c). Although Cd and Pb are highly toxic in trace amounts, yet known to be accumulated by earthworms. The deposition mainly occurs in their chlorogenous tissue along with reproductive tissue (seminal vesicles) including the fact of slow release in the environment (Hirano & Tamae, 2011). It is also known to induce chloragocytes to express metallothionein under metal-exposed conditions as stated earlier by many researchers (Morgan & Morgan, 1990; Hirano & Tamae, 2011). Concurrently, the present study also found a strong relationship by examining linear regression analysis between Cu (R^2=0.94), Cd (R^2=0.98), and Cr(R^2=0.98), with their respective loss at the end of trial, while Ni showed a strong inverse relationship (R^2=0.82) implying that Ni loss might occur

from leaching, adsorption or precipitation rather than earthworm bioaccumulation. The changes in available metal concentration are presented as the removal efficiency ratio (RE) depicted in Fig. 7.7d Interestingly, RE of vermicomposting was much higher than composting and was in the order Cd> Pb> Ni> Cr> Cu, however, RE of composting reactors was a little different in order i.e., Ni> Cd> Pb> Cu >Cr.

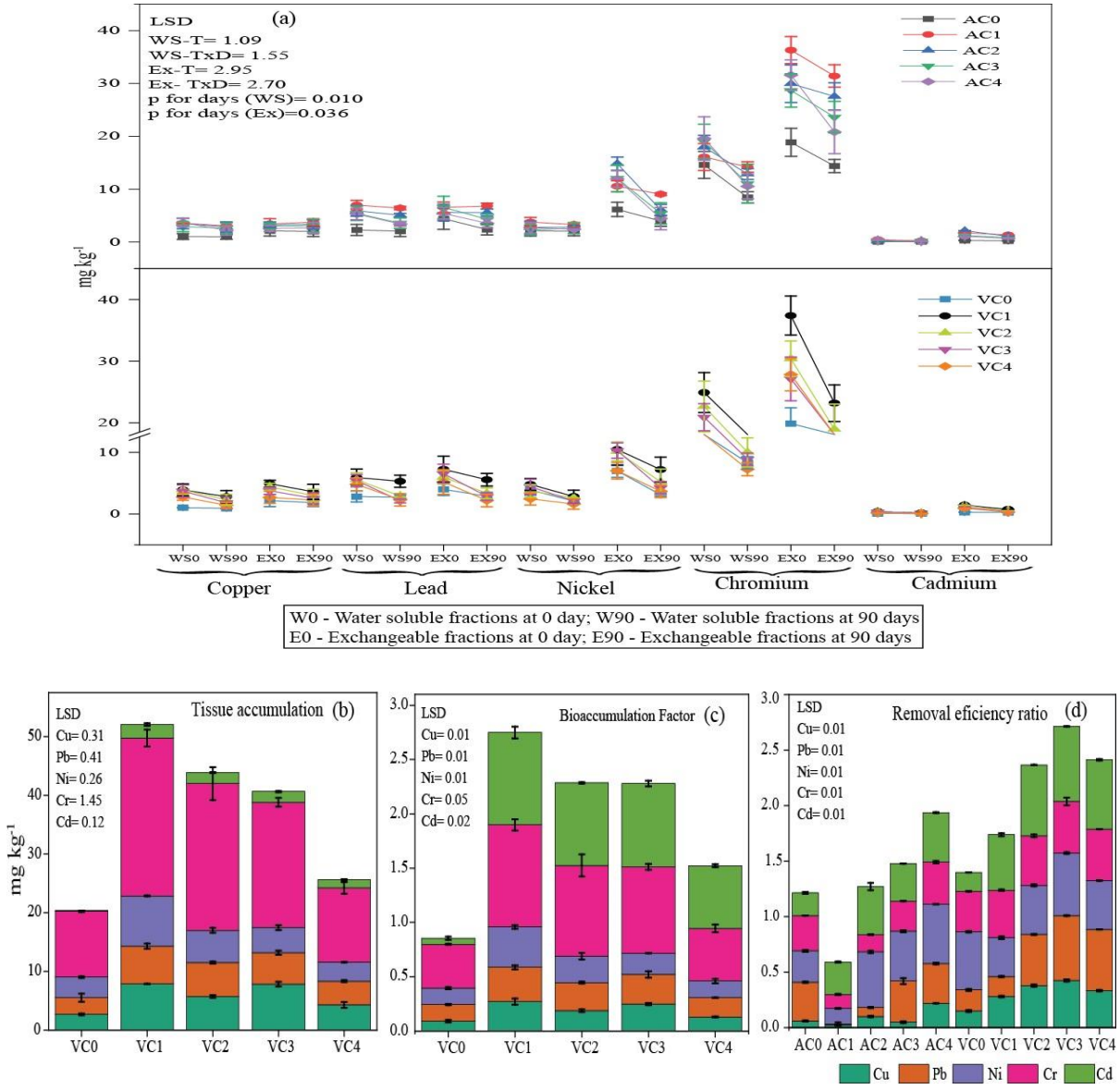

Fig. 7.7. (a) Variations in bioavailable fractions [water soluble (W) and exchangeable (E)] of different metals during bio-conversion (aerobic and vermiconversion). Magnitude of metal accumulation by *Eisenia fetida*. (b-c) Removal efficiency ratio (d) of composting and vermicomposting unit. (LSD= least significant deviation). Each error bar represents value ± standard error.

7.3.11. Microbe-metal synchrony – a correlation-based insight

Enzyme richness, reduced metal availability, advanced microbial activity, nutrient readiness, and high porosity make compost extremely beneficial for soil and plant nutrition. However, the presence of metal and its mobility create an imbalance owing to their detrimental impact on microbial survivability. Since microbes are the source system of nutrient cycling (C, N, P, S), their deficiency may lead to the barrenness of any system. Here, an attempt was made to justify the metal-microbe dynamics of prepared compost and vermicompost using Pearson's correlation statistics. According to Shi et al. (2013), correlation is the most authentic approach to understand metal-microbe synchronicity. It was performed by taking the microbial attributes (MBC, RQ, qCO_2), enzyme activities (urease, alkaline phosphatase, FDA, dehydrogenase, sulphatase, β-D-glucosidase), and water-soluble (WS) and exchangeable (Ex) fraction of metal (Cu, Cr, Pb, Ni, Cd). The result of correlation statistics is presented in Fig. 7.8. From analysed data in aforementioned sections demonstrate an abundant microbial proliferation with increased enzyme richness and a corresponding presence of metal in the bio-processed material. The correlation statistics unveiled how this microbial existence managed metallic acquaintance. Respiration quotient (RQ) and metabolic quotient (qCO_2) are the stress indicator of any system, which was positively correlated with all the water-soluble and exchangeable fractions of Cu, Pb, Ni, Cr, and Cd for all combinations of composting and vermicomposting reactors at 5% level (RQ, r: WS-Cu=0.67, Ex-Cu=0.77, WS-Pb=0.67, Ex-Pb=0.66, WS-Ni=0.70, Ex-Ni=0.75, WS-Cr=0.67, Ex-Cr=0.50, WS-Cd=0.68, Ex-CD=0.47; qCO_2, r: WS-Cu=0.76, Ex-Cu=0.77, WS-Pb=0.76, Ex-Pb=0.79; WS-Ni=0.78, Ex-Ni=0.71, WS-Cr=0.79, Ex-Cr=0.76, WS-Cd=0.72, Ex-CD=0.74). In contrast, a significant reverse relationship ($p<0.05$) among C_{mic} and other enzymatic activities with WS & Ex fraction of Cu, Pb, Ni, Cr, and Cd postulate that the concentration of available metal did not create any hindrances on microbial survivability, proliferation, and enzymatic exudation. Moreover, the positive correlation between stress indicators (RQ and qCO_2) and metal mobility has proved that the metal-microbe dynamics were in equilibrium.

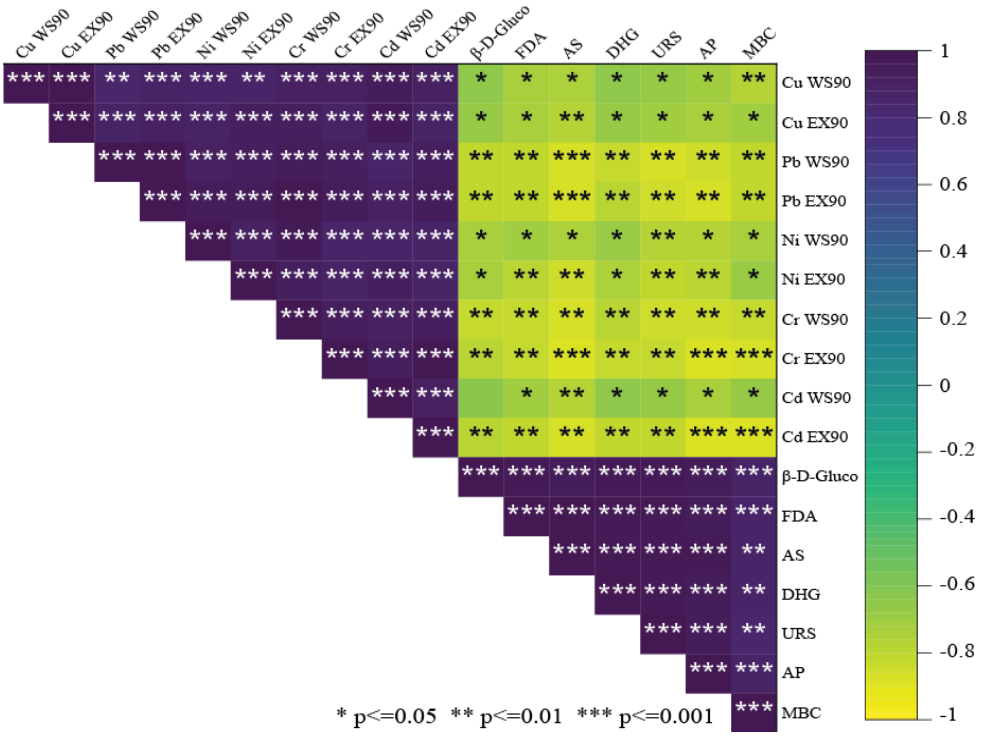

Fig. 7.8 Correlation-based metal bioavailability and microbial activity interactions (each point indicates the correlation coefficients and their significance levels are indicated by colour of the points).

7.3.12. Fate of metal in the compost- fractionation study

Leaching, element absorption, waste mass-volume reduction, and organic matter mineralization all played a role in the process' ability to change the overall metal concentration. However, vermicomposting is primarily driven by earthworm intervention, whereas composting merely deals with volume reduction. The distribution of heavy metal before and after bioprocessing is presented in Fig. 7.9. The dynamics were a little intricate during bioprocessing. A significant reduction in the water-soluble (WS) and exchangeable (Ex) fractions was extensively reported which is consistent with our findings (Hait & Tare 2012; Chakraborty et al., 2022). In vermireactors and aerobic reactors as well, there was a decline in the WS-Ex metal fraction. In the beginning, Cu mostly prevailed over WS, Ex, CBD, OXD, and ORG fractions, as composting proceeded the residual fraction (RS) augmented and oxide-bound (OXD) fractions decreased remarkedly. Similarly, as vermicomposting progressed, the organic bound fraction (ORG) and residual fractions (RS) elevated and conserved a greater amount of Cu. A substantial gaining of humic acid may account for it. Pb was extremely high in innate RM so, RM-based fed stock was also high. Likewise, their lability also decreased (WS, Ex & CBD). Metal was mostly shifted to ORG, OXD, and RS fractions since Pb become

immobilized when organic matter is broken down into insoluble salts or humic substances, which converts WS/Ex/CBD fractions into more stable ORG/OXD (He et al., 2009). A considerable presence of CBD fraction in aerobic reactors, even though it is reportedly unavailable, a reduced pH condition makes it available for cellular access which can be a threat to flora and fauna. The chemical partitioning of Ni after vermicompost was somewhat like the following: organic bound (ORG)> carbonate bound (CBD)> residual phase (RS)> oxide bound (OXD)>exchangeable (Ex)> water-soluble (WS) where, VC3 (1RM:3CD) and VC2 (1RM:2CD) exhibited the greatest decrease from WS, Ex, and CBD-bound metal likely due to the bioaccumulation of earthworms. Interestingly, in composting the metal was more prominent in carbonate, oxide, and residual phases than an organic fraction. Due to weight loss, CO_2 and water evolution, and the mineralization process, metals became concentrated during the composting process, leading to an increment in Ni, which is in line with Liu et al. (2007). Cr detected in vermicomposted RM, belonged to residual, oxide, and organically bound fractions, while in composting it was dominantly present in exchangeable, carbonate-bound, water-soluble, and residual fractions. Despite the fact of considerable early dominance in the WS and Ex fractions, they experienced a moderate drop in compost and a fair reduction in the vermicomposting system at the end of incubation. Reduction of Cr^{6+} to Cr^{3+} probably limits their bioavailability as Cr^{3+} is steadier and forms a stable complex with humic content, while Cr^{6+} is more soluble in water, thus available (Paul et al., 2020). This suggested that vermicompost could be a promising approach to augment stability by reducing their bioavailability. Other research also reported the increase of Cr in the residual fraction He et al. (2016) and Lv et al. (2016). Although the speciation of Cr in the compost and vermicompost reactors is a bit complicated, yet, environmental conditions, earthworm intervention, or microorganisms played a crucial role. The explanation for this is not quite evident, though. Cd was largely associated with carbonate bound and exchangeable fractions at the beginning which was shifted to organically bound fractions after vermicomposting in all the treatments along with an augmentation of the residual fraction. This finding partially contradicted He et al. (2016)'s observation of a rise in Ex- phase, but it was also somewhat similar as he also reported an increase in residual phase and a drop in reducible fraction. Considering, aerobic composting Cd was mostly found in carbonate bound, oxide bound, and residual fraction. Overall, humic substances handled the metal dynamics of both reactors, but in vermicomposting reactors, earthworms' gut/skin epithelial absorption of bioavailable metal operated as a possible influence.

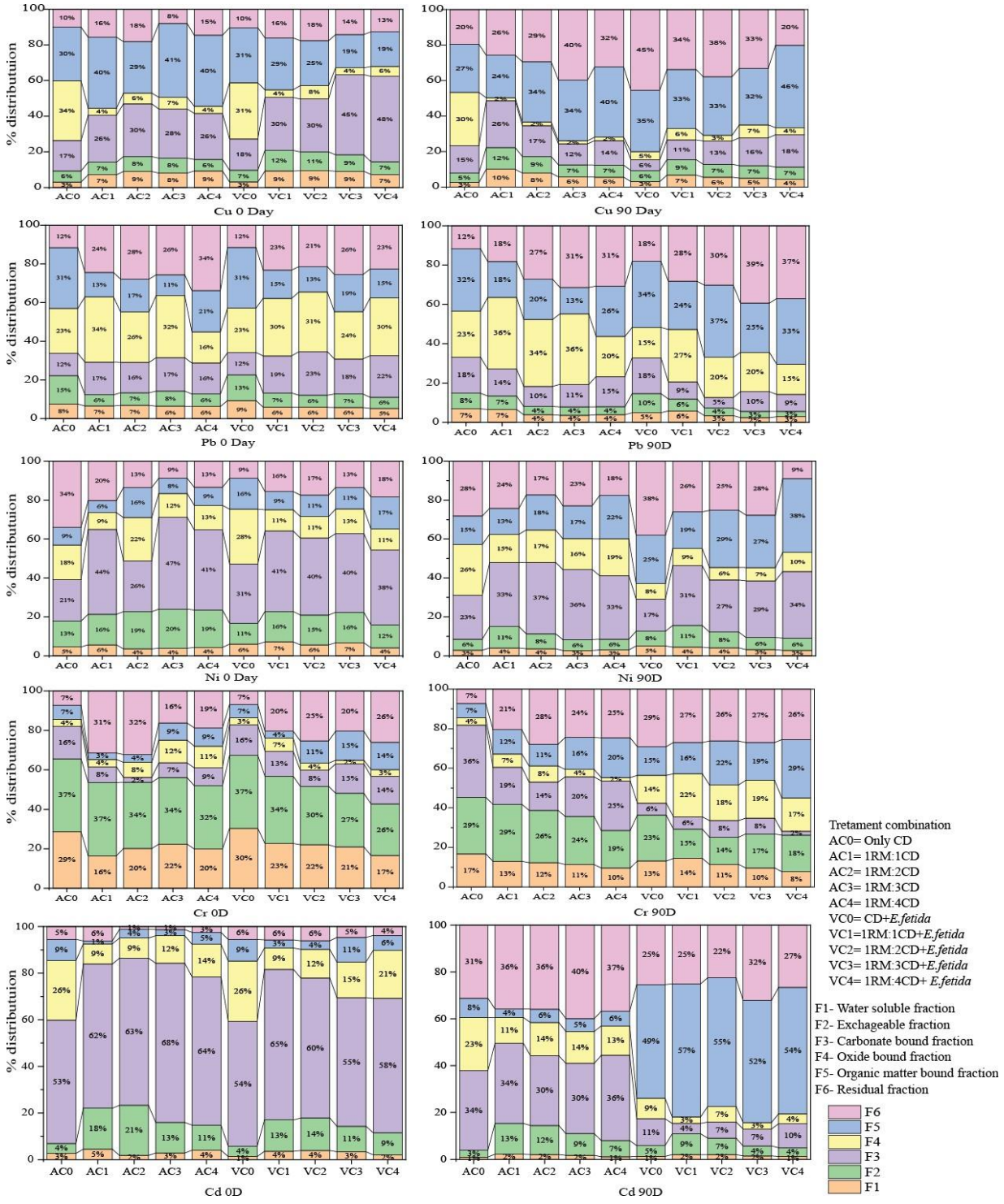

Fig. 7.9. Changes in different fractions of metal under aerobic and vermicomposting between initial and final days.

7.3.13. Mobility factor assessment (MF) and pollution load index (PLI)

An essential characteristic that clarifies the metals' effectiveness in migration is the mobility factor. All of the bioprocessing units showed a considerable decrease in MF (Fig. 7.10a). We recorded highest reduction for Cd in vermireactors (0.7-0.8-fold). The reduction was significant for days ($p < 0.05$) for all the metals under study, according to two-way ANOVA. In addition, metal removal considerably decreased the PLI in all vermireactors, although it increased in aerobic reactors for Cr and Ni (Fig. 7.10b). Among them, Cd (0.10-0.29-fold) experienced the greatest reduction, which was followed by Pb, Ni, Cu, and Cr. A similar kind of finding was obtained by Lv et al. (2016) and Mondal et al. (2020).

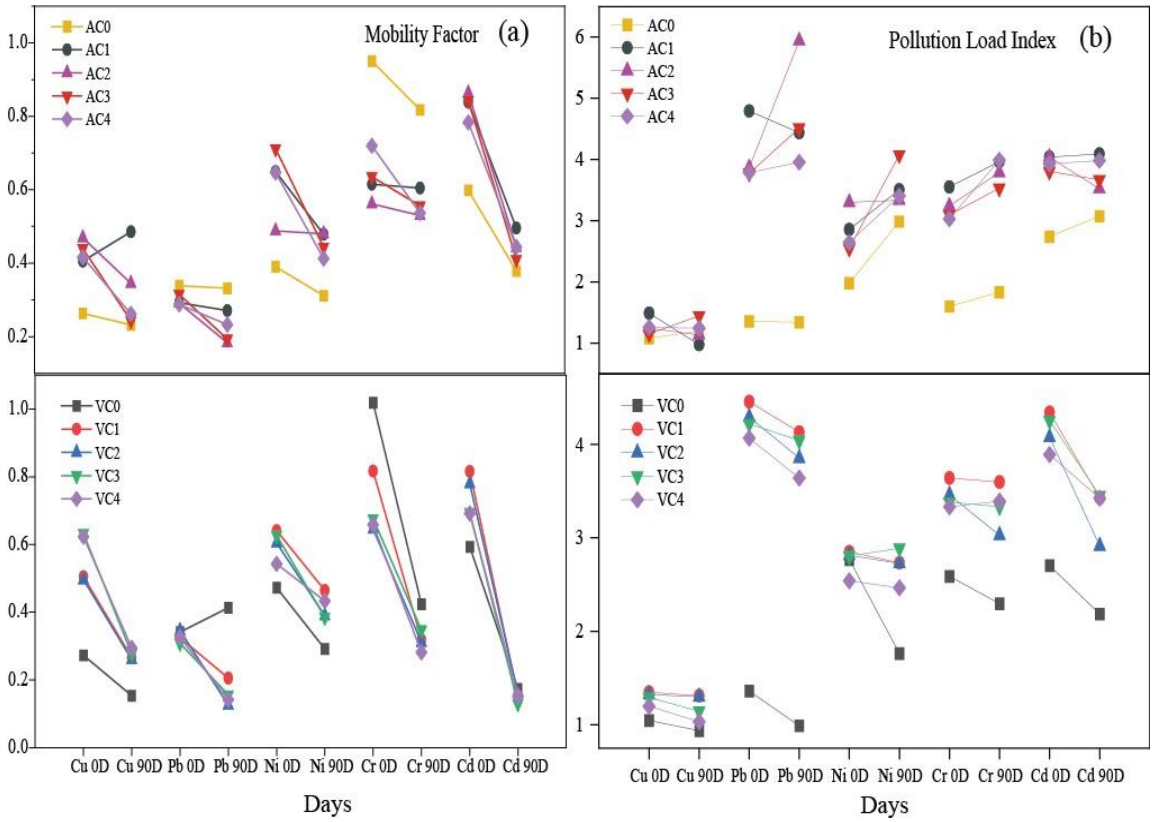

Fig. 7.10. Changes in mobility factor (MF) and pollution load index (PLI).

7.3.14. Compost quality indices (Biodegradability quotient, benefit ratio, compost quality quotient)

The biodegradability coefficient (K_b) suggests the intensity of organic matter degradation which is an indirect way of measuring compost maturity (Garg & Gupta, 2011). K_b was higher in vermicomposting compared (0.50-0.66) to aerobic composting (0.29-0.41), where VC2 (0.63) and VC3 (0.60) were highest after experimental control (VC0) (Fig. 7.11a).

This was likely earthworm-microbe's cooperative effort which led to maximum degradation of OM budget of waste (RM) based feedstock. The nutrient benefit ratio (N, P, K) was higher in vermi reactors, as anticipated. VC2 and VC3 showed a greater benefit compared to VC1 and VC4 (Fig. 7.11b). The ratio was highest for mineralizable N>available P> exchangeable K. Additionally, the CQQ was noticeably higher in vermi bins compared to their corresponding aerobic counterpart (Fig. 7.11c). The increment prolonged up to 90 days however it was sharper between 30 to 60 days in both systems. This was probably caused by persistent degradation that lasted up to 60 days, followed by a slower metabolism brought on due to substrate insufficiency. A two-way ANOVA demonstrates that increment was highly significant among days (p=0.0001). Even while the results did not significantly differ from those of Hussain et al. (2018) and Goswami et al., (2017), however, a slight increase between 60 and 90 days were nevertheless indicative of compost maturation.

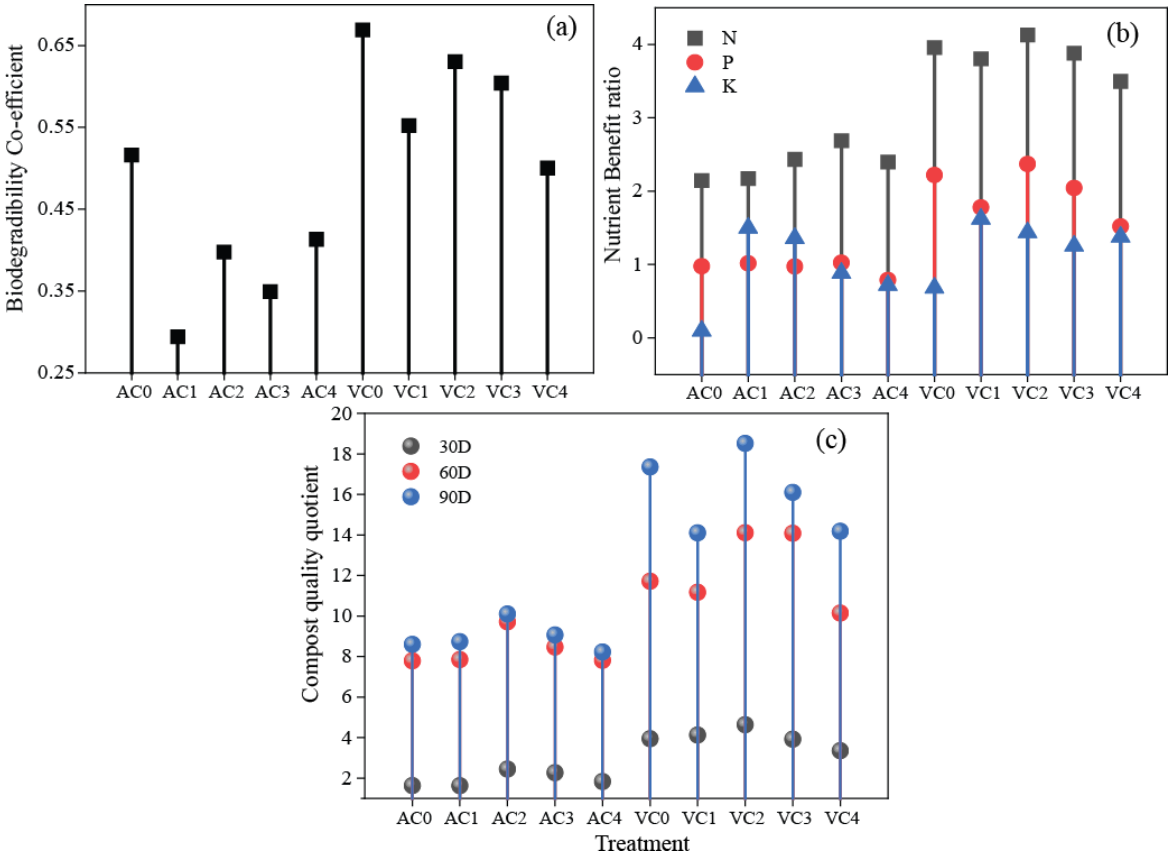

Fig.7.11. Different compost maturity indices and nutrient benefit ratio.

7.4. Conclusion

This study was the first attempt to assess the feasibility of using vermitechnology to convert the alkaline-sodic, metal-rich RMs into useful fertilizer. The trial demonstrated that

Eisenia fetida outperformed aerobic composting in terms of metal remediation, microbial community structure, activity, and enzymatic richness and correspondingly revealed, 1:2 and 1:3 (RM: CD) were equally palatable as RM-free substrate (only CD) for earthworm growth and nutrient mineralization. Alpha diversity analysis, PLFA study, and species indices delivered definite information on species distribution of vermibins and how they counteracted metabolic stress. Shifting of gram-negative to gram-positive bacterial community influenced stress ratio reduction. With respect to the enzyme input on the overall dissimilarity index between AC and VC and C-N limitation to the microbial utilization during vermiconversion, SIMPER, and vector analysis provided a piece of new scientific information. Correlation output demonstrated enzyme augmentation and microbial activity greatly reduced the bioavailability of metal (Cd, Cr, Ni, Pb, Cu), and earthworm bioaccumulation contributed significantly in declining in vermibins. Finally, a crop experiment showed that vermiconverted -RM could replace 50% of chemical fertilizers without lowering crop yield. Therefore, the key finding is that RMs can be detoxified into nutrient-rich fertilizers for agricultural applications using the *Eisenia*-mediated vermiconversion system, however, a dose-dependent mechanistic study will be needed for genotoxicity evaluation. Long-term effects of vermiconverted-RM on soil health would be a fascinating venture for future researchers.

Chapter 8

Efficacy of vermicomposted red mud (RM) on crop growth and soil health through pot and field-based assessment: A dual approach

Chapter 8

Efficacy of vermicomposted red mud (RM) on crop growth and soil health through pot and field-based assessment: A dual approach

8.1. Performance of vermicomposted RM on green gram (*Vigna radiata L.*) through pot experiment

8.1.1. Introduction

The 'Green revolution' brings a phenomenal change in today's agriculture practices. Over the last five decades, agronomic practices are continually changing with the inclusion of different modern techniques. However, to fulfil the upsurging demand of the population, agriculture practices are getting more inclined to the use of inorganic amendments for getting high productivity within less time. Extensive usage of agrochemicals along with their cumulative residue depositions in the soil give rise to nutrient-depletion conditions. Mostly, unscientific employment of imbalanced mineral fertilizers by farmers without considering any integrated nutrient management results in the deterioration of soil health, death of helpful microorganisms, and affects soil biodiversity (Rupani et al., 2018). Moreover, presence of synthetic chemicals and pesticides in agricultural runoff coupled with a high infiltration rate pollutes the environment and degrades the surface and groundwater quality. Although chemical NPK fertilizer instantly boosts plant health by refurbishing the depleted nutrients nevertheless high inputs of such fertilizers in crop cultivation led to an increased accumulation in the grain that exceeds the safety levels creating an alarming impact on the food chain (Bhattacharyya et al., 2003). Such a frame of adverse consequences demands developing some sustainable and eco-friendly nutrient management practices to ensure greater productivity without intimidating soil health. Commonly, proportionate nutrient supplementation is required by plants for the optimal growth and yield of any crop. A small deficiency or excess in nutrients may cause instabilities in the physiological and metabolic processes of plants. This necessitates the desirability of organic supplements as they are rich in carbon-nitrogen content. Since Indian soils are poor in organic matter content hence incorporation of organic supplements benefits the soil's organic carbon (SOC) status. Preservation of SOC is indispensable for long-term sustainable agriculture practices. Thus, agronomic practices that lift crop productivity as well as conserve the organic matter content in soil are highly appreciated. Organic manure moreover a combination of organic/inorganic manure could be an effective approach to nutrient

supplementation for maximal production of crops (Ibrahim et al., 2015). Such practices may take care of plants' health as well as protects the soil's health. Organic manure includes cattle dung, farm yard manure (FYM), crop residue, kitchen waste, and lignocellulosic deposits out of which cow dung manure is the most popular however currently faces scarcity owing to its diversified use in fuel supplementation (gobar gas production, cow dung cake etc.) in rural areas (Bhattacharyya et al., 2003). Application of biofertilizer and vermicompost is gaining familiarity nowadays for sustainable management. Vermitechnology is a classically recognized agricultural practice increasing crop yield by improving soil's physical, chemical, and biological properties. It is a non-thermophilic stabilized nutrient-rich end product of earthworm-microorganism interaction with high porosity, ventilation, and water retaining capacity. Vermicompost (VC hereafter) is a globular structure having a higher surface area for the strong retention of micronutrients and plays an effective role in plant growth and promotion. It contains nutrients like soluble potassium, nitrates, phosphates, exchangeable calcium, sodium etc. They are rich in microbial activity viz. bacterial, fungal, or actinomycetes and are considered nutritive organic fertilizers. Considering the origin of VC, it widely varies in chemical composition (Dume et al., 2022). Declining of traditional natural resources and emergence of waste invites us to pay attention to an alternative strategy where the waste could be recycled and reutilized. Presently vermiconversion is quite a well-known process to convert different industrial wastes into a value-added product. In general, the major limitation of using industrial wastes directly for agricultural purposes is presence of hazardous toxicants (Cd, Cr, Pb, Ni, As) although sometimes being rich in micronutrients (Fe, Cu, Mn, Zn, Ca, K, Mg) (Bhattacharya et al., 2012). These toxicants are not volatile and mostly remain in labile pools thus threatening sustenance. Earthworms together with microorganisms synergistically act on it during vermicast processing and produce a nutrient-rich product having dramatically reduced level contaminants. They as well unlock the micronutrients (Ca, K, Na, Mg, N, P, Fe, Zn, Mn) and make them into plant-available form for an easy uptake. Water soluble and exchangeable are the two most dicey fractions of any contaminants which enter into the food chain leading to bioaccumulation. Earthworm greatly sequesters them and shifts their availability state into a residual or organic bound fraction which lowers their toxicity (Goswami et al., 2017). The mineralization and humification process of earthworms and microorganisms is enhanced in presence of organic substrate (cow dung, cattle manure, rice straw, rice husk etc). A mixture of natural organic substrate and waste serves as beneficial feedstock material for earthworm growth and productivity. The approach gives a twining benefit of effective disposal and resource recovery and unveils a new avenue of compost application for sustainable agriculture.

Considering these perspectives, the present study is an endeavour of applying sanitized industrial waste (Red mud) using an epigeic earthworm species (*Eisenia fetida*) as a cost-effective fertilizer for crop cultivation. It is well-established that lateritic soils lack essential plant nutrients.

Pulses play a vital role in the Indian diet as a protein source, and green gram (*Vigna radiata L.*) holds the 3rd most important protein crop in India. It is also abundant in calcium, potassium, phosphorus, and vitamins A, B, and C, all of which are essential for human health. It was selected as the test crop in Giridih's depleted soil because of its brief lifespan (65–80 days), versatility in several intensive crop rotations, and ability to improve soil fertility by fixing atmospheric nitrogen through rhizobial symbiosis (Singh et al., 2017). Our study was designed to investigate the impact of such amendments in soil-plant systems and their relative toxicity towards human consumption. To comply with this objective a pot experiment was conducted for two consecutive years in summer season on a pulse crop (*Vigna radiata L.*) commonly known as green gram. It is quite a familiar crop in the tropics for intercropping systems with a short span of maturation time (65-80 days), which helps to increase the soil fertility status but can grow with a low fertile status of soil. Keeping these facts under consideration, the experiment was accomplished at agricultural farmhouse of the Indian Statistical Institute at Giridih, Jharkhand in the year 2020 and 2021. The hypothesis of this study is that a 50% substitution of inorganic fertilizer with organic (vermicompost) fertilizer will give enhanced crop productivity as well securing soil health.

8.1.2. Material and Methods

8.1.2.1 Processing of vermicompost (VC)

Vermicompost (VC) was prepared from industrial waste [red mud (RM)] in the year 2020 (September to November) by using an epigeic earthworm species (*Eisenia fetida*) at the vermicompost unit of the Indian Statistical Institute (ISI), Giridih, Jharkhand. Cow dung (CD was used as a bulking agent and collected from local cattle houses. Four different feedstock combinations were introduced to *E. fetida* with one positive control (only cow dung) and one negative control (only RM) and left for 90 days for conversion of waste to compost. The ratios (RM: CD) of the feedstock were (1:1, 1:2, 1:3, and 1:4) where 10 worms (healthy, non-ciliated, 35-40 days old) were employed per kg of substrate. Since worms introduced to RM died within one day, thus we maintained only RM for up to 90 days. At the end of November, the prepared VC was withdrawn from composting unit, sieved and preserved for crop trial.

8.1.2.2. Greenhouse pot experiment

A local summer variety of green gram (*Vigna radiata L.*) seeds was bought from the local market (variety -IPM-02-03). The seeds were sowed to a seedbed (30X50 cm) in the greenhouse of ISI, Giridih farmhouse for 10-12 days with 60% water holding condition. After 12 days the seedlings (6- 7 cm) got ready for the plantation, uprooted and transplanted in the experimental pot.

The pot experiment was conducted at the same greenhouse for crop trials for two consecutive years (2021 and 2022) in the month of March to June in order to check the efficacy of prepared vermicompost. The experimentation was laid out into twelve different combinations of treatments depicted in Table 8.1.1. Recommended fertilizer dose opted for the trial was 20:40:40 (N_2:P_2O_5: K_2O)/ha. In a nutshell, four replicates of each treatment were made where the earthen pots were filled up with 10kg of soil. Prior to sowing of the plant, the organic amendments were mixed (both full dose and half dose) in soil and left for 7 to 10 days. Only inorganic amendment (fertilizer) was added one day before the transplantation. Urea, super phosphate and muriate of potash were used as NPK precursors. 5-6 cm long seedlings were planted in each pot (2 plants/pot). The organic amendment was used in two doses 10 t/ha (VC 100%) and 5 t/ha (50% VC). Other agronomic practices like watering, drainage of excess water, weeding, and application of pesticides were followed uniformly for all the treatments recommended by the Department of Agriculture and Ecology, ISI, Giridih, Jharkhand.

Table 8.1.1. Treatment combinations for two-year crop trial (2021-2022)

Pot name	Treatment combination
T1	Control (No amendment)
T2	Fertilizer (NPK)100%
T3	Vermicompost (1:1) 100%
T4	Vermicompost (1:1) 50% + Fertilizer (NPK) 50%
T5	Vermicompost (1:2) 100%
T6	Vermicompost (1:2) 50%+ Fertilizer (NPK) 50%
T7	Vermicompost (1:3) 100%
T8	Vermicompost (1:3) 50% + Fertilizer (NPK) 50%
T9	Vermi compost (1:4) 100%
T10	Vermicompost (1:4) 50% + Fertilizer (NPK) 50%
T11	Cow dung 100%
T12	Cow dung 50% +Fertilizer (NPK) 50%

8.1.2.3. Soil sampling and analysis of soil and plant sample

The field moist samples were collected at four different stages of plant i.e., transplanting time, flowering time, maturation time and post-harvest for microbial parameter analysis (microbial biomass C, soil respiration, enzymatic activities). Soil samples were kept in a sterile plastic bag from each replicate of twelve treatments. The sowing stage sample was taken just before the transplantation and post-harvest samples were drawn ten days after harvesting. The key attribute microbial biomass C was measured following Jenkinson (1988). Soil respiration was estimated by measuring CO_2 released at the time of incubation of soil when induced with 0.5% glucose in a closed system, and the trapped CO_2 in NaOH solution was subsequently titrated with HCl. FDA activity was measured following Tabatabai (1994) involving estimation of fluorescein released when moist soil incubated with phosphate buffer (pH 7.6) and fluorescein diacetate solution at 25^0C. Dehydrogenase measured by taking 6g of moist soil

incubated with 3% TTC at 37^0C for 24 h subsequently triphenyl formazan (TPF) was extracted and filtered with aid of methanol and finally measured spectrophotometrically at 485nm.

To assess the physicochemical parameters, viz. pH, EC, organic carbon, available nitrogen (N), phosphorus (P) and potassium (K), soil samples were drawn from each replicate before sowing and after harvesting. The samples were air-dried, sieved through 2 mm mesh and preserved for analysis. All the parameters were analyzed following Page et al. (1982). Likewise, the vermicompost samples were also undergone for the measurement of available nutrients (N, P, K). Considering metal profiling, before addition of amendments composite soil sample representing the status of the soil of experimentation was collected to analyze the inherent metal distribution of soil. For treatments, only post-harvest samples were taken metal speciation study. Sequential extraction for speciation study was done by following Tessier et al. (1979) using air-dried, 0.2 mm sieved sample. Quantification of phytoaccumulated metal was done by digesting the dried root, shoot and grain in a 4:1 ratio (HNO_3:$HClO_4$) acid mixture and a subsequent volume makeup to 50 ml. Concentrations of metal in the digests were measured using atomic absorption spectrophotometer (Systronics AA S-816) and expressed in terms of dry weight basis. Standard solutions of the metals (Cr, Ni, Cd, Cu, Pb) were made from the stock solution (1000 mg/L, Merck grade) in 1% (v/v) HNO_3 for calibration. For quality checking, certified reference materials 2710 and blank extract were used. Total nutrient uptake (P, K) in different parts of plants was analysed using the same digest. Determination of K was done by using a flame photometer (Systronics) while P was measured spectrophotometrically.

8.1.2.4. Analysis of plant biochemical attributes

At the end of the complete life cycle, the green gram plants were harvested and growth parameters and yield characteristics were recorded. Biochemical attributes like chlorophyll a, chlorophyll b, and total chlorophyll were extracted by acetone-hexane mixture in a 4:1 ratio. Protein content was quantified by Lowry et al. (1951). Total soluble sugar (TSS) was measured following the phenol-sulfuric acid method proposed by Dubois et al. (1956). Agronomic parameters namely plant height, root length, shoot length, number of nodules, number of branches, pod number per plant, pod length, grain count per pod, 100 seed weight, and total no of seeds per plant were recorded.

A. Measurement of protein (Lowry et al., 1951)

The principle behind the Lowry method of determining protein concentrations lies in the reactivity of the peptide nitrogen with the copper ions under alkaline conditions and the

subsequent reduction of the Folin-Ciocalteay phosphomolybdic phosphotungstic acid to heteropolymolybdenum blue by the copper-catalysed oxidation of aromatic acids [Dunn, 13]. The Lowry method is sensitive to pH changes and therefore the pH of assay solution should be maintained at 10 - 10.5.

Reagents

1. 2% Na_2CO_3 in 0.1 N NaOH
2. 1% NaK Tartrate in H2O
3. 0.5% CuSO4.5 H2O in H2O
4. Reagent I: 48 ml of A, 1 ml of B, 1 ml C
5. Reagent II- 1-part Folin-Phenol [2 N]: 1 part water
6. BSA Standard - 1 mg/ ml

Procedure

1. 0.2 ml of BSA working standard in 5 test tubes and make up to 1ml using distilled water.
2. The test tube with 1 ml distilled water served as blank.
3. Added 4.5 ml of Reagent I and incubated for 10 minutes.
4. After incubation added 0.5 ml of reagent II and incubated for 30 minutes
5. Measured the absorbance at 660 nm and plot the standard graph.
6. Estimated the amount of protein present in the given sample from the standard graph.

B. Measurement of total soluble sugar (TSS) (Dubois et al., 1956)

Glucose is dehydrated to hydroxymethyl furfural in a hot acidic media. With phenol, this produces a green product with a peak absorption at 490 nm.

Reagents

1. Phenol 5%: Redistilled (reagent grade) phenol (50g) dissolved in water and diluted to one liter.
2. Sulphuric acid 96% reagent grade.
3. Standard Glucose: Stock – 100mg in 100mL of water. Working standard – 10mL of stock diluted to 100mL with distilled water.

Procedure

1. 100 mg of the green gram were weighed into a boiling tube.

2. Hydrolysed in a boiling water bath for three hours with five millilitres of 2.5 N-HCl before allowing to cool to room temperature.
3. Then neutralised it with solid sodium carbonate until the effervescence stops.
4. Made up the volume to 100mL and centrifuge.
5. Pipetted out 0.2, 0.4, 0.6, 0.8 and 1mL of the working standard into a series of test tube.
6. Pipetted out 0.1 and 0.2mL of the sample solution in two separate test tubes. Make up the volume in each tube to 1mL with water.
7. Set a blank with 1mL of water.
8. Added 1mL of phenol solution to each tube.
9. Added 5mL of 96% sulphuric acid to each tube and shake well.
10. After 10min shake the content in the tubes and placed in a water bath at 25-30°C for 20min.
11. Read the colour at 490nm.
12. Calculated the amount of total carbohydrate present in the sample solution using the standard graph

Calculation

Absorbance corresponds to 0.1mL of the test = 'x' mg of glucose

100mL of the sample solution contains = ('x' ÷ 0.1) × 100mg of glucose = % of total carbohydrate present.

C. Measurement chlorophyll A, chlorophyll B and total chlorophyll (**(**Ignat et al., 2013**)**

Reagents

1. 80% ethanol or 80% acetone (v/v) in water

Procedure

1. Weigh 700 mg fresh tissue and transfer to graduated sample tubes (10ml).
2. Add 80% ethanol or 80% acetone till the tissue gets immersed. It is then kept in freeze at -18ºC for 3 hrs.
3. Crush the tissue in a mortar. Filter the suspension through a membrane filter.
4. Read the absorbance at 664.2 nm, and 648.6 nm for Chlorophyll A, Chlorophyll B

Calculation (Unit: mg chl g^{-1} fresh tissue)

Chlorophyll A = $(13.36 \times A_{664.2}) - (519 \times A_{648.6})$

Chlorophyll B = $(27.43 \times A_{648.6}) - (8.12 \times A_{664.2})$

Total Chlorophyll = $(5.24 \times A_{664.2}) + (22.24 \times A_{648.6})$

8.1.2.5. Nutrient benefit ratio and metal mobility assessment

The potential benefit of using organic amendment (here VC) for enhancement of soil fertility status can be calculated by the following Eq. 1 (Sahariah et al., 2015). The nutrient benefit ratio (NBR) was computed for the variables TOC, available N, available K, and available P accountable for soil fertility factor.

$$Nutrient\ benifit\ ratio = \frac{Average\ concentration\ 60D - Average\ concentration\ 0D}{Average\ concentration\ 0D}$$

Apart from nutritional factors, presence of toxic components like heavy metals and their plausible movement towards plant systems was assessed and represented as bioconcentration factors (BCF), translocation factors (TF) and bioaccumulation factors (BAF) (Islam et al., 2020). The formulae are given below

$$Bioconcentration\ factors(BCF) = \frac{Croot}{Csoil}$$

$$Translocation\ factor\ (TF) = \frac{Cshoot}{Croot}$$

$$Bioaccumulation\ factor\ (BAF) = \frac{Cgrain}{Csoil}$$

8.1.2.6. Prediction of metal content in moong bean grain

Metal content in the edible part of green gram raised in organically amended soil was predicted by the solubility-free ion activity model (FIAM) without measuring metal solubility in practical. The model describes that metal uptake could be controlled by free metal ion activity in soil solution. Transfer factor (TF) is the ratio of metal content in plant (M_{plant}) to metal ion activity in soil (M^{n-}) solution. (Mirecki et al. 2015)

$$TF = \log \frac{[Mplant]}{(M^{n-})}.$$

Simple pH dependent Freundlich equation was employed to predict the free ion activity of three metallic species (Cr, Ni, Cu) as follows

$$p(M^{n-}) = \{p[Mc] + k_1 + k_2\ pH\}_{n/F}$$

where Mn- denotes the free ion activity in soil solution and Mc denotes the humic content (mol/kg carbon) to which the labile metal be adsorbed, k1 and k2 stands for the metal

coefficient and n_F is the power term of Freundlich equation. Predicted metal uptake was derived by combining equations presented above and depicted as follows

$p[M_{plant}]= C+\beta1p[M_c]+\beta2[pH])$

where C = k1/nF − log TF, β1 = 1/nF, β2 = k2/nF and C, β1 and β2 are empirical metal and plant-specific coefficients. Equation (7) was parameterized by nonlinear error minimization by means of the "SOLVER" facilities in Microsoft Excel 2019.

8.1.2.7. Risk assessment

A health risk assessment was done to confirm any associated health complications on consumption of cultivated crops. Estimated daily intake, carcinogenic and non-carcinogenic risk of the three metals (Cu, Ni, Cr) was computed.

Estimated daily intake was computed for three metals (Cu, Ni, Cr) by following equation 8 (Rashid et al., 2022) and the derived value was compared with maximum tolerable daily intake set by regulatory bodies. The equation used to derive the values based on US-EPA

$$EDI = \frac{IngR\ X\ C}{BW}$$

where EDI = estimated daily intake of metal from consumed crop (mg/d/ BW (kg), IngR = ingestion rate (kg) of, C = concentration of metal in the sample (mg/kg), and BW = body weight (kg). The average pulses consumption rate worldwide (0.021 kg/person/ day) and BW values for adults (70 kg) respectively (Rashid et al., 2022).

Non-carcinogenic health risks through metal consumption via intake of moon bean were calculated in terms of hazard quotient (HQ) following the USEPA (Rashid et al., 2022). If the HQ > 1, the average daily dose (ADD; mg kg/body weight/day) of metal exceeds the reference dose (R_fD; mg kg/body weight/day), demonstrating that there is a possible risk related with metal intake. The oral reference doses used for the calculation were 1.5, 0.02 and 0.04 mg/kg/day for Cr, Ni, and Cu respectively (USEPA 2010). Total hazard quotient is ∑HQ.

$$HQ = \frac{EDI}{RfD}$$

The carcinogenic risk factor is the dimensionless indicator that helps to assess the incremental lifetime cancer risk for the intake of moong bean calculated by equation given below.

CR= EDI X CSF

Where CSF is the cancer slope factor. The Carcinogenic slope (CSF) value of Ni and Cr is 0.84, and 0.5 respectively (USEPA; United State Environmental Protection Agency 2015). Carcinogenic Slope factor (CSF) has yet not been established for Cu since they are not recorded to cause any carcinogenic effect.

8.1.2.8. Statistical analysis

Analysis of variance (ANOVA) followed by least significant difference (LSD) calculation was used to explain the consequence of different amendments on crop growth, yield characteristics, soil fertility including the metal uptake by grains of green gram (*Vigna radiata L.*) employing SPSS statistical package (IBM SPSS 25.0 statistics). The data presented and discussed were mean of two years. All the data were represented in mean ±SE form.

8.1.3. Result and Discussion

8.1.3.1. General characterization of RM-based vermicompost

Vermicompost produced from industrial waste (red mud) was found to contain a significant amount of nutrients, which is elaborately discussed in chapter 7. The compost was rich in organic matter and other nutrients viz. nitrogen (N), phosphorus (P), potassium (K), etc. It not only contained nutrients but was also enriched with nitrogen-fixing and phosphate-solubilizing bacteria. The cow dung used in this study was having a neutral pH of 7.7, EC 1.1 mS/cm, available N 124 mg/kg, available P 35 mg/kg, and potassium 169 mg/kg.

8.1.3.2. Effect of amendments on crop growth, yield attributes, and biochemical quality

Overall, the beneficial effect of organic amendments was evidenced in growth and development of plants. A perusal of data (Table 8.1.2a and 8.1.2b) distinctively identified that application of VC50% + NPK50% logged maximum plant height, number of branches, nodule number, root and shoot length, and pod count. The organic + inorganic treatments were found to be significantly ($p<0.05$) superior to organic amendments alone. Significantly higher plant height was recorded in T12 (VC50%+NPK50%) followed by T6> T2> T8> T7> T11> T9> T10> T5> T4> T3 >T1 (LSD=1.25; $p<0.0001$; F= 37.50). The root length was in the order as follows T8> T10> T3> T11> T6> T12> T9> T5> T4> T2> T7> T1 (LSD=1.57; p=0.0309; F=2.47). On the other hand, highest shoot length was achieved in T12 (35.76 cm) followed by T2> T6> T7> T8> T11> T9> T10> T3> T5> T4 >T1 (LSD=1.84; $P<0.0001$; F=24.06). Root nodule formation is an important attribute that varied significantly ($p<0.05$). The higher number of nodules was found in T6 (28.00±1) and T8 (27.33±2.9), and had the order somewhat

like T6> T8> T12> T2> T10> T9> T11=T7> T5> T4> T3>T1 (LSD=4.27; p=0.047; F=2.24). The addition of organic amendments triggered the soil's organic matter content which possibly reduced the bulk density thereby improving the pore spaces that directly increased fertility of amended soil and facilitated better growth of plants (Rahman et al., 2019; Dong et al., 2021). Considering the grain (seeds) number per pod T8 produced a maximum of 8.33±0.33. It was distributed and differed among the treatments as T8> T2=T4=T6=T10> T12> T11=T5> T7> T2=T9> T1 (LSD=0.577; P<0.0001; F=11.56). Following similar trend pod numbers per plant varied significantly and were noted highest in T6 (29.67±2.86) followed by T2> T8> T12> T10> T4> T11> T9> T3=T5> T7>T1 (LSD=1.38; p<0.0001; F=16.13).). Significantly higher number of seeds per plant produced by T6 (50% VC+50% NPK) and T2(100%NPK) followed by T8> T4> T10> T12> T11> T9> T3> T5> T7> T1 (LSD=16.91; p<0.0001; F=11.95). Considering 100 seed weight which was also highest in 50%VC+50%NPK treatment (T6-6.7g±0.12). Nearly all the treatments showed >5.5 cm pod length except T1 showed 4.5 cm of pod length, which was the lowest among all. The highest pod length was recorded in T2 (6.3 cm±0.05) supplemented with 100%NPK. Yield was highest in T6 (15.90±0.88 g/plant) followed by T2> T8> T12> T10> T4> T11> T9> T7> T5> T3> T1 (LSD=2.88). The notable performance of composite treatments may be from the application of vermicompost which contains a balanced amount of nutrients, along with beneficial microbial consortia like N_2-fixing, phosphate, and potassium solubilizers (Hussain et al., 2016). They enhance nitrogen fixation with aid of enzyme nitrogenase thereby triggering the nodule formation, as well as solubilizing more insoluble P and K, and also producing secondary metabolites viz. stimulants, growth regulators, and enzymes that support plant growth and development. The result of our observation is consistent with earlier studies (AL-Dulimi et al., 2017; Mahmoud et al., 2015; Kaysha et al., 2020, and Blouin et al., 2019).

Photosynthetic pigments like chlorophyll a and b were found to be highest in T6 (11.21±0.55; 4.68±0.19 µg g^{-1}) while an elevated concentration of total chlorophyll was detected in T12 (33±0.45 µg g^{-1}). The data that a higher quantity of pigments exists in organic+inorganic and manure-treated soil (Fig. 8.1.1a) is in close agreement with the study of Manikandan and Thamizhiniyan (2016). Total soluble sugar (TSS) was highest in T10 (2908.20±7.3 µg g^{-1}) and lowest in T1(1155.93±5.93) while soluble protein content was highest in T12 (3030.81±0.81 µg g^{-1}) (Fig. 8.1.1b). A balanced NPK uptake of plants had a rewarding effect on plant nutrition that triggered photosynthesis for a suitable making of food. The results

of having high protein content in compost-treated plants coincide with the study of Gowda et al. (2008) who detected higher protein in wheat plants treated with vermicompost.

Table 8.1.2 (a-b). Effect of different treatments on growth and yield attributes (mean ±SE of two years)

(a)

Treatments	Plant Height (cm)	No. of Branches plant^{-1}	No. of nodules plant^{-1}	No. of Pods plant^{-1}	Total no of seeds plant^{-1}
T1	28.33±1.10	5.33±0.33	13.33±2.60	7.00±0.71	61.00±5.86
T2	39.74±0.70	11.67±0.33	22.67±2.91	29.00±2.12	237.33±8.84
T3	28.76±1.09	7.67±0.33	15.33±2.33	13.33±3.49	165.67±10.84
T4	28.81±0.67	10.33±0.88	16.00±3.00	17.67±3.49	196.33±4.18
T5	29.65±0.78	7.67±0.67	17.00±1.53	13.33±3.49	159.33±17.33
T6	39.98±0.50	11.33±0.67	28.00±1.00	29.67±2.86	239.00±5.77
T7	35.61±0.93	7.33±0.88	19.00±3.21	13.33±1.47	138.33±6.12
T8	38.19±0.54	8.33±0.88	27.33±2.91	26.33±1.78	206.00±8.33
T9	34.05±1.62	8.33±0.88	21.00±6.08	15.67±2.86	169.00±5.86
T10	33.58±0.72	9.33±0.88	21.67±3.18	19.00±0.71	192.67±8.97
T11	34.96±1.13	9.00±0.00	19.00±0.58	16.67±1.78	173.33±15.19
T12	45.92±0.49	10.67±0.67	22.00±3.21	24.00±2.12	177.33±16.83
LSD	1.25	0.96	4.27	1.38	1.3
p	<0.05	<0.05	0.047	<0.05	<0.05

(b)

Treatment	Root length (cm)	Shoot length (cm)	Pod length (cm)	No. of seeds pod^{-1}	100 seed weight (gram)	Yield (g/plant)
T1	6.97±0.12	20.63±0.82	4.50±0.60	3.00±0.58	3.07±0.36	0.64±0.88
T2	7.53±0.54	30.93±1.82	6.30±0.06	8.00±0.00	6.20±0.37	14.38±0.88
T3	9.70±0.56	20.93±0.79	5.13±0.13	6.67±0.33	4.67±0.08	4.15±0.88
T4	8.13±1.64	17.53±1.28	6.17±0.03	8.00±0.00	5.73±0.15	8.10±0.88
T5	9.07±1.49	19.13±0.81	5.90±0.06	7.33±0.67	5.13±0.29	10.11±0.88
T6	9.57±1.07	29.60±0.68	6.30±0.15	8.00±0.00	6.70±0.12	15.90±0.88
T7	7.40±0.45	29.03±1.47	5.93±0.29	7.00±0.58	5.47±0.43	11.65±0.88
T8	11.80±1.81	27.47±0.62	6.17±0.15	8.33±0.33	6.33±0.27	13.87±0.88
T9	9.10±1.63	27.07±1.56	5.97±0.12	6.67±0.33	5.33±0.27	9.88±0.88
T10	11.23±0.64	20.97±1.52	6.17±0.09	8.00±0.00	6.50±0.07	10.17±0.88
T11	9.60±0.10	27.17±1.27	6.00±0.15	7.33±0.67	5.87±0.04	11.14±0.88
T12	9.30±0.90	35.77±2.02	6.27±0.18	7.67±0.33	6.37±0.29	11.98±0.88
LSD	1.57	1.84	0.31	0.57	0.29	0.29
p	0.25	<0.05	<0.05	<0.05	<0.05	<0.05

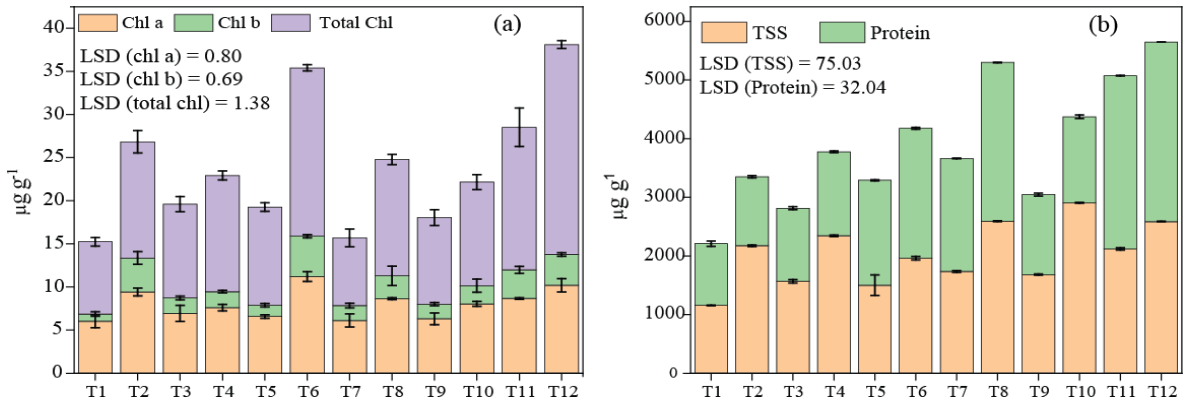

Fig. 8.1.1. Biochemical attributes Chlorophyll a, b and Total chlorophyll, protein and total soluble sugar (TSS).

8.1.3.3. Influence on soil physicochemical properties

Changes in the physicochemical parameter amid treatments are depicted in Fig. 8.1.2a-f. In general, addition of vermicompost raised the pH slightly due to release of alkaline humates from vermicompost (Das et al., 2018) hence, a small increment (average 0.06-fold) was observed in all the amended soil compared to control (Fig. 8.1.2a). After harvesting, soil pH was little altered among the treatments except in T9 which remained same ($LSD_{Treatment}$=0.16; p for time=0.012). Electrical conductivity (EC) was not much differed among treatments between pre-plantation and post-harvesting time ($LSD_{Treatment}$=0.07) (Fig. 8.1.2b). The present study evidenced an average of 18.09% increase in SOC content of soil after the addition of RM-vermicompost compared to control however there was no significant difference exists among the treatments. The post-harvest SOC content was as follows T12> T9> T6> =T7> T10>=T11> T8>T5 >T4 >T3> T2> T1 ($LSD_{Treatment}$=0.05; p for time=0.008). The findings are in accord with Antil and Singh (2007) and Dong et al. (2021). The mineralizable N content of amended soil increased considerably compared to control owing to microbial decomposition of the organic manure which in turn releases N thus increasing the plant available N in soil, supported by earlier studies (Laos et al., 2000; Abbasi et al., 2007). Mineralizable N in post-harvest soil was significantly high in treated soil compared to control nevertheless among the treatments it was insignificant ($LSD_{Treatment}$= 0.912; $p<0.05$; p for treatment × time=0.009). The N content was highest in T2 followed by T10 and T12 (Fig. 8.1.2f). Potassium (K) is another vital macronutrient for plant growth. Average 21.21% K content was elevated after the addition of NPK and VC, in which T2 gained maximum (Fig. 8.1.2d). The difference between pre-plantation and post-harvesting K content between control and treatments was highly significant ($p<0.0001$, $LSD_{Treatment}$=2.07; p for treatment × time=0.0002). At the end of cropping season

K was highest in T12 (277.61±2.83) and lowest in control soil (177.65±1.08). Potassium solubilizing bacteria (KSB) might be the major drivers of K availability in VC-treated soil. Our findings are supported by Bhattacharyya et al. (2007) and Warman and Termeer (2005). During vermicast processing earthworm converts insoluble Ca, Al bound P into soluble one. Consequently, application of VC in the soil helped to increase the availability of P. Incorporation of VC did not work immediately nevertheless a gradual increment resulted in an adequate amount of P at the post-harvesting time ($LSD_{Treatment}$=2.45). The change was significant between control and treatments ($p<0.0001$), as well as treatments and time. A significant build-up in P availability was evidenced in T2 while lowest in control soil (Fig. 8.1.2e). Overall advancement under VC-treated soil may be accredited from the steady release of NPK due to augmented microbial activity and the secondary metabolic enzyme in the vermicompost, that coincide with the study by Goswami et al. (2017). The higher nutrient-benefit ratio demonstrated the beneficiary role of vermicompost in enhancing soil fertility (Sahariah et al., 2015). Almost all the organically amended treatments exhibited a higher ratio except organic C. The benefit ratio was in the order of P> K=N> OC (Fig. 3e). Moreover, the incorporation of vermicompost increased soil fertility either by solubilizing the essential nutrients or liberating them from organic compounds upon decomposition.

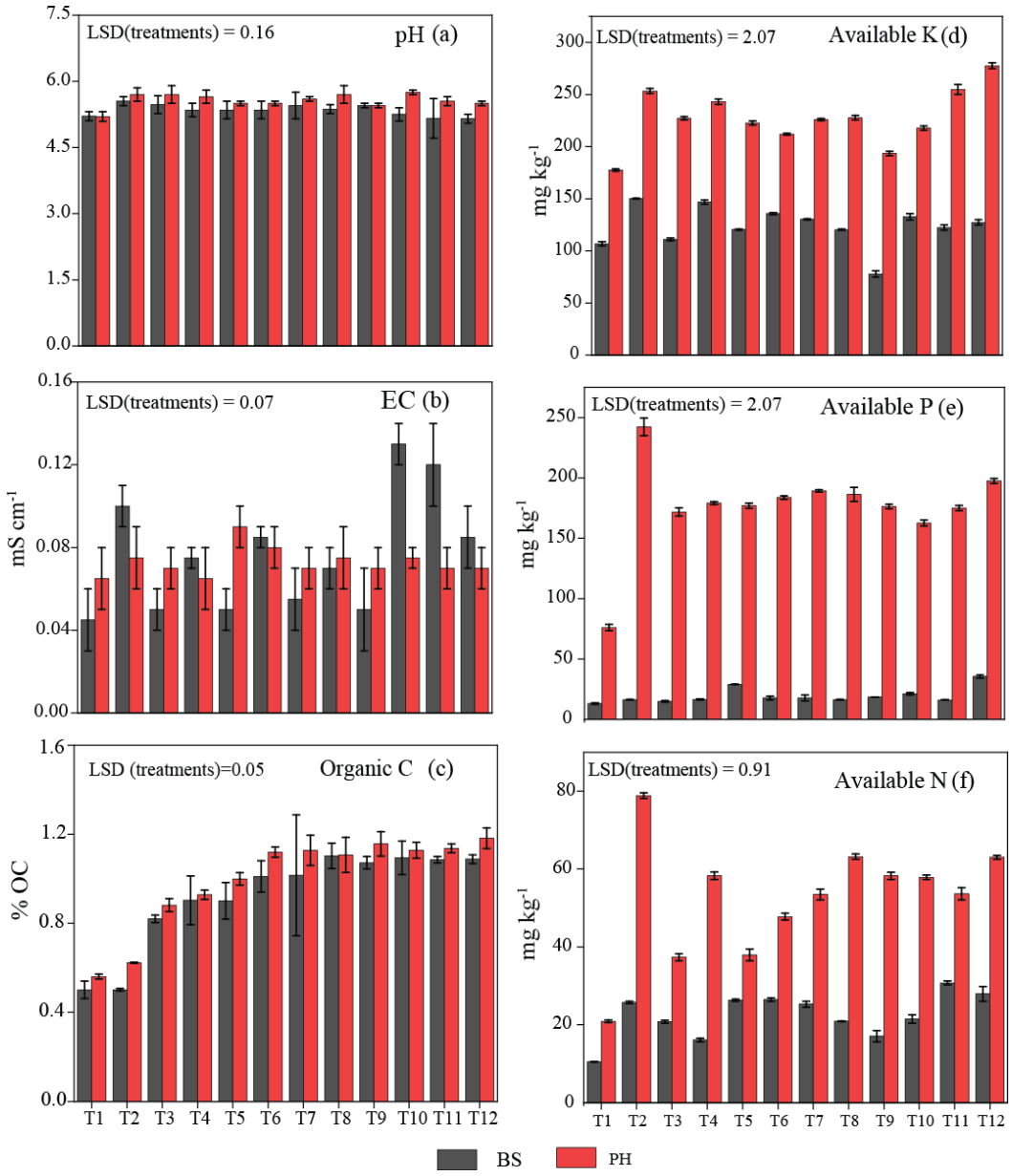

Fig. 8.1.2. Changes in the soil physicochemical properties and nutritional status before-transplantation (seedlings) and post-harvest soil.

8.1.3.4. Influence on temporal variation of soil microbial attributes

Considering the fact of securing soil quality, maintenance of OC from the microbial origin is highly important for sustenance. Addition of VC immediately augmented the microbial biomass (average 39%) compared to the control soil which further slowed down up to maturation time of the plant and thereafter increased at the end of cropping season (Fig. 8.1.3a). 100% NPK and 50%CD+50%NPK treated soil showed a maximum increase ($p<0.0001$). Periodically, the declining trend of microbial biomass content in all the treatments

might result from plant-microbe interaction (Kuzyakov & Xu, 2013; Bhattacharyya et al., 2003). The initial increase in microbial activity helps plant growth promotion by providing nutrition to the plant while the contrasting phenomena of increased plant growth and decreased microbial biomass generated with time might result from the competition for nutrients between plants and microbes (Kuzyakov & Xu, 2013; Bhattacharyya et al., 2003). An increase in biomass C after cropping irrespective of treatments may be the result of plant residues left in the soil, that restored microbial activity ($LSD_{Treatment}$=1.49, LSD_{time}=0.86). On a contrary note, dehydrogenase activity went higher up to flowering time (35 days) after the addition of the amendments and surprisingly got a reduction at maturation time (60 days) followed by an increase in post-harvesting soil (Fig. 8.1.3b). Although the initial increase was not significant among treatments nonetheless found significant ($p<0.05$) with control. The increase was an average of 37.62% (LSD_{time}= 0.36; $LSD_{Treatment}$=0.63, p for treatment × time =0.011). The improved microbial activity may be due to plant-microbe mutualism, where plant root exudates attracted the organism to colonize. The experimental results are supported by the findings of Pradhan and Sahoo (2012). Soil respiration (glucose-induced) is a direct measurement of active microbial population. It was increased up to flowering time (35 days) across the treatments followed by a substantial decrease during maturation time (at 60 days). The post-harvesting soil again produced good respiration owing to greater microbial activity (Fig. 8.1.3b). Addition of VC augmented cellular activity by more than 50% compared to control soil. Notably, soil amended with 50%VC+50%NPK and 50%CD+50%NPK exhibited a significant increase ($LSD_{Treatment}$=2.10, LSD_{time}=1.21, p for treatment x time=0.009). Likewise, fluorescein diacetate hydrolysing activity (FDA) elevated in the amended soil (average 48%; $p<0.0001$). Exceptionally FDA did not show much decrease during maturation time across the treatments (Fig. 8.1.4d), however, post-harvest activity was more impressive compared to other attributes ($LSD_{Treatment}$=0.89; LSD_{time}=0.52; p for treatment × time =0.0008). Such contrasting behaviour of FDA could be associated with active enzymes within dead biomass, related cell fragments along with active cells (Bhattacharyya et al., 2003). Results of the overall microbial attributes promptly indicated that composite treatments (50% VC+ 50% NPK) were indeed a good supplementation for both soil and plant nutrition.

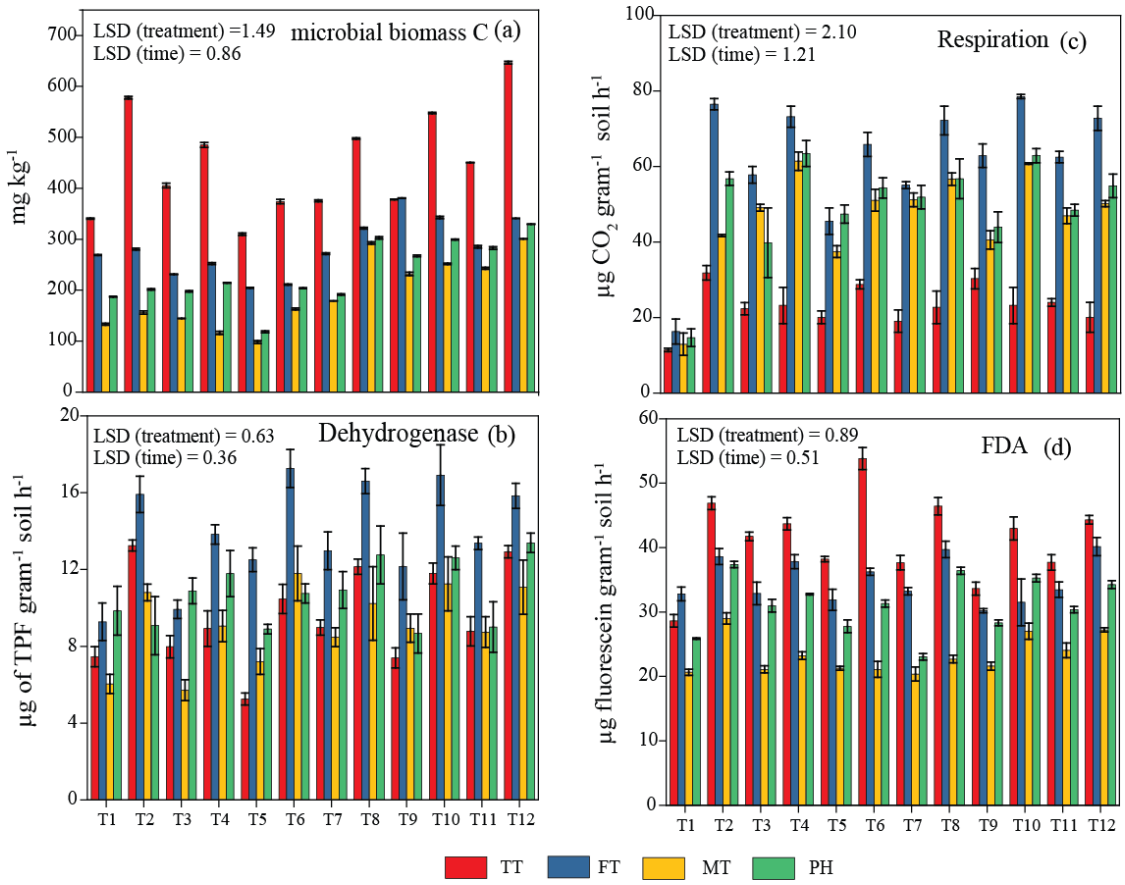

Fig. 8.1.3. Periodical changes in soil microbial properties during different stages of growth and development. TT- transplantation time; FT- flowering time; MT- maturation time, PH-post harvest.

8.1.3.5. Plant uptake of nutrients

Nutrient uptake (P and K) by the plant in root, shoot, and grain was assessed and depicted in Fig. 8.1.4a-b. The findings showed that composite treatment (VC+NPK) causes more nutrient uptake than soil treated with VC alone, however, the comparison was significant with control ($P<0.0001$). The K uptake was in the order of grain>shoot >root while P was highest in shoot > root>grain. Across the treatments, grain uptake of K was highest at T6 ($LSD_{grain}=7.32$, $p=0.0006$). On a contrary note, P uptake was highest in shoot followed by root and grain. The highest transfer took place in shoot of T12 plants that subsequently got the maximum amount of P in their grain compared to others. Gross P uptake by the plant under various treatments was in the order of T11> T12> T8> T2> T6> T7> T10> T5> T4> T9> T3> T1 ($LSD_{root}=17.99$, $p=0.0003$, $LSD_{shoot}=19.78$, $p=0.0012$; $LSD_{grain}=20.05$, $p=0.0061$). Availability of P was greatly induced in VC-aided soil which was not only the result of

insoluble P transformation but rather an augmentation of P-solubilizing microbes and their enzymatic activity. The findings concur with Mondal et al. (2020).

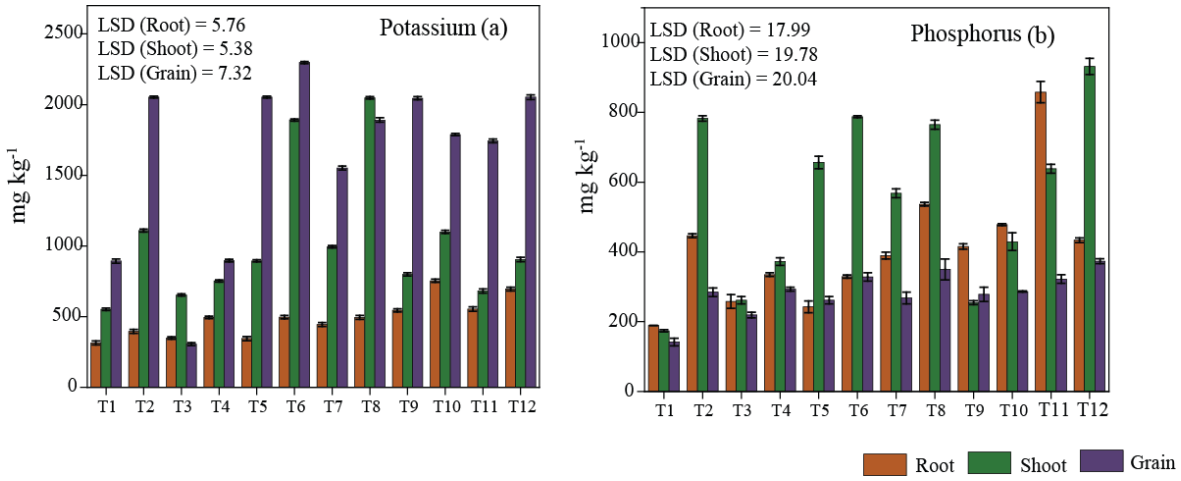

Fig. 8.1.4. Nutrient (K and P) uptake by plants after harvesting.

8.1.3.6. Metal distribution

Metal exists in the soil in six different fractions i.e., water-soluble, exchangeable, carbonate bound, Fe-oxide bound, organic bound, and residual fraction. The result (Fig. S1) showed that metals across VC-treated soil were most predominant in the organic bound phase and residual phase except in control soil. This might be due to the presence of humic content in VC which retained the metal through an organometallic complex (Hussain et al., 2016). Two metals Cd and Cu is widely distributed in carbonate phase while Pb was in Fe- oxide and residual phase. Considering the water-soluble and exchangeable fraction which was much higher in control soil for all the metal compared to treatments.

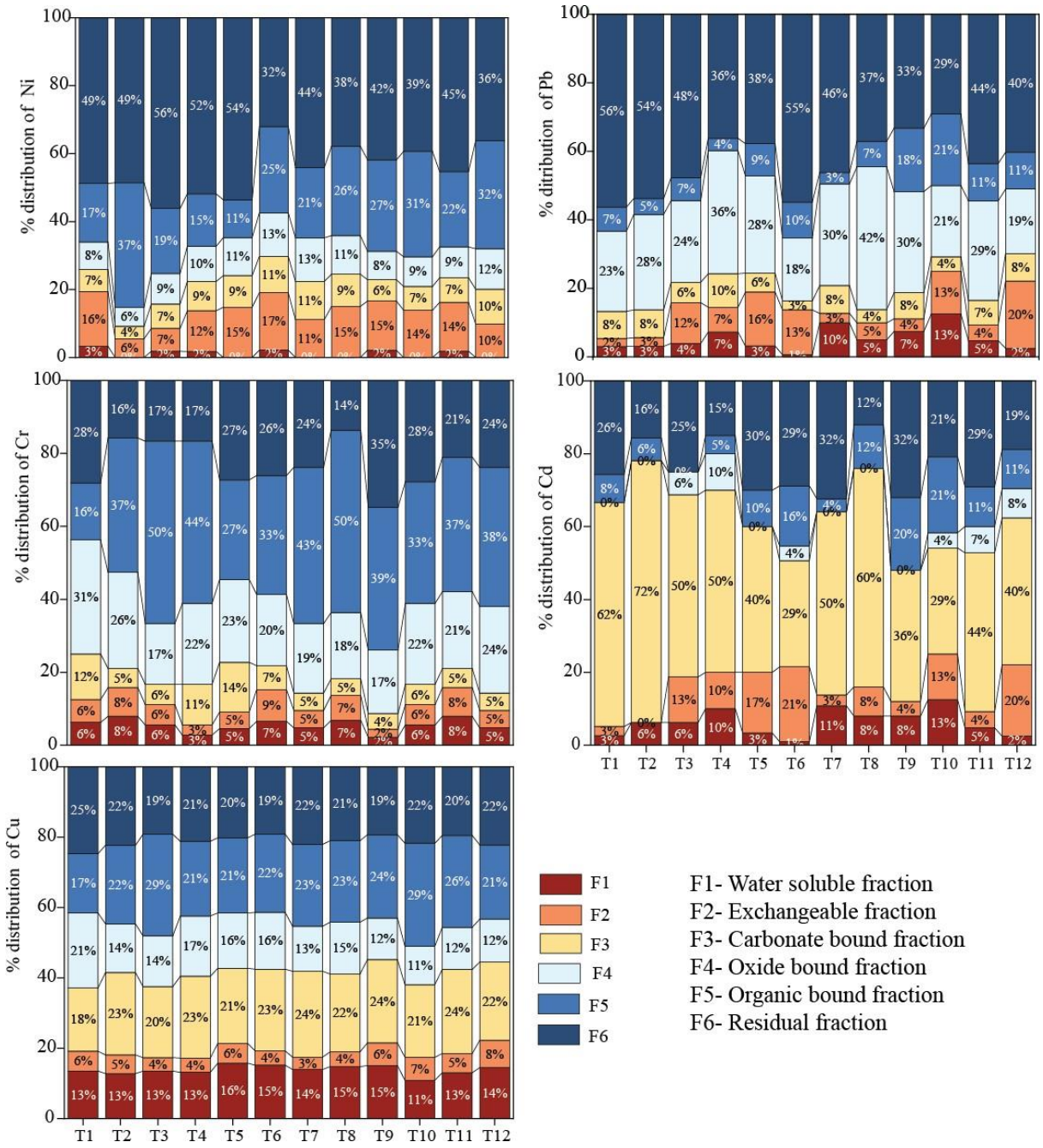

Fig. 8.1.5. Different fractional distributions of metal (Cu, Cr, Ni, Cd, Pb) across treatments after VC treatment.

8.1.3.7. Phytoavailability and bioaccumulation of metal

In the present study, we assessed the availability of metal in roots and their possible translocation in shoot and grain (Fig. 8.1.6.a-c). The uptake of five metals (Cr, Cu, Ni, Cd, and Pb) irrespective of plant parts (root, shoot, grain) was significantly lower compared to the control soil plants. Ni showed maximum accumulation in root followed by shoot and grain,

while Cu showed a maximum grain uptake followed by root and shoot except for T1 and T4. Cr got its highest accumulation in root in almost all the treatments (LSD=0.70) followed by shoot (LSD=0.42) and grain (LSD=0.06). Pb was below detection limit in root, shoot, and grain whereas Cd was poorly accumulated (0.1-0.5 mg/kg) in the root of the plant. However, the studied metal concentration in the edible part was within safe limits (WHO, 2007). Concentration of metals (Cu, Cr, Ni) in grain was significantly low compared to the control ($p<0.0001$). Similar trend was observed in case of root ($pCr<0.0001$, $F=63.80$; $pNi=0.0016$, $F=6.45$; $pCu<0.0001$, $F=19.57$) and shoot ($pCr<0.0001$, $F=61.56$; $pNi=0.0016$, $F=36.18$; $pCu=0.0010$, $F=7.95$). The availability of metal was significantly lowered in treatments under the influence of VC. Such reduction in metal migration from soil to plants might be due to the presence of increased organic matter which likely forms an organometallic complex thus lowering transfer (Mondal et al., 2020). However, a significant positive correlation at 5% and 1% levels, between water soluble, exchangeable phase and root, shoot, grain metal indicated that these two metal fractions were responsible for plant uptake, however, their concentration in the edible part within the safe limit is harmless. Root uptake was highly significant with Cr, Ni, and Cu (r-Cr=+0.65; r-Ni=+0.69; r-Cu= +0.91). For shoot it was as follows r-Cr= +0.66; r-Ni=+0.88; r-Cu= +0.90, while grain accumulation was highly significant with Cu followed by Ni and Cr (r-Cu= +0.93; r-Ni= +0.75, r-Cr= +0.59).

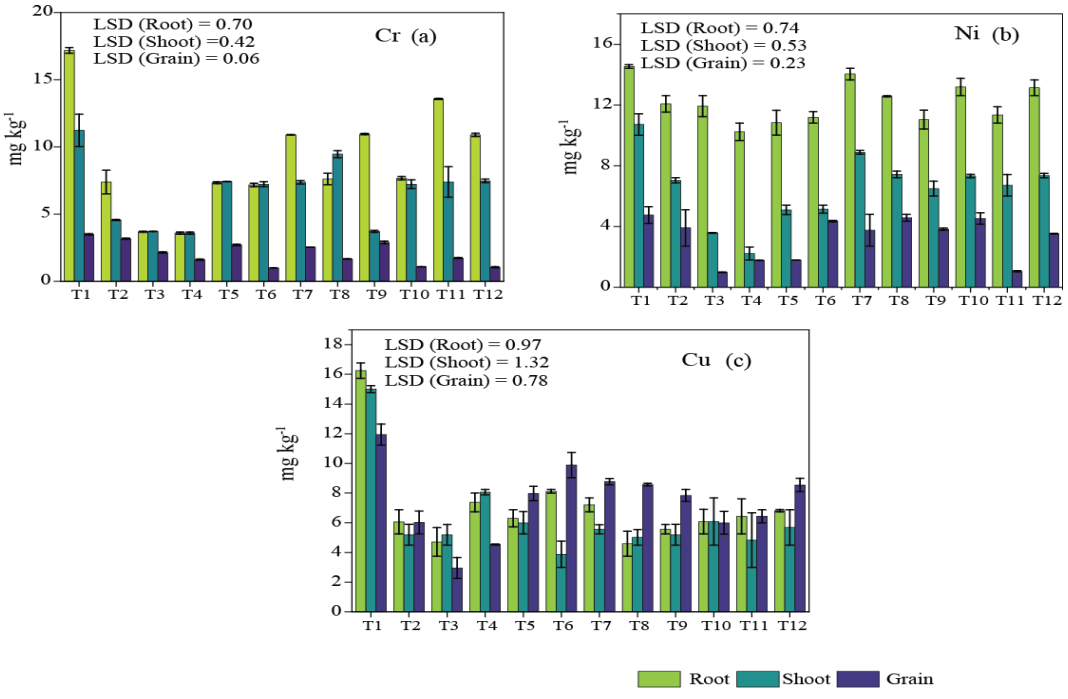

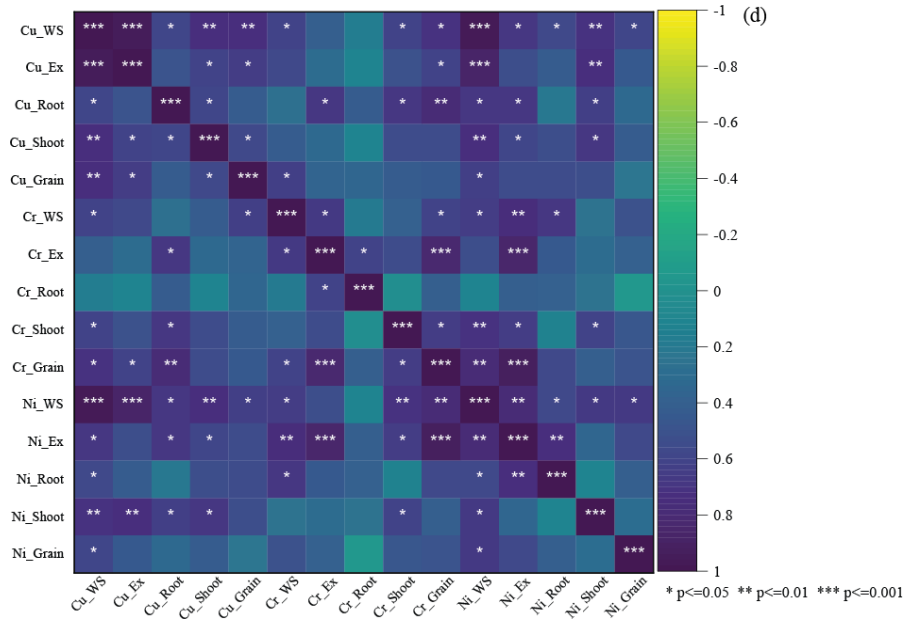

Fig. 8.1.6. Metal uptake in different parts of the plant (a-c); Correlation coefficient between plant uptake metal and water (WS) and exchangeable (Ex) fractions of metal (d).

8.1.3.8. Prediction of toxic metals in grain

Solubility-free ion activity model (FIAM) is a mechanistic approach through which grain metal content was predicted without actually measuring their solubility (Golui et al., 2014; Mandal et al., 2019). The values coefficient viz. C, β1, and β2 of FIAM for three metal Cr, Cu, and Ni was calculated and tabulated in Table 8.1.3. Results implied that approximate 88% variability of Cr, 95% variability of Cu, and 80% variability of Ni content was explainable by the model based upon pH, organic carbon, and extractable (labile pool) metal. These three measurements were used as input assuming that the organic matter adsorbs the extractable metal. From the result, it was well evident that pH and organic carbon had a negative effect on Cr and Ni solubility (β1 and β2 value positive) whereas organic carbon had a positive effect (β1 negative value) in Cu solubility. The negative effect explains that an increase in each organic carbon or pH will diminish the metal content (Cr, Ni) in mung bean grain, while, the negative β1 value demonstrated the positive impact of organic carbon in Cu uptake in grain. The uptake can be justified as Cu is a micronutrient required for many physiological processes. In addition, they affect membrane permeability. Since, humic substances contain both hydrophobic and hydrophilic sites they might have a strong interaction with phospholipid structure of cell membrane thereby reacting as a carrier of nutrients through them (David et al.,

1994; Govindasmy and Chandrasekaran, 1992). The observation of our study is well associated with the findings of Golui et al. (2014) who found a similar trend of Cu uptake in spinach.

Table 8.1.3. Prediction of metal (Cr, Ni, Cu) content in green-gram grains by solubility-free ion activity model.

	Model Parameters			
Metal	**C**	**β1**	**β2**	**R^2**
Cr	-2.25	0.29	0.18	0.88
Ni	-2.53	0.33	0.11	0.83
Cu	-1.79	-0.39	1.49	0.96

*Values of R^2 are significant at 5% probability level.

8.1.3.9. Bioconcentration, translocation, and bioaccumulation factors

Bioconcentration factor, translocation factor, and bioaccumulation factor are some calculative measures, used to ensure the metal distribution pattern among plant parts under different treatments (Fig. 8.1.7). The bioconcentration factor (BCF) majorly deals with root metal uptake, where the trend was Ni> Cr> Cu. In general, high concentrations of Ni trigger an easy movement to the xylem and phloem for better translocation, however, the minimal concentration of plant available (approximately 2-7 mg/kg) metal across the treatments may retarded its migration that can be further validated by an inconsequential translocation rate (TF<1). Root accumulation of Cr depends on its oxidation state. Commonly, Cr (VI) is soluble and can easily absorb by roots nevertheless a lower translocation (TF<1) was a benefit for the tested crop. A high translocation factor (TF) i.e., >1 concludes greater mobility from root to aerial parts. TF varies from 0.9-2.09 for Cu, 0.3-0.8 for Cr, and 0.2-0.7 for Ni which indicated Cu had higher translocation rate than Ni and Cr across the treatments. Cu use symplastic pathway for its translocation additionally it forms a metal complex with nicotianamine that get translocated toward developing organ and matured seeds (Islam et al., 2020; Pasricha et al., 2021). Metal mobilization turns crucial when it comes to bioaccumulation which was found to be lower for Cr (0.17-0.8) and Ni (0.2-1.2) except Cu (0.5-2.3) for the tested crop.

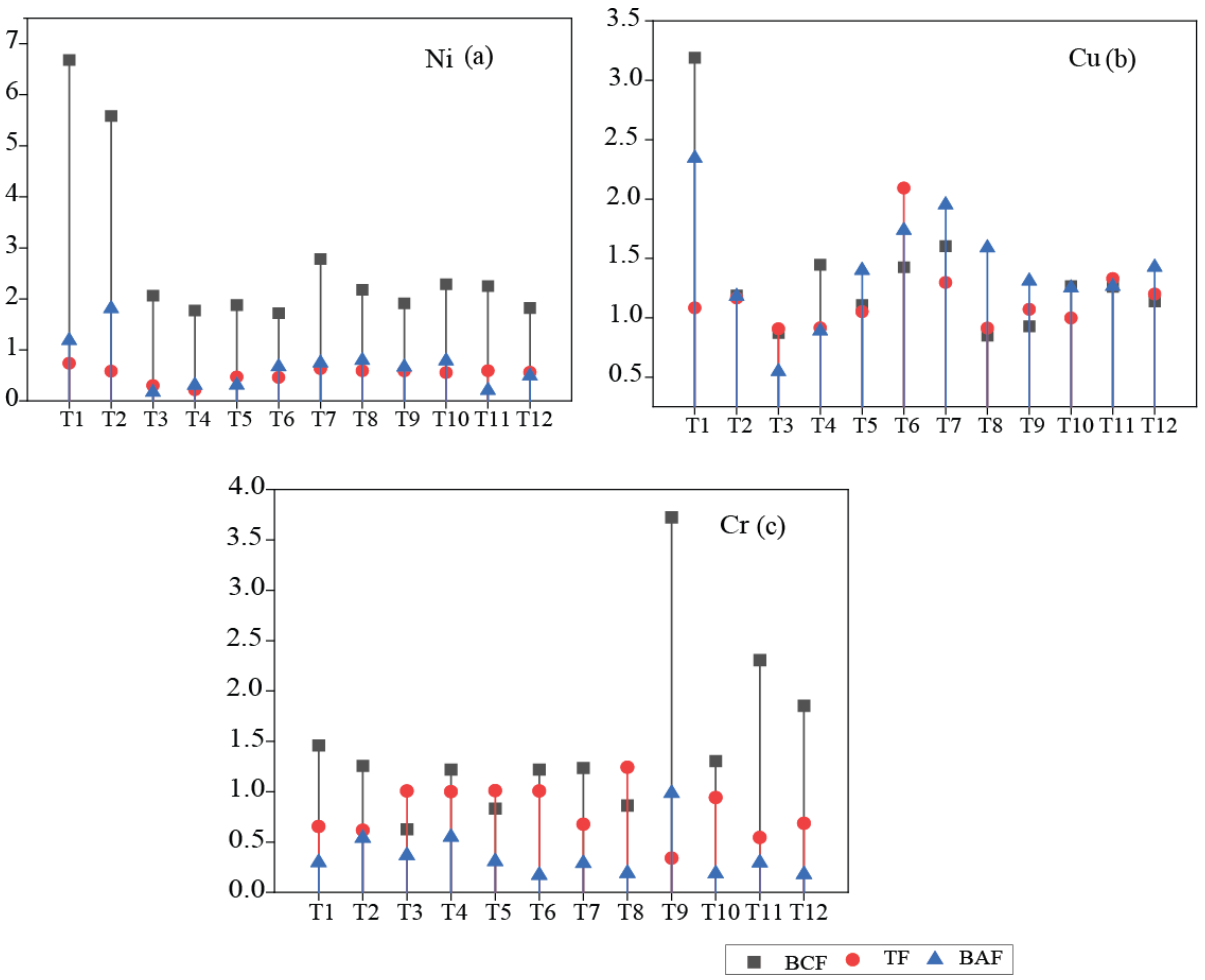

Fig. 8.1.7. BCF- bioconcentration factor; TF- translocation factor, BAF- bioaccumulation factor of Ni, Cu, and Cr.

8.1.3.10. Dietary exposure

The estimated daily risk (EDI) of the studied metal was found to be remarkedly lower across the treatments including control soil for all three metals (Table 8.1.4a). EDI for Cu ranged between 0.002-0.0008, Ni varied between 0.001-0.0003 and Cr ranged between 0.001-0.0003, which is significantly lower than the suggested values. Health risks associated with metal intake through grain feeding are presented in the corresponding HQ (Table S5). Results demonstrated that the HQ values were far less than 1 for all the metals amid the treatments, out of which Cr showed lowest HQ indicating that intake of VC and VC+NPK-fertilizer-treated mung bean will be safe for human consumption. Yet a brief comparison among treatments exhibited control soil had a higher HQ compared to the amended one. Our findings concur with Mandal et al. (2019), who found a reduced HQ for As in organically amended soil. On other

hand, the calculated CR of Cr ranged between 0.00003 to 3.8E-05 while Ni was from 0.0001 to 9.6E-05 which comes within limits (Table 8.1.4b). Thus, from a health perspective the cultivated crop receiving organic or composite (50%VC+50%NPK) treatments, was found to be hazard free for consumption.

Table 8.1.4 (a) Estimated daily intake of heavy metals (Cr, Ni, Cu) on consumption of *Vigna radiata L*. (b) Non-carcinogenic and Carcinogenic risk on consumption of *Vigna radiata L*.

(a)

	EDI		
Treatments	**Cr**	**Ni**	**Cu**
T1	0.001032	0.001591	0.003582
T2	0.000936	0.001531	0.001805
T3	0.00066	0.000287	0.000886
T4	0.00047	0.000534	0.001359
T5	0.00083	0.000537	0.002391
T6	0.000296	0.001321	0.002966
T7	0.000763	0.000813	0.002632
T8	0.000495	0.001306	0.002572
T9	0.000896	0.001126	0.002353
T10	0.000329	0.001246	0.001799
T11	0.000507	0.0003	0.001931
T12	0.000304	0.001066	0.002563

- MTDI Maximum tolerable daily intake Cu 30*, Ni 0.30**, Cr 0.20***

*(JECFA 2003)

**(WHO 1996)

***(RDA 1989

(b)

Treatment	HQ			CR	
	Cr	Ni	Cu	Cr	Ni
T1	0.000803	0.079541	0.071647	3.89E-05	0.000101
T2	0.000728	0.076541	0.036097	3.53E-05	9.69E-05
T3	0.000513	0.014332	0.017713	2.49E-05	1.82E-05
T4	0.000365	0.026714	0.027184	1.77E-05	3.38E-05
T5	0.000645	0.026864	0.047822	3.13E-05	3.4E-05
T6	0.00023	0.066034	0.059322	1.12E-05	8.36E-05
T7	0.000593	0.04067	0.052635	2.88E-05	5.15E-05
T8	0.000385	0.065284	0.051441	1.87E-05	8.27E-05
T9	0.000697	0.056277	0.047069	3.38E-05	7.13E-05
T10	0.000256	0.062291	0.035977	1.24E-05	7.89E-05
T11	0.000394	0.015007	0.038618	1.91E-05	1.9E-05
T12	0.000236	0.053277	0.051266	1.14E-05	6.75E-05

8.1.4. Conclusion

Application of two different dosages (100% organic; 50%NPK+ 50% organics) for two consecutive years provided a twining benefit to plant growth and soil fertility. Nutrient solubilization (N, P, K) and soil microbial activity was enhanced while migration of toxic metals got restricted determined by FIAM. Grain metal uptake within permissible limits ensures safe consumption. Composite treatments provided an improved pulse yield. Inclusively, vermitechnology could be a beneficial tool for turning poorly fertile soil into productive one, and recycled red mud could be an alternative nutritional source for plants. To ensure the suitability of RM-vermicompost, it was tested under field conditions with staple food like rice for its long-term applicability.

8.2. Performance of vermicomposted RM on rice (*Oryza sativa*) through field experiment

8.2.1. Introduction

More than half of the world's population relies on rice as a staple diet. India is one of the leading producers of this crucial cereal crop in the world. The rise of the population largely increases the demand for it. This has led to an increased usage of inorganic fertilizers and chemical supplements for rapid growth and high productivity of crops. Besides the quality of soil, precisely the red soil/lateritic zone of eastern India is extremely poor in terms of nutritional value and microbial activity. This large group of soil is generally gravelly and coarse-textured, have high acidity, deficient in soil organic matter (humus) and other macro and micronutrients viz. N, P, K, Ca, Zn, B etc. Cultivation practices mostly depend on rainwater in this semiarid region and nutrient loss is another limitation of agriculture practices. These contrasting issues led farmers to use more chemical fertilizers for greater productivity of crops (Ghosh, 2021). Extensive use of such inorganic fertilizer/supplements instantly boosts plant health by restoring the depleted nutrients however such high inputs directed to an increased accumulation in the grain which often exceeds the safety levels creating an alarming impact on the food chain (Bhattacharyya et al., 2003). This necessitates the desirability of organic supplements as they are rich in microbial activity, carbon-nitrogen content, humic substance etc. Hence, agronomic practices that lift crop productivity as well as conserve the organic matter content in soil are highly appreciated. Such practices may take care of plants' health as well as protects the soil's health.

Traditional composting methods focus on soil sustainability, replacing artificial fertilisers, and recycling different solid waste dumps in a way that is environmentally friendly. While vermicomposting technique that uses earthworms as its bio-engine for transforming waste materials into sanitized nutrient enriched products (Bhattacharya and Kim, 2016). Earthworm are regarded as an efficient waste to wealth converter. They not only enhance the microbial community structure, alongside, improve the organic content and make the substrate nutrient rich (Singh et al., 2008; Bhattacharya et al., 2012). Consequently, it is still a viable option for farmers seeking to practise sustainable agriculture.

In search of that efficacy of vermiconverted waste conducted a field study. In previous chapter, we presented and discussed a successful vermiconversion of red mud. Previously a pot experiment was conducted on green gram (*Vigna radiata L.*) in summer of consecutive two years. After this successful pot application, in present work, we applied the vermicomposted

RM on rice thorough field application. Since rice is a primary food of south east Asia including Indian subcontinent. So, it occupies a large part in Indian cropping system. Considering this perspective, we applied the vermicomposted red mud on large scale basis, as an alternative to traditional fertilizer. Alongside, we assessed the effect of combination of vermicomposted RM and chemical fertilizer on field condition to provide an integrated nutrient management approach to the farmers.

The main goals of the current study were to (a) assess the viability of using vermicomposted RMs as soil amendments and plant growth stimulants, and (b) determine the effects of vermicomposted RMs on environmental quality with regard to soil metal pollution. The test crop for these large-scale field tests was monsoon rice (*Oryza sativa*), which was cultivated, in the field of agricultural farm of Indian Statistical Institute, Giridih, Jharkhand.

8.2.2. Material and Methods

8.2.2.1. Experimental site

To verify the efficacy of vermicomposted RMs (RM-VC), a field study on monsoonal rice was carried out in at the Agricultural Farm of the Indian Statistical Institute in Giridih, Jharkhand (24.1913° N, 86.2996° E). Climatic condition of experimental site is given below Table 8.2.1.

Table 8.2.1. Climatic condition

Time Period	July-November
Temperature (Max-Min)	33^0C-20^0C
Annual rainfall	313mm-84mm
Relative humidity	82%-57%

The soil at the experimental location in Giridih, Jharkhand, was red loamy soil which comes under afisol type. Before transplantation, composite soil samples were taken from experimental site and tested for soil organic carbon, pH, EC, and accessible NPK.

8.2.2.2. Experimental design

Twelve different fertilizer treatments were used in the experiment. For this experiment, we used a randomised block design with three replicates and a $2m^2$ plot. In order to ensure that all the treatments and rice plants were grown throughout the rainy season, a total of 36 plots

(three replicates per treatment) were created for Giridih fields. Figure 8.2.1 shows the experiment's scheme of organisation.

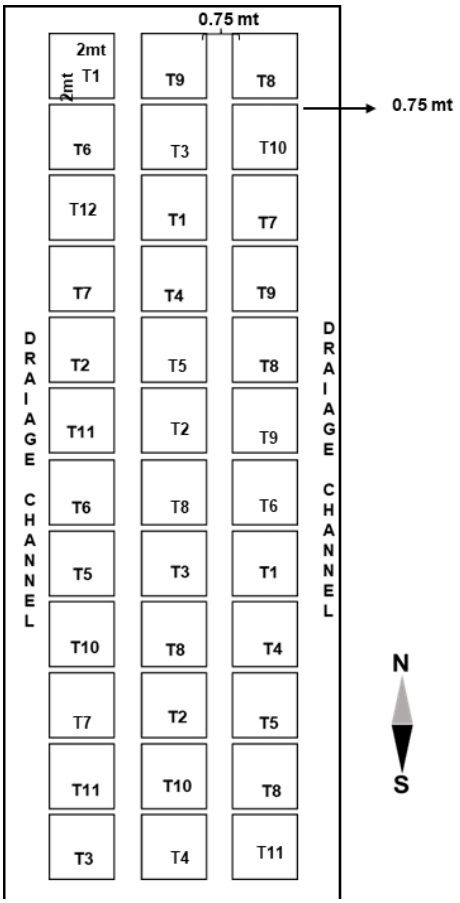

Fig. 8.2.1. Layout of the experimental plots.

8.2.2.3. Rice variety selection, dose preparation, and application in field

All the organic (Vermiconverted mixture of RM and Cow dung manure) were applied to the field 7 days before transplantation and fertilizer was at the time of transplanting (rice). Sita var. was used for the experiment with recommended dose (Fertilizer**)** - 60:30:30 Kg N: P_2O_5:K_2O / ha. Two recommended doses were selected 20t/ha and 10t/ha + NPK (1/2 dose). The modified doses are presented in Table 8.2.2.

Table 8.2.2. Detail of the treatment combinations applied during the rice cultivation.

Plot name	Treatment combinations
T1	Control (No amendment)
T2	Fertilizer (NPK)100%
T3	Vermicompost (1:1) 100%
T4	Vermicompost (1:1) 50% + Fertilizer (NPK) 50%
T5	Vermicompost (1:2) 100%
T6	Vermicompost (1:2) 50%+ Fertilizer (NPK) 50%
T7	Vermicompost (1:3) 100%
T8	Vermicompost (1:3) 50% + Fertilizer (NPK) 50%
T9	Vermi compost (1:4) 100%
T10	Vermicompost (1:4) 50% + Fertilizer (NPK) 50%
T11	Cow dung 100%
T12	Cow dung 50% +Fertilizer (NPK) 50%

During wet season cultivation, soil received incomplete applications of N, and complete application of P_2O_5, K_2O. During tillering and panicle initiation stages received equal distributions of the remaining N. All of the treatments suggested by the Agriculture and Ecological Division, ISI, Giridih India, were applied consistently using agronomic management practises including irrigation, pesticide application, etc. For every treatment during cultivation, other control managements including weeding, cleaning, and crop protection were also consistently maintained (Table 8.2.3.).

Table 8.2.3. Agronomic practice for wet season cultivation of rice.

Agronomic practices for the wet season cultivation (Monsoon Rice) : 2022	
Nursery Preparation	10.06.22
Sowing of the seeds in nursery	17.06.22
Land preparation 3-4 times ploughing followed by harrowing and laddering	20.06.22
Plot demarcation	28.06.22
Application of organic manures	05.07.22
Allocation of different treatments in demarcated plot	12.07.22
Transplanting and basal application of 1/2 N + full P_2O_5 + full K_2O	12.07.22
Application of 1/2 N at tillering	13.08.22
Application of 1/2 N at panicle initiation stage	17.09.22
Irrigation supplementary*	As per requirement
Harvesting	16.11.22

8.2.2.4. Collection of soil sample from experimental field before transplantation and after harvesting

Before transplanting, we randomly selected 36 soil samples from various locations in a rice field by cutting a slice that covered a depth of 0 to 15 cm. To create composite samples that accurately reflect the characteristics of the soils on each plot, these soil samples were correctly blended. Following harvest, we took soil samples from several locations on each plot. Following collection, soil samples were air dried at room temperature, ground with a mortar and pestle, sieved with a mesh size of 2mm and 0.2mm, and then stored in plastic containers for further examination.

8.2.2.5. Physico-chemical and microbial analysis of soil

Physicochemical attributes viz., pH, EC, TOC, and available NPK were analysed before and after cultivation, while microbial parameter viz, microbial biomass carbon, and soil respiration were carried out temporally viz, 0 days, 30 days, 60 days, and 90 days.

Soil samples were analysed through following protocols –

A. pH- Description detailed in chapter 4, section 4.2.2.
B. EC- Description detailed in chapter 4, section 4.2.2.
C. TOC- Description detailed in chapter 4, section 4.2.2.
D. Available N- Description detailed in chapter 4, section 4.2.2.
E. Available P- Description detailed in chapter 4, section 4.2.2.

F. Available K- Description detailed in chapter 4, section 4.2.2.

G. Plant metal uptake- Described in the chapter 8, section 8.1.2.3.

H. MBC- Description detailed in chapter 5; section 5.2.5

I. Soil respiration-Description detailed in chapter 7, section 7.2.4

8.2.2.6. Rice crop growth and yield assessment

A. Tiller number- We recorded tiller number manually at tillering and harvesting stages.

B. Nutrient uptake analysis- Plants uptake nutrients in their leaves, stems and roots. We analysed uptake of phosphorus (P) and potassium (K) by using following standard procedure.

C. Biochemical attributes viz., total soluble sugar (TSS) and protein was estimated.

D. Yield- Initially, the crop yield for each plot was considering the net plot area of $2m^2$ in Kg and subsequently converted into ton ha^{-1} as shown below:

If yield is x kg in a plot for treatment T, then,

The yield for average yield of T from three replicates in kg ha^{-1} is

$$T = \frac{(\sum_{i=1}^{3} Xi)\ X\ 10000}{Plot\ size\ X\ 3}$$

Where, Xi= yield in i^{th} replicate

Then converted to ton ha^{-1} as below:

Hence yield for specific treatment in ton ha^{-1} is; **Yield= T in kg X 1000**

8.2.2.7. Statistical analysis

We followed one and two-way ANOVA with the Least Significant Difference (LSD) test to analyse the soil and plant sample with the help of SPSS25 software.

8.2.3. Result and Discussion

8.2.3.1. The effect of RM vermicompost on soil fertility

In India, *Eisenia fetida* is extensively used for waste-based vermicomposting, where it is used to convert waste into a valuable nutrient-rich product. The vermicompost created in vermicompost unit of ISI, Giridih, was used as a source of nutrients for monsoon rice farming. The final outcome of this experiment was appreciable. It not only provided a good yield (4.92±1.65 t/ha), but also provided nutrients and nourishment to the soil.

8.2.3.2. Impact on physico-chemical attributes of the soil

Prior to and following cultivation, the soil fertility level was recorded (Table. 8.2.4). The soil was typically lateritic, acidic, and poor in organic carbon (SOC) and NPK levels. A slight rise (0.08-0.14-fold) in pH among the RM-VC treated soil was likely due to application of RM-VC that had a neutral pH. The humic content of RM-VC is frequently combined with intrinsic Al^{3+} and Fe^{3+} of soil to raise the pH (Sanyal, 1991). Similarly, a sharp increase was evinced in electrical conductivity (1.3-3.6-fold increase) of RM-VC applied soil compared to control soil possibly due to the mineral richness of vermicompost that induced such elevation. Regardless of treatments, there was a little increment in organic carbon content (0.05-0.33-fold increase) although insignificant, and the highest increase was in T6 (RM-$VC_{1:2}$ 50%+ NPK 50%). Vermicomposts are rich in humic content that could have led to the soil SOC status thereupon improved the net SOC of the potting soil (Mondal et al., 2020). The soil was inherently low in plant-available N (mineralizable N), nevertheless, application of RM-VC in combination with chemical fertilizer (NPK) improved the N-content (0.03-0.2-fold-increase) and was in the order T6> T10> T9> T8> T12> T5> T4> T11> T2> T3> T1 (LSD=3.08). The result showed a more prolific N-elevation in treatments with 50% chemical fertilizer substituted with RM-VC. The remarkable increment of P content was evinced under all the treatments (0.3-1.6-fold-increase) with most pronounced in T6 (118±1.50; RM-$VC_{1:2}$50%+50%NPK) and T12 (100.73±2.93; RM-$VC_{1:3}$50%+50%NPK). Organic compounds produced during vermicomposting are spontaneously introduced to the soil through amendments, limiting the P adsorption to the positively charged edges of soil particles by substituting organic anions (Brady and Weil, 2002). Additionally, P-solubilizing bacteria introduced upon RM-VC allocation expedite P mineralization thus increasing soil P content. Elevation in K level (1.6-3.7-fold-increase) under vermistabilized-RM treated soil alone or in combination with NPK ascribed to the steady release of nutrients coupled with augmented activity of microbes and their enzymes. A concurrent no-input treatment (T1) was run which also showed a marginal improvement at post-harvest stage, however, the progress was lower compared to RM-VC and FYM-treated soil in all aspects.

Table 8.2.4. Soil fertility before and after sesame cultivation under various treatments (mean ± SE).

Treatments	pH	EC	TOC (%)	Mineralizable N (mg kg^{-1})	Available K (mg kg^{-1})	Available P (mg kg^{-1})
Initial Soil	5.20±0.1	0.03±0.01	0.98±0.01	38.50±1.2	164.69±6.2	37.47±3.2
T1	5.22±0.3	0.03±0.001	0.98±0.03	39.09±3.5	295.21±3.9	51.17±2.9
T2	5.40±0.05	0.09±0.005	1.01±0.08	39.32±3.2	588.84±8.5	66.18±4.7
T3	5.40±0.03	0.06±0.003	1.14±0.01	39.04±2.5	584.41±15.1	71.14±3.1
T4	5.55±0.11	0.08±0.007	1.22±0.08	44.57±5.4	445.80±6.8	76.82±2.1
T5	5.50±0.12	0.07±0.001	1.26±0.08	43.41±5	569.41±6.1	75.01±6.0
T6	5.50±0.22	0.08±0.002	1.15±0.08	47.41±3.6	658.94±8.5	118.21±6.4
T7	5.60±0.10	0.06±0.001	1.24±0.1	44.73±3.2	544.37±8.8	86.74±4.9
T8	5.62±0.33	0.06±0.001	1.24±0.02	45.03±3.1	589.41±13.0	78.34±4.7
T9	5.45±0.02	0.05±0.003	1.20±0.04	49.06±2.2	495.34±7.9	87.07±5.1
T10	5.55±0.11	0.08±0.002	1.13±0.07	48.31±2.1	577.54±8.5	97.16±3.1
T11	5.55±0.11	0.07±0.001	1.18±0.08	40.31±1.9	544.87±11.2	96.03±6.7
T12	5.50±0.54	0.08±0.01	1.16±0.07	44.94±3.3	638.94±15.2	100.87±5.1
LSD	0.06	0.001	0.08	3.08	12.92	3.14
p	NS	NS	NS	NS	0.003	0.004

8.2.3.3. Impact on microbial attributes of the soil

For microbial analysis the soil sample were collected plot wise (T1-T12) in periodical manner. Microbial biomass C was high initially in all the treatment except no input treatment ($p<0.05$). The results are presented in Fig. 8.2.2 The trend of temporal variation was interesting. In general rice cultivation in mostly done under water logged condition, likewise the present study carried out water logged condition; thus, a significant variation was evident among the treatment. Concerning to their periodical distribution load, it was found that MBC was initially high, and followed by decline onwards. Among the treatment the MBC was as follows T10> T12> T8= T9> T6= T7> T11> T4> T5> T3> T2>T1. Significant decrease was observed between highest (547 mg/kg) and lowest was at 90 days (94 mg/kg) (p for days =0.0003). The increment was more in 100% vermicompost-RM treated plots. This is probably due to the addition of microorganism introduced through vermicompost. However, the continual decline

in microbial activity may be due to nutrient shortage, plant microbe interaction, additionally under water logged condition anoxic environment is formed which put detrimental impact on aerobic microflora (Ponnamperuma, 1972; Bhattacharyya et al., 2003). In water logged condition, anaerobic and facultatively organism predominant, which usually have minimal yield compared to aerobic organism. In contrast, soil respiration (glucose induced) was gradually increase up to 90 days and a significant difference ($p<0.05$) was observed between organic input amended and no input treatment, though among treatments their difference was not significant. Since waterlogged conditions are mostly dominated by anaerobes, they are not good assimilator of organic carbon hence release waste product like CO_2 and low molecular weight compounds. As a result, we got an increased trend of soil respiration.

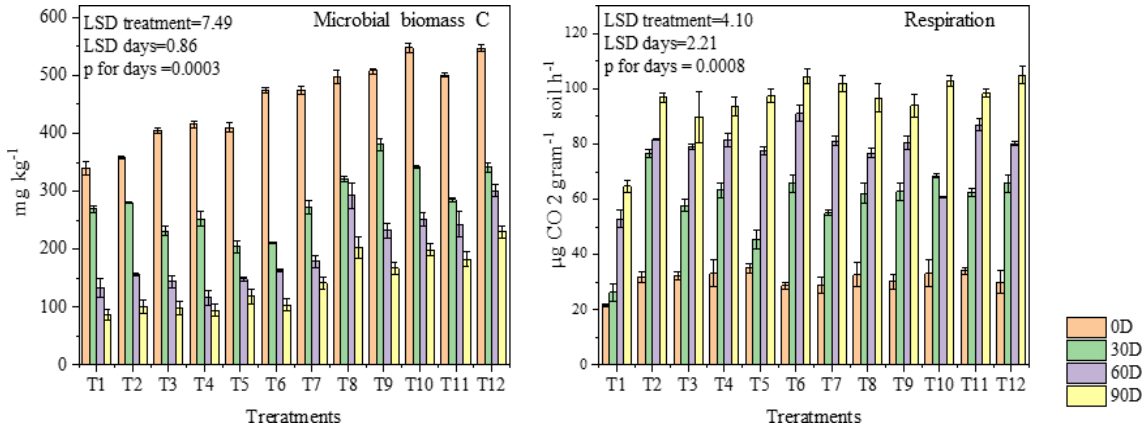

Fig. 8.2.2. Changes in the microbial biomass carbon and soil respiration during rice cultivation under different treatments.

8.2.3.4. Effect of vermicompost RM on crop productivity

- **Tillering habits**

Tillering is the important agronomic trait for grain production in rice (Li et. al., 2013). The adventitious roots on rice tillers allow them to grow independently of the culm and are used to produce specialised grain-bearing branches over the un-elongated basal internode (Li et al., 1979). Interestingly, overall rise in the number of tillers from the tillering to the harvesting stages was observed possibly due to the production of tertiary tiller which hardly contribute in grain production (Mohanan & Mini, 2008). The data on tiller production is presented in Table.8.2.5. A significantly tiller production was recorded in 50% NPK+50% RM-VC treatments compared. The highest tiller was observed in T6 16.01±0.7), while the tiller was lowest during no input treatment (6.09±0.6). The balanced enhancement of NPK probably

induced the growth and tiller development. Furthermore, addition of vermicompost augment the plant hormones like auxin, gibberellin, cytokinin which supports the plant growth (Lazcano & Dominguez, 2011). Our findings are in good agreement with Dash et al. (2011); Alim et al. (2012).

Table 8.2.5. Effect of different treatment combination on tiller number in tillering and harvesting stages (mean ±SE).

Treatment	No. of Tillers	
	Tillering stage	Harvesting stage
T1	6.09 ±2.65	6.09 ±1.12
T2	14.2 ±2.11	13.9 ±0.91
T3	8.55 ±3.21	8.98 ±2.10
T4	9.08 ±1.10	9.08 ±1.09
T5	11.66 ±3.11	12.09 ±2.09
T6	15.08 ±2.01	16.01 ±2.11
T7	14 ±2.01	14.88 ±2.2
T8	15 ±1.99	15.9 ±1.90
T9	14.15 ±2.01	14 ±2.91
T10	12.6 ±0.98	13.5 ±1.32
T11	13.2 ±2.11	13.99 ±1.19
T12	13.9 ±3.11	14.99±3.12
P for treatment (Tillering stage)	0.008	
LSD		1.88

- Biochemical attributes (Chlorophyll, protein and sugar content)

Interestingly chlorophyll content was high in vermicompost treated soil. However, 50%NPK+ 50% RM-VC showed a better result in plant growth and development. The result of the experiment in presented in Fig.8.2.3 Chlorophyll A, Chlorophyll B and total chlorophyll was significantly high in amended plot compared to non-amended treatment. Moreover, the overall beneficial impact of vermicompost can be justified, since, the humified substance enhance the secretion of auxin-like activity in plant, which supports the higher chlorophyll content (Da-Bing et al., 2012). Likewise, total sugar, and protein were found to be higher under RM-VC applied treatments (Fig. 8.2.3)

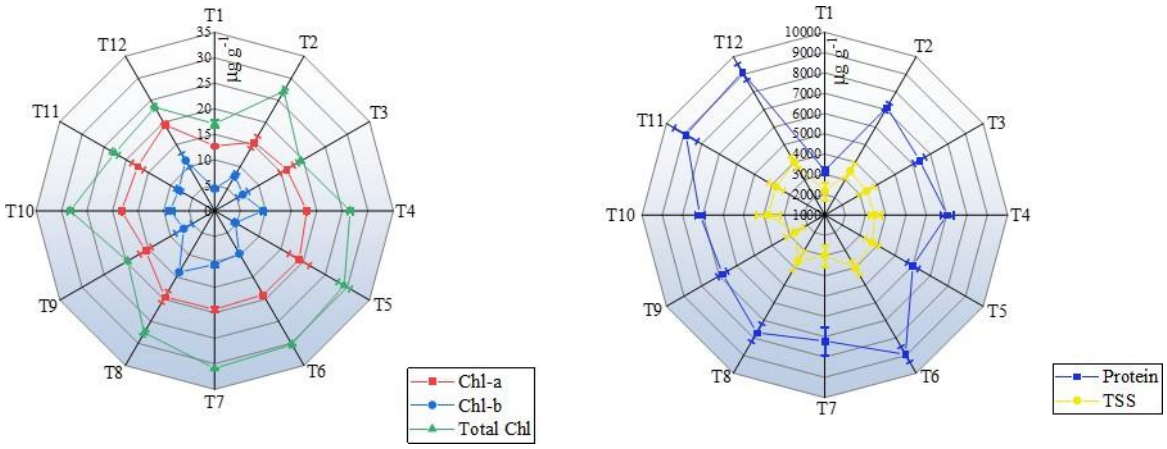

Fig. 8.2.3. Biochemical quality parameters of rice after harvesting.

8.2.3.5. Plant nutrient uptake

Nutrient uptake (P and K) by the plant in root, shoot, and grain was assessed and depicted in Fig. 8.2.4. The results demonstrated that soil treated with a composite of VC and NPK absorbs more nutrients than soil treated with VC alone, however the comparison was significant with control (p=0.0001). The K uptake was in the order of grain>shoot >root while P was highest in shoot > root>grain. Across the treatments, grain uptake of K was highest at T7 (LSD_{grain}=12.32, p=0.0006). On a contrary note, P uptake was highest in shoot followed by root and grain. The highest transfer took place in shoot of T8 plants that subsequently got the maximum amount of P in their grain compared to others. The increase in P availability in VC-aided soil was not only due to the transformation of insoluble P but also to an increase in P-solubilizing microorganisms and their enzymatic activity. The findings coincide with Mondal et al. (2020).

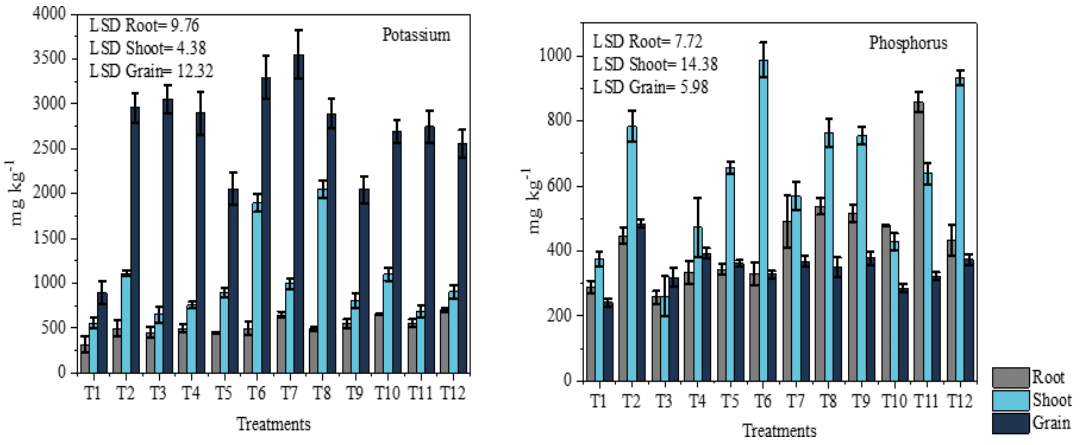

Fig. 8.2.4. Effect of different treatment combination on phosphorus (P) and potassium (K) uptake in rice plant (mean±standard error).

8.2.3.6. Metal availability and phytoaccumulation

A detailed fractionation study was done to check the distribution of metal in the studied soil (Fig. 8.2.5). Except Pb and Cd the other three metal Cu, Cr and Ni were dominantly present in organic bound fraction. This seemed to be formation of metal-organic complex. According to reports, metals have a greater affinity towards organic compound, specifically Cu, which make a stable coordination complex (Chirenje et al., 2002). Metals that are associated with Fe & Mn oxide bound state at the beginning, under water logged reduced conditions they become soluble and reacts with humic content of the organic matter and becomes poorly soluble, consequently loses mobility (Bhattacharyya et al., 2006). Cd is primely dominant in the carbonate bound fraction, and Pb was in residual fraction. In addition, a significant reduction ($p<0.05$) in DTPA extractable metal was evinced under all the treatments compared to initial concentration (Table 8.2.6). For all the metals an average >0.5-fold reduction was detected which is in contradiction with Da S Trentin et al. (2019) who found Mn triggered phytotoxicity occurred by using vermicompost, otherwise, the results are in good agreement with Mondal et al. (2020) and Goswami et al. (2017).

In the case of plant uptake there was no phytoaccumulation observed in shoot and grain, however a few amounts of metal are accumulated by root (Fig. 8.2.6.). Interestingly, like other parameters the accumulation was significantly higher in no input treatment (T1, $p<0.05$), and a trace amount of metal was detected in their shoot and grain of T1 (Cr shoot= 5.9 mg/kg, Cr grain= 3.2mg/kg; Ni shoot= 6.8 mg/kg, Ni grain= 5.4 mg/kg, Cu shoot 8 mg/kg, Cu grain= 6.9

mg/kg). A significant positive ($p<0.05$) correlation between WS & Ex metal and plant metal (root) indicated that these two metal fractions are responsible for plant uptake.

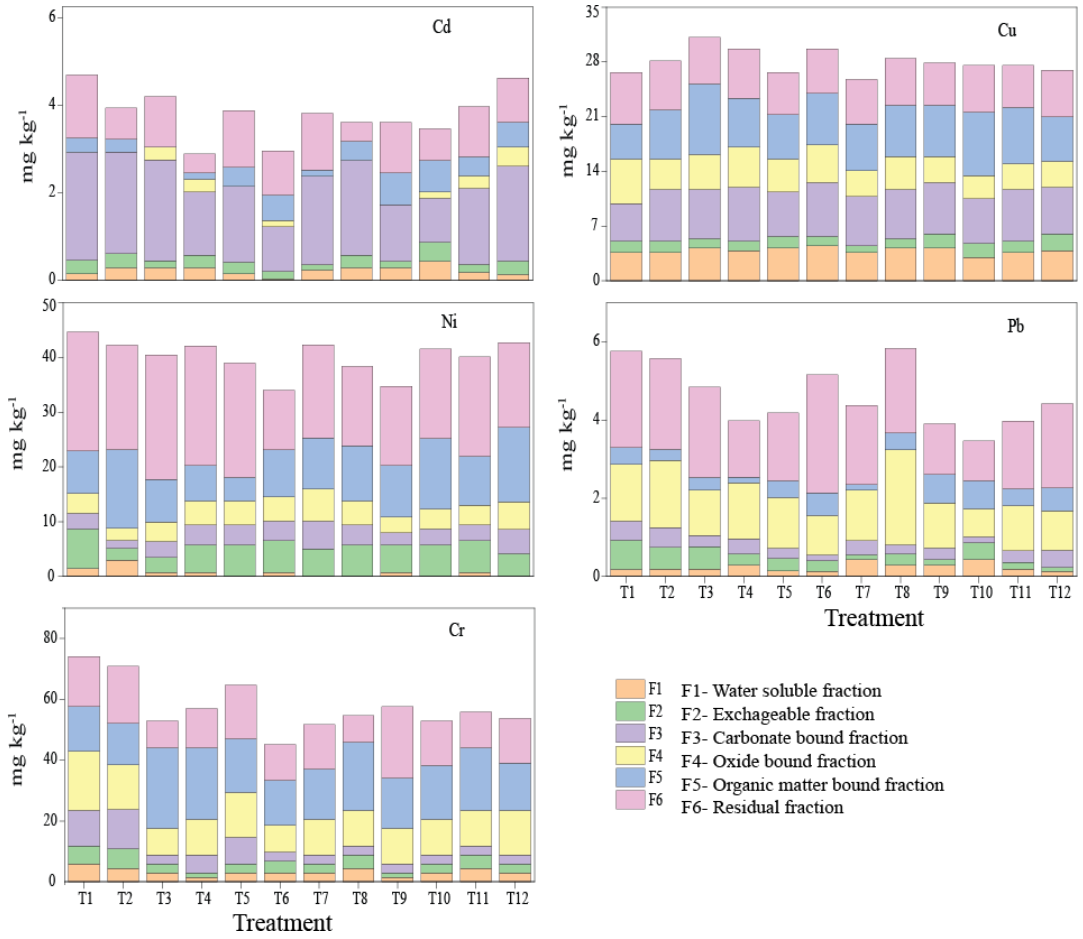

Fig. 8.2.5. Different fractional distributions of metal (Cu, Cr, Ni, Cd, Pb) across treatments.

Table 8.2.6. Soil metal status (DTPA-extractable) before and after sesame cultivation under various treatments (mean ± SE).

Treatments	Cr(mg/kg)	Ni (mg/kg)	Cu (mg/kg)	Cd (mg/kg)	Pb (mg/kg)
Initial Soil	10.47±0.99	7.93±1.09	16.99±2.32	1.89±0.05	3.55±0.88
T1	8.82±0.87	7.32±1.02	14.29±1.98	1.29±0.03	2.33±0.76
T2	8.88±0.76	6.88±0.98	13.29±3.98	1.29±0.12	2.34±1.01
T3	2.94±0.88	2.16±0.05	11.59±1.87	0.87±0.02	1.77±0.34
T4	2.94±1.01	1.44±0.06	6.29±1.08	0.58±0.04	1.58±0.87
T5	5.88±1.09	2.16±0.07	6.89±0.98	0.87±0.07	1.87±0.77
T6	2.94±0.88	1.44±0.08	9.89±1.11	0.75±0.09	0.95±0.06
T7	2.98±1.02	0.72±0.00	5.69±1.09	0.55±0.01	1.55±0.08
T8	2.90±0.76	1.44±0.08	6.59±1.11	0.58±0.02	1.58±0.39
T9	2.78±0.02	0.72±0.01	7.19±1.21	0.43±0.008	0.93±0.008
T10	5.88±0.09	2.88±1.0	5.99±0.87	0.87±0.06	0.97±0.002
T11	2.94±0.54	0.72±0.08	6.29±1.66	0.370.006	0.97±0.006
T12	2.94±0.22	0.72±0.08	7.19±2.43	1.19±0.88	1.19±0.10
LSD	0.36	0.48	0.18	0.08	0.21
p	0.001	0.035	0.0006	0.0004	0.003

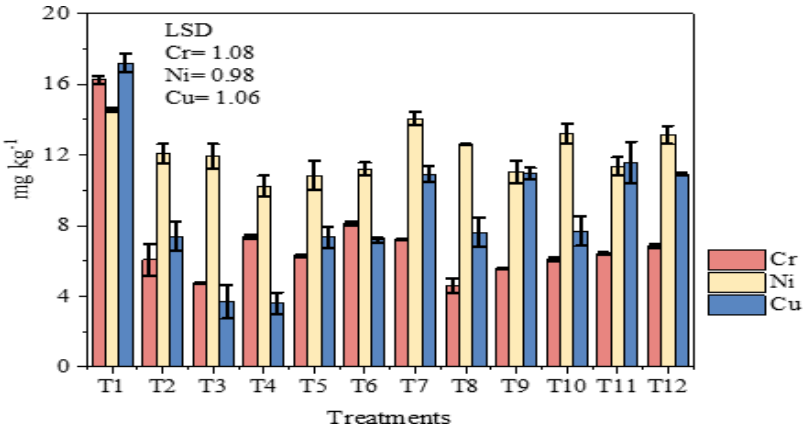

Fig. 8.2.6. Metal accumulation in the root of rice in different RM-VC treated plots after harvesting.

8.2.3.7. Grain yield

The result of the grain yield is depicted in Table 8.2.7. Significantly high grain yield was achieved in T8 and T6. Both the treatments were 50% reduction of chemical fertilizer and substituted with 50 % RM-VC (1:2 and 1:3). The result implied that vermicomposted RM application coupled with 50% dosage NPK fertilizer could produce a statistically similar or even better in as compared sole RM-VC or NPK or CD application in field scale. Due to the application of vermicompost, increased nutrient uptake by plants and improved bioavailability

in the root zone of standing crops increase grain yield (Banik and Bejbaruah, 2004). Vermicompost application has been shown to have a similar positive effect on rice yield recently (Sahariah et al., 2020).

Table 8.2.7. Effect of different treatments on rice grain yield (mean ±SE)

Treatments	yield (tons/ha)
T1	1.21±0.04
T2	4.09±1.21
T3	2.56±0.86
T4	3.06±0.04
T5	3.36±0.33
T6	4.22±1.65
T7	3.82±1.11
T8	4.27±1.02
T9	4.18±0.99
T10	3.94±0.14
T11	3.83±1.25
T12	3.92±1.11
LSD	0.42
p =	0.008

8.3.4. Conclusion

The present investigation summarizes that the crop trial using two different dosages (100% organic; 50%NPK+ 50% organics) turns out to be beneficial for both plant and soil health. Among treatments, T6 (50% 1:2RM-VC+50% NPK) and T8 (1:3 RM-VC 50%+ 50% NPK) were most effective for rice cultivation. Comparing the nutrient status of lateritic soil, the composite treatments work better than sole VC treatments. Solubility of the essential nutrients (N, P, K) enhanced coupled with soil microbial activity while migration of toxic metals got restricted under VC treatments. Intervention of organics improved total yield and

other yield attributes. Overall, this study proved vermitechnology could be a useful way of converting poorly fertile soil into a productive one and prolific recycling of hazardous waste like red mud on a large-scale basis might keep a potential nutritional value for a staple crop like rice.

Chapter 9

Summary and Conclusion

Chapter 9

Summary and Conclusion

9.1. Summary

The overall goal of this work was to characterize a red mud (RM) produced by aluminum processing factories and to investigate the viability of using vermicomposting technology to convert this industrial waste material into beneficial organic manure for use in agriculture. Although RM is extremely sodic and rich in potentially hazardous metals, there was no reliable information regarding the physicochemical qualities, metal distribution, or leaching characteristics previously to this research. Additionally, biological traits like enzyme content and microbial diversity were disregarded under the assumption that the high levels of sodicity and alkalinity would render the environment devoid of microbial activity. Furthermore, their secondary use is mostly in non-biological sectors such as chemical industry and engineering sectors, construction sector, however in present scenario, some environmental application of RM is emerging. In many countries, the RM is being ameliorated through revegetation using different amendments (gypsum, compost, soil/sand etc.,). Owing to its high sodicity, very few alkali-tolerant species viz., *Agrostis stolonifera*, *Holcus lanatus*, *Lolium perenne* can grow and thrive. On top of that, their reuse is scanty due to several obstacles (high Na, highly toxic metal, presence of radioactive compound). Continual disposal, landfilling, unscientific and open dumping imposed an increasing nuisance on the ecosystem by releasing large quantities of inorganic toxic substances into the environment, upsetting the ecological balance. India, the most populated and third-largest producer of RM, confronts a severe challenge as a result of its high land occupancy and the environmental hazards caused by the disposal of RM. Therefore, clean sustainable technology could save the environment to some extent.

In this regard, we have collected the RM from the HINDALCO aluminum plant, located at Muri, Jharkhand, and did an in-depth characterization for standardizing it for vermicomposting. The RM was found to have >6% Na content, which is threatening. Along with that abundance of other cations like Ca^{2+}, Mg^{2+} K^{+} were detected. Considering the heavy metal content, Cr was highest followed by Pb, Ni, and Cd. An adequate presence of these toxic metals in the mobile fraction (water soluble and exchangeable) intimidates the ecosystem. Elemental solubility and leaching properties exacerbated over time specifically, the increment in Na concentration was scary for the environment. The RM also underwent comparative

analysis with its native bauxite ore, which revealed, the detrimental impact of NaOH during industrial Bayer extraction. This high volume of NaOH changes the characteristics of RM, transforming it from acidic to hyper alkaline, destroying microbial activity, and increasing the availability of metal. Moreover, the ecological and human health hazard potential of the different types of RM was assessed to identify their suitability for agricultural application.

On the basis of the findings and understanding, the RM was pre-treated with gypsum and calcium chloride, and subsequently, mixed with cow dung (bulking agent) at four different ratios [1:1, as VC1; 1:2 as VC2; 1:3 as VC3; and 1:4 as VC4 (RM: CD)] and incubated with *Eisenia fetida* for 90 days. A corresponding aerobic composting was done for fair comparison and the significance of adding earthworms. The results portrayed the appreciable enhancement in plant nutrients (available N, P, K) microbial enzyme, microbial activity, and diversity in microbial community structure. And most importantly a significant ($p<0.05$) reduction in the bioavailability of metal was evidenced which is the result of earthworm gut accumulation. A substantial amount of Na (17.42 g/kg in a 1:1 ratio) was accumulated by earthworms, which caused the Na concentration to likewise decrease. The performance of VC2 and VC3 was noticeable with respect to metal removal efficiency, earthworm growth and fecundity, augmentation in microbial activity, and improvement of nutritional value. Overall, these studies showed that the ratio of the feedstock has a substantial impact on earthworm growth, waste digestion, and metal accumulation efficiency. Based on the obtained data in the vermicomposting experiment, this has provoked us to apply this compost for soil fertility and crop growth. A summer crop *Vigna radiata L.* (commonly green gram) was cultivated through a pot experiment and promising results subsequently led us to apply this vermicompost in staple food like rice (Oryza *sativa L.*) cultivation in field conditions. The vermicompost was applied in both solitary and integrated nutrient management schemes. The yield was highest in the integrated approach for VC3 (50% VC3+50% NPK) and VC2 (50% VC3+50% NPK) for rice, while green gram, it was VC2 ((50% VC3+50% NPK). Considering the metal uptake, in the case of rice there was no uptake in shoot and grain, however for green gram a small amount of uptake was detected in grain, though it was under permissible limit. The free ion activity model (FIAM) determined a restricted migration of the toxic metal. In addition to crop growth and yield, the soil nutrient status was also enhanced in RM-VC-treated plots.

On the other side, this study has explored the RM as a bowl of extremophilic bacteria, however, it probably does not harbour fungus according to our findings. Since fungi are acid-loving and grow moderately acidic to near neutral pH, high sodicity and alkalinity are a

hindrance to their growth in RM. Following this we ventured into the microbial community diversity through a metagenome approach, revealing a predominance of *Bacillus*, *Halomonas*, *Alcanovorax*, species. Satisfying this finding, through a culture-dependent approach, we isolated the polyextremophilic *Bacillus xiamenensis* ISIGRM16 that has metal adsorption ability. In the next phase, a biomass-biosorbent was prepared using this bacterium and showed an impressive removal efficiency of three potentially toxic elements Cd^{2+}, $Ni^{2+,}$ and Cr^{6+} from an aqueous solution. The removal was as follows Cd^{2+}(>99%), Ni^{2+}(>85%), and Cr^{6+}(>40%). The biosorbent was then tested in a multimetal (Cd+Cr+Ni) system, where it functioned equally well. The removal efficacy preservation up to the third cycle was validated by a consecutive adsorption-desorption experiment, making them profitable for wastewater treatment. Last but not least, the FESEM-EDX and FTIR analyses reveal the structural changes that occur after metal adsorption and demonstrate how functional groups (carboxyl, hydroxyl, and amide) on the cell surface are involved in metal adsorption.

9.2. Limitation of the study

Even though this study investigated RM from an unfamiliar viewpoint, certain topics are yet unexplored because of various limitations. This study discovered an explicable bioaccumulation tendency in earthworms, however further research is needed to fully grasp the mechanical approach from genetic perspective. Additionally, a dose-dependent study should be conducted to determine the earthworms' maximum tolerable dose by determining the threshold value for their absorption capacity. On the other hand, the prepared biomass-biosorbent from *Bacillus xiamenensis* ISIGRM16 should be used in actual wastewater treatment to check for any changes in their capacity to remove contaminants from a solution in a natural setting. Last but not least, heavy metal resistance mechanisms in bacteria should be investigated.

9.3. Prospect in the near future

Even though the study was carried out as thoroughly as feasible owing to time constraints, the scientific success of the research objective warrants further long-term research. From the current study, the optimization of vermitechnology concerning eco-friendly disposal of RM, the following avenue could be explored shortly:

1. If industries take responsibility for the complete removal of water-soluble Na along with the addition of amendments, then it can be directly vermicomposted without any pretreatment, which will speed up the process and broaden applicability.

2. As agriculture is often the backbone of a country's economy, using vermicomposted RM to increase crop yield will lower the cost of chemical fertilizer, and at the same time, widespread agricultural use will ease the pressure on RM disposal sites. The overpopulated country will benefit as a result of the decreased environmental risk and land occupancy.
3. Since RM is home to a diverse range of extremophilic organisms, it may be used in a number of various industrial fields. Being alkaliphilic, they have a significant potential to produce organic acid and numerous other bioactive substances that may be used for a variety of reasons. They can be employed for in-situ remediation processes as they are extremophilic and survive in extreme conditions.

List of Publication

Publication accepted:

1. Charan, K., Bhattacharyya, P. Vermicomposted red mud- A up-and-coming approach towards soil fertility. Journal of Crop and Weed. 19 (2).

Publication under communication:

1. Charan, K., Mandal, J., Bhattacharyya, P. Hazard remediation of wastewater by novel polyextremophilic *Bacillus xiamenensis* ISIGRM16 isolated from alkaline-sodic red mud- A sustainable sorptive approach. Submitted to Environmental Science and Pollution Research. Manuscript number: EMID: f0c275859e4accc7.

Seminars attended:

1. 9th Annual Convention and National Webinar "Managing Agro-Chemicals for Crop and Environmental Health". February 25-26, 2022.
   (Selected as the best paper presentation. Paper entitled as 'Impact of different pools of acidity on soil eco-physiological health of Bauxite mine over burden with reference to its trace elemental profiling")
2. National seminar on "Current perspective on Environmental Science & Technology", February 27-March 1, 2022.
3. National Conference on "Recent Trends on Microbial, Plant and Animal Research". September 15 -16, 2022
4. 10th Annual Convention and National Seminar on Next-gen Management of Agro-chemicals for Achieving Sustainable Development Goals, February 24-25, 2023

Bibliography

Bibliography:

Abbasi M. K., Hina M, Khalique A, Khan SR. (2007). Mineralization of three organic manures used as nitrogen source in a soil incubated under laboratory conditions. Communications in Soil Science and Plant Analysis, 38:1691–1711

Adamczyk-Szabela, D., & Wolf, W. M. (2022). The Impact of Soil pH on Heavy Metals Uptake and Photosynthesis Efficiency in *Melissa officinalis*, *Taraxacum officinalis*, *Ocimum basilicum*. Molecules, 27: 4671.

Adimalla, N. (2020). Heavy metals pollution assessment and its associated human health risk evaluation of urban soils from Indian cities: a review. Environmental Geochemistry and Health, 42:173–190.

Agnew, M. D., Koval, S. F., & Jarrell, K. F. (1995). Isolation and Characterization of Novel Alkaliphiles from Bauxite-Processing Waste and Description of *Bacillus vedderi* sp. nov., a New Obligate Alkaliphile. Systematic and Applied Microbiology, 18:221–230.

Agrawal, S., Rayapudi, V., & Dhawan, N. (2018). Microwave Reduction of Red Mud for Recovery of Iron Values. Journal of Sustainable Metallurgy, 4:427–436.

Ahad RIA, Syiem MB, Rai AN (2021) Cd(II) sorption by *Nostoc sp*. JRD1: Kinetic, thermodynamic and isotherm studies. Environmental Technology &Amp; Innovation, 21:101-283.

Ahadi, N., Sharifi, Z., Hossaini, S. M., Rostami, A., & Renella, G. (2020). Remediation of heavy metals and enhancement of fertilizing potential of a sewage sludge by the synergistic interaction of woodlice and earthworms. Journal of Hazardous Materials, 385:121573.

Ahemad, M. (2012). Implications of bacterial resistance against heavy metals in bioremediation: a review, *IIOAB-India*.

Ahn, Y., & Reddy, M. V. (2011). *Aspergillus tubingensis*Improves the Growth and Native Mycorrhizal Colonization of Bermudagrass in Bauxite Residue. Bioremediation Journal, 15:157–164.

Alam, M. Z., & Ahmad, S. (2012). Multi-metal biosorption and bioaccumulation by *Exiguobacterium* sp. ZM-2. Annals of Microbiology, 63:1137–1146.

Al-Dulaimi, N. H and M. A. Al-Jumaili. (2017). Response green beans to spray some Micronutrients and addition Organic fertilizer. The Iraqi Journal of Agricultural Sciences, 48: 444– 455.

Alekseev, K. N., Mymrin, V., Avanci, M. A., Klitzke, W., Magalhães, W. L. E., Silva, P., Catai, R. E., Da Silva, D. A., & Ferraz, F. a. P. (2019). Environmentally clean construction materials from hazardous bauxite waste red mud and spent foundry sand. Construction and Building Materials, 229:116860.

Ali, U., Sajid, N., Khalid, A., Riaz, L., Rabbani, M. S., Syed, J. H., & Malik, R. N. (2015). A review on vermicomposting of organic wastes. Environmental Progress & Sustainable Energy, 34:1050–1062.

Alim, M. A. (2012). Effect of Organic and Inorganic Sources and Doses of Nitrogen Fertilizer on the Yield of Boro Rice. Journal of Environmental Science and Natural Resources, 5:273–282.

Amer A, Hassan H., Ghozlan H. Sabry S. (2013). Nickel biosorption by alkali tolerant *Exiguobacterium* sp. 27 isolated from lake Mariout. Egypt. Life Science Journal, 4:1338-1347

Amin MT, Alazba AA, and Shafiq M (2017) Non-spontaneous and multilayer adsorption of malachite green dye by *Acacia nilotica* waste with dominance of physisorption. Water Science Technology, 76:1805–1815

Anderson, T. H., & Domsch, K. (1990). Application of eco-physiological quotients (qCO2 and qD) on microbial biomasses from soils of different cropping histories. Soil Biology and Biochemistry, 22:251–255.

Ansari, A., & Ismail, S. A. (2012). Role of Earthworms in Vermitechnology. *ResearchGate*.

Antil RS, Singh M. (2007). Effects of organic manures and fertilizers on organic matterand nutrients status of the soil. Archives of Agronomy and Soil Science, 53:519–528

Aono, R., & Horikoshi, K. (1983). Chemical Composition of Cell Walls of Alkalophilic Strains of *Bacillus*. Microbiology, 129:1083–1087.

Arief VO, Trilestari K, Sunarso J, Indraswati N, Ismadji S (2008). Recent progress on biosorption of heavy metals from liquids using low cost biosorbents: characterization, biosorption parameters and mechanism studies: A review. Clean, 36:937–962

Asha, S., & Vidyavathi, M. (2009). Cunninghamella – A microbial model for drug metabolism studies-A review. Biotechnology Advances, 27:16–29.

ATSDR (2012). Toxicological profile for chromium.

Ayangbenro, A. S., & Babalola, O. O. (2017). A New Strategy for Heavy Metal Polluted Environments: A Review of Microbial Biosorbents. International Journal of Environmental Research and Public Health, 14:94.

Balabantaray, S. K., Aravindan, S., & Ravi, R. (2020). Morphological, microstructural and mineralogical dataset of bauxite over Mainpat plateau from a part of Deccan traps, Surguja district, Chhattisgarh. SN Applied Sciences, 2:11.

Banik, P., & Bejbaruah, R. (2004). Effect of vermicompost on rice (*Oryza sativa*) yield and soil-fertility status of rainfed humid sub-tropics. Indian Journal of Agricultural Sciences, 74:488–491.

Banning, N., Phillips, I., Jones, D. R., & Murphy, D. (2011). Development of Microbial Diversity and Functional Potential in Bauxite Residue Sand under Rehabilitation. Restoration Ecology, 19:78–87.

Be, I., Okoduwa, S. I. R., Idoko, G., Akabuogu, E. P., Adeyi, A. O., & Ejiogu, I. K. (2018). Toxicity and Bioremediation of Heavy Metals Contaminated Ecosystem from Tannery Wastewater: A Review. Journal of Toxicology, 1–16.

Bhatnagar, A., Vilar, V. J., Botelho, C. M., & Boaventura, R. A. (2011). A review of the use of red mud as adsorbent for the removal of toxic pollutants from water and wastewater. Environmental Technology, 32:231–249.

Bhattacharya, S. S., & Kim, K. (2016). Utilization of coal ash: Is vermitechnology a sustainable avenue? Renewable & Sustainable Energy Reviews. 58:1376–1386.

Bhattacharya, S., Iftikar, W., Sahariah, B. P., & Chattopadhyay, G. N. (2012). Vermicomposting converts fly ash to enrich soil fertility and sustain crop growth in red and lateritic soils. Resources Conservation and Recycling, 65:100–106.

Bhattacharyya P, Chakrabarti K, Chakraborty A, Nayak DC, Tripathy S, Powell MA. (2007). Municipal waste compost as an alternative to cattle manure for supplying potassium to lowland rice. Chemosphere, 66:1789–1793.

Bhattacharyya, P., Chakrabarti, K., & Chakraborty, A. (2003). Effect of MSW Composton Microbiological and Biochemical Soil Quality Indicators. Compost Science & Utilization, 11:220–227.

Bhattacharyya, P., Chakraborty, A., Chakrabarti, K., Tripathy, S. K., & Powell, M. (2006). Copper and zinc uptake by rice and accumulation in soil amended with municipal solid waste compost. Environmental Earth Sciences, 49:1064–1070.

Bhattacharyya, P., Reddy, K. J., & Attili, V. S. S. (2011). Solubility and Fractionation of Different Metals in Fly Ash of Powder River Basin Coal. Water Air and Soil Pollution, 220:327–337.

Bhattacharyya, P., Tripathy, S., Chakrabarti, K., Chakraborty, A., & Banik, P. (2008). Fractionation and bioavailability of metals and their impacts on microbial properties in sewage irrigated soil. Chemosphere, 72:543–550.

Bish, D. L., & Post, J. E. (1989). Modern Powder Diffraction. In De Gruyter eBooks.

Blagodatskaya, E., & Kuzyakov, Y., (2011). Priming Effects in Relation to Soil Conditions – Mechanisms. Springer Netherlands EBooks, 657–667.

Blouin, M., Barrere, J., Meyer, N., Lartigue, S., Barot, S., & Mathieu, J. (2019). Vermicompost significantly affects plant growth. A meta-analysis. Agronomy for Sustainable Development, 39:4

Borah P, Singh P, Rangan L, Karak, T, Mitra S (2018) Mobility, bioavailability and ecological risk assessment of cadmium and chromium in soils contaminated by paper mill wastes. Groundwater for Sustainable Development, 6:189–199.

Boyer, S., & Wratten, S. D., (2010). The potential of earthworms to restore ecosystem services after opencast mining – A review. Basic and Applied Ecology,11:196–203.

Brady, N.C., Weil, R.R. (2002). The Nature and Properties of Soils, thirteenth ed. Prentice Hall, Upper Saddle River, NJ

Brandl, H. (2001). Microbial Leaching of Metals. Biotechnology Set, 191–224.

Brandl, H. (2002). Metal-microbe-interactions and their biotechnological applications for mineral waste treatment. ResearchGate. https://www.researchgate.net/publication/229048513

Bray, A. W., Stewart, D. I., Courtney, R., Rout, S. P., Humphreys, P. N., Mayes, W. M., & Burke, I. T., (2018). Sustained Bauxite Residue Rehabilitation with Gypsum and Organic Matter 16 years after Initial Treatment. Environmental Science & Technology, 52:52–161.

Brinton, W.F. (2000). Compost Quality Standards and Guidelines. Woods End ResearchLaboratory, USA, p. 42,

Burke, I. C., Mayes, W. M., Peacock, C. L., Brown, A. J., Jarvis, A. P., & Gruiz, K. (2012). Speciation of Arsenic, Chromium, and Vanadium in Red Mud Samples from the Ajka Spill Site, Hungary. Environmental Science & Technology, 46:3085–3092.

Burke, I. C., Peacock, C. L., Lockwood, C. L., Stewart, D. A., Mortimer, R. J., Ward, M. D., Renforth, P., Gruiz, K., & Mayes, W. M. (2013). Behavior of Aluminum, Arsenic, and Vanadium during the Neutralization of Red Mud Leachate by HCl, Gypsum, or Seawater. Environmental Science & Technology, 47:6527–6535.

Cain, A., Vannela, R., & Woo, L. K. (2008). Cyanobacteria as a biosorbent for mercuric ion. Bioresource Technology, 99:6578–6586.

Cánovas, D., Mukhopadhyay, R., Rosen, B. P., & De Lorenzo, V. (2003). Arsenate transport and reduction in the hyper-tolerant fungus *Aspergillus* sp. P37. Environmental Microbiology, 5:1087–1093.

Caravaca, F., Masciandaro, G., & Ceccanti, B. (2002). Land use in relation to soil chemical and biochemical properties in a semiarid Mediterranean environment. Soil & Tillage Research, 68:23–30.

Casida, L. E., Klein, D. A., & Santoro, T. J. (1964). Soil dehydrogenase activity. Soil Science, 98: 371–376.

Cayllahua, J. E. B., de Carvalho, R. J., & Torem, M. L. (2009). Evaluation of equilibrium, kinetic and thermodynamic parameters for biosorption of nickel(II) ions onto bacteria strain, *Rhodococcus opacus*. Minerals Engineering, 22:1318–1325.

Cha, J., & Cooksey, D. A. (1991). Copper resistance in Pseudomonas syringae mediated by periplasmic and outer membrane proteins. Proceedings of the National Academy of Sciences of the United States of America, 88:8915–8919.

Chakraborty, P., Sarkar, S., Mondal, S., Agarwal, B., Kumar, A., Bhattacharya, S., Bhattacharya, S. S., & Bhattacharyya, P., (2022). *Eisenia fetida* mediated vermi-transformation of tannery waste sludge into value added eco-friendly product: An insight on microbial diversity, enzyme activation, and metal detoxification. Journal of Cleaner Production, 348:131368.

Chandra, K. S., & Krishnaiah, S. (2022). Strength and leaching characteristics of red mud (bauxite residue) as a geomaterial in synergy with fly ash and gypsum. Transportation Research Interdisciplinary Perspectives, 13:100566.

Chang JS, Chen CC (1998) Quantitative Analysis and Equilibrium Models of Selective Adsorption in Multimetal Systems Using a Bacterial Biosorbent. Separation Science and Technology, 33:611–632.

Chang, J., & Chen, Y. (2010). Effects of bulking agents on food waste composting. Bioresource Technology, 101:5917–5924.

Channaveerswami, A. S. (2005). "Studies on integrated nutrient management and planting methods on seed yield and quality of groundnut". Ph.D. Thesis, Univ. Agric. Sci., Dharwad, Karnataka (India).

Chatterjee, S., Mahanty, S., Das, P., Chaudhuri, P., Das, S. (2020). Biofabrication of iron oxide nanoparticles using manglicolous fungus *Aspergillus niger* BSC-1 and removal of Cr(VI) fromaqueous solution. Chemical Engineering Journal, 385:123790.

Chatterjee, S., Kumari, S., Rath, S., Priyadarshanee, M., Das, S. (2020). Diversity, structure and regulation of microbial metallothionein: metal resistance and possible applications in sequestration of toxic metals. Metallomics, 12:1637–1655.

Chen, L., & Wu, C. (2012). Stockpiling and Comprehensive Utilization of Red Mud Research Progress. Materials, 5:1232–1246.

Chen, R., Senbayram, M., Blagodatsky, S., Myachina, O., Dittert, K., Lin, X., Blagodatskaya, E., & Kuzyakov, Y. (2014). Soil C and N availability determine the priming

effect: microbial N mining and stoichiometric decomposition theories. Global Change Biology, 20:2356–2367.

Cherian, M., & Nordberg, M. (1983). Cellular adaptation in metal toxicology and metallothionein. Toxicology, 28:1–15.

Cherono, F., Mburu, N., Kakoi, B. (2021) Adsorption of lead, copper and zinc in a multi- metal aqueous solution by waste rubber tires for the design of single batch adsorber. Heliyon, 7: e08254

Chiaverini, N., & De Ley, M. (2010). Protective effect of metallothionein on oxidative stress-induced DNA damage. Free Radical Research, 44:605–613.

Chirenje, T., Rivero, C., & Q, L., MA. (2002). Leachability of Cu and Ni in wood ash-amended soil as impacted by humic and fulvic acid. Geoderma, 108:31–47.

Cho, D., Yoon, K., Ahn, Y., Sun, Y., Kim, K., Hou, D., Kim, K., & Kim, K. (2019). Fabrication and environmental applications of multifunctional mixed metal-biochar composites (MMBC) from red mud and lignin wastes. Journal of Hazardous Materials, 374:412–419.

Cornelis, G., Poppe, S., Van Gerven, T., Van Den Broeck, E., Ceulemans, M., & Vandecasteele, C. (2008). Geochemical modelling of arsenic and selenium leaching in alkaline water treatment sludge from the production of non-ferrous metals. Journal of Hazardous Materials, 159: 271–279.

Cornish, P. S., Kumar, A., & Das, S. (2020). Soil fertility along toposequences of the East India Plateau and implications for productivity, fertiliser use, and sustainability. SOIL, 6:325–336

Courtney, R., & Kirwan, L. J. (2012). Gypsum amendment of alkaline bauxite residue – Plant available aluminium and implications for grassland restoration. Ecological Engineering, 42:279–282.

Courtney, R., & Xue, S. (2019). Rehabilitation of bauxite residue to support soil development and grassland establishment. Journal of Central South University, 26:353–360.

Courtney, R., Di Carlo, E., & Schmidt, O. (2020). Soil properties and earthworm populations associated with bauxite residue rehabilitation strategies. Environmental Science and Pollution Research, 27:33401–33409.

Courtney, R., Harrington, T. C., & Byrne, K. A. (2013). Indicators of soil formation in restored bauxite residues. Ecological Engineering, 58:63–68.

Courtney, R., Mullen, G. B., & Harrington, T. J. (2009). An Evaluation of Revegetation Success on Bauxite Residue. Restoration Ecology, 17:350–358.

Cumberland, S. A., Douglas, G., Grice, K., & Moreau, J. W. (2016). Uranium mobility in organic matter-rich sediments: A review of geological and geochemical processes. Earth-Science Reviews, 159:160–185.

Cusack, P. B., Courtney, R., Healy, M. G., Donoghue, L. M. O., & Ujaczki, É. (2019). An evaluation of the general composition and critical raw material content of bauxite residue in a storage area over a twelve-year period. Journal of Cleaner Production, 208:393–401.

Da S Trentin, A. W., Reddy, K. R., Kumar, G., Chetri, J. K., & Thomé, A., 2019. Quantitative Assessment of Life Cycle Sustainability (QUALICS): Framework and its application to assess electrokinetic remediation. Chemosphere, 230:92-106.

Da-Bing.X., Qiu-Jun,W., Yun-Cheng,W., Guang-Hui,Y., Qi-Rong, S., & QiWei,H. (2012). Humic-Like Substances from Different Compost Extracts Could Significantly Promote Cucumber Growth. Pedosphere, 22: 815–824.

Das, S., Dash, HR., Chakraborty, J. (2016) Genetic basis and importance of metal resistant genes in bacteria for bioremediation of contaminated environments with toxic metal pollutants.Applied Microbiology Biotechnology, 100:2967–2984.

Das, S., Charan, T., Mukherjee, S., Seal, S., Sah, R. K., Duary, B., Kim, K., Bhattacharya S. S. (2018). Impact of edaphic factors and nutrient management on the hepatoprotective efficiency of Carlinoside purified from pigeon pea leaves: an evaluation of UGT1A1 activity in hepatitis induced organelles. Environmental Research, 161:512-523

Das, D., Dwivedi, B., Datta, S., Datta, S., Meena, M., Agarwal, B., Shahi, D., Singh, M., Chakraborty, D., & Jaggi, S. (2019). Potassium supplying capacity of a red soil from eastern India after forty-two years of continuous cropping and fertilization. Geoderma, 341:76–92

Das, S., Goswami, L., & Bhattacharya, S. S. (2020). Vermicomposting. In Elsevier eBooks, 79–102.

Dash, D., Patro, H., Tiwari, R. C., & Shahid, M. (2010). Effect of Organic and Inorganic Sources of N on Yield Attributes, Grain Yield and Straw Yield of Rice (*Oryza sativa*). Research Journal of Agronomy, 4:18–23.

Datta, S. P., Subba Rao, A., & Ganeshamurthy, A. N. (1997). Effect of electrolytes coupled with variable stirring on soil pH. Journal of the Indian Society of Soil Science, 45:185–187.

David, P. P., Nelson, P. V., & Sanders, D. C. (1994). A humic acid improves growth of tomato seedling in solution culture. Journal of Plant Nutrition, 17:173–184.

De Oliveira Romano, R. C., Bernardo, H. M., Maciel, M. G., Pileggi, R. G., & Cincotto, M. A. (2019). Using isothermal calorimetry, X-ray diffraction, thermogravimetry and FTIR to monitor the hydration reaction of Portland cements associated with red mud as a supplementary material. Journal of Thermal Analysis and Calorimetry, 137:1877–1890.

Deka, H., Deka, S., Baruah, C., Das, J., Hoque, S., Sarma, H., & Sarma, N., (2011). Vermicomposting potentiality of *Perionyx excavatus* for recycling of waste biomass of java citronella - An aromatic oil yielding plant. Bioresource Technology, 102:11212–11217.

Del Busso Zampieri, B., Nogueira, E. W., Quaglio, O. A., & Brucha, G. (2019). Overview of Known Alkaliphilic Bacteria from Bauxite Residue. Journal of Mining and Mechanical Engineering, 1:2.

Desai, N. N., Tanksali, A., & Soraganvi, V. S. (2016). Vermicomposting – Solution for Milk Sludge. Procedia Environmental Sciences, 35:441–449.

Deshpande, S. P., Dafare, S. W., Batra, V., & Bhavsar, R. S. (2017). Properties, Utilization, and Characterization of Red Mud In Terms of Its Environmental Effects. International Journal of Researches In Biosciences, Agriculture And Technology, 2.

Devi, J., Deb, U., Barman, S., Das, S., Sundar Bhattacharya, S., Fai Tsang, Y., Lee, J. H., & Kim, K. H. (2020). Appraisal of lignocellusoic biomass degrading potential of three earthworm species using vermireactor mediated with spent mushroom substrate: Compost quality, crystallinity, and microbial community structural analysis. Science of the Total Environment, 716:135215.

Dey, S. (2021). Microbial Resources of Alkaline Bauxite Residue and Their Possible Exploitation in Remediation and Rehabilitation. Geomicrobiology Journal, 39:219–232.

Dey, S., & Paul, A. (2021). Evaluation of physio-biochemical potentials of alkaliphilic bacterial diversity in bauxite processing residues of diverse restoration history. Environmental Sustainability, 4:155–169.

Di Carlo, E., Boullemant, A., & Courtney, R. (2019). A field assessment of bauxite residue rehabilitation strategies. Science of the Total Environment, 663:915–926.

Di Carlo, E., Boullemant, A., & Courtney, R. (2020). Ecotoxicological risk assessment of revegetated bauxite residue: Implications for future rehabilitation programmes. Science of the Total Environment, 698:134344.

Di Carlo, E., Boullemant, A., Poynton, H., & Courtney, R. (2020). Exposure of earthworm (*Eisenia fetida*) to bauxite residue: Implications for future rehabilitation programmes. Science of the Total Environment, 716:137126.

Diaz, M., Madejón, E., López, F., López, R., & Cabrera, F. (2002). Optimization of the rate vinasse/grape marc for co-composting process. Process Biochemistry, 37:1143–1150.

Diaz-Burgos, M. A., Ceccanti, B., & Polo, A. (1993). Monitoring biochemical activity during sewage sludge composting. Biology and Fertility of Soils, 16:145–150.

Dimas, D., Giannopoulou, I., & Panias, D. (2009). Utilization of alumina red mud for synthesis of inorganic polymeric materials. Mineral Processing and Extractive Metallurgy Review, 30: 211–239.

Dodoo-Arhin, D. (2013). Fabrication and Characterisation of Ghanaian Bauxite Red Mud-Clay Composite Bricks for Construction Applications. American Journal of Materials Science, 3:110-119.

Dong, L., Wentong, Z., Xiong, Y., Zou, J., Huang, Q., Xu, X., Ren, P., & Huang, G. (2021). Impact of short-term organic amendments incorporation on soil structure and hydrology in semiarid agricultural lands. International Soil and Water Conservation Research, 10:457–469.

Dong, S., Zhang, S., Wang, L., Ma, G., Lu, X., & Li, X. (2020). Concentrations, Speciation, and Bioavailability of Heavy Metals in Street Dust as well as Relationships with Physiochemcal Properties: A Case Study of Jinan City in East China. Environmental Science and Pollution Research, 27:35724–35737.

Donoghue, A. M., Frisch, N., & Olney, D. (2014). Bauxite Mining and Alumina Refining. Journal of Occupational & Environmental Medicine, 56:12–17.

Dubey, A., Mishra, R. K., Hsieh, Y., Cheng, C., Wu, B., Chen, L., Gwo, S., & Yen, T. (2020). Aluminum Plasmonics Enriched Ultraviolet GaN Photodetector with Ultrahigh Responsivity, Detectivity, and Broad Bandwidth. Advanced Science,7: 2002274.

Dubinin MM, Zaverina ED, Radushkevich, LV (1947) Sorption, and structure of activated carbons I. Investigation of organic vapor adsorption. Zhurnal Fizicheskoi Khimii, 21:1351–1362

Dubnovitsky, A. P., Kapetaniou, E. G., & Papageorgiou, A. C. (2009). Enzyme adaptation to alkaline pH: Atomic resolution (1.08 Å) structure of phosphoserine aminotransferase from *Bacillus alcalophilus*. Protein Science, 14:97–110.

Dubois M K, Gilles J K, Robers P A and Smith F. (1951). Calorimetric determination of sugar and related substance. Analytical Chemistry, 26: 351-356.

Duckworth, A. (1996). Phylogenetic diversity of soda lake alkaliphiles. FEMS Microbiology Ecology, 19:181–191.

Dume, B., Hanc, A., Svehla, P., Michal, P., Chane, A. D., & Nigussie, A. (2022). Vermicomposting Technology as a Process Able to Reduce the Content of Potentially Toxic Elements in Sewage Sludge. Agronomy, 12:2049.

Easha, N. J., Rahaman, M. S., Zaman, T., & Uddin, M. K. (2015). Feasibility Study of Vermicomposting of Textile Sludge Mixed with Cow Dung and Seed Germination Bioassay for Toxicity Evaluation of the Produced Compost. International Journal of Environmental Protection and Policy, 3:27.

Eberlein, C., Baumgarten, T., Starke, S., & Heipieper, H. J. (2018). Immediate response mechanisms of Gram-negative solvent-tolerant bacteria to cope with environmental stress: cis- trans isomerization of unsaturated fatty acids and outer membrane vesicle secretion. Applied Microbiology and Biotechnology, 102:2583–2593.

Edraki, M., Baumgartl, T., Manlapig, E., Bradshaw, D., Franks, D. M., & Moran, C. (2014). Designing mine tailings for better environmental, social and economic outcomes: A review of alternative approaches. Journal of Cleaner Production, 84:411–420.

Edwards, C. A. (2004). The Use of Earthworms in the Breakdown of Organic Wastes to Produce Vermicomposts and Animal Feed Protein. Earthworm Ecology, 359–394.

Epstein, E. (1997). The Science of Composting. Technomic Publishing Co. Inc., Lancaster, PA

17604.

Erős, T., Takács, P., Czeglédi, I., Sály, P., & Specziár, A. (2015). Taxonomic- and trait-based recolonization dynamics of a riverine fish assemblage following a large-scale human-mediated disturbance: the red mud disaster in Hungary. Hydrobiologia, 758:31–45.

Ettler, V., Cihlová, M., Jarošíková, A., Mihaljevič, M., Drahota, P., Kříbek, B., Vaněk, A., Penížek, V., Sracek, O., Klementová, M., Engel, Z., Kamona, F., & Mapani, B. (2019). Oral bioaccessibility of metal(loid)s in dust materials from mining areas of northern Namibia. Environment International, 124:205–215.

Evans, K. E. (2016). The History, Challenges, and New Developments in the Management and Use of Bauxite Residue. Journal of Sustainable Metallurgy, 2:316–331.

Evans, K., Nordheim, E., & Tsesmelis, K. (2012). Bauxite Residue Management. In John Wiley & Sons, Inc. eBooks, 61–66.

Fahad, M., Ali, S., Shah, K. H., Shahzad, A., & Abrar, M. (2019). Quantitative elemental analysis of high silica bauxite using calibration-free laser-induced breakdown spectroscopy. Applied Optics, 58: 7588.

Fathollahi, A., Khasteganan, N., Coupe, SJ., Newman, AP (2021) A meta-analysis of metalbiosorption by suspended bacteria from three phyla. Chemosphere, 268:129290.

Feigl, V., Ujaczki, É., Vaszita, E., & Molnar, M. (2017). Influence of red mud on soil microbial communities: Application and comprehensive evaluation of the Biolog EcoPlate approach as a tool in soil microbiological studies. Science of the Total Environment, 595:903–911.

Feng, Y., & Yang, C. (2018). Analysis on Physical and Mechanical Properties of Red Mud Materials and Stockpile Stability after Dilatation. Advances in Materials Science and Engineering, 2018:1–14.

Fernández-Gómez, M. J., Díaz-Raviña, M., Romero, E., & Nogales, R. (2013). Recycling of environmentally problematic plant wastes generated from greenhouse tomato crops through vermicomposting. International Journal of Environmental Science and Technology, 10:697–708.

Fernández-Gómez, M. J., Romero, E., & Nogales, R., (2010). Feasibility of vermicomposting for vegetable greenhouse waste recycling. Bioresource Technology, 101:9654–9660.

Ferreira-Baptista, L., & De Miguel, E. (2005). Geochemistry and risk assessment of street dust in Luanda, Angola: A tropical urban environment. Atmospheric Environment, 39:4501–4512.

Filipović-Kovačević, Ž., Sipos, L., & Briški, F. (2000). Biosorption of Chromium, Copper, Nickel and Zinc Ions onto Fungal Pellets of *Aspergillus niger* 405 from Aqueous Solutions. Food Technology and Biotechnology, 38:211–216

Foday, E. H. I. N. G. H. A., Jr. (2019). Characterization of Bauxite Residue in Bukit Goh, Pahang, Malaysia. Journal for Studies in Management and Planning, 4:2395-0463.

Fomina, M., & Gadd, G. M. (2014). Biosorption: current perspectives on concept, definition and application. Bioresource Technology, 160:3–14.

Forey, E., Chauvat, M., Coulibaly, S. F., Langlois, E., Barot, S., & Clause, J. (2018). Inoculation of an ecosystem engineer (Earthworm: *Lumbricus terrestris*) during experimental grassland restoration: Consequences for above and belowground soil compartments. Applied Soil Ecology, 125:148–155.

Fuller, R. C., Nelson, E. S., & Richardson, C. J. (1982). Reclamation of Red Mud (Bauxite Residues) Using Alkaline-Tolerant Grasses with Organic Amendments. Journal of Environmental Quality, 11:533–539.

Garg, V. K., & Gupta, R. (2011). Effect of Temperature Variations on Vermicompostingof Household Solid Waste and Fecundity of *Eisenia fetida*. Bioremediation Journal, 15:165– 172.

Gautam, M., & Agrawal, M. (2017). Phytoremediation of metals using vetiver (*Chrysopogon zizanioides (L.)* Roberty) grown under different levels of red mud in sludge amended soil. Journal of Geochemical Exploration, 182:218–227.

Gautam, M., & Agrawal, M. (2019). Effects of Red Mud Addition in Soil Fertilized with Cowdung Manure on Growth Performance and Metal Accumulations in *Brassica juncea*

Cultivars Kranti and Pusa Bold. Communications in Soil Science and Plant Analysis, 50:1214–1231.

Gautam, M., Pandey, B., & Agrawal, M. (2018). Identification of indicator species at abandoned red mud dumps in comparison to residential and forest sites, accredited to soil properties. Ecological Indicators, 88:88–102.

Ge, M., Zhou, H., Shen, Y., Meng, H., Li, R., Zhou, J., Cheng, H., Zhang, X., Ding, J., Wang, J., & Wang, J. (2020). Effect of aeration rates on enzymatic activity and bacterial community succession during cattle manure composting. Bioresource Technology, 304:122928.

Gelencsér, A., Kováts, N., Turóczi, B., Rostási, Á., Hoffer, A., Imre, K., Nyirő-Kósa, I., Csákberényi-Malasics, D., Tóth, Á., Czitrovszky, A., Nagy, A., Nagy, S., Ács, A., Kovács, A., Ferincz, Á., Hartyáni, Z., & Pósfai, M. (2011). The Red Mud Accident in Ajka (Hungary): Characterization and Potential Health Effects of Fugitive Dust. Environmental Science & Technology, 45:1608–1615.

Geng, C., Liu, J., Wu, S., Jia, Y., Du, B., & Yu, S. (2020). Novel method for comprehensive utilization of MSWI fly ash through co-reduction with red mud to prepare crude alloy and cleaned slag. Journal of Hazardous Materials, 384:121315.

Geva, P., Kahta, R., Nakonechny, F., Aronov, S., & Nisnevitch, M. (2016). Increased copper bioremediation ability of new transgenic and adapted Saccharomyces cerevisiae strains. Environmental Science and Pollution Research, 23:19613–19625.

Ghaedi, M., Ansari, A., Habibi, M., Asghari, A. (2014). Removal of malachite green from aqueous solution by zinc oxide nanoparticle loaded on activated carbon: Kinetics and isothermstudy. Journal of Industrial and Engineering Chemistry, 20:17–28.

Ghosh, G. K. (2021). Red and Lateritic Soils and Agri-Productivity: Issues and Strategies. Journal of the Indian Society of Soil Science, 67:104-121.

Ghosh, I., Guha, S., Balasubramaniam, R., & Kumar, A. (2011). Leaching of metals from fresh and sintered red mud. Journal of Hazardous Materials, 185: 662–668.

Golui, D., Datta, S. P., Rattan, R. K., Dwivedi, B. S., & Meena, M. C. (2014). Predicting bioavailability of metals from sludge-amended soils. Environmental Monitoring and Assessment, 186:8541–8553.

Gomes, H. I., Mayes, W. M., Rogerson, M., Stewart, D. A., & Burke, I. C. (2016). Alkaline residues and the environment: a review of impacts, management practices and opportunities. Journal of Cleaner Production, 112:3571–3582.

Gonçalo Filho, F., da Silva Dias, N., Suddarth, S. R. P., Ferreira, J. F. S., Anderson, R. G., dos Santos Fernandes, C., de Lira, R. B., Neto, M. F., & Cosme, C. R., (2019). Reclaiming Tropical Saline-Sodic Soils with Gypsum and Cow Manure. Water, 12:57.

Goswami, L., Nath, A., Sutradhar, S., Bhattacharya, S. S., Kalamdhad, A., Vellingiri, K., & Kim, K. H. (2017). Application of drum compost and vermicompost to improve soil health,growth, and yield parameters for tomato and cabbage plants. Journal of Environmental Management, 200:243–252.

Goswami, L., Patel, A. K., Dutta, G., Bhattacharyya, P., Gogoi, N., & Bhattacharya, S. S. (2013). Hazard remediation and recycling of tea industry and paper mill bottom ash throughvermiconversion. Chemosphere, 92:708–713.

Goswami, L., Pratihar, S., Dasgupta, S., Bhattacharyya, P., Mudoi, P., Bora, J. K., Bhattacharya, S. S., & Kim, K. (2016). Exploring metal detoxification and accumulation potential during vermicomposting of Tea factory coal ash: sequential extraction and fluorescence probe analysis. Scientific Reports, 6:1.

Goswami, L., Raul, P. K., Sahariah, B., Bhattacharyya, P., & Bhattacharya, S. S. (2014). Characterization and Risk Evaluation of Tea Industry Coal Ash for Environmental Suitability. Clean-soil Air Water, 42:1470–1476.

Goswami, L., Sarkar, S., Mukherjee, S., Das, S., Barman, S. R., Raul, P. K., Bhattacharyya, P., Mandal, N., Bhattacharya, S., & Bhattacharya, S. (2014). Vermicomposting of Tea Factory Coal Ash: Metal accumulation and metallothionein response in *Eisenia fetida* (Savigny) and *Lampito mauritii* (Kinberg). Bioresource Technology, 166:6–102.

Goulding, K. W. T. (2016). Soil acidification and the importance of liming agricultural soils with particular reference to the United Kingdom. Soil Use and Management. 32:390–399.

Govindasmy, R., & Chandrasekaran, S. (1992). Effect of humic acids on the growth, yield and nutrient content of sugarcane. Science of the Total Environment, 117–118:575–581.

Gowda, C., Patil, N. K. B., Patil, B. N., Awaknavar, J. S., Ninganur, B. T. and Hunje, R. (2008). Effect of organic manures on growth, seed yield and quality of wheat. Journal of AgriculturalSciences, 21: 366-368.

Gräfe, M., & Klauber, C. (2011). Bauxite residue issues: IV. Old obstacles and new pathways for in situ residue bioremediation. Hydrometallurgy, 108:46–59.

Gray, N., Lumsdon, D. G., & Hillier, S. (2016). Effect of pH on the cation exchange capacity of some halloysite nanotubes. Clay Minerals, 51:373–383.

Groth, I., Schumann, P., Rainey, F. A., Martin, K., Schuetze, B., & Augsten, K. (1997). *Bogoriella caseilytica* gen. nov., sp. nov., a New Alkaliphilic Actinomycete from a Soda Lake in Africa. International Journal of Systematic Bacteriology, 47:788–794.

Gu, H., Wang, N., & Liu, S. (2012). Radiological restrictions of using red mud as building material additive. Waste Management & Research, 30:961–965.

Guibaud, G., Comte, S., Bordas, F., Dupuy, S., & Baudu, M. (2005). Comparison of the complexation potential of extracellular polymeric substances (EPS), extracted from activated sludges and produced by pure bacteria strains, for cadmium, lead and nickel. Chemosphere, 59:629–638.

Gupta S, Kumar A (2019). Removal of nickel (II) from aqueous solution by biosorption on *A. barbadensis* Miller waste leaves powder. Applied Water Science. 9:96.

Gupta, V. K., Nayak, A., & Agarwal, S. (2015). Bioadsorbents for remediation of heavy metals: Current status and their future prospects. Environmental Engineering Research, 20:1–18.

Hackenberger, D. K., Feigl, V., Lončarić, Ž., & Hackenberger, B. K. (2019). Biochemical and reproductive effects of red mud to earthworm *Eisenia fetida*. Ecotoxicology and Environmental Safety, 168:279–286.

Hait, S., & Tare, V. (2012). Transformation and availability of nutrients and heavy metals during integrated composting–vermicomposting of sewage sludges. Ecotoxicology and Environmental Safety, 79:214–224.

Hamdy, M. K., & Williams, F. S. (2001). Bacterial amelioration of bauxite residue waste of industrial alumina plants. Journal of Industrial Microbiology & Biotechnology, 27:228–233.

Hamidpour, M., Akbari, L., & Shirani, H. (2017). Effects of Co-Application of Zeolites and Vermicompost on Speciation and Phytoavailability of Cadmium, Lead, and Zinc in a Contaminated Soil. Communications in Soil Science and Plant Analysis, 48:262–273.

Han, Q., Wang, M., Cao, J., Gui, C., Liu, Y., He, X., He, Y., & Liu, Y. (2020). Health risk assessment and bioaccessibilities of heavy metals for children in soil and dust from urban parks and schools of Jiaozuo, China. Ecotoxicology and Environmental Safety, 191:110157.

Hanif, M. A, Nadeem, R., Bhatti, H. N, Ahmad, N. R, Ansari, T. M. (2007). Ni(II) biosorption by *Cassia fistula* (Golden Shower) biomass. Journal of Hazardous Materials, 139:345–355.

He, M. M., Tian, G. M., & Liang, X. Q. (2009). Phytotoxicity and speciation of copper,zinc and lead during the aerobic composting of sewage sludge. Journal of Hazardous Materials, 163:671–677.

He, X., Zhang, Y., Shen, M., Zeng, G., Zhou, M., & Li, M. (2016). Effect of vermicomposting on concentration and speciation of heavy metals in sewage sludge with additive materials. Bioresource Technology, 218:867–873.

Hill, G. E., & Baldwin, S. A. (2012). Vermicomposting toilets, an alternative to latrine style microbial composting toilets, prove far superior in mass reduction, pathogen destruction, compost quality, and operational cost. Waste Management, 32:1811–1820.

Hirano, T., & Tamae, K., 2011. Earthworms and Soil Pollutants. Sensors, 11:11157–11167.

Hsu, M., Selvaraj, K., & Agoramoorthy, G. (2006). Taiwan's industrial heavy metal pollution threatens terrestrial biota. Environmental Pollution, 143, 327–334.

Hua, Y., Heal, K. R., & Friesl-Hanl, W. (2017). The use of red mud as an immobiliser for metal/metalloid-contaminated soil: A review. Journal of Hazardous Materials, 325:17–30.

Hussain, N., Chatterjee, S. K., Maiti, T. K., Goswami, L., Das, S., Deb, U., & Bhattacharya, S. S. (2021). Metal induced non-metallothionein protein in earthworm: A new pathway for cadmium detoxification in chloragogenous tissue. Journal of Hazardous Materials, 401:123357.

Hussain, N., Das, S., Goswami, L., Das, P., Sahariah, B., & Bhattacharya, S. S. (2018). Intensification of vermitechnology for kitchen vegetable waste and paddy straw employing

earthworm consortium: Assessment of maturity time, microbial community structure, and economic benefit. Journal of Cleaner Production, 182:414–426.

Hussain, N., Singh, A., Saha, S., Venkata Satish Kumar, M., Bhattacharyya, P., & Bhattacharya, S. S. (2016). Excellent N-fixing and P-solubilizing traits in earthworm gut-isolated bacteria: A vermicompost based assessment with vegetable market waste and rice straw feed mixtures. Bioresource Technology, 222:165–174.

Hyun, J., Endoh, S., Masuda, K., Shin, H., & Ohya, H. (2005). Reduction of chlorine in bauxite residue by fine particle separation. International Journal of Mineral Processing. 76:13-20.

Ianieva, O. (2009). Mechanisms of bacteria resistance to heavy metals. Mikrobiolohichnyĭ zhurnal (Kiev, Ukraine: 1993). 71:54-65

Ibrahim, M. M., Mahmoud, E. K., & Ibrahim, D. A. (2015). Effects of Vermicompost and Water Treatment Residuals on Soil Physical Properties and Wheat Yield. International Agrophysics, 29:157–164.

Ignat, T. Schmilovitch, Z., Fefo¨ldi, J., Bernstein, N., Steiner, B. Egozi, H., Hoffman, A. (2013). Nonlinear methods for estimation of maturity stage, total chlorophyll, and carotenoid content in intact bell peppers. Biosystems engineering, 114: 414- 425.

Irvine, G. W., Summers, K. L., & Stillman, M. J. (2013). Cysteine accessibility during As3+ metalation of the α- and β-domains of recombinant human MT1a. Biochemical and Biophysical Research Communications, 433:477–483.

Islam, F., Gault, A. G., Boothman, C., Polya, D. A., Charnock, J. M., Chatterjee, D., & Lloyd, J. R. (2004). Role of metal-reducing bacteria in arsenic release from Bengal delta sediments. Nature, 430:68–71.

Islam, M. D., Hasan, M. M., Rahaman, A., Haque, P., Islam, M. S., & Rahman, M. M. (2020). Translocation and bioaccumulation of trace metals from industrial effluent to locally grown vegetables and assessment of human health risk in Bangladesh. SN Applied Sciences, 2:8.

Ismail, S.A. (1997) Vermicology: The biology of Earthworms. Orient Longman Limited, Chennai, 92.

Jackson, M.L. (1973). Soil Chemical Analysis. Prentice Hall of India Private Limited.

Jain M, Garg V K, Kadirvelu K, Sillanpaa M, (2015) Adsorption of heavy metals from multi-metal aqueous solution by sunflower plant biomass-based carbons. International Journal of Environmental Science and Technology, 13:493–500.

Jaishankar M, Tseten T, Anbalagan N, Mathew BB, Beeregowda KN (2014) Toxicity, mechanism and health effects of some heavy metals. Interdisciplinary Toxicology, 7:60–72.

Jeyakumar, P., Debnath, C., Vijayaraghavan, R., & Muthuraj, M. (2022). Trends in Bioremediation of Heavy Metal Contaminations. Environmental Engineering Research, 28:220631–0.

JECFA (2003). Summary and conclusions of the 61st meeting of the Joint FAO/WHO Expert Committee on Food Additives (JECFA). JECFA/61/SC. Rome

Jenkinson, D.S., 1988. Determination of microbial biomass carbon and nitrogen in soil. In: Wilson, J.R. (Ed.), Advances in Nitrogen Cycling in Agricultural Ecosystems. CAB, Wallingford, 368-386.

Jiang, C., Zhao, Q., Zheng, L., Chen, X., Li, C., & Ren, M. (2021). Distribution, source and health risk assessment based on the Monte Carlo method of heavy metals in shallow groundwater in an area affected by mining activities, China. Ecotoxicology and Environmental Safety, 224:112679.

Jiao, X., Teng, Y., Zhan, Y., Wu, J., & Lin, X. (2015). Soil Heavy Metal Pollution and Risk Assessment in Shenyang Industrial District, Northeast China. PLOS ONE, 10: e0127736.

Jones, B. E. H., & Haynes, R. J. (2011). Bauxite Processing Residue: A Critical Review of Its Formation, Properties, Storage, and Revegetation. Critical Reviews in Environmental Science and Technology, 41:271–315.

Joshi, A. A., Kanekar, P. P., Kelkar, A. A., Shouche, Y. S., Vani, A. A., Borgave, S. B., & Sarnaik, S. (2008). Cultivable Bacterial Diversity of Alkaline Lonar Lake, India. Microbial Ecology, 55:163–172.

K, S. B., Krishnaiah, S., & Sahile, K. (2021). Utilization of Red Mud-Fly Ash Reinforced with Cement in Road Construction Applications. Advances in Materials Science and Engineering, 2021:1–8.

Kabir, M. H., Wang, Q., Rashid, M. H., Wang, W., & Isobe, Y. (2022). Assessment of Bioaccessibility and Health Risks of Toxic Metals in Roadside Dust of Dhaka City, Bangladesh. Atmosphere, 13:488.

Kannan, P., Banat, F., Hasan, S. W., & Haija, M. A. (2021). Neutralization of Bayer bauxite residue (red mud) by various brines: A review of chemistry and engineering processes. Hydrometallurgy, 206:105758.

Kapoor, A., Viraraghavan, T., & Cullimore, D. (1999). Removal of heavy metals using the fungus *Aspergillus niger*. Bioresource Technology, 70:95–104.

Karigar, C. S., & Rao, S. D. (2011). Role of Microbial Enzymes in the Bioremediation of Pollutants: A Review. Enzyme Research, 2011:1–11.

Karwal, M., & Kaushik, A. (2020). Co-composting and vermicomposting of coal fly-ash with press mud: Changes in nutrients, micro-nutrients and enzyme activities. Environmental Technology & Innovation, 18:100708.

Kaur, A., Singh, J., Vig, A. P., Dhaliwal, S., & Rup, P. J. (2010). Cocomposting with and without *Eisenia fetida* for conversion of toxic paper mill sludge to a soil conditioner. Bioresource Technology, 101:8192–8198.

Kauben, F., & Friedrich, B. (2016). Methods for Alkaline Recovery of Aluminum from Bauxite Residue. Journal of Sustainable Metallurgy, 2:353–364.

Kavas, T. (2006). Use of boron waste as a fluxing agent in production of red mud brick. Building and Environment, 41:1779–1783.

Kaysha, K., Shanka, D., & Bibiso, M. (2020). Performance of mung bean (*Vigna radiata* L.) varieties at different NPS rates and row spacing at Kindo Koysha district, Southern Ethiopia. Cogent Food & Agriculture, 6:1771112.

Kazy, S. K., Sar, P., Singh, S. K., Sen, A. K., & D'Souza, S. F. (2002). Extracellular Polysaccharides of a Copper-Sensitive and a Copper-Resistant *Pseudomonas aeruginosa* Strain: Synthesis, Chemical Nature and Copper Binding. World Journal of Microbiology & Biotechnology, 18:583–588.

Ke, W., Zhang, X., Zhu, F., Wu, H., Zhang, Y., Shi, Y., & Hartley, W. (2021). Appropriate human intervention stimulates the development of microbial communities and soil

formation at a long-term weathered bauxite residue disposal area. Journal of Hazardous Materials, 405: 124689.

Keita, M., & Traore, O. (2020). Environmental Impact of Open PIT Mining: Case of Bauxite Mining in Guinea -- A Review. International Journal of Applied Environmental Sciences, 15:167-177.

Khairul, M., Zanganeh, J., & Moghtaderi, B. (2019). The composition, recycling and utilisation of Bayer red mud. Resources Conservation and Recycling, 141:483–498.

Khaitan, S., Anastas, P. T., & Lowry, G. V. (2009). Mechanisms of Neutralization of Bauxite Residue by Carbon Dioxide. Journal of Environmental Engineering, 135:433–438.

Khambhaty, Y., Mody, K., Basha, S., Jha, B. (2009). Kinetics, equilibrium and thermodynamic studies on biosorption of hexavalent chromium by dead fungal biomass of marine *Aspergillus niger*. Chemical Engineering Journal, 145:489–495.

Kim, J. B., & Chon, H. (2001). Pollution of a water course impacted by acid mine drainage in the Imgok creek of the Gangreung coal field, Korea. Applied Geochemistry, 16:1387–1396.

Kirwan, L. J., Hartshorn, A. J., McMonagle, J., Fleming, L. K., & Funnell, D. (2013). Chemistry of bauxite residue neutralisation and aspects to implementation. International Journal of Mineral Processing, 119:40–50.

Kishan, D., Kushwaha, S. P. S., & Dindorkar, N. (2018). Geo-Environmental Impact of Bauxite Residue Stabilized with Fly Ash and Gypsum to Mitigate the Leaching Problems. In Sustainable civil infrastructures. Springer International Publishing. ISBN: 978-3-030-01929-7.

Kong, X., Guo, Y., Xue, S., Hartley, W., Wu, C., Ye, Y., & Cheng, Q. (2017). Natural evolution of alkaline characteristics in bauxite residue. Journal of Cleaner Production, 143:224–230.

Krishna, P., Ahn, Y., & Reddy, M. V. (2014). Bacterial diversity of extremely alkaline bauxite residue site of alumina industrial plant using culturable bacteria and residue 16S rRNA gene clones. Extremophiles, 18:665–676.

Krishna, P., Arora, A., & Reddy, M. V. (2008). An alkaliphilic and xylanolytic strain of actinomycetes *Kocuria* sp. RM1 isolated from extremely alkaline bauxite residue sites. World Journal of Microbiology & Biotechnology, 24:3079–3085.

Krishna, P., Reddy, M. V., & Patnaik, S. K. (2005). *Aspergillus Tubingensis* Reduces the pH of the Bauxite Residue (Red Mud) Amended Soils. Water Air and Soil Pollution, 167: 201–209.

Król, A., Mizerna, K., & Bożym, M. (2020). An assessment of pH-dependent release and mobility of heavy metals from metallurgical slag. Journal of Hazardous Materials, 384:121502.

Kubicek, C. P., Röhr, M., & Rehm, H. (1985). Citric Acid Fermentation. Critical Reviews in Biotechnology, 3:331–373.

Kungolos, A., Samaras, P., Tsiridis, V., Petala, M., & Sakellaropoulos, G. (2006). Bioavailability and Toxicity of Heavy Metals in the Presence of Natural Organic Matter. Journal of Environmental Science and Health, 41:1509–1517.

Kunito, T., Isomura, I., Sumi, H., Park, H. D., Toda, H., Otsuka, S., Nagaoka, K., Saeki, K., & Senoo, K. (2016). Aluminum and acidity suppress microbial activity and biomass in acidic forest soils. Soil Biology and Biochemistry, 97:23–30.

Kurniawan, T. A., Chan, G. Y., Lo, W. H., & Babel, S. (2006). Comparisons of low-cost adsorbents for treating wastewaters laden with heavy metals. Science of the Total Environment, 366:409–426.

Kutchko, B., & Kim, A. H. (2006). Fly ash characterization by SEM–EDS. Fuel, 85:2537–2544.

Kuzyakov, Y., & Xu, X. (2013). Competition between roots and microorganisms for nitrogen: mechanisms and ecological relevance. New Phytologist, 198:656–669.

Laos F, Satti P, Walter I. (2000). Nutrient availability of composted and noncomposted residues in a Patagonian Xeric Mollisol. Biology and Fertility of Soils, 31:462–469

Lasheen, & Ammar, N. (2009). Assessment of metals speciation in sewage sludge and stabilized sludge from different Wastewater Treatment Plants, Greater Cairo, Egypt. Journal of Hazardous Materials, 164:740–749.

Lazcano, C., & Dominguez, J. (2011). The Use of Vermicompost in Sustainable Agriculture: Impact on Plant Growth and Soil Fertility. Soil Nutrients, 10:1–23.

Lazcano, C., Gómez-Brandón, M., & Domínguez, J. (2008). Comparison of the effectiveness of composting and vermicomposting for the biological stabilization of cattle manure. Chemosphere, 72:1013-1019.

Ledin, M. (1996). The environmental impact of mine wastes -- Roles of microorganisms and their significance in treatment of mine wastes. Earth-Science Reviews, 41:67–108.

Leenaers, H., Okx, J., & Burrough, P. A. (1990). Comparison of spatial prediction methods for mapping floodplain soil pollution. Catena, 17:535-550

Li, W., Chen, Y., Wang, T. (2021). Cadmium biosorption by lactic acid bacteria *Weissella viridescens* ZY-6. Food Control, 123:107747.

Li, X., Li, D., Yan, Z., Ao, Y. (2018) Adsorption of cadmium by live and dead biomass of plant growth-promoting rhizobacteria. RSC Advances, 8:33523–33533.

Li, G., Zhang, Z., Sun, H., Chen, J., An, T., & Li, B. (2013). Pollution profiles, health risk of VOCs and biohazards emitted from municipal solid waste transfer station and elimination by an integrated biological-photocatalytic flow system: A pilot-scale investigation. Journal of Hazardous Materials, 250–251:147–154.

Li, L., Shi, Z., Li, L., Shen, G., Wang, X., An, L., & Zhang, J. (2010). Overexpression of ACL1 (abaxially curled leaf 1) Increased Bulliform Cells and Induced Abaxial Curling of Leaf Blades in Rice. Molecular Plant, 3:807–817.

Li, S., Zhang, Y., Feng, R., Yu, H., Pan, J., & Bian, J. (2021). Environmental Safety Analysis of Red Mud-Based Cemented Backfill on Groundwater. International Journal of Environmental Research and Public Health, 18:8094.

Li, X., Wang, Y., Qiusheng, Z., Tiangui, Q., Liu, G., Zhihong, P., & Wang, H. (2017). Transformation of hematite in diasporic bauxite during reductive Bayer digestion and recovery of iron. Transactions of Nonferrous Metals Society of China, 27:2715–2726.

Li, Y., Jiang, J., Xue, S., Millar, G. J., Kong, X., Li, X., Liu, L., & Li, C. (2018). Effect of ammonium chloride on leaching behavior of alkaline anion and sodium ion in bauxite residue. Transactions of Nonferrous Metals Society of China, 28:2125–2134.

Li, Y., Liu, C., Luan, Z., Peng, X., Zhu, C., Chen, Z., Zhang, Z., Fan, J., & Jia, Z. (2006). Phosphate removal from aqueous solutions using raw and activated red mud and fly ash. Journal of Hazardous Materials, 137:374–383.

Li, Y-H. (1979). Morphology and Anatomy of Grass Family Crops. (Shanghai Science and Technology Press, Shanghai, 138–142

Liao, J., Jiang, J., Xue, S., Qingyu, C., Wu, H., Manikandan, R., Hartley, W., & Huang, L. (2018). A novel acid-producing fungus isolated from bauxite residue: the potential to reduce the alkalinity. Geomicrobiology Journal, 35:840–847.

Lim, P. S., Wu, T. Y., Sim, E. Y. S., & Lim, S. C. (2011). The potential reuse of soybean husk as feedstock of Eudrilus eugeniae in vermicomposting. Journal of the Science of Food and Agriculture, 91:2637–2642.

Lindsay, W. L., & Norvell, W. A. (1978). Development of a DTPA Soil Test for Zinc, Iron, Manganese, and Copper. Soil Science Society of America Journal, 42:421–428.

Liu, W., Chen, X., Li, W., Yu, Y., & Yang, W. (2014). Environmental assessment, management and utilization of red mud in China. Journal of Cleaner Production, 84:606–610.

Liu, W., Yang, J., & Xiao, B. (2009). Application of Bayer red mud for iron recovery and building material production from alumosilicate residues. Journal of Hazardous Materials, 161: 474–478.

Liu, X., & Zhang, N. (2011). Utilization of red mud in cement production: A review. Waste Management & Research, 29:1053–1063.

Liu, Y., & Naidu, R. (2014). Hidden values in bauxite residue (red mud): Recovery of metals. Waste Management, 34:2662–2673.

Liu, Y., Lin, C., & Wu, Y. (2007). Characterization of red mud derived from a combined Bayer Process and bauxite calcination method. Journal of Hazardous Materials, 146:255–261.

Liu, Y., Ma, L., Li, Y., & Zheng, L., 2007. Evolution of heavy metal speciation during the aerobic composting process of sewage sludge. Chemosphere, 67:1025–1032.

Liu, Y., Naidu, R., & Ming, H. (2011). Red mud as an amendment for pollutants in solid and liquid phases. Geoderma, 163:1–12.

Lloyd, J. R., & Lovley, D. R. (2001). Microbial detoxification of metals and radionuclides. Current Opinion in Biotechnology, 12:248–253.

Lockwood, C. L., Stewart, D. A., Mortimer, R. J., Mayes, W. M., Jarvis, A. P., Gruiz, K., & Burke, I. C. (2015). Leaching of copper and nickel in soil-water systems contaminated by bauxite residue (red mud) from Ajka, Hungary: the importance of soil organic matter. Environmental Science and Pollution Research, 22:10800–10810.

Lombi, E., Hamon, R., McGrath, S. P., & McLaughlin, M. J. (2003). Lability of Cd, Cu, and Zn in Polluted Soils Treated with Lime, Beringite, and Red Mud and Identification of a Non-Labile Colloidal Fraction of Metals Using Isotopic Techniques. Environmental Science & Technology, 37:979–984.

Lowry, O. H., Rogebrough, N. J., Farr, A. L., & Randall, R. J. (1951). Protein measurementwith the folin phenol reagent. Journal of Biological Chemistry, 193: 265-275.

Lünsdorf, H., Erb, R. W., Abraham, W., & Timmis, K. N. (2000). "Clay hutches": a novel interaction between bacteria and clay minerals. Environmental Microbiology, 2:161–168.

Luo, X., Fu, X., Yang, Y., Cai, P., Peng, S., Chen, W., & Huang, Q. (2016). Microbial communities play important roles in modulating paddy soil fertility. Scientific Reports, 6.

Lv, B., Xing, M., & Yang, J. (2016). Speciation and transformation of heavy metals during vermicomposting of animal manure. Bioresource Technology, 209:397–401.

Lv, B., Xing, M., Yang, J., Qi, W., & Lu, Y. (2013). Chemical and spectroscopic characterization of water extractable organic matter during vermicomposting of cattle dung. Bioresource Technology, 132:320–326.

Lyu, F., Hu, Y., Wang, L., & Sun, W. (2021). Dealkalization processes of bauxite residue: A comprehensive review. Journal of Hazardous Materials, 403:123671.

Lyu, F., Sun, N., Sun, W., Khoso, S. A., Tang, H., & Wang, L. (2019). Preliminary assessment of revegetation potential through ryegrass growing on bauxite residue. Journal of Central South University, 26:404–409

Ma, L., Wang, H., Wu, J., Wang, Y., Zhang, D., & Liu, X. (2019). Metatranscriptomics reveals microbial adaptation and resistance to extreme environment coupling with bioleaching performance. Bioresource Technology, 280:9–17.

Ma, L., Xu, J., Chen, N., & Li, M. (2019). Microbial reduction fate of chromium (Cr) in aqueous solution by mixed bacterial consortium. Ecotoxicology and Environmental Safety, 170:763–770.

Macías-Pérez, L. A., Levard, C., Barakat, M., Angeletti, B., Borschneck, D., Poizat, L., Achouak, W., & Auffan, M. (2022). Contrasted microbial community colonization of a bauxite residue deposit marked by a complex geochemical context. Journal of Hazardous Materials, 424:127470.

Madejová, J. (2003). FTIR techniques in clay mineral studies. Vibrational Spectroscopy, 31: 1–10.

Mahmoud, M., K. Essawy & A. Doaa. (2015). Effects of vermicompost and water treatment residuals on soil physical properties and wheat yield. International Agrophysics, 29: 157-164.

Manasi, Rajesh, V., Kumar, A., & Rajesh, N. (2014). Biosorption of cadmium using a novel bacterium isolated from an electronic industry effluent. Chemical Engineering Journal, 235: 176-185.

Mandal, J., Golui, D., Raj, A., & Ganguly, P. (2019). Risk Assessment of Arsenic in Wheat and Maize Grown in Organic Matter Amended Soils of Indo-Gangetic Plain of Bihar, India. Soil and Sediment Contamination: An International Journal, 28:757–772.

Manfroi, E. P., Cheriaf, M., & Rocha, J. C. (2014). Microstructure, mineralogy and environmental evaluation of cementitious composites produced with red mud waste. Construction and Building Materials, 67:29–36.

Manikandan, S., and Thamizhiniyan, P. (2016). Effect of organic and inorganic fertilizer on phytochemical constituents in sunflower. Journal of Applied Advanced Research, 1:18-20.

Martínez, C., Rivera-Hernández, M., Álvarez, L. J., Rodríguez, I. A., Ruiz, F., & Compeán-García, V. (2020). Biosynthesis and characterization of cadmium carbonate crystals by anaerobic granular sludge capable of precipitate cadmium. Materials Chemistry and Physics, 246:122797.

Masion, A., Vilgé-Ritter, A., Rose, J., Stone, W. E. E., Teppen, B. J., Rybacki, D., & Bottero, J. Y. (2000). Coagulation-Flocculation of Natural Organic Matter with Al Salts:

Speciation and Structure of the Aggregates. Environmental Science & Technology, 34:3242–3246.

Masoudi, R., Moghimi, H., Azin, E., Taheri, R.A. (2018) Adsorption of cadmium from aqueous solutions by novel Fe_3O_4- newly isolated *Actinomucor* sp. bio-nanoadsorbent: functional group study. Artificial Cells, Nanomedicine, and Biotechnology, 46: S1092–S1101.

Mathivanan, K., Chandirika, J. U., Mathimani, T., Rajaram, R., Annadurai, G., Yin, H. (2021) Production and functionality of exopolysaccharides in bacteria exposed to a toxic metal environment. Ecotoxicology and Environmental Safety, 208:111-567.

Mayes, W. M., Burke, I. C., Gomes, H. I., Anton, Á. D., Molnár, M., Feigl, V., & Ujaczki, É. (2016). Advances in Understanding Environmental Risks of Red Mud After the Ajka Spill, Hungary. Journal of Sustainable Metallurgy, 2:332–343.

Mayes, W. M., Jarvis, A. P., Burke, I. C., Walton, M., Feigl, V., Klebercz, O., & Gruiz, K. (2011). Dispersal and Attenuation of Trace Contaminants Downstream of the Ajka Bauxite Residue (Red Mud) Depository Failure, Hungary. Environmental Science & Technology. 45:5147–5155.

Mclean, E.O. (1965). Soil pH and lime requirement, in: C.A. Black (Ed.), Methods of Soil Analysis. Part II, American Society of Agronomy. Madison, WI, USA.

McMahon, P. L., & Chapelle, F. H. (1991). Microbial production of organic acids in aquitard sediments and its role in aquifer geochemistry. Nature, 349:233–235.

Medina-Sauza, R. M., Álvarez-Jiménez, M., Delhal, A., Reverchon, F., Blouin, M., Guerrero-Analco, J. A., Cerdan, C., Guevara, R., Villain, L., & Barois, I. (2019). Earthworms Building Up Soil Microbiota, a Review. Frontiers in Environmental Science, 7.

Mekonnen, E., Yitbarek, M., Soreta, T.R. (2015). Kinetic and thermodynamic studies of the adsorption of Cr(VI) onto some selected local adsorbents. South African Journal of Chemistry, 68.

Meyer, F. M. (2004). Availability of Bauxite Reserves. Natural Resources Research, 13:161–172.

Mihankhah, T., Saeedi, M., & Karbassi, A. (2020). A comparative study of elemental pollution and health risk assessment in urban dust of different land-uses in Tehran's urban area. Chemosphere, 241:124984.

Milačič, R., Zuliani, T., & Ščančar, J. (2012). Environmental impact of toxic elements in red mud studied by fractionation and speciation procedures. Science of the Total Environment, 426:359–365.

Mirecki, N., R. Agic, L. Sunic, L. Milenkovic, and Z. S. Ilic. (2015). Transfer factor as indicator of heavy metals content in plants. Fresenius Environmental Bulletin, 24:4212–19.

Mishra, N., & Das, N. (2017). Coal Mining and Local Environment: A Study in Talcher Coalfield of India. Air, Soil and Water Research. 10:117862211772891.

Mishra, T., & Pandey, V. C. (2019). Phytoremediation of Red Mud Deposits Through Natural Succession. In Elsevier eBooks, 409–424.

Misra, V., & Pandey, S. (2005). Hazardous waste, impact on health and environment for development of better waste management strategies in future in India. Environment International, 31:417–431.

Mohanan, K., & Mini, C. B. (2008). Relative Contribution of Rice Tillers of Different Status Towards Yield. International Journal of Plant Breeding and Genetics, 2:9–12.

Mohapatra, R.K., Parhi, P.K., Pandey, S., Bindhani, B.K., Thatoi, H., Panda, C.R. (2019). Active and passive biosorption of Pb(II)using live and dead biomass of marine bacterium *Bacillus xiamenensis* PbRPSD202: Kinetics and isotherm studies. Journal of Environmental Management, 247:121–134.

Mohy Eldin, M., Aly, K., Khan, Z., Mekky, A., Saleh, T., Al-Bogami, A. (2016). Removal of methylene blue from synthetic aqueous solutions with novel phosphoric acid-doped pyrazole- g-poly (glycidyl methacrylate) particles: kinetic and equilibrium studies. Desalination and Water Treatment, 57:27243–27258.

Mondal, A., Das, S., Sah, R. K., Bhattacharyya, P., & Bhattacharya, S. S. (2017). Environmental footprints of brick kiln bottom ashes: Geostatistical approach for assessment of metal toxicity. Science of The Total Environment, 609:215–224.

Mondal, A., Goswami, L., Hussain, N., Barman, S., Kalita, E., Bhattacharyya, P., & Bhattacharya, S. S. (2020). Detoxification and eco-friendly recycling of brick kiln coal ash using*Eisenia fetida*: A clean approach through vermitechnology, Chemosphere, 244:125470.

Mondal, N. K., Samanta, A., Dutta, S., & Chattoraj, S. (2017). Optimization of Cr(VI) biosorption onto *Aspergillus niger* using 3-level Box-Behnken design: Equilibrium, kinetic,

thermodynamic and regeneration studies. Journal of Genetic Engineering and Biotechnology, 15:151–160.

Moorhead, D. L., Sinsabaugh, R. L., Hill, B. H., & Weintraub, M. N. (2016). Vector analysis of ecoenzyme activities reveal constraints on coupled C, N and P dynamics. Soil Biology and Biochemistry, 93:1–7.

Moorhead, D.L., & Sinsabaugh, R.L. (2006). A theoretical model of litter decay and microbial interaction. Ecological Monographs, 76:151–174.

Morgan, J. E., & Morgan, A. J. (1990). The distribution of cadmium, copper, lead, zinc and calcium in the tissues of the earthworm *Lumbricus rubellus* sampled from one uncontaminated and four polluted soils. Oecologia, 84:559–566.

Mukiza, E., Zhang, L., Liu, X., & Zhang, N. (2019). Utilization of red mud in road base and subgrade materials: A review. Resources Conservation and Recycling, 141:187–199.

Muñoz, A, J., Espínola, F., Moya, M., Ruiz, E. (2015). Biosorption of Pb(II) Ions by *Klebsiella* sp. 3S1 Isolated from a Wastewater Treatment Plant: Kinetics and Mechanisms Studies. BioMed Research International, 719060:1–12.

Nagarajan, N., Gunasekaran, P., Rajendran, P. (2015). Genetic characterization, nickel tolerance, biosorption, kinetics, and uptake mechanism of a bacterium isolated from electroplating industrial effluent. Canadian Journal of Microbiology, 61:297–306.

Nagvenkar, G. S., & Ramaiah, N. (2010). Arsenite tolerance and biotransformation potential in estuarine bacteria. Ecotoxicology, 19:604–613.

Nanda, M., Kumar, V., & Sharma, D. (2019). Multimetal tolerance mechanisms in bacteria: The resistance strategies acquired by bacteria that can be exploited to 'clean-up' heavy metal contaminants from water. Aquatic Toxicology, 212:1–10.

Nannipieri, P., Ascher, J., Ceccherini, M. T., Landi, L., Pietramellara, G., & Renella, G. (2003). Microbial diversity and soil functions. European Journal of Soil Science, 54:655–670.

Naskar, A., Majumder, R., & Goswami, M. (2020). Bioaccumulation of Ni(II) on growing cells of Bacillus sp.: Response surface modeling and mechanistic insight. Environmental Technology and Innovation, 20:101057.

Naykodi, A., Patankar, S. C., & Thorat, B. N. (2022). Alkaliphiles for comprehensive utilization of red mud (bauxite residue)—an alkaline waste from the alumina refinery. Environmental Science and Pollution Research, 30:9350–9368.

Netzahuatl-Muñoz, A. R., Cristiani-Urbina, M. D. C., & Cristiani-Urbina, E. (2015). Chromium Biosorption from Cr (VI) Aqueous Solutions by *Cupressus lusitanica* Bark: Kinetics, Equilibrium and Thermodynamic Studies. PLOS ONE, 10: e0137086.

Newsome, L., & Falagán, C. (2021). The Microbiology of Metal Mine Waste: Bioremediation Applications and Implications for Planetary Health. Geohealth, 5.

Ni, F., Peng, X., Zhao, Y., He, J., Cao, Y., & Luan, Z. (2012). Preparation of coagulant from red mud and semi-product of polyaluminum chloride for removal of phosphate from water. Desalination and Water Treatment. 40:153–158.

Nie, Q., Liu, Y., Wang, G., & Bai, B. (2020). Physicochemical and Microstructural Properties of Red Muds under Acidic and Alkaline Conditions. Applied Sciences, 10:2993.

Nikaeen, M., Nafez, A. H., Bina, B., Nabavi, B. F., & Hassanzadeh, A., (2015). Respiration and enzymatic activities as indicators of stabilization of sewage sludge composting. Waste Management, 39:104–110.

Nikolova, R., Boteva, S., Kenarova, A., Dinev, N., & Radeva, G., 2023. Enzyme activities in soils under heavy metal pollution: a case study from the surroundings of a non-ferrous metal plant in Bulgaria. Biotechnology & Biotechnological Equipment, 37:49–57.

Nogueira, E.W., Hayash, E.A., Alves, E., Lima, C.A.D.A., Adorno, M.T., Brucha, G. (2017). Characterization of Alkaliphilic Bacteria Isolated from Bauxite Residue in the Southern Region of Minas Gerais, Brazil. Brazilian Archives of Biology and Technology, 60.

Noreen, Z., Hameed, A., & Faryal, R. (2010). Comparative Analysis of Biosorption Potential for Chromium Removal by Live and Dead Biomass of *Aspergillus niger* ZH2. International Journal of Chemical Reactor Engineering, 8.

Nucifora, G., Chu, L., Misra, T. K., & Silver, S. (1989). Cadmium resistance from *Staphylococcus aureus* plasmid pI258 *cadA* gene results from a cadmium-efflux ATPase. Proceedings of the National Academy of Sciences of the United States of America, 86:3544–3548.

Nuhoglu, Y., & Malkoc, E. (2009). Thermodynamic and kinetic studies for environmentaly friendly Ni(II) biosorption using waste pomace of olive oil factory. Bioresource Technology, 100:2375–2380.

Obhodas, J., Sudac, D., Matjacic, L., & Valkovic, V. (2012). Red Mud Characterization Using Atomic and Nuclear Analytical Techniques. IEEE Transactions on Nuclear Science, 59:1453–1457.

Opiso, E. M., Tabelin, C. B., Maestre, C. V., Aseniero, J. P. J., Park, I., & Villacorte-Tabelin, M. (2021). Synthesis and characterization of coal fly ash and palm oil fuel ash modified artisanal and small-scale gold mine (ASGM) tailings based geopolymer using sugar mill lime sludge as Ca-based activator. Heliyon, 7:e06654.

Ordóñez, S., Sastre, H., & Díez, F. V. (2001). Catalytic hydrodechlorination of tetrachloroethylene over red mud. Journal of Hazardous Materials, 81:103–114.

Osman, G., Abulreesh, H. H., Elbanna, K., Shaaban, M. R., Samreen, S., & Ahmad, I. (2019). Recent Progress in Metal-Microbe Interactions: Prospects in Bioremediation. Journal of Pure and Applied Microbiology, 13:13–26.

Oves, M., Khan, M.S., Zaidi, A. (2013). Biosorption of heavy metals by *Bacillus thuringiensis* strain OSM29 originating from industrial effluent contaminated north Indian soil. Saudi Journal of Biological Sciences, 20:121–129.

Özdemir, S., Kilinc, E., Poli, A., Nicolaus, B., & Güven, K. (2009). Biosorption of Cd, Cu, Ni, Mn and Zn from aqueous solutions by thermophilic bacteria, *Geobacillus toebii* sub.sp. *decanicus* and *Geobacillus thermoleovorans* sub.sp. *stromboliensis*: Equilibrium, kinetic and thermodynamic studies. Chemical Engineering Journal, 152:195–206.

Özden, B., Brennan, C., & Landsberger, S. (2019). Investigation of bauxite residue (red mud) in terms of its environmental risk. Journal of Radioanalytical and Nuclear Chemistry, 319: 339–346.

Page, A.L., Miller, R.H., Keeney, D.R. (1982) Methods of Soil Analysis - Part 2. Soil Sci Soc Am, Madison.

Page, V., & Feller, U. (2015). Heavy Metals in Crop Plants: Transport and Redistribution Processes on the Whole Plant Level. Agronomy, 5:447–463.

Pakade, V.E., Ntuli, T.D., Ofomaja, A.E. (2017) Biosorption of hexavalent chromium from aqueous solutions by Macadamia nutshell powder. Applied Water Science,7:3015-3030.

Pal, R., Bhattacharyya, P., Das, P., Chakrabarti, K., Chakraborty, A., & Kim, K. (2007). Relationship between acidity and microbiological properties in some tea soils. Biology and Fertility of Soils, 44:399–404.

Palmer, S. J., Nothling, M. D., Bakon, K. H., & Frost, R. L. (2010). Thermally activated seawater neutralised red mud used for the removal of arsenate, vanadate and molybdate from aqueous solutions. Journal of Colloid and Interface Science, 342:147–154.

Pande, V., Pandey, S. K., Sati, D., Bhatt, P., & Samant, M. (2022). Microbial Interventions in Bioremediation of Heavy Metal Contaminants in Agroecosystem. Frontiers in Microbiology, 13.

Pandey, A., & Prakash, R. (2020). Opportunities for sustainability improvement in aluminum industry. Engineering Reports, 2.

Pandey, B., Agrawal, M., & Singh, S. (2014). Coal mining activities change plant community structure due to air pollution and soil degradation. Ecotoxicology, 23:1474–1483.

Panias, D., Giannopoulos, I. P., Perraki, T. (2007). Effect of synthesis parameters on the mechanical properties of fly ash-based geopolymers. Colloids and Surfaces A: Physicochemical and Engineering Aspects, 301:246–254

Paramguru, R. K., Rath, P. C., & Misra, V. (2004). Trends in red mud utilization – A review. Mineral Processing and Extractive Metallurgy Review, 26:1–29.

Parbat, R. N. (1996). Emerging uses of aluminium in late 20th and early 21st century. Bulletin of Materials Science, 19:1017–1023.

Pardo, R., Herguedas, M., Barrado, E., & Vega, M. (2003). Biosorption of cadmium, copper, lead and zinc by inactive biomass of *Pseudomonas putida*. Analytical and Bioanalytical Chemistry, 376:26–32

Paredes, J. M., Ordóñez, S., Vega, A., & Díez, F. V. (2004). Catalytic combustion of methane over red mud-based catalysts. Applied Catalysis B-environmental, 47:37–45.

Pasricha, S., Mathur, V., Garg, A., Lenka, S., Verma, K., & Agarwal, S. (2021). Molecular mechanisms underlying heavy metal uptake, translocation and tolerance in hyperaccumulators-an analysis. Environmental Challenges, 4,

Patel, S., Pal, B. K., & Patel, R. K. (2018). A novel approach in red mud neutralization using cow dung. Environmental Science and Pollution Research, 25:12841–12848.

Paul, S., Das, S., Raul, P., & Bhattacharya, S. S., 2018. Vermi-sanitization of toxic silk industry waste employing *Eisenia fetida* and *Eudrilus eugeniae*: Substrate compatibility, nutrient enrichment and metal accumulation dynamics. Bioresource Technology, 266:267–274.

Paul, S., Goswami, L., Pegu, R., & Bhattacharya, S. S. (2020). Vermiremediation of cotton textile sludge by *Eudrilus eugeniae*: Insight into metal budgeting, chromium speciation, and humic substance interactions. Bioresource Technology, 314:123753.

Paul, S., Pegu, R., Das, S., Kim, K., & Bhattacharya, S. S. (2022). Eco-geological consequences of textile processing wastes: Risk assessment, elemental dissolution kinetics, and health hazard potential. Environmental Research, 216:114693.

Peech, M., Cowan, R. L., & Baker, J. H. (1962). A Critical Study of the BaCl2-Triethanolamine and the Ammonium Acetate Methods for Determining the Exchangeable Hydrogen Content of Soils. Soil Science Society of America Journal, 26:37–40.

Peng, F., Liang, K., Shao, H., & Hu, A. (2005). Nano-crystal glass-ceramics obtained by crystallization of vitrified red mud. Chemosphere, 59:899–903.

Pervaiz, I., Ahmad, S., Madni, M. A., Ahmad, H., & Khaliq, F. H. (2013). Microbial biotransformation: a tool for drug designing. Applied Biochemistry and Microbiology, 49: 437–450.

Piearce, T. G., Oates, K., & Carruthers, W. J. (1990). A fossil earthworm embryo (Oligochaeta) from beneath a Late Bronze Age midden at Potterne, Wiltshire, UK. Journal of Zoology, 220: 537–542.

Ponnamperuma, F. N. (1972). The Chemistry of Submerged Soils. Advances in Agronomy, 24:29–96.

Power, G., Gräfe, M., & Klauber, C. (2011). Bauxite residue issues: I. Current management, disposal and storage practices. Hydrometallurgy, 108:33–45.

Powlson, D., Brookes, P., & Christensen, B. (1987). Measurement of soil microbial biomass provides an early indication of changes in total soil organic matter due to straw incorporation. Soil Biology and Biochemistry, 19:159–164.

Prabha, M. (2007). Comparative studies on the digestive enzymes in the gut of earthworms, Eudrilus eugeniae and Eisenia fetida. Indian Journal of Biotechnology, 6:567-569.

Pradhan, A., & Sahoo, S.K. (2012). Effect of Rice Mill wastewater on soil respiration and enzyme activities under field and pot conditions. Asian Journal of Water, Environment & Pollution, 9:61-71

Pradhan, J., Das, S., & Thakur, R. S. (1999). Adsorption of Hexavalent Chromium from Aqueous Solution by Using Activated Red Mud. Journal of Colloid and Interface Science, 217:137–141.

Prasad, N. (2006). Development and Characterization of Metal Matrix Composite Using Red Mud an Industrial Waste for Wear Resistant Applications. Ph.D.-Thesis. NITRKL.

Priyadarshanee, M., & Das, S. (2021) Biosorption and removal of toxic heavy metals by metal tolerating bacteria for bioremediation of metal contamination: A comprehensive review. Journal of Environmental Chemical Engineering, 9:104686.

Qaidi, S. M. A., Tayeh, B. A., Isleem, H. F., De Azevedo, A. R. G., Ahmed, H. U., & Emad, W. (2022). Sustainable utilization of red mud waste (bauxite residue) and slag for the production of geopolymer composites: A review. Case Studies in Construction Materials,16: e00994-. 00994

Qi, Y. (2012). Vermiculture Technology: Earthworms, Organic Wastes, and Environmental Management. International Journal of Environmental Studies, 69:173–174.

Qi, Y. (2021). The neutralization and recycling of red mud –A review. Journal of Physics, 1759: 012004.

Qu, Y., Li, H., Wang, X., Tian, W., Shi, B., Yao, M., & Zhang, Y. (2019). Bioleaching of Major, Rare Earth, and Radioactive Elements from Red Mud by using Indigenous Chemoheterotrophic Bacterium *Acetobacter* sp. Minerals, 9:67.

Quintelas, C., Rocha, Z., Silva, B., Fonseca, B., Figueiredo, H., & Tavares, T., 2009. Removal of Cd(II), Cr(VI), Fe(III) and Ni(II) from aqueous solutions by an *E. coli* biofilm supported on kaolin. Chemical Engineering Journal, 149:319–324.

Rahman, A., Lee, S. Y., Ji, H., Kabir, A. H., Jones, C., & Lee, K. W. (2018). Importance of Mineral Nutrition for Mitigating Aluminum Toxicity in Plants on Acidic Soils: Current Status and Opportunities. International Journal of Molecular Sciences, 19:3073.

Rahman, M., Hossain, M., Ali, M., Anik, M., & Alam, F. (2019). Effects of arbuscular mycorrhizal fungi, rhizobium and phosphorus on mung bean (*Vigna radiata*) in saline soil. Bangladesh Journal of Agricultural Research, 44:153–165.

Rahman, Z., Thomas, L., & Singh, V. P. (2019). Biosorption of heavy metals by a lead (Pb) resistant bacterium, *Staphylococcus hominis* strain AMB-2. Journal of Basic Microbiology, 59: 477–486.

Rai, S., Wasewar, L. K., Mishra, R., S., Puttewar, S. P., Chaddha, M. J., Mukhopadhyay, J., Chang, K. Y. (2013). Neutralization of Red Mud Using Inorganic Acids. ResearchJournal of Chemistry and Environment, 17:10-17.

Rai, S., Bahadure, S., Chaddha, M. J., & Agnihotri, A. N. (2020). Disposal Practices and Utilization of Red Mud (Bauxite Residue): A Review in Indian Context and Abroad. Journal of Sustainable Metallurgy, 6:1–8.

Rai, S., Mukhopadhyay, J., Yoo, C., & Uslu, H. (2012). Neutralization and utilization of red mud for its better waste management. Archives of Environmental Science, 6:13-33.

Rai, S., Wasewar, K. L., Lataye, D. H., Mishra, R. S., Puttewar, S., Chaddha, M. J., Mahindiran, P., & Mukhopadhyay, J. (2012). Neutralization of red mud with pickling waste liquor using Taguchi's design of experimental methodology. Waste Management & Research, 30:922–930.

Raiesi, F., & Sadeghi, E. (2019). Interactive effect of salinity and cadmium toxicity on soil microbial properties and enzyme activities. Ecotoxicology and Environmental Safety, 168: 221–229.

Rajkhowa, D. J., Saikia, M., & Rajkhowa, K. (2002). Effect of vermicompost with and without fertilizer on green gram. Legume Research, 25:295–296.

Ramaswamy, P., Gomes, S. A., & Ravichander, N. (2019). Utilization of aluminum dross: Refractories from industrial waste. *IOP* Conference Series: Materials Science and Engineering, 577: 012101.

Ramírez, A., Gómez, L., Müller, A. J., & De Rojas De Gáscue, B. R. (2022). Characterization and Modification of Red Mud and Ferrosilicomanganese Fines and Their Application in the Synthesis of Hybrid Hydrogels. Polymers. 14:4330.

Rani, A. & Goel, R. (2009). Strategies for Crop Improvement in Contaminated Soils Using Metal Tolerant Bioinoculants. In: Khan, M.S., Zaidi, A. and Mussarat, J., Eds., Microbial Strategies for Crop Improvement, Springer, Berlin,105-132.

Rao, B. D., & Reddy, N. (2017). Zeta Potential and Particle Size Characteristics of Red Mud Waste. Developments in geotechnical engineering. Springer Nature. Eds., 1:69–89.

Rashid, M. H., Rahman, M. M., & Naidu, R. (2022). Zinc Biofortification through Basal Zinc Supply Reduces Grain Cadmium in Mung Beans: Metal Partitioning and Health Risks Assessment. Toxics, 10:689.

Rasulov, B. A., Aisa, H. A., & Aisa, H. A. (2013). Biosorption of Metal Ions by Exopolysaccharide Produced by *Azotobacter chroococcum* XU1. Indian Journal of Environmental Protection, 4:989-993

Ravindran, B., Wong, J. W. C., Selvam, A., & Sekaran, G. (2016). Influence of microbial diversity and plant growth hormones in compost and vermicompost from fermented tannery waste. Bioresource Technology, 217:200–204.

RDA (Recommended Dietary Allowance) (1989). Recommended Dietary Allowance. Eds., 10th. National Academic Press, Washington

Raghubanshi, A. S., Mudgal, M., Chouhan, R. K., Kumar, A., Srivastava, A. K. (2022) Recycling and potential utilization of red mud (Bauxite Residue) for construction industry applications. Indian Journal of Engineering and Materials Sciences, 29:4.

Ren, B., Zhang, Q., Zhang, X., Zhao, L., Li, H. (2018) Biosorption of Cr (VI) from aqueous solution using dormant spores of *Aspergillus niger*. RSC Advances. 8:38157–38165.

Ren, G., Jin, Y., Zhang, C., Gu, H., Qu, J. (2015). Characteristics of *Bacillus sp*. PZ-1 and its biosorption to Pb (II). Ecotoxicology Environment Safety, 117:141–148.

Richards, R. H., Heguy, A., & Karin, M. (1984). Structural and functional analysis of the human metallothionein-IA gene: Differential induction by metal ions and glucocorticoids. Cell, 37: 263–272.

Romera, E., González, F., Ballester, A., Blázquez, M., & Muñoz, J. (2007). Comparative study of biosorption of heavy metals using different types of algae. Bioresource Technology, 98: 3344–3353

Rosen, B. P. (2002). Biochemistry of arsenic detoxification. FEBS Letters, 529:86–92.

Rousk, J., Brookes, P. C., & Bååth, E. (2009). Contrasting Soil pH Effects on Fungal and Bacterial Growth Suggest Functional Redundancy in Carbon Mineralization. Applied and Environmental Microbiology, 75:1589–1596.

Rout, S. N., Sahoo, T., & Das, S. K. (2013). Design of tailing dam using red mud. Open Engineering, 3.

Roy, S., Sarkar, D., Datta, R., Bhattacharya, S. S., & Bhattacharyya, P. (2022). Assessing the arsenic-saturated biochar recycling potential of vermitechnology: Insights on nutrient recovery, metal benignity, and microbial activity. Chemosphere, 286:131660.

Rubinos, D. A., & Barral, M. T. (2013). Fractionation and mobility of metals in bauxite red mud. Environmental Science and Pollution Research, 20:7787–7802.

Ruby, M. V., Davis, A., Schoof, R., Eberle, S., & Sellstone, C. M. (1996). Estimation of Lead and Arsenic Bioavailability Using a Physiologically Based Extraction Test. Environmental Science & Technology, 30:422–430.

Rupani, P. F., Embrandiri, A., Ibrahim, M. H., Ghole, V., Lee, C. T., & Abbaspour, M. (2018). Effects of different vermicompost extracts of palm oil mill effluent and palm-pressed fibre mixture on seed germination of mung bean and its relative toxicity. Environmental Science and Pollution Research, 25:35805–35810.

Saha, P. D., & Datta, S. (2009). Assessment on thermodynamics and kinetics parameters on reduction of methylene blue dye using fly ash. Desalination and Water Treatment, 12:219–228.

Sahariah, B., Das, S., Goswami, L., Paul, S., Bhattacharyya, P., & Bhattacharya, S. S. (2020). An avenue for replacement of chemical fertilization under rice-rice cropping pattern: Sustaining soil health and organic C pool via MSW-based vermicomposts. Archives of Agronomy and Soil Science, 66:1449–1465.

Sahariah, B., Goswami, L., Farooqui, I. A., Raul, P., Bhattacharyya, P., & Bhattacharya, S. S. (2015). Solubility, hydrogeochemical impact, and health assessment of toxic metals in

municipal wastes of two differently populated cities. Journal of Geochemical Exploration, 157: 100–109.

Sahariah, B., Goswami, L., Kim, K. H., Bhattacharyya, P., & Bhattacharya, S. S., 2015. Metal remediation and biodegradation potential of earthworm species on municipal solid waste: A parallel analysis between *Metaphire posthuma* and *Eisenia fetida*. Bioresource Technology, 180:230–236.

Sahmoune, M. N. (2018). Performance of Streptomyces rimosus biomass in biosorption of heavy metals from aqueous solutions. Microchemical Journal, 141:87–95.

Sahoo, P. K., Bhattacharyya, P., Tripathy, S., Equeenuddin, S. M., & Panigrahi, M. (2010). Influence of different forms of acidities on soil microbiological properties and enzyme activities at an acid mine drainage contaminated site. Journal of Hazardous Materials, 179: 966–975.

Sahoo, S., Mishra, P., & Mohapatra, B. K. (2017). Morphological and microstructural characteristics of bauxite developed over a part of Precambrian Iron Ore Group of rocks, Sundergarh District, Eastern India. Arabian Journal of Geosciences, 10.

Sahu, R. C., Patel, R. K., & Ray, B. C. (2010). Neutralization of red mud using CO2 sequestration cycle. Journal of Hazardous Materials, 179:28–34.

Sahu, R. C., Patel, R. K., & Ray, B. C. (2011). Removal of hydrogen sulfide using red mud at ambient conditions. Fuel Processing Technology, 92:1587–1592.

Saikia, B. J., & Parthasarathy, G. (2010). Fourier Transform Infrared Spectroscopic Characterization of Kaolinite from Assam and Meghalaya, Northeastern India. Journal of Modern Physics, 01:206–210.

Sajjad, W., Zheng, G., Ma, X., Xu, W., Ali, B., Rafiq, M., Zada, S., Irfan, M., & Zeman, J. (2020). Dissolution of Cu and Zn-bearing ore by indigenous iron-oxidizing bacterial consortia supplemented with dried bamboo sawdust and variations in bacterial structural dynamics: A new concept in bioleaching. Science of the Total Environment, 709:136136.

Samal, S., Ray, A. K., & Bandopadhyay, A. (2013). Proposal for resources, utilization and processes of red mud in India — A review. International Journal of Mineral Processing. 118: 43–55.

Sambrook J (2001) Molecular Cloning: A Laboratory Manual, Third Edition (3 volume set) (3rd ed.). Cold Spring Harbor Laboratory Press.

Sanders, R. D. (2002). Aluminum and Aluminum Alloys. Kirk-Othmer Encyclopedia of Chemical Technology, 2:279-343

Santana, N. A., Ferreira, P. H., Tarouco, C. P., Schardong, I. S., Antoniolli, Z. I., Nicoloso, F. T., & Jacques, R. J. S. (2019). Earthworms and mycorrhization increase copper phytoextraction by *Canavalia ensiformis* in sandy soil. Ecotoxicology and Environmental Safety, 182:109383.

Santini, T. C., Kerr, J. M., & Warren, L. A. (2015). Microbially-driven strategies for bioremediation of bauxite residue. Journal of Hazardous Materials, 293:131–157.

Santini, T. C., Warren, L. A., & Kendra, K. E. (2015). Microbial Diversity in Engineered Haloalkaline Environments Shaped by Shared Geochemical Drivers Observed in Natural Analogues. Applied and Environmental Microbiology, 81:5026–5036.

Sanyal SK (1991) Ionic environment of acid soils. In: Mohsin MA, Sarkar AK, Mathur BS (eds) Acid soil management. Kalyani, New Delhi, India. 3–21

Saranya, K., Sundaramanickam, A., Shekhar, S., Meena, M., Sathishkumar, R. S., & Balasubramanian, T. (2018). Biosorption of multi-heavy metals by coral associated phosphate solubilising bacteria *Cronobacter muytjensii* KSCAS2. Journal of Environmental Management, 222:396–401.

Šarapatka, B. (2003). Phosphatase Activities (ACP, ALP) in Agroecosystem Soils. Ph.D. thesis.

Saravanane, R., Sundararajan, T., Sivamurthyreddy, S. (2002) Efficiency of chemically modified low-cost adsorbents for the removal of heavy metals from wastewater: a comparative study". Indian Journal of Environmental Health, 44:78–81

Schmalenberger, A., O'Sullivan, O., Gahan, J., Cotter, P. D., & Courtney, R. (2013). Bacterial Communities Established in Bauxite Residues with Different Restoration Histories. Environmental Science & Technology, 47:7110–7119.

Schmidt, M. W. I., Torn, M. S., Abiven, S., Dittmar, T., Guggenberger, G., Janssens, I. A., Kleber, M., Kögel-Knabner, I., Lehmann, J., Manning, D. A. C., Nannipieri, P., Rasse, D.

P., Weiner, S., & Trumbore, S. E. (2011). Persistence of soil organic matter as an ecosystem property. Nature, 478:49–56.

Schnürer, J., & Rosswall, T. (1982). Fluorescein Diacetate Hydrolysis as a Measure of Total Microbial Activity in Soil and Litter. Applied and Environmental Microbiology, 43:1256–1261.

Schwarz, M., & Lalík, V. (2012). Possibilities of Exploitation of Bauxite Residue from Alumina Production.

Senff, L., Hotza, D., & Labrincha, J. A. (2011). Effect of red mud addition on the rheological behaviour and on hardened state characteristics of cement mortars. Construction and Building Materials, 25:163–170.

Sglavo, V. M., Campostrini, R., Maurina, S., Carturan, G., Monagheddu, M., Budroni, G., & Cocco, G. (2000). Bauxite 'red mud' in the ceramic industry. Part 1: thermal behaviour. Journal of the European Ceramic Society, 20:235–244.

Shahpiri, A., & Mohammadzadeh, A. (2018). Mercury removal by engineered Escherichia coli cells expressing different rice metallothionein isoforms. Annals of Microbiology, 68:145–152.

Shankar, T., Mariappan, V., Isaiarasu, L. (2011). Screening Cellulolytic Bacteria from the Mid-Gut of the Popular Composting Earthworm, *Eudrilus eugeniae* (Kinberg). World Journal of Zoology, 6:142-148.

Shannon, C., 1948. A mathematical theory of communication. Bell System Technical Journal archives, 27:379–423.

Sharma, K., & Garg, V. K. (2017). Management of food and vegetable processing waste spiked with buffalo waste using earthworms (*Eisenia fetida*). Environmental Science and Pollution Research, 24:7829–7836

Sharma, P. K., Balkwill, D. L., Frenkel, A. I., & Vairavamurthy, M. A. (2000). A New *Klebsiella planticola* Strain (Cd-1) Grows Anaerobically at High Cadmium Concentrations and Precipitates Cadmium Sulfide. Applied and Environmental Microbiology, 66:3083–3087.

Sharma, S., Pradhan, K., Satya, S., Vasudevan, P., & Khas, H. (2005). Potentiality of Earthworms for Waste Management and in Other Uses - A Review. Journal of American Science. 1.

Shen, G., Cao, L., Lu, Y., & Hong, J. (2005). Influence of Phenanthrene on Cadmium Toxicity to Soil Enzymes and Microbial Growth. Environmental Science and Pollution Research, 12:259–263.

Shi, Z., Cao, Z., Qin, D., Zhu, W., Wang, Q., Li, M., & Wang, G. (2013). Correlation Models between Environmental Factors and Bacterial Resistance to Antimony and Copper. PLOS ONE. 8: e78533.

Siddiquee, S., Rovina, K., Azad, S. A., Naher, L., Suryani, S., & Chaikaew, P. (2015). Heavy Metal Contaminants Removal from Wastewater Using the Potential Filamentous Fungi Biomass: A Review. Journal of Microbial & Biochemical Technology, 07.

Siles, J. A., Ohlinger, B., Cajthaml, T., Kistler, E., & Margesin, R., (2018). Characterization of soil bacterial, archaeal and fungal communities inhabiting archaeological human-impacted layers at Monte Iato settlement (Sicily, Italy). Scientific Reports, 8:1.

Silveira, N. C. G., Martins, M. L. F., Da Silva Bezerra, A. C., & Araújo, F. (2021). Red Mud from the Aluminium Industry: Production, Characteristics, and Alternative Applications in Construction Materials—A Review. Sustainability, 13:12741.

Singh, S. R., & Singh, A. P. (2017). Adsorption of Heavy Metals from Waste Waters using Waste Biomass. International Journal of Engineering Research & Technology. 6.

Singh, A. K., Sharma, R., & Agrawal, S. B. (2008). Effects of fly ash incorporation on heavy metal accumulation, growth and yield responses of Beta vulgaris plants. Bioresource Technology, 99:7200–7207.

Singh, M., Deokaran, Mishra, J. S., & Bhatt, B. P. (2017). Effect of Integrated Nutrient Management on Production Potential and Quality of Summer Mungbean (*Vigna radiata L.).* Journal of Krishi Vigyan. 5:30-45

Singh, R., Singh, R., Soni, S. K., Singh, S. P., Chauhan, U., & Kalra, A. (2013). Vermicompost from biodegraded distillation waste improves soil properties and essential oil yield of Pogostemon cablin (patchouli) Benth. Applied Soil Ecology, 70:48–56.

Sinha, R., Chauhan, K., Valani, D., Chandran, V., Soni, B., & Patel, V. M. (2010). Earthworms: Charles Darwin's 'Unheralded Soldiers of Mankind': Protective & Productive for Man & Environment. Journal of Environmental Protection, 01:251– 260.

Skodras, G., Diamantopoulou, I., Pantoleontos, G., Sakellaropoulos, G. (2008). Kinetic studies of elemental mercury adsorption in activated carbon fixed bed reactor. Journal of Hazardous Materials, 1:1–13.

Smith, B., Wilson, J.B., 1996. A consumer's guide to evenness indices. Oikos 76:70–82.

Somlai, J., Jobbágy, V., Kovács, J., Tarjan, S., & Kovács, T. (2008). Radiological aspects of the usability of red mud as building material additive. Journal of Hazardous Materials, 150:541–545.

Sorokin, D. Y., Kuenen, J., & Muyzer, G. (2011). The Microbial Sulfur Cycle at Extremely Haloalkaline Conditions of Soda Lakes. Frontiers in Microbiology, 2.

Souza, M. J. B., Simão, L., Montedo, O. R. K., Pereira, F. V., & De Oliveira, A. C. (2019). Aluminum anodizing waste and its uses: An overview of potential applications and market opportunities. Waste Management, 84:286–301.

Srivastava, V. C., Mall, I. D., & Mishra, I. M. (2006). Modelling Individual and Competitive Adsorption of Cadmium(II) and Zinc(II) Metal Ions from Aqueous Solution onto Bagasse Fly Ash. Separation Science and Technology, 41:2685–2710.

Stehouwer, R. (2004). Soil chemistry and the quality of humus. BioCycle, 45:41-46.

Stiling, P., (2011). Ecology: Global Insights and Investigations (1st ed.). McGraw-Hill Education.

Stürzenbaum, S. R., Höckner, M., Panneerselvam, A., Levitt, J., Bouillard, J. S., Taniguchi, S., Dailey, L. A., Khanbeigi, R. A., Rosca, E. V., Thanou, M., Suhling, K., Zayats, A. V., & Green, M. (2012). Biosynthesis of luminescent quantum dots in an earthworm. Nature Nanotechnology, 8:57–60.

Sun, C., Chen, J., Tian, K., Peng, D., Liao, X., & Wu, X. (2019). Geochemical Characteristics and Toxic Elements in Alumina Refining Wastes and Leachates from Management Facilities. International Journal of Environmental Research and Public Health. 16:1297.

Sutar, H., Mishra, S. C., Sahoo, S. K., Chakraverty, A., & Maharana, H. (2014). Progress of Red Mud Utilization: An Overview. American Chemical Science Journal. 4:255–279.

Suthar, S. (2007). Nutrient changes and biodynamics of epigeic earthworm Perionyx excavatus (Perrier) during recycling of some agriculture wastes. Bioresource Technology, 98:1608–1614.

Suthar, S., 2009. Vermicomposting of vegetable-market solid waste using *Eisenia fetida*: Impact of bulking material on earthworm growth and decomposition rate. Ecological Engineering, 35:914–920.

Swain, B., Lee, C. G., & Park, J. Y. (2022). Assessment of bauxite residue as secondary resource for rare earth metal and valorization challenges: A perspective. Resources, Conservation & Recycling Advances, 14: 200078.

Tabatabai, M.A. (1994). Soil enzymes. In: Weaver, R.W., Angel, J.S., Bottomley, P.S.(Eds.), Methods of Soil Analysis. Part 2. Microbiological and Biochemical Properties. Soil Science Society of America, Madison, WI, 775–833.

Talukdar, D., Jasrotia, T., Sharma, R., Jaglan, S., Kumar, R., Vats, R., Kumar, R., Mahnashi, M. H., & Umar, A. (2020). Evaluation of novel indigenous fungal consortium for enhanced bioremediation of heavy metals from contaminated sites. Environmental Technology and Innovation, 20:101050.

Tamilselvan, N., Saurav, K., & Kannabiran, K. (2011). Biosorption of Cr (VI), Cr (III), Pb (II) and Cd (II) from aqueous solutions by *Sargassum wightii* and *Caulerpa racemosa* algal biomass. Journal of Ocean University of China,11:52–58

Teitzel, G., & Parsek, M. R. (2003). Heavy Metal Resistance of Biofilm and Planktonic *Pseudomonas aeruginosa*. Applied and Environmental Microbiology, 69:2313–2320.

Tessier, A., Campbell, P. G. C., & M, B. (1979). Sequential extraction procedure for the speciation of particulate trace metals. Analytical Chemistry, 51:844–851.

Thapar, R. K. (2022). Evaluation of the biosorption potential of *Aspergillus flavus* biomass for removal of chromium (VI) from an aqueous solution. Journal of Applied Biology and Biotechnology, 10:59-67

Thatoi, H., Das, S., Mishra, J., Rath, B. P., & Das, N. (2014). Bacterial chromate reductase, a potential enzyme for bioremediation of hexavalent chromium: A review. Journal of Environmental Management, 146:383–399.

Tiago, I., Chung, A. P., & Veríssimo, A. (2004). Bacterial Diversity in a Nonsaline Alkaline Environment: Heterotrophic Aerobic Populations. Applied and Environmental Microbiology, 70:7378–7387.

Tom, A., Djonga, P. N. D., Tsamo, C., Valery, H. A., Azangueu, J., & Noukelack, S. K. (2022). Structural Characterization of Bauxite Red Mud to Utilization in Ceramic Wall/Roofing Tile: Effect of Temperature on Mechanical Properties and Physic-Chemical Stability. Advances in Materials Physics and Chemistry, 12:1–18.

Tordoff, G. M., Baker, A. J. M., & Willis, A. J. (2000). Current approaches to the revegetation and reclamation of metalliferous mine wastes. Chemosphere, 41:219–228.

Tripathy, B., & Raha, S. (2019). Formation Of Soil. Thematics Journal of Geography. 8:144–150.

Tripathy, S., Bhattacharyya, P., Mohapatra, R., Som, A., & Chowdhury, D. (2014). Influence of different fractions of heavy metals on microbial ecophysiological indicators and enzyme activities in century old municipal solid waste amended soil. Ecological Engineering,70:25–34.

USEPA (United State Environmental Protection Agency) 2015. Risk based screening table. Composite table: summary Table 0615.

USEPA. (1992). Method 1311, Toxicity Characteristic Leaching Procedure (TCLP). PublicationSW) 846: Test Methods for Evaluating Solid Wast, Physical/Chemical Methods.

USEPA. (2002). Supplemental guidance for developing soil screening levels for superfund sites. Washington, DC: U. S. Environmental Protection Agency, Office of Emergency and Remedial Response.

Usmani, Z., Kumar, V., & Mritunjay, S. K. (2017). Vermicomposting of coal fly ash using epigeic and epi-endogeic earthworm species: nutrient dynamics and metal remediation. RSC Advances, 7:4876–4890.

Van Beers, D., Bossilkov, A., & Lund, C. (2009). Development of large scale reuses of inorganic by-products in Australia: The case study of Kwinana, Western Australia. Resources Conservation and Recycling, 53: 365-367.

Vasseur, P., & Bonnard, M., 2014. Ecogenotoxicology in earthworms: A review. Current Zoology, 60:255–272.

Verma, A., Suri, N. M., & Kant, S. (2017). Applications of bauxite residue: A mini-review. Waste Management & Research. 35:999–1012.

Verma, S., & Kuila, A. (2019). Bioremediation of heavy metals by microbial process. Environmental Technology and Innovation,14:100369.

Vig, A. P., & Singh, J. (2018). Earthworms as Organic Waste Managers and Biofertilizer Producers. Waste and Biomass Valorization, 9:1073–1086.

Vig, A. P., Singh, S., Singh, J., Kumar, S., & Bhawana. (2018). Bioremediation and detoxification of industrial wastes by earthworms: Vermicompost as powerful crop nutrient in sustainable agriculture. Bioresource Technology, 252:172–179.

Vijver, M. G., Vink, J. P., Miermans, C. J. H., & Van Gestel, C. A. (2007). Metal accumulation in earthworms inhabiting floodplain soils. Environmental Pollution, 148:132–140.

Walkley, Y.A., Black, I.A. (1934). An examination of the method for determining soil organic matter and a proposed modification of the chromic acid titration method. Soil Science. 37:29–38,

Wang, D., Shi, Q., Wang, X., Wei, M., Hu, J., Liu, J., & Yang, F. (2010). Influence of cow manure vermicompost on the growth, metabolite contents, and antioxidant activities of Chinese cabbage (Brassica campestris ssp. chinensis). Biology and Fertility of Soils, 46:689–696.

Wang, L., Chen, L. Q., Cho, D., Kim, K., Yang, J., Hou, D., Baek, K., Kua, H. W., & Poon, C. S. (2019). Novel synergy of Si-rich minerals and reactive MgO for stabilisation/solidification of contaminated sediment. Journal of Hazardous Materials, 365:695–706.

Wang, L., Sun, N., Tang, H., & Sun, W. (2019). A Review on Comprehensive Utilization of Red Mud and Prospect Analysis. Minerals, 9:362.

Wang, L., Sun, N., Wang, Z., Han, H., Yang, Y., Liu, R., Hu, Y., Tang, H., & Sun, W. (2019). Self-assembly of mixed dodecylamine–dodecanol molecules at the air/water interface based on large-scale molecular dynamics. Journal of Molecular Liquids, 276:867–874.

Wang, M., & Liu, X. (2021). Applications of red mud as an environmental remediation material: A review. Journal of Hazardous Materials, 408:124420.

Wang, S., Ang, H. M., & Tadé, M. O. (2008). Novel applications of red mud as coagulant, adsorbent and catalyst for environmentally benign processes. Chemosphere, 72:1621–1635.

Wang, W., Pranolo, Y., & Cheng, C. Y. (2013). Recovery of scandium from synthetic red mud leach solutions by solvent extraction with D2EHPA. Separation and Purification Technology, 108:96–102.

Wang, X., Sun, T., Wu, S., Chen, C., Kou, J., & Zhen, L. (2019). A novel utilization of Bayer red mud through co-reduction with a limonitic laterite ore to prepare ferronickel. Journal of Cleaner Production, 216:33–41.

Wang, X., Zhang, Y., Lu, R., Zhou, F., An, Q., Meng, Z., Yu, B., & Lv, F. (2015). Novel multiple coagulant from Bayer red mud for oily sewage treatment. Desalination and Water Treatment, 54:690–698.

Warman PR, Termeer WC. 2005. Evaluation of sewage sludge, septic waste and sludge compost applications to corn and forage: yields and N, P and K contents of crops and soils. Bioresource Technology, 96:955–961

WHO 1996. Guidelines for drinking-water quality, vol 2, 22nd edn. World Health Organization, Geneva.

WHO/FAO (2007) Joint FAO/WHO Food Standard Programme Codex Alimentarious Commission 13th Session. Report of the Thirty-Eight Session of the Codex Committee on Food Hygiene, Houstan, United States of America, ALINORM 07/30/13.

Wiercigroch, E., Szafraniec, E., Czamara, K., Pacia, M. Z., Majzner, K., Kochan, K., Kaczor, A., Baranska, M., Malek, K. (2017). Raman and infrared spectroscopy of carbohydrates: A review. Spectrochimica Acta Part A: Molecular and Biomolecular Spectroscopy, 185:317–335.

Wierzba, S. (2017) Biosorption of nickel (II) and zinc (II) from aqueous solutions by thebiomass of yeast *Yarrowia lipolytica*. Polish Journal of Chemical Technology, 19:1–10.

Witek-Krowiak, A. (2012). Analysis of temperature-dependent biosorption of Cu^{2+} ions on sunflower hulls: Kinetics, equilibrium and mechanism of the process. Chemical EngineeringJournal, 192:13–20.

Wright, R. O. (1989). Soil aluminum toxicity and plant growth. Communications in Soil Science and Plant Analysis. 20:1479–1497.

Wu, H., Liao, J. X., Zhu, F., Millar, G., Courtney, R., Xue, S. G. (2019). Isolation of an acid- producing *Bacillus sp*. EEEL02: Potential for bauxite residue neutralization. Journal of CentralSouth University, 26:343–352.

Xiu, W., Guo, H., Liu, Q., Liu, Z., Zou, Y., & Zhang, B. (2015). Arsenic Removal and Transformation by *Pseudomonas* sp. Strain GE-1-Induced Ferrihydrite: Co-precipitation Versus Adsorption. Water Air and Soil Pollution, 226:6.

Xu, D., Wang, Q., Wu, Y., Yu, G., Shen, Q., & Huang, Q. (2012). Humic-Like Substances from Different Compost Extracts Could Significantly Promote Cucumber Growth. Pedosphere, 22:815–824.

Xue, S., Kong, X., Wu, C., Huang, L., Huang, N., & Hartley, W. (2016). A review of the characterization and revegetation of bauxite residues (Red mud). Environmental Science and Pollution Research, 23:1120–1132.

Xue, S., Kong, X., Zhu, F., Hartley, W., Li, X., & Li, Y. (2016). Proposal for management and alkalinity transformation of bauxite residue in China. Environmental Science and Pollution Research, 23:12822–12834

Yadav, A. K., & Garg, V. K. (2013). Nutrient Recycling from Industrial Solid Wastes and Weeds by Vermiprocessing Using Earthworms. Pedosphere, 23, 668–677.

Yadav, A., & Garg, V. K. (2019). Biotransformation of bakery industry sludge into valuable product using vermicomposting. Bioresource Technology, 274:512–517.

Yadav, K. D., Tare, V., & Ahammed, M. M. (2010). Vermicomposting of source-separated human faeces for nutrient recycling. Waste Management, 30:50–56.

Yalçın, N., & Sevinç, V. (2000). Utilization of bauxite waste in ceramic glazes. Ceramics International, 26:485–493.

Yang, C., Niu, Y., Su, H., Wang, Z., Tao, F., Wang, X., Tang, H., Ma, C., & Xu, P. (2010). A novel microbial habitat of alkaline black liquor with very high pollution load: Microbial diversity and the key members in application potentials. Bioresource Technology, 101:1737–1744.

Yang, S., Deng, W., Liu, S., Yu, X., Mustafa, G., Chen, S., He, L., Ao, X., Yang, Y., Zhou, K., Li, B., Han, X., Xu, X., & Zou, L. (2020). Presence of heavy metal resistance genes

in Escherichia coli and Salmonella isolates and analysis of resistance gene structure in *E. coli* E308. Journal of Global Antimicrobial Resistance, 21:420–426.

Yang, Z., Wang, Y., Shen, Z., Niu, J., & Tang, Z. (2009). Distribution and speciation of heavy metals in sediments from the mainstream, tributaries, and lakes of the Yangtze River catchment of Wuhan, China. Journal of Hazardous Materials, 166:1186–1194.

Ye, N., Yang, J., Ke, X., Zhu, J., Li, Y., Xiang, C., Wang, H., Li, L., & Xiao, B. (2014). Synthesis and Characterization of Geopolymer from Bayer Red Mud with Thermal Pretreatment. Journal of the American Ceramic Society, 97:1652–1660.

Yilmaz, E. I., & Ensari, N. Y. (2005). Cadmium biosorption by *Bacillus circulans* strain EB1. World Journal of Microbiology and Biotechnology, 21:777–779

Yin, K., Wang, Q., Lv, M., & Chen, L. (2019). Microorganism remediation strategies towards heavy metals. Chemical Engineering Journal, 360:1553–1563.

Yuan, X., Huang, H., Zeng, G., Li, H., Wang, J., Zhou, C., Zhu, H., Pei, X., Tang, L., & Liu, Z. (2011). Total concentrations and chemical speciation of heavy metals in liquefaction residues of sewage sludge. Bioresource Technology, 102:4104–4110.

Yuvaraj, A., Thangaraj, R., Karmegam, N., Ravindran, B., Chang, S. H., Awasthi, M. K., & Kannan, S. (2021). Activation of biochar through exoenzymes prompted by earthworms for vermibiochar production: A viable resource recovery option for heavy metal contaminated soils and water. Chemosphere, 278:130458.

Zeb, A., Li, S., Wu, J., Lian, J., Liu, W., & Sun, Y. (2020). Insights into the mechanisms underlying the remediation potential of earthworms in contaminated soil: A critical review of research progress and prospects. Science of the Total Environment. 740:140145.

Zeng, H. C., Lyu, F., Sun, W., Zhang, H., Wang, L., & Wang, Y. (2020). Progress on the Industrial Applications of Red Mud with a Focus on China. Minerals, 10:773.

Zhang, M., Song, L., Jiang, H., Li, S., Shao, Y., Yang, J., & Li, J. (2017) Biomass based hydrogel as an adsorbent for the fast removal of heavy metal ions from aqueous solutions. Journal of Materials Chemistry, 5:3434–3446

Zhang, M., Yin, Q., Ji, X., Wang, F., Gao, X., & Zhao, M. (2020). High and fast adsorption of Cd(II) and Pb(II) ions from aqueous solutions by a waste biomass based hydrogel. Scientific Reports 10.

Zhang, G., He, J., & Gambrell, R. P. (2010). Synthesis, Characterization, and Mechanical Properties of Red Mud–Based Geopolymers. Transportation Research Record, 2167:1–9.

Zhang, L. (2013). Production of bricks from waste materials – A review. Construction and Building Materials, 47:643–655.

Zhang, S., Liu, D., Deng, W., & Que, G. (2007). A Review of Slurry-Phase Hydrocracking Heavy Oil Technology. Energy & Fuels, 21:3057–3062.

Zhang, T., Wang, Y., Lu, G., Liu, Y., Zhang, W., & Zhao, Q. (2018). Comprehensive Utilization of Red Mud: Current Research Status and a Possible Way Forward for Non-hazardous Treatment. 131-142.

Zhang, Y., Atopkin, D., Wang, L., & Wu, D. (2021). Description of a new earthworm species of the genus Drawida (Oligochaeta: Moniligastridae) from Northeast China and Far East Russia. Journal of Asia-Pacific Biodiversity,14:425–429.

Zhang, Y., Jiang, J., & Chen, M. (2008). MINTEQ modeling for evaluating the leaching behavior of heavy metals in MSWI fly ash. Journal of Environmental Sciences-china, 20: 1398–1402.

Zhao, C., Wang, Y., Wang, Y., Wu, F., Zhang, J., Cui, R., Wang, L., & Mu, H. (2018). Insights into the role of earthworms on the optimization of microbial community structure during vermicomposting of sewage sludge by PLFA analysis. Waste Management, 79, 700– 708.

Zhong, H., & Wang, W. (2009). Controls of Dissolved Organic Matter and Chloride on Mercury Uptake by a Marine Diatom. Environmental Science & Technology, 43:8998–9003.

Zhou, B., Cao, S., Chen, F., Zhang, F., & Zhang, Y. (2019). Recovery of Alkali from Bayer Red Mud Using CaO and/or MgO. Minerals, 9:269.

Zhou, H., Zhou, X., Zeng, M., Liao, B. H., Liu, L., Yang, W. T., Wu, Y. M., Qiu, Q. Y., & Wang, Y. J. (2014). Effects of combined amendments on heavy metal accumulation in rice (*Oryza sativa L.)* planted on contaminated paddy soil. Ecotoxicology and Environmental Safety, 101: 226–232.

Zhu, D., Chun, T., Pan, J., & He, Z. (2012). Recovery of Iron From High-Iron Red Mud by Reduction Roasting With Adding Sodium Salt. Journal of Iron and Steel Research International, 19:1–5.

Zhu, F., Li, Y., Xue, S., Hartley, W., & Wu, H. (2016). Effects of iron-aluminium oxides and organic carbon on aggregate stability of bauxite residues. Environmental Science and Pollution Research, 23:9073–9081.

Zhu, F., Xue, S., Hartley, W., Huang, L., Wu, C., & Li, X. (2016). Novel predictors of soil genesis following natural weathering processes of bauxite residues. Environmental Science and Pollution Research, 23:2856–2863.

Zhu, F., Zhou, J., Hartley, W., Wu, C., & Guo, Y. (2016). Aging of bauxite residue in association of regeneration: a comparison of methods to determine aggregate stability & erosion resistance. Ecological Engineering, 92:47–54.

Annexure A

Table 1: **Relative standard deviations for various elements analysed in UV Visible spectrophotometer (Systronics 117) and Flame photometer (Systronics 130).**

Instrument	Parameter	Method detection limit	Relative standard deviation (%)
UV-VIS Spectrophotometer	Dehydrogenase	0.5 µmol g^{-1} h^{-1}	2.1
	Phosphatase	0.1 µg g^{-1} h^{-1}	4.9
	Phosphorus	0.5 mg kg^{-1}	1.6
	Leucine	0.1 µg g^{-1}	0.9
Flame Photometer	Potassium (K)	0.5 mg kg^{-1}	6.2
	Sodium (Na)	0.5 mg kg^{-1}	4.8
	Calcium (Ca)	0.5 mg kg^{-1}	4.3

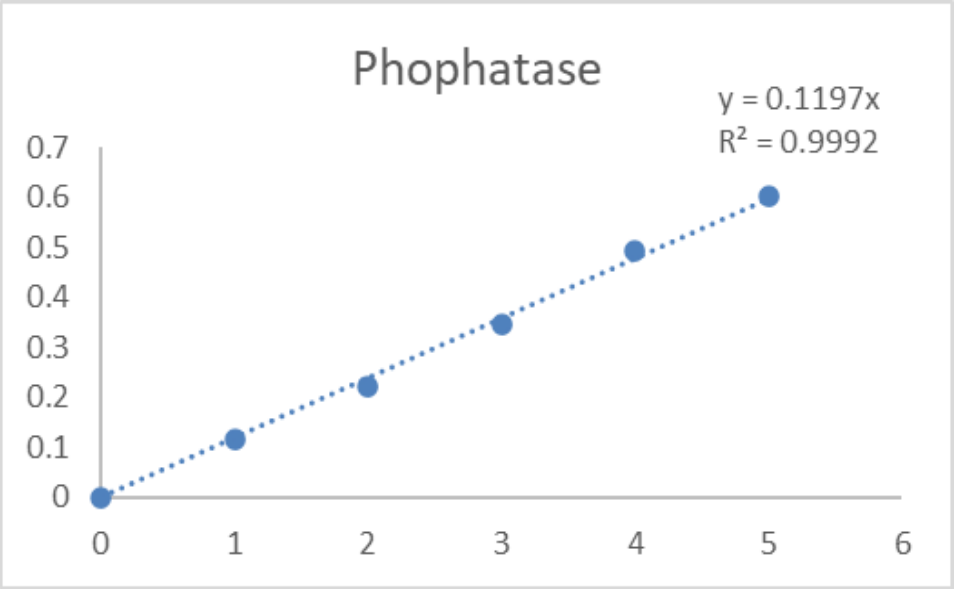

Fig. 1: Calibration curve of phosphatase activity

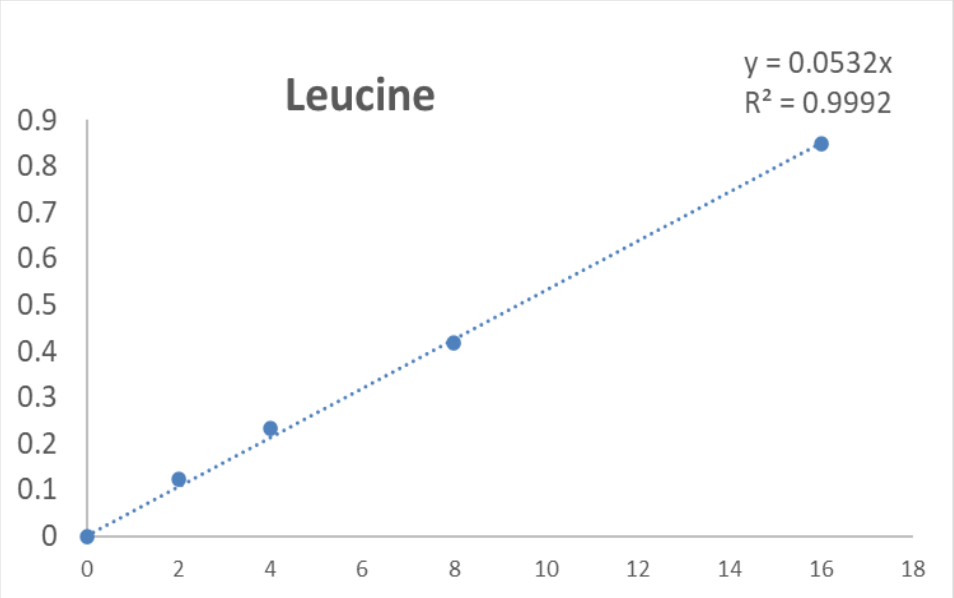

Fig. 2: Calibration curve of leucine

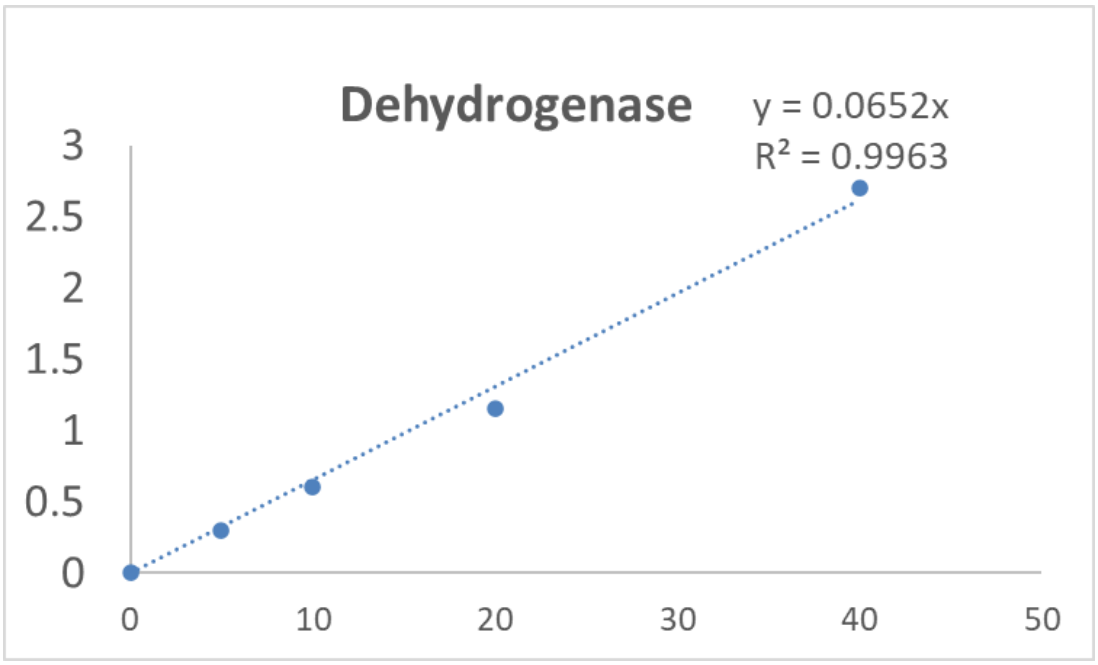

Fig. 3: Calibration curve of dehydrogenase

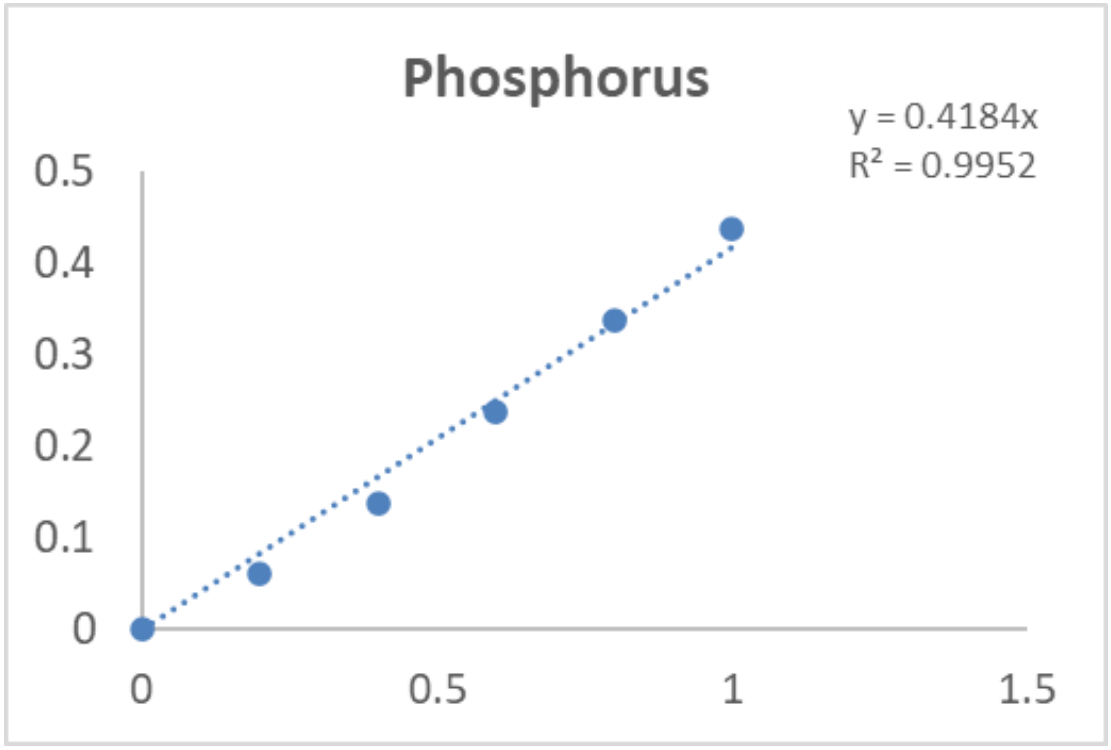

Fig. 4: Calibration curve of phosphorus.

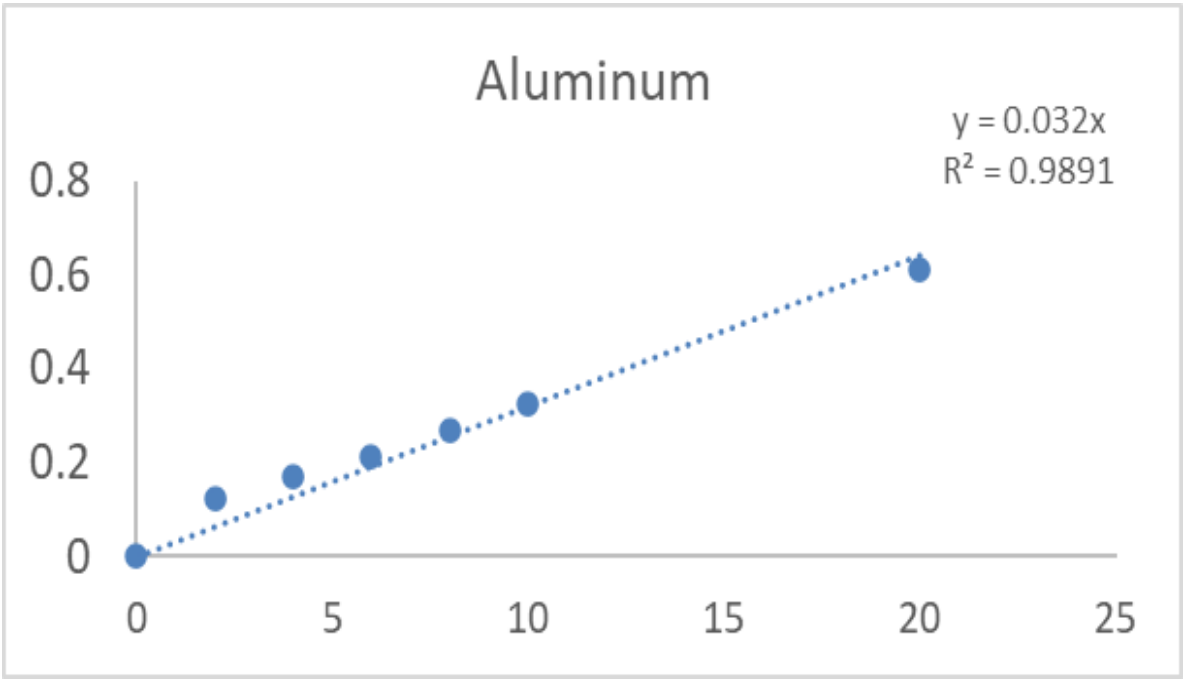

Fig. 5: Calibration curve of aluminum.

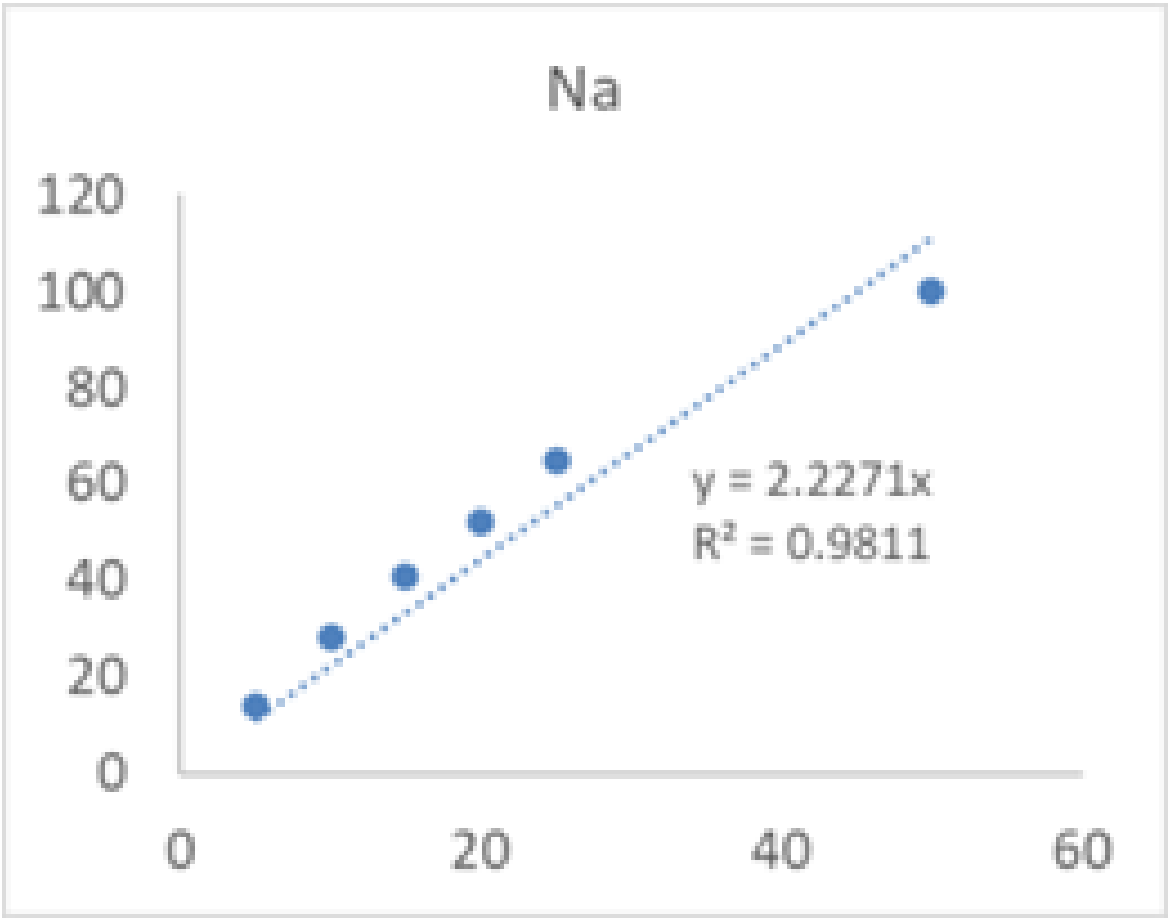

Fig. 6: Calibration curve of Na.

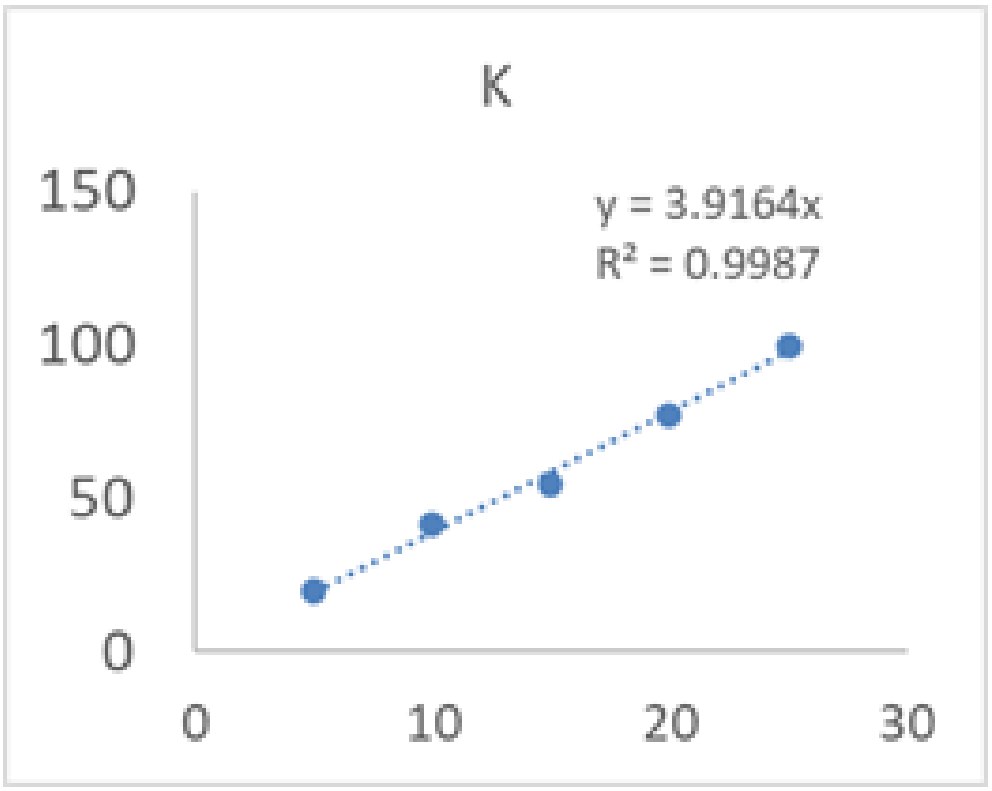

Fig. 6: Calibration curve of K.

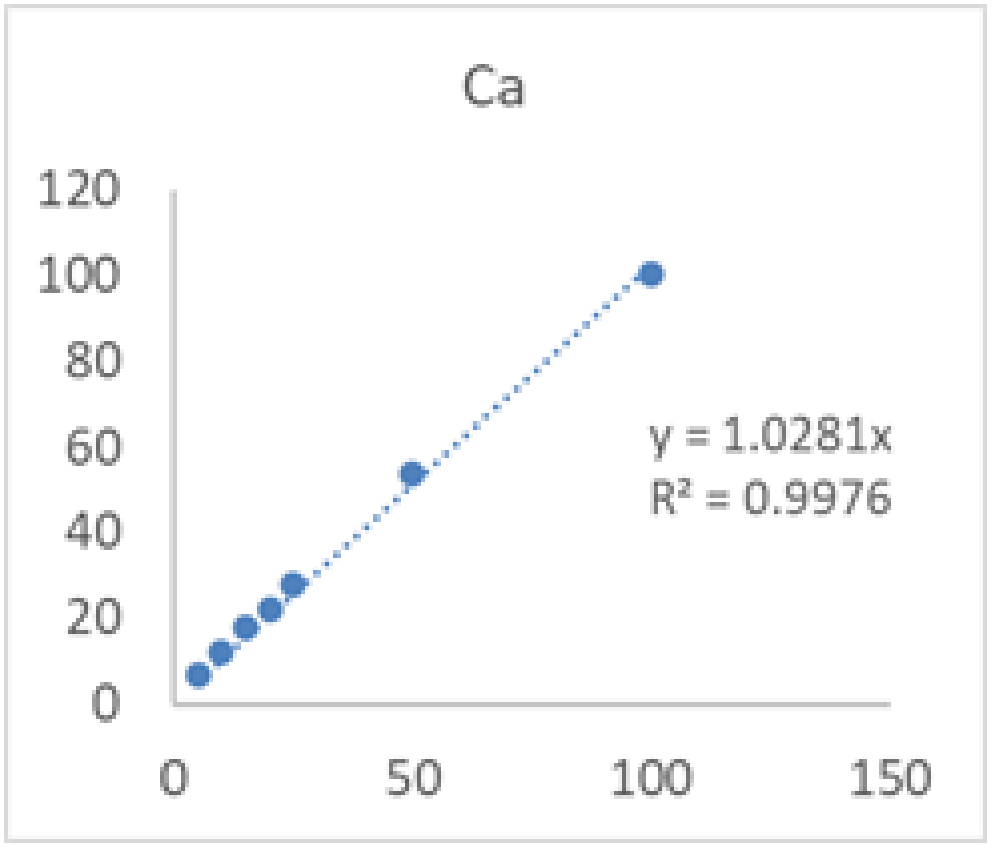

Fig. 6: Calibration curve of Ca.

PHOTOGRAPHS

Picture 1: Red mud (RM) sample collection from HINDALCO, Muri, Jharkhand.

Picture 2: Earthworm inoculation and vermicomposting of red mud (RM).

Picture 3: Pot application of vermicomposted red mud (RM-VC) for *Vigna radiata L.*

Picture 4: Field application of RM-VC for monsoonal rice (*Oryza sativa L.*)

Picture 5: Plot design, application and production of monsoonal rice.

Crop and Weed Science Society
(CWSS) Registration No. S/IL/24559 - 2004
Secretariat : Department of Agronomy, Faculty of Agriculture, Bidhan Chandra Krishi Viswavidyalaya (BCKV).
Mohanpur - 741252, Nadia, West Bengal, India, Tel : (03473) 222269 Ext.-89 and Fax: (03472) 222273 / 75 / 77

Ref. No. : ..... Date : .....

Date: 20-02-23

Acceptance Letter for Articles Submitted for Publication in J. Crop and Weed

Dear Author,

Greetings!

We are happy to inform you that the following article has been accepted as Full Paper article for publication in volume 19 (2) of the Journal of Crop and Weed scheduled to be published during August 2023 subject to the fulfillment of the following requirements.

Title	*Author*	*Affiliation*
Vermicomposted red mud- A up-and-coming approach towards soil fertility	**K. CHARAN, P. BHATTACHARYYA***	**Agricultural and Ecological Research Unit, Indian Statistical Institute, Giridih, Jharkhand 815301, India pradip.bhattacharyya@gmail.com**

Sl No	*Requirement*	*Comment*
1	Submission of signed 'No Objection Certificate' from all the authors clearly stating that they have no objection in publishing the article in the Journal of Crop and Weed transferring the copyright to the Secretary, CWSS and the article is not published or not being considered for publication in any other journal and is devoid of any conflict of interest.	If not submitted already
2	Membership fees for all the authors (Life membership fee Rs5000)	If not paid already
3	Processing fee of Rs500/=	If not paid already
4	Publication Charge @ Rs 1000 per author	If not paid already

Thank you very much for selecting the Journal of Crop and Weed as the outlet for your valuable research work to the world.

With regards,

Sd/.
Md. Nasim Ali
Executive Editor
Journal of Crop and Weed